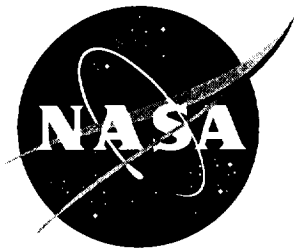

NASA Technical Memorandum 108522

Project ORION: Orbital Debris Removal Using Ground-Based Sensors and Lasers

J.W. Campbell

October 1996

NASA Technical Memorandum 108522

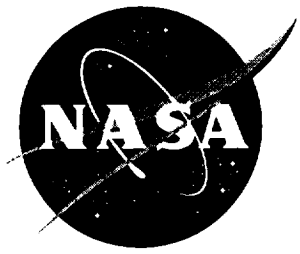

Project ORION: Orbital Debris Removal Using Ground-Based Sensors and Lasers

J.W. Campbell, Project Manager
Marshall Space Flight Center • MSFC, Alabama

National Aeronautics and Space Administration
Marshall Space Flight Center • MSFC, Alabama 35812

October 1996

TABLE OF CONTENTS

TABLE OF CONTENTS

LIST OF ILLUSTRATIONS

TECHNICAL MEMORANDUM

PROJECT ORION: ORBITAL DEBRIS REMOVAL USING GROUND-BASED SENSORS AND LASERS

EXECUTIVE SUMMARY

A study was initiated in 1995 by NASA, co-sponsored by the U.S. Air Force (USAF) Space Command, to determine the feasibility of removing the bulk of the threatening orbital debris in low-Earth orbit (LEO) by irradiating it with a ground-based laser. The laser energy ablates a thin surface layer from a debris particle, causing plasma blowoff. The dynamic reaction from one or more laser hits lowers the perigee of the orbit and hastens reentry.

The study was undertaken as an initiative of the Advanced Concepts Office at NASA Headquarters (HQ), and managed by the NASA Marshall Space Flight Center (MSFC). The study team included USAF Phillips Laboratory, MIT Lincoln Laboratories, NASA MSFC, Northeast Science and Technology, Photonic Associates, and the Sirius Group.

A wide range of objects in orbit are characterized as orbital debris. The size range of greatest interest is 1 to 10 cm. While objects smaller than 1 cm are extremely numerous and difficult to detect, shielding against them is straightforward, although somewhat expensive. Objects larger than about 10 cm are routinely tracked, and their numbers are small enough that operational spacecraft can maneuver to avoid them. There remain about 150,000 objects between 1 and 10 cm in size. They are problematic to track, too numerous to avoid, and shielding against them is very difficult or expensive.

NASA believes that the debris population likely to exist during the life of the *International Space Station* (*ISS*) is high enough that limited protection measures are being incorporated into the *ISS* program. These will protect it against objects up to about 2 cm in diameter.

Various strategies for irradiating the debris objects were analyzed, including those that engage objects in several passes over the laser, and those in which immediate reentry is caused by irradiation during a single pass. The latter is operationally the simplest: fire at any debris object the sensors show to be approaching in favorable circumstances, without regard to whether it has been previously irradiated or not. The former requires a plan such as our "steady rain" approach to guarantee that the risk to space assets does not temporarily increase at any orbital altitude.

The statistical characteristics of the debris population are reasonably well known. Five different representative debris objects were defined as reference targets to deorbit. The orbital distribution of the debris particles was addressed, and the velocity change needed was determined to be a few hundred meters per second—sufficient to cause the perigee to drop to 200 km. Achieving a 200-km perigee reduces a particle's expected lifetime in orbit to a few days.

The interaction of laser beams with these debris objects was characterized, and the range of coupling coefficients of the resulting plasma blowoff determined from both experiment and theory. The required incident beam intensity and duration at the objects was then determined in order to cause the velocity change necessary for reentry within a few orbits. It was determined that the laser has to place many very short pulses on the objects to avoid self-shielding of the generated plasma at the object. The intensity of the irradiation was also determined.

Once the requirements at the debris objects were understood, the required ground laser characteristics were then defined, considering the effects of the atmosphere on the beam. Effects included in the calculations were turbulence, absorption, stimulated Raman scattering (SRS), stimulated thermal Rayleigh

scattering (STRS), whole-beam thermal blooming, and nonlinear refractive index. A graphical technique was developed that enables selection of the optimum laser for this system.

A number of options for detection, acquisition, tracking, and handoff of debris targets to the laser were investigated. These included radar, passive optical, active optical using the laser itself, and combinations of these. In addition, a novel detection technique was analyzed that uses the many communications spacecraft that are or will soon be in orbit as "free" illuminators to form a bistatic surveillance system.

A spectrum of system concepts was developed, each of which meets some or all the system goals. These concepts span a range of costs and technology challenges. In addition, a demonstration of the capability on actual debris could be mounted using mostly existing assets for about $20 million.

The nearest term operational system would consist of a Nd:glass laser operating at 1.06 mm with a pulse width of 5 ns operating at a rate of 1 to 5 Hz. It would have 3.5-m diameter optics, operate with a sodium guide star, and produce 5-kJ pulses. This system would cost about $60 million, and would cause the reentry of essentially all debris in the desired size range in 2 years of operation, up to an altitude of 800 km. This system would be sufficient to protect the *ISS* as well as all other satellites in LEO below 800 km, including the planned Iridium and Teledesic systems.

More ambitious technology systems were defined that have the ability to remove all such debris objects up to an altitude of 1,500 km. This would extend protection to the Globalstar system as well as other civilian and defense assets. This more advanced system would require an additional $80 million and an additional year of operation.

A cursory analysis indicated that a system of this type is not inherently an antisatellite weapon, being relatively very weak. It would have to illuminate a typical spacecraft continuously for years to destroy its structure, and months to make major changes in its orbit, though unintentional damage to some sensors and other subsystems would be possible.

Due to the inherently national character of such a system, if serious interest develops to pursue the capability, it is likely that the Department of Defense (DOD) should be the preferred agency to develop and operate it for the benefit of all spacecraft, be they commercial, civil, or defense.

The study concluded that the capability to remove essentially all dangerous orbital debris in the targeted size range is not only feasible in the near term, but its costs are modest relative to the likely costs to shield, repair, or replace high-value spacecraft that could otherwise be lost due to debris impacts for debris particles greater than about 1 cm in size. Due to the difficulty in detecting debris smaller than about 1 cm, and their great numbers, the presence of an ORION system would not obviate the need to shield high-value, large, long-lived spacecraft to resist impacts of debris particles that are about 1 cm in size and smaller.

The study concluded that a demonstration system should be undertaken to demonstrate, at low cost, the ability to detect, track, illuminate, and perturb the orbit of an existing particle of debris.

The study also concluded that the bistatic detection technique could form a needed augmentation to the current space surveillance systems, particularly in the Southern Hemisphere.

PROJECT ORION TEAM

Ivan Bekey, Senior Executive, Advanced Concepts Office	NASA/HQ
John Rather, Study Advisor	NASA/HQ
Jonathan W. Campbell, Project Manager	NASA/MSFC
William Dent	Dent International Research Inc.
Claude R. Phipps	Photonic Associates
Richard C. Raup	MIT Lincoln Laboratories
James P. Reilly	Northeast Science and Technology
David Spencer	USAF Phillips Laboratory
Ramaswamy Sridharan	MIT Lincoln Laboratories
Charles R. Taylor	Western Oregon State College
Glenn Zeiders	The Sirius Group

1. INTRODUCTION

Project ORION was undertaken as an initiative of the Advanced Concepts Office at NASA Headquarters, and managed by NASA MSFC. The study team included USAF Phillips Laboratory, MIT Lincoln Laboratories, NASA MSFC, Northeast Science and Technology, Photonic Associates, and the Sirius Group.

The orbital debris population has increased at a linear rate since the exploration of space began. Most of the mass of the debris in orbit is in the form of large objects: inactive payloads and rocket bodies. Most of the risk to space assets, however, comes from smaller objects. The small objects are mission-related debris, such as bolts that separate in the deployment of payloads and, most importantly, fragments resulting from degradation, explosions, and collisions in space.

If enough large objects are placed in orbit, the growth in the debris population will change from linear to exponential. This is a result of the collisions between large and small objects. The population may already have reached the threshold for exponential growth in certain altitude ranges. Some mitigation measures have, therefore, been put into place and others are being discussed.

One mitigation measure already being used is spacecraft shielding. This technology reduces the risk of catastrophic damage, and the production of more fragments in orbit, in collisions with debris up to about 1 cm in diameter. For the *ISS* this protection will be extended up to about 2 cm for critical areas. There is no technology presently available at a reasonable cost to shield against debris greater than about 2 cm and traveling at 10 km/s mean relative speed. This is because the shielding weight penalty is an exponentially increasing function of the maximum size of the debris.

The additional shielding required just to extend the *ISS* protection envelope from 1-cm debris particles to 2 cm weighs about 10,000 lb. For a launch cost of $10,000 per lb, the cost simply to launch this shielding is on the order of $100 million. Development, fabrication, and integration could double the cost.

Avoidance maneuvers are another measure already being used to deal with orbital debris. These are effective for avoiding objects larger than about 10 cm in diameter. Objects this size or larger can be tracked reliably and their orbits predicted well enough to allow the debris to be avoided. This method only applies to assets that are maneuverable, and is relatively expensive in that it requires additional propellant.

Presently on the drawing board are a few other concepts that may eventually be useful. These include a maneuverable "catcher's mitt" unattached payload for the space station. Devices such as these are inherently expensive and may not be able to respond quickly enough to prevent collisions.

Neither shielding (due to the weight penalty) nor maneuvers (because of the difficulty of tracking and generating reliable orbit elements) are sufficient to mitigate debris in the 2- to 10-cm regime. Approximately 150,000 1- to 10-cm debris particles are currently estimated to be orbiting the Earth. The majority of this debris is found from 200 to 1,500 km in altitude. The maximum of the distribution as a function of altitude is found around 1,000 km. This peak is thought to be due primarily to a single event, the leakage of metal coolant from the damaged reactor of a Russian satellite. The remainder of the distribution reveals a more uniform distribution with altitude. The maximum density as a function of inclination is at roughly 40° to 60°.

A natural mechanism for the removal of objects in LEO is drag in the upper atmosphere. Drag brings objects gradually to lower orbits until they eventually burn up in the lower atmosphere. The natural decay time for a particle decreases rapidly for lower orbits, but in orbits above 500 km many years are required. This study explores ways of accelerating this natural mechanism by altering the orbits of debris particles with laser energy beamed from the ground.

Heating the surface of a debris particle with a sufficiently intense laser beam ablates and ionizes a thin layer of material. The particle experiences a small but significant momentum change. A sufficient number of such interactions, delivered at well-chosen times and positions, can change the particle's orbit and cause it to reenter sooner than it would otherwise.

At the energies we are considering in this study, we will not be completely vaporizing the debris particles, nor will they be fragmented into a large number of smaller bits. Instead, we have found a means of deorbiting the debris in the 1- to 10-cm range, the range that is expensive to shield against and difficult to track reliably. It will still be necessary to study mitigation options (such as more powerful laser systems) to address the longer-term but lower-risk problem of larger debris.

It is also recognized that large, long-lived spacecraft such as the *ISS* will need some shielding even if an ORION system is deployed. This is because the flux of debris particles smaller than 1 cm is relatively large, and the small particles are nearly impossible to detect with present technology. Collisions can result in extensive damage to unshielded spacecraft.

The overall objective of the study was to determine the technical feasibility, the cost, and the development time for using ground-based lasers and sensors to remove 1- to 10-cm sized debris from LEO. This was further divided into the following specific subobjectives:

A. Protect the *ISS* and other assets in LEO to an 800-km altitude

B. Protect all Earth-orbiting assets to a 1,500-km altitude.

We will show that ORION systems that accomplish these objectives may cost less than the amount needed just to shield the *ISS* from debris between 1 and 2 cm in size, and would have the potential to protect not just the space station but all other assets in LEO below about 1,500 km.

This report is in the form of a summary followed by seven technical appendices. The appendices provide a deeper technical discussion of our analyses.

Sections 2, 3, and 4, which follow this introduction, develop three sets of physical constraints on the ORION system. Section 2 is concerned with the debris properties: their sizes, compositions, and distribution in space, and their optical and radar properties. The interaction of solid targets with intense laser

beams is considered in section 3. Section 4 is concerned with the propagation of an intense laser beam through the atmosphere. In section 5, we synthesize the physical and programmatic constraints into a set of requirements for a system. In sections 6 and 7, we discuss existing technology as it relates to the system requirements. Section 6 deals with high-energy lasers and related technology, while section 7 is concerned with sensors and tracking. Section 8 contains our feasible options along with cost estimates. In section 9, we distinguish the ORION concept from anti-satellite weapons. Section 10 summarizes the study, and section 11 presents our conclusions. We follow this with our recommendations in section 12.

Appendix A was prepared by Dr. James P. Reilly of Northeast Science and Technology. It is a thorough analysis of solid-state laser technology as it applies to ORION. In particular, it addresses issues of allowable pulse duration versus extracted energy density, and the cooling requirements of repetitively pulsed solid-state lasers as functions of pulse energy. The cooling requirements take into account both beam quality reduction and fracture. Appendix B, also by Dr. Reilly, is a unified evaluation and side-by-side comparison of all debris-object acquisition schemes. These analyses all used a common analysis approach, current state-of -the-art focal plane and optical telescope technology capabilities, and current state-of-the-art microwave detectors and transmitter technologies. Common success criteria are applied to all detection techniques.

Appendix C, prepared by R. Sridharan of MIT Lincoln Laboratories, expands on microwave and optical tracking systems for ORION. The present orbital debris environment and engagement strategies are discussed.

Claude Phipps of Photonic Associates prepared appendix D. It contains a complete discussion of the laser-target interaction. In addition, it deals with the critical effects of nonlinear processes in the atmosphere on pulsed laser beam propagation. These effects include SRS, STRS, and nonlinear refraction and self-focusing (n_2). Appendix C also deals with the relationship between laser-produced impulse and reduction of debris orbital lifetime, laser and systems design, system demonstration, and first-order cost models.

Appendix E was contributed by Glenn Zeiders of the Sirius Group. Atmospheric linear propagation and adaptive optics are treated thoroughly. Also in appendix D are discussions of lifetime of debris in orbit and engagement geometries that reduce the lifetime. Optical system design, including a coelostat design for the laser installation, is included.

Appendix F, by William Dent of Dent International Research, Inc., compares the options available in high-power lasers. It concludes with an indepth review of Nd:glass laser technology.

The bistatic detection of orbital debris with communications satellites is treated in appendix G. It was prepared by Richard C. Raup of MIT Lincoln Laboratories.

2. THE DEBRIS PARTICLE

One set of constraints on the design of both the laser and the sensor systems is the range of characteristics of the debris particles. The microwave reflectance sets the size and power needed if a radar facility is to acquire and track objects. Similarly, the optical reflectance determines the size of an optical tracking system. The optical reflectance also plays a role in the laser system design, since laser reflection from a target decreases the momentum transfer. The ablation and ionization properties of the particle surfaces also set requirements on the size, pulse duration, and power of the laser.

The roughly 150,000 particles in the size range from 1 to 10 cm, which are the object of this study, can be classified into five distinct groups. Our approach was to examine each category in order to establish minimum requirements for the sensor and laser systems. The requirements for the categories can then be compared and the requirements assembled for a system that deals with all five categories.

2.1 Debris Distribution in the 1- to 10-cm Size Regime

A great deal of work has already been accomplished in characterizing the debris cloud surrounding the Earth. The Haystack radar system of MIT Lincoln Laboratories has done pivotal work in this regard. The work is described more fully in appendix C and is illustrated below.

A sample of the Haystack debris measurements is shown in figure 1. The top part of the figure shows the number of particles detected per hour in bins of 50-km altitude each. It shows that relatively few particles are detected below 500 km, and that the number of detections per hour rises to a level of about 0.1 per hour per 50-km altitude bin between 500 and 1,500 km. The flux of detectable objects is defined as the ratio of the rate of passage of detectable objects to the cross-sectional area through which they pass. The flux must be calculated from the detection rate in each altitude bin, taking the geometry into account. The derived flux is shown in the lower part of figure 1. It shows a distinct peak in the flux at an altitude of 1,000 km.

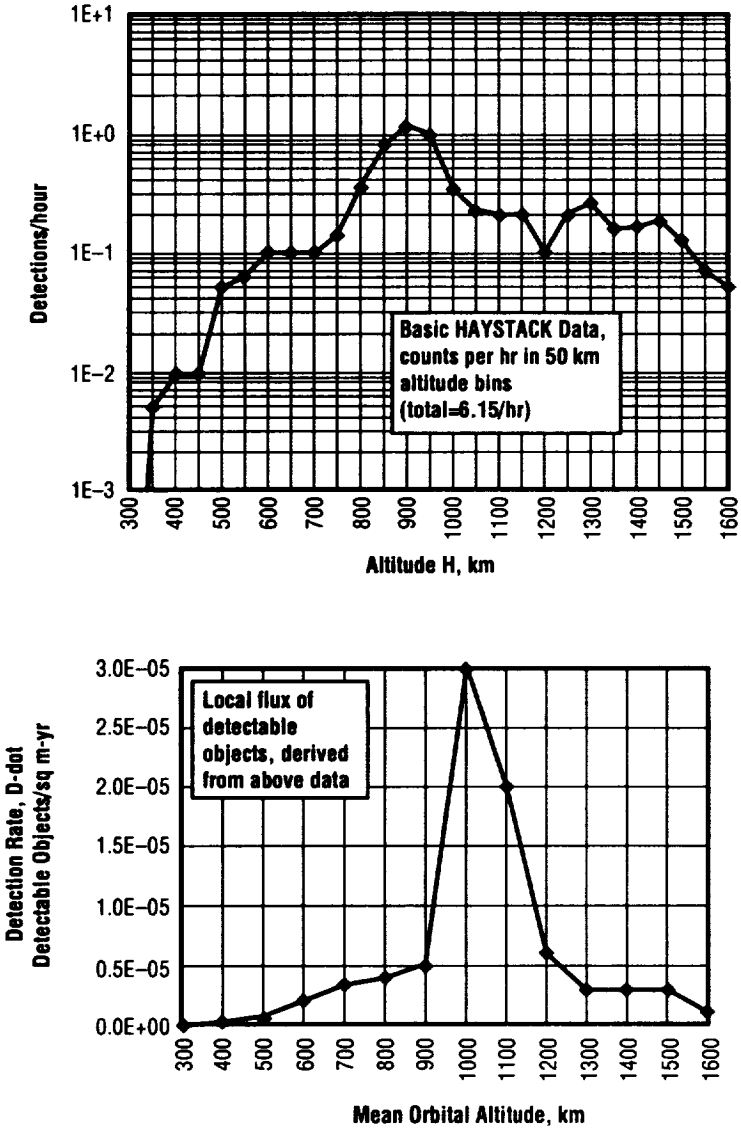

Figure 1. Haystack measurements of debris count versus altitude in 50-km altitude bins and derived flux of objects into cylindrical beam.

There are several implications of the orbital debris measurements from the ground. First, debris is found at all altitudes ranging from below 200 km to above 1,500 km. Flux varies with altitude, with a maximum at about 1,000 km. Recall that debris above 500 km will remain a threat for years due to minimal drag. Debris below 200 km will reenter in a few hours or days due to drag. Finally, and perhaps the most important point, is that there is an existing radar, Haystack, which has proven that radar can detect and track 1- to 10-cm debris in the altitude range of interest to the ORION study.

With respect to the distribution of particles, two requirements were set for ORION. System A, corresponding to subobjective A, is intended to protect the *ISS* and over 300 other satellites below 800 km. Configuration B is intended to protect all assets below 1,500 km. Figure 2 compares the orbital debris population in LEO, the present and projected near-term LEO satellite distribution, and the ranges of ORION subobjectives A and B. The left-hand graph displays Haystack estimates of total numbers of debris particles in 100-km altitude shells. Altitude is now on the vertical axis. The center graph shows the distribution of present and near-term space assets on the same altitude scale. The bar graphs on the right show the altitude ranges addressed by ORION systems.

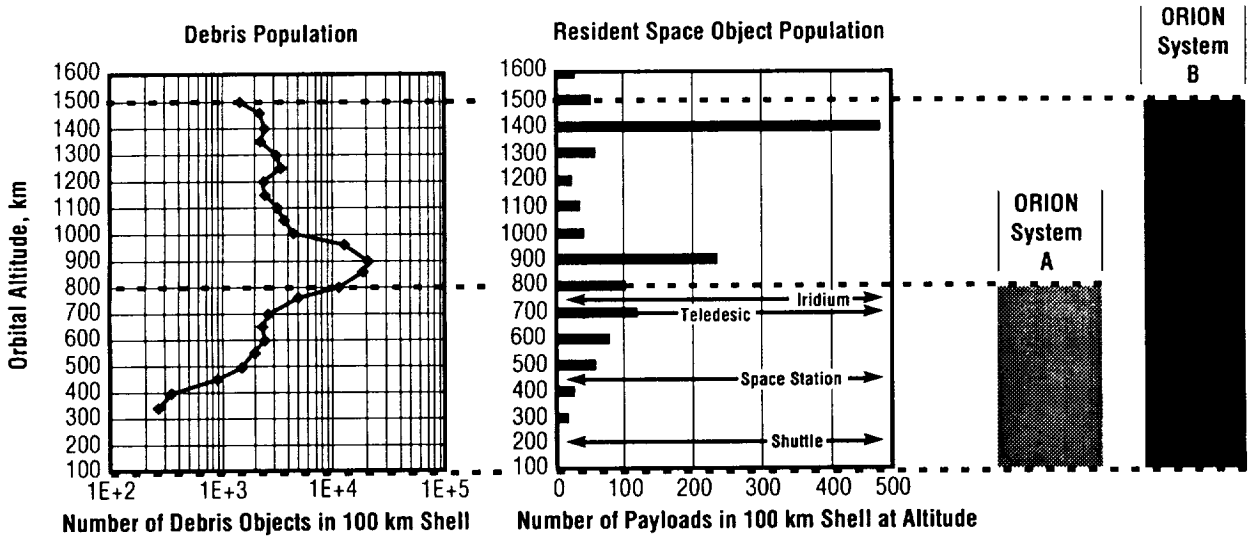

ORION Systems will provide protection both for existing low-altitude assets and near-term government and commercial payloads

System A: 200 km to 800 km orbital altitude cleared of debris
System B: 200 km to 1500 km orbital altitude cleared of debris

Figure 2. Comparison of ORION protection for existing LEO assets with debris distribution.

2.2 Debris Categories

Surprisingly, the existing debris distribution can reasonably be organized into as few as five major categories: Na/K spheroids (reactor coolant), carbon phenolic fragments, multilayered insulation (MLI), crumpled aluminum, and steel tank rib supports. The laser interactions with and radar characteristics of these categories are part of the first set of parametric requirements on the laser and the sensor systems. The characteristics are displayed in figure 3. They include the inclination, apogee, perigee, area-to-mass ratio, actual size, Bond albedo, Dv required for deorbit, and the estimated number of particles.

Debris Target Matrix

Target	A	B	C	D	E
Description	Na/K Sphere	Carbon Phenolic Fragment	MLI (Plastic/Al Surfaces)	Crumpled Aluminum	Steel Tank Rib Support
Inclination (deg)	65	87	99	30	82
Apogee (km) Perigee (km)	930 870	1190 610	1020 725	800 520	1500 820
A/m (cm^2/gm) Actual size (cm)	1.75 1.0	0.7 1×5	25 0.05×30	0.37 1×5	0.15 1×10
Bond albedo	0.4	0.02	0.05/0.7	0.05/0.7	0.5
Optimum C_m(dyne-s/J)	6±2	7.5±2	5.5±2	4±1.5	4±1.5
Δv required (m/s)	190	110	140	90	160
Estimated number of targets	50 k	20 k	60 k	10 k	10 k

Figure 3. Orbital debris particle characteristics matrix.

Most of the estimated 150,000 debris particles in the 1- to 10-cm size range are in orbits at inclinations ranging from 30° to 99°. This has implications for the laser site selection. The latitude requirements are somewhat relaxed. The use of Haystack itself, in remote association with a laser site at a clear weather, clear sky location (such as Albuquerque or China Lake) becomes an intriguing possibility.

Only the Na/K spheres (about 50,000 particles) are in nearly circular orbits. The remainder of the debris particles travel in elliptical orbits ranging from 1,500-km apogee to 520-km perigee. For example, the bulk of the carbon phenolic fragments are in highly elliptical orbits with apogees around 1,190 km and perigees around 610 km. Since the inclination of these orbits is about 87°, they constitute a risk to all space-based assets in this range; and, since the main source of debris in orbits from 200 to 500 km is material entering this range from above, they are a risk to practically all assets with orbits below about 1,200 km.

The multispectral reflectivity of the debris particles has been investigated. The requirements presented to the sensor and laser systems hold no major surprises. The microwave reflectivity of about 0.1 is manageable to more than a 2,000-km slant range by current, proven radar technology such as Haystack. Reflection at 1.06 microns to more than a 2,000-km slant range is expected to be sufficient to enable fine tracking using a laser radar. Reflection in visible light is expected to be more than sufficient to allow sunlight tracking at appropriate times during the day to more than a 2,000-km slant range. A 2,000-km range in these categories is the maximum needed to track debris at 45° in elevation and 1,500 km in altitude.

A final conclusion from figure 3 bears on the laser system requirements. Orbital calculations of the cumulative Dv required to deorbit particles from the five categories on a single pass found them to be in the range from 90 to 190 m/s. For more detail, refer to appendix D.

2.3 Particle Engagement Strategies

The 200-km altitude is defined as ORION's threshold for success based on independent results from orbital models developed at the USAF Phillips Laboratory, NASA/MSFC, and NASA/Johnson Space Center (JSC). The product TA/m (lifetime times cross-sectional-area-to-mass ratio) is graphed in figure 4. As an example of the use of the figure, first find the 200-km perigee altitude on the horizontal axis. Read up to the curves and find that TA/m[a] 1 cm^2 day/g. Next, as a worst case, look up the lowest A/m in figure 4, which is 0.15 cm^2 /g for a steel part. Finally, divide this into TA/m and find that the expected life in orbit is about 7 days. In other words, a typical debris particle will reenter in a few days due to atmospheric drag as it approaches a perigee less than 200 km. For the same A/m at 500 km perigee, the natural decay time is approximately 18 years.

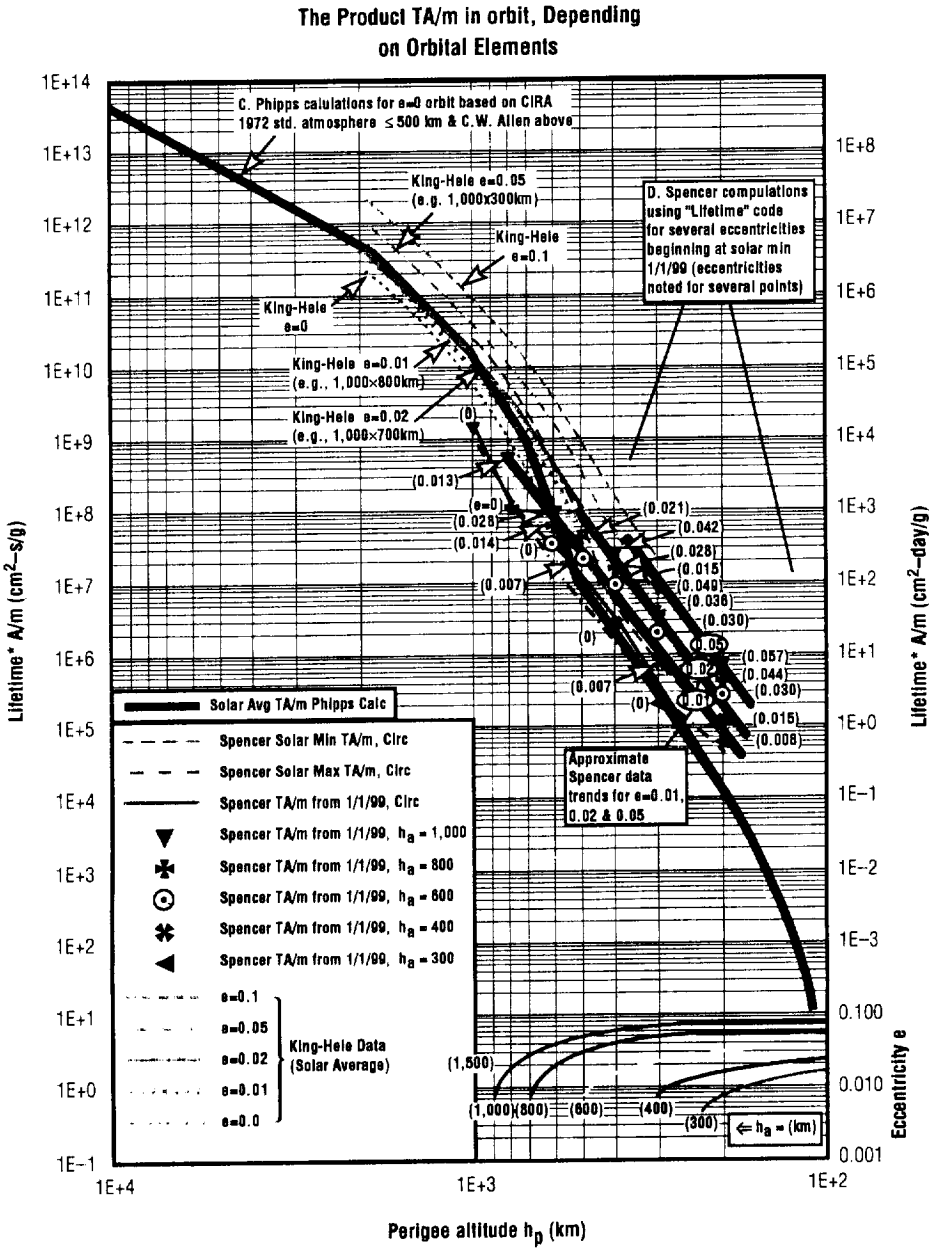

Figure 4. The product of lifetime and area-to-mass ratio as a function of perigee altitude.

The increase in lifetime with increasing altitude is one ingredient in a recipe for modeling the time evolution of the debris population. It is true that a particle in the lower part of the 200-500 km altitude range exits in a short time due to drag. It takes a much longer time for any one particle to move into the upper part of the range from above. This is offset by the greater number of particles at the top part of the range. Also, it is the more hazardous particles, with low area-to-mass ratios, that traverse the altitude range most slowly. In the 18 years it takes the particle of the previous example to move through the 200- to 500-km altitude range, many more space operations take place, with the predictable result that the debris population grows linearly or exponentially in time. One finding of the NRC Committee on Space Debris[1] is that even with current mitigation measures, the orbital debris population in LEO will continue to grow at a linear rate (if not an exponential rate) until well into the next century. Only after many years of both current and new mitigation measures could the population begin to fall.

High laser intensity on the surface of the particle is a key requirement for generating sufficient Dv for deorbit. Two basic operational strategies are available. The first is called one pass, one deorbit, and the second is called steady rain. In the former strategy, the particle is detected soon after it rises above the horizon and a sufficient number of high energy laser pulses are brought to bear on the surface of the particle. Each pulse ablates a thin layer of the surface and subsequently ionizes it. The reaction causes a small change in the particle's orbit. Sufficient pulses on one pass bring the perigee below 200 km, which is our definition of a successful deorbit.

The second strategy is to engage lower altitude particles before higher altitude ones. The idea is to walk down, from high to low, a train of particles while actually reducing the risk to space-based assets. For example, 100-km bands could be established. First, only particles in the 200- to 300-km range would be allowable targets. A particle would be lowered from the 200- to 300-km band to below 200 km. Only when a particle is removed from this range would it be permissible to engage a particle in the 300- to 400-km band. As a particle from the 300- to 400-km band falls into the lower band, the risk to assets in the lower band is no higher than it had been at first, for one particle was removed at the beginning.

Then, particles in both the 200- to 300-km and the 300- to 400-km bands would be eligible to be engaged. However, the prerequisite for engagement in the 400- to 500-km would be a particle lowered from the 300- to 400-km bands and the 200- to 300-km bands. This same scheme would be followed in moving to higher altitudes. This steady-rain strategy eliminates the possibility of a temporary increase in risk to space assets caused by failure to deorbit a particle in a single pass. Post-engagement tracking is desirable in this case, to verify that the particles have indeed been moved to lower orbits.

As will be discussed later, the Dv's required are such that the one-pass, one-deorbit strategy should be workable for the majority of the debris we have categorized. This means that substantive technical margin is offered by having the steady-rain option as a backup operational approach. More details on the strategies are supplied in appendix C.

3. THE PARTICLE/LASER INTERACTION

The previous section dealt mainly with the debris characteristics that set limits on their detection, identification, and tracking. This section deals with the characteristics of materials thought to be present in the debris when they are exposed to high intensity light. The pulse energy, mirror size, and repetition rate requirements for an ORION laser stem from the surface characteristics of the debris particles being irradiated and the momentum transfer needed for perigee reduction. The requirements on pointing are related to the appropriate times for engagement of debris in elliptical orbits.

---

[1] National Research Council Committee on Space Debris, *Orbital debris: a technical assessment*, National Academy of Sciences, 1995.

3.1 The Particle's Surface

Ablation of a microthin layer of the particle's surface is crucial to providing a significant change in momentum to the particle. Ionization and plasma formation further enhance the momentum transfer. We ignore the much weaker radiation pressure that exists in the absence of ablation. A substantial amount of work has been published by the fusion community over the past decade, pertaining to these interactions for various materials. A wealth of detail can be found in appendix D.

The coupling coefficient C_m is the ratio of the momentum transferred to the energy delivered. The laser intensity on the target is the ratio of the power in the beam to its cross-sectional area, and the coupling coefficient is a nonlinear function of intensity for a particular material. The peak of the function corresponds to the laser intensity at which the maximum change in the particle's momentum occurs for the least amount of energy input.

Figure 5 illustrates the coupling coefficient for a single material, nylon, irradiated by varying intensities of KrF laser radiation. In this experiment, the pulse duration was fixed at 22 ns. At an intensity of 2.5×10^8 W/cm^2, the laser energy is most efficiently coupled to the momentum change of the particle. Reducing the intensity by as much as 50 percent only reduces the coupling coefficient from a maximum of 6.5 to about 6 dyne s/J. Even if the vaporized material is not ionized, there is good momentum coupling by simple evaporation. This illustrates that there is a relatively forgiving threshold intensity requirement for the laser at the particle, since large (50 percent) variations in intensity mean only a small change in coupling efficiency.

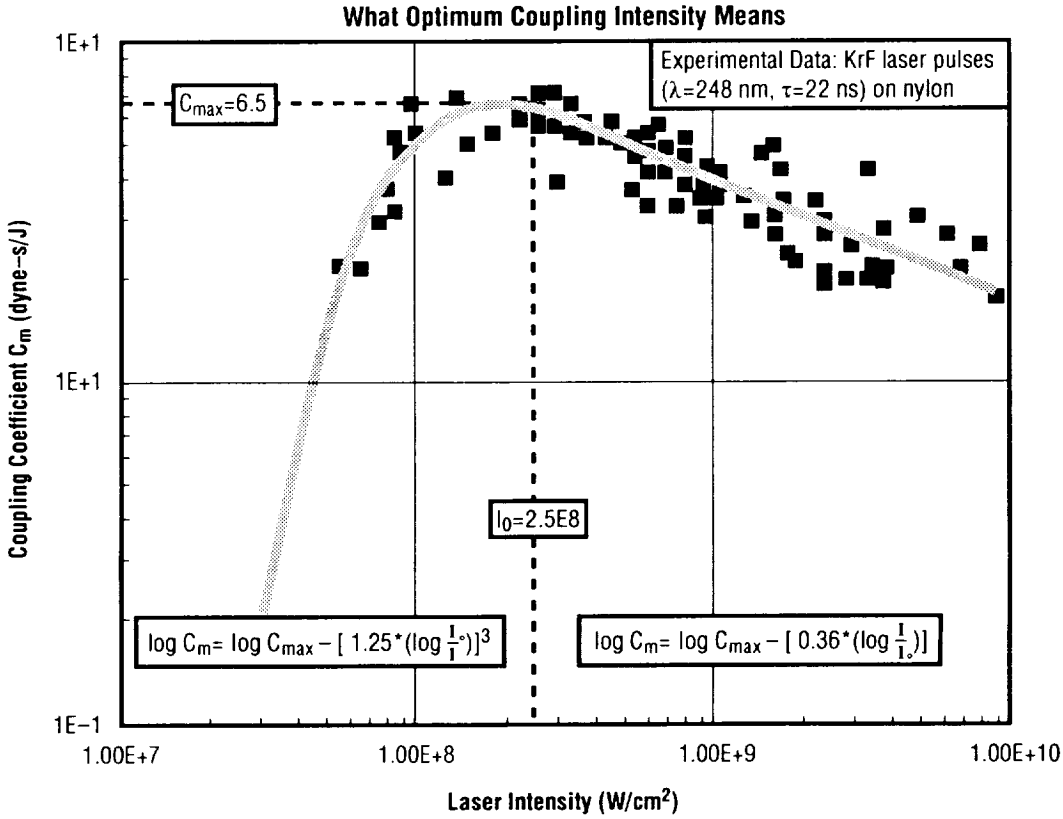

Figure 5. What optimum coupling intensity means.

The intensity of a laser pulse of a given energy depends on the pulse duration. A shorter pulse of a given energy has a higher intensity. To put it precisely, the intensity on the target is the fluence divided by the pulse duration, where the fluence is the ratio of the energy reaching the target to its cross-sectional area.

Figure 5 illustrates the coupling coefficient for a single material and a single pulse duration. The intensity needed for peak coupling efficiency actually depends on both the pulse duration and the material. As the pulse duration decreases, there is less time for energy reaching the target surface to be conducted to the interior, and the intensity for peak efficiency decreases. Also, metals require a somewhat higher intensity for maximum coupling than nonmetals because they are better thermal conductors.

Remarkably, we found that a simple relationship predicts the fluence required for most efficient coupling for all pulse durations and all materials for which there are sufficient data. The relationship is shown in figure 6. To use this graph, one chooses a pulse duration on the basis of available technology or atmospheric factors, and then reads the most efficient fluence within a factor of 3 or so. For example, for pulse durations on the order of 5 to 10 ns, an incident fluence of about 4 to 6 J/cm^2 provides the optimum momentum coupling for the five categories of debris. Recall that the coupling coefficient depends only weakly on the intensity in the vicinity of the peak, so the fluence requirements are quite forgiving.

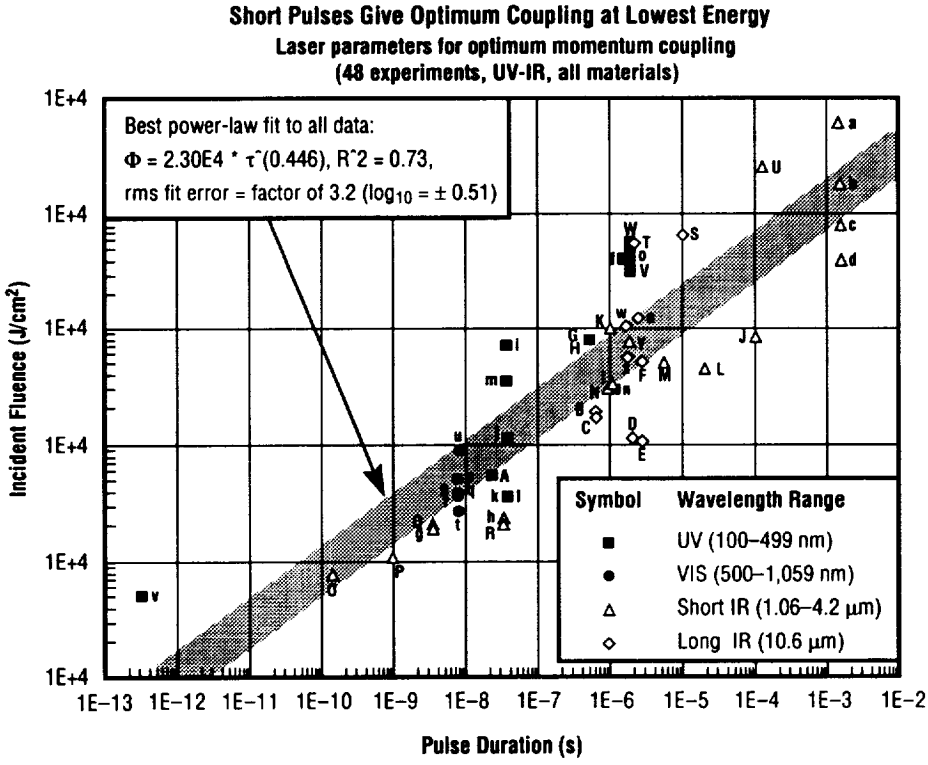

Figure 6. Laser fluence for optimum momentum coupling at various pulse durations.

The intensity of a continuous wave (CW) laser is less than the peak intensity of a pulsed laser of the same average power and wavelength. Our models of the CW systems are based on simple vaporization of the debris surface. This study pointed out the need for experimental studies of CW photoablation of materials more complex than elemental surfaces. Also, we have found no studies of laser interactions with surfaces having shapes more complex than flat plates.

3.2 When And How Often To Engage

As we showed in the previous section, short laser pulses give efficient momentum coupling at reasonably low fluences. In section 6, we will argue that such fluences are within the capabilities of near-future technology pulsed lasers operating from the ground. Here we present our estimates of the number of pulses needed to remove debris in various orbits.

It is crucial to engage the particle at the proper point of its orbit and in the right direction, or the resulting Dv will not have the desired effect. In some circumstances, it could raise the perigee. Engaging the particle as it is rising above the laser's horizon is typically the best. For any engagement, Dv will occur along the normal to the particle's surface being irradiated. This is not necessarily (and normally will not be) in exactly the same direction as the laser beam. However, for many particles, due both to spin and random orientations, the average direction for the momentum change is expected to be along the line of sight of the laser. Engaging as the particle is rising above the horizon normally gives a vector momentum component opposite the orbital motion, hence lowering the perigee. However, there are special cases (e.g., perigee over the laser) in which one should not engage at debris rise, which places a requirement on the sensor system design that a particle's orbit parameters must be determined before and after engagement. The primary engagement rule found in this study is that any pulse that tends to increase the tangential velocity should be avoided. More detail on the geometric factors for successful laser engagement can be found in appendix E.

The final key piece to the laser/particle interaction puzzle deals with whether sufficient time would be available to engage the particle on orbit with sufficient pulses to lower its perigee below 200 km. Figure 7 shows the Dv needed to deorbit debris as a function of altitude for various orbits. To use the figure, start with the initial altitude, such as 500 km. For this altitude, we read a required Dv change of about 90 m/s. The relation between the Dv and the fluence is:

$$\mathrm{Dv} = C_m F A/m$$

where C_m is the coupling coefficient and F is the fluence. With the figures in the previous section (steel part with A/m = 0.15 cm^2/g, F = 4.6 J/cm^2, C_m = 6.5 dyne s/J) we find Dv = 4.5 cm/s. Therefore, it would require 2,000 pulses to bring the perigee below 200 km in this example. If the pulse rate is 10 Hz

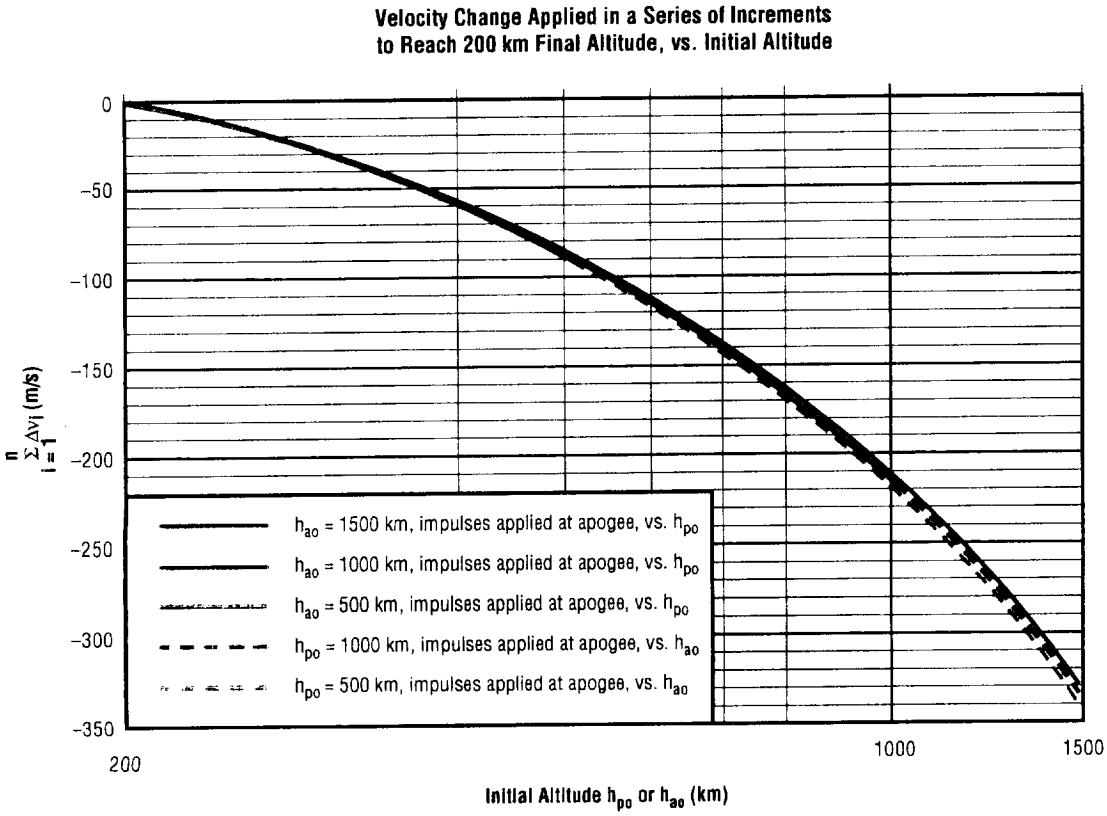

Figure 7. Velocity change applied in a series of increments to reach 200 km final altitude versus initial altitude.

or more, only about 3 min or less are required for the engagement. This is easily within the time interval any debris particle remains in sight.

The analysis of the previous paragraph is a worst case, since the steel parts have the lowest A/m of all the debris in orbit. We will consider issues of laser propagation in the next section, but we note here that a fluence of 4.6 J/cm^2 provided by a laser at 1 mm launched by a 4.5 m adaptive optic would require an energy of at least 3,600 J per pulse at 0° zenith angle, or at least 12,000 J per pulse at 60° zenith angle. If such energies are not available, or not available at such a high pulse rate, then it may be necessary to deorbit the steel parts in multiple passes. The other target types will be much easier to deorbit in a single pass.

4. LASER ATMOSPHERIC PROPAGATION

This section deals with a third set of physical constraints on the ORION laser and sensor systems. First, the relationship between diffraction-limited mirror size and spot size on the particle will be discussed. Next, we consider the intensity and beam quality losses associated with operating through the atmosphere. These losses can be severe unless properly handled in the design of the laser system. The physical mechanisms considered are atmospheric absorption, turbulence, and nonlinear effects.

4.1 Linear Propagation

As we showed in the previous section, a sufficiently high laser beam intensity on the particle surface is needed to impart the desired momentum change. For a given amount of energy in a pulse of a given duration, the intensity is inversely proportional to the cross-sectional area of the beam at range. We now consider the lower limit on the beam diameter in the regime of linear propagation.

The spot size is fundamentally limited by diffraction. The diffraction-limited diameter of the spot is proportional to the wavelength and inversely proportional to the diameter of the telescope used to focus it. The smallest spot size is obtained, in principle, by using the shortest wavelength and the largest mirror diameter available.

The largest mirrors in existence are 10 m in diameter, but for a moment let us consider a much less expensive 3.5-m mirror as an illustration. Also, let us take 0.5 mm, which is in the visible part of the spectrum, as a typical "short" wavelength. At the longest slant range of interest, 2,000 km, the spot diameter is about 70 cm. Recall that a fluence of about 5 J/cm^2 is required for most efficient coupling with a 10-ns pulse. With these numbers, we arrive at a pulse energy of 20 kJ. Pulse energies considerably higher than this have been obtained with existing lasers. Thus, a simple calculation shows that existing technology, in principle, can easily provide the intensity needed for momentum transfer to the most distant pieces of debris under consideration.

While smaller spot sizes further relax the laser power requirement, the fine tracking challenge grows, as does the size of the mirror. For primary mirrors larger than about 3.5 m, aperture size becomes a primary driver to the cost of the laser system. Designing to shorter wavelengths reduces the aperture size requirement proportionally, but raises serious issues relating both to turbulence and the surface accuracy of the mirror.

4.2 Turbulence and Atmospheric Absorption

The air through which the laser beam passes before leaving the atmosphere is not a uniform medium. The index of refraction is a function of the air density. The lower layer of the atmosphere, or troposphere, is characterized by turbulent motion of cells of air with varying density. As convection cells

move through the beam, or the beam moves through cells, the beam tends to spread and lose coherence because of the density variations.

For the ORION project, it is important to maintain the beam quality in order to place sufficient intensity on the particle at range. This places the requirement for adaptive wavefront correction on the beam director design. Appendix E treats these issues in great detail, and we summarize them here.

The effects of turbulence on the beam can be nullified by distorting the optics of the beam directing telescope in a controlled way. This is "adaptive optics." The size of the independently controlled zones on the correcting optic (assumed to be equal in size to the aperture) should be on the order of the Fried scale r_0. The Fried scale is on the order of 10 cm for a wavelength of 1 mm. It decreases with decreasing wavelength. From this we can see that one thousand or more independently controlled, primary mirror segments will be needed to correct a 3.5-m mirror in a 1-mm laser beam director.

Adaptive optics with over 100 segments are already in use for astronomical imaging. Larger systems are now under development, including a system for the 3.5-m STARFIRE telescope.

The information on atmospheric conditions needed to correct the mirror cannot come from the debris itself. The light travel time is such that the laser must be pointed up to 100 m ahead of the particle. An artificial beacon, or guide star, must be used instead. A guide star is made with a laser much lower in power than the "pusher" laser. The beacon will be aimed ahead of the particle and used to sample the column of air through which the pusher laser must pass.

The guide star is not effective unless some of its energy is scattered back to the ground to return the phase information necessary to distort the correcting optics. The beacon laser's wavelength can be chosen so that some of its energy is scattered back to the telescope from a distinct layer high in the atmosphere. Astronomical systems in use today typically make use of the presence of sodium in a layer about 90 km above the ground. It is fortuitous that sodium can be found in this layer, for it is not difficult to build a laser that can excite the sodium atoms into resonance fluorescence and return a usable signal to the ground.

At the position of the intended laser spot in the sky, the area over which the beam can be corrected by a guide star is known as the "coverage size." The coverage size decreases as wavelength decreases. If diffraction alone were considered, one would use the shortest wavelength available. But once the coverage size is smaller than the intended beam spot size, it is no longer possible to use the guide star to correct completely for atmospheric turbulence, and the beam would spread and fall in intensity. One way around this would be to use more than one guide star. Several closely spaced guide stars could provide the phase information needed to correct the optics. While this is possible in principle, it has not been demonstrated.

We have found that for adaptive primary mirrors 3.5 m in diameter and smaller, a single sodium guide star is sufficient to provide the necessary corrections for a wavelength of 1.06 mm. If a shorter wavelength were used, then a minimum of four closely spaced guide stars would be needed to provide sufficient information to make the necessary wavefront corrections for a mirror this size.

A full analysis of the tradeoffs in laser wavelength must take atmospheric transmission into account. The atmosphere is highly absorptive for most wavelengths of the electromagnetic spectrum. Fortunately, transparent and partially transparent windows exist in which the laser beam will propagate without serious attenuation. The visible and near infrared from 0.4 to 1.3 mm is one window, as is the infrared band from 9.5 to 12 mm.

Although the technology exists for powerful lasers at 10 mm, the mirror size required to produce a small spot on a target is prohibitively large. There is well-developed technology for powerful lasers in the visible to near infrared, and it is within this window that the most reasonable options are to be found. Further discussion of existing laser technology may be found in section 6.

4.3 Atmospheric Nonlinear Effects

Even though the laser wavelength is chosen in a window of atmospheric transparency, one must consider the possibility of beam spreading and energy loss by nonlinear mechanisms. These are mechanisms that grow in importance as the intensity of the beam in the atmosphere increases, or as the path length in the atmosphere increases. We have made an extensive study of these effects, including nonlinear refractive index, STRS, SRS, and whole-beam thermal blooming.

Nonlinear refractive index tends to degrade beam quality by spreading the beam, since the refractive index tends to increase at high intensity. STRS attenuates the beam by breaking it up and scattering it in different directions. SRS attenuates the beam by scattering it in different directions at different wavelengths. Whole-beam thermal blooming spreads the beam as it heats the air through which it passes. The nonlinear mechanisms are depicted in figure 8. Our modeling of these effects is treated completely in appendix D. The limits imposed by the nonlinear mechanisms on the ORION laser are graphed in figure 9. The beam is assumed to be propagating vertically through the atmosphere, so that the near-field intensity on the vertical axis refers to the beam as it leaves the laser. The beam is also assumed to originate at sea level. The graph would appear somewhat altered at angles other than vertical, and if the laser were located at a high altitude above sea level. The laser pulse duration is shown on the horizontal axis. The graph is for a specific wavelength, 1.06 mm, but it has the same basic shape for other wavelengths.

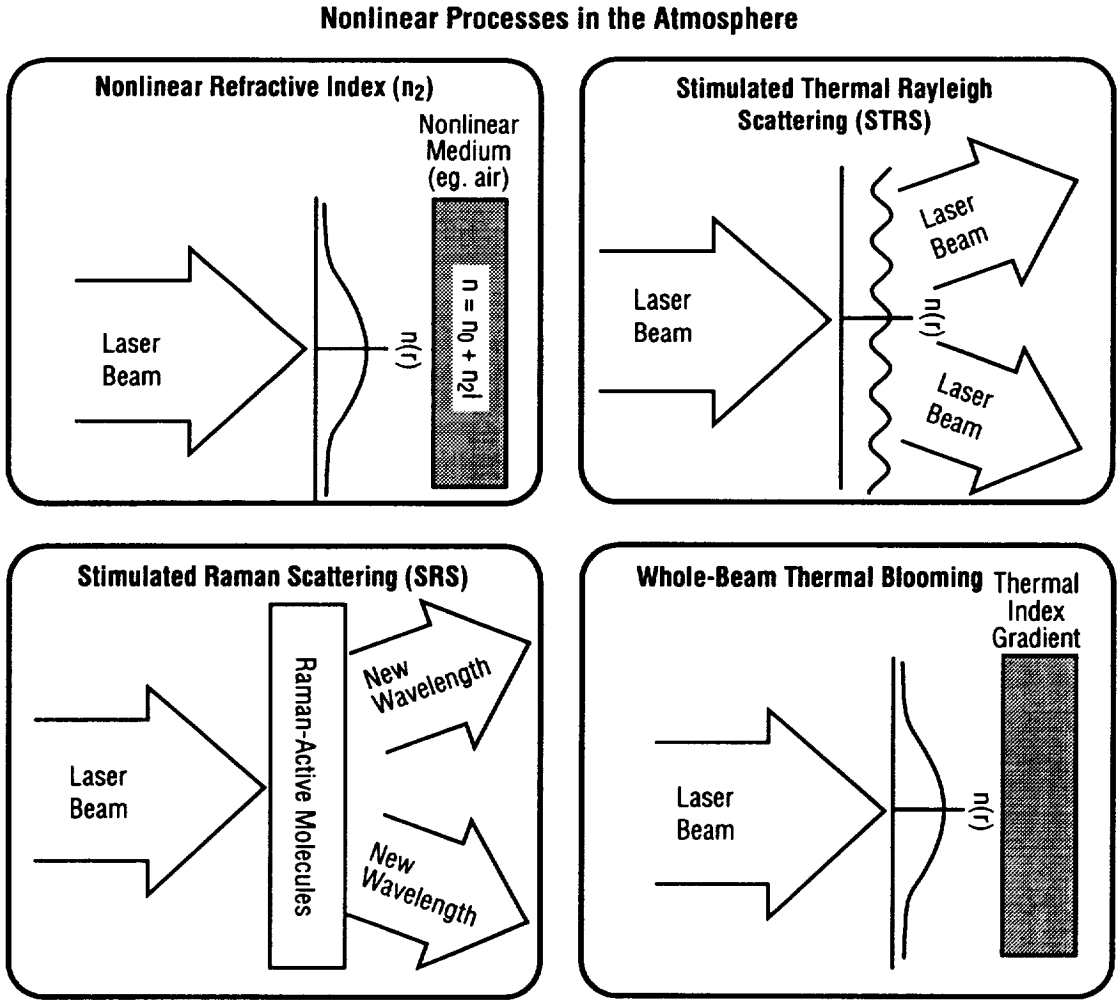

Figure 8. Nonlinear processes in the atmosphere.

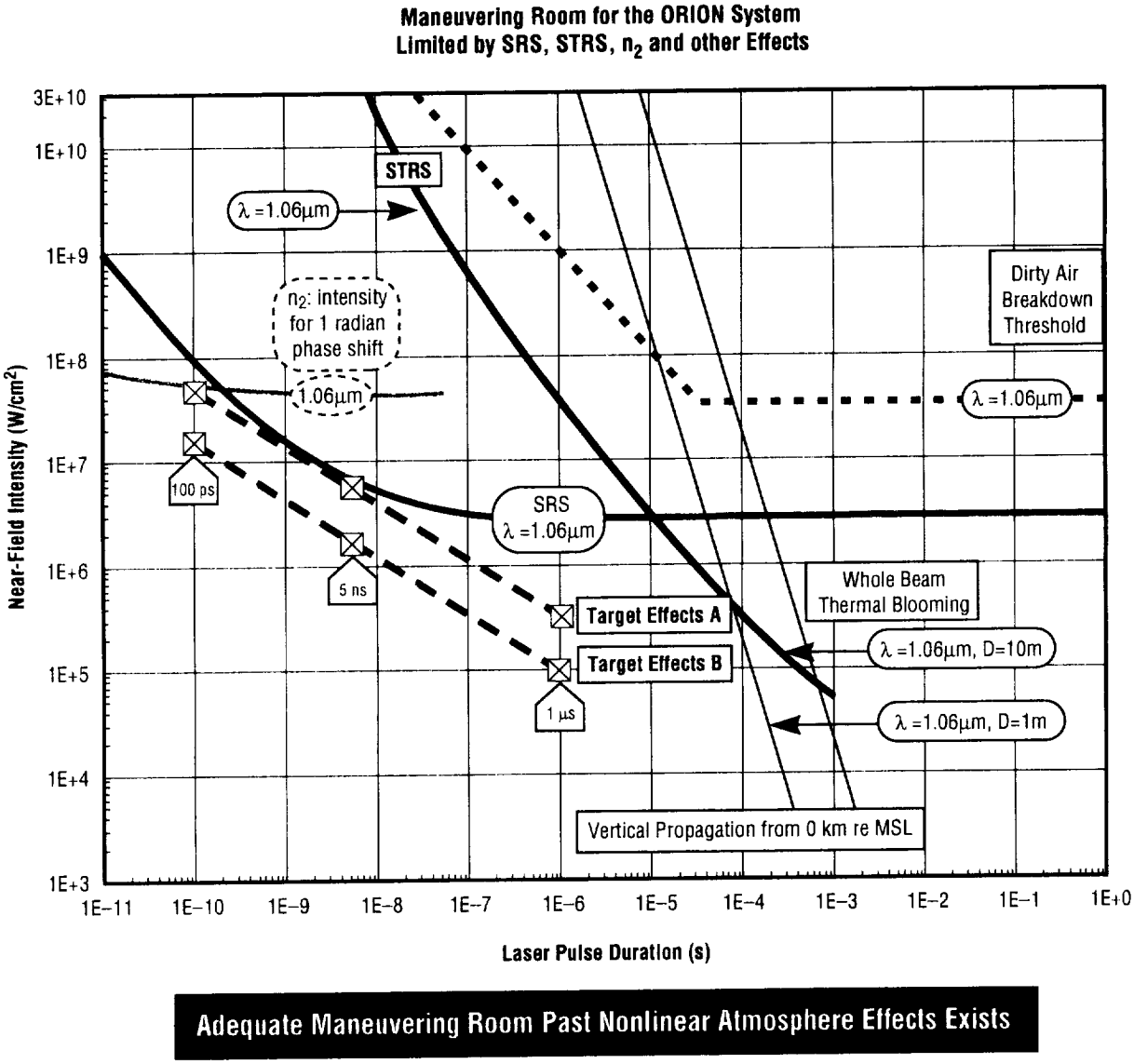

Figure 9. Maneuvering room for the ORION system limited by SRS, STRS, n_2, and other effects.

The intensity limit imposed by whole-beam thermal blooming is shown with two light solid lines, one each for telescopes of 1 m and 10 m in diameter. Since it takes time for the air density to change in response to heating, this effect can be eliminated by using short pulses. The allowed intensity for whole-beam thermal blooming rises to extremely high levels for pulses shorter than 1 ms, where other limiting mechanisms come into play.

The limit imposed by STRS is shown with a heavy solid line. It, too, can be avoided by choosing a short pulse duration. If the duration is kept below 10 ns, then both STRS and whole-beam thermal blooming are displaced by another intensity-limiting mechanism.

Nonlinear refractive index is not so well understood for long pulses, but for pulses less than about 100 ns, it imposes an intensity limit of about 5×10^7 W/cm^2. Our best prediction is that the limit increases slightly with shorter pulses.

For pulses between 200 ps and 10 ms, the most stringent limit is set by SRS. This limit is shown in the figure with the lower heavy solid line. With the limits imposed by the four nonlinear mechanisms combined on one graph, a region of operability or "corner of opportunity" stands out. The corner, for this wavelength, is at an intensity of 3×10^6 W/cm^2 and a duration of 10 ms. Pulses shorter than this or lower in intensity should not be significantly affected by the nonlinear mechanisms.

One possible exception to this "corner of opportunity" view will be considered later for the attainment of subobjective B. When the SRS intensity limit first begins to rise for short pulses, it rises so slowly that the higher allowed intensity is too little to compensate for the decrease in fluence due to the shorter pulse. But, recall that the intensity needed for most efficient momentum coupling decreases with decreasing pulse length. There is a possible operating point near 100 ps pulse duration where the SRS limit has risen enough to make such operation attractive, and where the nonlinear index effect is not yet the limiting consideration.

It is important to note how the situation of figure 9 changes when a different wavelength is used. As the wavelength decreases, the near-field intensity limits also decrease for a given pulse length. This implies that the smaller apertures permitted by diffraction for smaller wavelengths can only be realized up to a point. Beyond that point, smaller apertures are forbidden by near-field intensities beyond those allowed by nonlinear atmospheric effects.

5. LASER AND SENSOR SYSTEM REQUIREMENTS

The particle characteristics, the laser/particle interaction, and the atmospheric propagation form a set of physical design constraints for ORION. In this section, the requirements are folded together into a complete set of requirements for the laser and sensor systems. Also included are the programmatic considerations of cost and schedule. The requirements on the laser system will be compared with existing technology in section 6. In section 7, the sensor requirements will be related to existing technology.

The requirements for the laser are summarized in the top row of figure 10. The laser system must operate in one of the atmospheric transmission windows, such as the one shown by the dark band from 0.4 to 1.3 mm. Beam effects due to turbulence must be minimized by active correction in which the area of coverage is as large as the laser spot at range.

In order to place the critical intensity on the particle at range, nonlinear effects must be minimized by operating in the region of opportunity defined by short pulse duration (e.g., 10 ms for 1 mm) and below the critical near field intensity (e.g., 3 MW/cm^2 for 1 mm). The laser and corrective optics must be capable of achieving the critical intensity and fluence (e.g., 600 to 850 MW/cm^2, 4 to 6 J/cm^2) on the debris particle at least at 800 km altitude and preferably to 1,500 km.

If we take the number of debris particles to be 150,000, appropriate for subobjective B, then the time required to remove all the debris is about 0.3 year/min times the time for each piece of debris. The time for each piece is an average, which must include off-duty time. For example, if the average operating time to remove one piece of debris is 10 min, then the time to remove all the debris is 3 years. The time to acquire suitable targets, and the repetition rate and maintainability of the laser, are all constrained by this together with the programmatic requirement that all debris to be cleared in some definite time, such as 5 years.

The Haystack radar has shown that in a field-of-view of 0.05°, the rate of detection of debris particles is about 6/h. Of these, only about 1/h is in circumstances suitable for targeting. The rate must be an order of magnitude higher, or the laser will be idle most of the time as it waits for a new target to be identified. Therefore, we recognize that the field of regard for the ORION sensor should measure on the order of 0.5°. If a sensor has a very high sensitivity and can be moved rapidly, then the field of regard can be

ORION System Requirements

Laser	Atmospheric Windows	Nonlinear Effects (SRS,STRS, n_2)	Debris Alt. (km)	1–20-cm Clear Time (yrs)	Debris Intensity (MW/cm^2)	Debris Fluence (J/cm^2)
⇒	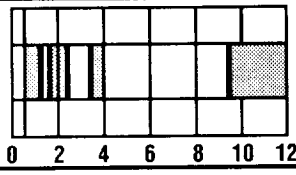	**$\tau \geq 10ns$: $I_{atm} \geq 3MW/cm^2$**	**500–1500**	**<5**	**$\tau \geq 5$–10ns: 600–850**	**$\tau \geq 5$–10ns: 4-6**

Radar Sensor	Field of View	Sensitivity	Discrimination	Assessment	Operability	S/N Ratio	Handover
⇒	**≥0.5°**	**d = 1 cm h = 1500 km R ≥ 0.3**	**X-section Orbit**	**Immediate Spin Orbit**	**24 hours**	**Limited by Noise**	**d_s = 200 m**

Laser Sensor	Search Wide Field of View	Sensitivity	Discrimination	Assessment	Operability	S/N Ratio	Handover
⇒	**≥0.5°**	**d = 1 cm h = 1500 km R ≥ 0.3**	**X-section Orbit**	**Immediate Spin Orbit**	**24 hours**	**Limited by Photon Count**	**d_s = 200 m**

Passive Optics Sensor	Search Wide Field of View	Sensitivity	Discrimination	Assessment	Operability	Adequate Signal-to-Noise Ratio	Handover
⇒	**≥0.5°**	**d = 1 cm h = 1500 km**	**X-section Orbit**	**Immediate Spin**	**4 hours (twilight)**	**Limited by Photon Count**	**d_s = 200 m**

Figure 10. ORION system requirements.

built up by sweeping rapidly through several fields of view. The Haystack radar, for example, with its high sensitivity, could scan a 0.5° wide field in a bowtie pattern that would be virtually "leak proof."

Ultimately, the position of the particle must be determined to within about 0.4 mrad (70 cm beam width at 2,000-km slant range). The field of regard of 0.5° (9,000 mrad) is so much larger that a fine tracking mechanism will be needed. To distinguish coarse from fine tracking, we set a somewhat arbitrary crossover of 100 mrad. This corresponds to about 200 m at a distance of 2,000 km. The actual crossover could be larger if the fine tracking is capable of finding the object in a larger field, or smaller if the coarse tracking mechanism is very precise.

Twenty-four hour, remote operability in all weather conditions would be ideal. If the sensor does not operate at all times or in all conditions, then either the laser average power must be made higher or the

time to remove the debris population grows. Remote operability is needed for handoff of the tracking information to the laser.

The sensitivity must be sufficient to see 1-cm debris in each category at a slant range of 2,000 km. The sensor system requirements are summarized below the laser requirements in figure 10. The full analysis appears in appendices B and C.

6. THE ENGAGEMENT LASER SYSTEM

Three sets of constraints on the laser concept imposed by the debris characteristics, the laser-target interaction, and atmospheric propagation were discussed in sections 2, 3, and 4. In section 5, these were synthesized to form a full set of constraints. In this section, we review existing laser technology in the light of the constraints. Laser technology is reviewed in appendix F. We will see that the requirements converge on a wavelength near 1 mm and either a pulsed solid state laser or a CW gas laser.

6.1 Pulsed Solid-State Lasers

Solid-state lasers have the highest pulse energies available at this time. Each of 10 beams of the Nova laser at Lawrence Livermore National Laboratory (LLNL) produces 10 kJ per pulse. The Beamlet laser at LLNL produces 20 kJ per pulse. Both of these are Nd:glass lasers. Pulse durations of about 1 to 50 ns are typical for Nd:glass lasers. Thus, these lasers operate in the ORION corner of opportunity for reasonably sized apertures. For example, for a 10-kJ pulse lasting 10 ns, SRS can be avoided (at 1 mm) for apertures larger than about 0.4 m.

The fundamental wavelength of the Nd:glass laser is 1.06 mm, which is in the visible/near infrared window. The visible wavelength, 0.53 mm, is derived with high efficiency by frequency doubling in a KDP crystal. The shorter wavelength initially appears attractive, since a smaller aperture is required to produce a given spot size. The SRS limit is more stringent for the shorter wavelength, however, and the beam correction would require unproven multiple guide star technology. For the near term, then, the 1.06 mm wavelength is favored, with the shorter wavelength a strong future possibility.

The highest power lasers today are designed for low repetition rates. Beamlet, for example, operates at under 0.02 pulses per second. The difficulty with higher rates is that nonuniform heating of the amplifying medium degrades the optical quality of the beam. Beamlet can be operated continuously at its designed rate because the cooling system minimizes nonuniform heating as long as its maximum repetition rate is not exceeded.

If we are to accomplish ORION's task without proposing lasers much more powerful than those in existence, we must increase the repetition rate, or else the deorbiting of the debris will take far too long. We are aware of two ways to overcome the repetition rate limitation. One is to fire the laser rapidly without cooling and to allow the amplifying medium to heat up uniformly so that optical quality is not affected. This is called the "hot rod" mode. It is modeled in detail in appendix A. It should be possible to fire up to 1,000 pulses in a short time interval before the laser is cooled for the next round.

Smaller lasers have proven that higher continuous rates are possible. At LLNL, for example, a laser that produces 100 J per pulse operates at 6 pulses per second, and is being upgraded to 12 pulses per second. Although cooling of the medium results in nonuniformities, the optical quality is actively corrected with a stimulated Brillouin scattering (SBS) mirror. The design of such a system is treated in appendix F.

Overall, the Nd:glass laser at 1.06 mm was found to be the laser with the best potential for accomplishing the mission. The technology is widespread and developing rapidly because of activity in fusion research.

6.2 Pulsed Chemical and Gas Lasers

CO_2 gas lasers operate in the mid-infrared (IR) band, at wavelengths of 10.6 and 11.2 mm. In order to be competitive with solid-state lasers, they must either be made much more powerful or a much larger aperture must be used. For example, since the wavelength is 10 times that of the Nd:glass laser, a telescope 10 times larger would be needed to produce the same diffraction-limited spot size. This would make the telescope diameter on the order of 40 m. If, instead, the same size telescope were contemplated for both lasers, the power of the CO_2 laser would have to be 100 times greater to produce the same fluence on the target. SRS would then become a limiting factor. Either solution would be very expensive.

Two other lasers that operate between the near- and mid-IF regions are HF/DF chemical and the CO lasers. Neither is as well developed as Nd:glass or CO_2 lasers. They suffer, to a lesser degree, from the same limitations as the CO_2 laser at longer wavelengths. The DF laser is included in figure 11 for reference.

Technical Basis for Choosing ORION Laser Device (Longer-term Example)

Laser	Atmospheric Windows	Nonlinear Effects (SRS,STRS, n_2)	Debris alt. (km)	1–20–cm Clear Time (yrs)	Debris Intensity (MW/cm^2)	Debris Fluence (J/cm^2)
⇒	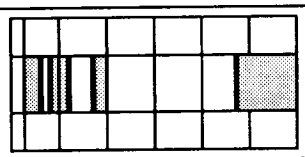	**$\tau \geq 10$ns: $I_{atm} \geq 3MW/cm^2$**	**500–1500**	**<5**	**$\tau \geq 5$–10ns: 600-850**	**$\tau \geq 5$–10ns: 4-6**

Rep-Pulsed Laser Options	λ (μm)	Beam Size at 1500 km (cm)	Laser Pulse Energy for Efficient Thrust (kJ)		Beam Fluence in Atmosphere (J/cm^2)		SRS-Safe Beam Fluence in Atmosphere (J/cm^2)		Guide-stars Needed	Cost ($M)		Laser Device Choice Basis
Pulse Width: ⇒			1 μs	10 ns	1 μs	10 ns	1 μs	10 ns		1 μs	**10 ns**	
Nd Solid State	0.53	24	24	3.0	0.085	0.011	2	0.04	4* (difficult)	54	**23**	* Cheaper But Guidestar Kluge
Nd Solid State	**1.06**	**48**	**97**	**12**	**0.34**	**0.043**	**2.5**	**0.05**	**1**	**100**	**40**	**Best Cost That Works**
DF Chemical	4±	180	1370	170	4.9	0.61	2.5	0.06	0	1920	290	High Cost, Won't Work (SRS)
CO_2 Gas	10.6	480	9700	1200	34	4.3	3	0.07	0	11400	1700	High Cost, Won't Work (SRS)

CW Laser Option	Wave-Length μm	1500 km Beam dia (cm)	Laser Power for Efficient Thrust (kw)	Intensity in Atmosphere (W/cm^2)	Blooming-safe Intensity in Atmos. (W/cm^2)	Guide-stars Needed	Cost ($M)	Basis for Laser Device Choice
Iodine Gas	1.3 CW	59	3200 (Power Overkill Necessary for Thrust)	11	8?	1	68	Blooming? Beam Quality? Target interaction? Next Lower Cost

Figure 11. Technical basis for choosing the ORION laser.

6.3 Continuous Wave Gas Laser

An iodine laser operating at 50 J per pulse has been demonstrated in the United States. The long pulse duration of 10 ms would place it well below the intensity for most efficient coupling. The wavelength of 1.3 mm is not far from the Nd:glass wavelength and just inside the near infrared window.

The repetition rates of iodine lasers are as high as 1 pulse per second, with higher rates under development. It is interesting to note that these lasers can be made to operate in a CW mode. The ROTOCOIL laser at the USAF Phillips Laboratory is an iodine laser at 1.3 mm with a continuous power of 40 kW. Although this is somewhat different from the pulsed mode of operation we had envisioned for ORION, our preliminary study indicates that it could accomplish its objectives.

In a CW mode, the intensity must be kept well below the peak intensity of a pulsed laser in order to avoid thermal blooming and STRS. Even so, the average power must be greater than for the pulsed laser, since short pulses couple most efficiently at lower fluences. These two conditions can be met, since the CW laser is constantly in use, where the duty cycle of the pulsed laser can be 10^{-6} or less. We will include an iodine CW option in one of our systems to consider for subobjective B.

Data on all the lasers considered are included in figure 11.

6.4 Relevant Electro-Optical Technology

The laser system consists primarily of a beam director, a guide star subsystem for optical correction, a coarse track handoff system, a fine track subsystem, and a high-energy, pulsed laser. Large aperture systems with corrective optics were identified as part of this study. Many of the details are reserved for appendix E.

The Advanced Electro-Optical System (AEOS) located in Maui, HI, is shown in figure 12. It employs a 3.6-m primary mirror. This facility's mission is high-accuracy, high-sensitivity satellite detection and tracking. The STARFIRE facility located near Albuquerque, NM, is intended for a similar mission. It employs a 3.5-m aperture for high-sensitivity, high-accuracy tracking.

AEOS and STARFIRE use adaptive optics with a single guide star to correct wavefront aberrations due to atmospheric turbulence. The tracking rates are about 18° per second in azimuth and 5° per second in elevation. These rates are sufficient to accomplish the ORION objectives. Although costs will be considered in more detail in section 8, it is interesting to note that STARFIRE costs included $7 million for the primary mirror and $10.5 million for the telescope mount. Total facility costs came to about $27 million.

Analyses such as this have shown that there are several possible directions one might take to accomplish subobjectives A and B. Subobjective A could be accomplished with a 1.06-mm laser using a 3.5-m mirror. Operation would be within the corner of opportunity with 5-ns, 5-kJ pulses. The time needed to do this depends on the tracking and handoff system, which will be discussed in the next section. If the sensor system were not capable of 24-h operation, the subobjective A could still be accomplished by using a somewhat larger telescope to obtain a more intense beam.

Recall that subobjective B raises the coverage from 800 km to 1,500 km. This will require more energy on target at greater range. Three laser systems are promising in this regard. One is to develop a Beamlet-type Nd:glass laser for high pulse rates at 10 to 20 kJ per pulse. A 6-m diameter mirror would be needed to avoid SRS. Alternatively, a 0.1-ns pulsed Nd:glass laser could be developed to take advantage of the increase in the SRS threshold with decreasing pulse duration. The third option that seems feasible for this subobjective is the CW iodine laser. This would also require a 6-m adaptive optics telescope.

Advanced Electro-Optical System
3.67 m Telescope Facility

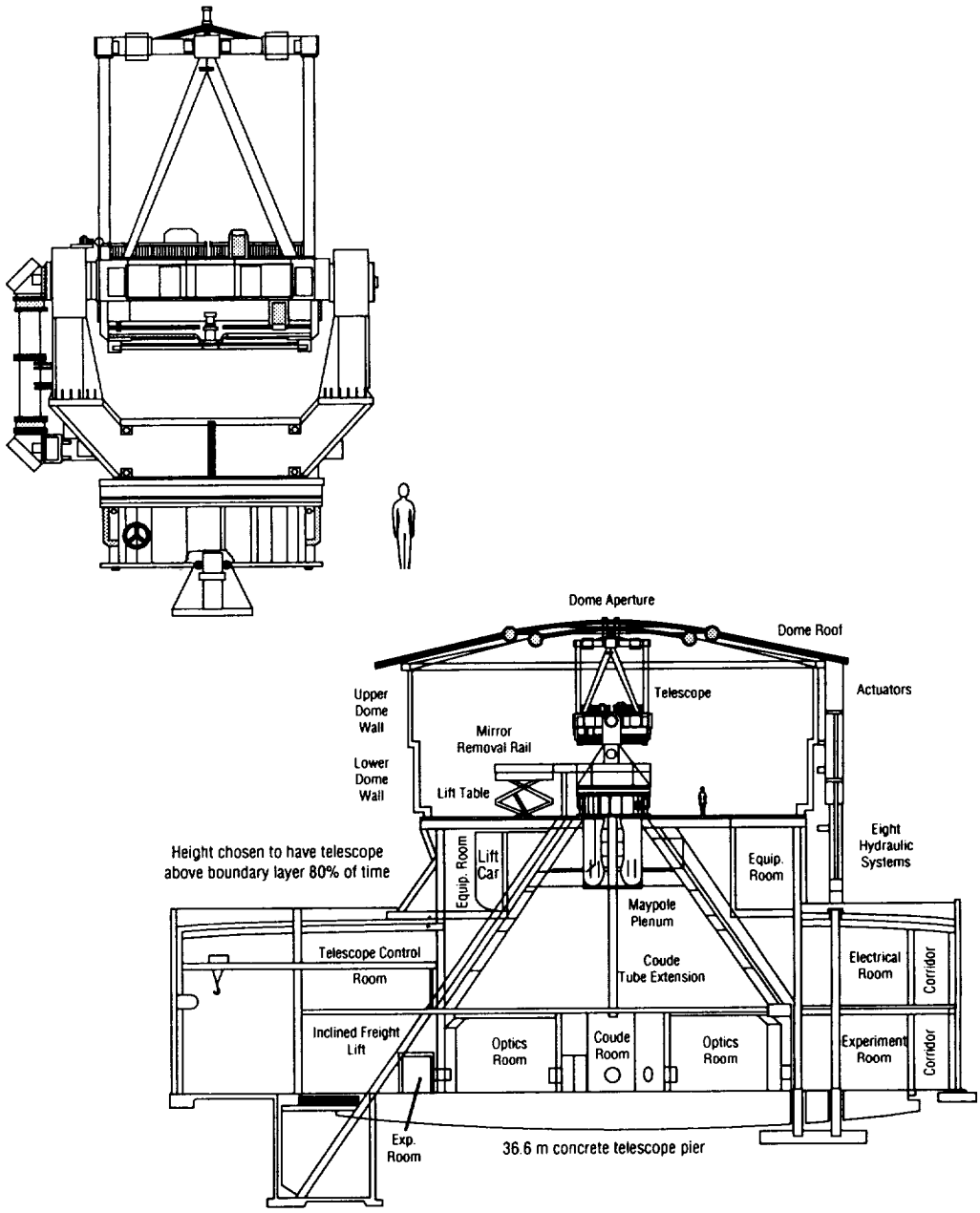

3.63 m c.a. F/1.51 Zerodur parabolic primary
84 active supports + 48 lateral supports
18.3 deg/sec azimuth, 4.75 deg/sec elevation
Maui system (shown) under construction with very expensive site-associated costs

25 cm c.a. secondary:
a. F/200, 0.3 m rad Fov Coude system
b. F/32, 1 m rad Bent Cassegrain

Starfire in operation: $7M primary mirror (R&D for stress lapping)
$10.5M telescope mount
$27M total with facilities

200 W $3.55M LLNL Na guidestar on hold
Adaptive optics not ready yet
Intensified 30 cm 0.3" acquisition scope

Figure 12. AEOS.

7. THE ACQUISITION AND TRACKING SENSOR SYSTEM

In this section, we review current detection and tracking technology in connection with the system requirements already set forth in section 5. Detecting, acquiring, and coarse tracking a particle the size of a marble at 2,000 km is a challenging requirement. Handing off to a laser engagement system is another challenging undertaking. Several options have been identified that can satisfy the requirements dictated by the debris population characteristics. One proven technology option has been the MIT Lincoln Laboratories Haystack radar. Another is the STARFIRE passive optical satellite tracking system in Albuquerque, NM. Thus, there is substantive technical margin for this aspect of the problem.

It is logical to consider active optical tracking, with either a pulsed or CW laser, making use of the pusher laser in a defocused mode. We will see that this has the potential to extend the availability of optical tracking from the 4 h per day of the passive option to nearly 24 h per day.

Also considered in this section is the possibility of using existing communications satellite technology to perform debris detection. The forward scattering enhancement, made possible by the location of satellites in orbit, makes this scheme possible. The fact that existing systems might be used parasitically makes this option attractive from a cost standpoint.

Along with the foregoing, it is important to consider the handoff to the laser system and whether the radar can be used remotely. For example, building a clone of Haystack at an optimum laser site would cost on the order of $80 to $100 million. Remote radar support during operations promises to save the cost of building a new radar. With all the requirements in mind, we now explore radar, passive optics, bistatic radio frequency (RF) detection (using communication satellites to illuminate the particles), and laser radar.

7.1 Microwave Radar Option

The advantages of radar include all-weather operation and relatively high accuracy in position and signature. As mentioned previously, the Haystack radar developed and operated by MIT Lincoln Laboratories at Tyngsboro, MA, (42.6° N latitude) is an example of proven radar technology with the potential to accomplish the ORION mission. The facility is depicted in figure 13. Haystack is probably the most sensitive radar in the world capable of achieving the tracking rates necessary for ORION. Haystack operates at 10 GHz with a range resolution of 1 to 10 m and an angular resolution of 10 to 50 mrad. Its range rate performance is 0.1 to 1 cm/s. Given these performance values, Haystack would be suitable for use in the ORION sensor mission.

With Haystack, the disadvantage of being in a nonoptimum environment for the laser may be ameliorated by remote handoff. In principle, this is primarily a software development and integration task, which Lincoln Laboratories believes can be done with existing technology. The advantage of this development would be to utilize the advantages of Haystack without having to clone it at the laser facility site (a very expensive undertaking).

The general importance of this development is that the handoff technique could be applied to any radar. ORION could use any radar that might be available and suitable. One penalty for using Haystack remotely would be its latitude, which constrains the minimum inclination. This is expected to be only a minor disadvantage since it can see the majority of the debris populations.

Search and acquisition could be accomplished using a two-dimensional bowtie scan to build up the field of regard. Such a scan pattern at 30° elevation would be virtually leak proof. The radar would provide tracking and discrimination of the target with a resolution less than 200 m. A resolution cell on the order of the laser beam size (about 1 m) is needed for laser engagement with the particle, so the radar would be required to hand off to a fine track system.

Canonical Microwave Radar for ORION

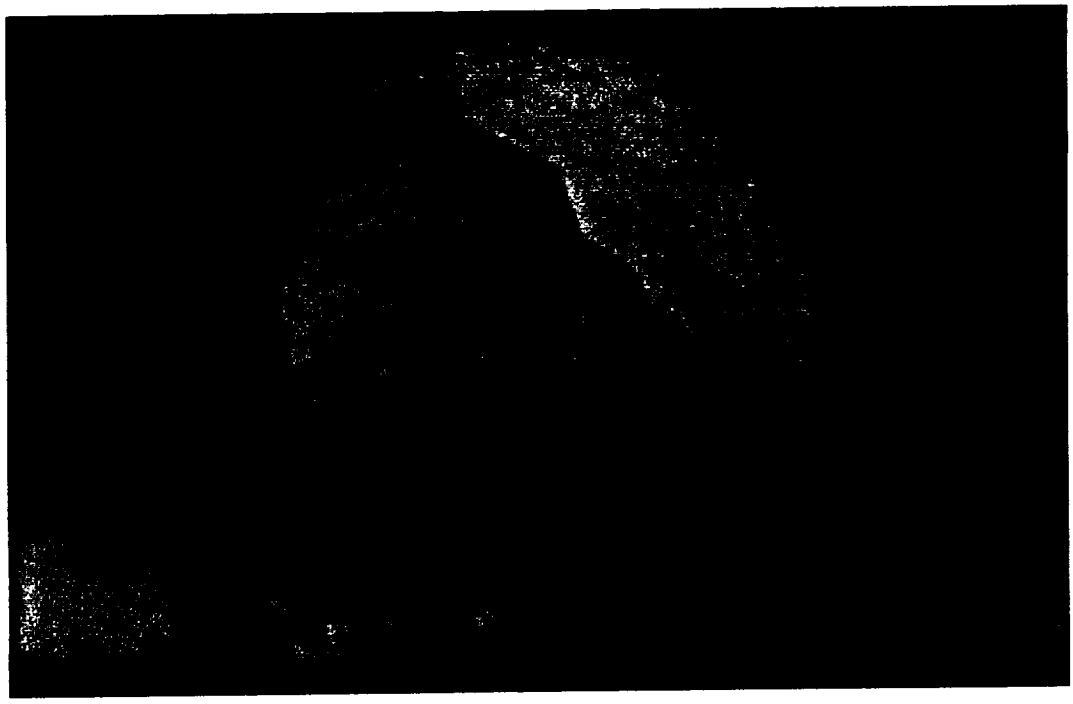

Long Range Imaging Radar

High Power Transmitter (200 kW)
Large, Precise Antenna (120 ft)
Wideband Capability (1 GHz)
Sensitive Receiver

Location Tyngsboro, MA (42.6° N, 272° E)

Radar Frequency 10 GHz

Sensitivity (S/N on 1 sq. mile target at 1000 km range)

Pulse Length (ms)	**S/N Ratio** (db)
2.0	61
5.0	65

Tracking Precision

Range	1–10 m
Angles	50 μrad
Range rate	.1–1 cm/s

Figure 13. Haystack: canonical microwave radar for ORION.

Of course, the engagement laser itself could be used in the fine track role by simply defocusing the beam to capture the particle in the 200-m pixel provided by the radar, and then walking the resolution cell size down to 1 m. At this point, the laser would engage the particle in order to lower its perigee. In addition to the other advantages discussed, radar provides knowledge after the engagement as to how a particle's orbit was affected.

Of course, the engagement laser itself could be used in the fine track role by simply defocusing the beam to capture the particle in the 200-m pixel provided by the radar, and then walking the resolution cell size down to 1 m. At this point, the laser would engage the particle in order to lower its perigee. In addition to the other advantages discussed, radar provides knowledge after the engagement as to how a particle's orbit was affected.

Remote handoff is extremely promising. It is expected that a reasonably straightforward development will resolve information transfer concerns and minimize information transfer time lags. Coordinate conversions could be accomplished by modern computers in near-real time either at Haystack or at the laser facility. The USAF Phillips Laboratory is presently investigating predictive accuracy in using such an approach. A demonstration project would be needed to complete a detailed solution.

Although Haystack is the flagship of operational USAF radar, other existing radars including the USAF HAVE STARE (with significant modification) would be viable candidates for accomplishing the ORION sensor mission, either collocated or in the remote mode.

Microwave radar approaches the ideal of 24 h per day operation in all weather. It can operate in the day or at night, and even in cloudy conditions. We have estimated that Haystack or another radar would provide up to a 20-h operating window per day, allowing for severe weather and maintenance time.

7.2 Passive Optics Option

Using Sun reflection from the debris particle, high-sensitivity, high-resolution passive optics offers the advantage of low cost as compared to building a new radar. Developing a remote handoff capability for the radar offers the attractive approach of a complementary radar/optics approach. This is important, since surveys show that some debris detected in visible light is not detected by radar, and vice versa. Passive optics also provide immediate feedback that the particle was successfully engaged by the laser, since plasma ignition produces a bright flash in the visible.

The disadvantage to passive optics alone is that it only operates during times of clear weather when the Sun/particle/observer angles are appropriate. This alignment typically provides a 4 h per day window for operations. As will be shown later in discussing ORION system options, using passive optics alone will extend the clearing time beyond 2 years for the debris population under 800 km. We have been able to keep it to 3 years by using a larger mirror than for the microwave radar option. Another disadvantage is that orbit assessment would be difficult with a passive optics system alone. Orbit assessment is proven technology existing at Lincoln Laboratories and also used with STARFIRE and AMOS.

Figure 14 shows the STARFIRE facility. A single facility this size located in a suitable location (e.g., China Lake) could accomplish both the detection and tracking mission and the particle engagement mission. In short, a single $50 million facility such as this could protect *ISS* and all other assets under 800 km.

7.3 The Bistatic Detection Option

Orbital debris is continuously being illuminated by a number of communications transmitters located on the ground, in LEO, and in geosynchronous orbit (GEO). This illumination is due to the normal functions of such satellites, and is available to ORION at no cost. Dramatic increases are expected in the numbers of communications satellites in the next few years, particularly in LEO, and thus in the number of potential illuminators for use in ORION surveillance.

Example Optical System

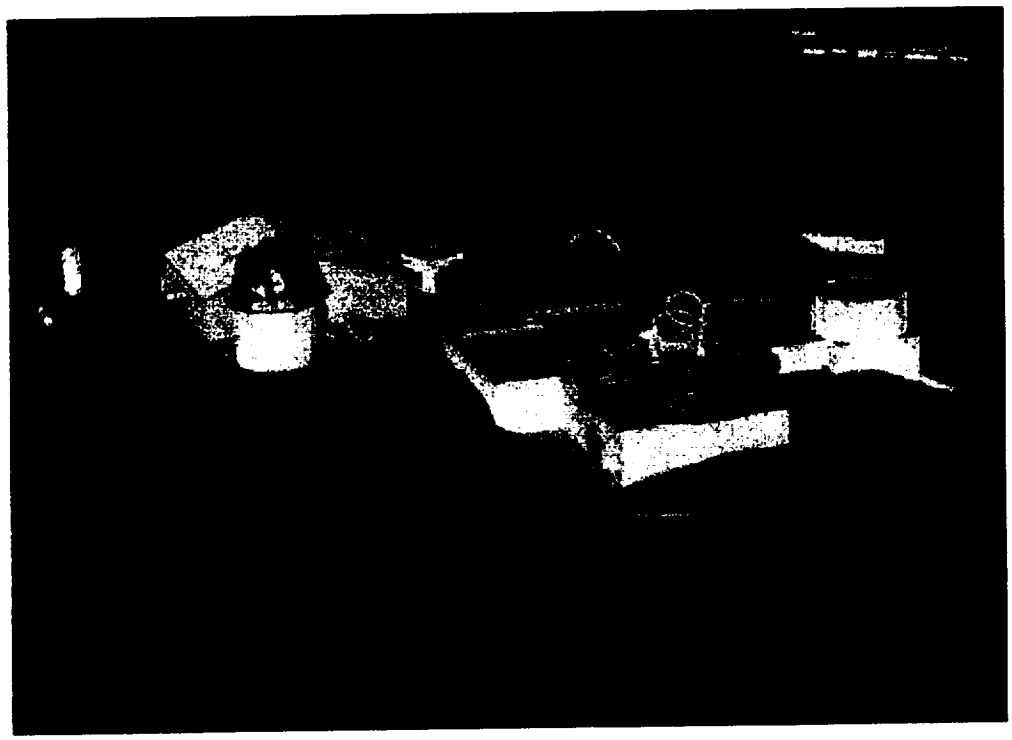

- **STARFIRE, Albuquerque**
- **3.5 meter F/32 Telescope (Narrow FOV)**
- **Satellite Tracking**
- **High Sensitivity**
- **High Accuracy**, Angles 10 μrad

Figure 14. STARFIRE: example optical system.

One major implementation option makes use of the fact that the debris target forward-scatter cross section can be much larger than the back-scatter cross section usually used for surveillance. This is true when the target is large compared with the wavelength of the radiation, and is nearly in line between the transmitter and the receiver (i.e., scatter angle close to 180°). The most interesting such application of the forward-scattering enhancement, without placing any requirements on the communications satellite, is to place a special antenna array on the ground that would look for radiation scattered or diffracted by debris from any normal satellite downlink signal. The large numbers of satellites (close to 1,000 in LEO in the time frame of the year 2000) would assure that favorable geometries for detection of debris objects occur frequently.

Another implementation option is to use a ground receiver to detect the radiation scattered forward by the debris from the communications satellite's uplink signal. This differs from conventional radar only in that the transmitter and receiver are not collocated, with the forward scattering angle being between 0° and 180°. While with this option the transmitter is much more powerful than the typical spacecraft transmitter, most large radars are still more powerful than communications uplinks. Nonetheless, these uplinks are "free" to ORION, and so will also be considered for debris detection.

The details of our analysis of the bistatic detection option are contained in appendix G. Main results were the characterization of the detectable debris size as a function of the downlink frequency, satellite altitude, and receiving array size and geometry. The detectable debris size decreases as the array size increases and as the frequency increases. Further improvement can be made if the target is illuminated over several receiver beam widths. The forward-scattering enhancement is greatest for shorter path lengths, and when the target is near either the transmitter or the receiver. The implications are that for a given power density reaching the ground, the debris is more easily detected with signals from LEO satellites than GEO satellites. This is true even taking into account the larger antennas and powers of GEO satellites.

In order to model the potential of the bistatic detection, a baseline calculation was performed for a debris particle orbiting at 500-km altitude. The baseline frequency is taken to be 20 GHz, with the satellite placing 10^{-12} W/m^2 on the ground from an altitude of 800 km. The numbers are consistent with existing communications satellites. The theoretical limit for a 25-m detector antenna is 0.1 m^2, or 30-cm debris particles.

The situation improves for other communications satellite sources. There is an unusually powerful transmitter on the ACTS satellite in GEO. For a target in high-Earth orbit (HEO), the disadvantage of greater altitude is compensated by the fact that its effective radiated power is greater, a debris particle would spend a greater time in its beam than for a satellite at a lower altitude, and the forward-scattering effect is enhanced by the proximity of the target to the transmitter. This case is also shown as a curve in figure 15, even though debris at this height was not the subject of the ORION study. With the ACTS spacecraft, debris particles of 0.03 m^2, or 17 cm across, would be detectable near GEO with a 25-m ground receiver array.

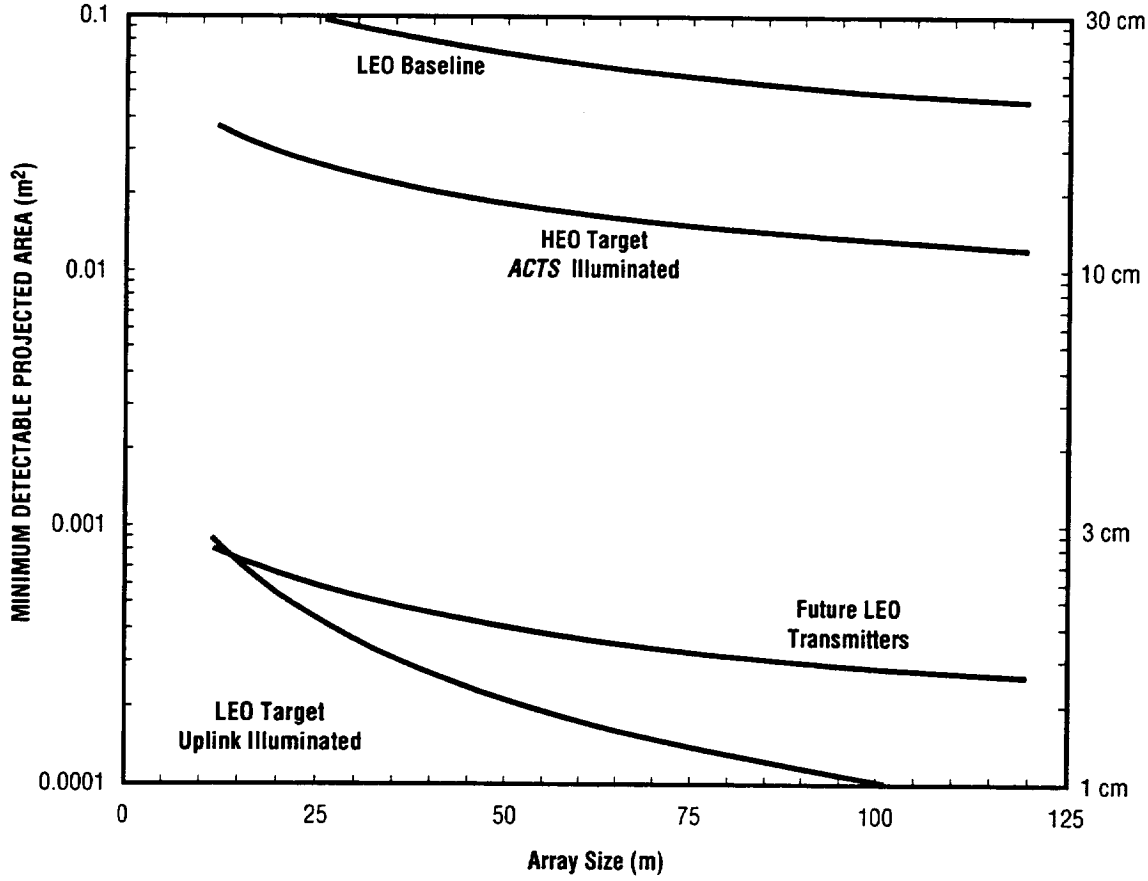

Figure 15. Performance prediction for bistatic detection.

Planned LEO communications satellites such as Iridium or Teledesic will deliver a much greater power density to the ground, principally in order to work with portable and other small terminals. Frequencies may also increase to 30 GHz. If a piece of orbital debris were to pass between such a satellite and an array on the ground in a favorable alignment for forward-scattering enhancement, the threshold detectable area would fall dramatically. For an object passing within 50 km of the transmitter, the threshold detectable size is 0.001 m^2, or 3-cm size, when using a 25-m detector array. Equally dramatic is the theoretical threshold for detection of a target passing through the uplink beam of a powerful ground uplink transmitter to a GEO satellite. In this case, the same detector array could detect 0.0004 m^2, or 2-cm size debris particles at 500-km altitude, even though the forward-scattering enhancement is absent in this case.

The calculations of detection performance do not account for some losses in signal processing and are somewhat idealized, and thus practical systems would probably have lower performances. While practical systems would thus only be able to detect larger debris than indicated above, the use of larger antenna arrays could compensate for the losses. These larger arrays would be more costly, though they would still be receive-only. The implication is that bistatic detection can probably be effective for debris particles of a few centimeters or larger. Further study must be done to see if a system concept is possible that would extend this performance down to 1-cm size.

In summary, bistatic detection using communications satellites, radar satellites, and other tracking radars on the ground is very promising and needs to be investigated further.

7.4 Laser Radar Option

With this option, the laser system itself would simply be used to perform both the sensing and the particle engagement functions. As the altitude range to be searched increases, the laser energy must by focused into smaller and smaller spots in order to give an adequate signal-to-noise ratio. This requirement is in conflict with the need to search wider areas at higher altitudes. The conflict can be addressed by increasing the pulse repetition frequency of a pulsed laser, but at some point the round-trip light travel time will become larger than the time between successive pulses. At this point, the next outgoing pulse threatens to blind the detector to the return from the previous pulse. For altitudes above about 600 km, this might require a detecting telescope separate from the beam launching telescope.

This laser radar option, while it appears to be feasible, greatly increases the complexity of the laser system. The sensing requirements dictated by the characteristics of the debris population would drive the design to a 5- to 10-m mirror with multiple guide stars. Clearly, a remote radar and/or passive optics offers more technological and cost margin for the 800-km objective. Choosing the objective of removing all debris below 1,500 km makes the laser radar approach more attractive as one would already be forced to larger apertures to keep the engagement laser spot size small at the longer ranges.

7.5 Sensor Conclusions

Four sensor approaches have significant capability applicable to the ORION mission, thus substantive technological margin has been found in the sensor technology. As was shown previously, this was found to be true for the laser area as well. The findings are summarized in figure 16.

The two most promising near-future options are the radar and the passive optics. Both offer good tracking capabilities, good to excellent discrimination capabilities, and excellent handover accuracy. Both can search wide areas of space to detect 1-cm debris out to 2,000 km. Both offer some damage assessment. Either option can satisfy ORION mission requirements. For a demonstration, it may be advantageous to have both radar and optics operating together hand in hand. As will be shown later, the radar option is slightly higher in cost than the passive optics. Nevertheless, the radar can operate in all-weather/day/night conditions, so the rate of detection and hence the rate of debris removal is higher than with the passive optics.

Sensor Conclusions

Parameter	Radar	Passive Optics	Bistatic System	Laser Radar
Search	Bowtie	Wide FOV	None	Defocus or Fence
Detection				
500 km	1 cm	1cm	**> 5 cm**	1cm
1000 km	1 cm	1cm	**> 10 cm**	1cm
1500 km	**2 cm**	1cm	**> 20 cm**	1cm
Tracking	Yes	Yes	**No**	Yes
Discrimination	Excellent	Good	**Unknown**	Excellent
Handover Accuracy	Excellent	Excellent	NA	Excellent
Damage Assessment	Excellent	**Partial**	No	Excellent
Utilization	24 h/day	**< 4 h/day**	24 h/day	24 h/day
Availability	Exists	**Buildable**	**New**	**ORION**
Cost	Low for Haystack	Low for STARFIRE	Unknown	ORION +
	High/New	Moderate/New		

Figure 16. Sensor conclusions.

While the bistatic detection system offers high potential for reduced costs, the technique is not as well analyzed. The finding that this approach has the capability to detect at least 5-cm debris at 500 km holds implications for several applications, including augmentation of the USAF space surveillance systems, and warrants further study. Since we need reliable detection of 1-cm objects, it was not selected for ORION at this time, though it may prove to be a viable contender upon more detailed analysis.

The laser radar meets ORION requirements. Yet, the technology is not as mature as radar or passive optics, hence the cost growth risk is higher. A large (6-m) mirror would be required, with the associated requirement for multiple guide stars. As discussed previously, this is future technology requiring substantive development.

7.6 Handoff

A smooth transition from coarse to fine tracking is vital to ORION. The radar provides particle location and velocity to a resolution cell about 200 m across at 2,000 km. Once the particle's orbital parameters are determined by the radar (about 10 s after detection), a laser beam defocused to the same resolution as the radar will be precisely pointed to illuminate the same region of space. The debris particle will then be simultaneously illuminated by both the radar and the fine track laser. An automatic, computer-controlled, step-by-step focusing procedure will then commence in which the beam is incrementally

focused down to the minimum attainable spot size. Radar (or passive optics) coverage will be continuous during this procedure to complement fine tracking.

Once the laser is pointed at the predicted location of the particle with an uncertainty corresponding to the minimum spot size of the engagement laser, engagement occurs and is repeated as long as the particle remains in the window of opportunity. Radar tracking and handoff (i.e., tracking information updates) continue throughout the multiple engagements. Once the particle leaves the window of opportunity, the radar assesses the post-engagement orbit for bookkeeping purposes.

8. SYSTEM COSTS

The first crucial finding provided by this study is that ground-based lasers and sensors are a feasible approach to orbital debris removal. As the study unfolded, it became clear that a number of technical approaches were feasible, adding confidence. Finally, these technical approaches were found to have reasonable costs as compared to other orbital debris mitigation approaches.

Throughout the study, cost was viewed as a key factor in developing configurations. Costs were primarily determined by analogy, supported by NASA costing models. As a result, two demonstration experiments have been identified, and five affordable systems may work, pending the results of a demonstration. Hence, we are confident that the ORION mission can be accomplished with substantive programmatic margin.

Either the AEOS or the STARFIRE facility could relatively easily be adapted to do an active ORION demonstration. This would consist of detecting and tracking a cataloged particle with a perigee of approximately 200 km and then modifying its orbit to a measurable degree. An existing Nd:YAG or Nd:glass providing 100 J per pulse would be sufficient for the demonstration, assuming a pulse duration of 1 to 10 ns and a repetition rate of one pulse per second. Guide stars would be needed for adaptive optics.

Although the beam intensity on the primary mirror would be moderate, the mirrors would probably have to be coated to handle the flux. No cooling of the mirror is expected to be needed.

One demonstration series we have envisioned would use passive optics only and operate just 4 h per day. This is the least expensive option. The other demonstration series would involve an existing radar and remote handoff. Either demonstration could best be controlled with the use of special space shuttle-deployed targets, as described in appendix D.

An overview of the systems we believe are feasible for subobjectives A and B is shown in figure 17. It also shows the estimated cost ranges and percentages of the debris population included for each system graphically.

The cost estimates for an ORION demonstration converge around $20 million. For a cost on the order of $80 million, orbital debris removal can be demonstrated as part of a phased program and most debris below 800 km removed. One system option, A1, employs a passive optics sensor in conjunction with a Nd:glass laser at 1.06 mm, uses a 3.5-m primary mirror, and should cost about $65 million. Cost details are shown in figure 18, and models are explained in detail in appendix D.

Option A2 employs a Haystack-type radar operating remotely in conjunction with a Nd:glass laser at 1.06 mm. It uses a 3.5 m primary mirror, and should cost about $100 million. A2 clears all the debris below 800 km (about 30,000 particles) in 2 years, while A1 takes 3 years.

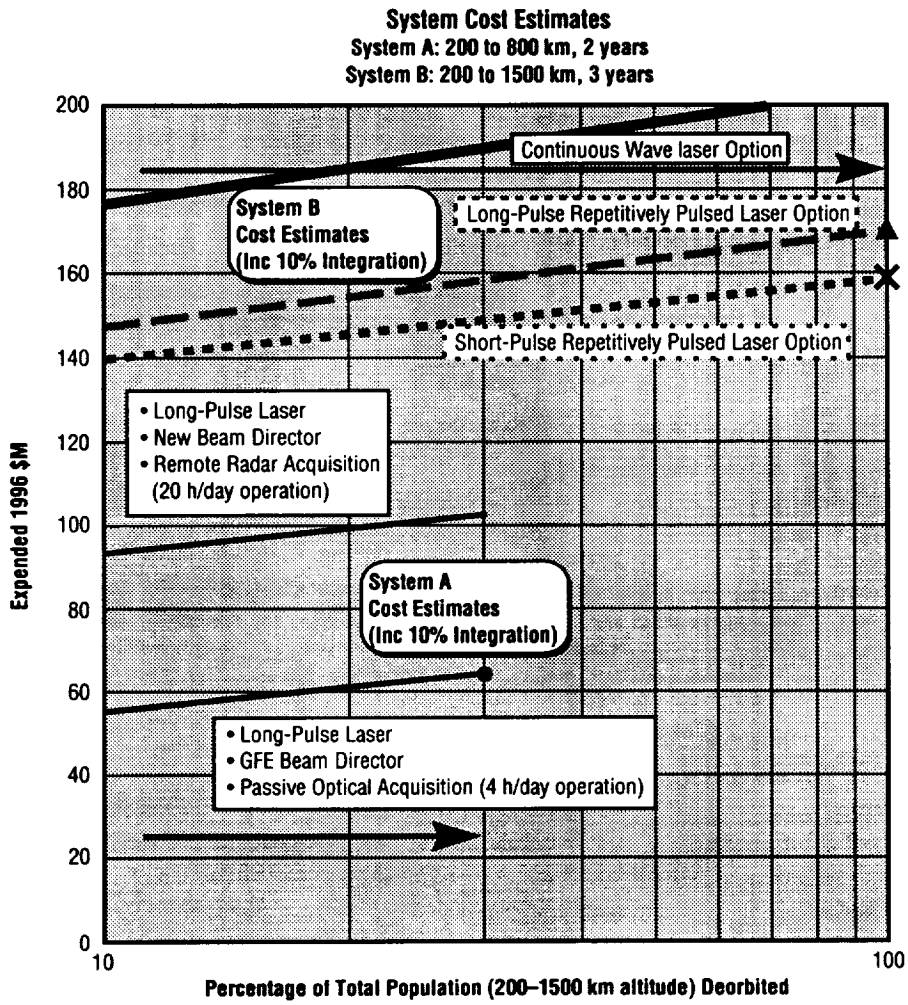

System A Designed to clear altitudes up to 800 km in 2 years after On-Orbit Demonstration Program (approximately 30,000 debris objects)

System B Designed to clear altitudes up to 1500 km in 3 years after On-Orbit Demonstration Program (approximately 115,000 debris objects)

	Option A1	Option A2	Option B1	Option B2	Option B3
Operations	4 h/day	20 h/day	20 h/day	20 h/day	20 h/day
Pusher Laser	Cooled bursts 5 ns, 1–5 Hz	Cooled bursts 5 ns, 1–5 Hz	Actively cooled Nd 100 ps,1–5 Hz modified LLNL system	Actively cooled Nd 10 ns,1–5 Hz one NIF module	CW Iodine ground-based recycled gas
Beam Director	Government furnished equipment (GFE) with modifications	New	New	New	New
Guide Star	Existing	Existing	New	New	New
Acquisition Assessment	Passive Electro-optical (EO) • At site	Radar • At remote location	Radar options • Government furnished equipment, relocated • New (max $) • Remote location	• Laser illuminator at site or • Remote radar	• Laser illuminator at site or • Remote radar

Figure 17. Cost summary graph.

Top-Level Program/Cost Matrix—ORION

	Near-Term On-Orbit Demo Options (using Proven Technologies) Demonstrate acquisition, track, handover, irradiate, spot maintaince, de-orbit in approximately 1 year from go-ahead		System A Clear out 200-800 km altitude range in less than 3 years from approval Options for near Term System (using Proven Technologies)	
System Component	**Demo Option 1**	**Demo Option 2**	**Option A1** (4 hrs/day operation)	**Option A2** (20 hrs/day operation)
Laser Device	1–10 ns pulsed NdYag (100 J) (GFE L. Hackel Laser at PL)	1–10 ns pulsed NdYag (100 J) (GFE L. Hackel Laser at PL)	5 ns pulsed NdYag (5 KJ, 1–5 Hz) (Beamlet Design, Hot Rod mode, Cooled between bursts)	5 ns pulsed NdYag (5 KJ, 1–5 Hz) (Beamlet Design, Hot Rod mode, Cooled between bursts)
Estimated Cost	1.3–3.0	1.3–3.0	28.6–31.6	33.3–37.3
Beam Director Optic	GFE 3.5M Telescope with modifications required	GFE 3.5M Telescope with modifications required	GFE 3.5M Telescope with modifications required	New 3.5M Telescope
Estimated Cost	3.4–6.3	5.2–9.9	4.0–6.0	35.0–40.0
Guide Star System	GFE LLNL Sodium System & SOR Rayleigh System	GFE LLNL Sodium System & SOR Rayleigh System	New Sodium System	New Sodium System
Estimated Cost	1.4–2.3	2.0–4.0	4.9–6.5	6.5–9.7
Acquisition/Tracking	GFE passive EO (sunlight illumination) (4 h/day operation) GFE 3.5 M telescope **1)** demo acquisition/ handover to remote low-power illuminator with retro-reflector orbiter	Haystack/Have Stare/Millstone (24 h/day operation) **1)** demo acquisition/handover to remote low-power illuminator with retro-reflector orbiter **2)** demo acquisition/handover to remote pusher laser with orbiter target	Passive Electro-optical (sunlight illumination) (4 h/day operation-1 crew shift) acquisition/handover by small telescope at Pusher site with real debris Targets	Haystack/Have Stare/Millstone (existing radars @ need sole` use)(24 h/day operation – 3 shifts) acquisition/handover to remote pusher laser with real debris targets
Estimated Cost	5.0–9.0	5.5–9.8	5.4–8.1	7.2–12.3
Target Set	Up to 300 km altitude special demo targets (shuttle–deployed)	Up to 300 km altitude special demo targets (shuttle–deployed)	Up to 800 km altitudes existing debris populations	Up to 800 km altitudes existing debris populations
Estimated Cost	0.5–1	0.5–1	0	0
Integration				
Estimated Cost	1.2–2.1	1.5–2.6	4.0–5.0	8.3–9.7
TOTAL P. E. Cost Range	**$13M–$23M**	**$16M–$28M**	**$57M–$69M**	**$93M–$108M**

Figure 18. Detailed cost breakdown.

Top-Level Program/Cost Matrix–ORION

System B Options for Advanced Technology System (using Near-Term Technologies) Clear out 200-1500 km altitude range in less than 3 years from approval		
Option B1 (20 h/day operation)	**Option B2** (20 h/day operation)	**Option B3** (20 h/day operation)
100 ps repped-pulse pulsed NdYag (2–4 kJ cooled, 1-5 Hz) (requires demonstration) 45.9–66.9	10 ps repped-pulse pulsed NdYag (10–20 kJ cooled, 1-5 Hz) (193rd module of 192-laser NIF) 50.9–79.9	CW Iodine (2–4 MW, ground-based, recycled gas) 67.9–105.9
New 6 meter beam director 57.3–60.3	New 6 meter beam director 57.3–60.3	New 6 meter beam director 57.3–60.3
New Sodium Guidestar 7.1–10.7	New Sodium Guidestar 7.1–10.7	New Sodium System 7.1–10.7
Microwave radar; remote or located near Pusher site (24h/day operation) **A)** New radar near site $80M or **B)** remote radar handover $5M or **C)** GFE Have Stare equipment guess transp., setup, use $5M 16.9–21.9	Pusher Laser as active illuminator and ranging radar (24h/day operation) estimated additional staff, consumables, ADP= $16.9M-$25.9M or **B)** Remote redar handover $5M 16.9–25.9	Pusher Laser as active illuminator (24h/day operation) estimated additional staff, consumables, ADP= $23.9M-$39.9M or **B)** Remote redar handover $5M 23.9–39.9
Up to 1500 km altitude existing debris populations 0	Up to 1500 km altitude existing debris populations 0	Up to 1500 km altitude existing debris populations 0
12.2–15.5	12.5–17.2	15.6–21.7
$140M–$176M	**$145M–$195M**	**$172M–$239M**

Figure 18. Detailed cost breakdown (continued).

For a cost on the order of $160 million, orbital debris removal can be demonstrated as part of a phased program and the envelope of coverage extended to 1,500 km. Configurations B1, B2, and B3 remove all debris below 1,500 km (about 150,000 particles). Costs grow because requirements dictate larger primary mirrors (5 to 10 m).

For example, option B1 total costs were derived to be $140 to $176 million. The breakdown for this configuration includes a 0.1-ns pulsed Nd:glass laser operating at 2 to 4 kJ and 1 to 5 Hz and costing $45.9 to $66.9 million. Also included is a Government-furnished telescope with a 6-m adaptive primary mirror costing $57.3 to $60.3 million. A new sodium guide star subsystem costs $7.1 to $10.7 million. The radar subsystem costs $16.9 to $21.9 million. Integration costs are expected to range from $12.2 to $15.5 million. This is a summary of a more detailed breakdown. The total costs for the other configurations were derived in a similar manner.

Option B2 would use a 10-ns Nd:glass laser both as a pusher and as a laser radar. The total cost is estimated to be about the same as for option B1. For option B3, we have assumed the development of an iodine CW laser operating at 2- to 4-MW average power. Our best estimate of the system cost is in the range $172 to $239 million.

9. NOT A WEAPON

ORION would make a poor antisatellite weapon. Each laser pulse ablates a layer only a few molecules thick. Thus, at the energy levels delivered, burning a hole through the skin of a satellite would take years. Deorbiting a satellite might be accomplished, but it would take months of dedicated operation. Hence, accidentally bringing down a satellite is not possible. Satellite sensors looking directly at the laser site may be blinded, and some other spacecraft components damaged, but this can easily be avoided with the proper operating procedures at the laser site. The procedures would include avoidance of illumination of known spacecraft, which is a technique being used today with complete success. As a result, the ORION system could be operated without endangering any declared active spacecraft.

10. SUMMARY

The orbital debris population poses a significant threat to the *ISS* and other assets in LEO. Currently, millions of dollars are planned toward mitigating the risk, which includes curtailing debris production as well as shielding and maneuvers.

The characteristics of the orbital debris population including size, shape, composition, reflectivity, altitude, and inclination are reasonably well known. The laser/particle interaction and plasma dynamics on extremely short timescales are sufficiently understood. Laser propagation through the atmosphere is constrained by many effects including turbulence, absorption, and SRS. Very short pulses allow us to work within the limits imposed by these physical phenomena.

Several proven ground-based laser and sensor technology options have been found to allow construction of feasible systems. Sensor technology includes ground-based radar systems (e.g., Haystack) and high-sensitivity passive optics that will provide the detection and coarse tracking. Laser options include a repetitively pulsed Nd:glass laser operating at 1.06 mm with a 3.5-m adaptive optics primary mirror and a single sodium beacon. The integration of the sensor and laser options were more than sufficient to remove all debris below 800 km. An advanced system using technology becoming available in the next 5 years will extend this envelope to 1,500 km.

For a cost on the order of $20 million, orbital debris removal can be demonstrated. For an additional cost on the order of $60 million, or $80 million total, essentially all orbital debris in the 1- to 10-cm size range below 800 km can be eliminated over 2 to 3 years of operation, thus protecting the *ISS* and other assets (e.g., Iridium, Teledesic) against debris of these sizes. A cheaper system capable of debris removal only to 500-km altitude could be used if the sole objective were to protect the *ISS*. For a total cost on the order of $160 million and an additional year of operation, this envelope can be extended to 1,500 km, thus protecting both *ISS* and Globalstar.

The bistatic detection technique using communications satellites, though not selected for inclusion in the recommended system architecture at present, may prove to be an inexpensive and readily implemented means to augment the nation's space surveillance capability. It may be particularly useful to detect and catalog debris in the southern hemisphere, where there is a dearth of sensors at present.

11. CONCLUSIONS

Removing 1- to 10-cm debris from LEO using ground-based lasers and ground-based sensors is feasible. All five debris categories can be brought down in 2 to 3 years of ORION operations.

The study objectives have been achieved. Reasonable confidence exists that the systems are feasible in the near term. Suitable hardware and facilities exist in the United States to accomplish a demonstration experiment. Given the high cost of shielding individual orbiting assets, particularly against debris larger than 2 cm, it is strongly recommended that a demonstration be initiated immediately as an alternative or complementary debris mitigation approach.

Russian progress in ORION-related technological areas has been impressive. They presently enjoy substantive capabilities and facilities, and are eager to apply these to an international project. This should be considered in any plan of action.

Due to the inherently national character of an ORION-type system, if serious interest develops to pursue the capability, it is likely that the DOD should be the preferred agency to develop and operate it for the benefit of all spacecraft, be they commercial, civil, or defense, with NASA playing a supporting role to ensure benefits to the *ISS*. There may be sufficient motivation to pursue the bistatic detection surveillance technique, whether an ORION system is deployed or not.

12. RECOMMENDATIONS

Maximizing the use of Government-furnished equipment hardware, initiate a demonstration program to find, track, and push a suitable particle presently in LEO and verify the change in orbital parameters.

This demonstration should focus on using an existing high energy laser. Preferably, a Nd:glass laser operating at 1.06 mm should be used in conjunction with an existing adaptive mirror such as STARFIRE or AEOS. The remote application of Haystack should be demonstrated as part of this, as well as the application of passive optics.

A few existing, cataloged (i.e., tracked by U.S. Space Command) debris targets with suitable characteristics should be identified. Both Haystack and the passive optical tracker should be demonstrated against these targets. The laser should then be used to engage the debris, and the resulting change in orbit parameters should be measured.

Based on further study, demonstration findings, and accurate cost estimates, select a configuration option either to accomplish the 800- or the 1,500-km mission.

Perform a definitive study of bistatic detection as a surveillance technique and its application to augment debris detection capability, particularly in the Southern Hemisphere.

TECHNICAL APPENDICES

A. Advanced ORION Laser System Concept, Prepared by James P. Reilly (Northeast Science and Technology)

B. Target Acquisition for ORION, Prepared by James P. Reilly (Northeast Science and Technology)

C. Engagement Strategies and Risk, Prepared by R. Sridharan (MIT, Lincoln Laboratories)

D. Analysis of the ORION System Concept, Prepared by Claude R. Phipps (Photonic Associates)

E. ORION Optics and Target Engagement, Prepared by Glenn Zeiders (The Sirius Group)

F. Selection of Laser Devices and Neodymium Glass Laser System Analysis, Prepared by William Dent (Dent International Research, Inc.)

G. Bistatic Detection of Space Objects Using a Communications Satellite System, Prepared by Richard C. Raup (MIT, Lincoln Laboratories)

APPENDIX A

ADVANCED ORION LASER SYSTEM CONCEPT

Dr. James P. Reilly
Northeast Science and Technology

ADVANCED ORION LASER SYSTEM CONCEPT

Dr. James P. Reilly
Northeast Science & Technology

Introduction

The purpose of this brief study is to analyze the complete potential of the solid state laser in a very long pulse/high energy mode of operation as well as in a very short / lower energy mode of operation, operating in an actively-uncooled (termed "Hot-Rod" mode or "Heat Capacity" mode) method of operation. Concentrating on the phase aberrations to be expected by operating in such manner, the study presented here reports on estimating the bulk phase and intensity aberration distribution in the laser output beam during a single repped-pulse train. Recommendations are made for mitigating such aberrations.

Summary of Results; Conclusions and Recommendations

In this study, we have analyzed the optical performance of an uncooled solid state laser, and for reasons of reliability of performance, have chosen a slab-geometry, flashlamp-pumped MOPA design. In the pulse-width regime required (5-50 ns) the single pulse output fluences allowed by LLNL demonstrations, but degraded for repped operation, allow reasonable-shaped MO pulses to be amplified to the reuquireed energy level with little or no extraction-induced phase aberrations. Further, using LLNL data on thermal gain limitations, 100 -1000 pulses should be extractable from the laser device before gain reduction and other spectroscopic effects begin in the gain medium. At this point, optical pumping and lasing should be ceased, and cooling begun to return the medium to its original state. The analysis indicates that pump-nonuniformities and intrinsic gain medium nonuniformities will probably be the limiting causes of beam phase aberrations, as well as those in associated optical elements---all of which point to engineering design and perhaps adaptive optics to ameliorate those effects which cannot be eliminated by quality control and good engineering.

Statement of the Problem

In designing single-pulse solid-state uncooled lasers, the concentration typically is on the extraction of maximum single-pulse energy at the desired pulse width with the desired beam average phase uniformity. In designing repetitively -pulsed solid-state actively-cooled lasers, the concentration is typically on the extraction of maximum long-term average power at the given pulse width and desired pulse repetition rate, all with the desired beam average phase uniformity.

In the present study, however, the concentration is on the design of uncooled solid-state lasers with the extraction of maximum total emitted laser energy (single-pulse energy X pulse rep rate X run-time) with a specified pulse width and with minimum area-integrated beam phase aberration, all with an eye toward systems which can be cooled down relatively quickly to repeat this repped-pulse lasing cycle in a reasonably fast turn-around time.

Method of Approach

In this analysis, we :

1. first lay out the alternatives to the modes of operation
   - geometry of the gain medium (slab vs rod)
   -amplifier vs oscillator operation
2. then outline the key issues affecting the present problem

3. then discuss heat deposition and its effects on phase differences across the beam
4. then analyze the sources of phase aberration in the output beam, and
5. finally identify potential mitigation approaches

Technical Analysis

A) Mode of Operation

Figure 1 shows the basic geometries of solid-state lasers :

1. rod gain medium :axial extraction, radial pumping, radial cooling
2. slab gain medium: long-dimension extraction, short-dimension pumping and cooling
3. slab gain medium: Brewster's-angle extraction and pumping, short-dimension cooling

Figure 2 shows the laser design trade-off parameters . One of the important parameters is the maximum extractable fluence (joules/cm^2 of output) which the gain medium material can handle without important irreversible damage in bulk or at the surface. The current values of maximum damage threshold for SINGLE-PULSE operation at various pulse-widths are showing **Figure 3.** Note that in the region attractive to ORION (5 to 50 ns) the allowable output fluence at 1.06 microns is between 10 and 20 joules/cm^2 for glass and YAG hosts doped with Nd ions.

It is well known for both gas lasers and solid-state lasers, that oscillator or resonator extraction techniques produce the highest extraction efficiency and the most compact and lighter-weight laser designs, while master-oscillator/power-amplifier (MOPA) extraction techniques can provide higher beam quality, more flexibility and tighter control of the output waveform and phase / frequency content of the output beam at the price of larger, heavier and more cumbersome laser system designs.

SINCE MINIMIZING FLOOR-SPACE AND WEIGHT IS NOT AN OVER-RIDING CONSIDERATION FOR THE GROUND-BASED ORION CONCEPT, WHILE MAXIMUM FLEXIBILITY AND CONTROL AT HIGH BEAM QUALITY IS OF UTMOST IMPORTANCE, WE HAVE CHOSEN THE MOPA AS OUR RECOMMENDED LASER ARCHITECTURE.

The next mode of operation to be chosen is the cooled vs uncooled version of the solid state laser. Clearly for single-pulse operation, no cooling is considered. For rep-rated operation however, whether to cool or not IS an issue. Clearly for continuous 24 hrs / day operation, we require active cooling. However, for an operating mode where one 30 second debris engagement occurs every 10 minutes or so in one two-hour period at dawn and another at dusk (a very real possibility for a viable near-term system), one must question whether ACTIVE cooling is necessary during lasing, or just a rapid cooldown between shots. These two operating scenarios can result in VERY different laser designs, with the former (active cooling while lasing) being a MUCH more difficult (and hence time-consuming and hence expensive) laser design than a simpler, cheaper and potentially more robust system which simply needs to be cooled down between bursts. It is the latter system which is discussed in this report.

B) Key Issues

Figure 4 lists the issues which must be considered in any solid-state laser design as to damage, performance as a simple laser energy source, and performance as a source of coherent radiation. We assume in this report that issues of damage and performance as an energy source are taken care of by good engineering design. We discuss her those issues concerning beam quality, especially those important to an active optical system whose function it is to compensate for these in real time, either open-loop (by pre-programming) or in closed-loop operation using sensors and feedback loops.

NST

Northeast Science & Technology

Repped Solid State Geometries

a) Radial temperature profile

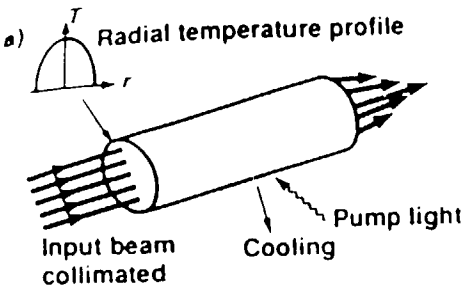

b) Axial temperature profile

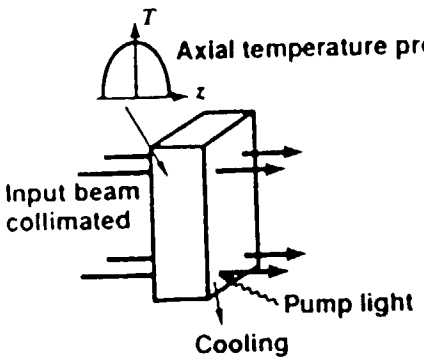

c) "Zig–zag" amplifier

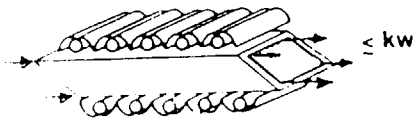

d) "Disk" amplifier, gas cooled

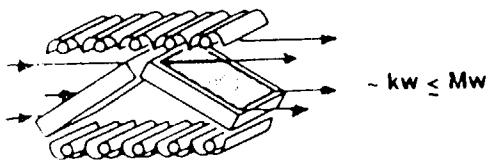

FIG 2

NST

Northeast Science and Technology

SOLID STATE LASER DESIGN TRADE-OFF PARAMETERS

Material Damage Limits pulsed Joule/cm^2 and watt/cm^2 of output. Both scale with pulse length

Pump-Radiation Attenuation Scales gain medium cross-section dimensions and doping fraction

Above parameters limit maximum energy per pulse

Gain Parasitics Limit cavity length at achievable small signal gain

Crystal Fracture Limits mean temperature rise for a given material. Beam quality degrades before rods fracture.

Optical Path (temperature) In homogeneities Limits temperature "ripple" for allowable cavity length

Thermal Diffusion / Conduction Limit pulse repetition rate for required temperature uniformity which drives phase uniformity

Upper State Natural Decay Rates Limit maximum rep rate for raw power output (may not be high-quality beam)

Above parameters dictate maximum rep rate

System Efficiencies Drive power and energy requirements

Platform Payload Capacity Limits allowable weight, volume and consumables

No Limit to Run Time For steady-state-cooling designs

FIG 5

NST

Northeast Science and Technology

Limiting Single Pulse Fluence in ND:Glass Beamlet Train

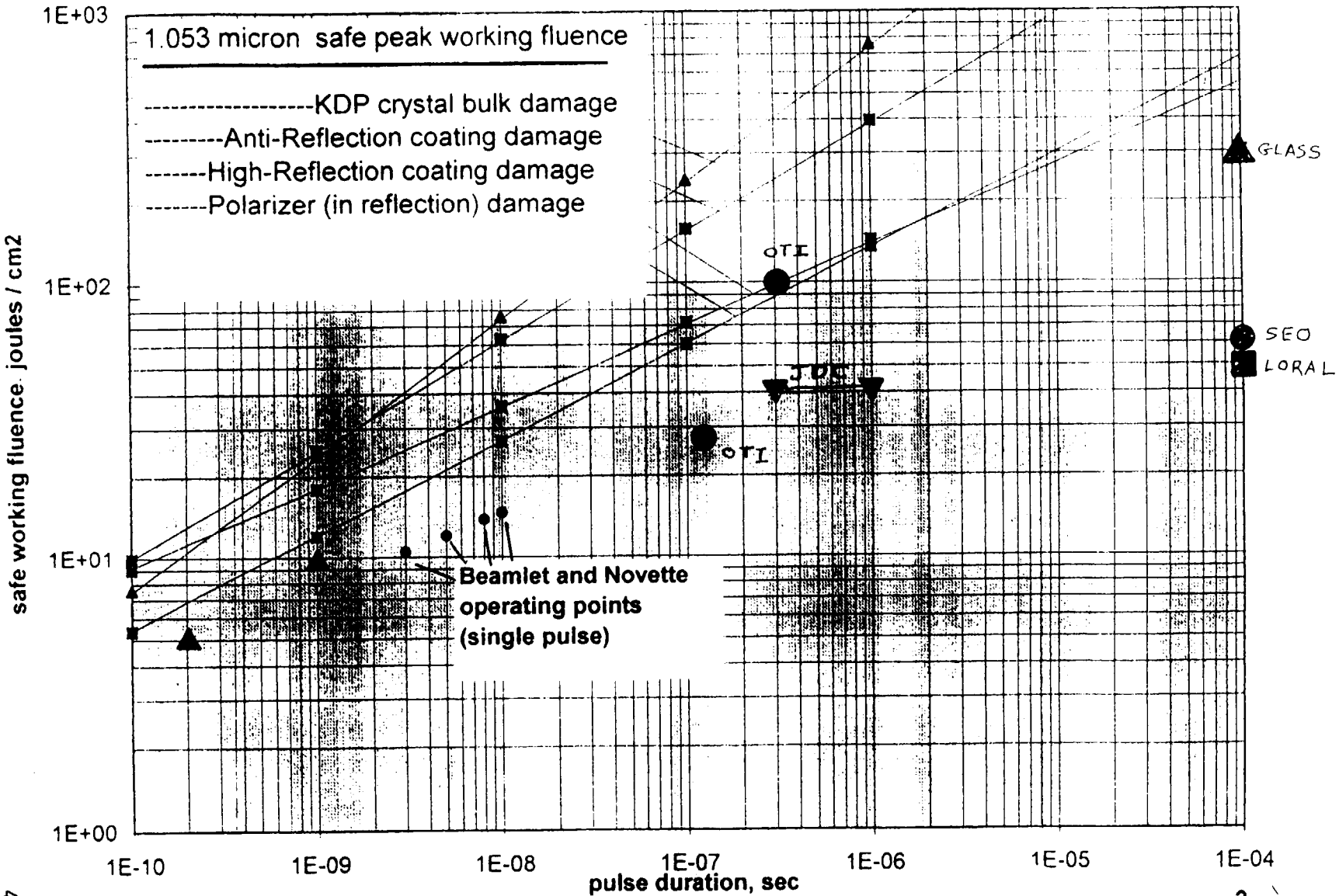

LLNL Beamlet and Novette Lasers have Demonstrated 10-20 j/cm^2 Optics

FIG 4

NST

Northeast Science & Technology

Rep-rate issues for Solid State Lasers

Damage limits stemming from Thermal Deposition and Inadequate Thermal Management

Fracture	differential thermal profile buildup induces-- tension in outer (free) edges -- compression in center (free) region
Differential Expansion	between gain mat'l and transmission-face coatings as well as edge-band coatings
Inclusions / Interfaces	surface and bulk sites show --higher linear absorption than bulk deposition, and/or --higher electric field concentrations with local heating higher than bulk deposition

Phase Aberrations resulting from *Differential* Thermal Deposition

Thermally-induced phase shifts- change of index of refraction with temperature
- thermal expansion induces different physical path lengths for optical raypaths

Photoelastic	stress-induced changes in refractive index at laser wavelength
Thermal Lensing	symmetrical thermal change in refractive index causes whole-beam divergence
Stress Bi-Refringence	stress-induced changes in refractive index over range of wavelengths
Beam Steering	asymmetric thermal changes in refractive index causes beam steering

Performance Limits due to *Absolute* Temperature Levels Reached

Redistribution of Population among Stark levels (ie, gain is a function of temperature level)

Resonance Re-Absorption (more important at high gain values and high absolute temperature levels)

Line-Width Dependence on Temperature Level (higher temperatures mean wider linewidths)

C) Heat Deposition Analysis

The discussion of heat deposition in the solid state laser is dominated by the line spectrum of the absorption by the solid state laser's gain medium convolved with the power spectrum of the pump source, and to a lesser extent the design of the optical cavity which traps (or does not trap) the pump radiation for ultimate absorption by the gain medium. The conventional mode of operation fro small lasers and/or CW lasers is to use efficient CW Diode lasers as pump sources. Because the CW diode laser is tuned exactly to the desired absorption bands in the solid state laser, waste heat is limited to quantum efficiency effects in the pumped solid-state laser. However, these CW diode lasers are too low in power to pump the multi-kilojoule lasers required for ORION, so we are left with the conventional pump sources ---dominated by doped Xenon flashlamps. **Figure 5 (ref 1)** shows typical energy deposition fractions compared to typical laser extraction. Perhaps only 8% of the input lamp power is absorbed by the laser gain medium, and only 2% of the input lamp energy appears as output laser energy. Hence, this figure would indicate that of the deposited energy in the solid state medium, 25% is emitted as radiation and 75% remains as heat. **Figure 6 and 7 (from refs. 2,3 and 4)** show more recent achievements in efficiencies, including the additional efficiency levels for cooled systems, either real-time actively-cooled or between-burst cooling as is discussed here. Note the efficiencies for diode pumping in **Figure 7**, and summarized below.

Pump Scheme	Diode Pump	Flashlamp Pump
Electrical Power Into Pump	100 units (U)	100 U
Power Absorbed by Laser	70 U-90 U	50 U-75 U
Power emitted by laser	1 U-14 U	0.3 U - 7 U
Power Remaining as Heat	50 U- 90 U	45 U - 75 U

It is these inefficiencies which must be addressed in the laser design , because it is the waste heat LEVEL and its DISTRIBUTION which dictate the phase aberrations produced in the beam. Note however, that the differences in diode pumping and flashlamp pumping are minimal as far as phase aberrations go. The major difference is in the size and complexity of the power supplies which power them.

Figure 8 sketches the energy level diagram for 3-level and 4-level solid state lasers., and sets the nomenclature for the gain terms. **Figure 9** sketched the thermal profiles in an amplifier stage which is ***relatively*** well-filled with laser intensity, but which (as it must) has zero intensity near the edges of the gain medium. Note the thermal profiles immediately after the extraction and the slower-timescale deposition (leakage) between extraction pulses due to the slow upper-state decay which being excited by the pump light. **Figure 10** shows the expressions for the time-dependent heat deposition in the solid state laser medium. **Figures 11 and 12** list the equations used here to analyze the time-dependent thermal profiles . **Figure 13** shows the temperature change all along the optical axis of the final amplifier stage immediately after an extraction pulse. Clearly, the more solid medium is used (ie, the longer the gain medium "L") the less is the temperature change, because of the increased heat capacity of the laser medium . After the extraction, heat continues to be deposited, because of the finite-rate leakage out of the upper states of the laser medium between pulses. **Figure 14** shows the temperature change all along the optical axis of the last amplifier stage JUST BEFORE the next extraction pulse (when the gain has been pumped up to design value). In the next Section, we will use these temperature changes to scope the requirements on beam phase homogeneity.

NST

Northeast Science & Technology

System Efficiency Drives Power Supply Cost

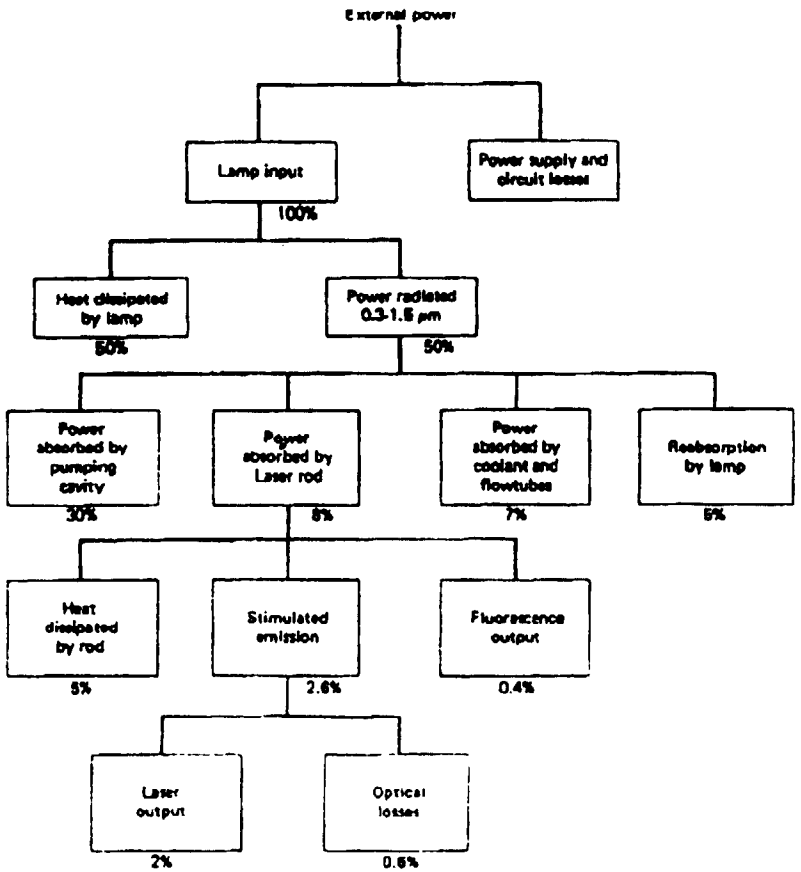

Fig. 6.75. Energy balance in an optically pumped solid-state laser system. (The percentages are fractions of electrical energy supplied to the lamp)

NST
NORTHEAST SCIENCE & TECHNOLOGY

SOLID STATE SYSTEM EFFICIENCY

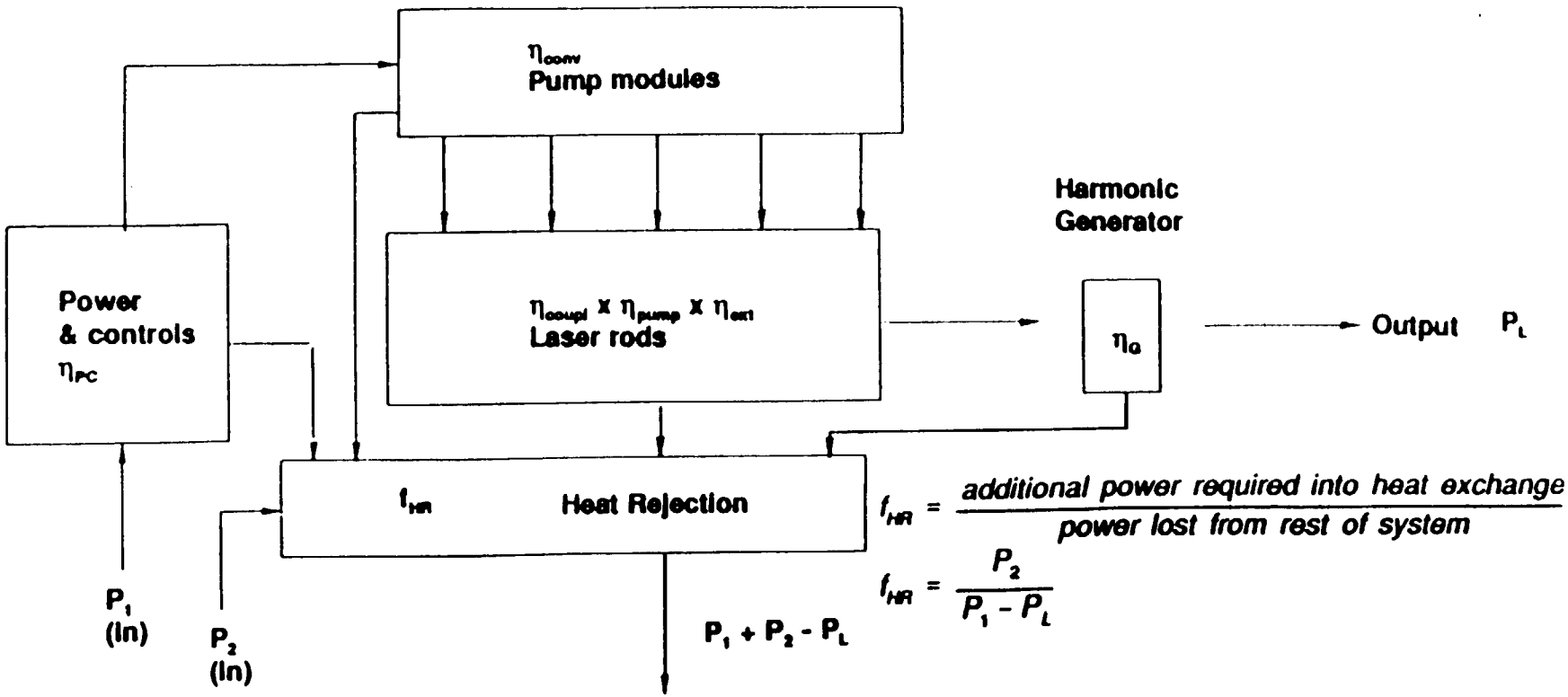

$$f_{HR} = \frac{\textit{additional power required into heat exchange}}{\textit{power lost from rest of system}}$$

$$f_{HR} = \frac{P_2}{P_1 - P_L}$$

$$\eta_{tot} = \frac{\textit{laser power out}}{\textit{total power in}} = \frac{P_L}{P_1 + P_2} = \frac{P_1 \times \eta_{PC}\,\eta_{conv}\,\eta_{coupl}\,\eta_{pump}\,\eta_{ext}\,\eta_G}{P_1 + P_1(1 - \eta_{PC}\,\eta_{conv}\,\eta_{coupl}\,\eta_{pump}\,\eta_{ext}\,\eta_G)\,(1 + f_{HR})}$$

NST

NORTHEAST SCIENCE & TECHNOLOGY

DIODE-PUMPED SOLID-STATE LASER SYSTEM EFFICIENCY AND TYPICAL VALUES

$$\eta_{total} = \frac{\eta_{PC}\ \eta_{conv}\ \eta_{coupl}\ \eta_{ext}\ \eta_G}{1 + (1 - \eta_{PC}\ \eta_{conv}\ \eta_{coupl}\ \eta_{pump}\ \eta_{ext}\ \eta_G)\ (1 + f_{HR})}$$

System range
1.1%-14.1%

Power conditioning and controls
80%-90%

Conversion to diode output in pump band
30%-50%

Optical coupling
70%-90%

Absorbed pump x quantum effic. x Stokes shift
(70%-90%) x 90% x 76%

Extraction
70%-90%

Harmonic generation
40%-70%

Heat rejection
50%-90% efficiency
($0.1 \leq f_{HR} < 0.5$)

Diode conversion and heat rejection efficiency show biggest payoff potential for system efficiency

NST

Northeast Science & Technology

SCALING SOLID STATE LASER

Three Level System

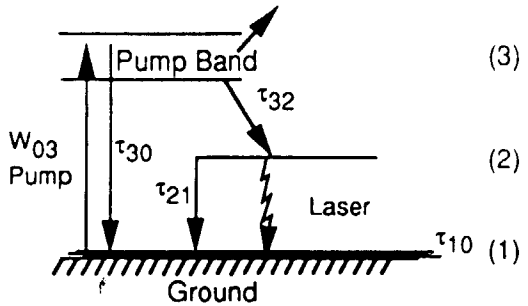

Example: Ruby ($\lambda = 0.63$)
H_o in YAG, YLF ($\lambda = 2\ \mu m$)

Four Level System

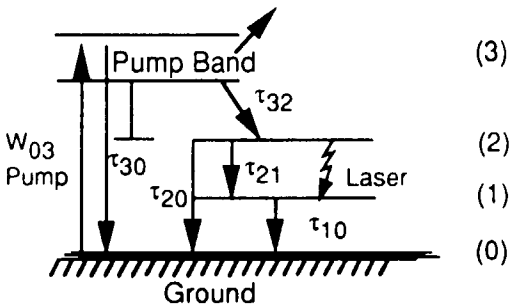

Example: N_D in YAG, YLF ($\lambda = 1.06\ \mu m$)
($\lambda = 2\ \mu m$)

Small signal gain $$g_o = \sigma_{21}\ \eta_{tot}\ \frac{W_{03}\ \tau_{21} - g_2/g_1}{W_{03}\ \tau_{21} + 1}$$

$$g_o = \sigma_{21}\ \eta_{tot} \left(\frac{W_{03}\ \tau_{21}}{W_{03}\ \tau_{21} + 1} \right)$$

Requires $\geq$ 50% of ground level of ruby must be exited
- τ_{32} fast (1-2 ns)
- τ_{21} slow (500 µsec) (Ho:YLF)
- τ_{10} very fast (< 1 ns)

Typically, $W_{03}\ \tau_{21} \leq 10^{-2}$ (YAG) (slow pump, fast pulse)
- τ_{32} fast (1-2 ns)
- τ_{21} slow (250 µsec) (N_D)
- τ_{100} fast (1-10 ns)

FIG 9

NST

AMPLIFIER THERMAL INHOMOGENEITIES

Northeast Science and Technology

52

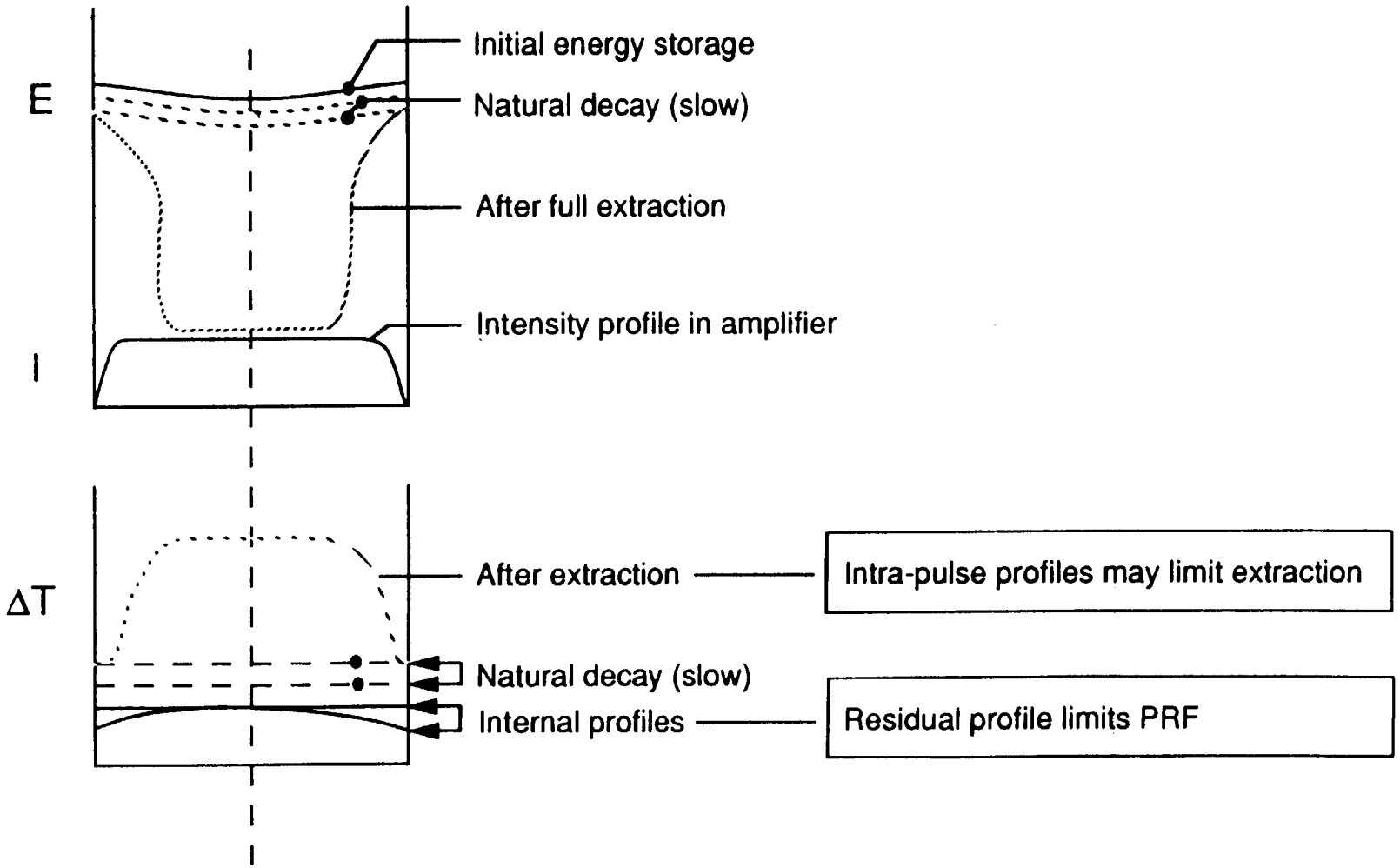

NST

Northeast Science & Technology

DOMINANT THERMAL RELAXATION PROCESSES IN SOLID STATE LASER

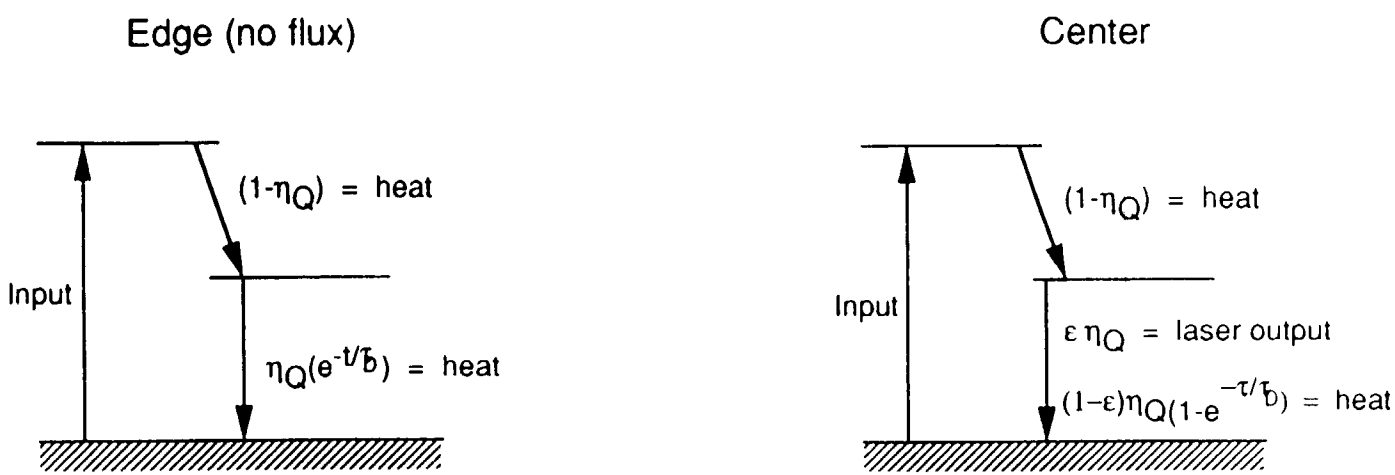

- Quantum inefficiency $(1-\eta_Q)$ appears "instantly" as heat
- Upper laser state
  - Extracted energy $(\varepsilon\,\eta_Q)$ leaves "instantly"
  - Un-extracted energy $((1-\varepsilon)\eta_Q)$ relaxes slowly into heat

NST

AMPLIFIER HEATING ON A SINGLE PULSE

Northeast Science & Technology

- Heating of amplifier during pump pulse

$$\rho\, C\, \frac{dT_1}{dt} = N_{upper}\, E_{upper}\, \frac{1}{\tau_D} + (1 - \eta_Q)\, P_{pump}$$

$$@\ \frac{d}{dt}(N_{upper}\, E_{upper}) = \eta_Q\, P_{pump} \quad (N_{upper}\, E_{upper})/\tau_D$$

Note: $E_{stored} = N_{upper}\, E_{upper} = \eta_Q\, P_{pump}\, \tau_D\, (1 - e^{-t_{pump}/\tau_D})$

For a constant pump power during pump pulse t_{pump}

$$\rho\, C\, \Delta T, = \eta_Q\, P_{pump}\, \tau_D \left(\frac{t_{pump}}{T_D} - e^{-\frac{t_{pump}}{T_D}} \right) + (1 - \eta_Q)\, P_{pump}\, t_{pump}$$

Note: $t_{pump} \leq \tau_D$ for minimum pump input energy efficiency and minimum heating

- Heating of amplifier after amplifier extraction and subsequent decay of remaining upper state

$$\rho\, C\, \Delta\, T_2 = \left(\frac{E_{stored}}{\eta_Q} - \frac{J_{out}}{\eta_Q L} \right) \left(1 - e^{-t/\tau_D}\right) + \left(\frac{1 - \eta_Q}{\eta_Q} \right) \frac{J_{out}}{L}$$

NST

AMPLIFIER HEATING FOR REPPED-PULSE AMPLIFIERS

Northeast Science & Technology

Amplifier designed to be operated when gain has reached design level for each pulse

$$g_o = \beta E_{storage} = \beta N_{upper} \hbar\nu = \beta \eta_Q P_{pump} \tau_D (1 - e^{-t/\tau_D}) \rightarrow \beta \eta_Q P_{pump} t_{pump} \quad (t_{pump} << \tau_D)$$

- Heating of amplifier during pump phase

$$\rho C \Delta T_1 = P_{pump} t_{pump} (1 - \eta_Q e^{-t_{pump}/\tau_D}) \rightarrow P_{pump} t_{pump} (1 - \eta_Q) \quad (t_{pulse} << \tau_D)$$

- Heating of amplifier due to extraction and natural decay during interpulse time

$$\rho C \Delta T_2 = \frac{1}{\eta_Q} (1 - \eta_Q) \frac{J_{out}}{L} + \frac{1}{\eta_Q} \left[E_{stored} - \frac{J_{out}}{L} \right] [1 - e^{-t/\tau_D}]_{interpulse}$$

$$\rightarrow \frac{E_{stored}}{\eta_Q} - \frac{J_{out}}{L} \qquad (t_{interpulse} >> \tau_D)$$

Bulk heating

$$\Delta T = \Delta T_1 + \Delta T_2 = \frac{1}{\rho C} \left[\frac{g_o}{\beta \eta_Q} (1 - \eta_Q) + \left(\frac{g_o}{\beta \eta_Q} - \frac{J_{out}}{L} \right) \right]$$

pump phase extraction decay

Max radial difference

$$\Delta T^{\bullet} \text{ (center to edge)} = \frac{1}{\rho C} \frac{g_o}{\beta \eta_Q} (2 - \eta_Q)$$

NST

BULK AND RADIAL ΔT DURING EXTRACTION PULSE

Northeast Science & Technology

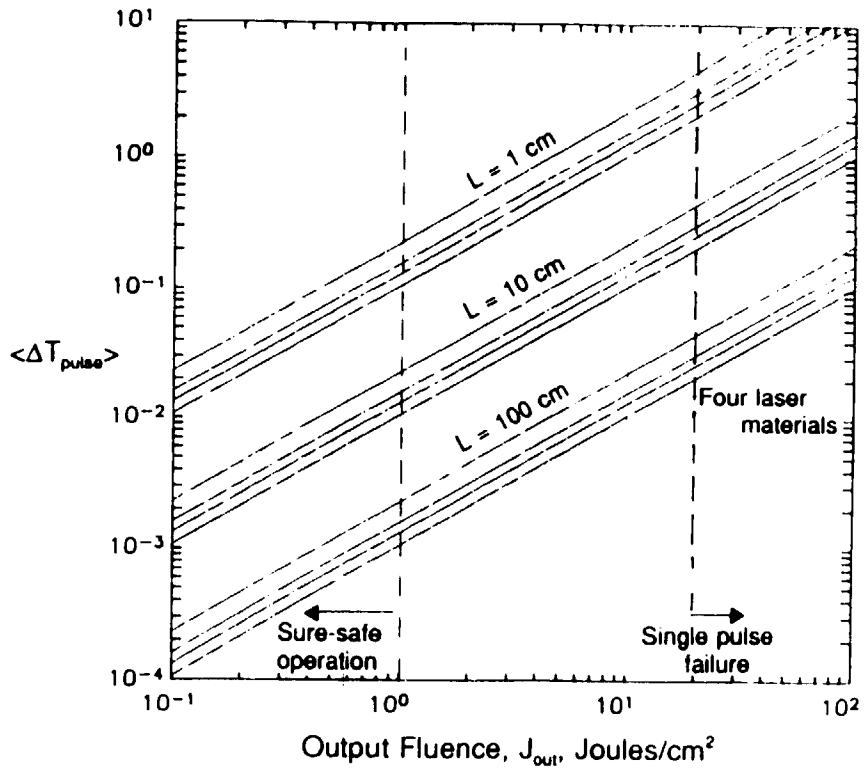

During extraction pulse

$$\Delta T_{pulse} = \frac{1}{\rho C} \frac{J_{out}}{L} \frac{1 - \eta_Q}{\eta_Q}$$

- occurs during output pulse
- results in bulk optical path change in center
- no extraction near edge implies
  $\Delta T = 0$
  $\Delta T_{radial} = \Delta T_{bulk}$

L = TOTAL PHYSICAL GAIN MEDIUM LENGTH IN OPTICAL DIRECTION IN FINAL AMPLIFIER STAGE

NST

RADIAL ΔT IN AMPLIFIER BETWEEN PULSES

Northeast Science & Technology

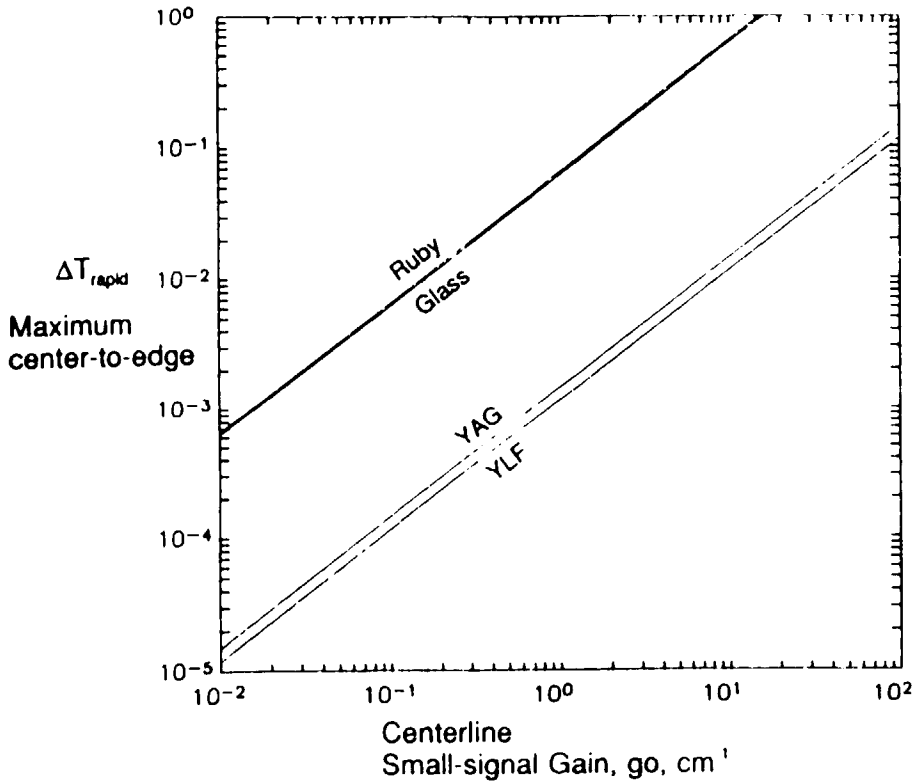

$$\Delta T_{max} = \frac{1}{\rho C} \frac{g_o}{\beta \eta_Q} (2 - \eta_Q)$$

- occurs between output pulses
- assumes no extraction near edge of MO beam

	ρC	β	η_Q
Phosphate glass	2.68x.168	0.16 cm^2/J	75%
Ruby	0.42/0.13	0.088	70%
N_D:YAG	4.56x0.59	4.73	65%
HO:YLF	3.95x0.79	0.5	75%

D) Phase Aberration Analysis

Figure 15 shows the relations which give rise to phase inomogeneities $\Delta \Psi$ --the temperature-dependent index of refraction of the gain medium and its thermal expansion (ie physical length growth) due to heating in the center of the medium as compared to the region near the edge of the medium which has been pumped optically just as hard as the center, but has had no laser extraction (so it will tend to get hotter than the center after upper-state relaxation to ground). **Figure 16** shows the phase difference between the optical axis and the medium edge resulting from various Δ T 's along various length gain media. *The very simple relation tells a very powerful story* -- keep either the temperature difference between center and edge very small (ie DO NOT COOL, and FILL THE GAIN MEDIUM) or keep the medium very short. Or both. A value of $\Delta \Psi$ of 0.3 keeps the far-field intensity within 10% of that of a diffraction-limited beam. The simple formula below described this relationship.

$$I / Io = 1 / (1 + (\Delta \Psi)^2)$$

Figure 17 uses $\Delta\Psi = 0.3$ as a limit, and relates the temperature rise in the slab center to the extracted single-pulse fluence. For Nd Yag, up to 20 joules /cm^2 are allowed (ie UP TO MATERIAL DAMAGE THRESHOLDS !!!) before the temperature differences are noticeable. If we limit the beam to the 1-20 joules/cm^2 region, no gross extraction effects should be seen in uncooled amplifiers. The major thermal differences will therefor be dominated by pump uniformity --that is good engineering of the pump lamps and their optical cavities. Another cut at this conclusion is shown in **Figure 18**, which indicates that flat-top (or equivalently super-gaussian shaped) amplifier pulses are not required for radial thermal uniformity at the 10 joule/cm^2 output level.

As to temperature level, the "Hot Rod"(**ref 4**) or "Heat Capacity Mode" (**ref 5**) or Thermal Inertial Laser" (**ref 3**) methods of operation ----all equivalent ,simply different names given to the same concept--- has very reasonable upper temperature-level limits before the gain begins to decrease. **Figure 19** shows the centerline temperature rise after a single pulse as functions of the gain slab thickness and pump pulse irradiance. Clearly, the more solid gain medium we have (ie the thicker the slab) the less the temperature rise produces in the slab by the given energy delivery. The LLNL Beamlet laser and others at LLNL used as models in this study pump in the region 0.2 to 2 joules of pump light per square cm of slab surface area, have been successful cooling this energy density with active gas or liquid flows for truly-continuous repetititve-pulse operation of Beamlet laser designs for the National Ignition Facility (**Ref 7**) . **Figure 20** shows the successfully-demonstrated cooling rates on laser slabs at LLNL and the operational laser slab optical pumping heat loadings at LLNL (**Refs 6 & 7**) , and the implication for CONTINUOUS rep-rated operation of the Beamlet laser, and this bodes well for cool-down between bursts for the "Hot-Rod" mode of operation. Using these pump fluence levels and gain slabs in the 0.5 to 2 cm thick region will produce small (0.1-1 °C) termperature rises in the slabs for each pulse. This temperature rise per pulse will allow 100 to 1000 pulses to be emitted from the UNCOOLED medium until the temperature level of 350 K to 400K (**ref 6**) is reached, where gain reduction begins as well as Stark level redistribution, resonant re-absorption and line spreading (mentioned in **Figure 4** as considerations) begin to become important (**ref 5** , where 390 K is recommended as an upper limit)

Conclusions

In the above, we have analyzed the optical performance of an uncooled solid state laser, and for reasons of reliability of performance, have chosen a slab-geometry, flashlamp-pumped MOPA design. In the pulse-width regime required (5-50 ns) the single pulse output fluences allowed by LLNL demonstrations, but degraded for repped operation, allow reasonable-shaped MO pulses to be amplified to the reuquireed energy level with little or no extraction-induced phase aberrations. Further, using LLNL data on thermal gain limitations, 100 -1000 pulses should be extractable from the laser device

FIG 15

NST

Northeast Science and Technology

LIMITS ON BEAM PHASE HOMOGENEITY

W.J. Schafer Associates

- **Assume**
  - **perfect pump-light irradiation of entire crystal**
  - **only quantum defect inefficiency appears as heat**

$$\left.\begin{array}{l} E_{lasing} \leq 0.76\ E_{absorbed} \\ E_{heat} \geq 0.24\ E_{absorbed} \end{array}\right\rangle\ E_{heat} > 0.32\ E_{lasing}$$

  - **resonator configuration <u>not</u> used because strong radial internal flux gradients cause strong local dn/dt values even with variable reflectivity outcoupling**
  - **amplifier configuration using super Gaussians allows <u>small</u> radial gradients**

- **RMS phase non-uniformity given by**

$$\langle \Delta\psi \rangle = \frac{2\pi}{\lambda}\left(\frac{dn}{dT} + (n-1)\alpha\right) L\ \langle \Delta T \rangle$$

- **RMS thermal non-uniformity given by heat balance**

$$E_{heat} + \rho C\ \Delta T_{bulk}\ \pi R^2 L \geq 0.32\ E_{laser} = 0.32\ J \pi R^2$$

$$\Delta T|_{bulk} L = \frac{\geq 0.32\ J_{output}}{\rho C}$$

$$\boxed{\langle \Delta\psi \rangle = \frac{2\pi}{\lambda}\left(\frac{dn}{dT} + (n-1)\alpha\right)\left(0.32\ \frac{J_{out}}{\rho C}\right)\frac{\langle \Delta T \rangle}{(\Delta T)_{bulk}}}$$

NST

Northeast Science and Technology

THERMAL MANAGEMENT IN SOLID STATE LASER MEDIUM

60

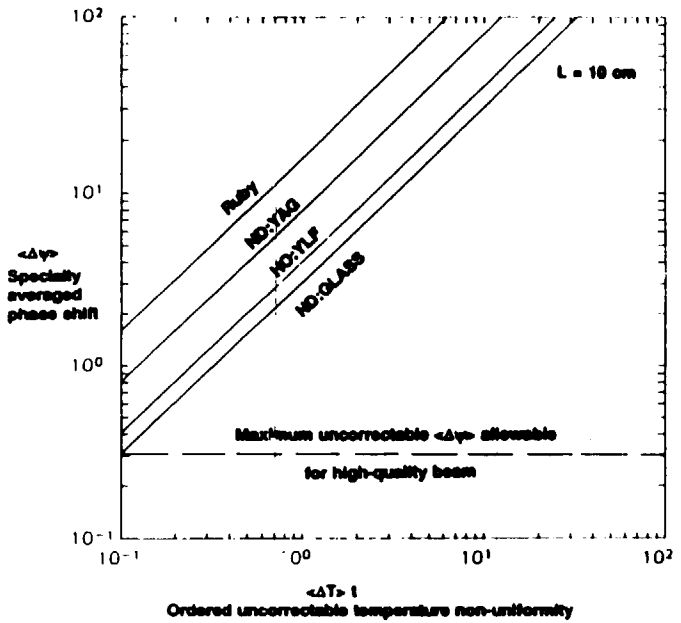

Phase shift due to optical path difference

$$\langle \Delta\psi \rangle = \frac{2\pi}{\lambda}\left[\frac{dn}{dT} + (n-1)\alpha\right] L\langle \Delta T \rangle$$

For near-perfect beam, ($I/I_o > 0.90$) require small phase shift in medium:

$$\langle \Delta\psi \rangle \leq 0.3$$

	λ	$\frac{dn^*}{dT}$	α^*	*D Thermal Diffusion Coefficient*
Ruby	**0.69 μm**	**13×10^{-6}/°C**	**6×10^{-6}/°C**	**0.13 cm^2/S**
ND:YAG	**1.06 μm**	**7×10^{-6}/°C**	**8×10^{-6}/°C**	**0.05 cm^2/S**
ND:phosphate glass	**1.06 μm**	**2-3×10^{-6}/°C**	**9.8×10^{-6}/°C**	**0.006 cm^2/S**
HO:YLF	**2.1 μm**	**7×10^{-6}**	**8×10^{-6}**	**~0.05 cm^2/S**

Because of longer wavelength, holmium (2 μm) lasers can handle more heat deposition than YAG
Because of faster thermal diffusion, Holmium-YLF and ND:YAG have higher PRF than glass host materials

*Ref. Koechner, "Solid State Laser Engineering"

NST
Northeast Science and Technology

GOOD QUALITY BEAM - USABLE OUTPUT FLUENCES

J
Joules/cm^2

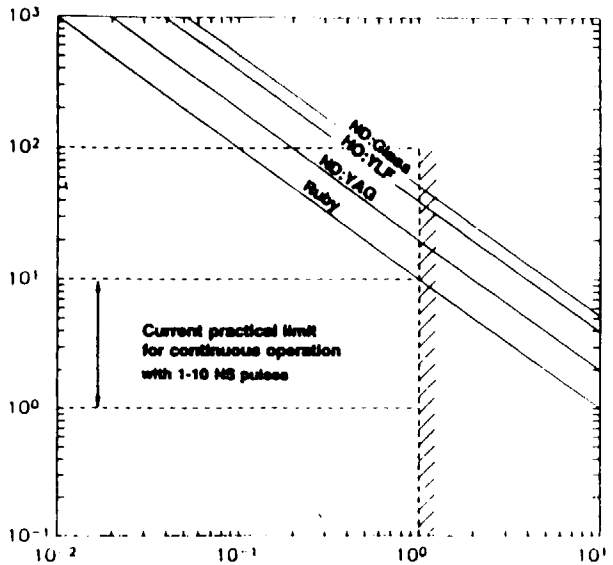

$<\Delta T> / \Delta T_{bulk}$

$$0.3 = \frac{2\pi}{\lambda}\left(\frac{dn}{dT} + (n-1)\alpha\right)\frac{\langle\Delta T\rangle}{(\Delta T_{bulk})}\left(\frac{0.32\,J}{\rho C}\right)$$

- **Output fluence from amplifier limited by surface damage, small phase in homogeneity and quantum defect heating**

Temperature "ripple" in laser rod prior to next pulse/peak bulk temperature rise after pulse extraction

- **Quantum-defect heating allows higher output fluences than current output reflector surface damage limits**
- **Output fluence limited by surface damage, not medium heating and phase shifts**

NST

Northeast Science and Technology

AMPLIFIER OUTPUT - BEAM PHASE HOMOGENEITY

W.J. Schafer Associates

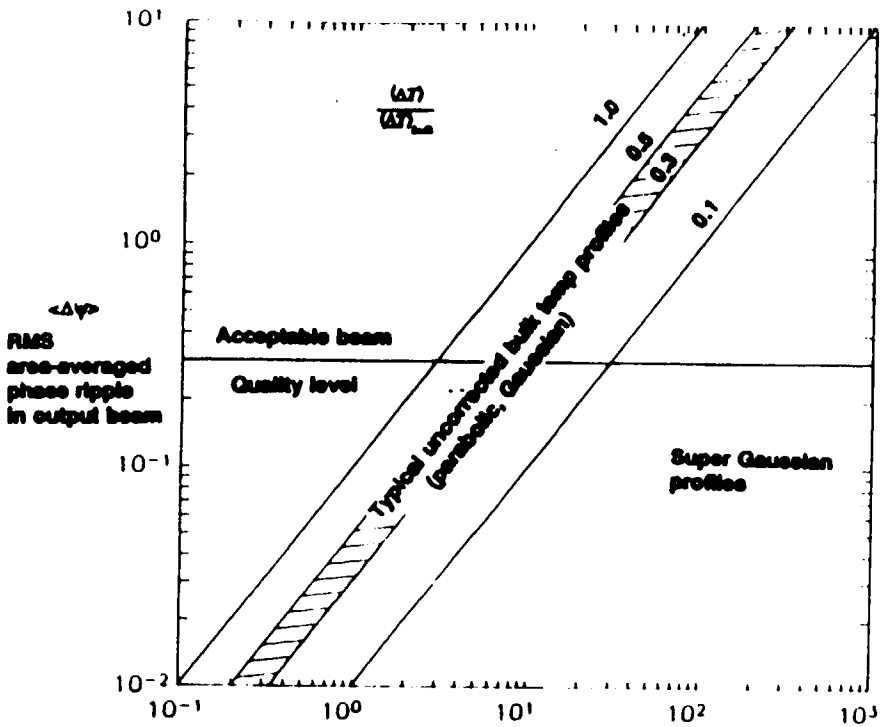

Output fluence, J, Joules/cm²

$$\langle\Delta\psi\rangle = \frac{2\pi}{\lambda}\langle\Delta(nL)\rangle \qquad (1)$$

$$\geq \frac{2\pi}{\lambda}\left(\frac{dn}{dT} + (n-1)\,\alpha\right)\left(0.32\,\frac{J_{out}}{\rho C}\right)\frac{\langle\Delta T\rangle}{\langle\Delta T\rangle_{bulk}}$$

- **For damage-limited extraction fluences and cool-down allowed from initial bulk temperature level to low RMS temperature ripple $\langle\Delta T\rangle$ just prior to next pulse**
- **Requires care in engineering diode light deposition profiles and radial absorption**
- **2 micron wavelength has 1/2 $\langle\Delta\Psi\rangle$ as 1 micron for same output fluence and temperature ripple**

Careful beam shaping and output-beam corrections allow use of output fluences above 10 J/cm²

NST
NORTHEAST SCIENCE & TECHNOLOGY

UNCOOLED-BURST OPERATION
– A POSSIBLE NEAR-TERM DEMO

"HOT ROD" CONCEPT FOR NEAR-TERM DEMO OF SOLID-STATE LASER
- REF: BATTELLE COLUMBUS PROPOSAL / SMALL-SCALE DEMO
- REF: LLNL DESIGN / PROPOSAL TO P.L.'S ABL PROGRAM OFFICE

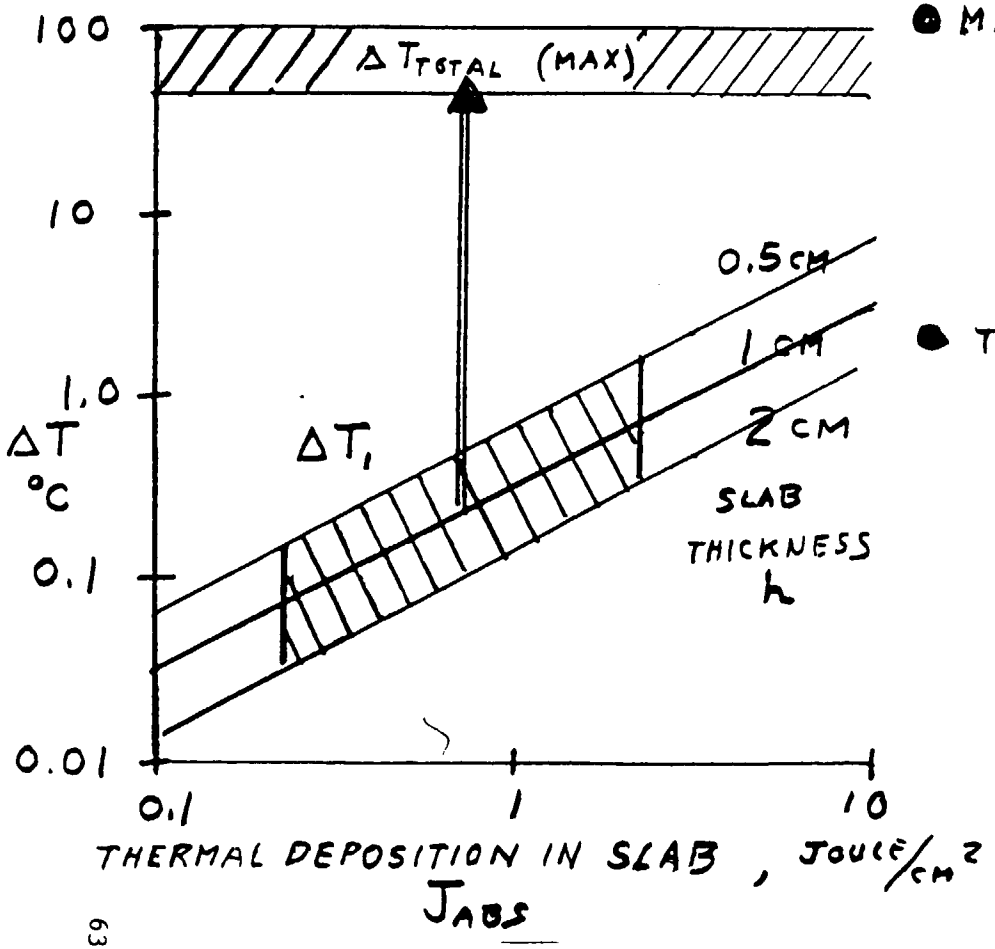

- MAX TOTAL ΔT FOR 10% GAIN LOSS

  3.3% Nd_2O_3 LHG-5 GLASS

  $T_{MAX} = 350°K$ ($g_0 = 0.01/CM$)

  $T_{MAX} = 400°K$ ($g_0 = 0.05/CM$)

- TEMPERATUR RISE PER PULSE

  $J_{ABS} = \rho C \Delta T_1 h$

100 – 1000 PULSE BURST
WITHOUT COOLING
ALLOWS POSSIBLE NEAR-TERM DEMO

NST

Northeast Science and Technology

Required and Demonstrated Heat Transfer Rates

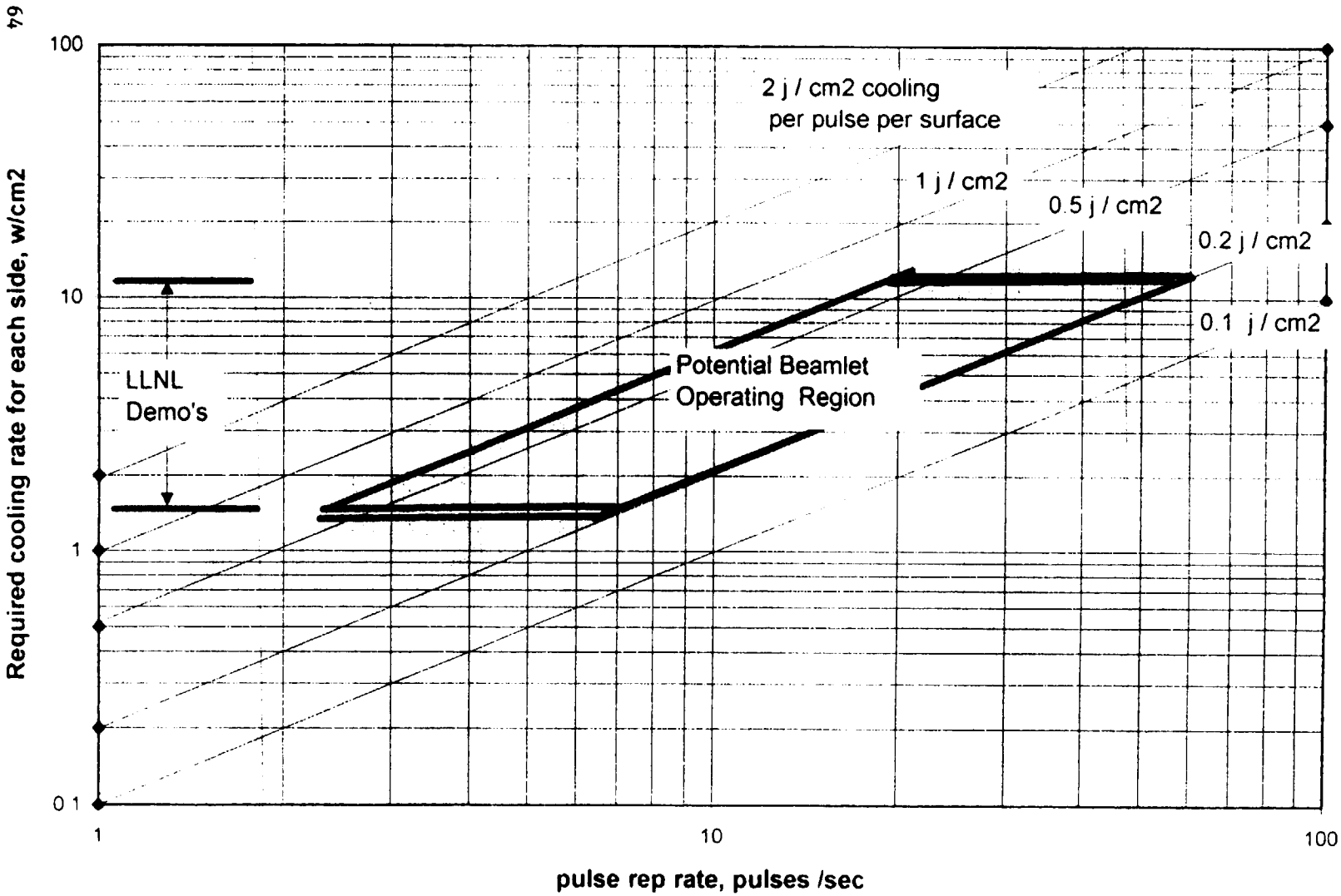

LLNL Demonstrated Cooling Rates and Energy Deposition Indicates 10 - 20 hz Appears Feasible

before gain reduction and other spectroscopic effects begin in the gain medium. At this point, optical pumping and lasing should be ceased, and cooling begun to return the medium to its original state. The analysis indicates that pump-nonuniformities and intrinsic gain medium nonuniformities will probably be the limiting causes of beam phase aberrations, as well as those in associated optical elements---all of which point to engineering design and perhaps adaptive optics to ameliorate those effects which cannot be eliminated by quality control and good engineering.

List of References

1. W. Koechner, "Solid State Laser Engineering", Springer-Verlag, 1976
2. G.Zeiders, "A Critique of High Rep-Rate Glass Lasers for ICF" , WJSA Report WJSA 77-15, TR1
3. C.Walters et al., "Nd-Glass Burst Laser with kW Average Power Output", IEEE Journal of Quantum Electronics, Vol. 31. No. Feb. 1995
4. J.Reilly, "Laser Transmitter Sizing and State-of the-Art Review", WJSA Report WJSA-R-93-B-001
5. G.Albrecht, "A 4 MJ Diode-Pumped, Heat Capacity Disc Amplifier - Defender" , briefing by LLNL , LLNL Document 99-50-0193, 12 GFA/fwh
6. A.Erlandson et al., "Model Predicting the Temperature Dependance of the Gain Coefficient and the Extractable Stored Energy Density in Nd:Phosphate Glass Lasers", J.Opt. Soc. Am. B / Vol 9, No. 2 / February 1992
7. S.Sutton et al, "Optimim Peformance Considerations for a Large-Aperture Average Power Solid-State Laser Amplifier", J.Appl.Phys, 69 (3), 1 February 1991

APPENDIX B

TARGET ACQUISITION FOR ORION

Dr. James P. Reilly
Northeast Science and Technology

Target Acquisition for ORION

Dr. James P. Reilly

Northeast Science and Technology
117 North Shore Blvd
East Sandwich, Ma 02537
508-833-8980

Introduction

The purpose of this section is to define the capability of purely-optical techniques to provide the initial acquisition of the debris targets, with subsequent handover to the "pusher" laser system for causing its demise by inducing de-orbiting.

We first repeat the target set definition to insure consistency with the other analyses performed by ORION Team members. We then use MIT/LL Haystack data to produce a debris number density distribution, this to be used in conjunction to the basic debris flux density distribution derived by MIT . These two models (number density and flux density distributions) are then used to obtain the requirements on a purely-radar system as well as a purely-optical system to provide acquisition of all targets of interest (currently estimated at between 30,000 to 100,000 in number) in the orbital altitude regions of interest to NASA .

Definition of the Target Set

As can be seen in **Figure 1** (ref. 1&2) , the 6 canonical objects of interest to ORION are varied in size, shape, material, orbital parameters and optical properties. Since the majority of the debris population is currently believed to be Target Class A (the NaK spherical solids), *we shall concentrate on the acquisition of these objects*, knowing that we will have to examine the robustness of the acquisition systems proposed for consideration as a result of these analyses. Examination of **Figure 2** shows a model for the current estimates of the population distribution function (ie, the number densities of debris objects larger than a given size). Note that current estimates indicate more than 100,000 objects in the 1 cm diameter object class analyzed here or larger.

Figure 3 (taken from MIT/LL presentation at the October 1995 ORION review) show the actual measures counts per hour as well as the derived flux of objects larger than 1 cm in diameter through a stationary HAYSTACK beam set up with a 1 millirad FWHM beam divergence, pointed vertically. The data was plotted by MIT in 100-km-high altitude bins from an orbital altitude of 300 km to 1500m. As a check on the total detection rate quoted by MIT for the 300-1500 km range, the mean flux of objects through the cylindrical measurement area would have to be given by :

$$\text{Flux} = \frac{6 \text{ objects / hr}}{\pi \times 1 \text{ km} \times 1200 \text{ km}} = 1.4 \times 10^{-5} \text{ objects / m}^2 \text{ - year}$$

which is in good agreement with the general scale of detected objects shown in **Figure 3.**

Ref. 1 ORION review, 16 October, 1995
Ref. 2 ORION review, 12 December, 1995

Target:	A	B	C	D	E	F
Description	Na/K sphere	carbon phenolic	MLI	crumpled aluminum	steel tank rib support	steel tank
inclination, deg	65	87	99	30	82	60
apogee, km	1020	930	1190	1020	800	1500
perigee, km	870	610	725	520	820	980
Area/Mass, cm^2/gm	1.75	0.7	25	0.37	0.15	0.13
actual size, cm	1	1 x 5	0.05 x 30	1 x 5	1 x 10	100x100x0.2
actual mass, gm	0.45	28	28	54	65	75,000
periodicity, sec	----	10	0.2	1	---	30
surface	metal	quasi / metallic	dielectric / metal	charred / shiny	metallic	metallic
Bond albedo	0.4	0.02	0.05-0.7	0.05-0.7	0.5	0.1
% of population	40%		significant	significant		

Figure 1 : ORION target classes : identification and important characteristics

If , on the other hand, we assume a total of N = 100,000 such objects orbiting the earth in a spherical shell of thickness ΔH and extending from an orbital altitude H of 300 to 1500 km, and uniformly filling the shell, we would expect a mean flux Q (ie, objects / m^2-year) averaged over the entire shell to be given by:

$$Q = \frac{N \text{ (objects)} \times V \text{ (orbital velocity)}}{4\pi \left(R_{earth} + \bar{H} \right)^2 (\Delta H) \text{ (ie, the shell volume)}}$$

$$= \frac{100{,}000 \text{ objects} \times 7 \text{ km/sec}}{4\pi \left(6378 \text{ km} + 950 \text{ km} \right)^2 (1200 \text{ km})} = 2.7 \times 10^{-5} \text{ obj/m}^2\text{-year}$$

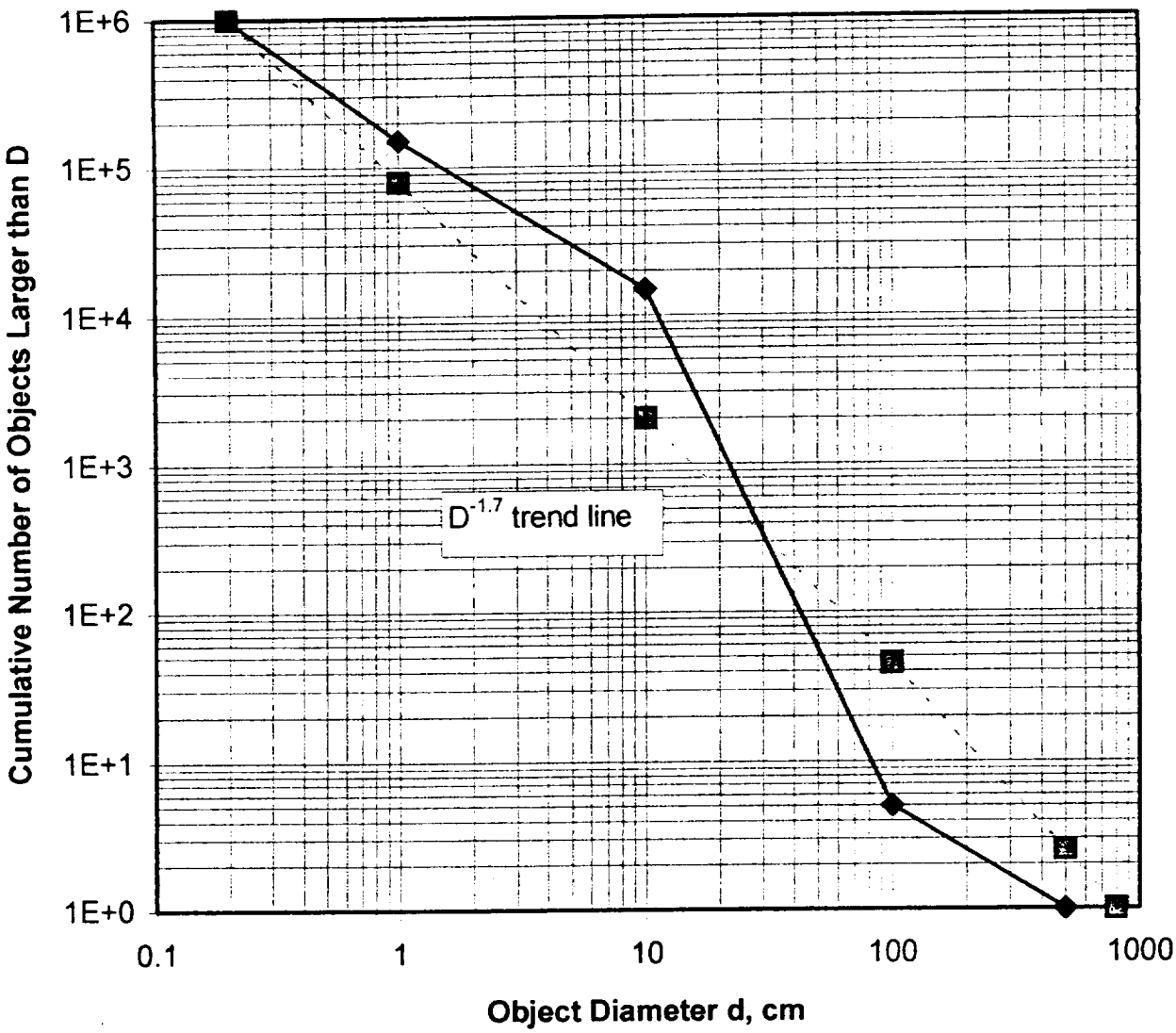

Figure 2: Debris Distribution Function (taken from ORION Project Review, 12/12/95)

This value is sufficiently close to the measured detection rate by HAYSTACK that the uniformly-filled shell (or more accurately, layers of uniformly-filled shells) debris-distribution model will be used here to investigate alternate Radar and Electro-Optic (EO) detection strategies in the following sections.

We can use this uniformly-filled but layered-shell model to evaluate postulated search strategies for acquiring a major fraction of the debris population in a reasonable
(for example , less than one year) time .

Figure 3 shows the measured flux Q of space debris objects larger than approximately 1 cm diameter vs orbital altitude (in 100 km altitude bins) as estimated from HAYSTACK data (the details are described in the next Section). Using the above discussion, we can estimate the effective 3D inter-object spacing between debris objects in this altitude region, as well as the projected 2D inter-objects spacing between those objects.

The "snapshot" 3D spatial distance between objects is of use to estimate the instantaneous line-of-sight mean separation between debris objects as well as the instantaneous azimuthal separation between those objects for a acquisition systems with high-resolution LOS range resolution and high angular resolution pulse, such as a laser radar or high-resolution microwave radar. The mean azimuthal 2D spatial distance is of use to estimate the angular separation between objects for acquisition systems with poor LOS resolution and good angular resolution, such as passive (or quasi-CW active optical illuminator) systems.

The "snapshot" 3D spatial distance between objects can be obtained simply by tasking the measured detection rate (Q) of objects larger than 1 cm diameter and dividing by the orbital velocity at that altitude. That is, since

$$Q \text{ (objects/ sq. meter -sec)} = n \text{ (objects / cubic meter)} \times V \text{ (meter / sec)}$$

and since

$$n \text{ (objects / cubic meter)} = 1 \text{ object} / [\, 4/3\ \pi\ (S \text{ (radial separation, meters)})^3 \,]$$

we have

$$S \text{ (3D radial separation, meters)} = [\pi\ 3/4\ (\ V / Q\ )^{0.33}\ ]$$

Likewise, we can radially project the population of the debris belt and find a mean expectation value for the 2D separation . The total number of debris objects in a thin shell of thickness Δ H is

$$N \text{ (objects)} = n \text{ (objects / cubic meter)} \times 4\pi\, [\, R_{earth} + H \text{ (orbital altitude)}]^2 \times \Delta H$$

We can projects how many of these objects will appear on a sensor pixel at any given time by projecting the radial distribution of debris objects onto a plane, and the calculating the mean 2D radial spacing L of the projected images. This will be a measure of the mean radial spacing seen by a sensor system with poor LOS resolution and good angular resolution. Equating the total area occupied by these particles to the surface area of the shell at the orbital altitude of interest, we get

$$N\, \pi/4\ L^2 = 4\pi\, [\, R_{earth} + H \text{ (orbital altitude)}]^2$$

and substituting the previous equation relating N to n and Δ H, we obtain an expression for the 2D projected azimuthal separation :

$$L = [\, 4/\pi\ \ V\ /\Delta H \times Q\ ]^{0.5}$$

The characteristic 2D separation L in 100 km thick altitude bins in which the MIT data was reported,, and the characteristic 3D separation S also in 100 km thick altitude regions, are plotted in **Figures 4 & 5.** Note that at

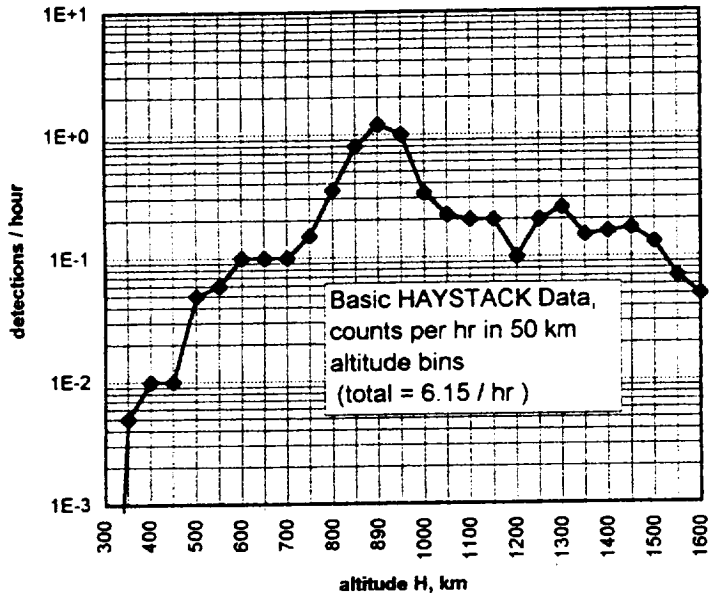

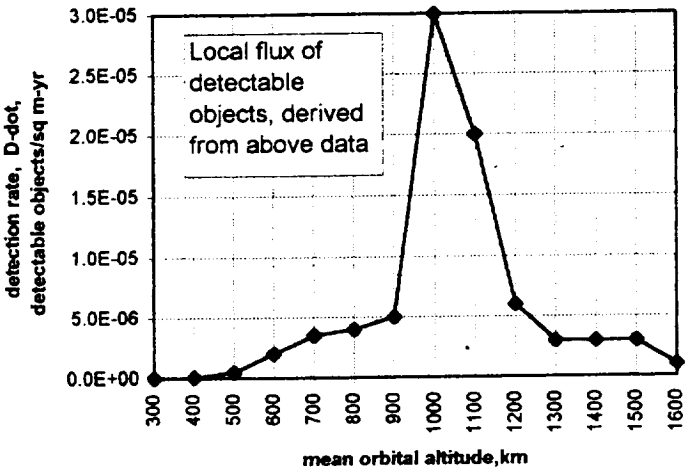

FIGURE 3 : HAYSTACK measurements of debris count vs altitude in 50 km altitude bins and derived flux of objects into cylindrical beam

the orbital altitude where the highest debris density is expected from the HAYSTACK measurements, the mean 3D spacing between debris objects is on the order of 100 km apart, in which case we could estimate a lower bound for detection as 100 km / 7 km/sec = 14 sec between object-detections. Since however the cylindrical measurement area of the beam has a diameter only 1 km wide azimuthally , it is much narrower than the lateral spacing between objects in our model, and so the time between two detections could be ***as long as*** 100 (ie, 100 km lateral particle spacing / 1 km beam width) times the 14 seconds, or 0.39 hours. Hence the LOWEST detection rate for debris in the high-density orbits would be 2.6 detections / hour. This is consistent with the HAYSTACK measurement of 6 detections / hour. The model is within a factor of about 2 of reproducing the HAYSTACK results, and gives us a more general tool to examine detection techniques and strategies.

As an example, a general search over the entire 300 to 1500 km altitude band set up on the basis of the TOTAL number of objects expected (nominally 100,000) spread uniformly over the band would expect the objects to have a 3D spacing of about 125 km, and a 2D separation of about 50 km . As seen on **Figures 4 and 5** The beam sizes and scan rates so determined would find it very difficult to search the lower altitude region (where the debris density is far lower than the ensemble mean), and would produce much higher detection rates than expected in the high-debris-density region around 1000 km. For example, a narrow beam passive optical system (ie, one with no range resolution) searching for debris in the 400 - 600 km altitude region would , from **Figure 4,** want to have a search Field Of Regard with a radius of about 200 km, and it would scan inside that radius with a Field Of View set by debris signature Signal-to-Noise and Signal-to Background ratios with optimized integration times and scan patterns. These will be discussed below.

General Discussion of Acquisition Approaches

In general, acquisition of remote objects for observation and tracking is accomplished by the observation of either self-emitted or reflected optical energy, RF energy, acoustic energy or other quanta in comparison to some background level. In particular, only optical and radar sensors are usable to acquire ORION targets. The three approaches below are ones which currently appear to even have a chance, given the slant ranges, object sizes and sensor characteristics involved.

1. **a microwave radar** - with characteristics similar to the MIT /LL HAYSTACK radar, but with a scanned beam (repeated linear one-dimensional scan) or a "bow tie" (repeated two-axis scan).
2. **a passive optical system** - an astronomical-class telescope perhaps with an angle-scanning capability along the lines suggested by MIT/LL for a modified HAYSTACK-type radar. The illumination of the objects would be by sunlight. The size of the instantaneous Field of View of the system fixes the instantaneous spot size being viewed, while the angle-scanning capability determines the search Field of Regard.
3. **an active illuminator laser system** - economy dictates that if this option is chosen, the transmitter would use the Pusher laser as the energy source, but would use a de-focused beam to interrogate a large spot in space for the detection function.

In the sections below, we discuss in detail the driving parameters for each of the above approaches, and using experimental data and demonstrated characteristics of operational hardware, suggest approaches to acquire and track the ORION target set debris objects.

Summary of MIT / LL's All-Radar Acquisition Approach

The all-radar approach has been extensively analyzed by MIT/LL during the course of the first phase of ORION. A radar system with beam parameters similar to those existing at the HAYSTACK facility is required for detection, acquisition , identification, track and handover to the "pusher" laser system. HAYSTACK has been used by NASA to detect, acquire, identify and track space debris objects down to approximately 1 cm diameter at orbital altitudes from 300 km to over 1500 km. Using HAYSTACK in a staring mode at 0° zenith angle (ie, 90° elevation angle) with 1 millisecond pulses, a 40 - 50 hz rep rate and a 1 milliradian FWHM beam divergence, detection rates of up to 6 / hr were recorded on objects larger than 1 cm (estimated from RCS data). This means that 6 objects 1 cm in diameter or larger entered the beam with a measurement area of

Mean 2D Debris Spacing

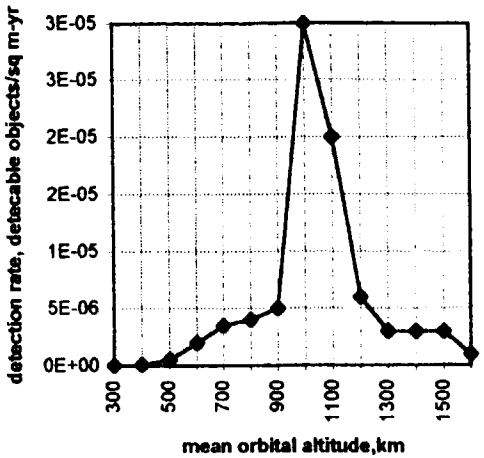

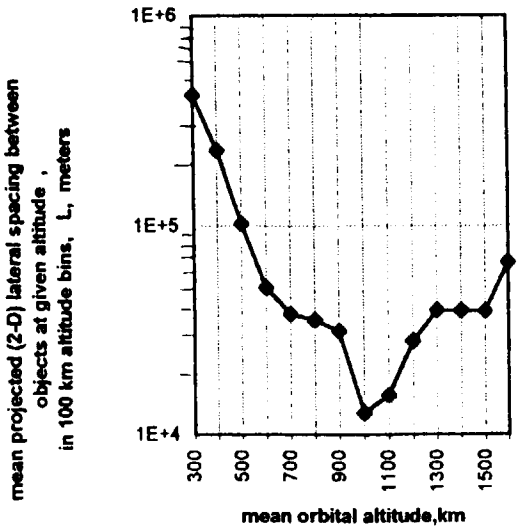

2D radial projection through 100 km thich spherical shell

Total number in shell = mean number density (objects / cubic meter)
x shell volume (cubic meters)

$$N = n \times 4\pi (R_{earth} + H)^2 \Delta H$$

Mean 2D projected spacing L around each object in 100 km thick thell

$$N \pi/4 L^2 = \text{sherical shell surface area} = 4\pi (R_{earth} + H)^2$$

Mean flux in shell = number density x orbital velocity

$$Q = nV$$

Mean 2D spacing

$$L = [4/\pi \ V \ / \ (\Delta H \times Q)]^{0.5}$$

NST

Northeast Science and Technology

Mean 3D Debris Spacing

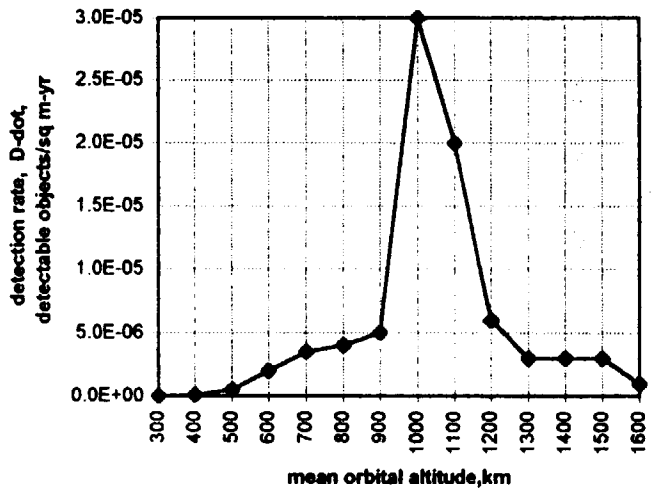

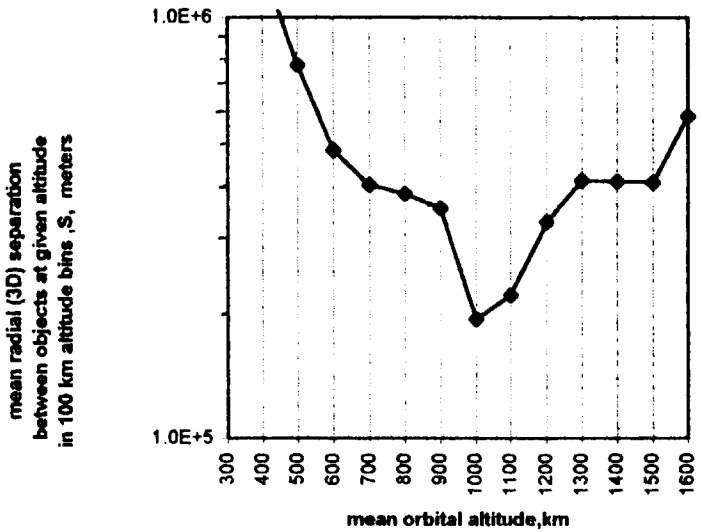

3D volumetric separation in each 100 km spherical shell

Mean 3D volumetric spacing S around each object in 100 km thick thell

$$n = 1 \text{ object} / 4\pi/3\ S^3$$

Mean flux in shell = number density x orbital velocity

$$Q = n V$$

Mean 3D spacing

$$S = 3\pi/4\ (V/Q)^{0.5}$$

approximately 1 km in diameter (ie, 1 millirad x approximately 1000 km range) by approximately 1200 k m high (ie, 1500 km max. altitude minus 300 km min. altitude). Since the length of the radar pulse used was 1 millisecond, the length of the "slug of light" moving along the radar line-of-sight (LOS) was 300 km, hence range resolution is only on the order of 150 km in LOS. At orbital velocities of 7 km/sec (appropriate to the 300 to 1500 km altitude range), the stay time of a debris object in a 1 km wide beam is no longer than 0.14 second, so one would think that high PRF's could be used to yield more data when a debris object entered the beam. However, since the round-trip time between the transmitter and the debris band was only 2 millisec (for 300 km altitude) to 10 milliseconds (for 1500 km altitudes), PRF's less than only 100 hz were allowed without "blinding " the received signal with the next outgoing pulse.

The achieved total detection rate of 6 / hr is too low for ORION, especially considering the fact than about 50% of these will be climbing toward zenith (and hence a candidate for the Pusher laser), but 50% will be expected to be descending from zenith ,and so are not candidates. In fact, at a useful detection rate of 3/hr, it would take 33,000 hrs (4 years at 24 hrs/day, 365 days/years of dedicated operation) to detect 100,000 debris objects of interest, EVEN ASSUMING THERE WERE NO REPEATED DETECTION OF THE SAME OBJECT ON SOME SUBSEQUENT PASS OVERHEAD. Clearly, a different approach is required.

MIT has proposed that another approach to the use of the radar be considered to dramatically increase the detection rate : that of a "picket fence" rather than a stationary staring beam be used , along with a longer pulse, to increase the measurement area from the single-beam 1 km x 100 km to one with 10 km (or more) x 100 km .

In the picket fence (or as MIT/LL terms it, the "bow tie" mode) the beam would scan the sky at its current scan rate so that effectively 10 or more angular beam positions are used to define a broader area through which the debris must pass. Since the debris orbital velocity is on the order of 7 km/sec. and the inertial velocity of a staring radar beam at the debris altitude is only on the order of 0.5 km/sec (inertial velocity = earth rotation rate x earth-radius-plus-orbit-altitude), it is appropriate to scale the measured entrance rate of detectable debris from the existing HAYSTACK data to the debris entrance rate into a beam "array" linearly with the measurement area interrogated by the beam.

The fence would be erected not at zenith, but rather at a low elevation angle, perhaps at 30° elevation or less , to allow subsequent time for handover to the Pusher laser and for impulse delivery prior to debris reaching zenith. At 1000 km orbital altitude, the 1 millirad beam with 30° elevation angle would be approximately 2 km wide. A scan pattern 10 beams wide increases the azimuthal size of the area from the previous 1 km (one vertical beam) to 20 km (10 osculating beam positions each 2 km wide), and using the longer-pulse option (ie 5 millisecond, not 1 or 2) gives higher S/N ratio for increased delectability and tracking precision. **Figure 6** shows the benefit of this approach to object detection, which reduces to total detection time down to a few months. **Figure 6** uses the recommended 20 hr / day operation suggested by MIT.

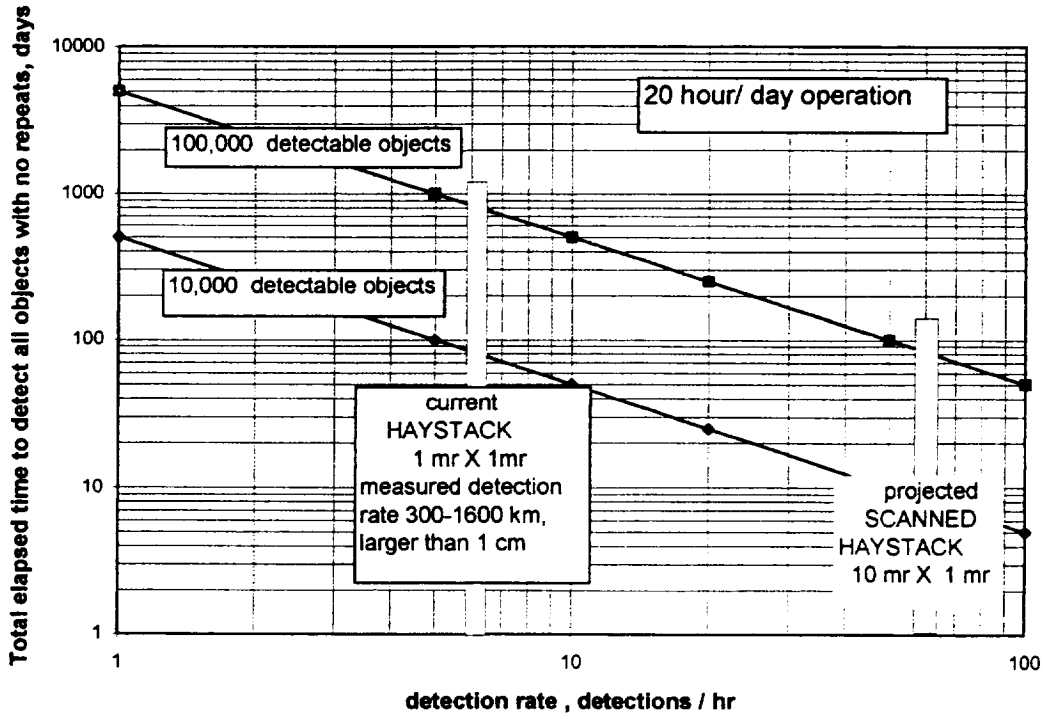

Figure 6: Total Detection Time is Faster with Scanned RADAR Beam Concept

The HAYSTACK 120 ft. diameter antenna is capable of a sustained angular velocity of 35-40 millirad/sec and angular accelerations of 35-40 millirad/sec^2. Radar antennas can be built to have even higher rates. MIT/LL indicates that the ALTAIR 150 ft diameter radar antenna has angular velocities and accelerations five (5 !!) times those of HAYSTACK. With the HAYSTACK rates, the antenna could complete a 10-non-overlapping-spot scan (10 x 1 millirad) and return to its original beam position in:

$$t_{return} = 2 \times 10 \text{ millirad} / 37 \text{ millirad/sec} = 0.54 \text{ sec}$$

A higher scan rate (and/or using a scan doctrine with overlapping beam positions) would ALWAYS allow the radar to return to the original spot BEFORE A DETECTED OBJECT HAD LEFT THE MEASUREMENT AREA , since the transit time of an orbital object at these altitudes across a stationary 2 km-diameter beam is :

$$t_{transit} = 2 \text{ km} / 7 \text{ km/sec} = 0.28 \text{ sec}$$

A higher scan rate (say 50 -75 millirad/sec - still substantially less than that of the ALTAIR radar's 150-200 millirad/sec angular velocity capability) would allow return interrogations prior to the debris leaving the scan region , which would be useful for verification, further discrimination and increased tracking precision.

General Discussion of the Acquisition Approach and Requirements

As we discussed above, the search rate must be such as to detect, acquire, discriminate and hand over a debris target in a time no longer than it takes the object to climb say less than about 20° or 30° toward zenith from its original detection elevation angle. Because we are discussing ground-based systems (or at best elevations less than or equal to that of the AMOS facility in Hawaii -- ie, 10,000 ft above mean sea level), the optical system will not be able to operate much below about 10° to 20° elevation angle. This set of practical limits however still allows the Pusher laser a range of elevation angles from about 40° or 50° all the way to 90°

to accomplish its impulse delivery function --a maximum of about 20 to 30 seconds. This will be important in helping to scope the required energy level, spot size and pulse repetition rate required of the Pusher function for the ORION laser.

The detection, acquisition and discrimination function could be accomplished by:

1. **a microwave radar** - with characteristics discussed above, similar to the MIT /LL HAYSTACK radar, but with a scanned "picket fence" (repeated linear one-dimensional scan) or a "bow tie" (repeated two-axis scan).
2. **a passive optical system** - an astronomical-class telescope perhaps with an angle-scanning capability along the lines suggested by MIT/LL for a modified HAYSTACK-type radar. The illumination of the objects would be by sunlight. The size of the instantaneous Field of View of the system fixes the instantaneous spot size being viewed, while the angle-scanning capability determines the search Field of Regard.
3. **an active illuminator laser system** - economy dictates that if this option is chosen, the transmitter would use the Pusher laser as the energy source, but would use a de-focused beam to interrogate a large spot in space for the detection function.

The size of the interrogated spot, the rate of active interrogation (by either the illuminator laser or by the microwave radar) and both the spacing and the number of objects expected to be present scales the total time to detect the objects. For example, the HAYSTACK radar, in the mode used for NASA for the detection of 6 objects/hour, used:

1. a stationary beam at 90° elevation angle
2. a beam divergence of 1 milliradians FWHM
3. an interrogation range of from 300 km out to 1600 km
4. a pulse repetition rate less than about 50 hz

For these conditions, the beam was about 1 km in diameter (FWHM points of the intensity profile). The orbital velocity at 1000 km is about 7 km/sec, and so the stay-time of a potential debris particle is less than 1 km / 7 km/sec = 0.14 sec. At 50 hz, the radar can illuminate the object up to 7 times, making for a more precise determination of tracking data, but at the same time slowing up the detection process. Substantially higher PRF's, however, can NOT be used because the round-trip time limits the PRF to less than 100 hz beyond which the return signal from the debris is "blinded" by the next outgoing radar pulse. This would not be the case if separate transmitter and receiver dishes were used, but these instruments are extremely expensive, and the option is not considered further in this discussion.

Dividing the surface area of the spherical shell of debris around the Earth at an altitude of 1000 km by the area of the 1 km radar spot gives 8.7×10^8 such spots. If the radar or laser illuminator tried to interrogate each of these 1 km spots WITH JUST ONE PULSE at a PRF of 50 hz, slewing to a new angular position between each and every pulse, it would take 1.7×10^7 seconds, or about 6 months. In reality, 2 or 3 "hits" are required to verify detection and to acquire even a rudimentary velocity vector for handover, so the required time to cover the sky is 1 to 2 years, 24 hrs each day, 365 days each year. Note that at these conditions, the required overall slew rate would be smoothly moving one full beam position (1 millirad) in two-to-three interpulse times (2 to 3 x 1/50 of a second) or 15-25 millirad/ sec. This is NOT impossible, since the 150 ft diameter ALTAIR radar dish has a slew rate of up to 200 millirad/sec, and even HAYSTACK's slew rate capability is 40 millirad/sec. The angular rate capability of large optical systems is even higher (see **Figure 7**).

Clearly, the way to shorter total detection times is with larger measurement volumes, either with large single-pulse beams (which may require high energy pulses) or with slewed beams (which require controllable-slewrate beam directors) for either radars or laser illuminators. The total detection time T*, interrogation rate ω (new beam positions per sec), pulse repetition frequency PRF, single-pulse interrogation area $\pi/4\ d_s^2$, debris *altitude H and total number* of debris objects N , can be related by the following simple equations:

1. For solar illumination or irradiation by a CW radar or laser illuminator (ie, no range information, just angular resolution), the characteristic time to search the entire sky with no repeat-interrogations is :

NST

Northeast Science and Technology

Angular Rate Capabilities
Radar and Optical Mounts

80

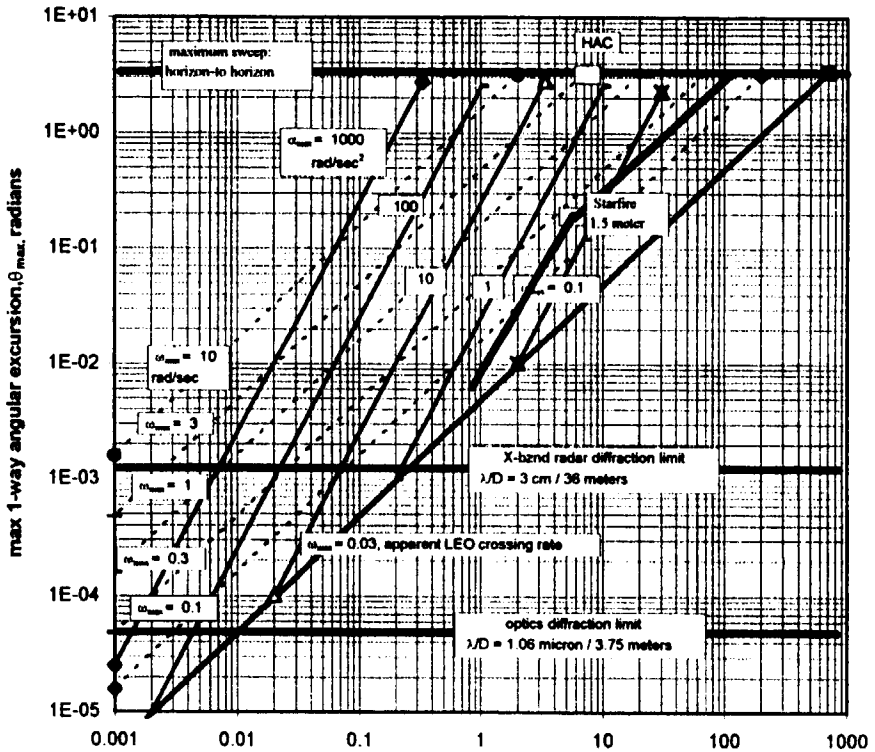

Angular Motion

$\theta = \theta_{max} \sin(ft)$

Angular Velocity

$\omega = f\,\theta_{max} \cos(ft)$

$\omega = \omega_{max} \cos(ft)$

Angular Acceleration

$\alpha = f^2\,\theta_{max} \sin(ft)$

$\alpha = \alpha_{max} \sin(ft)$

Cycle Time

$t_{cycle} = 2\pi / f$

Standard	30 cm Fast-Steering Mirrors	1000 rad/sec^2	
Thermotrex ROBS	1-Meter Telescope	100 rad/sec^2	
STARFIRE	3.75 Meter Telescope	0.26 rad/sec^2	0.26 rad/sec
STARFIRE	1.5 Meter Telescope	0.265 rad/sec^2	0.26 rad/sec
Firepond	1.23 Meter Telescope	0.26 rad/sec^2	0.26 rad/sec
AMOS	1.6 Meter Telescope	0.17 rad/sec^2	0.17 rad/sec
AMOS twin	1.2 Meter Telescope	0.17 rad/sec^2	0.17 rad/sec
AMOS LBD	0.6 Meter Telescope	0.17 rad/sec^2	0.17 rad/sec
HAC / AOA	0.6 Meter Telescope	4.0 rad/sec^2	4.0 rad/sec
HAYSTACK	36-ft RADAR	0.035 rad/sec^2	0.04 rad/sec
ALTAIR	80-ft RADAR		0.20 rad/sec
HAVE STARE	80-ft RADAR	0.035 rad/sec^2	0.04 rad/sec

$$T_{cw}^{*} = \frac{4\pi \text{ steradians} \,/\, \text{FWHM beam resolution angle (sterradians)}}{[\omega \text{ (new resolved spot positions /sec)}]}$$

A nomograph of this equation is presented in **Figure 8** , including also the stay time of a debris object in the resolution angle as a function of orbital altitude (ie, orbital velocity) and resolved spot diameter at altitude

$$t_{stay} = d_{spot} / V_{orbit}$$

and also the time elapsed for a slewing receiver to move one spot width (ie, the time between completely new measurement areas)

$$t_{switch} = \text{FWHM resolution angle} / \text{receiver slew rate}$$

We'll discuss **Figure 8** further in a later section, but for now we can point out a few things of interest. The Figure shows that the HAYSTACK radar beam divergence is 1 millirad, and so produces a 1-km-diameter spot 1000 km range. The stay-time of an orbital object in that beam at that altitude is no longer than 0.14 seconds, allowing lots of pulses to illuminate it and provide better information. Since the HAYSTACK has a maximum slew rate of about 40 millirad/sec (0.04 rad/sec), it COULD be used to search the complete sky in about 90 hours of operation (in 4.5 days of 20 hr/day operation). In such a mode of operation, the time the beam would take to move one millirad would be about 0.025 seconds, and so would take a "snapshot" of the debris content of that 1 milliradian solid angle. There would be a low probability of an object entering (or leaving) the measurement area before the beam moved on .

2. For active irradiation with a repped-pulse radar or laser illuminator (ie, with both range and angular resolution) the characteristic time to search one range of orbital altitudes with REPEATED interrogations is:

$$T_{p}^{*} = \frac{\text{surface area of specific debris sphere } [4\pi (R_{earth}+H)^2] \,/\, \text{beam area } [\pi/4\, d^2_{spot}]}{\omega \text{ (new beam positions / sec) } [= \text{PRF} / 3 \text{ ("hits" per beam position)}]}$$

the resolved measurement area. We have assumed here that three (3) pulses are necessary This relation is virtually identical to that for a CW sensor, with the exception that the RP sensor does not have the advantage of collecting return photons during the entire stay of a debris object for the required measurement accuracy, so the RP laser or RP radar illuminator has an interpulse time which is 1/3 that of the time it takes the beam director to move to a brand-new measurement area (ie, the illuminator PRF is equal to 3 x the beam director 's "new frame" rate , or PRF = 3 θ_{spot} (ie, d_{spot} / H) / S (ie, slew rate)). The RP version of **Figure 9** is shown as **Figure 9.**

As mentioned above, the stay-time of a debris object in a given beam is NO LONGER THAN d_{spot} / Orbital velocity ,and is usually (ie for a 1 km diameter spot and 7 km / sec) relatively long (0.1 to 0.2 seconds) . Hence rep rates of 5 - 10 hz are required at a minimum to insure 3 "hits" per transit of a debris object through a stationary beam with a diameter of 1 km. If, as the **Figure** assumes, the beam is slewing , higher illuminator PRF's are required, as we shall discuss in great detail in a later section. We assume here that the receiver dish is co-located with the transmitter dish (for economy, one dish will probably have to serve both transmit and receive functions) and so the round-trip time of a pulse from transmitter to debris orbit back to receiver must also be factored into the choice of PRF. Since the round-trip time is in the range :

NST

Northeast Science and Technology

Acquisition Capability for CW Sensing

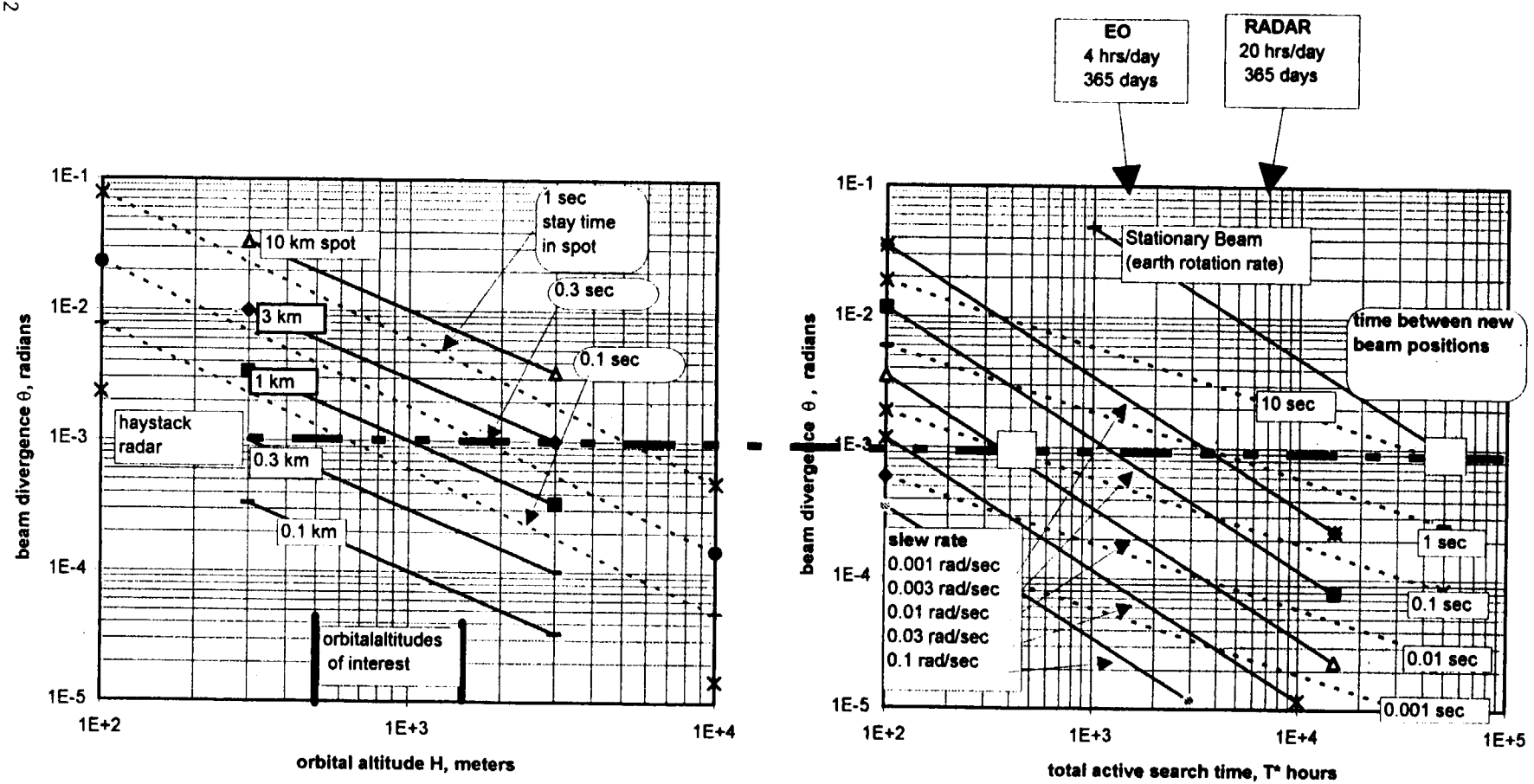

FIG 1-1

NST

Northeast Science and Technology

Acquisition Capability for RP Sensing

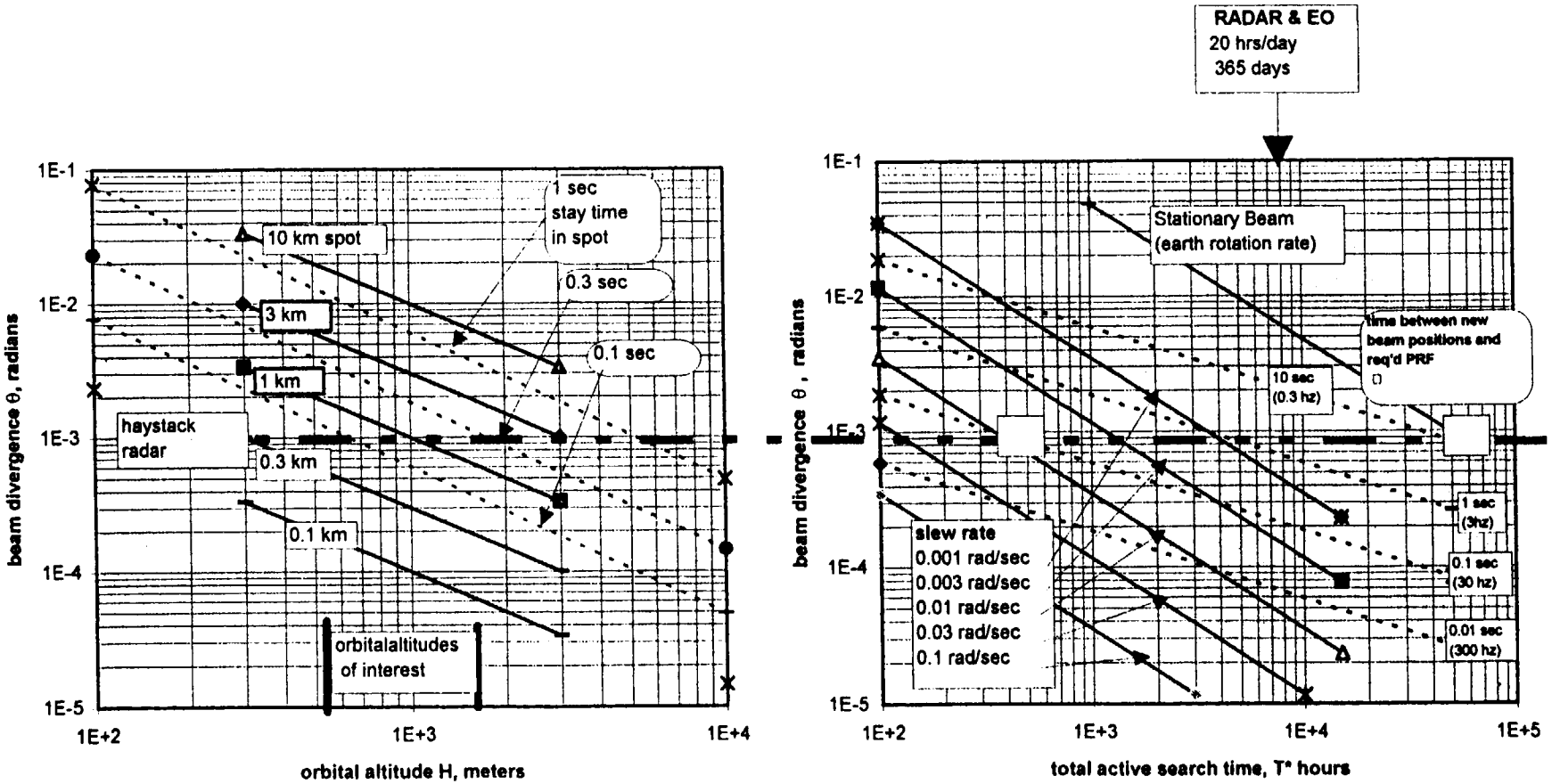

detect',.xls

from minimum round-trip time = 400 km x 2 / 3E8 m/s = 5 millisec = 1/ (200 hz)
to maximum round-trip time = 3000 km x 2 / 3E8 m/s = 40 millisec = 1/ (25 hz)

and the laser illuminator pulses are short (the HAYSTACK radar has pulses of 1-5 millisec, and the postulated Pusher laser has 100 ps to 100 ns pulses) there should be little or no overlap "blinding" of the weak incoming reflected signals by the strong outgoing pulse. However, the hardware should be protected by gating closed the receiver during the transmission pulse, and slightly increasing the illuminator PRF (by say 30%-40%) to compensate for the potential of lost information during the "receiver-closed" period.

3. Picket Fence analysis for debris acquisition

As discussed above, MIT/LL has suggested the use of a HAYSTACK-type radar in a scanning mode to increase the effective measurement area for detecting debris, and so to decrease the total time for detection of a large majority of the estimated 100,000 dangerous debris objects. In section what follows , we took the HAYSTACK detection data, and its estimated local debris flux Q (objects / sq. meter per year) vs altitude (in 100 km bins from 350 km to 1600 km orbital altitude), and computed characteristic 3D separations between debris objects assuming uniformly-filled spherical shells 100 km thick over this altitude range. Using this information, we can calculate the time required to detect N objects above 1 cm in characteristic diameter by the following simple relation

$$T^* = \frac{N \text{ (total no. of objects estimated to exist in shell } \Delta H \text{ thick at altitude H)}}{Q \text{ (objects/ sq meter per yr.)} \times (M\, d_{spot}) \times \Delta H}$$

where M is the number of side-by-side FWHM beam spot diameters making up the picket fence, d_{spot} is the instantaneous FWHM diameter of the actively pulsed and slewed illuminator beam itself, and ΔH is the Line-of-Sight range bin used for data reduction (100 km for the HAYSTACK data). The above is plotted as a 4-box nomogragh in **Figure 10.** The Figure shows that:

1. Searching with a single beam (Fence Area = 1 km diameter x 100 km high data bin) would take years, even in the highest-density debris region .
2. Searching with a MIT/LL "Bow Tie" pattern (a version of the picket fence) only 10 beams wide drops the search time to about 1 year, using MIT/LL's 20 hr/day estimate for useful search time. Since the beam needs only one back-and-forth sweep to get data from ALL altitudes, the entire 300-1600 km altitude region can be surveyed in about one year of continuous 20-hr-per-day operation.
3. Searching the lower altitude (very-low-density) region of 300-500 km would take about the same time (ie, less than one year), even though the total number of objects in this region so low. This is because the arrival rate at the measurement region is correspondingly low.

4.Passive Optical Acquisition

The concept of using reflected solar radiation to detect and acquire the debris is an attractive idea, since the illumination (while weak) is continuous. This section evaluates its use along with existing telescopes and focal planes to find, track and handover the selected ORION targets to the Pusher laser.

NST

Northeast Science and Technology

"Picket Fence" Detection Scheme Scaling ---RADAR Sensor

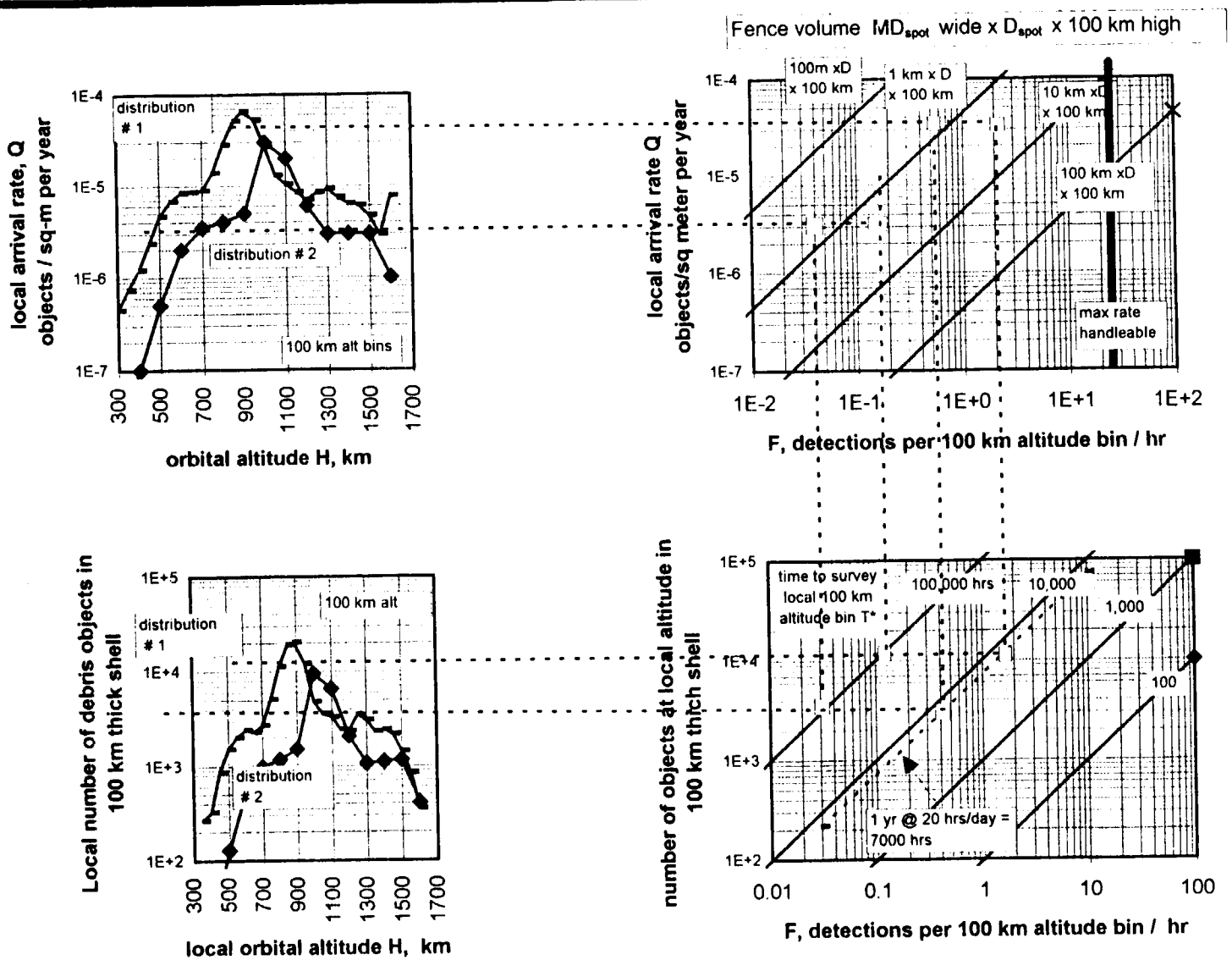

detect'n.xls

The reflected radiant intensity (watt / steradian) from a diffuse sphere with reflectivity-area product rA_{sph} illuminated by the sun, is given by:

$$I_{sph}(\text{W/sr}) = \frac{rA_{sph}}{\pi} \quad \frac{2}{3\pi} \quad (\sin\sigma + (\pi - \sigma)\cos\sigma)\ E_{sun}(W/cm^2)$$

where σ is the angle between the detector optical axis and the sun. At $\sigma = 90°$ (equivalent to a "half-moon" configuration as viewed by the sensor) the above reduces to

$$I_{sph}(\text{W/sr}) = \frac{rA_{sph}}{1.5\,\pi^2} \quad E_{sun}(W/cm^2) \quad , \qquad \text{at } \sigma = 90°$$

Thus, the signal photons on a pixel are:

$$N_{sig} = I_{sph}(\text{W/sr }\mu\text{m}) \quad \frac{A_{rcvr}}{R^2}\Delta\lambda \quad \frac{t_{integ}}{h\nu} \quad T_{opt}\,T_{prop}$$

where it is assumed that all the signal photons collected during the integration time t_{integ} by the receiver aperture A_{rcvr} are collected by a single pixel.

The sky photon counts on this same pixel are given by:

$$N_{sky} = I_{sky}(\text{W/sr-cm}^2\text{-}\mu\text{m}) \quad \frac{d^2_{pixel}}{f^2} \quad A_{rcvr} \quad \Delta\lambda \quad \frac{t_{integ}}{h\nu} \quad T_{opt}$$

The signal and sky background photons count numbers per integration time must be multiplied by the detector quantum efficiency η_{QE} to get the electron counts per integration time.

The pixel-with-target output is then approximately $N_{sig} + N_{sky}$ and the photon signal -to-noise ratio is given by

$$SNR = \frac{(N_{sig} + N_{sky}) - N_{sky}}{\text{sqrt}\,[(N_{sig} + N_{sky}) + N_{read}{}^2]}$$

where the readout photon noise N_{read} = CCD readout noise electrons per readout / η_{QE}. In astronomical telescopes this has been driven down to only 4 electrons per readout using cooled (- 40 C) systems, but typical good fielded-sensor noise levels are up at 8 - 12 noise electrons per readout. Quantum efficiency of detectors in the visible region of the spectrum for commercially-available detectors is 65 % .

The signal-to-background ratio (determining the noise - free contrast of the signal against the background) is defined as:

$$SBR = \frac{(N_{sig} + N_{sky}) - N_{sky}}{N_{sky}}$$

These two sensor criteria are sketched in **Figure 11** .

Typical values for the parameters of the debris spheres, the solar source and the sky background, along with those of the optical telescope's photon collection characteristics as well as those of the sensor's detector elements at the focal plane are listed in **Table 1.** These values were used to scope the application of various sensor / telescope combinations in acquiring and tracking the solar-illuminated debris objects, using SNR and SBR as simultaneous criteria, and varying sensor parameters to achieve acceptable levels of both SNR and SBR simultaneously.

Figures 12, 13 and 14 give the results of these calculations. These three Figures all display the following information, calculated from the above relations and parameter values :

1.
2. Number of signal photons received during the integration time from the 50% illuminated diffuse sphere,
3. SNR (signal-to-noise ratio) for both full daytime sky background, as well as for full moonless-night sky background,
4. SBR (signal-to-background ratio) for both full daytime sky background, as well as for full moonless-night sky background,

On-Chip Binning integration times-that is, the time the image spends on a single 40 micron detector, on a "binned" array (really a macro-pixel) of 10 x 10 and 100 x 100 detectors. In addition the stay-time of an orbital debris particle in a 1-km-diameter spot at altitude is shown (0.14 seconds)

Inspection of the three Figures :

Figure 12 --- 400 km slant range
Figure 13 --- 1200 km slant range
Figure 14 --- 3000 km slant range

shows that the really difficult problem with sun-illuminated ORION targets is SBR, or signal-to-background (ie, contrast). SNR can be made high enough to satisfy most data acquisition and data reduction systems / techniques by varying integration time between readouts, requiring the "on-chip-binning" approach suggested by MIT/LL.

Looking at the plots shown in these three **Figures,** we find that detection during full daylight using sun illumination is extremely difficult, if not impossible due to the bright day-sky optical background:

400 km slant range -- full daytime: SBR = 5E-4
1200 km slant range -- full daytime: SBR = 5E-5
3000 km slant range -- full daytime: SBR = 8E-6

while searching at Dawn or Dusk with a sun-illuminated target against a dark sky background produces extremely high contrast ratios (or SBR's) :

400 km slant range -- full night-sky SBR = >1E20
1200 km slant range -- full night-sky SBR = >1E20
3000 km slant range -- full night-sky SBR = >1E20

In addition, the **Figures** show the strength that on-chip binning adds to the passive detection technique. Signal-to-Noise ratio rises as the square-root of integration time, and with a dark sky background (all but eliminating sky-generated photons), the only serious noise sources are read-out noise and shot noise. Longer integration times mean more signal photons into the receiver aperture, and hence more shot noise, but on-chip-binning allows all these photons to be collected on an adjustable-size "macro-pixel", which produces less readout noise when the pixels are read out as one "macro-pixel" instead of as individual units. Including all these noise sources

Signal to Noise Ratio and Signal to Background Ratio

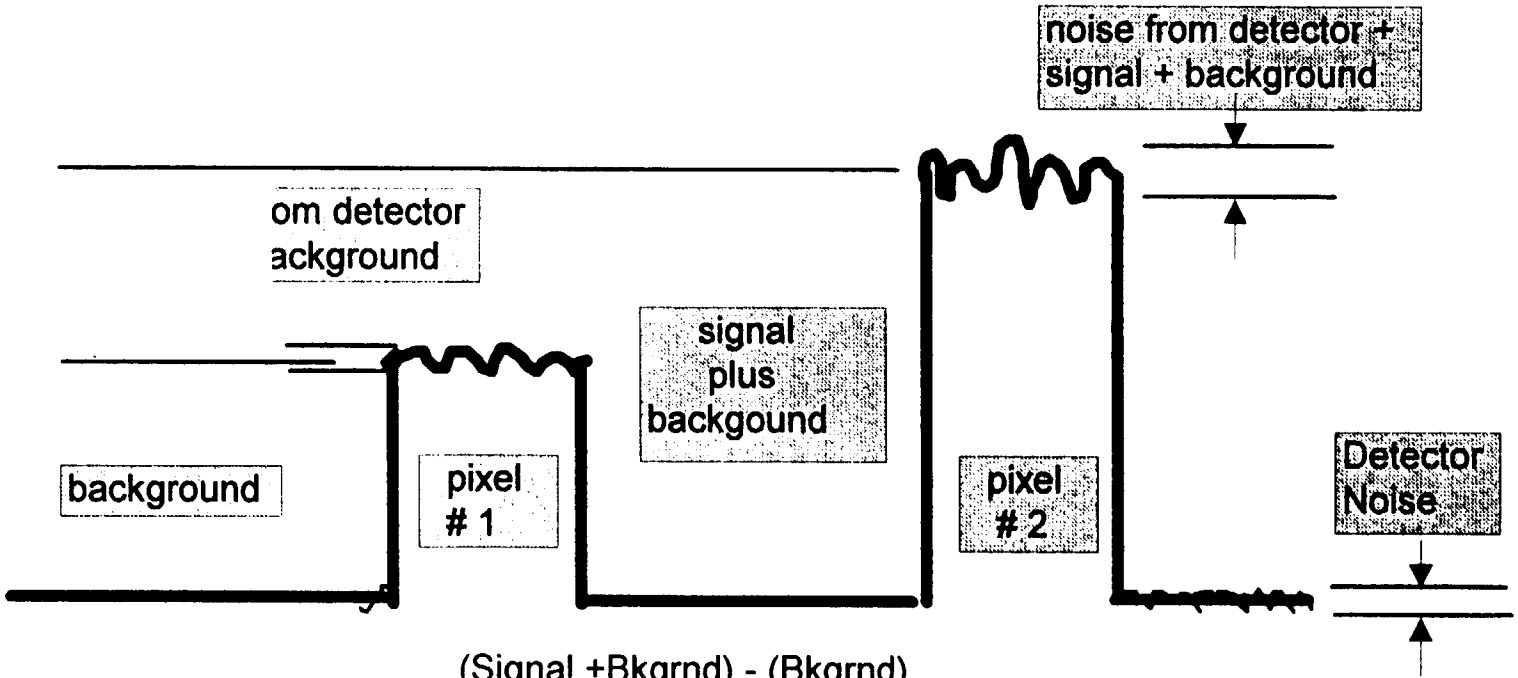

$$SNR = \frac{(\text{Signal} + \text{Bkgrnd}) - (\text{Bkgrnd})}{\sqrt{\text{Detector Noise}^2 + (\text{Signal Photelectrons}) + (\text{Background Photoelectrons})}}$$

$$SBR = \frac{(\text{Signal} + \text{Bkgrnd}) - (\text{Bkgrnd})}{\text{Background}}$$

Table 1
Debris, Illumination and Sensor System Characteristics for Sun-Lit Search Calculations

Debris Sphere	shape	spherical	
	diameter	1 cm	
	surface	diffuse	
	diffuse reflectivity	0.5	
	specular reflectivity	0	
Solar Source	irradiance in visible (0.4-0.9 microns)	0.2 W/ cm^2-micron	
Atmosphere	one-way transmission	70%	
Sky Background	daytime, no aerosols, no clouds	1.0 e-4 w/cm^2-ster-micron	ref 3
(0.4-0.7 micron)	daytime, with aerosols, no clouds	2.0 e-3 w/cm^2-ster-micron	ref 3,4,5
	15 min past sunset, no moon,no stars	2 e-8 w/cm^2-ster-micron	ref 4,5
	nighttime,no moon, with stars	2 e-11 w/cm^2-ster-micron	ref 4,5
	nightime, full moon, with stars	2 e-9 w/cm^2-ster-micron	ref 4,5
Collection Telescope	Effective Clear Aperture Diameter	3.5 meter	
	Visible transmission to focal plane	70%	
	Focal Length	f 30 (112.5 meters)	
	Maximum Slew rate	0.100 rad/sec	
	Maximum Angular Accelleration	0.100 rad/sec^2	
Focal Plane Detector	Wavelength Region	0.3-0.9 microns	
	Quantum Efficiency	65%	
	Notch Filter Width	0.05 microns	
	Individual Detector Size	40 microns	
	N x M Array size	1050 x 1050	
	readout noise	10 electrons/readout	
	D*	not used in present calculation	
	Integration Time	1E-6 to 3E-2 sec	
	Readout Time	1e-2 sec	
	Frame Rate	30 frames/sec	

ref 3 : MODTRAN II AFGL, Phillips Laboratory, Hanscom AFB, Massachusetts 1994

ref 4 : Infrared Handbook, ERIM, 1989 p 3-71

ref 5 : RCA Electro-Optics Handbook, RCA EO Div, Lancaster Pa 1974, p 62,68,70

FIG 12

NST

Northeast Science and Technology

Sunlit Acquisition ---400 km slant range

06

Debris Detection using Solar Illumination, Sunrise & Twilight Search , 400 km Slant Range

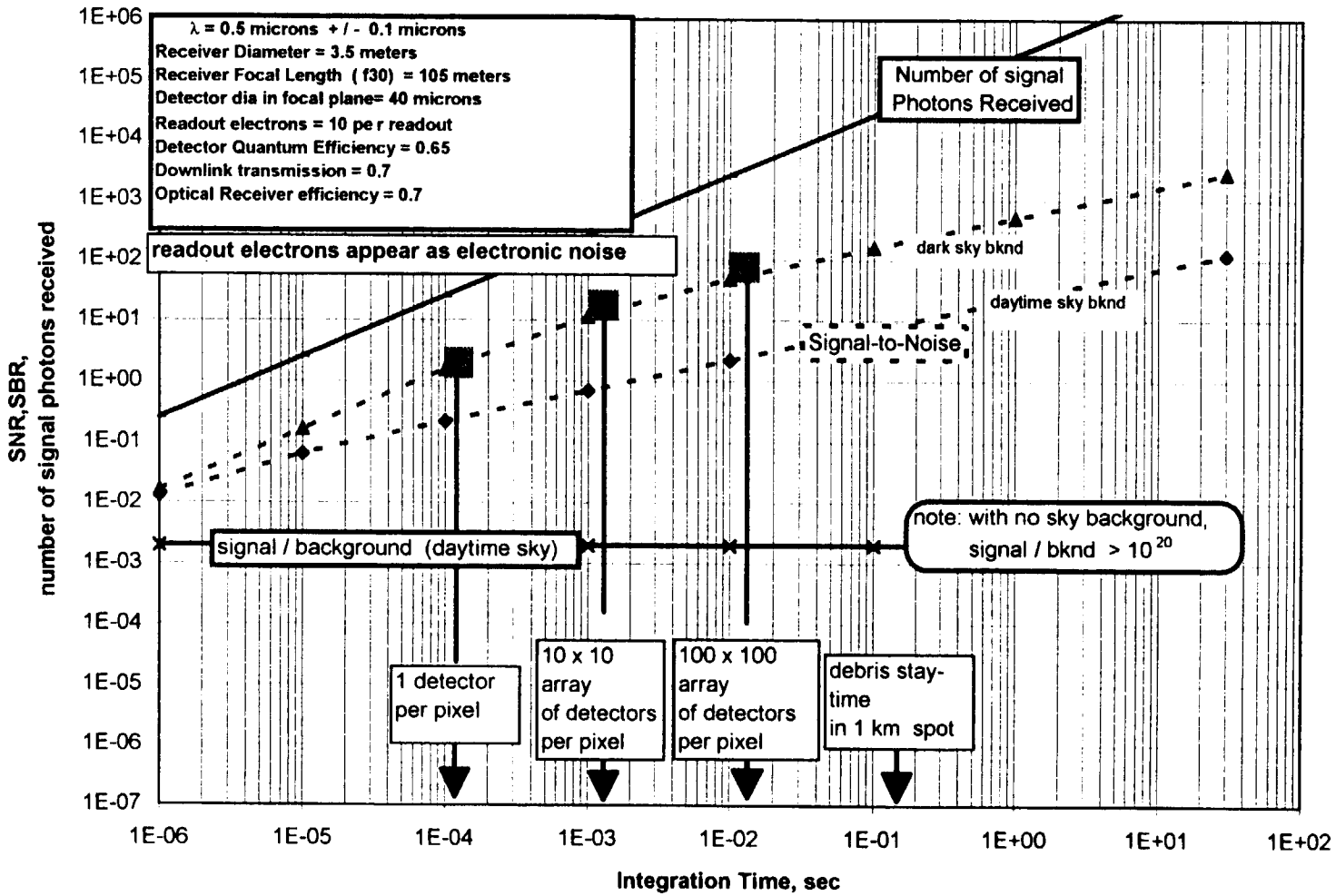

sencalc2.xlx

NST
Northeast Science and Technology

Sunlit Acquisition
---1200 km slant range

Debris Detection using Solar Illumination, Sunrise & Twilight Search, 1200 km Slant Range

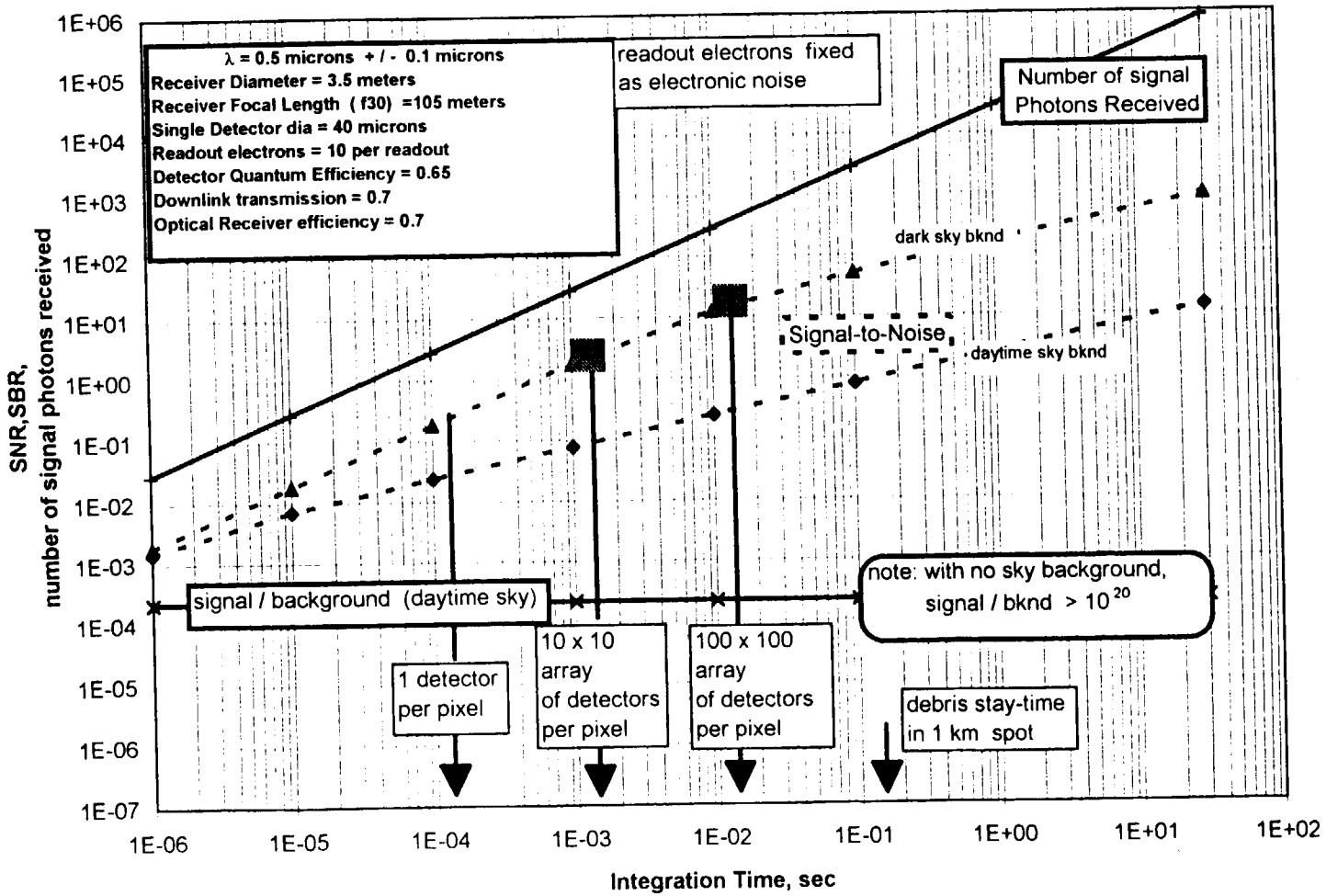

sencalc2.xlx

NST
Northeast Science and Technology

Sunlit Acquisition
----3000 km slant range

92

Debris Detection using Solar Illumination, Sunrise & Twilight Search , 3000 km Slant Range

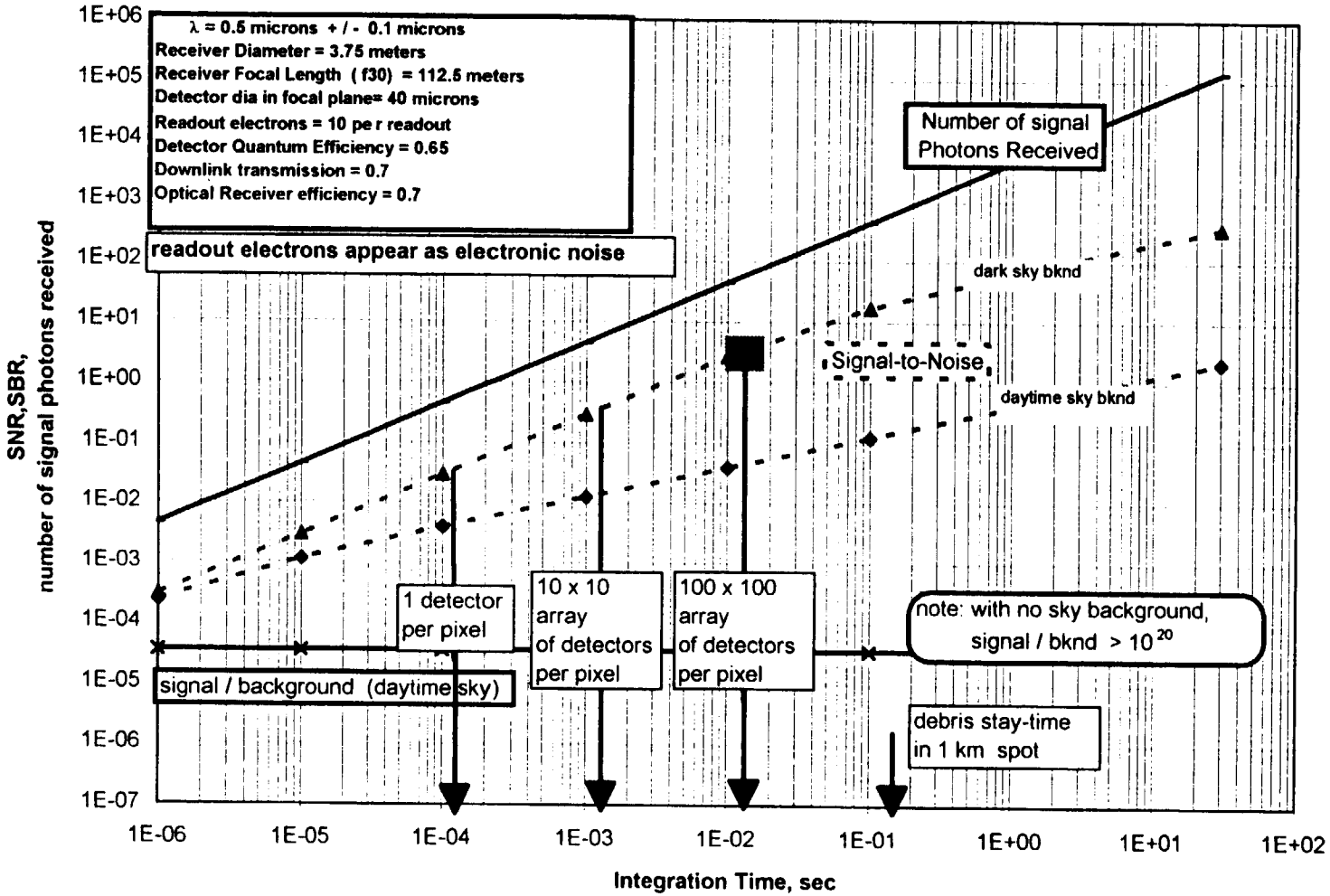

sencalc2.xlx

and dependencies, the three sensor-to-target range values considered here show that a single array, utilizing the adaptive capability of ganging pixels (to provide more signal photoelectrons for the same readout-noise electrons) can perform equally effectively with the same telescope and same detector chips in acquiring sunlit ORION targets.

Table 2
Capability of "On-Chip Binning" in Detection of Sun-Lit Debris

400 km slant range -- 1 single pixel has SNR ~2
3 x 3 pixel "array" has SNR ~5

1200 km slant range --10 x 10 pixel "array" has SNR ~2
30 x 30 pixel "array" has SNR ~7

3000 km slant range --100 x 100 pixel "array" has SNR ~2
300 x 300 pixel "array" has SNR ~10

At the 400 km range, the instantaneous-field-of-view of a single detector is the detector diameter / focal length of the telescope's focusing optics. For the telescope design considered here,

$\theta_{detector}$ = 40 microns / 112.5 meters = 3.55E-7 radians approximately

and the instantaneous-field-of-view of the array is simply the number of detectors in an array row or column times that value :

$\theta_{array} = \theta_{detector} \times N = 3.55E\text{-}7 \times 1050 = 4E\text{-}4$ radians approximately.

At 400 km slant range, the measurement spot area viewed by the entire focal plane array is 400 km x θ_{array} = 400 km x 4E-5 radians = 160 meters in diameter. At 1200 km slant range, the spot is 480 m in diameter and at 3000 km slant range, the spot is 1200 m in diameter. Using a single stationary (non-slewing) position for this beam to search the sky for debris would take an excessive amount of time, as is shown both in **Figure 8** (cf. "Stationary Beam" line) and in **Figure 10** (cf. lines at fence area of 0.7 - 1 km x 100 km) ---about 3-6 years. At slew rates capable of tracking LEO satellites (approximately 0.030 radians/sec or better). the search time reduces by at least a factor of 10 to a few months. The time to complete one full slew cycle. at a slew rate of .030 rad/sec is:

altitude	beam angle	spot dia	fence width	slew rate	time to complete one slew cycle
200 km	4E-4 rad	160 m	100 km = .250 rad	.030 rad/sec	8.3 sec
600 km	4E-4 rad	480 m	100 km = .083 rad	.030 rad/sec	2.8 sec
1500 km	4E-4 rad/sec	1200 m	100 km = .033 rad	.030 rad sec	1.1 sec

It must be noted that in the above, we have not taken into account atmospheric turbulence effects. The atmosphere is known to have integrated optical path angular fluctuations in the 100-to 1000 hz frequency range, with a characteristic long-term RMS spatial coherence scale r_o of between 2 and 10 cm, depending on the altitude of the abserver, day or night conditions , wavelength and wind conditions. This translates to a few microradians angular amplitude uncertainty (5 cm / 30 kM), and may preclude the utility of single-pixel detection (since a typical single-pixel FOV is on the order of 40 microns/ 40 meters focal length) and may even compromise the data from a 10x10 pixel "super-pixel" sub-array.

Purely passive tracking using sunlit targets for ORION appears do-able out to slant ranges of 3000 km, using slewed beams, current existing adaptive-optics telescopes, and "on-chip-binning" as a method of making adaptive sensor focal planes produce high-contrast signals (high SBR) as well as high SNR signals . Although searching is only possible for the total of 4 hours per day at dawn and dusk, the entire altitude range 300 -1600 km can be completely searched to acquire the (currently-estimated from the MIT/LL data) 100,000 or so debris objects 1 cm or larger in diameter in a period of less than nine to twelve months at current slew-rate capabilities. The follwing **Figure , Figure 14-A** shows that to detect all of the objects in any given altitude bin (an hence all the objects in all bins) in under 1 year requires a fence about 10 km wide at altitude -about .010 radian. At slew rates of .030 rad/sec, acomplete raster scan would take 0.67 seconds, an easy task as can be seen in **Fig 7.**

5.Active Optical Acquisition using a Repped-Pulse Laser Illuminator

In the above sections , the validity of the passive optical acquisition system was established using sunlight as the illumination and slewed telescope as a collector so as to provide as much detection area as possible , leading to a total search time requirement less than 9-12 months. The active-slewing approach was necessary, since the debris objects are only visible against a dark-sky background (ie at dawn and dusk) for a total of up to 4 hours per day. The advantage of an active repped-pulse laser illuminator is to provide illumination on demand, not just at dawn and dusk as with the Passive Optical Acquisition system described above. The equations describing the return signal photons are identical to those above, with the exception that the illumination is single-frequency (the laser wavelength) not broadband (like sunlight), and that we have direct control on its intensity and duration, via the illumination spot size and laser pulse width.

The reflected radiant intensity (watt / steradian) from a diffuse sphere with reflectivity-area product rA_{sph} illuminated by the sun, is given by:

$$I_f(\text{W/SR}) = \frac{rA_{sph}}{\pi} \quad \frac{T_{prop}\, E_{laser}}{(\pi/4)\, D^2_{spot}\, \tau_{pulse}}$$

where $T_{rpop}\, E_{laser}$ is the laser pulse energy transmitted up to the target through the atmosphere with transmission T_{prop}, D_{spot} is the laser spot size chosen specifically for the search function, and τ_{pulse} is the duration of the laser pulse. Thus, the signal photons on a pixel are:

$$N_{sig} = I_{sph}(\text{W/sr}) \frac{A_{rcvr}}{R^2} \frac{\tau_{pulse}}{h\nu} T_{opt}\, T_{prop}$$

where it is assumed that all the signal photons collected during the integration time t_{integ} by the receiver aperture A_{rcvr} are collected by a single pixel.

The sky photon counts on this same pixel are given by:

$$N_{sky} = I_{sky}(\text{W/sr-cm}^2\text{-}\mu\text{m}) \frac{d^2_{pixel}}{f^2} A_{rcvr}\, \Delta\lambda \frac{t_{integ}}{h\nu} T_{opt}$$

where t_{integ} is the integration time (probably somewhat longer than the laser pulse width to allow for uncertainties in arrival time and/or electronic response times).The signal and sky background photons count numbers per integration time must be multiplied by the detector quantum efficiency η_{QE} to get the electron counts per integration time.

NST

Northeast Science and Technology

"Picket Fence" Detection Scheme Scaling ---Passive EO Sensor

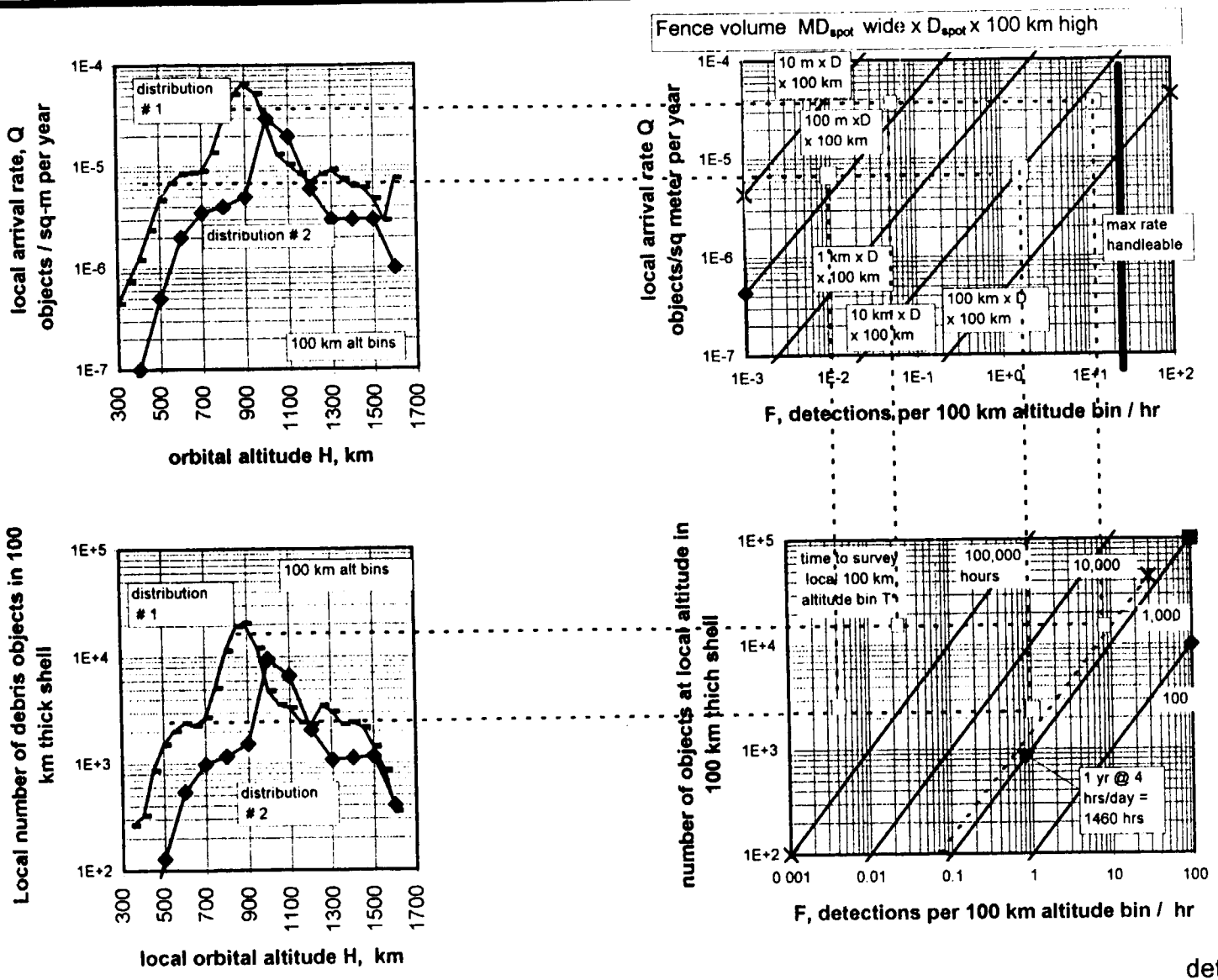

detect'n.xls

The pixel-with-target output is then approximately $N_{sig} + N_{sky}$ and the photon signal -to-noise ratio is given, as it was above, by

$$SNR = \frac{(N_{sig} + N_{sky}) - N_{sky}}{\text{sqrt}\,[(N_{sig} + N_{sky}) + N_{read}{}^2]}$$

where the readout photon noise N_{read} = CCD readout noise electrons per readout / η_e. In astronomical telescopes this has been driven down to only 4 electrons per readout using cooled (- 40 C) systems, but typical good fielded-sensor noise levels are up at 8 - 12 noise electrons per readout. Quantum efficiency of detectors for 1.06 micron commercially-available detectors is 65 % .

The signal-to-background ratio (determining the noise - free contrast of the signal against the background) is defined, as it was above, as:

$$SBR = \frac{(N_{SIG} + N_{sky}) - N_{sky}}{N_{sky}}$$

These two sensor criteria were discussed previously, and are sketched in **Figure 11** .

Typical values for the parameters of the debris spheres, the solar source and the sky background, along with those of the optical telescope's photon collection characteristics as well as those of the sensor's detector elements at the focal plane are listed in **Table 3.** These values were used to scope the application of various sensor / telescope combinations in acquiring and tracking the laser-illuminated debris objects, using SNR and SBR as simultaneous criteria, and varying sensor parameters to achieve acceptable levels of both SNR and SBR simultaneously.

Figures 15, 16 and 17 give the results of the calculations for the number of photons captured by the 3.75 meter diameter telescope. These three **Figures** all display the number of signal photons received during the integration time from the laser-illuminated diffuse sphere,
calculated from the above relations and parameter values :

Figure 15 --- 400 km slant range
Figure 16 --- 1200 km slant range
Figure 17 --- 3000 km slant range

The calculations indicate that in order to receive back from the illuminated 1 cm spherical object a minimum of 10 signal photons (ie, an equal number to the number of spurious "noise" electrons generated by the readout process on each detector), there is a trade-off between laser pulse energy, laser spot size and slant range. These are illustrated in **Table 4** below.

Table 4
Characteristic Laser Spot Sizes and Pulse Energies for Detection

400 km slant range	100 joules	130 meter dia spot
	1000 joules	500 meter dia spot
1200 km slant range	100 joules	50 meter dia spot
	1000 joules	180 meter dia spot
3000 km slant range	100 joules	20 meter dia spot
	1000 joules	60 meter dia spot

Table 3
Parameters Used for the Analysis of an Active Laser Illuminator for ORION Debris

Debris Sphere	shape	spherical	
	diameter	1 cm	
	surface	diffuse	
	diffuse reflectivity	0.5	
	specular reflectivity	0	
Solar Source	irradiance in laser band (1-2 microns)	0.01 W/ cm^2-micron	
Atmosphere	one-way transmission	85%	
Sky Background	daytime, no aerosols, no clouds	<1.0 e-8 w/cm^2-ster-micron	ref 3
(1-2 micron)	daytime, with aerosols, no clouds	5.0 e-4 w/cm^2-ster-micron	ref 3,4,5
	nightime, no moon,no stars	<1.0 e-10 w/cm^2-ster-micron	ref 4,5
	nighttime,no moon, with stars	1.5 e-10 w/cm^2-ster-micron	ref 4,5
	nightime, full moon, with stars	1.5 e-9 w/cm^2-ster-micron	ref 4,5
Collection Telescope	Effective Clear Aperture Diameter	3.5 meter	
	IR transmission to focal plane	70%	
	Focal Length	f 30 (112.5 meters)	
	Maximum Slew rate	0.100 rad/sec	
	Maximum Angular Accelleration	0.100 rad/sec^2	
Focal Plane Detector	Wavelength Region	1.06 microns	
	Quantum Efficiency	20%	
	Notch Filter Width	0.05 microns	
	Individual Detector Size	40 microns	
	N x M Array size	not required for present calculation	
	readout noise	10 electrons/readout	
	D*	not used in present calculation	
	Integration Time	1E-10 to 30 sec	
	Readout Time	not used in present calculation	
	Frame Rate	not used in present calculation	

ref 3 : MODTRAN II, AFGL, Phillips Laboratory, Hanscom AFB, Massachusetts, 1994
ref 4 : Infrared Handbook, ERIM Handbook, ERIM, 1989 p 3-71,72,73
ref 5 : RCA Electro-Optics Handbook, RCA EO Div, Lancaster Pa 1974, p 62,68,70

FIG 15

NST

Northeast Science and Technology

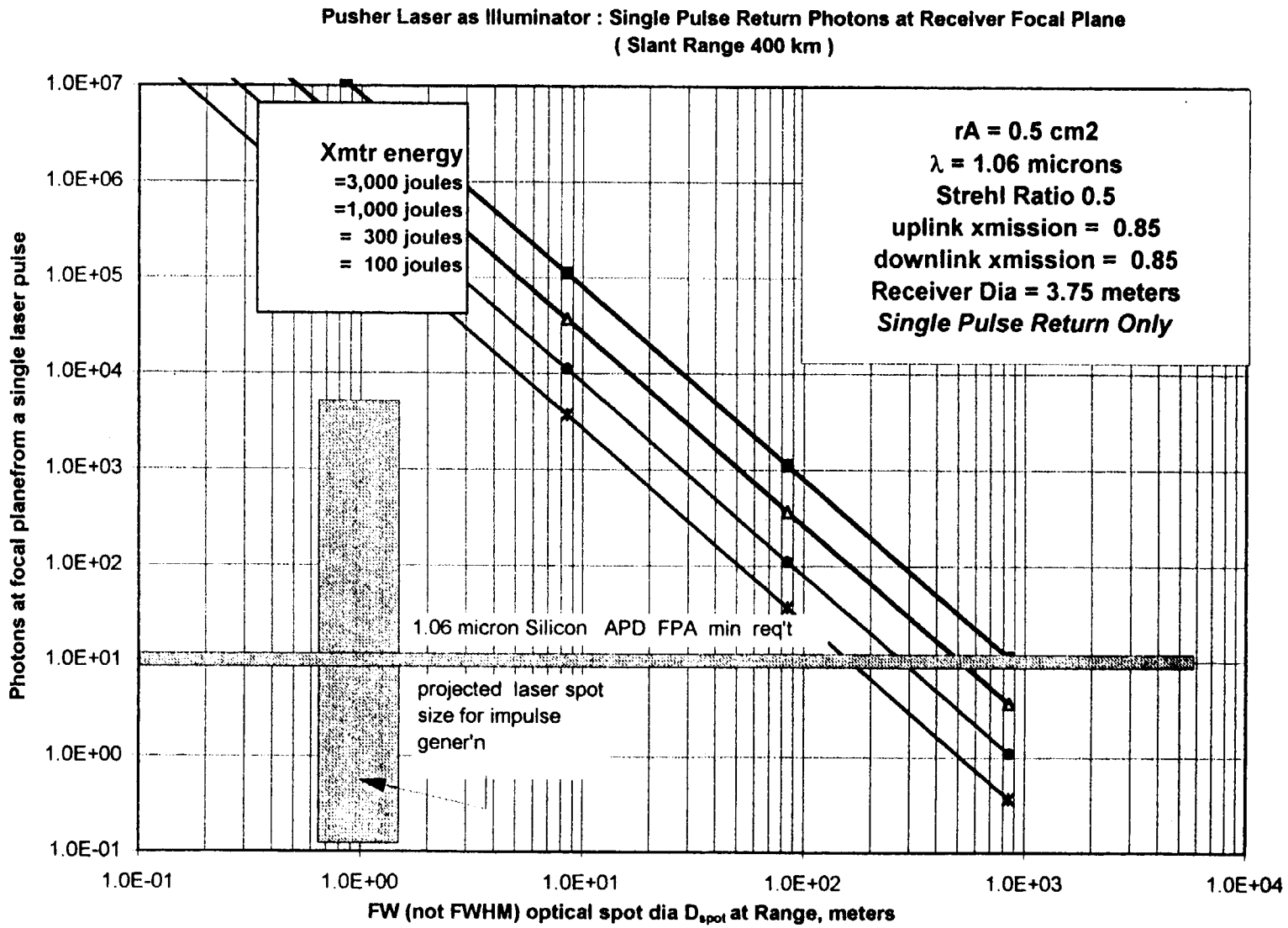

Pusher Laser and Its Optics can act in Autonomous Search Mode or as Handover from Microwave Radar

NST

Northeast Science and Technology

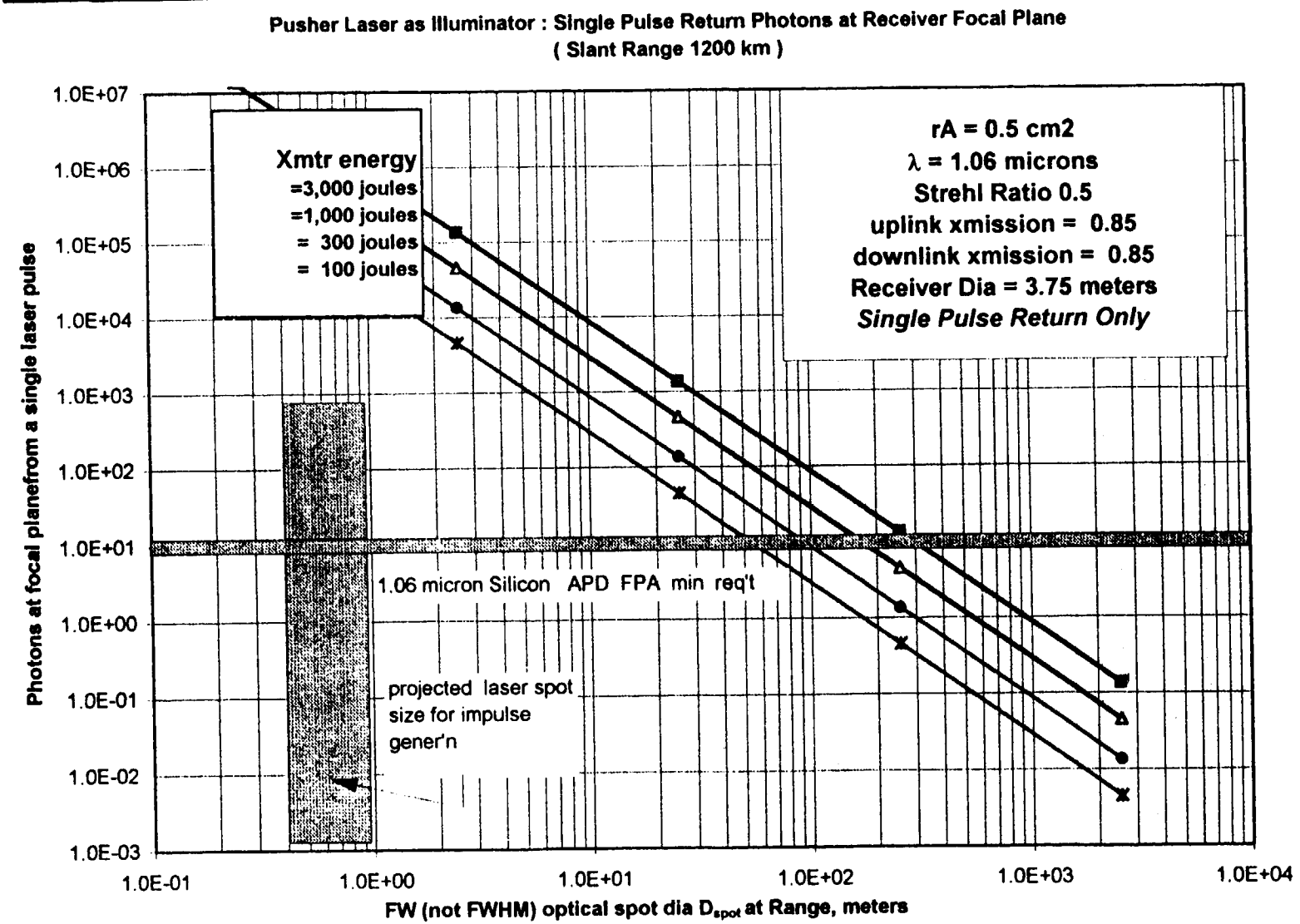

66

Pusher Laser and Its Optics can act in Autonomous Search Mode or as Handover from Microwave Radar

100

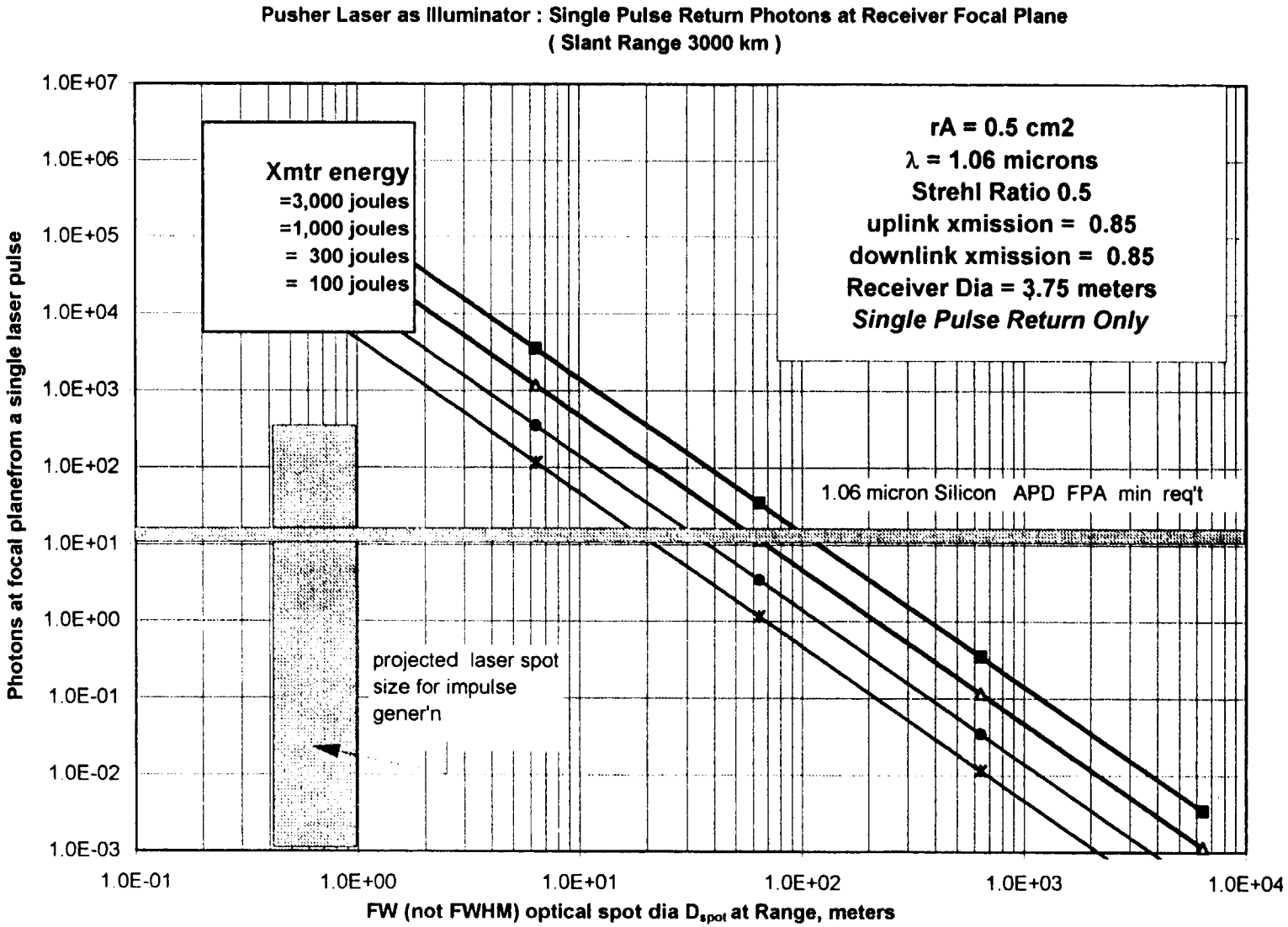

Pusher Laser and Its Optics can act in Autonomous Search Mode or as Handover from Microwave Radar

The SNR (signal-to-noise ratio) for both full daytime sky background, as well as for full moonless-night sky background, as well as the SBR (signal-to-background ratio) for both full daytime sky background and for full moonless-night sky background is shown in **Figures 18, 19 and 20.** Because of the variation of the spot size / pulse energy requirement with slant range, we choose a spot size characteristic of each of the slant ranges above. Since the laser illuminator spot is truly a quantity which can be varied from pass to pass of target objects, this is a valid exercise to help choose the required pulse energy and hence size the laser device hardware required

Table 5
Characteristic Spot Size Requirements for SNR > 1
Along with Target Stay Time in Spot (Spot Diameter / Orbital Velocity)

Figure 15 --- 400 km slant range ---300 meter dia spot ---<0.040 sec stay time in spot
Figure 16 --- 1200 km slant range --- 120 meter dia spot---<0.019 sec stay time in spot
Figure 17 --- 3000 km slant range -----40 meter dia spot----<0.007 sec stay time in spot

Inspection of **Figures 18, 19 and 20** rapidly shows that signal-to background ratio (SBR or contrast ration) is not the problem we face here----it is signal-to-noise ratio SNR. At energy levels below about 300 joules per pulse, the SNR is always less than unity, and only is above about 2 at energy levels above about 1000 joules per pulse , using this small receiver dish (3.75 meters). Our attempt to adjust integration time has no effect, and actually *HURTS* the SNR for pulses longer than about 1 microsecond. **Table 5** above shows the spot sizes required for this 1 kilojoule active illuminator (min energy for SNR > 1). In addition ,if we detect a potential target debris object in the spot , we would like to hit it at least 3 times to build confidence that it is a real object and not a spurious signal. **Table 5** also shows a rough estimate of the maximum time a debris object will stay in the beam (spot diameter / orbital velocity), in order to estimate the burst-mode capability the illuminator should have, to provide not only repped-pulse active scanning but also a burst of pulses to provide low false-alarm and high detection probability data that that given by a single return. A burst rep rate capability of 75 hz (i.e., 1 / (.040 sec / 3) to 425 hz (1 / (0.007 sec / 3) may be required of this 1 kj or greater laser used as an illuminator.

We conclude that initial detection by active illumination of the small 1 cm diameter debris objects in the orbital altitude region of interest 200-1500 km, with a 3.75 meter receiver dish at an elevation angle of 30 degree is not very effective for small laser pulse energies. At laser illumination energies above 1000 joules, however, the concept does become effective, but with small 40-300 meter diameter spots for the 400 - 3000 km slant ranges required. It would probably require pulse rep rates in excess of a few hundred hertz. If we now wish to use such a system (pulse energies above 1 kilojoule , 3.75 meter collector dish, pulse durations less than 1 microsecond), then in order to survey the entire sky and acquire the estimated 100,000 objects in less than 1 year, the picket fence approach discussed above for the radar and passive-optics approach must be used. **Figure 21** is a nomograph which calculates the side-to-side scanning requirements for these small (40-300 meter diameter beams. This Figure shows that in order to achieve the required sky coverage over the altitude region of interest requires a scan width of 1 beam dia by about 50 km, or about 100 to 1000 beamwidths. **Table 6** below shows the angular side-to-side scan angle requirements as functions of the altitude being searched with a 1 kj laser (SNR > 1).

Table 6
Lateral Width required for the EO Picket Fence

altitude	required spot diameter	beam angle D / R	scan width required M D	lateral scan width M D	lateral scan angle MD x D/R
200 km	300 m	1.5e-3	50 km	167 beamwidths	0.206 radians
600 km	120 m	2.0e-4	50 km	417 beamwidths	0.083 radians
1500 km	40 m	2.7e-5	50 km	1250 beamwidths	0.034 radians

FIG 1.8

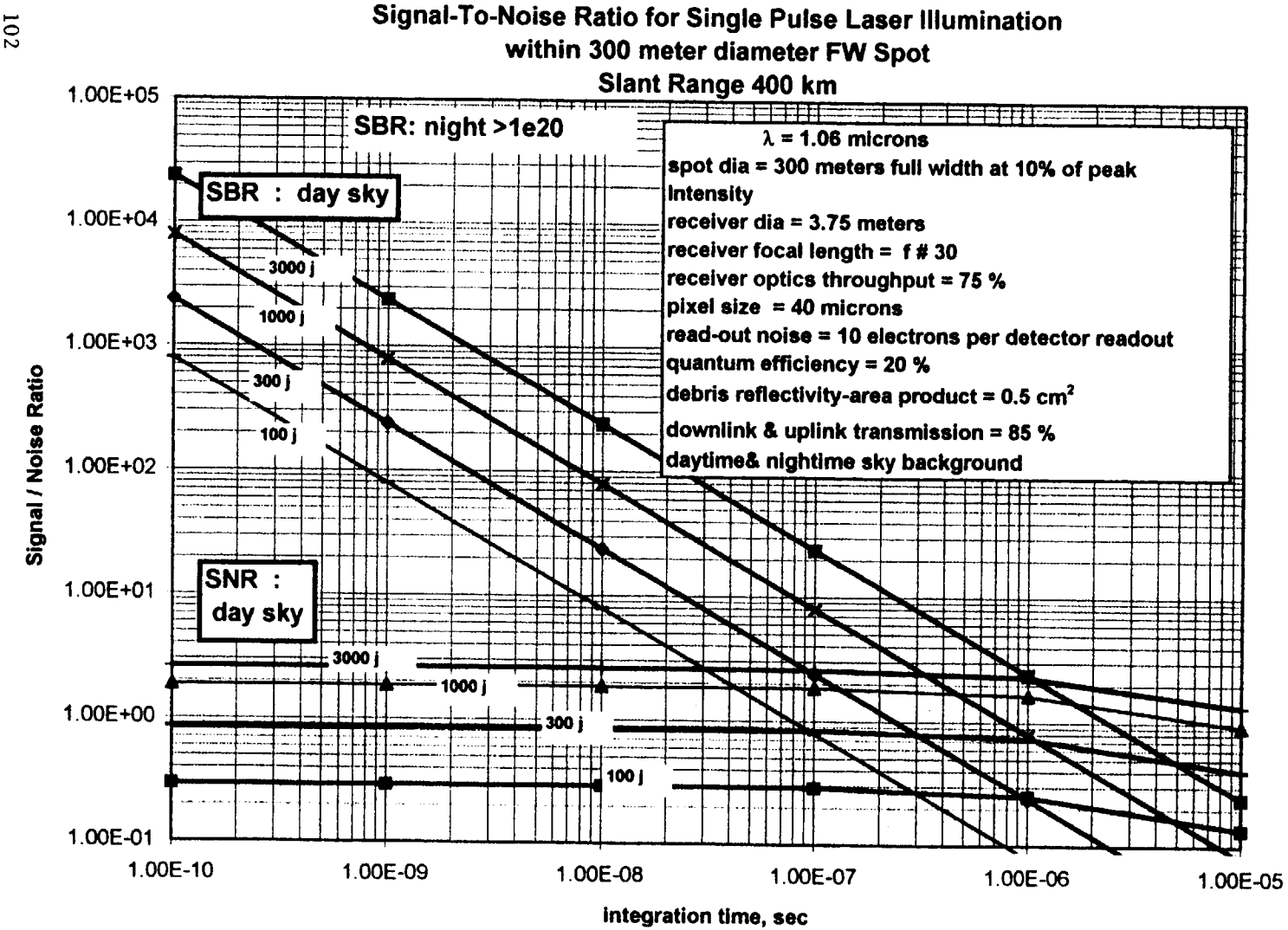
Signal-To-Noise Ratio for Single Pulse Laser Illumination
within 300 meter diameter FW Spot
Slant Range 400 km
SBR: night >1e20
SBR : day sky
3000 j
1000 j
300 j
100 j
λ = 1.06 microns
spot dia = 300 meters full width at 10% of peak Intensity
receiver dia = 3.75 meters
receiver focal length = f # 30
receiver optics throughput = 75 %
pixel size = 40 microns
read-out noise = 10 electrons per detector readout
quantum efficiency = 20 %
debris reflectivity-area product = 0.5 cm²
downlink & uplink transmission = 85 %
daytime& nightime sky background
SNR : day sky
3000 j
1000 j
300 j
100 j
Signal / Noise Ratio
1.00E+05
1.00E+04
1.00E+03
1.00E+02
1.00E+01
1.00E+00
1.00E-01
1.00E-10
1.00E-09
1.00E-08
1.00E-07
1.00E-06
1.00E-05
integration time, sec

NST

Northeast Science Technology

Signal-To-Noise Ratio for Single Pulse Laser Illumination
within 120 meter diameter FW Spot
Slant Range 1200 km

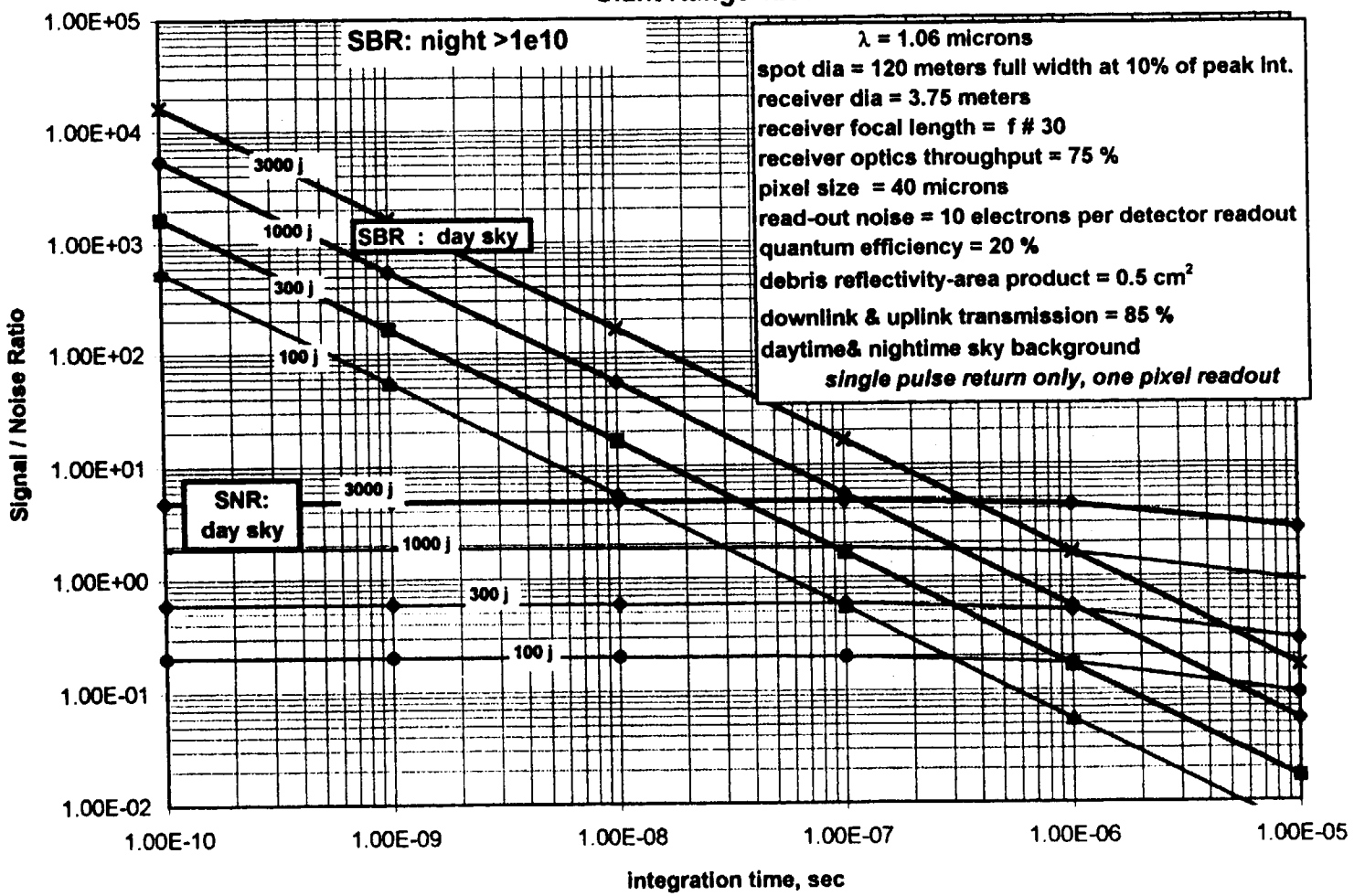

NST

Northeast Science Technology

FIG 20

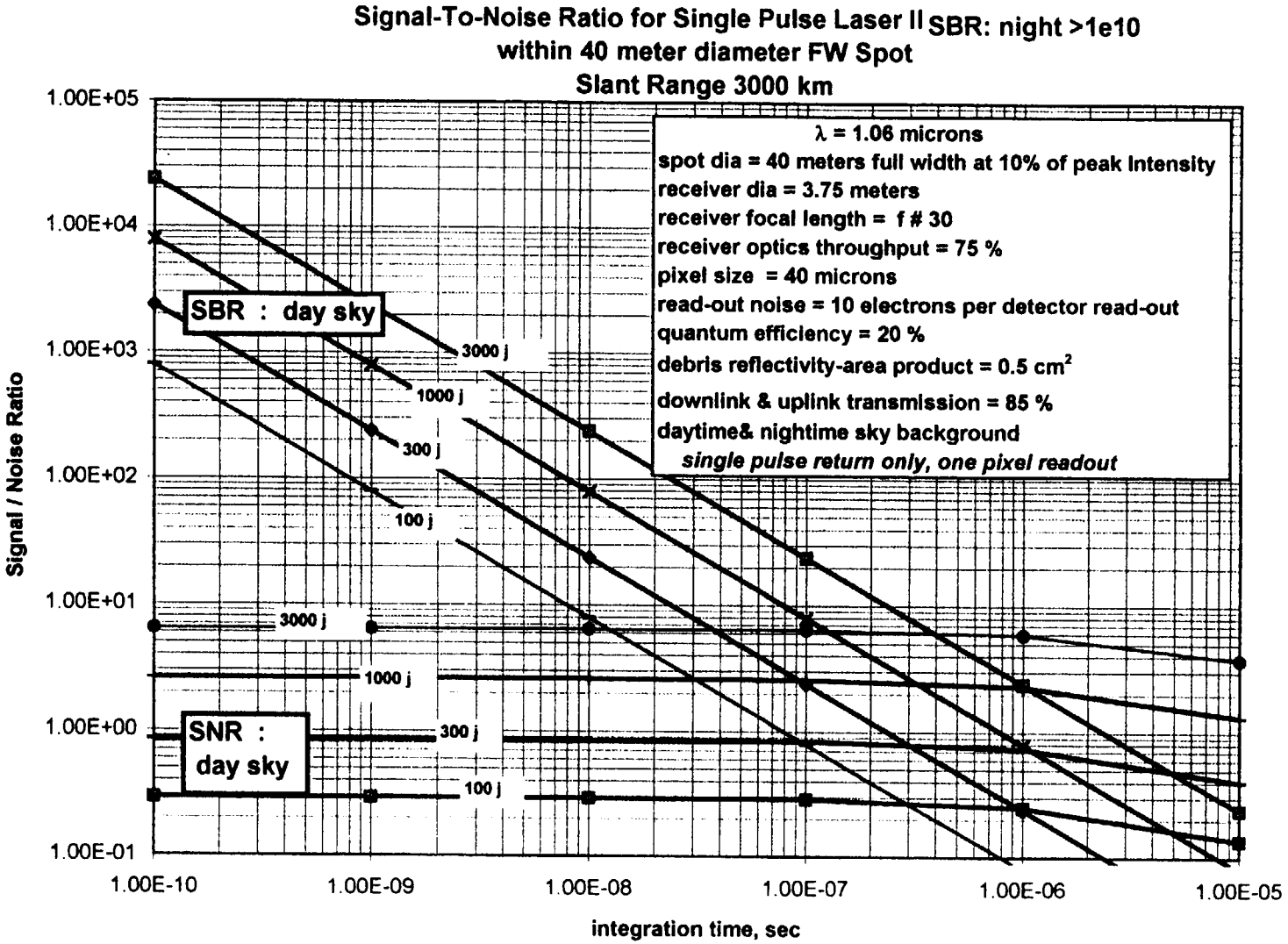

Fig 2.

NST

Northeast Science and Technology

"Picket Fence" Detection Scheme Scaling --- Laser Illuminator Sensor

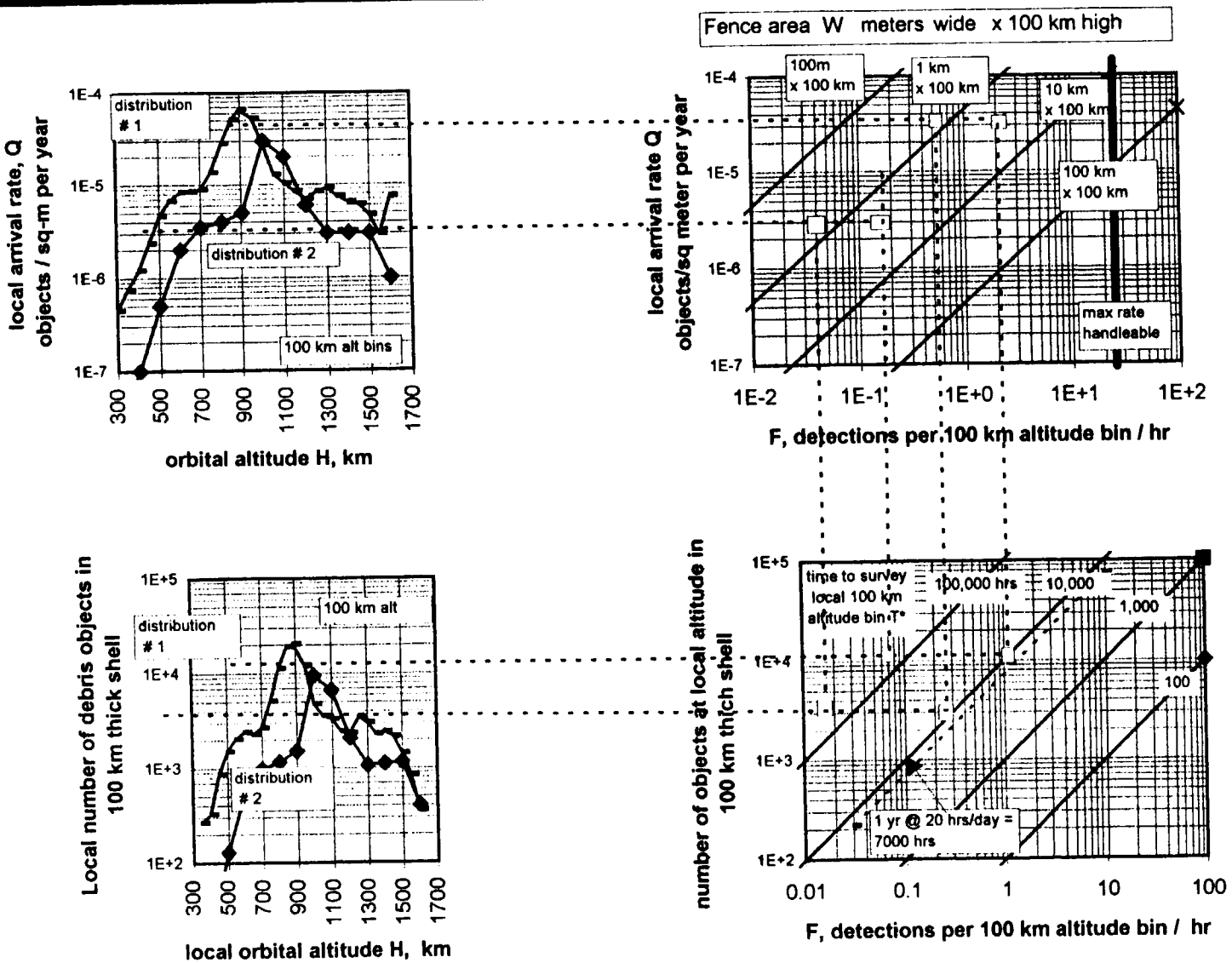

detect'n.xls

The amplitude of the side-to-side angle scan required is not extensive, but the question is how fast must it be accomplished. At angular rates required to track LEO objects, approximately 0.03 rad/sec, the Table below show how long a time accomplishing the above scans would take, along with the round-trip time for signals to leave and return to the receiver:

Table 7
Important Time-scales for Erecting the EO Picket-Fence

orbital altitude	total lateral scan angle MD x D/R	angular rate rad/sec	time for 1 full scan cycle	optical signal rnd-trip	time between beam positions time
200 km	0.206 radians	0.030	13.8 sec	0.003 sec	0.050 sec
600 km	0.083 radians	0.030	5.4 sec	0.008 sec	0.0067 sec
1500 km	0.034 radians	0.030	2.2 sec	0.020 sec	0.0009 sec

Comparing the last two columns in **Table 7** above , we see that the low altitude system (200 km orbital altitude searcher, having a slant range of 400 km) would be reasonable, requiring a telescope capable of tracking LEO objects (only 0.030 rad/sec, far less than current demonstrated technology ; see **Figure 7**), with a laser rep rate of 20 hz, and lots of time between pulses for the signal to get back to the receiver before the next pulse is launched.

However, at the 600 km altitude (1200 km slant range), the required PRF is 150 hz (1/ 0.0067 sec) , and the round-trip time is just a bit LONGER than the required interpulse time, indicating the beginnings of possible difficulty with using the same dish as both transmitter and receiver. A separate transmitter and receiver dish would, of course, work but is more expensive. At the longer range (1500 km altitude, or 3000 km slant range), the required laser is 1000 hz (and at least 1000 joules per pulse !!!) , and because the optical round-trip time is now 0.02 sec with an interpulse time of 0.001 sec, a separate dish for the transmitter and receiver is a necessity.

We must conclude from this that initials debris detection by an active illuminator appears to be a difficult task, if it is to be used to acquire all the objects within a one-year time frame over the orbital altitude ranges of interest.

6.Active Optical Acquisition using a CW Laser Illuminator

In the above , the validity of the passive optical acquisition system was established using sunlight as the illumination and slewed telescope as a collector so as to provide as much detection area as possible , leading to a total search time requirement less than 9-12 months (see **Figure 21** ; 20 hrs day operation for 1 year results in 7300 hours of search time). The active-slewing approach was necessary, since the debris objects are only visible against a dark-sky background (ie at dawn and dusk) for a total of up to 4 hours per day. The advantage of an active CW laser illuminator is to provide illumination on demand all during the day and night if necessary, not just at dawn and dusk as with the Passive Optical Acquisition system described above. The equations describing the return signal photons are identical to those of the repped-pulse illuminator, with the exception that the illumination is continuos , not pulsed. It is , as was the repped pulse illuminator, single-frequency (the laser wavelength) not broadband (like sunlight), and we have the same direct control on its intensity and duration, via the illumination spot size and laser pulse width.

The intensity levels which can be delivered to the interrogation volume depends of course on the laser power level, the Strehl ratio for the beam at interrogation range, the laser spot size chosen to do the searching and the atmospheric transmission from the transmitter to the range in question. The MINIMUM beam divergence angle will be that of a diffraction-limited beam

$$\theta_{min} = \lambda / D \quad , \text{FWHM angle for a diffraction-limited beam}$$

and at 1000km range, the FWHM spot diameter for a 3.5 meter diameter transmitter aperture with a 1.3 micron (i.e., a CW Iodine laser) or a 1.06 micron (CW glass laser , which exist at power levels below 1 kw) wavelength is about 0.3 meters in diameter. The mean power densities in the FWHM spot are functions of the chosen range, spot size (with 0.3 meters as a lower limit) , illuminator power level , and are shown **Figure 22** for a Strehl ratio of 0.5 and an atmospheric transmission of 89% (calculated with the MODTRAN II code (**ref 3**) for Iodine, and 80% for the solid-state laser wavelength.

The Figure illustrates that in order to produce irradiances higher than those of sunlight by AT LEAST the ratio of sensor quantum efficiencies at 1 micron vs 0.5 micron:

$$I_{breakeven} = 0.1 \text{ w/cm}^2 \text{ (sunlight) x } 65\% / 20\% = 0.33 \text{ w/cm}^2 \text{ (Laser req'm'nt)}$$

with the minimum spot deliverable at the chosen 1200 km slant range, the laser must be just under 1 kilowatt at 1 micron. Such lasers exist in the industrial laser community. However, the spot diameter is only 30 cm in diameter, and so the beam will have to be slewed rapidly to cover the entire sky in the picket fence search pattern in under one year.

Figures 23 & 24 show the SNR and SBR for a 1 micron CW illuminator producing 20, 200 and 2000 w/cm2 at a 1200 km slant range against a daylight-sky background (**Figure 23**) and against a moonless-night sky background (**Figure 24**). The parameters for the calculation are shown in **Table 3.** Neither background appears to pose a problem for a CW illuminator delivering 2 to 2000 watt / cm^2 at range, using relatively short integration times. **Table 8** below shows the illuminator and sensor focal plane requirements for this kind of system.

Table 8
Spot Size, Power Levels and Sensor Paramters for the CW Illuminator

Mean Irradiance in FWHM Spot	Required Illumination Time for SNR=5	Minimum Spot Dia Required at 7 km/sec	Minimum Spot Dia Deliverable (3.5 M,1200 km, 1 μm)	Minimum Laser Power Required at 1200 km Slant Range	Minimum Focal Plane FOV Req'd (Vt /R)	Possible Focal Plane FOV 2000 X 40 micron det'r & 105 M FL
w / cm^2	sec	meters	meters	watts	radians	radians
2	4E-4	2.8	0.3	1.2 E+5	2.33 E-6	7.6 E-6
20	4e-5	0.28	0.3	1.4 E+4	2.33 E-7	7.6 E-6
200	4E-6	0.028	0.3	1.4 E+5	2.5 E-7	7.6 E-6
2000	4E-8	0.0028	0.3	1.4 E+6	2.5 E-7	7.6 E-6

As can be seen the minimum power required at the debris altitude is 14 kw and with a Strehl ratio of 0.5 and atmosheric uplink transmission of 0.85, the minimum power out of the ground transmitter is about 33 kw of CW 1 micron radiation. No such 1.06 micron laser exists, but one could envision ganging 33 of the existing 1 kw 1.06 micron lasers, phase-locking them and using the net beam. Rather than go through such heroic efforts, it shoul be noted that the Phillips Lab at Kirtland AFB in NM has two CW 1.3 micron lasers which have been operating for years in this power range:

ROTOCOIL 40 kw CW Iodine at 1.3 microns
RADICL 20 kw CW Iodine at 1.3 microns

Hence this illumination scheme could work, using these lasers, 3.5 meter optics for both transmitter and receiver, and a focal plane similar to the one used by MIT LL in the visible, but made of detectors optimized for 1.3 microns.

NST

Northeast Science and Technology

Minimum Power Levels Required to Deliver Irradiance

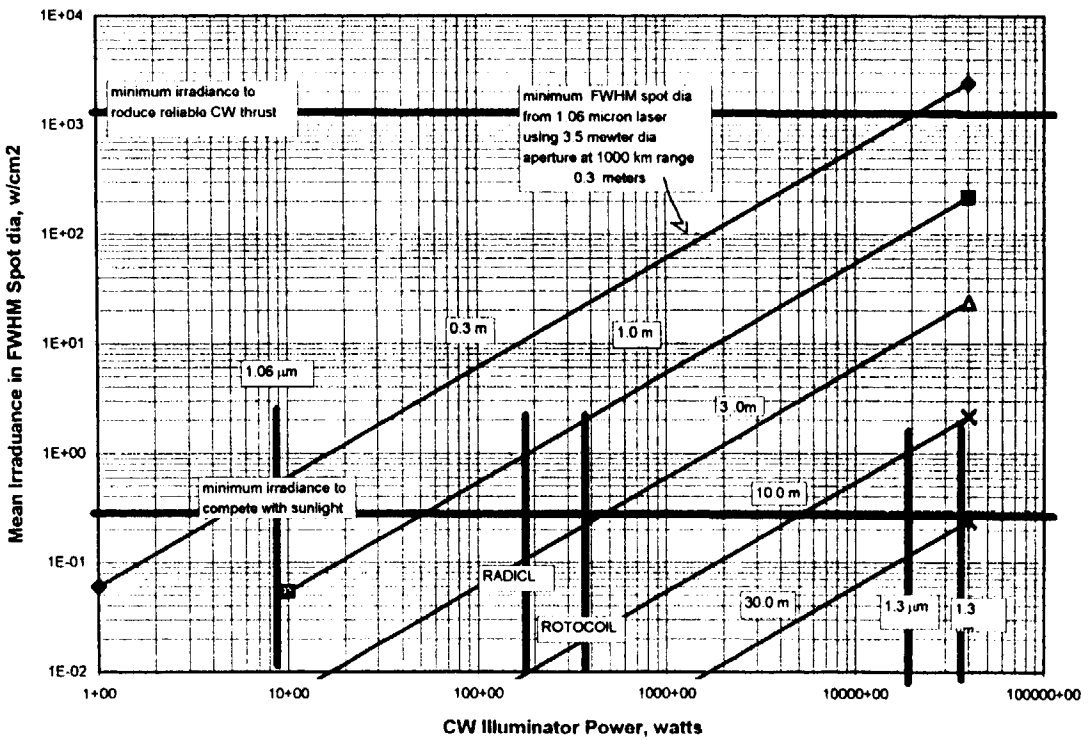

FIG 23

NST

Northeast Science and Technology

CW Illuminator:Performance against Day Sky Background

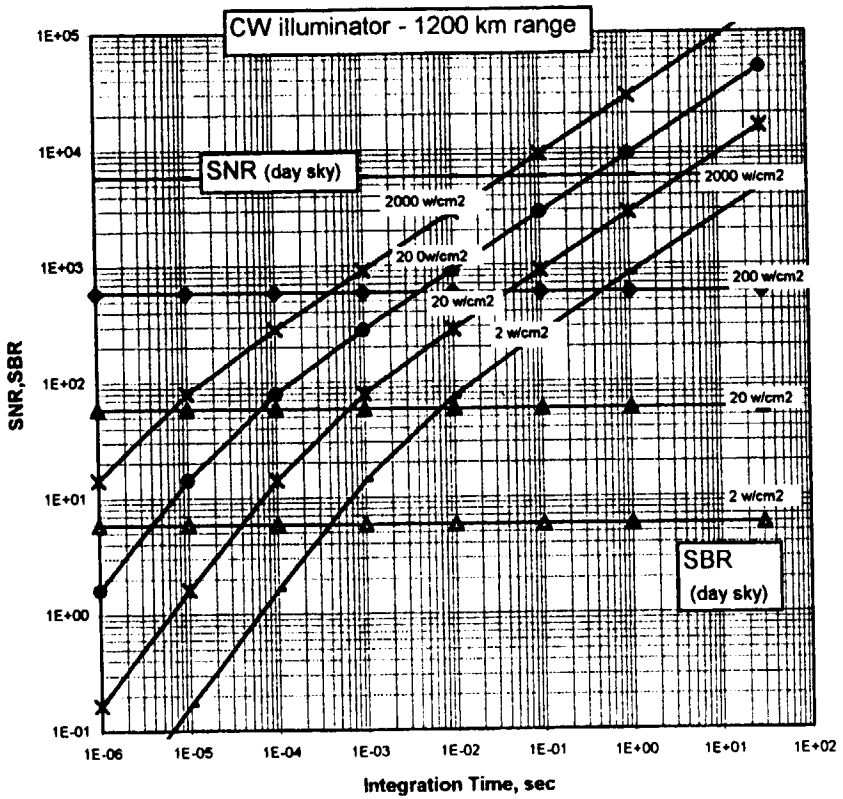

CW illuminator

1200 km range

1.06 - 1.3 micron laser

transmission = 70 %
debris reflectivty-area = 0.5 cm2
optical receiver 3.5 meter diameter
40 micron detector size
f 30 optics
10 electrons noise per readout
20 % quantum efficiency
75 % optical efficiency
day-sky bkgnd at 1 - 2 micron
= 5 E-4 w/cm^2-sr-μm

senscalc2.xls

FIG 24

NST

CW Illuminator: Performance against a Night Sky Background

Northeast Science and Technology

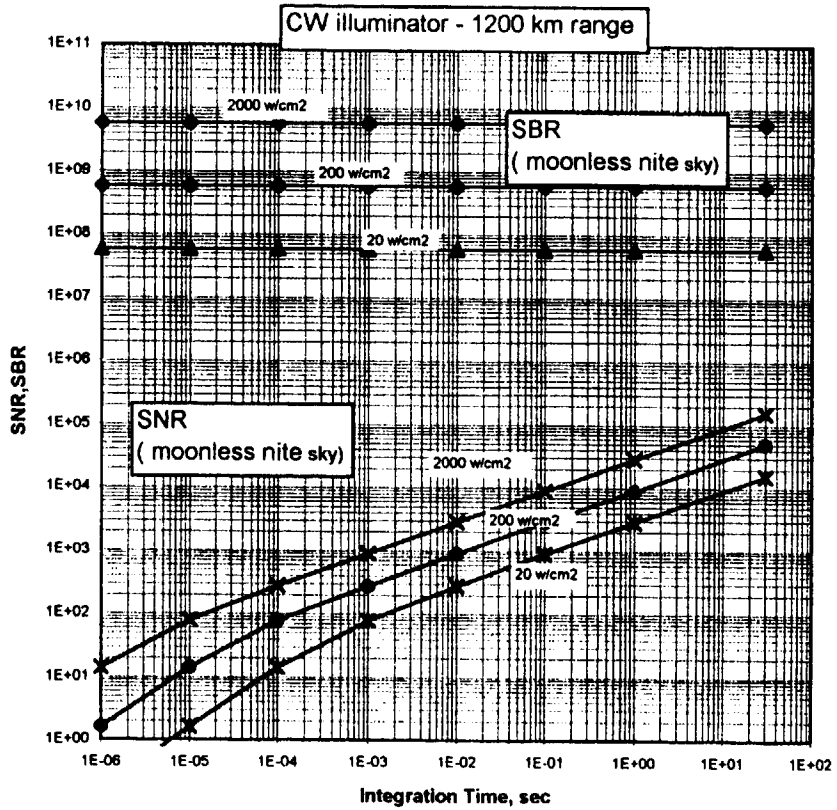

CW illuminator

200 km range

1.06 - 1.3 micron laser

transmission = 70 %
debris reflectivty-area = 0.5 cm2
optical receiver 3.5 meter diameter
40 microm detector size
f 30 optics
10 electrons noise per readout
20 % quantum efficiency
75 % optical efficiency
nite sky bkgrnd at 1 - 2 micron =
1 E -10 w / cm^2-sr-μm
(moonless clear night sky)
(from Ref 5 p 70)
(1 E -9 for full moon)

Conclusions

1. **The scanned RADAR beam** concept, using a HAYSTACK-like microwave radar appears able to accomplish the detection of the estimated 100,000 debris objects of interest to ORION in less than 1 year's time of dedicated operation (20 hrs / day, 365 days / year). To accomplish this, the current HAYSTACK detection data on this class of debris objects over the orbital altitude region of interest dictates that the beam be scanned laterally in a pattern termed a "bow tie" pattern to minimize leakage through the large planar measurement area approximately 1 beamwidth thick, 10 (or more) beamwidths wide (azimuthal sinusoidal scan) and the full orbital range high (300 km to 1500 km), controllably-oriented to put the large-area face perpendicular to the dominant debris stream being measured. The RADAR would point at about 30° elevation angle from the horizon, to provide sufficient time for Pusher Laser irradiation before the detected debris has risen in the sky from horizon to zenith.

2. **The angle-scanned passive-receiver optical system,** using sunlight to illuminate the debris objects at both dawn and dusk for approximately two hours each period also appears capable of the same success as the RADAR system described above by MIT/LL. This approach would use sunlight as the illuminator source and detect the diffuse scattering against a dark-sky background. We expect that a similar (low---say 30°) elevation angle from the horizon would be used as with the RADAR, for the same reasons. Detection in daylight using reflected sunlight appears impossible against the background of the bright day sky. The same concept of a controlled azimuthal scan to produce a "picket fence" measurement area (configured as was the RADAR "bow tie") produces a large measurement area. However, it is also necessary to used a focal plane array which is capable of "on-chip binning", to allow the collection of reflected signal photons from the debris object to be collected on an addressable sub-array of pixels on the focal plane (with correspondingly-longer integration times) and reading this sub-array out as a single "macro-pixel", so minimizing electronic read-out noise photoelectrons while maximizing signal photoelectrons. The angle-scanned passive receiver dish (the same 3.75 meter system used for the Pusher Laser) appears able to accomplish the detection of the estimated 100,000 debris objects of interest to ORION in less than 1 year's time of dedicated operation (4 hrs / day, 365 days year).

3. Initial debris detection by an **active rep-pulsed laser illuminator** , while possible according to this analysis, is very difficult. While it offers the opportunity of 24 hr / day operation(since it uses the laser to illuminate the debris, not the sun), the active illuminator detection concept appears to require substantial fluence (joules/cm^2) on target to achieve Signal-to-Noise Ratios greater than unity. We find that Signal-to-Background Ratio (ie, the contrast between the day sky and the reflected signal) is not a problem at all in this sensing technique. The high required fluence implies high laser pulse energies and/or small illumination spots---however small spots imply high pulse repetition frequencies to achieve the desired detection of the 100,000 object set in less than 1 year, even with the "picket fence" detection scheme. Trade-off studies reported here indicate that for very low orbits (the approximately 200 km Space Shuttle altitude), the laser illuminator's pulse energy and rep rate are low (300 to 1000 joule per pulse, at 20 hz using 300 meter diameter spots for illuminating, and a picket fence pattern approximately 167 beamwidths wide) .Attempting to achieve to same 1-year total detection time for objects at 600 km orbital altitudes (1200 km slant range), the laser energy could be the same, but the illumination spot has to decrease in size to provide more reflected photons which, over the longer path to the receiver, would give the same SNR as for the lower altitude detection. Calculated requirements for the 600 km

altitude region are for a 300 - 1000 joule laser pulse at 150 hz, using a 120 meter diameter illumination spot diameter at the slant range of 1200 km and a picket fence pattern approximately 420 beamwidths wide. The requirements for an illuminator useful at the 1500 km altitude (3000 km slant range) are much more demanding.

4. Initial debris detection by an **active CW laser illuminator** , while not extensively studied in this analysis, appears certainly do-able. It offers the opportunity of 24 hr / day operation at moderate transmitter power levels. It's function is to simply act as a brighter sun in the measurement area, using the same "picket fence" scanned beam and same on-chip binning concepts as the sun-illuminated detection scheme, and while suffers a bit due to the lower quantum efficiency of detectors at 1 micron as compared to those in the visible (0.4-0.7 micron), merely has to overcome sky background. It offers an additional plus--the transmitter might also act as a crude laser ranger, to assess the performance of the Pusher Laser after impulse delivery.

APPENDIX C

ENGAGEMENT STRATEGIES AND RISK

Ramaswamy Sridharan,
MIT, Lincoln Laboratories

2. ENGAGEMENT STRATEGIES AND RISK

2.1. The Problem

The mission of the ORION system is to reduce significantly the risk to manned assets in space and, to a lesser extent, provide a cleaner environment in space for satellite operations. Extensive work by NASA/JSC has resulted in a model of debris density and flux in space parameterized in various ways. Chapter 1 of this report contains a review of these models. Chapter 2 addresses strategies for removing debris from space using ORION.

The obvious strategy for removal of debris is to reduce the perigee height to below 200 Km. in a single period of irradiation. This might be called the "deluge" strategy. An alternative strategy could be to reduce the perigee height in steps of say 200 Km. This might be called "steady rain" strategy. In particular, the latter strategy might be forced on the ORION system if an adequately powerful laser cannot be found. This chapter will analyze the risk entailed in either strategy and make recommendations for one or more strategies to be tested/followed.

2.2. Debris Flux and Risk to Spacecraft

The most extensive set of data on debris of sizes > 8 mm. has been collected by the Haystack radar during the last four years. These data have been extensively analyzed by NASA/JSC[1]. There are several ways the potential risk to space assets can be derived and represented from these data. Fig. 2.1 below is

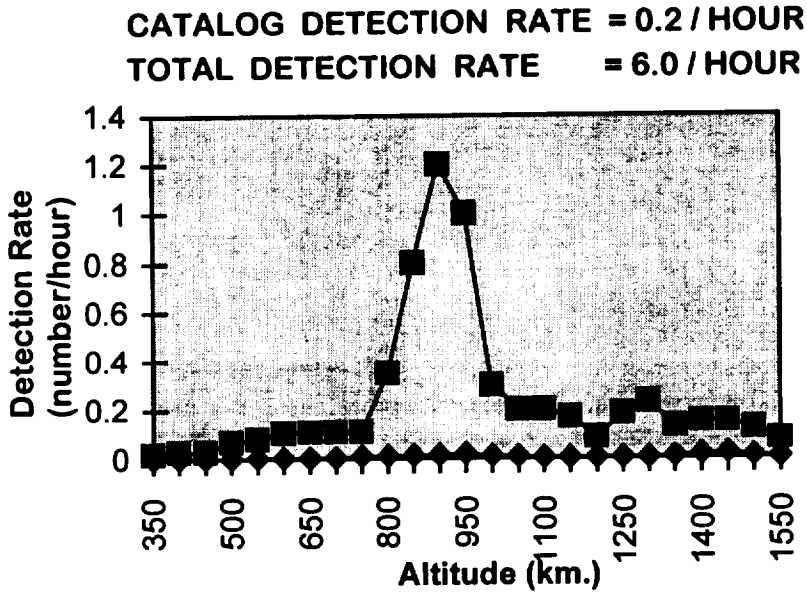

Fig. 2.1. Debris Detection Rate at Haystack Radar

drawn from the reference cited above. The two graphs represent the penetration rate by RSOs against the altitude of penetration of the Haystack radar beam when it is pointed straight up. The upper graph

[1]E.G.Stansbery, T.E.Tracy, D.J.Kessler, M.Matney, J.F.Stanley : "Haystack radar Measurements of the Orbital Debris Environment", JSC-26655, May 20, 1994.

(squares) is the actual detections and the lower graph (diamonds) is the detection rate of cataloged RSOs. The cumulative detection rate is ~6 / hour most of which are debris and hence of interest to the ORION system.

Fig. 2.2. below interprets the detection rate as a flux through a square meter of cross-section per year. This is a conventional way of representing *risk* to an orbiting resident space object (RSO). The obvious inference from the graph of debris flux is that the *population is peaked at 800-1000 Km.* Consequently, the risk to any operational spacecraft at this altitude regime(measured as flux/m^2/year) is significantly higher than at other altitudes. Further, it is estimated that there are approximately 120000 debris larger than 1 cm. characteristic size in orbit between the altitudes of 300 and 1500 Km. *Over one half (approximately 70000) of these debris are estimated to reside in the 800-1000 Km. altitude bin.* Also, most of the debris in this altitude bin are in near-circular orbits inclined to the Equator at approximately 65^0. Finally, it is important to note that *the debris in this bin correspond to debris type A* in our debris target matrix.

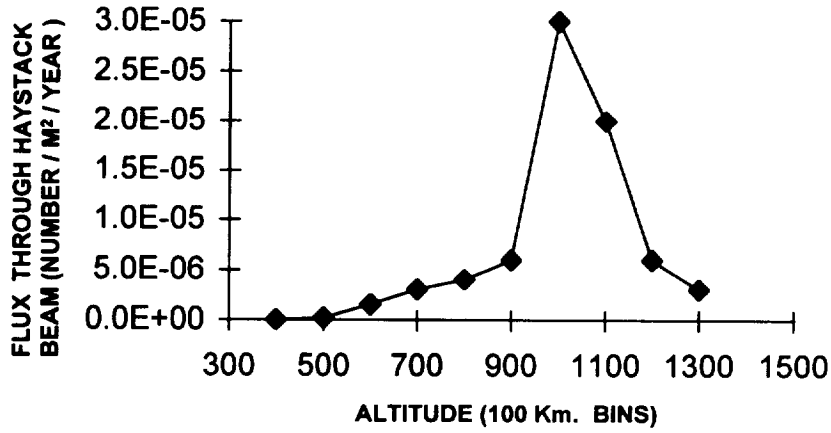

Fig. 2.2 : Flux through Haystack Beam

2.2. The Deluge Strategy

Given an ORION laser of sufficient power, this strategy would require the system to track and irradiate any debris piece that is detected. Per Glenn Zeiders' calculations, it is adequate to reduce the perigee height to ≤200 Km. for a rapid re-entry and decay (in less than a day) of the debris in the atmosphere. The risk of such a strategy is the marginal increase in collision probability with the International Space Station due to debris transiting the 400 Km. altitude regime. However, as is evident from the figures above, the risk due to the current environment is very low - in fact the collision probability of a International Space Station with a debris piece of >1 cm. size is estimated to be 1 in 70 years. Hence, despite the fact that an ORION system could "remove" ~ 100 debris objects per day, the increase in risk to the International Space Station is minimal. *Thus, the best strategy for ORION is the reduction of perigee heights of irradiated objects to below 200 Km.* However, according to Zeiders and Phipps, the penalty of this strategy is a requirement of laser average power of 150 kW. (for debris of Type A) to 500 kW. (for debris of Type D).

2.3. The "Steady Rain" Strategy

The major reason to look at an alternative strategy is the possible limitation on the power output of the laser. There is no extant laser that will meet the average and peak power requirements of the ORION system but lasers that can be scaled to meet the requirements may be available. Given such a system, it is essential to derive a strategy for debris removal that achieves the following:

1. A "staircase" type reduction of perigee height or altitude of debris.
2. Risk reduction in high risk environment.
3. No significant enhancement of risk in low risk environment.
4. No enhancement of risk to manned assets at ~400 Km. altitudes.

The recommended strategy derives directly from the distribution of debris as portrayed by Figures 2.1 and 2.2 based on extensive analyses by NASA / JSC[2].

Per the model, there are approximately 70000 pieces of debris in the 800 Km. - 1100 Km. altitude band (three altitude bins using 100 Km. bins). These are largely in the 65^0 inclination, near-circular orbits with sizes > 1 cm. Based on the putative parentage of these debris, they are expected to be near-spherical[3]. Type A in the debris matrix is representative of these objects.

The strategy then is to focus on the debris in the three altitude bins between 800 Km. and 1100 Km. The acquisition sensor should develop and use a search strategy that maximizes the probability of detection of these debris and should preferentially hand these debris off to the laser for irradiation.

The laser should ensure that the debris is irradiated adequately to reduce the perigee height by 100 - 200 Km. The laser system or the radar should then track the debris so as to assess the change in perigee height to facilitate book-keeping and to ensure that the perigee has not been put into or below the International Space Station altitude bin. If it has, then more tracking resources must be brought to bear to assess any risk to the International Space Station until the perigee height decreases below 200 Km.

A great advantage of this strategy is that the point of irradiation becomes the apogee of the orbit. Further, because the inclination of the orbit is close to the critical inclination, the argument of perigee moves very slowly. Thus, further apparitions of the same debris over the laser would be near the apogee of the orbit which, according to Zeiders, is the preferred point of irradiation for maximal effect on reducing the perigee height.

Once the perigee altitude of the debris piece has been reduced in steps to the 400 Km. bin., any further irradiation should seek to lower the perigee to 200 Km. so that the debris can decay rapidly.

The implications of the "steady rain" strategy are as follows:

1. Risk at lower altitudes is increased slightly. However, the risk is a factor of 5 - 10 times lower to begin with because of the debris distribution and hence the increase in risk is negligible.

2. Debris must be classified as to altitude bin and perhaps orbit type as soon as it is acquired by the detection sensor. Debris of interest for perigee reduction must be distinguished from other debris.

2. Post-irradiation tracking of the debris will be required so that the destination altitude bin can be identified and the effect of the laser quantified.

3. Some form of book-keeping would be required to ensure that risk in low risk environment is not unduly increased and the International Space Station is adequately safe. *However, cataloging*

---

[2] *Ibid* : E.G. Stansbery *et al*

[3] Sphericity is expected but not established - see M.J.Matney *et al* : "Observations of RORSAT debris using the Haystack Radar", presented at the Space Surveillance Workshop, MIT Lincoln Laboratory, March 95. Experiments with the Lincoln radars will answer this question.

of the debris is not required except in case the risk to the International Space Station has been increased.

Apart from the International Space Station, there is significant concern about the operational safety of unmanned payloads in orbit. The distribution of these payloads in the current space surveillance catalog is depicted in Fig. 2.3. It is evident that active payloads are concentrated in the 700- 900 Km. altitude bins while the population of inert payloads peaks at these altitudes too. Hence the strategy recommended above is deemed safe from the safety of operational unmanned payloads.

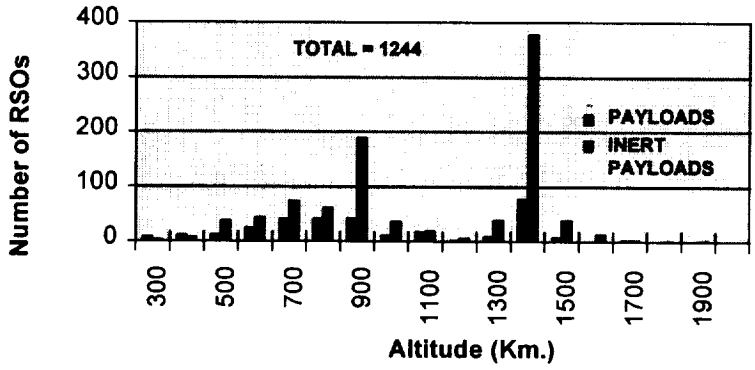

Fig. 2.3. Distribution of Cataloged Payloads

It is evident from the figures in this section that there is a secondary peak of both payloads and debris in the 1400 Km. altitude bin. If the ORION system were capable of irradiating these debris, a similar strategy to that outlined above is appropriate. *However it must be ensured that before these debris occupy the 900-110 Km. perigee bins, an adequate number have been removed from these lower bins so that operational safety of unmanned spacecraft at these altitudes is not worsened.*

2.4. Recommendations

The removal of debris in one irradiation remains the best strategy for debris mitigation. However, no such laser of adequate power and operational capability is expected to exist in the near future. Hence, a strategy for operations is recommended for the ORION system that will enhance its effectiveness in its task of cleaning out the debris environment. This strategy takes advantage of the debris density concentration in the 800 - 1000 Km. altitude band and recommends a staircase mode or "steady rain" technique of removing debris.

6. DEBRIS ACQUISITION AND TRACKING WITH MICROWAVE RADARS

6.1. The Problem

The ORION laser faces significant technical and political problems in autonomously acquiring debris for irradiation. Hence, a system is needed whose function would be "to seek, to find and to hand-off" to the laser. Specifically, the functions to be performed by the acquisition system are:

1. Autonomous detection of debris of interest to ORION.
2. Precision tracking of the debris.
3. Rapid discrimination using orbital and signature data.
4. Handover to the ORION laser for irradiation.
5. Assessment of the effects of the laser on the debris.
6. Book-keeping of debris, particularly in case the "steady rain" strategy of debris removal is used.
7. Adequate throughput to match the appetite of the laser.

There are at least three possible types of systems that can achieve these objectives. They are conventional microwave radars, conventional visible wavelength optical systems and unconventional serendipitous detection systems using communication satellites as transmitters. This chapter analyzes the use of microwave radars as acquisition systems for ORION.

6.2. Why Radars ?

The advantages of microwave radars are the following:
1. There are high sensitivity radars available in the inventory of AF and Army Space Commands and at least at one other location in Germany.
2. Radars are generally capable of all-weather day/night operation thus enabling the ORION laser to work in cloudless day and night conditions.
3. Microwave radars generally have high metric precision and near-real-time signature processing capability thus supporting the discrimination and handover requirements.
4. The mechanical /electronic dynamics of the radar permit stare-and-chase operations as are needed for ORION and also permit a high throughput of debris tracking.

The disadvantages of microwave radars are:
1. The radars are high cost items if a new system has to be procured (see Chapter 12).
2. Generally, the high sensitivity radars have a narrow instantaneous field-of-view which complicates the search and acquisition process and requires creative techniques for enhancing throughput.
3. Existing radars are not optimally located for laser operations.

On balance, microwave radars are an attractive option for the ORION system.

6.3. The Choice of Radars

Microwave radars operate at a range of frequencies from VHF (150 MHz) to W-band (95 GHz) in discrete frequency regions. The debris sizes (1 - 10 cm.) that we are considering is a major driver in the choice of frequency. Below L-band (~1300 MHz), the radar cross-section of debris smaller than 5 cm. is so small as to preclude effective detection. Further, for a given small debris (1 - 5 cm.), the radar cross-section at > 10 GHz. frequency is ~10 dB higher than at L-band or S-band (2 GHz.). Hence, the desirable range of frequency of operation of a radar is X-band (10 GHz.) or higher.

At present, the high power tubes for X-band radars are easily available while for higher frequencies, such tubes are experimental, particularly for the high powers (~> 100 kW) required by this applica-

tion. Hence a X-band radar is the ideal option with a C-band (4 GHz.) being an attractive alternative. Higher frequencies of the order of Ku-band (16 GHz) and K-band (35 GHz.) may be attractive alternatives in a few years.

There are weather considerations to be taken into account in radars too. Below C band, the weather has negligible effect on the radar. At X-band and above, moisture in the air and rain take an increasing toll on the sensitivity of the system. For example, the sensitivity of an X-band radar could decrease by 3 dB. in heavy rain while the K- and W-band radars would suffer substantially larger attenuation in humid atmospheres. Hence it is preferable to operate a radar for the ORION system at lower frequencies.

The available radars and their parameters in the frequency ranges of interest are given in Table 6.1. Notice that a UHF radar has been included because it is a high sensitivity phased array radar. The sensitivity of these radars is portrayed in the conventional manner as the S/N ratio obtained on a single pulse on a 0 dBsm.(or a 1 sq. meter) target at a slant range of 1000 Km. from the radar. A brief description of the radars and their operating characteristics is included in Appendix 6.1. Table 1 only lists the existing radars. Raytheon Company has paper designs for an upgraded X-band phased array radar and for a X-band interferometric radar system both of which would be suitable for the ORION system; however, these are unfunded at present. Further, existing C-band radars have not been included because they are not sensitive enough to detect the small debris of interest to the ORION system. It is quite conceivable that an existing C-band radar could be upgraded with a bigger antenna (say 25 meter) in which case it would be a viable candidate.

The Haystack radar is the most sensitive of the lot. It is exceeded only by the Arecibo and Goldstone radars neither of which are capable of tracking near-earth satellites and hence are not included in the table. The HAVE STARE system is intermediate in sensitivity between Haystack and HAX. Haystack, HAVE STARE and HAX operate in the desired frequency range. The TRADEX radar, which is located on the Kwajalein atoll, has the same sensitivity as Millstone. There is a German radar (FGAN) that is sensitive enough for the ORION system requirements but was not pursued further because of its location, its status as a University research radar and the lack of information on its detailed operating characteristics (this could be pursued in Phase 2 if desired).

TABLE 6.1 : AVAILABLE RADARS

	HAY STACK	HAVE STARE	HAX	MHR*	FPS-85
SENSITIVITY (dB/pulse) (S/N on 0 dBsm at 1000 Km)	61-65		47	48	50
PULSE LENGTH (ms)	2 - 5	0.175	2	1	0.25
FREQUENCY (GHz)	10	10	16	1.3	0.44
RANGE PRECISION (m)	1-10		1-10	10-25	25
BEAMWIDTH (deg)	0.05	0.075	0.1	0.44	1.0
ANGULAR RATE (deg/sec)	2, 2^	5, 3	10, 10	3, 3**	NA
ENCODER LSB (mdeg)	0.3	0.3	0.15	1.7	NA
TRACK PRECISION (mdeg)	0.5-1.0		1-2	3.0	25
PRF (Hz)	40 -100		40-100	40	20
LOCATION (deg. Latitude)	42.6	32?	42.6	42.6^^	28

*TRADEX SIMILAR TO MH
**TRADEX RATES 10° / sec.
^RATES IN AZIMUTH, ELEVATION
^^TRADEX LOCATION 8° LATITUDE

Table 6.2 below gives the expected radar cross-section of the debris matrix targets. Note that Target F is omitted from the table as it is a rocket body that is large and hence easily detectable by all the ra-

dars. Table 6.3 gives the expected S/N ratio on the debris matrix targets at a range corresponding to an elevation of 30^0.

TABLE 6.2. RADAR CROSS SECTION OF DEBRIS MATRIX TARGETS

RADAR	FREQ (GHz.)	A	B	C	D	E
			(RCS in dBsm.)			
Haystack^	10	-40	-40	-35	-30	-18 /-30*
HAX	16	-40	-40	-35	-30	-18/-30
MHR	1.3	-50	-50	-43	-35	-18/-35
FPS-85	0.44	ND	ND	ND	ND	-23/ND

^ HAVE STARE = Haystack * Maximum / Minimum
ND = Not Detectable

TABLE 6.3 : S / N RATIOS FOR DEBRIS MATRIX TARGETS AT ACQUISITION

Debris Type	A	B	C	D	E
Avg. Altitude (Km.)	907	875	663	1170	1002
Range at 30^0 Elevn. (Km.)	1560	1510	1180	1955	1705
S/N for Haystack (dB) (appropriate pulse)	17.3	17.8	23.1	19.3	25 - 37
S/N for HAX (dB) (2 ms. pulse)	0	0	9.1	1.3	7 - 19
S/N for TRADEX (dB)	-10	-9.5	2	1.5	18 / 1.5

It is evident from Table 6.3 that a radar similar to Haystack is the instrument of choice for the debris matrix targets as the expected S/N ratio is over the threshold of delectability (12 dB). The HAVE STARE radar can be upgraded to nearly Haystack's performance and would then be viable for the task.

6.4. Operation of Haystack (or similar) Radar for ORION

A concept of operations will be described in this section for a radar to act as the "debris finder" for the ORION laser. As part of the concept, the requirements/capability to perform all the functions tabulated in 6.1 will be stated.

6.4.1. Autonomous Detection of Debris

It is essential for the radar to have adequate time to acquire, track, discriminate and handover the target to the laser. The discrimination task will take several minutes to complete and hence it is essential for the radar to acquire the debris early in its apparition. Hence, the optimum strategy is for the radar to point at ~30^0 elevation and conduct a small scan. The choice of azimuth is dictated by the location of the radar and the inclinations of the orbits that are of prime interest. Since most of the debris are in high inclination orbits, a radar on or near the equator could point due north or south at 30^0 elevation for detection. However, Haystack is located at 42.6^0 north latitude and hence pointing due south is recommended as it improves the inclination coverage significantly (see Appendix 6.1).

The Haystack radar (or an upgraded HAVE STARE radar) has a very small beamwidth (instantaneous field-of-view) of the order of 0.05^0. Long experience with Haystack has established that in a stare mode pointing straight up, the radar detects, using a 1 ms. pulse, an average of 6 debris targets/hour (see Chapter 2) between the altitudes of 500 Km. and 1500 Km. At an elevation of 30^0, the radar loses ~9.5 dB in sensitivity due to the increase in range for the same altitude range. However, using a 5 ms. pulse mode, the radar can regain 7 dB in sensitivity. Additionally, the debris targets transit through the beam at a slower angular rate (see appendix 6.1) thus allowing multi-pulse summation to retrieve the remaining sensitivity "loss". Hence, we expect that the rate of detection would be of the order of 6 targets/hour in this mode. *However, this has to be established by experiment in Phase 2.* Unfortunately, half of these targets will be setting. Out of the three left, only one might come into the field-of-view of the laser. Therefore, methods have to be sought to enhance the rate of detection.

Detection statistics can be enhanced by conducting a scan with the radar. There are three modes for such a scan:

1. A mechanical "bow-tie" scan of ~20 beamwidths which can be essentially "leakproof" and will cover a 1^0 swath in azimuth. Since there is no requirement for the scan to be leak-proof, a larger scan can be employed if it is consistent with antenna dynamics.
2. An electronic scan that can be imposed on the beam by building a phased-array "lens" into the high power beam path between the feed and the Cassegrainian subreflector. Such a capability was designed for the HAVE STARE but was never built. It is fairly expensive and also reduces the sensitivity by about 2 dB.
3. An electronic scan that is generated by redesigning the high power feed as a small phased array. This has the advantage of avoiding the sensitivity loss but is still a complex upgrade.

It is our recommendation that the mechanical scan be tested in Phase 2. The other techniques are expensive (several million) and complex and should be resorted to only if the mechanical scan cannot satisfy the appetite of the laser. The gain in detection statistics to be expected increases at least linearly with the scan width and should be verified in Phase 2.

6.4.2. Precision Tracking of Debris

Once a debris target is detected the radar has to initiate tracking in what is essentially a transition from a 'stare" mode to a "chase" mode. This is a classic capability of most radars for detecting space objects with large radar cross-section. However, the chase operation for a debris with small RCS of the types of interest to ORION system is more challenging because the S/N ratio in the monopulse angle channels is not large. It is the signal in these channels over several pulses that enable the radar to determine the direction and rate of movement and initiate a chase.

The HAX radar, collocated with the Haystack radar has recently developed a "stare-and-chase" capability for debris targets. Since both Haystack and HAX share the same control system, the "stare-and-chase" algorithms can be transitioned to Haystack with small modifications. While the Haystack radar does not support the high angular rates of the HAX (see Table 6.1), we believe that it is still capable of the "stare-and-chase" mode. *Again, this is amenable to test in Phase 2.*

The Haystack radar can track in four dimensions - azimuth, elevation, range and range rate. The current precision in these dimensions is:

Elevation	10 - 35 μrad.
Azimuth	((10 - 35)/cos(elevation)) μrad.
Range	0.25 - 2 meters
Range Rate	1 - 10 millimeters/second.

Bias uncertainties in the metric data from the Haystack radar are of the same order as the precision.

Accurate tracking of the debris is required to ensure that the acquisition window for the laser is not large. The handover volume is dominated by the angle uncertainty and, at worst, is of the order of 35 μrad which translates to 35 meters at 1000 Km. This is certainly acceptable to the acquisition mode of the laser. *If a smaller handover volume is required, near-real-time processing of the metric data is required with a Kalman-type filter, along with better calibration techniques. These are available and amenable to testing in Phase 2.*

6.4.3. Discrimination

This is probably the most time-consuming and complex task for the radar. The requirements are as follows:

1. Verify that the debris is in an ascending pass.
2. Ascertain the catalog status of the debris in track.
3. Ensure that the estimated size and, if required, dynamics of the debris are within the capability of the laser.
4. Measure periodicities in the signature.
5. Check whether the debris will transit the laser field-of-view for the time interval required by the laser system to successfully irradiate it.
6. *Guarantee that no other resident space object, and in particular, no payloads will be illuminated by the laser inadvertently during the engagement.*
7. *Guarantee that no airplane intercepts the laser beam during the engagement.*

6.4.3.1. Correlation with the Catalog

The monopulse data recorded during the transit of the debris through the beam is adequate to discern whether the target is in an ascending pass. If not, the search can be resumed. As soon as ~ 30 seconds of metric data (or ~5 observations) are taken, an initial orbit can be estimated and checked to see if the debris will be within the field-of-view of the laser for the required time interval during this apparition. If not, the radar can return to its search scan. A correlation with the catalog should be done next. The data quality is adequate to yield a good estimate of the orbit of the debris which can be checked against all the RSOs in the catalog. This task should take no more than 5 seconds with a modern work station and appropriate architecture of the software. If it is a known large RSO, the search for debris can be resumed. If it is a cataloged piece of debris, a real-time decision needs to be made based on the following:

1. Is it of interest to the ORION system - depending on strategy and size?
2. Who nominally "owns" the cataloged debris? Does the ORION system have "permission" from the "owners" to irradiate their debris?

Given a positive answer to both questions, the next step can be taken.

6.4.3.2. RCS, Size and Dynamics

As the tracking of the debris piece continues, the radar must estimate the mean RCS and perhaps a variance. The signature data must also be analyzed through the mechanics of algorithms like auto-correlation or Fourier transform to determine any periodicities.

The mean RCS is used to estimate a characteristic size for the object in track. A quick method is to use the graphical relationship established by NASA/JSC by measuring 39 debris-like targets at various radar wavelengths[1] (see Fig. 6.2). It must be realized that this is quite approximate as the estimate of mean

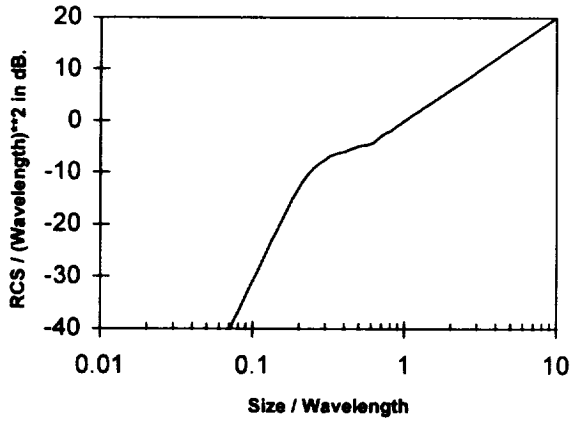

Fig. 6.1 : RCS - to - Size Scaling Chart

RCS is significantly affected by periodicity in the signature and, further, debris are known to have periodicities ranging from ~0.1 sec. to >>30 sec. which will significantly affect the estimates (see Appendix 6.2 on the characteristics of debris).

The value of estimated periodicity in the signature lies in the fact that it will be significantly affected by the impact of the laser energy and, hence, it can be used as an indicator of the success of the engagement.

The inferred size of the debris must be compared to a threshold set for the ORION system to decide on the engagement. The periodicity may prove useful for the same purpose.

6.4.3.3. Inadvertent Illumination of RSOs

A major concern with the ORION system is its potential for inadvertently illuminating and damaging a payload in orbit. This concern is motivated by both treaty implications and the cost of "friendly fire".

Once the debris has passed the filters in the previous sections and deemed suitable for engagement by the ORION system, a detailed prediction needs to be made of the part of the trajectory that the laser would illuminate. *This prediction has to be compared with the known position of the entire catalog of payloads to guarantee that inadvertent illumination does not occur. Further, US Space Command may require that a real-time check be made with a small catalog of important domestic payloads to preclude damage or interference.*

A question that remains is whether it is adequate to check against the locations of payloads or whether rocket bodies and other large objects in the catalog must be included in this check. The concern stems from the possibility of inadvertently causing a rocket body with left-over fuel to explode. Part of the answer is political. *The technical part of the answer will come from an analysis of the impact of the laser on the debris Matrix Target F.*

---

[1] E.G.Stansbery *et al* : "Haystack Radar Measurements of the Orbital Debris Environment", NASA/JSC-26655, May 20, 1994, p. a29.

One method of guarding against inadvertent illumination is for the acquisition radar to examine the space along the trajectory a little ahead of the ORION laser (an advance guard) with the ability to positively cut the laser off in case of a low altitude RSO detected in the beam (of course, this works only when the laser and the radar can simultaneously observe the debris). However, it is unlikely that RSOs at all altitudes can be detected in this mode and the catalog will have to be relied on for avoidance of the high altitude satellites. Since the ratio of low altitude to high altitude RSOs is ~5:1, this will be an effective technique that will reduce computational complexity. *This is a capability that could be demonstrated in Phase 2 at the Lincoln Space Surveillance Complex using Haystack radar and the Firepond laser.*

The Airborne Ballistic Missile Defense Laser (ABL) being built by AF Phillips Laboratory faces some of the same issues and the solution would be useful to ORION. Other systems like SBV/MSX, SWAT, Firepond laser and AMOS/Maui laser system have faced some of the same issues.

This is a major issue for the ORION system. It will affect decisions on site location and modes of operation.

6.4.3.4. Aircraft Avoidance

Regardless of the wavelength of operation of the laser, the ORION system has to ensure that it does not inadvertently illuminate an aircraft. Unlike RSOs, aircraft do not follow predictable trajectories. It is prudent to choose a site where major air traffic lanes can be avoided. But, in any case, the ORION system needs a real-time means of detection and avoidance of aircraft.

The technique postulated in the last section for avoiding RSOs by running an advance guard with the radar will not work for aircraft avoidance because of pulse lengths used except in case a new phased array radar operating at X-band is built for the ORION system. Optical guard bands using small telescopes will work or an aircraft detection radar can be built into the system. Since the FAA is shutting down a significant part of their radar system due to reliance on GPS technology, such a radar may be available to the ORION system "free".

This is a major issue for the ORION system. It will affect decisions on site location and modes of operation.

6.4.4. Radar - Laser Handover

Once a debris has passed all the filters listed above, it has to be handed off to the ORION laser for irradiation. The process in concept is very simple as the precision tracking of a Haystack-like radar is adequate to narrow the search volume for the laser. There are two types of handover.

A real-time handover occurs when the radar and laser are collocated. In this case, the only issue is the mutual calibration of the laser and the microwave radar pointing systems. This is not a major issue as substantial experience exists at MIT Lincoln Laboratory and other places. The radar continues to track the object until a successful handover has taken place. Note that this has a small impact on the concept of advance guard for avoidance of inadvertent illumination. However the fact that the beamwidth of the radar is significantly larger than that of the laser mitigates this impact.

A non-real- time handover occurs when the radar and the laser are not collocated. In such a case, the radar will have to determine a precise orbit and transmit it in some form to the laser system. The accuracy of the prediction is an issue that is being studied by AF Phillips Laboratory. Again, precise pointing calibration of both systems is a solvable concern. Note that in this case, the concept of using the radar in a guard band mode for avoiding inadvertent illumination does not apply.

Concerns pertaining to the handover for both real-time and non-real-time can be addressed in Phase 2 using the collocated and spatially dispersed set of MIT Lincoln installations.

6.4.5. Assessment

A critical issue is the assessment of the effects of the laser irradiation on the debris. The questions that need to be answered are:

1. Did the target interact with the laser energy?
2. Can the mass, area/mass ratio or some similar parameter for the debris be estimated?
3. Can the characteristics of the laser-debris interaction be measured or inferred?
4. What is the perigee bin of the target post-irradiation?
5. Is there a threat to a manned asset as a result of the orbit change?

There are four methods that can be used to perform these assessment tasks:

1. Measure the plasma "flash" created by the laser-particle interaction.
2. Measure the "instantaneous" Doppler change of the target as a result of the interaction.
3. Measure the change in the periodicity of the signature.
4. Compare the estimated orbits pre- and post-irradiation.

The plasma "flash" is expected to occur on every pulse of the laser that hits the target. A visible wavelength optical system, if collocated with the laser, can measure this effect. It is unknown whether there will be an enhancement of the radar cross-section as a result of the plasma though experience with observing large transtage thrusts indicates otherwise. The flash will clearly indicate that the target has been hit. It is unknown whether the plasma will be quenched rapidly enough such that the interaction due to each pulse can be monitored.

The Doppler of a target can be measured very precisely by a microwave or laser radar using techniques of Fourier Transforms. Also, depending on the accuracy of the track, Doppler can be inferred from range measurements. In either case, if the target is monitored while being irradiated by the laser, the departure of the measured Doppler from prediction based on the pre-radiation orbit is a clear and rapid indicator of laser effects. This technique is routinely applied at Lincoln radars for monitoring orbital maneuvers. However, it must be remembered that if the radar tracks the debris along with the laser, it cannot provide an advance guard to protect against inadvertent radiation of RSOs.

Continued tracking of the debris post-radiation will yield an estimate of the periodicity of the signature. This is very likely to have changed as a result of the laser-debris interaction and can both confirm the interaction and, perhaps, provide a quick but poor estimate of the moment of inertia of the debris. Further, the tracking data can be processed into an estimate of the orbit which, when compared with the pre-radiation orbit, can yield the following.

1. An estimate of the total velocity change imparted to the debris.
2. The perigee bin into which the debris has been moved.
3. An estimate of the mass of the debris if the intensity of the laser at the location of the debris is known and the size of the debris is known.

The new orbit must be used immediately to assess whether the threat to a manned satellite has been increased. If the new perigee height is lower than that of the manned asset, but is >200 Km., cataloging of the debris by further tracking is essential so as to provide adequate warning of close approaches.

6.4.6. Miscellany

Book-keeping of the debris merely refers to creating a histogram of the number of objects irradiated vs. the perigee bin in say 100 Km. steps before and after. This is to ensure that the risk in lower altitudes is not unduly increased and applies only in the case of the "steady rain strategy".

The throughput of the radar is governed by the approximately 10 minutes of total tracking plus the search time to find the debris. *The best it can be with one radar is 4-6 objects per hour or ~100 objects/day given 24 hour operation.*

6.5. Summary

This chapter has presented a solution for the problem of acquiring and handing off debris to the laser system and also suggested techniques for verification and assessment off the laser-debris interaction. Existing radars have been examined along with a few near-term new radars and a specific radar (Haystack) has been recommended for near-term use. There remain several issues that need to be addressed by some study and experimentation in a Phase 2. These are:

1. Detection statistics of debris :
Depending on the appetite of the laser, a high rate of detection of debris may be needed. Techniques have to be investigated for using a narrow beam radar in appropriate modes to enhance the detection of desirable debris.

2. Stare-and-chase of debris at Haystack:
The Haystack radar was designed with reasonable angular rates but has not ever been tested in a stare-and-chase mode. Since this is crucial to the use of the radar for ORION, it has to be tested.

3. Inadvertent Illumination of RSOs:
This is critical issue for ORION system. Techniques have been suggested in this section including prescreening of laser pointing and a "advance guard" approach. It is crucial to test these prior to any decision to design and field a laser system.

4. Radar-Laser Handover

Handover between collocated sensors has been amply demonstrated at the Lincoln space Surveillance Complex and also at Lincoln's KREMS facility. However, if the laser is not collocated with the radar, the handover is a slightly more difficult issue. Experiments can be conducted using Lincoln's dispersed facilities to demonstrate the accuracy, calibration and hand-off systems needed for the purpose.

A radar -based detection, acquisition, handover and assessment system seems quite feasible for the ORION system. There is at least one available radar system that fits the requirements. A few issues and concerns remain that can be answered with some study and experimentation.

Appendix 6.1 : Description of Radars

6.1.1. Haystack radar

This flagship of the radars built and operated by MIT Lincoln Laboratory is by far the most sensitive satellite tracking radar available today. The only radars with higher sensitivity are Arecibo and Goldstone, both of which do not have the angular rate dynamics to support satellite tracking. Located in Tyngsboro, Massachusetts, this radar is part of the Lincoln Space Surveillance Complex and operates at 10 GHz. with a 35 meter antenna. Its advantage is its high sensitivity. Its disadvantage is the relatively northern location which will preclude its effective tracking of debris in low inclinations.

Haystack, HAX and Millstone Hill radars are part of the Lincoln Space Surveillance Complex located at ~42.6^0 North latitude. The preferred mode of operation cited in Chapter 6 for the Haystack radar is to point due South at 30^0 elevation. The location and the pointing impose a restriction on the inclinations of the orbits o f the debris that will be seen by the radar. If h is the altitude of the circular orbit, θ is the latitude of the site, φ the minimum inclination of the orbit detectable at 300 elevation and R the radius f the earth, then the relationship of these quantities is given by

$$\sin (60^0 - \theta - \varphi) = (R \sin (120^0) / (R+h)$$

Figure 6.1.1. below illustrates this relationship for Haystack radar.

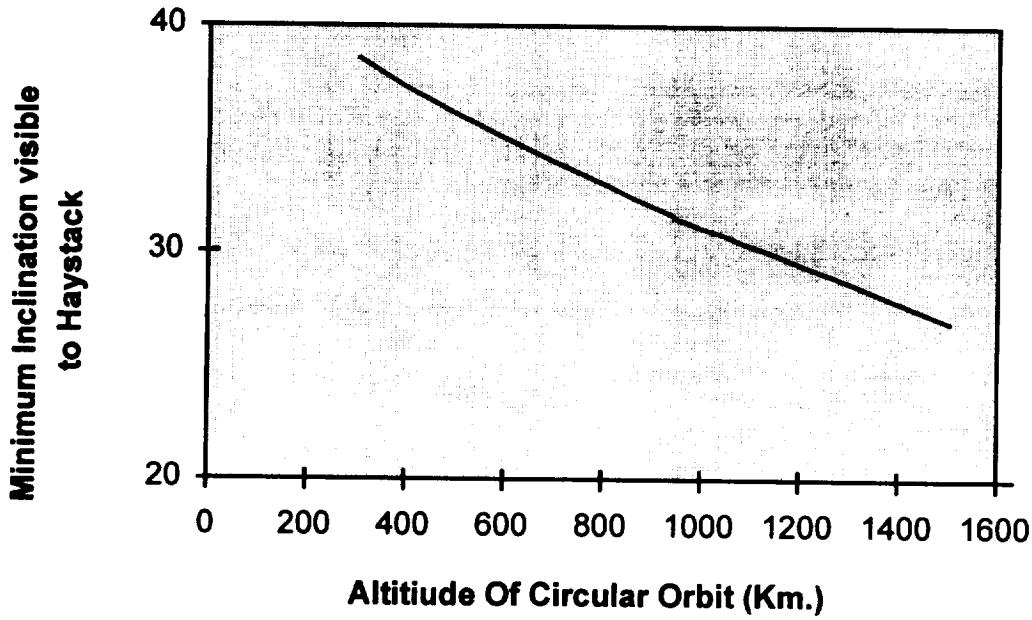

FIG. 6.1.1 : INCLINATION LIMITATION FOR HAYSTACK RADAR

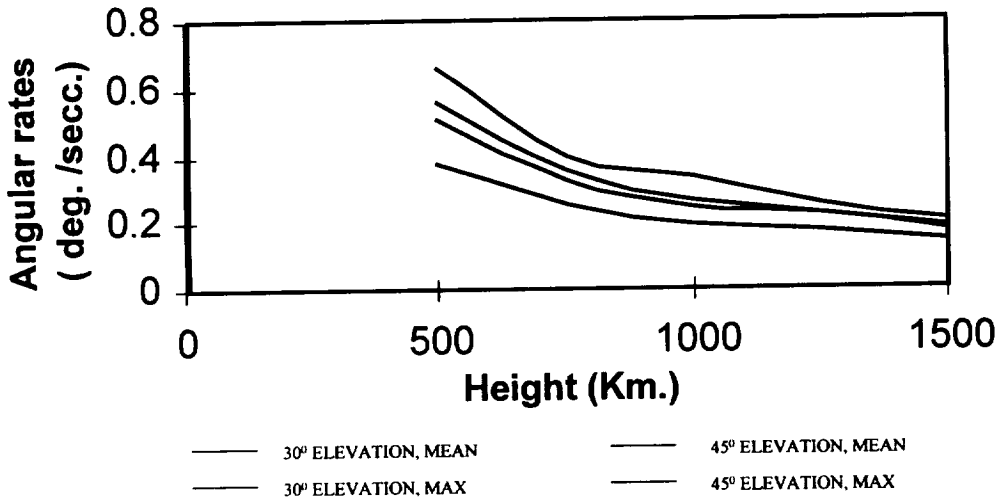

FIG. 6.1.2. : ANGULAR RATES OF DEBRIS

The Haystack radar has many waveforms: from 5 ms. CW for high single pulse detection sensitivity to 256 μs. pulse with 1 GHz. of bandwidth for high resolution imaging. The antenna rate are adequate to support stare-and-chase operations at reasonable ranges(altitudes). Fig. 6.1.2. shows the angular rates expected of debris in near-circular orbits at 30 deg. and 45 deg. elevations.

6.1.2. HAX radar

HAX is an adjunct to the Haystack radar that was built under NASA sponsorship. It operates at Ku-band at 16 GHz. with a 2 GHz. bandwidth for high resolution imaging. HAX and Haystack share the same control and processing system thus restricting their use to only one system at a time. HAX has high angular rates and accelerations that render it suitable for easy stare-and-chase operations. The sensitivity of the radar is restricted by the size of its antenna and hence is not usable for the ORION mission except in the low altitude regime (for >5 cm. objects at <1000 Km.).

6.1.3. Millstone Hill radar

This radar is collocated with Haystack. It operates at L-band (1295 MHz) which is a frequency lower than desirable for the ORION mission. If for any reason, cataloging of debris objects >3 cm. upto 1500 Km. altitude is required, this radar would play an important part. Further, if, as a result of ORION laser action, there is concern about hazard to a manned asset, this radar would be brought into play, along with its sister radar TRADEX on the Kwajalein atoll, for refining the orbit estimate of the debris.

6.1.4. The FPS-85 radar

This is a large phased-array radar that operates at 440 MHz. and is located in the Florida panhandle. While its relatively southern location and electronic agility offer great advantages, its frequency of operation precludes it from being an effective detection sensor for the ORION system.

Appendix 6.2 : Some Characteristics of Debris

NASA/JSC has been collecting debris data with a variety of sensors over the years. Chief among these is the Haystack radar whose data have begun to condition the debris models substantially. Collocated with Haystack are the HAX and the Millstone hill radars both of which are tracking radars but with somewhat less sensitivity than Haystack. The description below of the characteristics of debris is derived largely from the participation of the Millstone hill radar in the debris campaigns run by AF Space Command. Hence, the results are from a biased sample of debris with characteristic sizes larger than ~5 cm.

The periodicities in the signatures of debris presumably equal to or a fraction of the spin period) range from as low as 0.1 sec. to tens of seconds. There are inadequate statistics to assign a probability function to the spin period. All that can be stated at this point is that it would be invalid to assume that the thrust due to ablation caused by the interaction of the laser energy with the surface of the debris would be in the line-of-sight direction on an average. This will be true only if the debris is irradiated over several spin periods at a rapid rate compared to the spin period.

The radar cross section of the debris particle is not always a clear indicator of the size of the debris as there are objects that seem to be brighter (and larger) at optical wavelengths and dim (and smaller) at microwave frequencies. The percentage of such debris is an unknown at present. If it is a small percentage, it does not affect the functioning of the ORION system. If, in the unlikely event, it is a large percentage, then the ORION system must employ an optical acquisition system in addition to a radar system. Or the importance of the laser as an acquisition system is enhanced.

7.0 ACQUISITION AND TRACKING OF DEBRIS WITH VISIBLE WAVELENGTH OPTICAL SYSTEM

7.1 The Problem

The ORION laser faces significant technical problems in autonomously acquiring debris for irradiation. Hence, a system is needed whose function would be "to seek, to find and to hand-off" to the laser. Specifically, the functions to be performed by the acquisition system are:

a) Autonomous detection of debris of interest to ORION,
b) Coarse tracking of the debris,
c) Rapid discrimination using orbital and signature data,
d) Handover to ORION tracker to point laser for irradiation (this precision tracker will almost certainly be optical)
e) Assessment of the effects of the laser on the debris,
f) Book-keeping of debris, particularly in case the "steady rain" strategy of debris removal is used, and
g) Adequate throughput to match the appetite of the laser.

There are at least three possible types of system that can achieve these acquisition and assessment objectives. They are conventional microwave radars, conventional visible wavelength optical systems and unconventional serendipitous detection systems using communication satellites as transmitters. This chapter analyzes the use of visible wavelength optics as acquisition system for ORION.

7.2 Why Optical Systems?

The advantages of optical systems are the following:

a) High sensitivity optical systems can be built for significantly lower cost than similar microwave radars.

b) Optical systems can be designed with a significantly larger instantaneous field-of-view than conventional microwave radars.

c) High throughput of debris detection is achievable.

d) Adequate capability for metric tracking is available.

The disadvantage of optical systems are as follows:

a) Optical systems will work only at night in clear weather, thus reducing the available hours per day.

b) There are no immediately available optical systems of the kind needed for ORION.

c) Discrimination capability of broadband optical systems is somewhat more limited than that of radar.

7.3 Requirements

The major requirements for autonomous acquisition include being able to acquire and (coarse) track the specified range of debris particles, to provide an adequate acquisition rate so that targets can be dealt with at a reasonable rate, and to hand-over to a precision (optical) tracker for beam pointing. The additional

functions noted above — discrimination, assessment of effects, bookkeeping — can be provided by an optical system. In particular a precision tracker operating on handover from the optical acquisition system could provide target angle position information to better than microradian accuracy from which good target orbit information could be deduced. Target velocity would not be available (unless an active coherent system were being used) as would be the case for a radar tracker. Target optical signature time history would provide some good discrimination information. When illuminated by the Pusher Laser, the backscatter and the radiation from a plasma could be sensed for additional information.

For optical acquisition, the most stressing of the targets optically is the smallest/dimmest — a 1 cm sized particle with a reflectivity (albedo) of 0.1. An optical system must be able to acquire and track these targets at daily rates comparable to or greater than that achieved by a radar (Haystack) in order to be a viable alternative. Haystack has demonstrated acquiring small targets at a rate of about 6 per hour, essentially at any time during the day. Haystack, in acquiring and tracking such targets, could provide track information to an accuracy of about 40 μrad. Table 7.1 below gives the expected V_M of the debris matrix targets.

Table 7.1 : Expected Brightness of Debris Targets

Target	DEBRIS A (-40 dBsm)		DEBRIS B (-40 dBsm)		DEBRIS C (-35 dBsm)		DEBRIS D (-30 dBsm)		DEBRIS E (-18 to -30 dBsm)	
Avg. Altitude (Km)	907		875		663		1170		1002	
30 deg.	1560*	18.2^	1510	16.3	1180	8.1	1955	13.0	1705	13.7
60 deg. ELEVATION	1030	17.2	990	15.3	760	7.1	1320	12.1	1130	13.3

* Slant Range (Km) ^Estimated V_m

There are two possible optical acquisition approaches: an active system where an illuminating beam is used to irradiate the target with a ground receiver detecting the backscattered radiation or a passive system which detects the target when illuminated by the sun. The active system would require an illuminating laser of a size similar to that of the Pusher Laser. Such a system has been considered and is reported elsewhere. Invoking such a major element to provide acquisition and tracking looked difficult so a passive system was also examined in some detail.

7.4 Passive Optical Acquisition

Passive acquisition and tracking of (large) space objects in low altitude orbits can be accomplished when the objects are in terminator illumination around sunrise and sunset. Acquiring and tracking in the terminator mode means that the sky background is dark so that the dim target light doesn't have to compete with sunlight scattered by the atmosphere. Such acquisition has been routinely accomplished for large objects — typically satellites or spacecraft — and less routinely for small objects. The stressing target in the ORION group of targets is quite dim corresponding to a star of visual magnitude around 18 or 19. This is not routine.

The anticipated operation of an autonomous passive optical acquisition system is "stare and chase." The system will be pointed at a fixed position in the sky "staring" over its field of view with a fixed integration time (frame rate). When a target is detected, the system will continue to stare for several frames

as the target moves through the field of view. As detection frames accrue, a target is declared and a preliminary track file established. This track file is used to predict the target's future position (of the order of a second) and the telescope mount is accelerated to the correct (future) position and velocity. The target moves to the camera (tracker) boresight and stays there as the tracker takes control of the mount and automatically tracks (chases) the target.

A suitable acquisition system would operate for about 2 hours around sunrise and sunset each with a background consisting of sky background radiation, stars and possibly scattered light from the moon. A detailed analysis of time available as a function of latitude and time of year is presented in Appendix 7.1. The dimmest target ($\rho A = 0.1$ cm^2) was used to represent the most stressing case. Target orbits were reviewed in the 500 km to 1500 km altitude regime for acquisition at zenith angles of up to 60°. From this, the most stressing orbit selected was for a debris particle at an altitude of 1500 km and 60° zenith angle resulting in a desired acquisition range of 2500 km and an angular rate of 2.4 mrad/sec. This corresponds to a star having a visual magnitude of 18 or 19; quite dim.

Acquisition background information was taken from several sources. Sky glow information was derived from a review article by Gerald Daniels ("A Night Sky Model for Satellite Search Systems,"*Optical Engineering*," v16 no.1, Jan-Feb 1977) and from Gene Rork of Lincoln Laboratory (private communication) resulting in a value for airglow of 1.6×10^{-6} watts/cm^2-s within the wavelength band of 0.4 μm - 0.7 μm. Scattered moonlight several degrees away from the direct moonlight is of the order of 10×10^{-6} w/m^2-sr in the same band. Finally, the density of stars of magnitude 18 or 19 or brighter that would be seen by the camera while staring for debris particles was calculated. These densities are shown in Figure 7.1. The right hand ordinate in the figure shows the number of stars of the specified magnitude or greater that would fall into 50 μrad and 100 μrad pixel FOV-sizes appropriate to this system. This indicates that a large fraction of detector pixels will contain a star as bright or brighter than the target. Fixed background processing (such as frame-to-frame subtraction) will be required to eliminate these returns.

7.4.1 Canonical Passive Acquisition System

A preliminary study of requirements and hardware for providing the necessary acquisition and tracking for ORION was undertaken and indicates that a system utilizing current technology could provide the requisite acquisition and tracking. A baseline set of parameters for an operational system is shown in Table 7.2.

The wavelength band appropriate to sun illuminated tracking was taken to be from 0.4 μm to 0.7 μm. No attempt was made at this stage to optimize the receive band with detector responsivity and background noise.

Table 7.2
Baseline Parameters for Passive Optical Acquisition System

TELESCOPE
3.5 m Diameter (area - 9.6 m^2)
Angular velocity maximum > 0.5 °/sec
FOCAL PLANE
Pixel Size ~ 50-100 μrad
Number of Pixels ~ (25 x 25) to (50 x 50)
Dwell Time ~ 10^{-2} secs
Pixel Noise < 10 electrons/pixel

FIGURE 7.1

DENSITIES OF STARS VISIBLE TO ACQUISITION SYSTEM

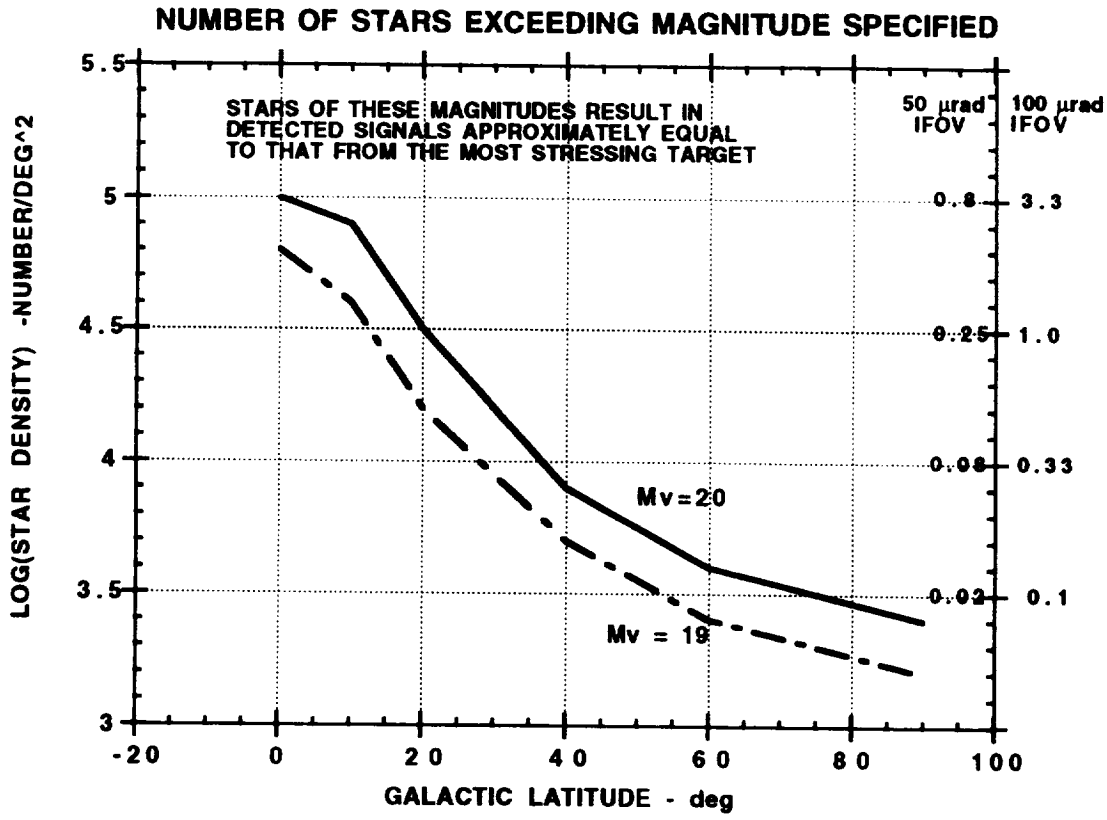

The diameter of the receiver (telescope) was selected as 3.5 m — reasonably large but not extraordinary. The Air Force is currently procuring two such systems, one for Kirtland AFB and one for the Maui Optical Station. The mount needs to be able to accelerate for the transition from "stare" to "chase" and to follow the target acceleration as it moves along its orbit. The transition acceleration will dominate; an estimated few degrees/sec^2 should suffice to permit the telescope mount to catch up to the moving target within a fraction of a second and within an angle not much greater than the tracker field of view. The Firepond telescope with its 1.2 m diameter aperture has a capability of 15 deg/sec angular velocity and 10 deg/sec^2 acceleration.

Atmospheric transmission at zenith angles of 60° over this visible band was taken as 0.69 (0.83 at zenith) based upon models used here at Lincoln Laboratory. A MODTRAN calculation done by Jim Reilly for this study indicated a higher zenith transmission of 0.9 so we chose the more conservative value. At these levels of trans-mission, the effect is not strong. The system optics were taken to have a transmission of 0.5.

Focal plane parameters were taken from those of current Lincoln Laboratory fabricated CCD focal planes. The quantum efficiency is 0.65 in the visible and the pixel read noise is 10 electrons/pixel for rates of 2 megapixels/sec. Current arrays are 2500 x 2000 pixels with 8 readout ports. The pixels are 25 μm square and would utilize on-chip binning (available on these chips) for this application.

The system parameters used in this study are listed in Table 7.3.

Table 7.3
Reflected Sunlight Acquisition Parameters
(Baseline Stand-alone Optical System)

TARGET	SYSTEM PARAMETERS
Area = 1 cm^2	Aperture area = 9.6 m^2 (3.5 m dia)
Reflectivity = 0.1	Obscuration < 10%
Angular Velocity = 2.4 mrad/sec	Optical transmission = 0.5
SUNLIGHT ILLUMINATION	
Wavelength band 0.4-0.7 μm	Detector Array:
Intensity = 1000 w/m^2	Quantum efficiency = 0.65
Atmospheric transmission = 0.83 (zenith)	Read Noise = 10 electrons / pixel
BACKGROUND	
— 1.63 E-10 w/cm^2 — dark night	
— 10 E-10 * — moonlight	Dwell Time = Pixel IFOV / Target angular rate
— 2.5 E-4 — daylight	

* Moonlight background depends primarily on the LOS zenith angle. Above a zenith of 60° the in-band moon background is less than 10E-10 w/cm^2.

The performance of such a system as a function of pixel field of view (FOV) is shown in Figure 7.2. In this figure, the target is the smallest (dimmest) target in the target set (1 cm diameter, 0.1 reflectivity). It is at an altitude of 1500 km and being observed (acquired) at a zenith angle of 60° and range of 2500 km. In this analysis, the telescope is pointing to a fixed position in space (staring mode) and the

FIGURE 7.2

REFLECTED SUNLIGHT ACQUISITION CANONICAL SYSTEM

TARGET @2500 km, OMEGA=2.4 mrad/sec
DARK BACKGROUND, ZENITH ANGLE = 60 deg

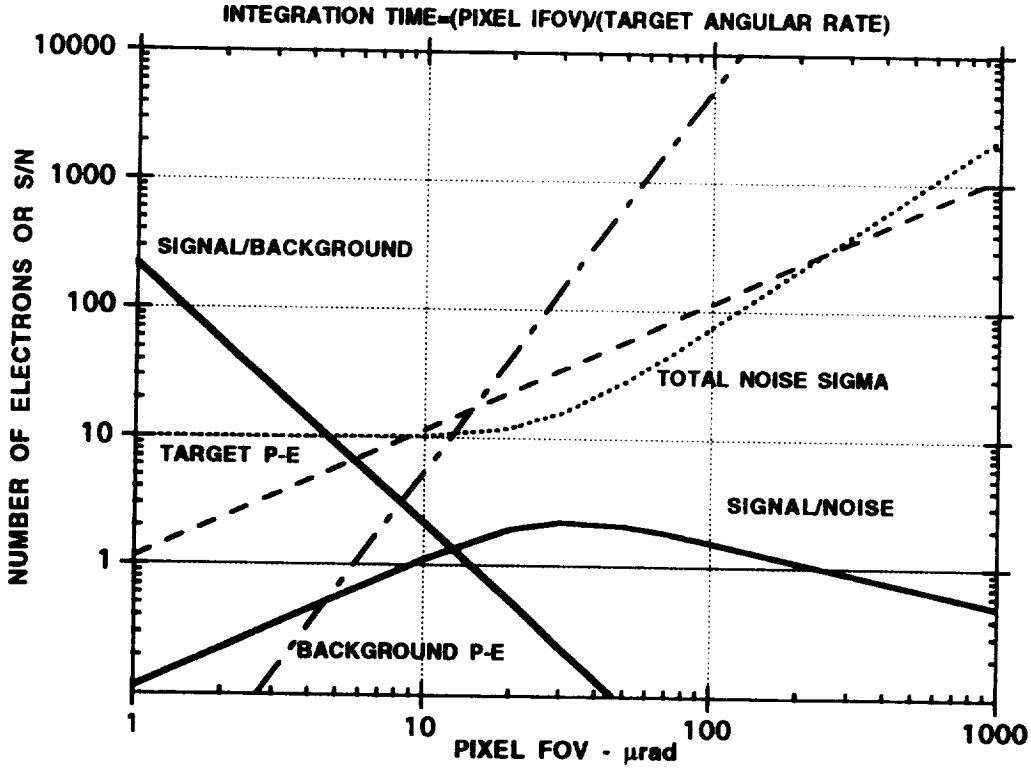

target moves across its field of view. The dwell time of the array is set equal to the time it takes this target, at its range and zenith angle, to cross the pixel FOV represented on the abscissa. Since this target is the dimmest in the set and at longest desired range, this figure represents the most stressing limit. Other targets will be brighter and thus give a larger signal or be the same brightness but closer resulting in a stronger collected signal. In operation, the dwell time would be constant at a value corresponding to that most stressing target and the specific pixel FOV for the focal plane.

Figure 7.2 shows a number of curves. The number of photo-electrons from the target and from the (dark) background are shown as broken lines. A total noise standard deviation (sigma) is calculated from adding the variances of the background photon noise in electrons and the focal plane read noise (σ_R = 10 electrons) and is shown as a dotted line. The solid line represents the S/N ratio: the ratio of signal photo-electrons to the total noise standard deviation (sigma) also in photo-electrons.

As indicated, the maximum signal-to-noise ratio is about 2 for this most-stressing case and occurs at a pixel FOV of about 20-60 μrad (with dwell times of about 8-25 msec). It is recognized that operation at this signal-to-noise ratio is marginal. It represents a probability of detection of 0.7 and a false alarm probability of 0.1. (Adjusting the threshold to increase the probability of detection would also increase the probability of false alarm.) However, it is anticipated that a fairly simple multiple hit track initiation algorithm could be used to process multiple detections which would increase the probability of detection without increasing the probability of false alarm. Furthermore, the target chosen is extremely dim (at the range chosen it corresponds to about a 19th magnitude star) and an increase in brightness by only 50% would increase the probability of detection to about 0.99 with no increase in false alarm probability for single pulse detection.

In Figure 7.3 is shown the same plots for a small target at an altitude of 1000 km with a range of 1700 km at a zenith angle of 60°. The peak S/N ratio remains at about 2 since, while the range decreases, the angular rate increases and the dwell time decreases.

Figures 7.4 and 7.5 show the effects of zenith angle and background. As can be seen in Figure 7.4, the effects of zenith angle from 0° to 60° are not large giving good flexibility in locating targets as early as possible. In Figure 7.5 is shown the effect of full moonlit night on background which drops the signal-to-noise ratio by about a factor of 2 at the maximum of the signal-to-noise curve. This is significant but not overwhelming; somewhat brighter targets than the most stressing would still be detected and tracked.

7.4.2 Acquisition Rates

The current Lincoln Laboratory CCD focal plane referred to above is a 2500 x 2000 pixel array with a pixel size of 25 μm. Using this size directly for a 40 μrad pixel FOV would imply, for a 3.5 m telescope, an f/number of 0.15 — quite impractical optically. However, if 12x12 sub-arrays of these pixels were binned into a super-pixel, it would be 300 μm on a side and for a 40 μrad super-pixel FOV, the optical system would be about f/2 — much more practical. This binning can take place on the chip so that the read-out noise for a super-pixel remains at 10 electrons/read. With 12x12 pixels per super-pixel, the whole array would have 200x167 super-pixels. The array FOV becomes 8 mrad x 6.67 mrad which is about 50 times that of Haystack. The acquisition rate will depend upon the shape of the FOV and the distribution of orbit angles but it will be at least 8 times that of Haystack thus essentially equalling (perhaps exceeding) the number of targets acquired by Haystack per day.

7.5. Operation of an optical acquisition system for ORION

A concept of operations will be described in this section for the canonical optical system defined earlier to act as the "debris finder" for the ORION laser. As part of the concept, the requirements/capability to perform all the functions tabulated in 7.1 will be stated.

FIGURE 7.3

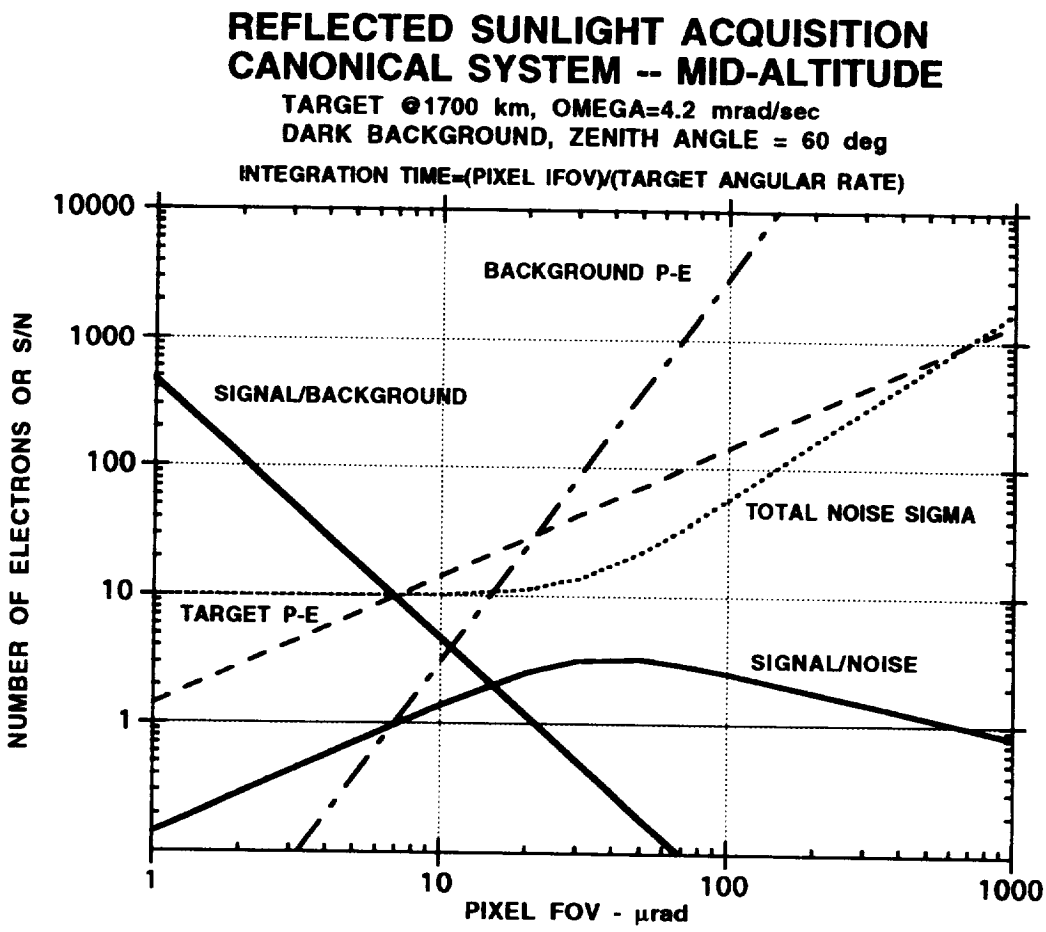
REFLECTED SUNLIGHT ACQUISITION
CANONICAL SYSTEM -- MID-ALTITUDE
TARGET @1700 km, OMEGA=4.2 mrad/sec
DARK BACKGROUND, ZENITH ANGLE = 60 deg
INTEGRATION TIME=(PIXEL IFOV)/(TARGET ANGULAR RATE)
NUMBER OF ELECTRONS OR S/N
10000
1000
100
10
1
BACKGROUND P-E
SIGNAL/BACKGROUND
TOTAL NOISE SIGMA
TARGET P-E
SIGNAL/NOISE
1
10
100
1000
PIXEL FOV - μrad

FIGURE 7.4

REFLECTED SUNLIGHT ACQUISITION ZENITH EFFECTS

DARK BACKGROUND

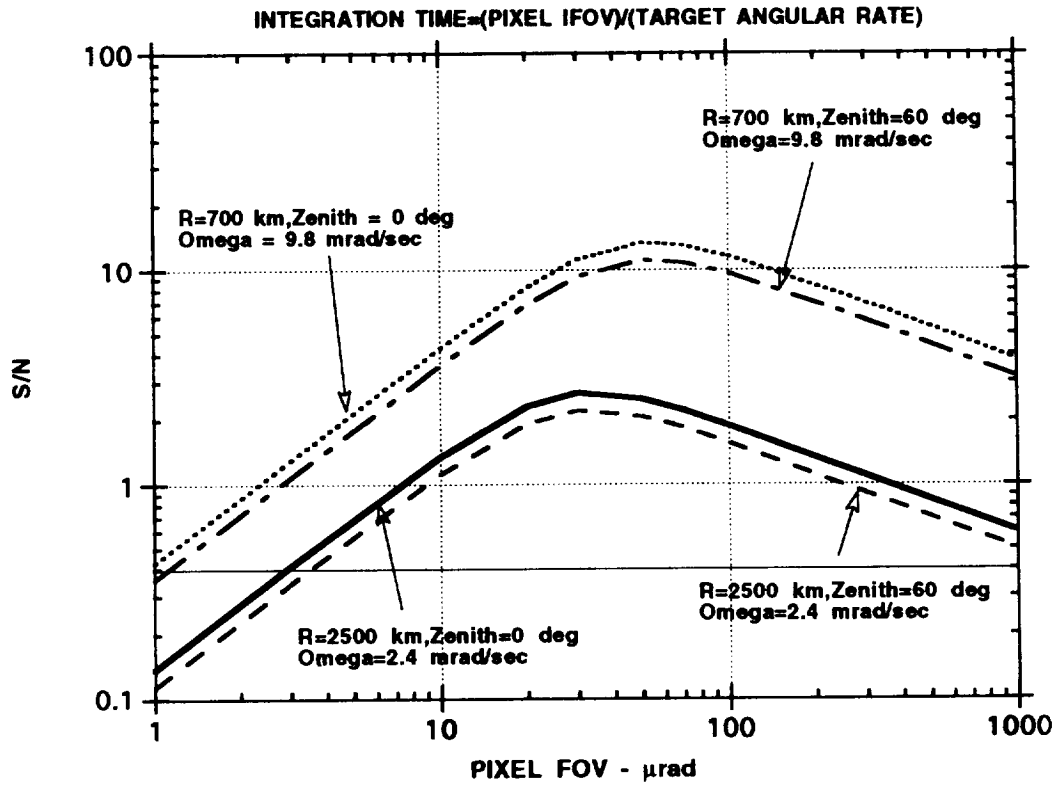

FIGURE 7.5

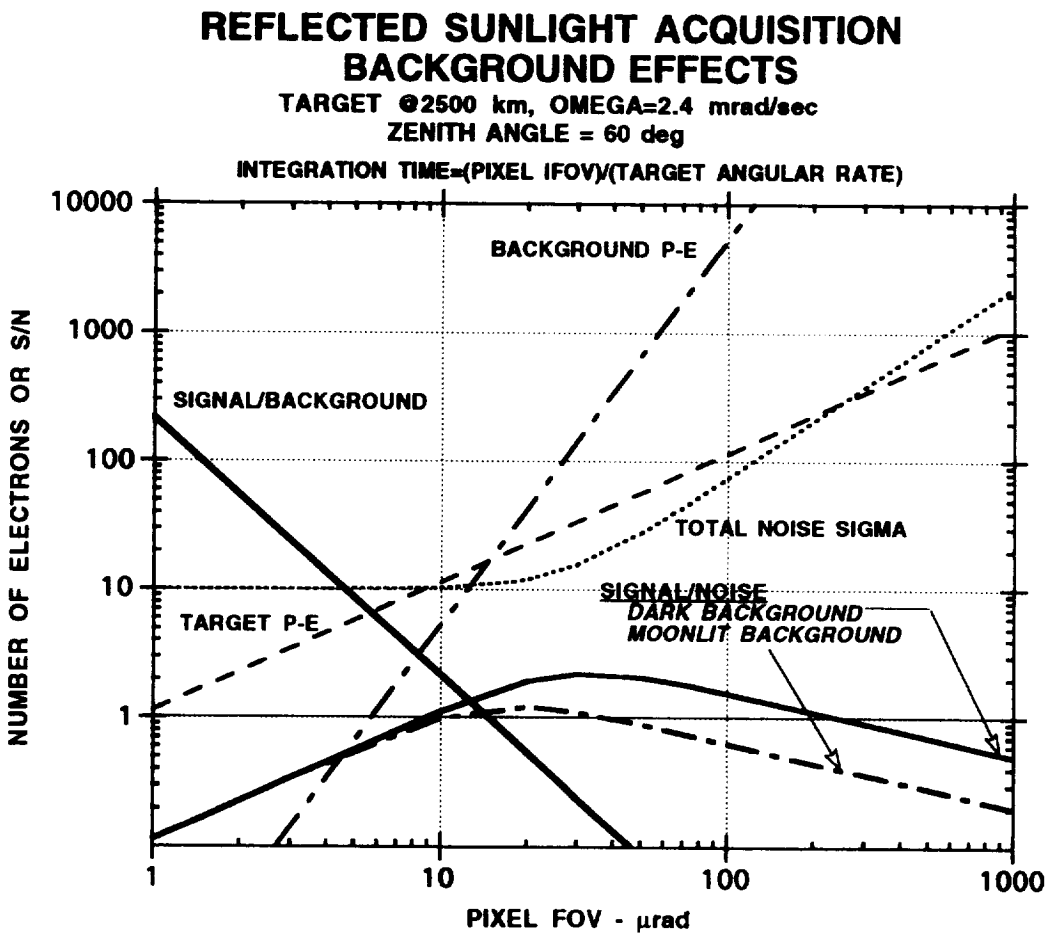
REFLECTED SUNLIGHT ACQUISITION
BACKGROUND EFFECTS
TARGET @2500 km, OMEGA=2.4 mrad/sec
ZENITH ANGLE = 60 deg
INTEGRATION TIME=(PIXEL IFOV)/(TARGET ANGULAR RATE)
NUMBER OF ELECTRONS OR S/N
10000
1000
100
10
1
BACKGROUND P-E
SIGNAL/BACKGROUND
TOTAL NOISE SIGMA
TARGET P-E
SIGNAL/NOISE
DARK BACKGROUND
MOONLIT BACKGROUND
1
10
100
1000
PIXEL FOV - μrad

7.5.1. Autonomous Detection of Debris

It is essential for the optical system to have adequate time to acquire, track, discriminate and handover the target to the laser. The discrimination task will take several minutes to complete and hence it is essential for the optical system to acquire the debris early in its apparition. Hence, the optimum strategy is for the optical system to stare at ~30^0 - 45^0 elevation. Since the optical system has a FOV of ~0.5^0, a scan is not needed though a "step-stare" scan could be used. The stare will keep the stars invariant in the FOV. The choice of azimuth is dictated by the location of the optical system and the inclinations of the orbits that are of prime interest. Since most of the debris are in high inclination orbits, a optical system on or near the equator could point due north or south at 30^0 elevation for detection. If however, the optical system is located in say New Mexico, at 32^0 north latitude, pointing due south is recommended as it improves the inclination coverage significantly (see Appendix 6.1).

The optical system should detect an average of 40 - 60 debris targets/hour between the altitudes of 500 Km. and 1500 Km. *However, this has to be established by experiment in Phase 2.* Unfortunately, half of these targets will be setting. Out of those left, only 1/3 might come into the field-of-view of the laser. If a higher detection rate is desired, the optical system could conduct a "step-stare" scan.

7.5.2. Precision Tracking of Debris

Once a debris target is detected the optical system has to initiate tracking in what is essentially a transition from a 'stare" mode to a "chase" mode. Such stare and chase operation for debris has been developed and demonstrated at the Experimental Test System (ETS) in New Mexico.

After the transition to "chase," the acquisition system will be continuously tracking the debris target. In the acquisition mode, with super-pixels of the order of 100 μrad, the tracking accuracy can be expected to be in the range of a fraction of the super-pixel size — the fraction depending on the S/N.

The Pusher Laser will most likely require a pointing accuracy in the region of 1 μrad. This could be accomplished by a separate optical tracker (passive or active) with appropriately sized detectors or focal plane arrays so that the overall field of view is sufficient to accept handover from the acquisition system (with its tracking jitter/accuracy) and sufficient resolution to achieve the required precision tracking accuracy. Indeed, with the focal plane array used in the acquisition system as described above, it may be quite feasible to reconfigure the focal plane array while still in acquisition track to utilize the much smaller pixels (non-super-pixels). These might have a pixel field of view in the few μrad region and would afford the required precision tracking required..

7.5.3. Discrimination

This is probably the most time-consuming and complex task for the optical system. The requirements are as follows:

1. Verify that the debris is in an ascending pass.
2. Ascertain the catalog status of the debris in track.
3. Ensure that the estimated size and, if required, dynamics of the debris are within the capability of the laser.
4. Measure periodicities in the signature.
5. Check whether the debris will transit the laser field of regard for the time interval required by the laser system to successfully irradiate it.
6. Check that the debris will be sun illuminated until handover is complete.
7. *Guarantee that no other resident space object, and in particular, no payloads will be illuminated by the laser inadvertently during the engagement.*
8. *Guarantee that no airplane intercepts the laser beam during the engagement.*

The first six of these can readily be accomplished by the optical system during the acquisition and track period.

7.5.3.1. Correlation with the Catalog

The data recorded during the transit of the debris through the FOV is adequate to discern whether the target is in an ascending pass. If not, the search can be resumed. As soon as ~ 75 seconds of metric data (or ~15 observations) are taken, an initial orbit can be estimated and checked to see if the debris will be within the field-of-view of the laser for the required time interval during this apparition. If not, the optical system can return to its search. A correlation with the catalog should be done next. The data quality is adequate to yield a good estimate of the orbital plane of the debris and of its position in space, both of which can be checked against all the RSOs in the catalog. This task should take no more than 5 seconds with a modern work station and appropriate architecture of the software. If it is a known large RSO, the search for debris can be resumed. If it is a cataloged piece of debris, a real-time decision needs to be made based on the following:

1. Is it of interest to the ORION system - depending on strategy and size?
2. Who nominally "owns" the cataloged debris? Does the ORION system have "permission" from the "owners" to irradiate their debris?

Given a positive answer to both questions, the next step can be taken.

7.5.3.2. Size and Dynamics

As the tracking of the debris piece continues, the optical system must estimate the mean size and perhaps a variance. The size can be approximately estimated using an average photometric phase model for debris. There is considerable doubt about the "average" value for albedo to be used which directly affects the estimate of size. *It is recommended that, during Phase 2, a large sample of debris be examined with particular bias towards the denser population regions to assess an average albedo. Techniques for decoupling the area and albedo have been developed*[1]. The signature data must also be analyzed through the mechanics of algorithms like auto-correlation or Fourier transform to determine any periodicities. The estimation of size is significantly affected by periodicity in the signature and, further, debris are known to have periodicities ranging from ~0.1 sec. to >>30 sec.

The value of estimated periodicity in the signature lies in the fact that it will be significantly affected by the impact of the laser energy and, hence, it can be used as an indicator of the success of the engagement.

The inferred size of the debris must be compared to a threshold set for the ORION system to decide on the engagement. The periodicity may prove useful for the same purpose.

7.5.3.3. Inadvertent Illumination of RSOs

A major concern with the ORION system is its potential for inadvertently illuminating and damaging a payload in orbit. This concern is motivated by both treaty implications and the cost of "friendly fire".

Once the debris has passed the filters in the previous sections and deemed suitable for engagement by the ORION system, a detailed prediction needs to be made of the part of the trajectory that the laser would illuminate. *This prediction has to be compared with the known position of the entire catalog of payloads to guarantee that inadvertent illumination does not occur. Further, US Space Command may*

[1] W.I.Beavers, L.W.Swezey : "Photopolarimetric Object Characterization and Size Measurement", MIT Lincoln Laboratory Project Report STK-234, 11 April 95.

require that a real-time check be made with a small catalog of important domestic payloads to preclude damage or interference.

A question that remains is whether it is adequate to check against the locations of payloads or whether rocket bodies and other large objects in the catalog must be included in this check. The concern stems from the possibility of inadvertently causing a rocket body with left-over fuel to explode. Part of the answer is political. *The technical part of the answer will come from an analysis of the impact of the laser on the debris Matrix Target F.*

The Airborne Ballistic Missile Defense Laser (ABL) being built by AF Phillips Laboratory faces some of the same issues and the solution would be useful to ORION. Other systems like SBV/MSX, SWAT, Firepond laser and AMOS/Maui laser system have resolved many of the same issues.

This is a major issue for the ORION system. It will affect decisions on site location and modes of operation.

7.5.3.4. Aircraft Avoidance

Regardless of the wavelength of operation of the laser, the ORION system has to ensure that it does not inadvertently illuminate an aircraft. Unlike RSOs, aircraft do not follow predictable trajectories. It is prudent to choose a site where major air traffic lanes can be avoided. But, in any case, the ORION system needs a real-time means of detection and avoidance of aircraft.

Often a local search radar is used to minitor aircraft in the area, to warn them off or to avoid illumination in their direction. Since the FAA is shutting down a significant part of their radar system due to reliance on GPS technology, such a system may be available to the ORION system "free". In addition, it may be possible to include a wide FOV optical system operating in advance of the main laser to provide additional target avoidance capability.

This is a major issue for the ORION system. It will affect decisions on site location and modes of operation.

7.5.4. Optical System - Laser Handover

Once a debris has passed all the filters listed above, it has to be handed off to the ORION laser for irradiation. The process in concept is very simple as the precision tracking of an optical system is adequate to narrow the search volume for the laser. There are two types of handover.

A real-time handover occurs when the optical system and laser are collocated. In this case, the only issue is the mutual calibration of the laser and the optical system. This is not a major issue as substantial experience exists at MIT Lincoln Laboratory and other places. The optical system continues to track the object until a successful handover has taken place.

A non-real- time handover occurs when the optical system and the laser are not collocated. In such a case, the optical system will have to determine a precise orbit and transmit it in some form to the laser system. The accuracy of the prediction is an issue that is being studied by AF Phillips Laboratory. Again, precise pointing calibration of both systems is a solvable concern.

Concerns pertaining to the handover for both real-time and non-real-time can be addressed in Phase 2 using the collocated and spatially dispersed set of MIT Lincoln installations.

7.5.5. Assessment

A critical issue is the assessment of the effects of the laser irradiation on the debris. The questions that need to be answered are:

1. Did the target interact with the laser energy?
2. Can the mass, area/mass ratio or some similar parameter for the debris be estimated?
3. Can the characteristics of the laser-debris interaction be measured or inferred?
4. What is the perigee bin of the target post-irradiation?
5. Is there a threat to a manned asset as a result of the orbit change?

There are four methods that can be used to perform these assessment tasks:

1. Measure the plasma "flash" created by the laser-particle interaction.
2. Measure the "instantaneous" Doppler change of the target as a result of the interaction.
3. Measure the change in the periodicity of the signature.
4. Compare the estimated orbits pre- and post-irradiation.

The plasma "flash" is expected to occur on every pulse of the laser that hits the target. A visible wavelength optical system, if collocated with the laser, can measure this effect. The flash will clearly indicate that the target has been hit. It is unknown whether the plasma will be quenched rapidly enough such that the interaction due to each pulse can be monitored.

The Doppler of a target can be measured very precisely by a coherent laser. Also, depending on the accuracy of the track, Doppler can be inferred from range measurements. In either case, if the target is monitored while being irradiated by the laser, the departure of the measured Doppler from prediction based on the pre-radiation orbit is a clear and rapid indicator of laser effects. This technique is routinely applied at Lincoln radar systems for monitoring orbital maneuvers.

Continued tracking of the debris post-radiation will yield an estimate of the periodicity of the signature. *However, it is quite unlikely that the debris target will continue to be illuminated by the sun and probably a laser or microwave radar system would have to provide the tracking.* The periodicity is very likely to have changed as a result of the laser-debris interaction and can both confirm the interaction and, perhaps, provide a quick but poor estimate of the moment of inertia of the debris. Further, the laser tracking data can be processed into an estimate of the orbit which, when compared with the pre-radiation orbit, can yield the following.

1. An estimate of the total velocity change imparted to the debris.
2. The perigee bin into which the debris has been moved.
3. An estimate of the mass of the debris if the intensity of the laser at the location of the debris is known and the size of the debris is known.

The new orbit must be used immediately to assess whether the threat to a manned satellite has been increased. If the new perigee height is lower than that of the manned asset, but is >200 Km., cataloging of the debris by further tracking is essential so as to provide adequate warning of close approaches.

7.5.6. Miscellany

Book-keeping of the debris merely refers to creating a histogram of the number of objects irradiated vs. the perigee bin in say 100 Km. steps before and after. This is to ensure that the risk in lower altitudes is not unduly increased and applies only in the case of the "steady rain strategy".

The throughput of the optical system is governed by the approximately 5 minutes of total tracking plus the search time to find the debris. *The best it can be with one optical system is 12 objects per hour or ~50 objects/day given the requirement of dawn and dusk conditions.*

7.6 Summary and Conclusions

The ORION system has a requirement for an autonomous system or systems to acquire the debris targets of interest and to track them well enough to hand over to a precision optical tracker which will point the Pusher Laser. The Haystack radar has the capability of acquiring the most stressing of these targets (reflectivity r = 0.1, area A = 1 cm^2) at a rate of about 6 per hour.

A passive optical system operating in the visible band detecting reflected sunlight in the terminator mode has been analyzed. An optical system with a 3.5 meter aperture utilizing current technology can detect these targets at altitudes of 1500 km and zenith angles of 60° corresponding to a range of 2500 km. With an existing focal plane, and a lot of processing, a total FOV of 8 mrad x 6.67 mrad could be implemented which could result in useful acquisition rates of at least 12 per hour or ~50 per day (~4 hours of terminator observation time per day). This is probably more than enough to saturate the capabilities of the Pusher Laser and remain reasonably competitive with a radar system.

APPENDIX D

ANALYSIS OF THE ORION SYSTEM CONCEPT

Claude Phipps
Photonic Associates

Table of Contents

TOPIC 1: OVERVIEW OF INTERRELATIONSHIP AMONG LASER AND TARGET PARAMETERS

The purpose of this section is to tie together the various laser and target illumination parameters in the ORION problem in such a way that the operating points we have selected make some kind of sense, and so other operating points can be selected with clear awareness of the "maneuvering room" in ORION's multi-parameter space.

This note uses relationships developed in later sections, but its proper place is at the beginning to provide a roadmap to tie those pieces together conceptually.

Diffraction

In vacuum, the relationship between near and far field irradiance scale parameters is governed by diffraction.

We use Siegman's beam quality factor N [he calls it M^2: see Siegman 1993] to describe the inevitable degradation of beam quality from the ideal, a concept which is really only appropriate for Gaussian beam propagation, entering propagation expressions for such beams as if the wavelength were N times longer than it is.

There are two special near and far planes at which it is easy to relate beam intensity distributions to each other. For Gaussian beams, it is the pupil plane of the focusing optic at z=0 and the plane at the Rayleigh range

$$z_R = \frac{\pi D_b^2}{8N\lambda} \qquad [1]$$

where $d_s = D_b/\sqrt{2}$. If one focuses harder than that, the focal spot moves in to $z<z_R$, but never gets smaller than

Diffraction: $$d_s = \frac{a N \lambda z}{D_b} \qquad [2]$$

where $a = 4/\pi$. In this case, if it is not true that $d_s << D_b$, Eqn. (2) is also not exactly true either and some larger spot size results from going through the exact analysis. If we define a fictitious quantity d_{so} according to:

$$d_{so} = \frac{D_b}{z/z_R}\left[1 - \sqrt{1 - \left(\frac{z}{z_R}\right)^2}\right] \qquad [3]$$

then d_s itself can be found from:

$$\frac{1}{d_s^2} = \frac{1}{d_{so}^2} + \frac{1}{D_b^2} \qquad [4]$$

This distinction is important because Eqn. [2] is in error by several percent for the ORION case. However, for scaling purposes, we will use Eqn. [2] as if it were exact.

From Eqn. [2] we can then state:

$$\frac{I_s}{I_b} = T\left(\frac{D_b}{d_s}\right)^2 = T\left(\frac{D_b^2}{a\,N\,\lambda\,z}\right)^2 \qquad [5]$$

where T is the one-way atmospheric transmission.

The Target Effects trendline linking beam intensity in the atmosphere to pulse duration

In section 1, we show that the fluence Φ_o or intensity I_o which are optimum for producing maximum momentum coupling coefficient $C_m = m\Delta v/W$ is given by

$$\Phi_o = C\tau^{\alpha} \qquad [6]$$

or $$I_o = C/\tau^{1-\alpha}$$

where $\alpha \approx 0.45$ for all materials as pulse duration τ varies from about 1ps to 1ms, and $C \approx 2.3E4$.

We also fit the response of an individual absorber around $I_{s\,o}$ in §2, showing that a good fitting function is

$$\log C_m = \log C_{max} - [1.25\,(\log \frac{I_o}{I})^3\,,\ I \le I_o$$
$$\log C_m = \log C_{max} - [0.36\,(\log \frac{I}{I_o})]\,,\ I > I_o \qquad [7]$$

It is important to realize that Eqn. [7] means that C_m goes like $I^{-\beta}$ for $I>>I_o$, [where β = 0.36 in the example plotted and 1/3 typically] and that this means that the actual momentum transferred continues to increase as I increases, going like

$$m\Delta v \propto I^{1-\beta} \approx I^{2/3}.$$

The optimum intensity is the one for which the expensive laser joules are used most efficiently; howver, in a situation where there is energy to burn and the situation is urgent, higher intensities than I_o do more work.

Assuming we want to achieve optimum coupling rather than maximum momentum transfer, Eqn. [6] implies that $I_s = C/\tau^{1-\alpha}$, which can be combined with Eqn. [5] to give an expression which relates near-field beam intensity to laser pulsewidth given a choice of range, wavelength and mirror diameter D_b:

$$I_b\tau^{1-\alpha} = \frac{C(aN)^2}{T}\left[\frac{\lambda z}{D_b^2}\right]^2 = \frac{Ca^2}{ST}\left[\frac{\lambda z}{D_b^2}\right]^2 \qquad . \quad [8]$$

where $S = 1/N^2$ is the so-called "Strehl Ratio". We have expressed this relationship leaving D_b rather than d_s a free variable because we believe the choice of D_b should be based on economics rather than falling out of some physics relationship. Note the strong D_b^{-4} dependence.

In § 5 and § 9, the dotted "target effects" line is based on an assumed choice of D_b, and that choice is the smallest mirror which can just avoid causing I_b to exceed the

threshold for Stimulated Raman Scattering and nonlinear phase shift in the atmosphere.

As an example, if $\alpha = 0.45$, $a = 4/\pi$, $\lambda = 1.06\ \mu m$, $z = 1500$ km, $T = 0.85$, $N = \sqrt{2}$ (Strehl ratio = 0.5) and $D_b = 600$ cm, the target effects trendline is $I_b\tau^{0.55} = 143$, which is approximately the dashed line plotted in the "maneuvering room" figure of §9. In that Figure, maneuvering room for the laser operating point is nearly absent, by design, to produce the most efficient and least costly design. However, choice of a larger mirror provides a lot more maneuvering room. The overall decision is a cost tradeoff, which is beyond the scope of this subsection, but which is treated in §0A following.

What are the limits to I_b?

Limits to I_b in the atmosphere are Stimulated Raman Scattering (SRS), Stimulated Brillouin Scattering (SBS), Stimulated Thermal Rayleigh Scattering (STRS) and nonlinear refraction (n_2).

SRS is a nonlinear process occurring with strong optical electric fields in which two photons - a laser photon and, usually, a red-shifted photon called the Stokes wave, are coupled by momentum contributed by vibration of a Raman-active molecule. Monatomic gases like argon do not produce SRS. In the atmosphere, nitrogen is the main contributor. For pulses longer than 1μs, starting from sea level, SRS limits I_b at 530 nm to about 1.3 MW/cm^2. This limit is proportional to the reciprocal of the SRS gain, which is in turn proportional to the Stokes frequency, so the I_b limit is approximately proportional to wavelength, and becomes about 30MW/cm^2 for long pulses at 11μm. As pulse durations become equal to and then shorter than the relaxation time of the molecular vibrations responsible for SRS gain, a gradual rolloff occurs as shown in the "maneuvering room" figure, eventually allowing much higher intensities to propagate. By the time 100ps is reached, $I_b = 50$ MW/cm^2 is permissible at 530 nm. This choice exceeds our n_2 limit (see below) at sea level, but is very acceptable when the beam starts from 6km elevation.

SBS is a nonlinear process in which the laser photon and the Stokes photon are coupled by a sound wave (phonon) in the Brillouin-active medium. One hears of SBS happening in liquids more often than in gases, but SBS competes with SRS at high gas pressures, and is in fact a main contributor to the procedure we will suggest (§ 11) for building a 100-ps laser. On a vertical path through the atmosphere for our laser parameters, SRS is effectively the only concern, since pressure drops so quickly, and pressure of a few atmospheres is required for SBS to be competitive with SRS in gases.

STRS is the result of the formation of minute diffraction gratings in the air due to minute intensity differences in the beam causing thermal density variations on the scale of a few wavelengths. These stimulate their own growth by causing greater intensity ripples downstream. The resulting grating can scatter the beam dramatically if conditions favorable to strong growth are not avoided.

Nonlinear refraction is the process whereby molecules or atoms of a medium are distorted by the high electric fields of an intense optical wave sufficiently to change the refractive index - usually by increasing it. The result is an optical phase shift in the beam proportional to local beam intensity, which results in beam breakup in solid state laser

systems. We have set a limit of one radian phase shift as being the limit of concern because as beam intensity varies from zero at the edge to maximum in the beam center, $\phi = 1$ corresponds to $\lambda/6$ wavefront error and, depending on assumptions about the beam profile, can cause a 10% loss in central beam intensity on target. We have used the best combination of theory and experiment available at the moment to estimate that half of the long pulse n_2 relaxes away for very short pulses. However, accurate resolution of this question from a theoretical standpoint should definitely be a subject of near-term future work. For long pulses, the n_2 limit is more than an order of magnitude above that placed by SRS.

However, a very attractive operating point exists at 100ps where the SRS limit has abated by about an order of magnitude, and here, n_2 is the deciding factor for all wavelengths.

Why this operating point is attractive will be discussed in the following subsection.

Why short pulses go with reduced pulse energy

We now ask what Eqn. [8] implies for laser pulse energy W. This is important because the cost of a laser tends to scale much more strongly with W than with total power P = fW in the range up to perhaps 10 or 15 Hz in which we are interested.

Since $W = I_b(\pi D_b^2/4)\tau$, Eqn. [8] can be re-expressed

$$W = \frac{\pi C (aN)^2}{4T}\left[\frac{\lambda z}{D_b}\right]^2 \tau^\alpha \quad = \frac{Ca}{ST}\left[\frac{\lambda z}{D_b}\right]^2 \tau^\alpha \quad . \quad [9]$$

This relationship shows that if mirror size D_b is fixed, dropping the pulsewidth from 40 ns to 100 ps will reduce laser pulse energy from 23 kJ to 1.5 kJ. This change should produce a much less expensive laser, providng that complex (e.g., grating pair) designs are avoided and simple (e.g., SBS-SRS cascade) designs are employed.

Universal Maneuvering Room plot

We are now in a position to make a "universal maneuvering room plot" based on the detailed work in the subequent sections §4-6 regarding STRS. Several of the boundaries limiting ORION laser design maneuvering room show the approximate behavior $I_b \propto \lambda$. Accordingly, the final two figures attached are plots of I_b/λ, on which the SRS limits, the n_2 limits and the whole beam thermal blooming limits for a particular mirror size are very nearly single lines and the STRS limit is much more closely bunched.

In order to show the target effects lines as single lines for two mirror diameters, we note that Eqn. [8] of this section shows that if **I_b/λ is constant**, $D_b \propto \lambda^{1/4}$. So, we have selected mirrors of the appropriate relative size: a 6-m diameter mirror at 1.06 μm corresponds to a 11-m mirror at 11.1μm in its ability to produce a target illuminance distribution for optimum coupling when we hold I_b/λ constant.

Using this plot, the $I_b \propto \lambda^2$ behavior for target effects at a fixed D_b is made more clear.

Glossary

a	Constant relating far field to near field parameters = $4/\pi$ for Gaussian radial profile beam = 2.44 for uniform "tophat" radial profile beam
α	exponent in Eqn. [6] expression for optimum coupling fluence
b	subscript describing the "beam" or near field irradiance pattern
C	constant in Eqn. [6] expression for optimum coupling intensity, =2.3E4 averaged over all metals and nonmetals
D_b	near field laser beam diameter (in the atmosphere)
d_s	far field laser spot diameter (on the target)
f	laser repetition frequency
$\Phi = I\tau$	fluence, J/cm^2
λ	laser wavelength, cm
s	subscript describing the "spot" or far field irradiance pattern
S	$1/N^2$, the Strehl ratio
τ	laser pulse duration
T	one-way atmospheric transmission
Δv	velocity increment imparted to target, cm/s
W	laser pulse energy
z	range to target, cm

References

Siegman, A. E. 1993 in *SPIE* **1910** *Proc Ninth International Symposium on Gas Flow an Chemical Lasers*

ORION ROADMAP

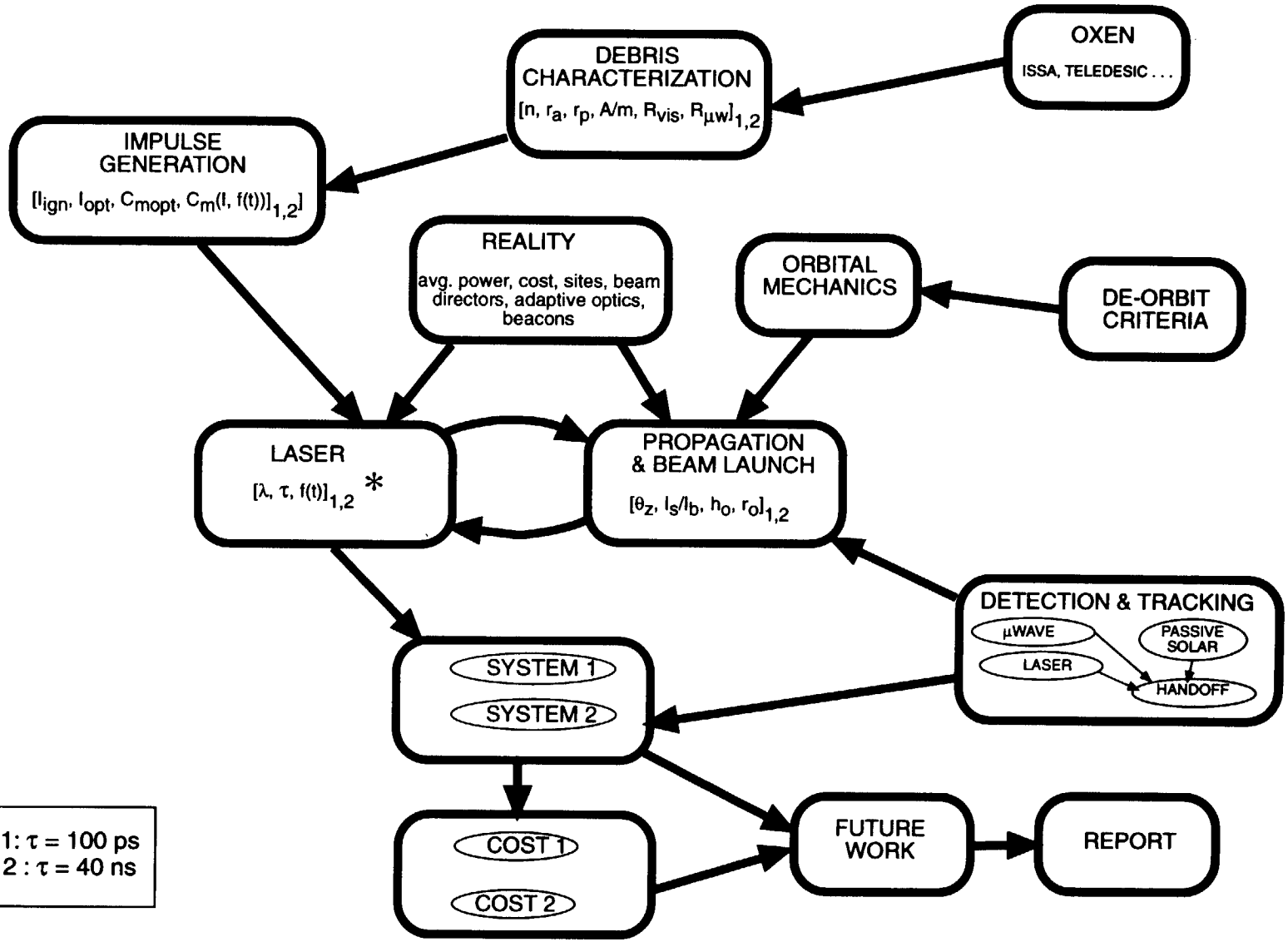

CRP 6/30/95

Universal ORION Maneuvering Room Chart

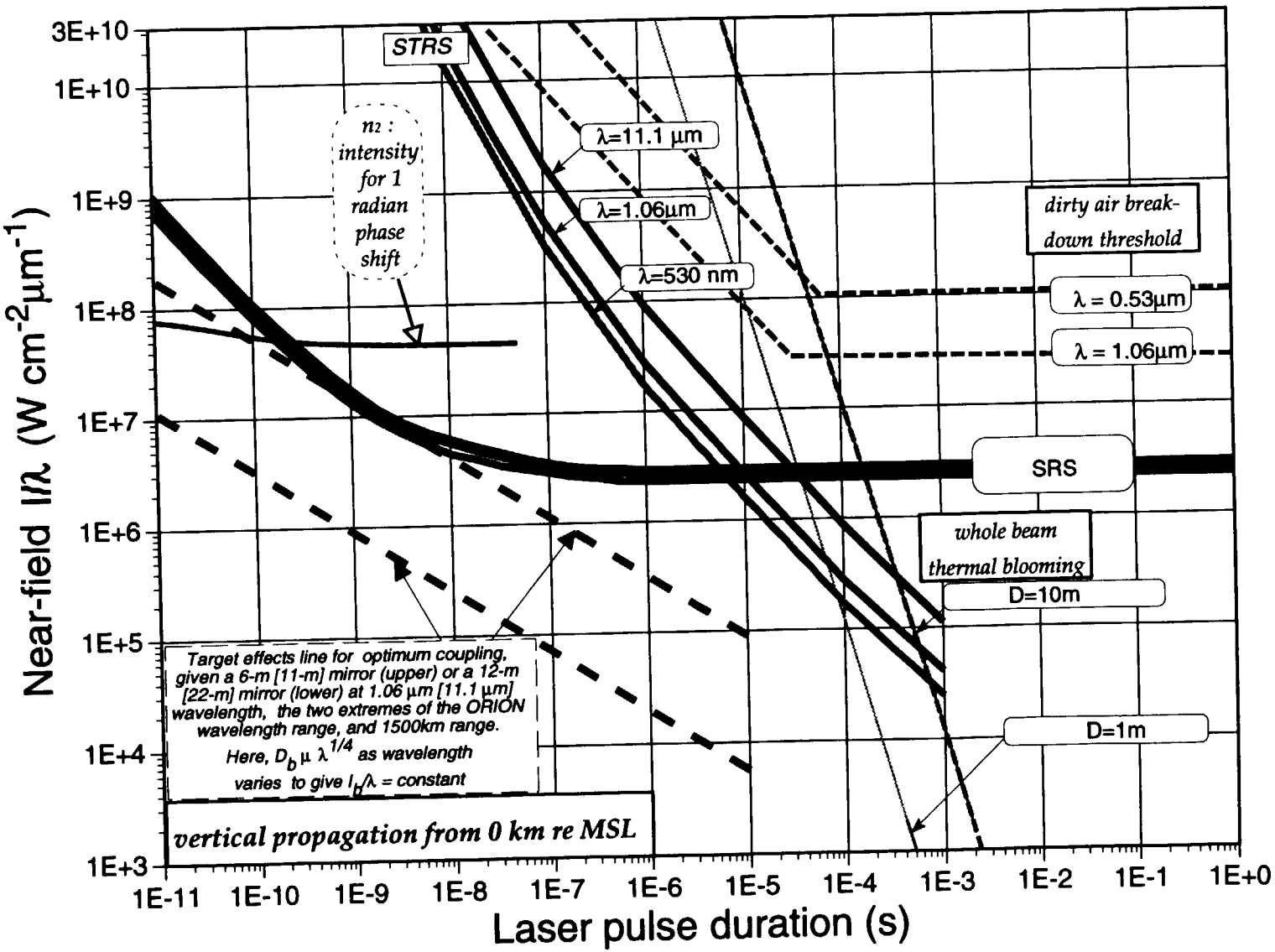

TOPIC 2: HOW PHYSICS & COST ALGORITHMS INTERACT TO PICK MIRROR DIAMETER

Executive Summary

The purpose of this monograph is to indicate how we can use approximate costing information to estimate optimum diameter of the ground-based beam launch mirror, given the goal of minimizing total system cost. This section is expanded and revised from the first version which you received earlier, to include a very important group of cost algorithms developed by Jim Reilly, which enabled us to measure the cost of repetitivelly pulsing the ORION laser.

Previously, laser cost was estimated single pulse cost alone. The new results for optimum D_b and system cost with solid state lasers are not very much different from the old ones.

What has changed can be summarized in 6 statements:

1. **Our results tend toward smaller mirrors than we considered to be desirable at the beginning of ORION Phase I**, motivated as we all were by an instinctual hatred of wasting laser energy. Optimum mirror sizes vary from about 3.5 m at 400km range to about 7m for 3000 km laser range, when the lowest-cost system options are considered.

1. **It is cheapest to achieve a given average laser power level (for lasers suitable for ORION) by going to the highest feasible repetition rate.** For example, a laser average power of 30kW is more cheaply achieved by building a 300-J-per-pulse laser operating at 100Hz rather than a 30-kJ, 1Hz unit. All cases we calculated gave similar results: you want the highest repetition rate you can get to achieve lowest laser cost (Figure 1). For the present analysis, we chose 100Hz repetition rate for all cases, because the costing algorithms may not be trustworthy much above this frequency, and because experience indicates that much higher rep rate is difficult to achieve in large systems.

2. **It is far cheaper to use the shortest feasible pulsewidth.** This point is illustrated by comparing the cost of 100-ps and 100-ns solid state laser options in Table 1, which shows that the optimum mirror diameter is about 50% greater, and the cost for any given laser range about 3 times greater, for the longer pulse option.

3. **Continuous (cw) lasers are competitive with repetitively pulsed solid state lasers for the ORION project.** We studied a 1.3-μm iodine laser option, and found it to be competitive with the Nd:glass option. We do not yet have reliable costing algorithms for RF-FEL's, and there is no *a priori* reason to assume they cost out the same as a high power cw laser. However, if they do, and if an RF-FEL can be built whose output is a continuous string of micropulses (100% duty cycle, not a series of macropulses), then coupling to the target should behave like cw, and the RF-FEL would also be competititve. The missing piece is costing for RF-FEL's.

4. **For the lowest cost alternatives studied, the optimum mirror diameter is about 4 m, and minimum system cost for 600 km laser range about $30M.** This mirror diameter is essentially identical to the 3.5-m diameter of the system at the Starfire Optical Range.

The details are summarized below.

Table 1: Summarizing Optimum ORION Parameters

Laser Type	Range (km)	Mirror Diameter D_b(m)	Total Cost (FY95 $)	Laser Average Power (W)
cw (iodine, 1.3μm)	400	4.2	25 M$	500 kW
	800	5.8	46 M$	900 kW
	1500	7.8	81 M$	1.8 MW
	3000	10.5	150 M$	4.6 MW
Solid State (1.06μm, 100ps)	400	3.5	25 M$	32 kW
	800	4.5	39 M$	80 kW
	1500	5.8	60 M$	160 kW
	3000	7.2	98 M$	430 kW
Solid State (1.06μm, 100ns)	400	6.5	71 M$	210 kW
	800	8.2	116 M$	525 kW
	1500	11	184 M$	1.0 MW
	3000	15	312 M$	2.2 MW

5. **Average power level required for the cw case is about 10 times that for the solid state option.** It was apparent many months ago that, because 1kW/cm^2 must be delivered to the target to obtain efficient thrust, the cw case involved MW-level power. We assumed, incorrectly, that the cost of achieving such a power level would exclude this option. There has been no change in the underlying target coupling calculations during this time.

Comments:

So why do the costs for the solid state laser case still come out about the same as before? Because the cost of the laser head for those dominates the cost of repetitively pulsing. (Just the opposite is true for repetitively pulsed gas lasers: Figure 2 attached illustrates this point.) This means that cost optimization gives the same answer as when flow loop costs were not included for the solid state case. Note that output power at 100Hz rather than output pulse energy is now plotted on the right-hand vertical axis.

Why are the minimum numbers for a particular range a little higher than before? Because we added a 10% contingency factor to the costs this time.

Caveats:

1. *This analysis will not necessarily minimize system operating cost.*
2. *The work has not yet been done to permit this analysis to include detailed cost breakdown for guidestars, adaptive optics and target tracking. This fact prevents us from extending this analysis to excimer lasers at the present time. It is assumed that laser rather than radar acquisition is implemented.*
3. *This analysis does include implicit assumptions such as location of the laser station on*

Earth, choice of laser parameters to achieve best momentum generation on the distant target together with avoidance of SRS and other nonlinear optical processes in the atmosphere, and choice of average power level appropriate to clear the 1 – 20-cm debris population in 2 years, but not adequate for single-pass knockdown of the majority of debris targets in our Target Matrix.

As more detailed cost algorithms become available, new data can be put into this procedure, and better estimates obtained. However, it is useful to point out what ORION cost estimates indicate right now.

Basis for Costs Quoted

There are two main costs in the ORION system, $\mathbb{C}_L$ and $\mathbb{C}_m$, respectively the cost of the laser system and the ground-based beam director with adaptive optics. First-cut evaluations of these are now possible due to the efforts of Linda Vestal, and inputs from Claude Phipps and Jim Reilly.

For the laser, 4% electrical efficiency is assumed.

Beam Director

For the mirror:

Take $$\mathbb{C}_m = B\, D_b^q \qquad [1]$$

D_b = mirror diameter in cm

At this moment, the best numbers we have for the coefficients and exponents in mirror cost are [please note, I have converted meters to cm in Linda Vestal's mirror cost formula for consistency]

$B = 74.5$
$q = 1.9556$

Solid state laser cost

Where W = laser energy in joules

we have $$\mathbb{C}_L = 1.1 \sum_{i=1}^{4} C_i \qquad [2]$$

with the following cost elements:

Laser head[a]: $C_1 = \$1.02E6 * W^{0.45}$. [2a]

Power supply[b]: $C_2 = \$3.2E4 * (fW/1000)^{0.85}$ [2b]

Cooling gas flow loop[b]: $C_3 = \$6.8E4 * (fW/1000)^{0.88} * (f/1000)^{0.083}$ [2c]

System integration[b]: $C_4 = \$6.0E4 * (fW/1000)^{0.256}$ [2d]

---

[a] Source: C. Phipps study of the Lawrence Livermore (LLNL) Nova-Athena-NIF (National Ignition Facility) construction and engineering design sequence, plus recent input from Lloyd Hackel at LLNL regarding 100-J, 30Hz, 10-ns laser system he has built for an illuminator at Starfire Optical Range.

[b] Source: J. P. Reilly

Gas laser (excimer or CO_2) cost

Where W = laser energy in joules

we have $$\mathbb{C}_L = 1.1 \sum_{i=1}^{7} C_i \qquad [3]$$

with the following cost elements:

Laser head[b]: $C_1 = \$1.2E4*(25W)^{0.19}$. [3a]

Power supply[b]: $C_2 = \$3.2E4*(fW/1000)^{0.85}$ [3b]

Cooling gas flow loop[b]: $C_3 = \$6.8E4*(fW/1000)^{0.88}*(f/1000)^{0.083}$ [3c]

Pulse forming network[b]: $C_4 = \$4.0E3*W^{0.918}$ [3d]

Switches[b]: $C_5 = \$6.0E3*W^{0.875}(f/1000)^{0.4.}$ [3e]

Optics[b]: $C_6 = \$1.8E4*W^{0.14}$ [3f]

System integration[b]: $C_7 = \$6.0E4*(fW/1000)^{0.256}$ [3g]

Pulsed laser cost determination

Now, we use the analysis in in §0 which employs the physics of the problem, to connect the required laser parameters on the ground to the target intensity required to form plasma and obtain optimum coupling, particularly to relate laser pulse energy W to mirror diameter D_b:

$$W = \frac{Ca}{ST}\left[\frac{\lambda z}{D_b}\right]^2 \tau^{\alpha} \quad . \qquad [4]$$

In this expression,

C = 2.3E4 is a constant derived from optimum target coupling

α = 0.45 is an exponent derived from optimum target couling

τ is laser pulse width

T is atmospheric transmission (0.85 for a vertical path)

S is Strehl ratio ($1/N^2$ in § 0) = 0.5

$a = 4/\pi$

λ is laser wavelength in cm

and z is range to target in cm.

To obtain our total system cost estimate, we add laser cost to beam director cost

$$\mathbb{C}_{tot} = \mathbb{C}_L + \mathbb{C}_M. \qquad [5]$$

Substituting Eqn. [4] into Eqn. [5] gives a plot of ORION system cost versus mirror diameter D_b, for which there is always a minimum. (See Figures 3 and 4).

The physical reason for this arises from what happens at the two extremes: for very large mirrors, a small spot on the target results in a small laser pulse energy, but these huge mirrors are very expensive (and probably impossible to build). In the limit, system cost dominated by mirror cost goes up about like D_b^2. At the other extreme, a very small mirror gives a large laser spot diameter in space, requiring huge laser energy to ignite a plasma. In this limit, system cost dominated by laser cost goes up about like $1/D_b$, because Eqn. [3] requires $W \propto 1/D_b^2$, but cost (Eqn. [2a]) goes up about like $\sqrt{W}$.

Visible Region CW laser

We consider the case of a cw iodine laser (λ=1.3 μm), a case currently receiving strong attention in the USAF.

Elsewhere, calculations by J. P. Reilly have shown that I_s = 1 kW/cm^2 is the appropriate target intensity for the cw case. Extensive data taken by O'Dean P. Judd completely supports this statement.[c] For cw lasers, Eqn. [5] of section zero can be recast:

$$I_b = \frac{I_s}{ST}\left(\frac{a\,\lambda\,z}{D_b^2}\right)^2$$

from which we have $$P = \left(\frac{\pi D_b^2}{4}\right) I_b = \frac{4\,I_s}{\pi\,S\,T}\left(\frac{\lambda\,z}{D_b}\right)^2 \qquad [6]$$

which is the analog of Eqn. [4] for the required cw output (optical) laser power level on the ground.

Reilly has shown that $$\mathbb{C}_L = 1E5\,(P/1000)^{0.81} \qquad [7]$$

Eqn. [1] already covers visible region mirror costs. Combining these results and varying D_b, as we did for repetitively pulsed lasers above gives the surprising result shown in Figure 5. In fact, a cw laser operating at 1.3μm has minimum cost which is not unfavorable compared to the minimum cost of repetitively-pulsed counterparts in the above sections!

It will be noticed that the corresponding power for 800km range is in the tens of MW level. Our result is surprising to us because we had not imagined that a tens-of-MW laser could be built for a reasonable cost, and dismissed this alternative out of hand, prior to having Reilly's cost figures.

[c] O'Dean P. Judd, private communication 6/17/95.

Photonic Associates
excellence in photonics

ORION Laser Cost vs. Rep Rate

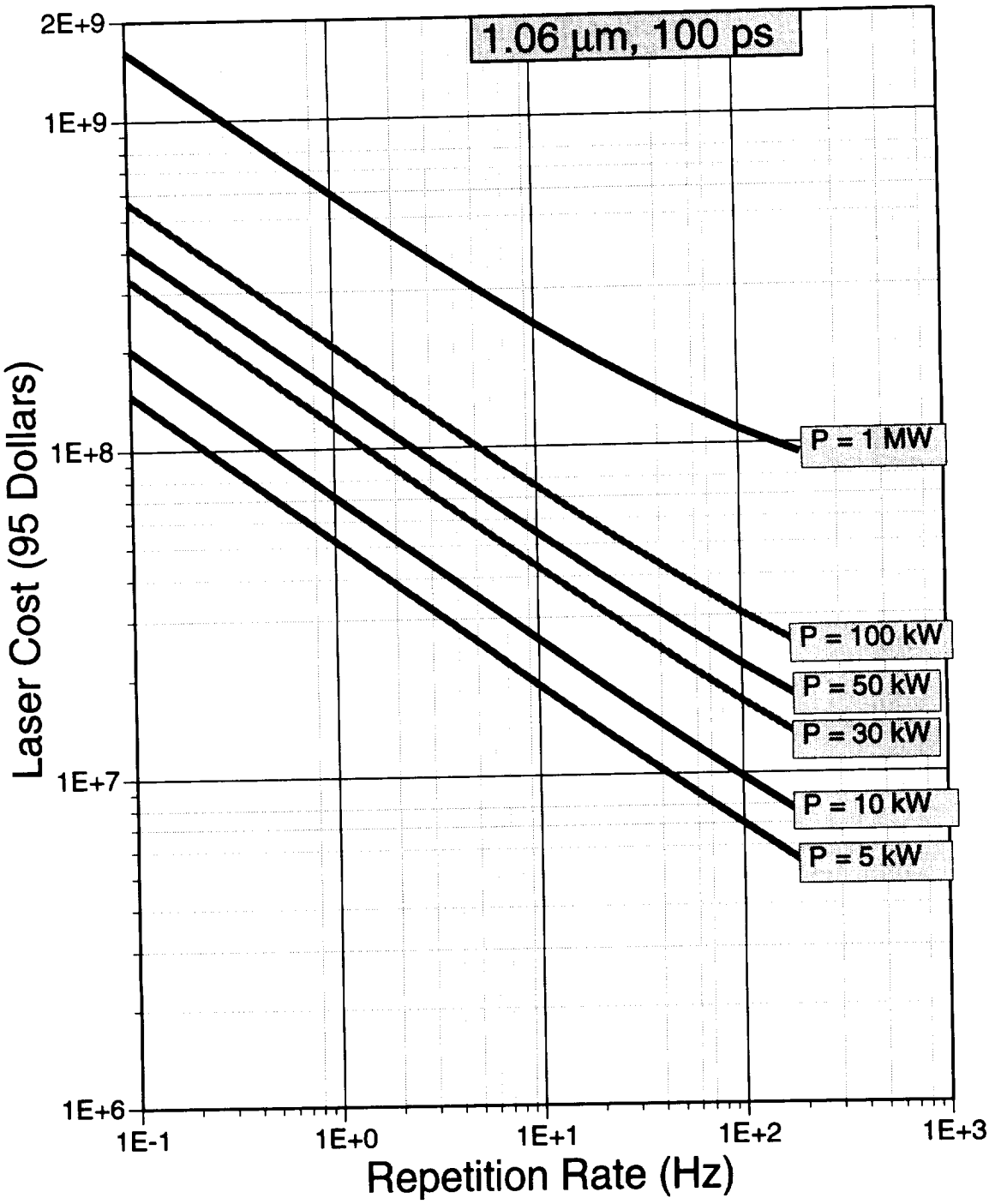

ORION Laser Cost Breakdown

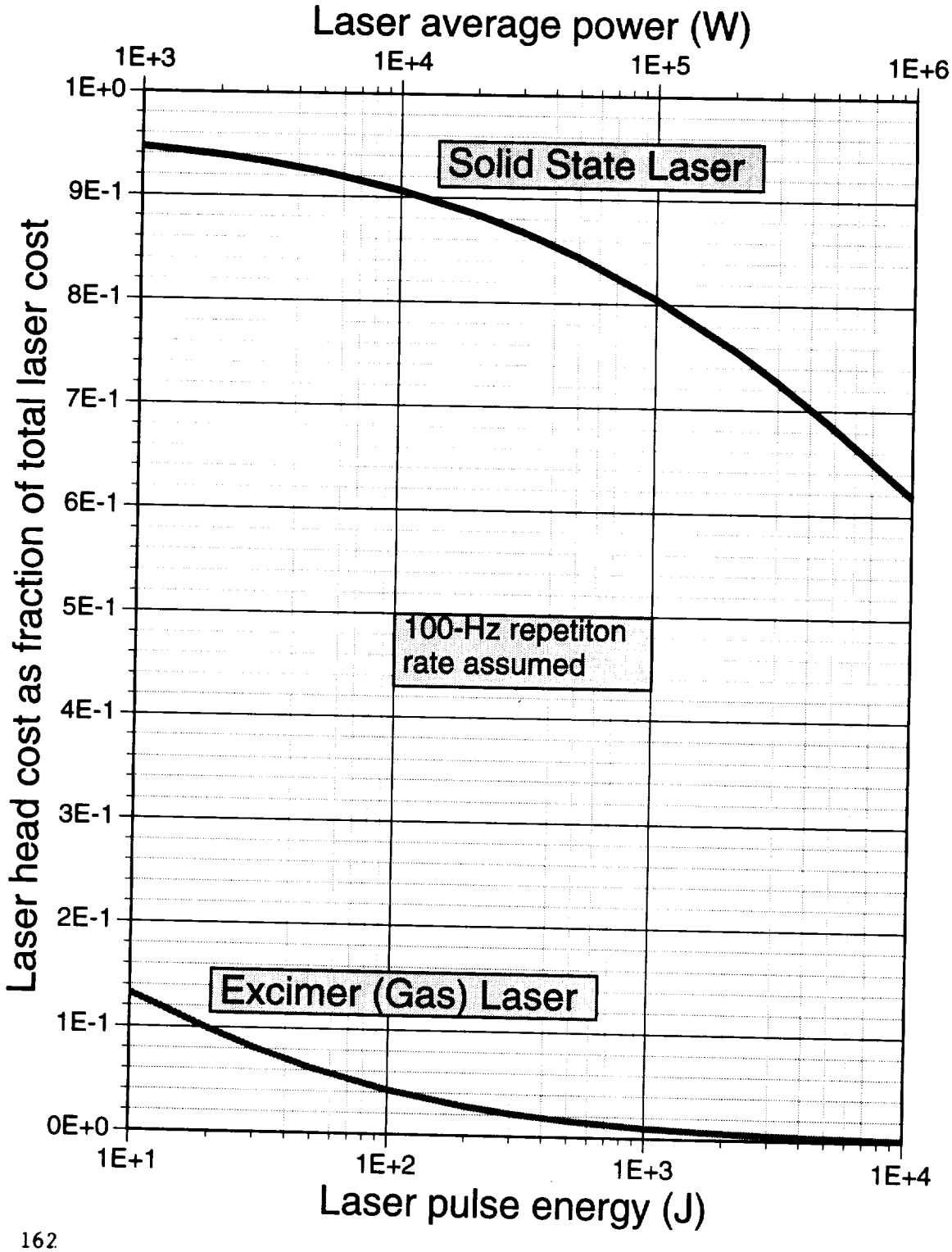

Photonic Associates
excellence in photonics

ORION System Cost vs. Mirror Diameter

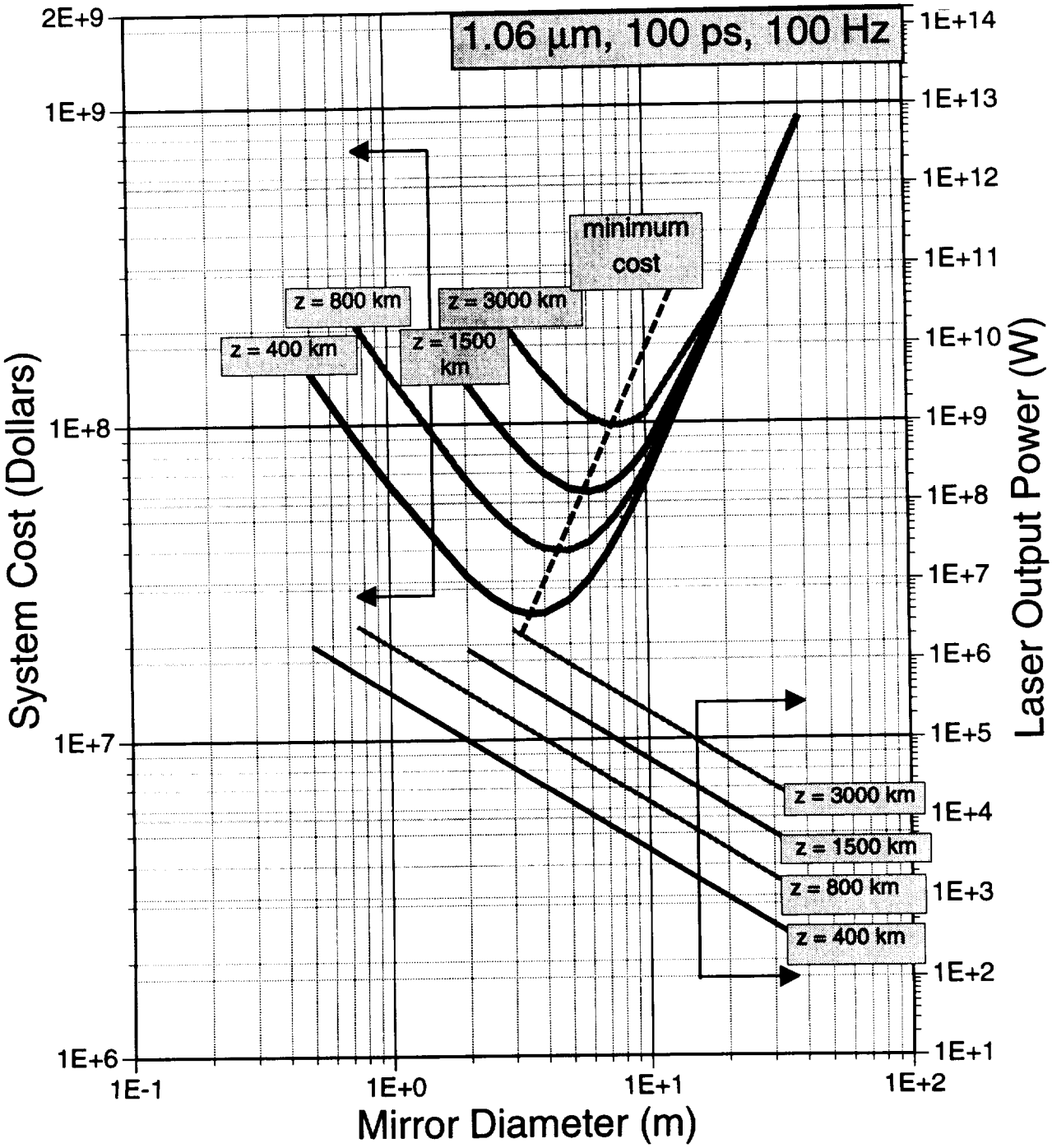

Photonic Associates
excellence in photonics

ORION System Cost vs. Mirror Diameter

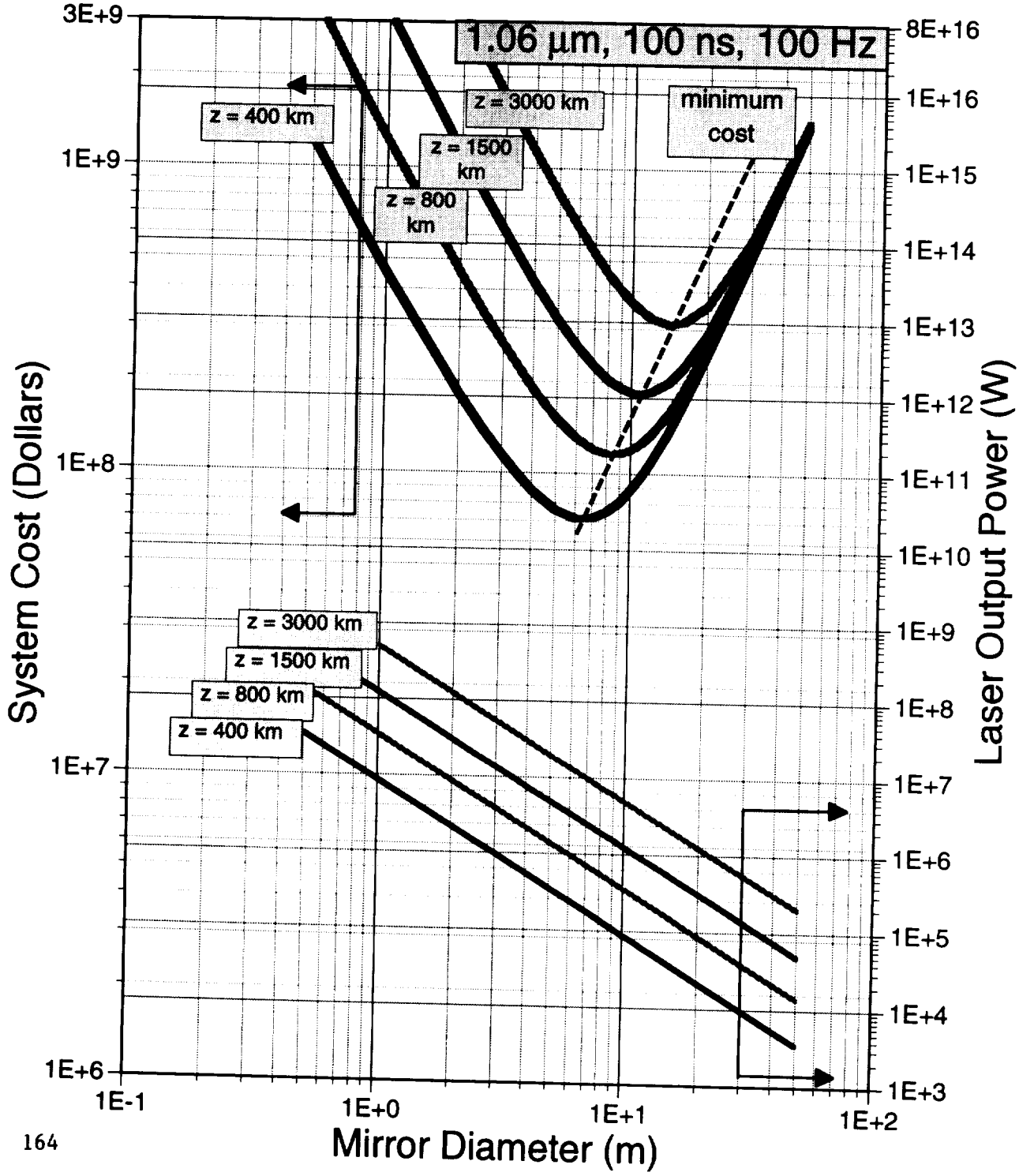

Photonic Associates
excellence in photonics

cw laser ORION costs

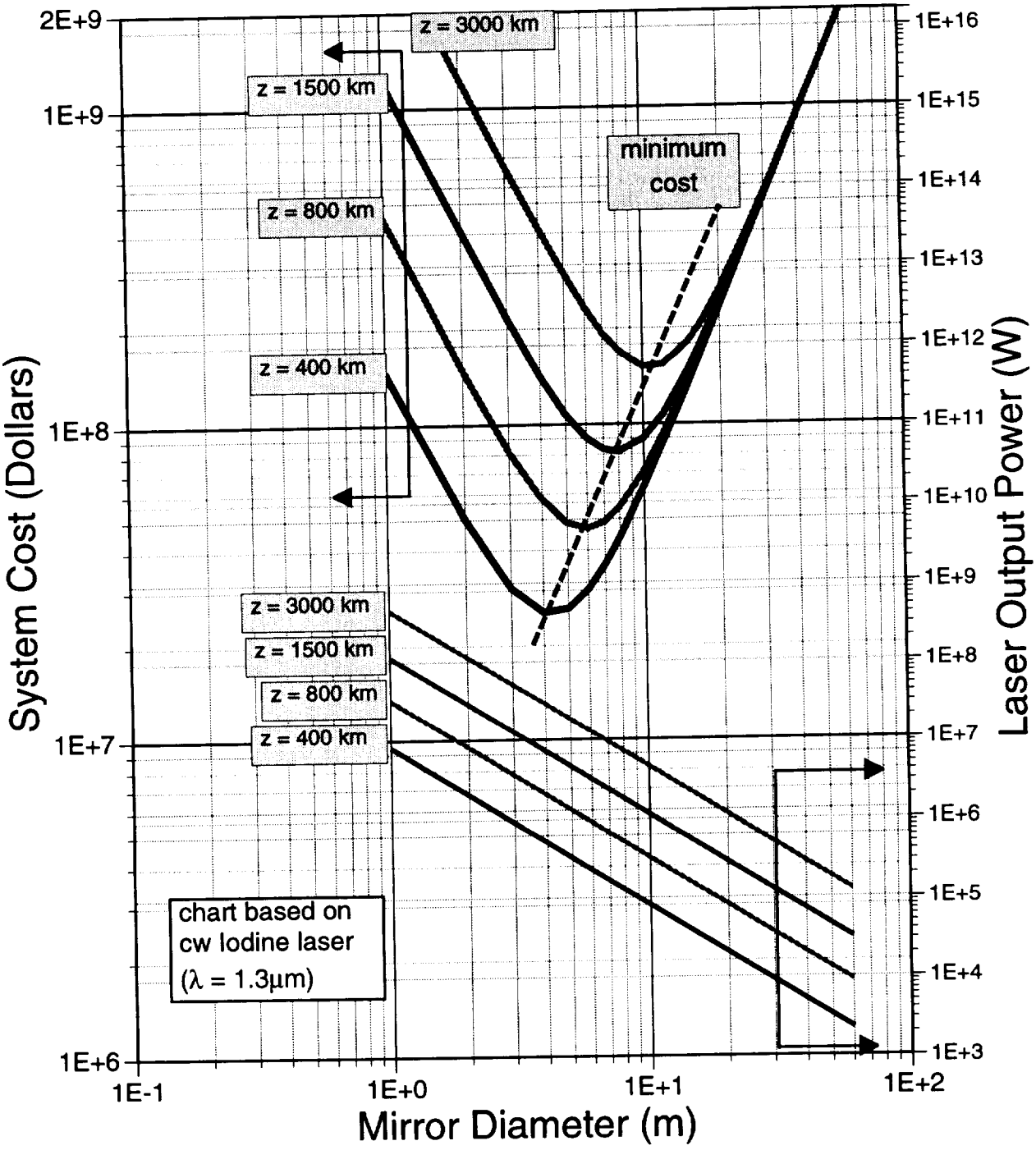

TOPIC 3: DOES A USEFUL SCALING GIVING LASER INTENSITY FOR MAXIMUM MOMENTUM COUPLING I_{MAX} IN VACUUM EXIST?

Such a relationship, if it exists, should describe, within a factor of 2 or 3, the relationship between laser fluence incident on the target (J/cm^2) and pulse duraton for a wide variety of possible debris surface characteristics and laser wavelengths, at the point where maximum impulse is generated. It would be surprising if such a universal relationship could be more accurate than a factor of 2 or 3, due to the variety of conditions under one hat. The relationship is highly useful for back-of-the-envelope scaling exercises such as led to the suggestion for a new candidate laser operating at 100 ps rather than 40 ns, which came up at the Washington kickoff meeting. Greater accuracy is not required (see Figure 1) since the typical curve for coupling vs. intensity (or fluence) changes fairly slowly near the peak. I want to reiterate that this graph gives peak coupling intensity, not plasma formation threshold, which we have been using a little too interchangeably.

Up to now, we have been using $\Phi_{max} = 8E4\sqrt{\tau}$ for the relationship, based on a quick study of a few experiments several years ago.

Now, after reviewing the data from 48 experiments spanning laser pulse durations from 300 fs (3E-13) to 1.5 ms (1.5E-3) from the UV to the IR, the answer is: yes it does exist.

Where $\Phi = c\,\tau^{\alpha}$ we have found:

Material (Expts)	c	α	rms log deviation from trend is a factor of:
All (48)	2.30 E4	0.446	3.2
Metals (30)	8.01 E5	0.648	2.4
Nonmetals (15)	5.97 E3	0.408	1.8

The index following the graph gives references for the work. For the metals graph, the 300 fs data point was deleted as not clearly relevant to our work, as were the Afanasev Cu and Pb points (b & d).

A word about scatter: The variation of coupling among materials in a carefully done experiment (take, e.g., points p,q,r,s,t,u which represent 694 nm on Be, C, Al, Zn, Ag and W) is often less than the variation among experimenters with the same materials (compare, e,g, points W,f,o,V,H,n which are all 351 nm on Al).

To qualify as relevant data, a curve like Figure 2 of §2 showing a clear maximum must have been generated, for a target in vacuum. Unfortunately, this requirement eliminates a lot of C_m vs. I data in the literature reported as single points or a trend, or where the target was in air. Coupling in air is usually quite different from vacuum coupling. I am currently including one air point in Figure 1 at 300 fs, since plasma expansion during such a very short pulse (at the sound speed) should be about 1000 times less than the mean free path of an air molecule. A table which elaborates this "index" is included.

Note that the intensity for maximum coupling is a factor of two or so above threshold for momentum production. It is also slightly above the intensity threshold for plasma ignition. The onset of plasma formation marks the onset of reduced efficiency of surface heating by the laser. This is due to two plasma-

related effects whose relative importance varies with wavelength and pulse duration: 1) surface shielding, in which the plasma becomes opaque to laser radiation, preventing it from reaching the surface and 2) reradiation, electron thermal conduction and energetic charged particle production which convert the absorbed laser energy to forms which do not reach the surface. The situation is complex, since plasma reradiation and thermal conduction also carry energy to the surface even when laser energy does not arrive there, but it is clear that more energy would arrive at the surface without the plasma.

In vacuum, plasma ignition intensity is closely related to the intensity for maximum coupling, tending to lie about a factor of two below it and following a similar trend with laser pulse duration and wavelength [see Figure 2, section 2] for the typical relationship between I_{max} and the threshold intensity for momentum production].

The 4th figure in this section shows the calculated plasma ignition threshold for aluminum with excimer laser pulses in vacuum after Rosen, *et al.* 1982.

This figure is evidence that, for a particular material and set of laser parameters in our range of interest, $I_{max}\sqrt{\tau}$ = constant is not a bad approximation.

There is a good physical reason to expect such behavior. To achieve a certain temperature (say that for vaporization and plasma formation) at x = 0 on the front surface of a single material, or on various other materials with the same product ρCK, using various combinations of I and τ, requires that $I\sqrt{\tau}$ be constant.

This can be seen from the well-known equation for the prompt temperature response of a semi-infinite solid with thermal diffusivity κ to a heat pulse $I\tau/J_o$ [see Carslaw and Jäger 1959 or Zeldovich and Raizer 1963]:

$$\{\lim|_{x<<2\sqrt{\kappa\tau}} T(x,\tau)\} = \frac{2\,I\sqrt{\tau}}{J_o \rho C \sqrt{\pi\kappa}} \exp\left(-\frac{x^2}{4\kappa\tau}\right) \qquad [1]$$

[In Eqn. (1), x is the dimension perpendicular to the solid surface, τ is laser pulsewidth, J_o = 4.185 J/cal, ρ is the material's density (g/cm^3), κ = K/(ρC) is its thermal diffusivity, K is its thermal conductivity and C is its specific heat (cal g^{-1}K^{-1})].

Finally, to avoid confusion, please be aware that the relationship for laser fluence Φ = Iτ

$$\Phi = c\,\tau^{\alpha}$$

is equivalent to $I\,\tau^{(1-\alpha)} = c$.

French Data: I finally got a response from the French on my request for the actual C_m values in their data with aluminum, particularly in the 100-ps range. Their published data[1] had arbitrary units for the coupling coefficients.

---

[1] Combis, David & Nierat, *Revue Scientifique et Technique de la Defense* , CEL-Valenton report no. 4 (1992)

It apparently took them 3 months to get approval. My interpretations of their data are summarized in the following table:

Table: C_{mopt} and I_{opt} for 1.06-μm pulses on 2024 aluminum[2]

Pulsewidth	C_{mopt}(dyne-s/J)	I_{opt}(W/cm^2)
160 ps	5.5	5.0E9
900 ps	7.0	1.3E9
4 ns	7.5	3.0E8
30 ns	6.5	6.9E7

Please see the attached, for examples of the actual 160-ps and 30-ns data sets.

The final figure shows all the French data plotted vs. the fit parameter ($I\lambda\sqrt{\tau}$), illustrating:
a) A comparison model calculated from first principles with no adjustable parameters can fit coupling data covering, in this case, a factor of 200 in pulsewidth, within a factor of 1.8 near peak coupling
b) The scatter between two different methods of taking the same data spans a (vertical) factor of 1.5., even with the most careful experimentalists in the French CEA.

References, section 1

Rosen, D. I., Mitteldorf, J., Kothandaraman, G., Pirri, A. N. and Pugh, E. R. 1982 J. Appl. Phys. **53**, 3190-3200

Zeldovitch, Ya. B. and Raizer, Yu. P. 1963*Physics of Shockwaves and High-temperature Hydrodynamic Phenomena* Moscow

Carslaw, H. S. and Jäger, J. C. 1959 *Conduction of Heat in Solids, 2nd ed.* Clarendon, Oxford

[2] P. Combis, CEL-Valenton, France (private communication)

Laser parameters for optimum momentum coupling (46 experiments, UV-IR, all materials)

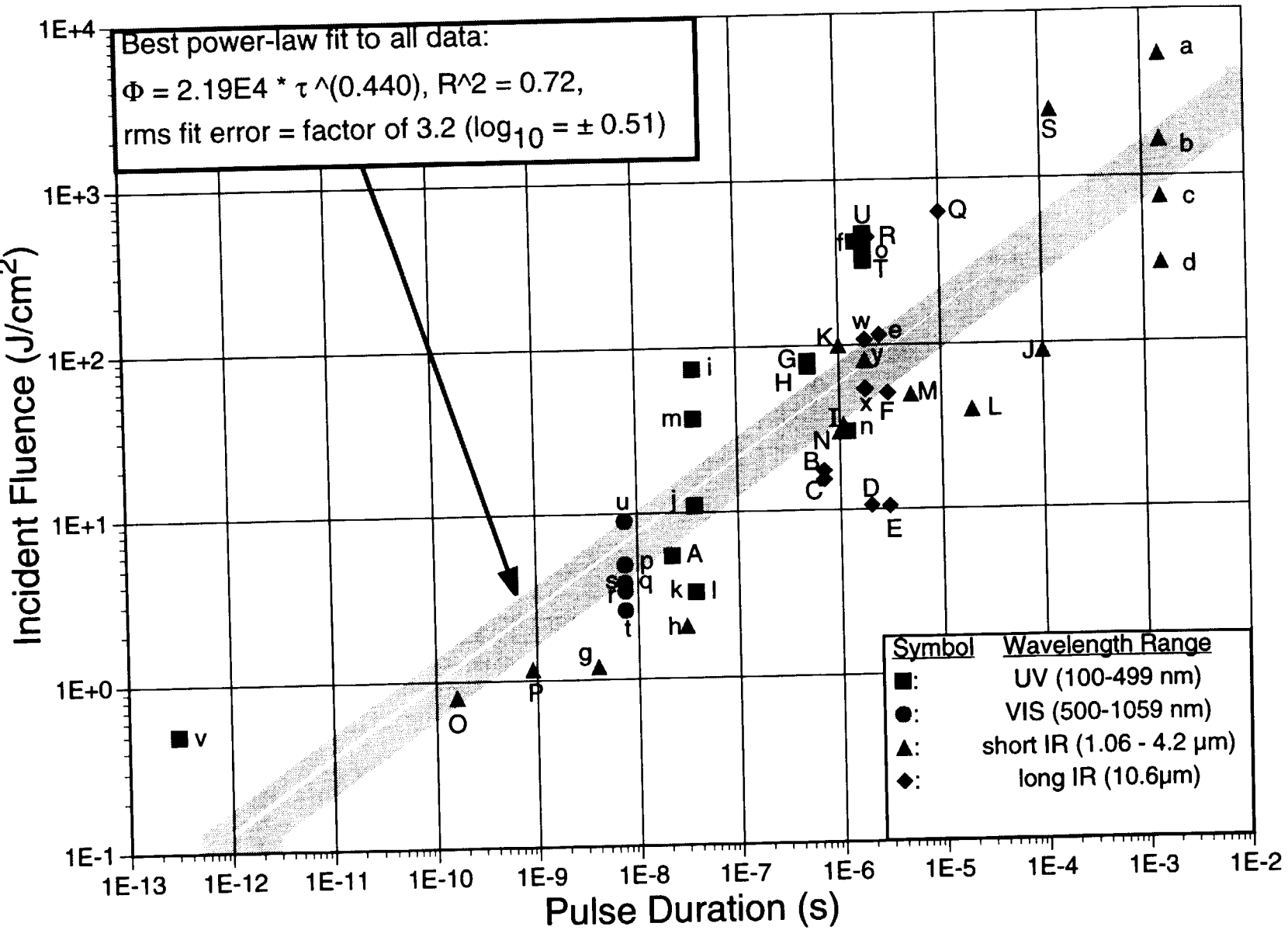

Sym	Author	λ	τ	Target
a	Afanasev	1.06μm	1.5 ms	Al
b	Afanasev	1.06μm	1.5 ms	Cu
c	Afanasev	1.06μm	1.5 ms	C
d	Afanasev	1.06μm	1.5 ms	Pb
e	Apostol	10.6μm	2.5μs	Bi
f	Augustoni	351nm	1.5μs	Al
g	Combis	1.06μm	4.0ns	Al
h	Combis	1.06μm	30ns	Al
i	Dingus	248nm	37ns	Ta
j	Dingus	248nm	37ns	Al
k	Dingus	248nm	37ns	Ti
l	Dingus	248nm	37ns	PMMA
m	Dingus	248nm	37ns	Al
n	Duzy	351nm	1.2μs	Al
o	Ermer	351nm	1.8μs	Al
p	Gregg	694nm	7.5ns	Be
q	Gregg	694nm	7.5ns	C
r	Gregg	694nm	7.5ns	Al
s	Gregg	694nm	7.5ns	Zn
t	Gregg	694nm	7.5ns	Ag
u	Gregg	694nm	7.5ns	W
v	Küper	248nm	300fs	Teflon
w	Phipps	10.6μm	1.8μs	Al
x	Phipps	10.6μm	1.8μs	Kevlar Epoxy
y	Phipps	3.0μm	1.8μs	Kevlar Epoxy

A	Phipps	248nm	22ns	Nylon
B	Phipps	10.6μm	700ns	Cellulose Nitrate
C	Phipps	10.6μm	700ns	Cellulose Acetate
D	Phipps	10.6μm	2.0μs	Pyroxylin
E	Rosen	10.6μm	3μs	Carbon Phenolic
F	Rosen	10.6μm	3 μs	C
G	Rosen	351 nm	500ns	Ti
H	Rosen	351 nm	500ns	Al
I	Rudder	1.06μm	1.1μs	Ti
J	Rudder	1.06μm	100μs	Grafoil
K	Rudder	1.06μm	1.0μs	Al
L	Rudder	1.06μm	20μs	Grafoil
M	Rudder	1.06μm	5.0μs	Grafoil
N	Rudder	1.06μm	1.0μs	Grafoil
O	Combis	1.06μm	160ps	Al
P	Combis	1.06μm	900ps	Al
Q	Shui	10.6μm	10μs	Al
R	Ursu	10.6μm	2.0μs	SS
S	Watt	1.06μm	128μs	Al
T	Wilson	351nm	1.8μs	Al
U	Wilson	351nm	1.8μs	Al

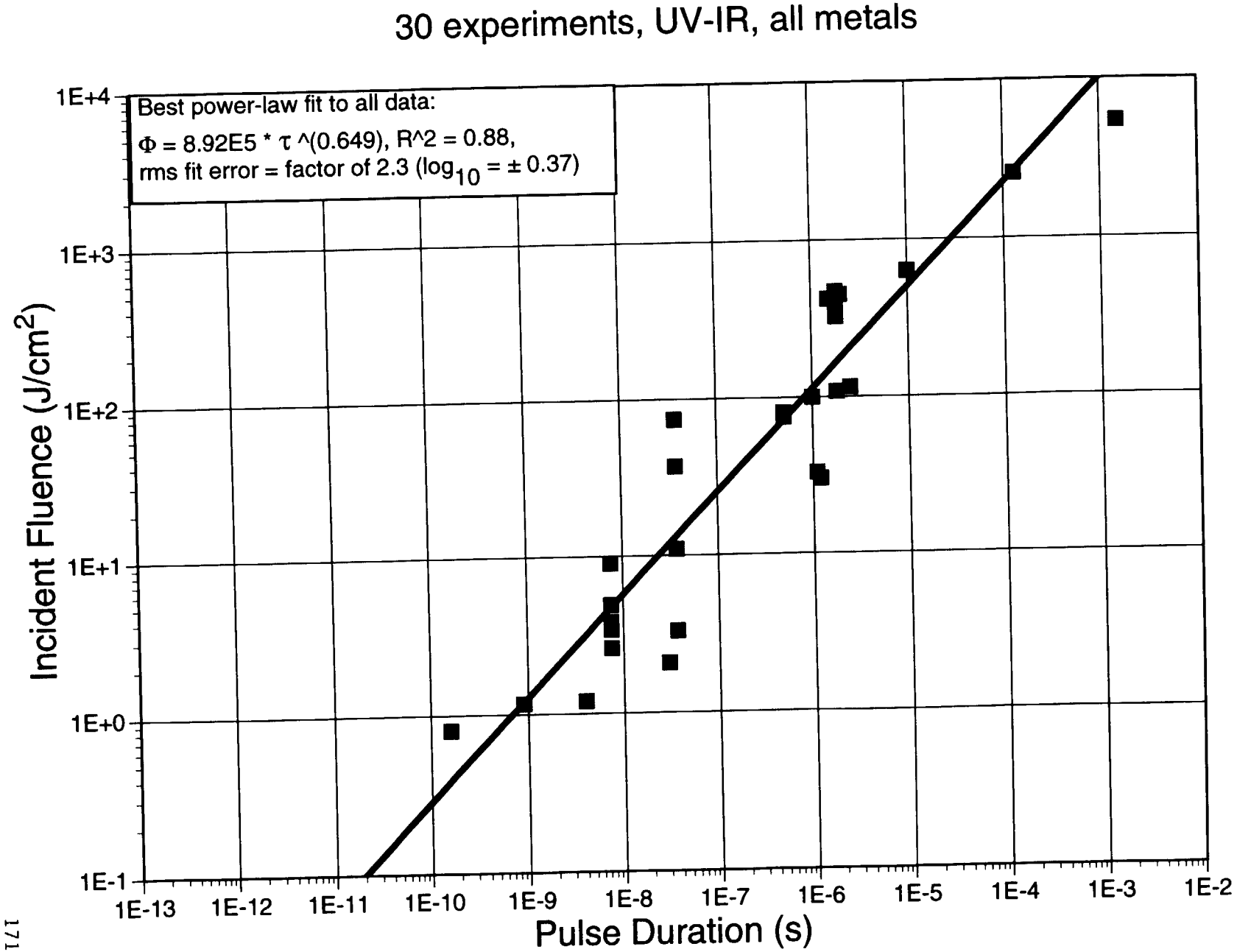
30 experiments, UV-IR, all metals
Best power-law fit to all data:
Φ = 8.92E5 * τ ^(0.649), R^2 = 0.88,
rms fit error = factor of 2.3 (log10 = ± 0.37)
Incident Fluence (J/cm2)
1E+4
1E+3
1E+2
1E+1
1E+0
1E-1
1E-13
1E-12
1E-11
1E-10
1E-9
1E-8
1E-7
1E-6
1E-5
1E-4
1E-3
1E-2
Pulse Duration (s)

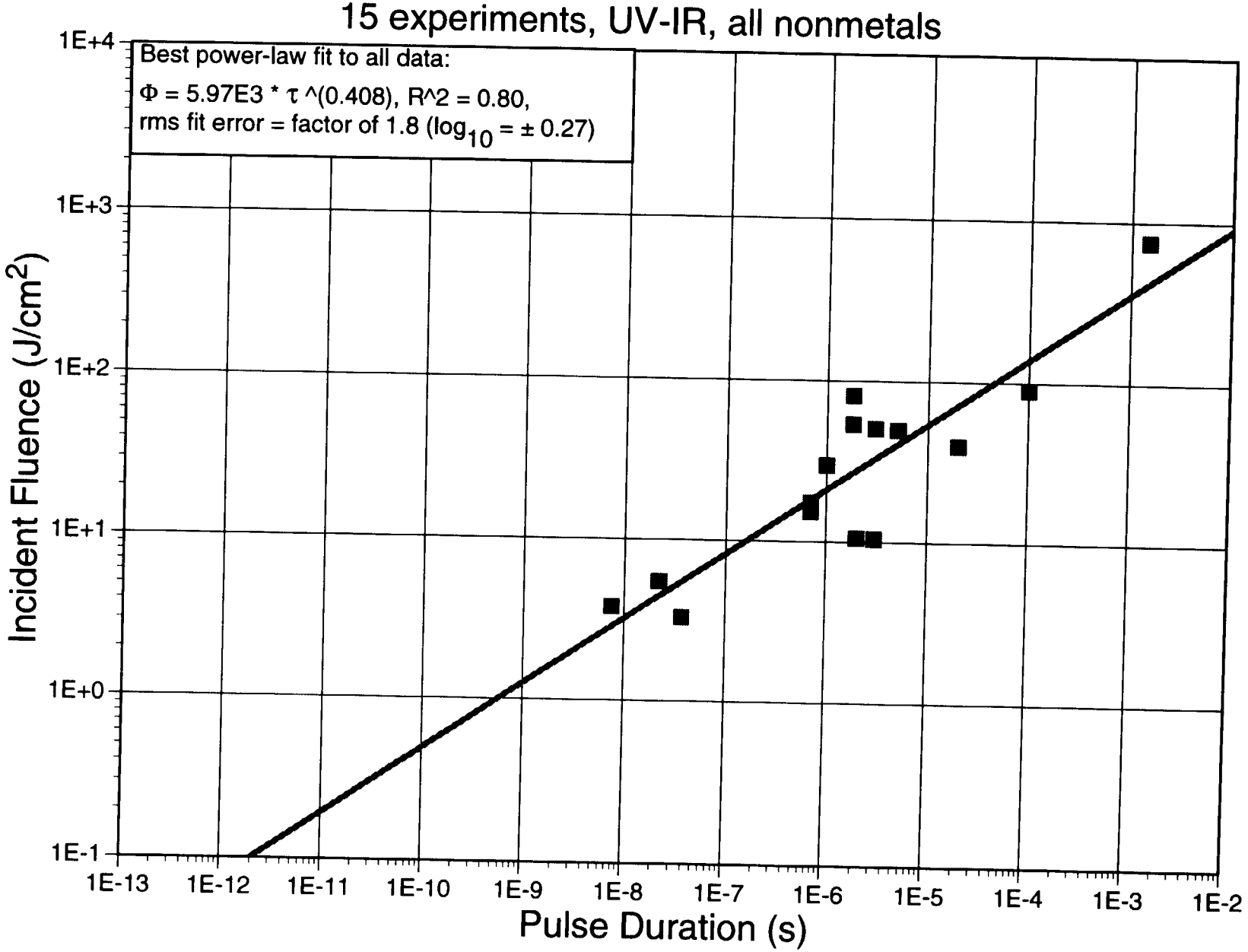
15 experiments, UV-IR, all nonmetals
Best power-law fit to all data:
Φ = 5.97E3 * τ ^(0.408), R^2 = 0.80,
rms fit error = factor of 1.8 (log10 = ± 0.27)
Incident Fluence (J/cm2)
1E+4
1E+3
1E+2
1E+1
1E+0
1E-1
1E-13
1E-12
1E-11
1E-10
1E-9
1E-8
1E-7
1E-6
1E-5
1E-4
1E-3
1E-2
Pulse Duration (s)

Predicted plasma ignition threshold for aluminum in vacuum at 350 nm wavelength, after Rosen, *et al., J. Appl. Phys.* **53,** 3190-3200 (1982)

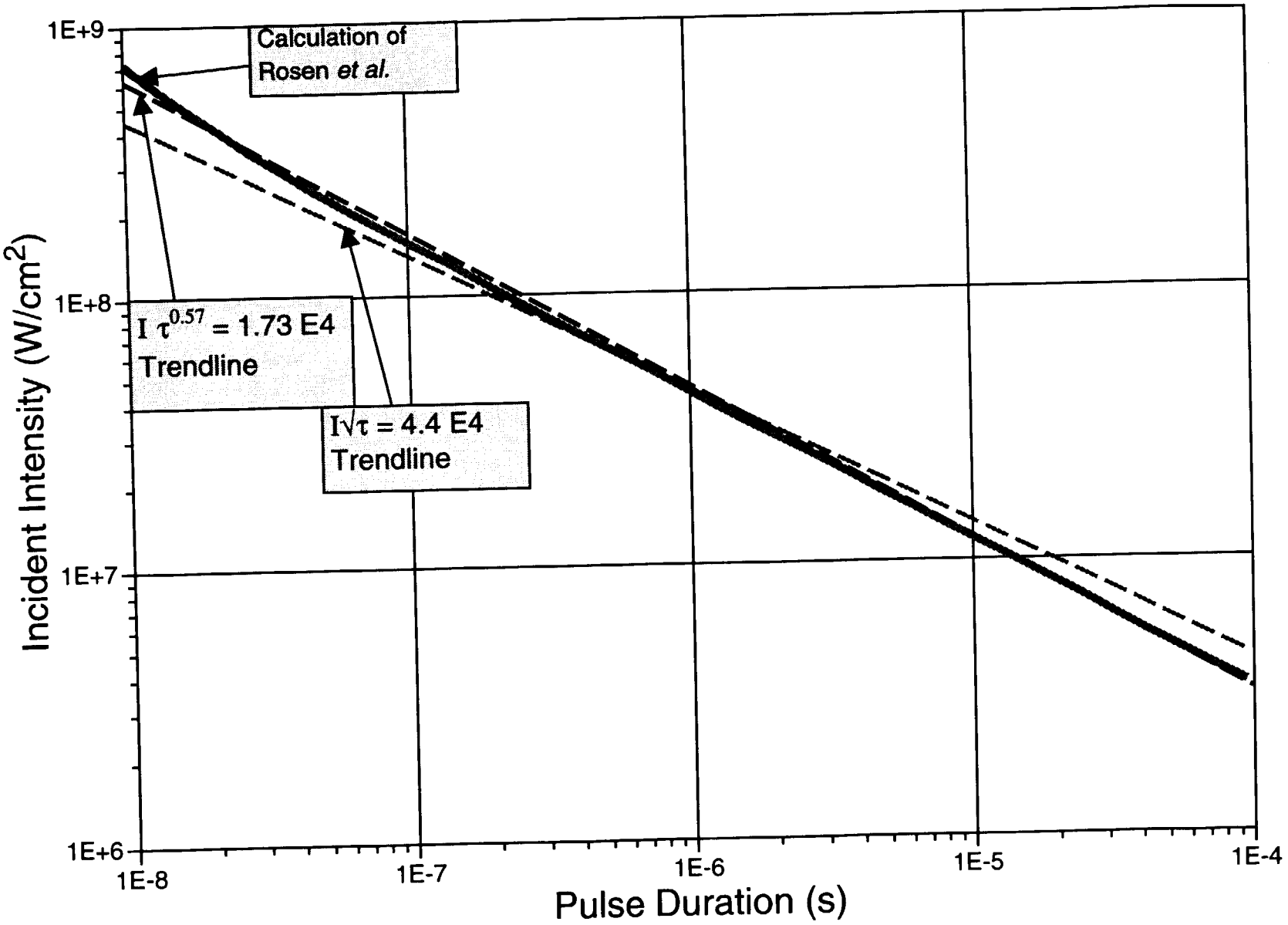

SURVEY OF LASER FLUENCE AND PULSEWIDTH FOR MAXIMUM COUPLING

λ	τ s	I_o Wcm^{-2}	Φ_o Jcm^{-2}	$I_o\sqrt{\tau}$	Target	C_m (dyne -s/J)	SYM	Comments	Source
248 E-7	37 E-9	3E8	11.1	5.8E4	Aluminum	5.7	j	5E-2 torr. Exptl data showing C_m peak	Dingus, unpublished; Phipps, et al. J. Appl. Phys. **64** 1083-96 (1988)
248 E-7	37 E-9	1E9	37	1.9E5	Aluminum	2.3	m	Vacuum. Exptl data showing C_m peak	Dingus, unpublished; Physical Sciences, Inc. final report, contract no. N00014-86-C-2241 (1987), J. McKay and P. Laufer, auth.
351 E-7	500 E-9	1.5E8	75	1.06E5	Aluminum (2024)	2.5	H	1E-4 torr. Experimental data showing peaking of C_m.	Rosen, et al. J. Appl. Phys. **53** 3190-3200 (1982)
351 E-7	1.2 E-6	2.5E7	30	2.7E4	Aluminum	3.2	n	0.1 torr Experimental data showing C_m peak	Duzy, et al. Appl. Phys. Lett. **37**, 542-4 (1980)
351 E-7	1.5 E-6	2.8E8	423	3.5E5	Aluminum	1.9	e	3E-2 torr. Exptl data showing C_m peak	Augustoni, et al. report AFWL-TR-85-126 (1986)
351 E-7	1.8 E-6	2.2E8	402	3.0E5	Aluminum	3.0	o	Vacuum. Exptl data showing C_m peak	Ermer, et al. in Physical Sciences, Inc. final report, contract no. N00014-86-C-2241 (1987), J. McKay and P. Laufer, auth.
351 E-7	1.8E-6	1.8E8	324	2.4E5	Aluminum	3.2	U	Vacuum. Exptl data showing C_m peak	Wilson 1986a in Pucik, "Optical Laser Impulse Coupling Data Package", RDA report 2/28/90
351 E-7	1.8E-6	2.6E8	470	3.5E5	Aluminum	6.0	T	Vacuum. Exptl data showing C_m peak	Wilson 1986b in Pucik, "Optical Laser Impulse Coupling Data Package", RDA report 2/28/90
694 E-7	7.5 E-9	4.5E8	3.4	3.9E4	Aluminum	6.0	r	1E-5 torr. Exptl data showing C_m peak	Gregg & Thomas J. Appl. Phys. **37** 2787-9 (1966)
1.06E-4	160 E-12	5E9	0.8	6.3E4	Aluminum 2024	5.5	O	Vacuum. Exptl data showing C_m peak	Combis, et al., Revue Scientifique et Technique de la Defense, CEL-Valenton no. 4 (1992)
1.06E-4	900 E-12	1.3E9	1.17	3.9E4	Aluminum 2024	7.0	P	Vacuum. Exptl data showing C_m peak	Combis, et al., Revue Scientifique et Technique de la Defense, CEL-Valenton no. 4 (1992)
1.06 E-4	4 E-9	3E8	1.2	1.9E4	Aluminum 2024	9.0	g	Vacuum. Exptl data showing C_m peak	Combis, David & Nierat, Revue Scientifique et Technique de la Defense, CEL-Valenton no.4 (1992)
1.06 E-4	30 E-9	6.9E7	2.07	1.2E4	Aluminum 2024	6.5	h	Vacuum. Exptl data showing C_m peak	Combis, David & Nierat, Revue Scien-tifique et Technique de la Defense, CEL-Valenton no.4 (1992)

SURVEY OF LASER FLUENCE AND PULSEWIDTH FOR MAXIMUM COUPLING

λ	τ s	I_o Wcm^{-2}	Φ_o Jcm^{-2}	$I_o\sqrt{\tau}$	Target	C_m (dyne-s/J)	SYM	Comments	Source
1.06E-4	1E-6	1E8	100	1E5	Aluminum (2024-T3)	2.0	K	Vacuum. Exptl data showing C_m peak.	Rudder, report AFWL-TR-74-100, pp 189-198 (1974)
1.06 E-4	128 E-6	2E7	2560	2.3E5	Aluminum	3.0	S	Vaccum. Exptl data showing C_m max but not a peak.	Watt, unpublished; in Pucik, "Optical Laser Impulse Coupling Data Package", RDA report 2/28/90
1.06E-4	1.5 E-3	3.6E6	5400	1.4E5	Aluminum	3.8	a	Vacuum. Exptl data showing C_m peak.	Afanasev, et al. Sov. Phys. Tech. Phys. **14** 669 (1969)[Zh. Tekh. Fiz. **39** 894 (1969)
10.6 E-4	1.8 E-6	6E7	108	8.0E4	Aluminum	1.7	w	Vacuum. Exptl data showing C_m peak	Phipps, et al, J. Appl. Phys. **64** 1083-96 (1988); unpublished presentation to USAF Space Div 10/18/84
10.6 E-4	10 E-6	6.3E7	630	2E5	Aluminum	2.05	Q	0.5 torr. Exptl data showng C_m peak	Shui, Young & Reilly, AIAA Journal **16** 649-50 (1978)
694 E-7	7.5 E-9	6.5E8	4.9	5.6E4	Berylium	3.4	p	1E-5 torr. Exptl data showing C_m peak	Gregg & Thomas J. Appl. Phys. **37** 2787-9 (1966)
10.6 E-4	2.5 E-6	4.6E7	115	7.3E4	Bismuth	7.7	d	1E-3 torr. Exptl data showing C_m peak	Apostol, et al. So.v J. Quant. Electron. **6** 1119-20 (1976)
10.6E-4	3 E-6	3.5E6	10.5	6.1E3	carbon phenolic	7.7	E	0.03-0.2 torr	Rosen, Nebolsine & Wu paper V1, AIAA Conf. Dynamics High Power Lasers, Cambridge, MA (1978)
10.6 E-4	700 E-9	2.2E7	15.4	1.8E4	cellulose acetate	11	C	1E-5 torr. Exptl data showing C_m peak	Phipps, et al. J.Lasers & Particle Beams **8** 281-97 (1990)
10.6 E-4	700 E-9	2.5E7	17.5	2.1E4	cellulose nitrate	33	B	1E-5 torr. Exptl data showing C_m peak	Phipps, et al. J. Lasers & Particle Beams **8** 281-97 (1990)
1.06E-4	1.5 E-3	1.1E6	1650	4.3E4	Copper	3.4	b	Vacuum. Exptl data showing C_m peak.	Afanasev, et al. Sov. Phys. Tech. Phys. **14** 669 (1969)[Zh. Tekh. Fiz. **39** 894 (1969)
1.06E-4	1 E-6	3E7	30	3.0E4	Grafoil	5.0	M	Vacuum. Exptl data showing C_m peak.	Rudder, report AFWL-TR-74-100, pp 189-198 (1974)
1.06E-4	5 E-6	1E7	50	2.2E4	Grafoil	4.55	L	Vacuum. Exptl data showing C_m peak.	Rudder, report AFWL-TR-74-100, pp 189-198 (1974)

SURVEY OF LASER FLUENCE AND PULSEWIDTH FOR MAXIMUM COUPLING

λ	τ s	I_o Wcm^{-2}	Φ_o Jcm^{-2}	$I_o\sqrt{\tau}$	Target	C_m (dyne-s/J)	SYM	Comments	Source
1.06E-4	20 E-6	2E6	40	8.9E3	Grafoil	4.7	K	Vacuum. Exptl data showing C_m peak.	Rudder, report AFWL-TR-74-100, pp 189-198 (1974)
1.06E-4	100E-6	9E5	90	9E3	Grafoil	4.7	J	Vacuum. Exptl data showing C_m peak.	Rudder, report AFWL-TR-74-100 , pp 189-198 (1974)
694 E-7	7.5 E-9	5E8	3.8	4.3E4	Graphite	7.5	q	1E-5 torr. Exptl data showing C_m peak	Gregg & Thomas J. Appl. Phys. **37** 2787-9 (1966)
1.06 E-4	1.5 E-3	5.0E5	750	1.9E4	Graphite	5.4	c	Vacuum. Exptl data showing C_m peak.	Afanasev, et al. Sov. Phys. Tech. Phys. **14** 669 (1969)[Zh. Tekh. Fiz. **39** 894 (1969)
10.6E-4	3 E-6	1.7E7	51	1.7E7	Graphite (ATJ-S)	3.8	F	0.03-0.2 torr	Rosen, Nebolsine & Wu paper V1, AIAA Conf. Dynamics High Power Lasers, Cambridge, MA (1978)
3E-4	1.8E-6	4.5E7	81	4.3E4	kevlar epoxy	15.6	y	1E-4 torr. Exptl data showing C_m peak	Phipps, et al. (unpublished)
10.6 E-4	1.8E-6	3E7	54	4.0E4	kevlar epoxy	2.4	x	Vacuum. Exptl data showing C_m peak	Phipps, et al, J. Appl. Phys. **64** 1083-96 (1988); unpublished pre-sentation to USAF Space Div 10/84
1.06 E-4	1.5 E-3	2.0E5	300	7.7E3	Lead	16	d	Vacuum. Exptl data showing C_m peak.	Afanasev, et al. Sov. Phys. Tech. Phys. **14** 669 (1969)[Zh. Tekh. Fiz. **39** 894 (1969)
248 E-7	22 E-9	2.5E8	5.5	3.7E4	nylon	6.5	A	1E-5 torr. Exptl data showing C_m peak. Same data as for I_{opt} fitting fn.	Phipps, et al. J. Appl. Phys. **64** 1083-1096 (1988)
248 E-7	37 E-9	9E7	3.3	1.7E4	PMMA (lucite)	11.8	l	5E-2 torr. Exptl data showing C_m peak	Dingus, unpublished; Physical Sciences, Inc. final report, contract no. N00014-86-C-2241 (1987), J. McKay and P. Laufer, auth.
10.6 E-4	2 E-6	5.3E6	10.6	7.5E3	pyroxylin	93	D	1E-5 torr. Exptl data showing C_m peak	Phipps, et al.J. Lasers & Particle Beams **8** 281-97 (1990)
694 E-7	7.5 E-9	3.5E8	2.6	3.0E4	Silver	6.3	t	1E-5 torr. Exptl data showing C_m peak	Gregg & Thomas J. Appl. Phys. **37** 2787-9 (1966)

SURVEY OF LASER FLUENCE AND PULSEWIDTH FOR MAXIMUM COUPLING

λ	τ s	I_o Wcm^{-2}	Φ_o Jcm^{-2}	$I_o\sqrt{\tau}$	Target	C_m (dyne-s/J)	SYM	Comments	Source
10.6 E-4	2 E-6	1.2E8	450	1.6E5	Stainless Steel	1.5	R	1E-2 torr. Exptl data showing C_m peak	Ursu, et al. Opt. Comm. **39** 180-185 (1981)
248 E-7	37 E-9	2E9	74	3.9E5	Tantalum	3.2	i	Vacuum. Exptl data showing C_m peak	Dingus, unpublished; in Physical Sciences, Inc. final report, contract no. N00014-86-C-2241 (1987), J. McKay and P. Laufer, auth.
248 E-7	300 E-15	1.7E12	0.5	9.1E5	Teflon	---	v	AIR. Included because of scarcity of very short pulse data. Criterion: Q* min = C_m max.	Küper & Stuke, Appl. Phys. Lett. 54, 4-6 (1989)
248 E-7	37 E-9	9E7	3.3	1.7E4	Titanium	4.2	k	5E-2 torr. Exptl data showing C_m peak	Dingus, unpublished; Physical Sciences, Inc. final report, contract no. N00014-86-C-2241 (1987), J. McKay and P. Laufer, auth.
351 E-7	500 E-9	1.6E8	80	1.1E5	Titanium (6Al4V)	3.6	G	1E-4 torr. Experimental data showing peaking of C_m.	Rosen, Hastings & Weyl J. Appl. Phys. 53 5882-5890 (1982)
1.06E-4	1.1E-6	3E7	33	3.1E4	Titanium (6Al-4V)	2.4	I	Vacuum. Exptl data showing C_m peak.	Rudder, report AFWL-TR-72-243, pp. 92-6(1972)
694 E-7	7.5 E-9	1.2E9	9.0	1.0E5	Tungsten	5.7	u	1E-5 torr. Exptl data showing C_m peak	Gregg & Thomas J. Appl. Phys. **37** 2787-9 (1966)
694 E-7	7.5 E-9	5E8	3.8	4.3E4	Zinc	9.5	s	1E-5 torr. Exptl data showing C_m peak	Gregg & Thomas J. Appl. Phys. **37** 2787-9 (1966)

DATA FROM OTHER SOURCES: LASER FLUENCE AND PULSEWIDTH FOR PLASMA INITIATION

Source	λ	τ s	I_o Wcm^{-2}	Φ_o Jcm^{-2}	$I_o\sqrt{\tau}$	Target	SYM	Ablation data $Q^*=\Phi/\rho x_v$	Comments
Benkov, et al. Sov. Tech. Phys. Lett 10,290-1(1984) [Pisma Zh. Tekh. Fiz. 10,689-2]	694 nm	60 ns	1.3E8	7.83	3.2E4	W	α		1E-4 torr collapse of surface reflectance at plasma threshold
Benkov, et al. Sov. Tech. Phys. Lett 10,290-1(1984) [Pisma Zh. Tekh. Fiz. 10,689-2]	694 nm	250 μs	2.0E6	506	3.2E4	W	β		1E-4 torr collapse of surface reflectance at plasma threshold
Beverly & Walters J. Appl. Phys. **47**, 3485-95 (1976)	10.6 μm	80 ns	1.5E8	12	4.2E4	Cellulose acetate	δ		2 torr. Plasma initiation time $\lessapprox$ pulse "spike" duration
Beverly & Walters J. Appl. Phys. **47**, 3485-95 (1976)	10.6 μm	80 ns	1.6E8	13	4.5E4	Aluminum	ε		2 torr. Plasma initiation time $\lessapprox$ pulse "spike" duration
Dreyfus, et al. SPIE **71C** 46-51 (1987)	248 nm	20 ns	5.5E7	1.1	7.8E3	Al_2O_3	ϕ		1E-6 torr. "significant plasma formation in the plume"
Dreyfus, J. Appl. Phys. **69**, 1721-1729 (1990)	193 nm	10 ns	4E8	4.0	4E4	Cu OFHC	γ		1E-6 torr. "spark". saturation of Cu^o in plume
Dreyfus, J. Appl. Phys. **69**, 1721-1729 (1990)	351 nm	10 ns	8E8	8.0	8E4	Cu OFHC	κ		1E-6 torr. "plasma". saturation of Cu^o in plume
Rothenberg & Kelly, Nucl. Inst. Meth. B. **229** 293-300 (1984)	248nm	12ns	8.32E7	1.0	9E3	Al_2O_3	λ	x_v=20nm ρ=2.77 Q^* =1.8E5 J/g	1E-6 torr. surface flash, Al I spectrum
Rothenberg & Kelly, Nucl. Inst. Meth. B. **229** 293-300 (1984)	532 nm	7ns	7.14E8	5.0	6.0E4	Al_2O_3	μ		1E-6 torr. surface flash, Al I spectrum

DATA FROM OTHER SOURCES: LASER FLUENCE AND PULSEWIDTH FOR PLASMA INITIATION

Source	λ	τ s	I_o Wcm^{-2}	Φ_o Jcm^{-2}	$I_o\sqrt{\tau}$	Target	SYM	Ablation data $Q^*=\Phi/\rho x_v$	Comments
Sutcliffe & Srinivasan, J. Appl. Phys. **60**, 3315-3322 (1986)	308 nm	15 ns	1.67E7	0.25	2.0E3	poly-imide		x_v=200nm ρ=1.44 Q^* =8.7E3 J/g	AIR. arbitrary: max etch depth recorded. Included for pulse comparison, not plotted.
Sutcliffe & Srinivasan, J. Appl. Phys. **60**, 3315-3322 (1986)	308 nm	5 ps	8E11	4.0	1.8E6	poly-imide		x_v=200nm ρ=1.44 Q^* =1.4E5 J/g	AIR. arbitrary: max etch depth recorded for 5ps pulse. Included for pulse comparison, not plotted.
Viswanathan & Hussla, J. Opt. Soc. Am. B 3 796-800 (1986)	248 nm	15 ns	500E6	7.5	6.12E4	Cu polyxtal	ν		UHV onset of Cu^+; "visual observation of green plume"
von Gutfeld & Dreyfus, Appl. Phys. Lett. 54, 1212-14 (1989)	248 nm	10 ns	1.5E8	1.5	1.5E4	Cu	ω		5E-5 torr. collapse of ion velocity below this fluence.

Coupling Coefficient vs. Intensity

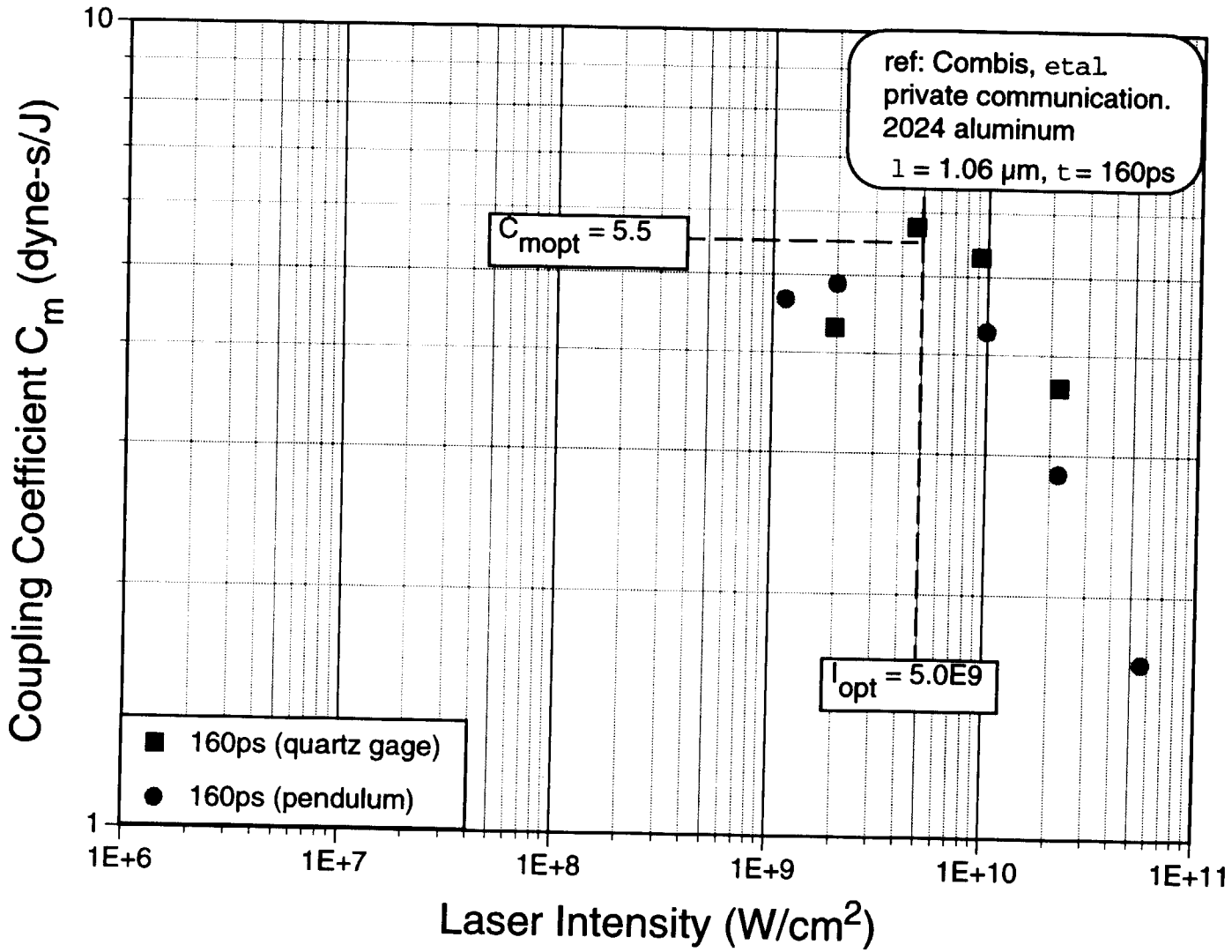

Photonic Associates
excellence in photonics

Coupling Coefficient vs. Intensity

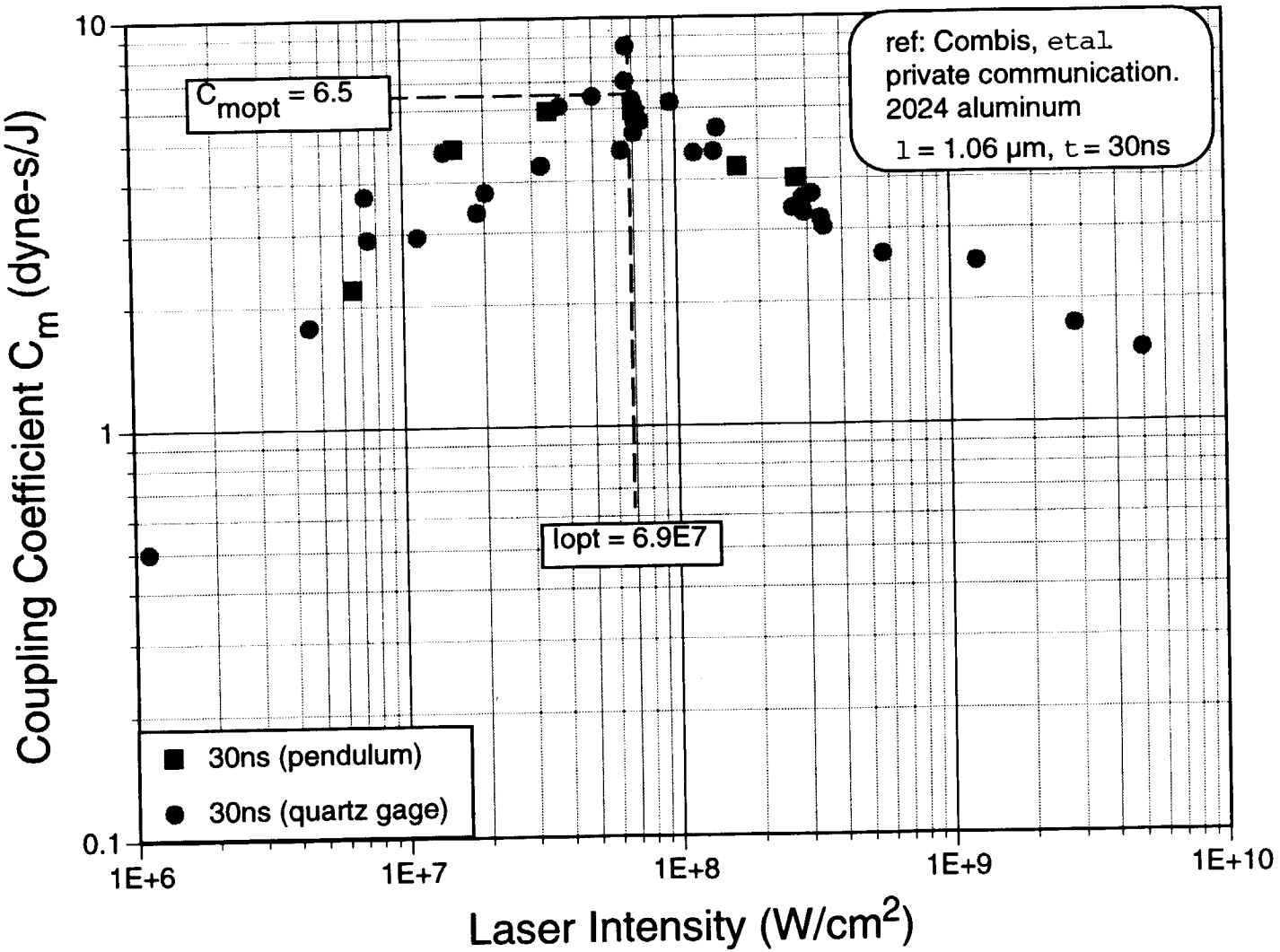

Coupling Coefficient vs. Intensity

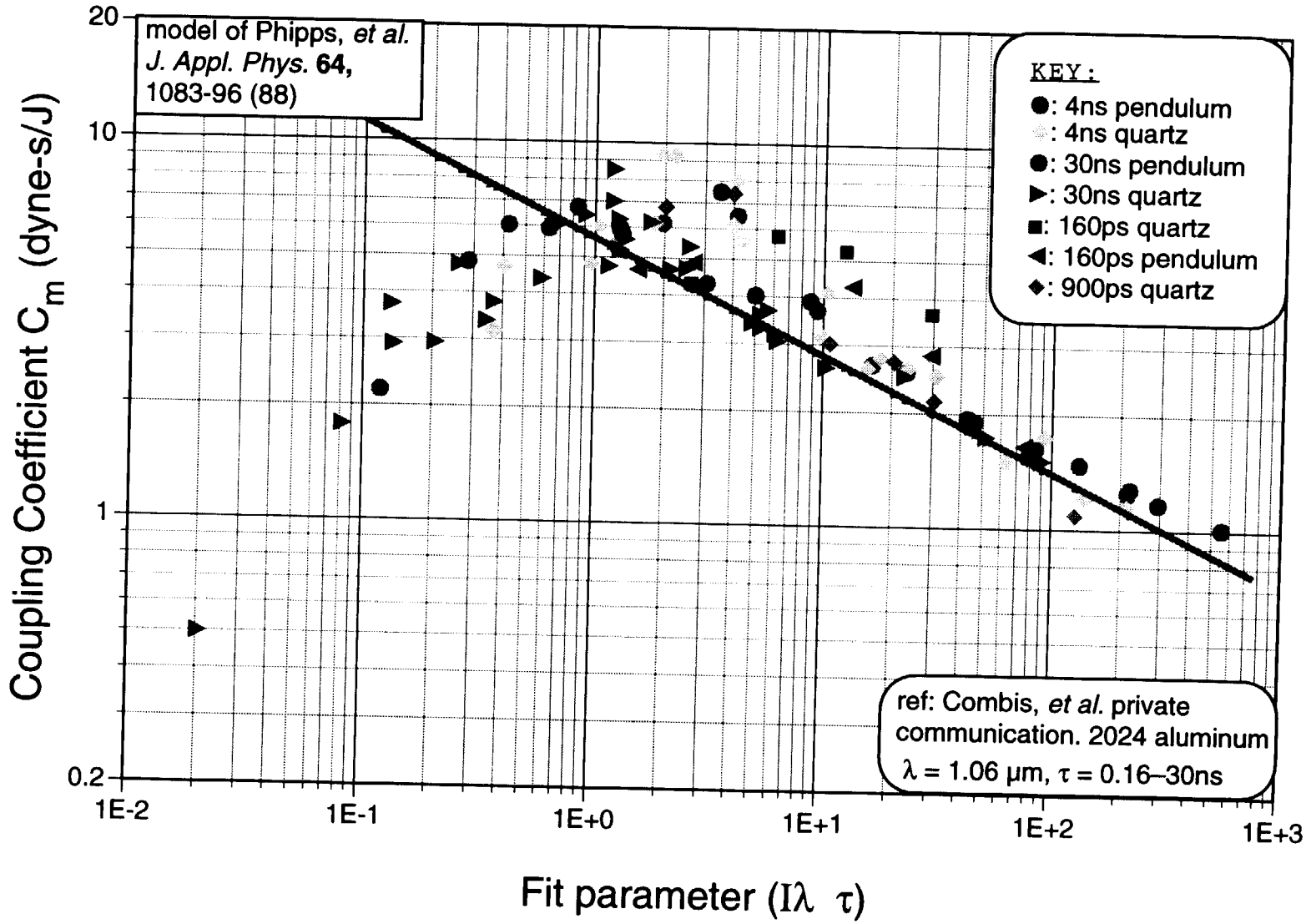

Photonic Associates
excellence in photonics

We have the pieces

Required laser pulse energy on the ground **W**

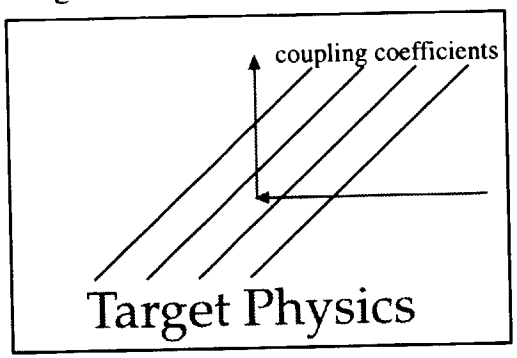

$\leftarrow \Delta v$

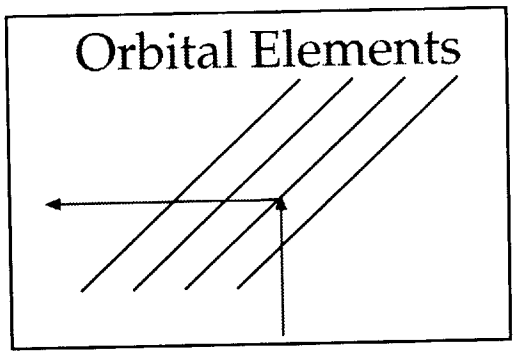

Δh_p

Debris size d, ρ

Shape $\Rightarrow \frac{A}{m}$:

Cube $\frac{1}{\rho d}$ Plate $\frac{1}{\rho t}$

Sphere $\frac{3}{2\rho d}$ Rod, side–on $\frac{4}{\pi\rho d}$

$\frac{A}{m}$ $\frac{TA}{m}$

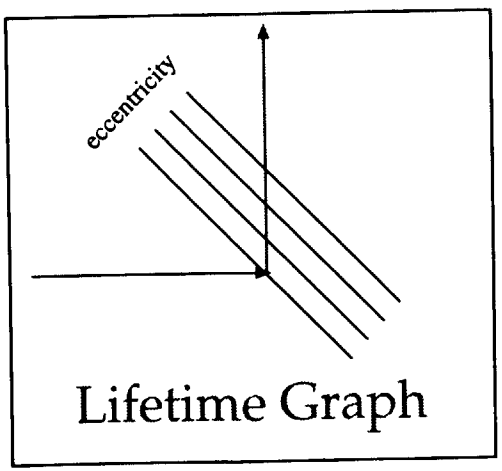

Desired Lifetime T

TOPIC 4: NONLINEAR RESPONSE OF AIR AT 100 ps.

NOTE: this section supersedes the previous handout on nonlinear index. Please discard your copy of the old section 5.

As pointed out in the kickoff meeting, an attractive short-pulse option (τ =100 ps) exists for the ORION laser which offers some advantages.

The preliminary analysis presented there indicated that this pulsewidth will allow us to use a smaller mirror as well as a smaller laser while still igniting a plasma and coupling well to the debris target and - because the Raman intensity threshold goes up for short pulses - still avoid stimulated Raman scattering in the atmosphere.

However, *nonlinear refraction* in the atmosphere may replace SRS as a concern for this laser. This note considers that possibility.

As illustrated in the inset figure, n_2 causes an instantaneous increase in the refractive index of the medium through which the pulsed laser beam passes which is proportional to the local intensity. Of course, we could take pains to make the beam intensity I(r) uniform in the near field (where a is the beam radius, the "near field" is defined as propagation distance z such that $z < a^2/\lambda$, about 6000 km). In this case n_2 would only add some additional frequency components to the beam due to the rapid change of phase during the rising and falling part of the pulse. However, this is normally an inefficient way of apodizing a beam, diffracting away energy which could have reached the target. Usually, we want a rounded beam shape, like the gaussian shown for illustrative purposes, which then causes the medium (air) to look like a lens.

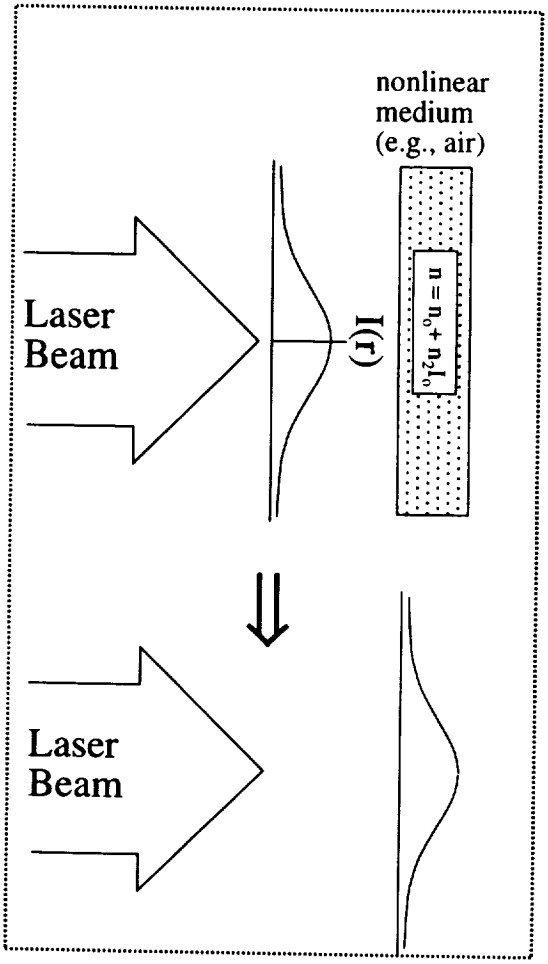

The nonlinear index n_2 in 1 atmosphre of air at standard temperature has been measured at 1.053μm [see Pennington, Henesian and Hellwarth 1988], and is

$$n_2 = (1.0 \pm 0.1)\ \text{E-16 esu} = 4.19\ \text{E-10 cm}^2/\text{GW}. \quad [1]$$

If, as in the kickoff meeting notes, we use a laser energy W = 1.2 kJ in a D_b = 500 cm beam with pulse duration τ = 100 ps, then the near field beam intensity is I_b = 60 MW/cm^2. This intensity would give 1 radian of phase shift in a distance

$$z = (k n_2 I_o)^{-1} = 6.33\ \text{km}/\lambda_{\mu m} \quad [2]$$

which, even at 1μm wavelength, is similar to the effective total thickness of the atmosphere. Previously, we used the fact that the rotational relaxation time T in atmospheric pressure air is about 100 ps [Pennington, *et al.* 1988] and theory for incorporating relaxation times which are similar to or longer than the laser pulsewidth [Marburger 1975] to conclude that the phenomena responsible for n_2 would not be able to follow a 100-ps

Nevertheless, it is now clear that this analysis was incorrect. A recent paper [Shaw, *et al.* 1990] clearly shows very little relaxation in measurements of phase shift in the atmosphere made with a τ=10ps KrF laser (248 nm). Shaw, et al. estimate the relevant relaxation times to be of order 1 or 2 ps rather than 100 ps.

Of course, in assessing relaxation processes, there are normally two separate time constants which are relevant. One is T_2, the dephasing time. This is related to the Raman linewidth $\Delta\nu$ (Hz, not radian frequency) by

$$T_2 = (\pi\Delta\nu_2)^{-1} \qquad [3]$$

The Raman linewidth in nitrogen, the main constituent of air, is pressure broadened for altitudes below about 40km in the atmosphere (pressures larger than about 2 torr), above which Doppler broadening is dominant [Kurnit, Ackerhalt and Watkins 1987]. In the pressure broadened regime,

$$\Delta\nu_2 = pB \qquad [4]$$

and B for room temperature N_2 is 3270 Mhz/amagat [Herring, Dyer and Bischel 1986] for the dominant rotational Raman lines, hence the $T_2 \approx 100$ ps estimate.

The other important relaxation time is T_1, the so-called longitudinal relaxation time, which is the time constant for the population difference between two states to decay. Shaw, *et al.* use the frequency difference between the rovibrational bands in nitrogen and oxygen

$$\Delta\nu_1 = 2.36\sqrt{bT} \qquad [5]$$

to estimate what is effectively $T_1 \approx 1 - 2$ ps for air.

There is even a third time constant which is much faster than these two, that for relaxation of electronic effects in air, that is, the nonlinear susceptibility which would still be present if the molecules were not free to rotate, but these are only 8% of the total nonlinear susceptibility [Pennington, Henesian and Hellwarth 1989].

Using the results of the previous section 5 analysis without dwelling on them, the picture that emerges for n_2 in vertical propagation through the atmosphere, as pulsewidth τ drops from a few ns to a few fs, is:

1. Relaxation of that part of n_2 due to T_2 after the fashion shown in the following Figure:

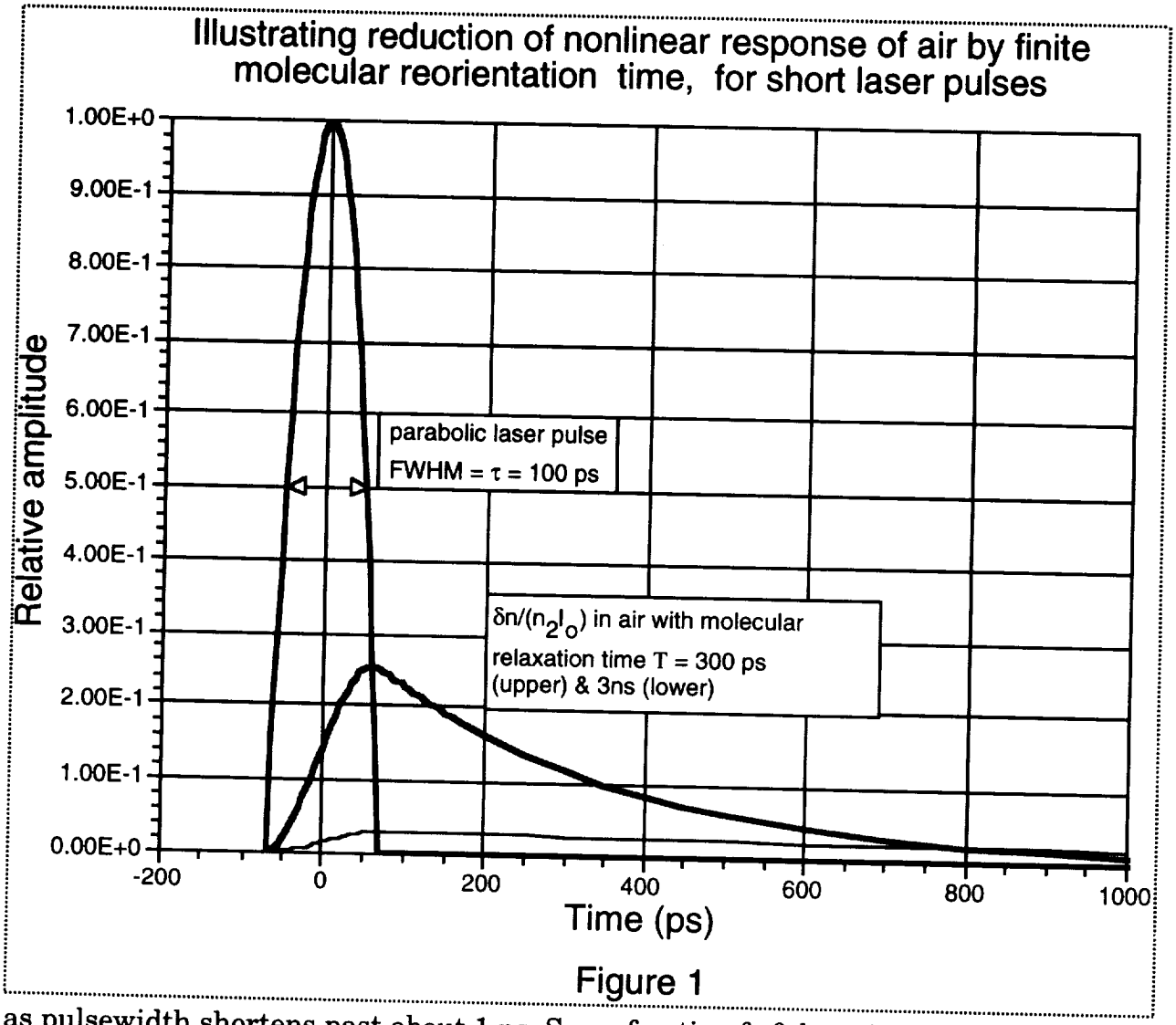

Figure 1

as pulsewidth shortens past about 1 ns. Some fraction f of the original n_2 will remain.

2. Relaxation of that part of n_2 due to T_1 after the same fashion, as pulsewidth τ shortens past about 1ps, leaving about 8% of the long pulse value.

3. Disappearance of n_2 as τ becomes short compared to 1fs.

The latter two cases do not concern us. The question is, how much of the n_2 on the vertical atmospheric path is due to T_2, and how much to T_1? Despite lots of conversations and literature search in the last week, this question does not have a simple answer, and the complicated analysis required has never been done [Hellwarth 1995].

What is required is to use Kramers-Kronig techniques to assess the relative contribution of the high frequency vibrational spectrum in nitrogen around 2330 cm^{-1} and that of the rotational spectrum around 80 – 100 cm^{-1} to its nonlinear index, following a prescription outlined in Hellwarth 1975.

Especially since the recent measurements of Shaw, *et al.* demonstrate that the fraction f is about 0.5, and because of the amount of work involved, it is my judgment that this task should not be completed now, but assigned to the follow-on R&D program.

In what follows, we will assume the fraction of n_2 which decays with the long time constant T_2 is exactly 0.5.

To show how this relaxation is done, follow the analysis of Marburger 1975], using a parabolic pulse shape with full width at half maximum (FWHM) τ, and parameter $\tau_o = \sqrt{2}\tau$ = the halfwidth of this pulse at the baseline:

$$I(t) = I_b\,(1 - \frac{t^2}{\tau_o^2}) \qquad \text{for } t <= \tau_o. \qquad [6]$$

The laser-induced refractive index change is given by:

$$\delta n = n_2 \left\{ I(t) + \frac{2T^2}{\tau_o^2} I_b \left[(\frac{t}{T} - 1) + (\frac{\tau_o}{T} + 1)\, e^{-(\tau_o + t)/T} \right] \right\} \qquad \text{for } t <= \tau_o$$

and

$$\delta n = n_2\, I_b \frac{2T^2}{\tau_o^2}\, e^{-t/T} \left[e^{\tau_o/T}\ (\frac{\tau_o}{T} - 1) + e^{-\tau_o/T} (\frac{\tau_o}{T} + 1) \right] \text{ for } t > \tau_o. \qquad [7b]$$

As in the above figure, there is a maximum value of δn in time, which is what we consider to be the nonlinear refractive index. Then, we numerically integrate Eqns. 7a and 7b, using the actual atmospheric pressure profile [Wolfe and Zyssis, 1978] broken into 20 layers for 11 different laser pulse durations ranging from 7ps to 50ns.

Hellwarth, et al. 1990 give a recipe for scaling this n_2 calculation to wavelengths other than the one for which n_2 was measured. The numerical results of their calculation are the basis for the following table, scaled to 1.06μm = 1.0. The column for I_o threshold scaling reflects the fact that phase shift $\Delta\phi = kn_2I_oz$, where $k = 2\pi/\lambda$.

λ	Scaled n_2	Scaled I_o threshold
353 nm	1.68	0.2
530 nm	1.05	0.475
1.053 μm	1.0	1.0
11 μm (long λ limit)	0.96	10.9

The calculated results for the n_2 limit are shown in the two new "Maneuvering Room" figures attached. The curves begin flattening out again at the left of the Figures because of the assumption that 50% of the nonlinear index does not relax with T_2 but rather with T_1. These figures also include the new SRS results whose derivation will be described in section 9.

The new n_2 curves portray the near field laser intensity required to just give one radian net phase shift ($\lambda/6$ wavefront distortion) between the center and edge of the laser beam at peak phase shift, while propagating on a vertical path through the atmosphere. The vertical path assumption is made for all calculations represented in the Figures. Clearly, the limits are 40% lower for a 45° zenith angle, for those features such as SRS, STRS and n_2, which an undesirable result is proportional to the product of intensity and path length. All the effects which are of concern to us share this behavior.

This is a good time to ask the question: how much phase error is acceptable? For a simple gaussian near-field radial intensity distribution in the laser beam, the Strehl ratio (ratio of on-axis intensity to that for perfect propagation) is [Phipps, *et al.* 1979]

$$|g_2(0)|^2 = \frac{\pi}{2\Delta\phi}\left[C_2^2(\Delta\phi) + S_2^2(\Delta\phi)\right] \qquad [8]$$

where C_2 and S_2 are Fresnel integrals. This expression was used to generate the Strehl ratio in the Table. The index (2) in Eqn. [8] comes from setting p=2 in the expression for a general hypergaussian beam radial intensity distribution:

$$\frac{I(r)}{I_o} = \exp[-2ar^p] \qquad [9]$$

Exact expressions for Strehl for shapes with $p \neq 2$ that give better exit pupil filling are also given in Phipps, *et al.* 1979.

We clearly would not want to accept as much as a 10% intensity loss on target due to nonlinear refraction. One radian phase shift in a simple gaussian radial intensity distribution, by Eqn. [8], just gives 9% loss in on axis Strehl. This is a worst case limit in two senses: (a) For the shorter pulses, average phase shift during the pulse is about half ot the peak value, and (b) hypergaussian profiles with better pupil filling, say p = 6, give less loss of Strehl ratio.

The conclusion of this preliminary study is that nonlinear refraction should not be a problem with the laser system parameters given here, for wavelengths $\lambda \geq 530$ nm although the parameters chosen turn out to be right on a new boundary for 530 nm. *We also note some really obvious advantages of the infrared wavelength 11.1μm.*

Topic 4 References:

Pennington, D. M., Henesian, M. A., and Hellwarth, R. W., 1988 *Phys. Rev. A* **39** pp. 3003-9

Marburger 1975, *Prog. Quant. Electr.* **4**, p. 40

Shaw, M. J., Hooker, C. J. and Wilson, D. C. 1990 *Opt. Commun.* **103**, pp. 153-160

Herring, G. C., Dyer, M. J. and Bischel, W. K. 1986 *Phys. Rev. A* **34** pp. 1944-51

Kurnit, N., Ackerhalt, J. and Watkins, D. E. 1987 *Stimulated Raman Scattering in the Atmosphere*, Los Alamos white paper (unpublished)

Hellwarth, R. W. 1995 *private communication*

Hellwarth, R. W. 1975 *Prog. Quant. Electron.* **5**, pp. 1-68.

Hellwarth, R. W., Pennington, D. M. and Henesian, M. A. *Phys. Rev. A* **41**, pp. 2766-2777

Phipps, *et al. 1979 Proc. Internat. Conf. Lasers '79,* SOQUE, McLean, VA (1979), p. 881]

Wolfe and Zyssis 1978 *The Infrared Handbook,* Office of Naval Research, Washington DC p. 5-107.

TOPIC 5: INTENSITY LIMITS DUE TO STIMULATED RAMAN SCATTERING

The main reason Stimulated Raman scattering (SRS) is bad for ORION beam propagation is that it can be shown to result in a cone-shaped beam with zero on-axis intensity in our configuration [Kurnit, *et al.* 1987]. Henesian, *et al.* 1985 also did experiments on SRS conversion over a 150-m air path in which they found that beam quality deteriorates severely above Raman threshold. Otherwise, one might decide to let the beam convert to a new wavelength and not worry about it.

The SRS interaction is one in which two electromagnetic waves E_L and E_S and a nonlinear polarization wave Q are coupled by an optical phonon wave above threshold in a Raman medium:

$$\mathcal{E}_L = E_L(z,t)\exp(ik_L z - i\omega_L t) \qquad [1]$$

$$\mathcal{E}_s = E_S(z,t)\exp(ik_s z - i\omega_s t)$$

$$Q = Q(z,t)\exp(ik_{ph} z - i\omega_{ph} t)$$

Practically, SRS is a nonlinear optical effect which redshifts sufficiently intense radiation to a new "Stokes" wavelength given by

$$\omega_s = \omega_L - \omega_R \quad . \qquad [2a]$$

while

$$\mathbf{k}_s = \mathbf{k}_L - \mathbf{k}_R \qquad [2b]$$

for the propagation vectors (whose magnitude is $k=2\pi/\lambda$) provides the other of the two required matching conditions. The Stokes shift $\omega_R = 2\pi c\nu_R$ depends on the Raman medium. For air, ν_R is about $80cm^{-1}$.

Ordinary SRS is already a fairly complex matter. The present problem requires a theory for Transient Stimulated Raman scattering, by definition, and that is even more complex. But first, let's review the steady state results.

In steady state, SRS intensity gain for the Stokes frequency depends on laser intensity I_L, SRS gain g_R and range z as:

$$\frac{I_s(z)}{I_{so}} = \frac{\exp(g_R I_L z)}{1 + (\omega_L I_{so}/\omega_s I_L)\exp(g_R I_L z)} \approx \exp(g_R I_L z) \qquad [3]$$

in the normal circumstance where the Raman seed intensity has not yet become as large as the laser intensity $I_{so}\exp(g_R I_L z) << I_L$ [Fulghum, *et al.* 1984].

The SRS gain coefficient is given by [Wang 1975]

$$g_R = \left(\frac{\partial\alpha}{\partial q}\right)^2 \frac{8\pi^3 N}{c^2}\frac{\omega_s}{\omega_R \gamma} \qquad [4]$$

in the atmosphere (n=1).

Note that gain is scaled between wavelengths via its proportionality to ω_s.

In Eqn. [4], γ is the Raman linewidth,

$$\gamma = \frac{1}{\pi T_2} \qquad [5]$$

δ the offset from the two-photon resonance, N is the molecular density and $(\partial\alpha/\partial q)$ the derivative of the molecular polarizability with respect to the normal coordinate q of displacement in a Raman-active vibrational mode.

For transient SRS, the situation is more complex. We follow the analysis of Ori, *et al.* 1990, with some help from Carman, *et al.* 1970.

In the transient regime, Eqn.s [1] become coupled field equations with coupling coefficients η_1 andη_2:

$$\frac{\partial Q^*}{\partial t} + (\gamma - i\delta)Q^* = i\eta_1 E_L^* E_s \qquad [6]$$

$$\frac{\partial E_s}{\partial z} + \frac{1}{c}\frac{\partial E_s}{\partial t} = -i\eta_2 Q^* E_L$$

In Eqns. [6], δ the offset from the two-photon resonance.

In the large amplification limit, transient SRS gain g_t can be related to the steady state value given by [Heeman and Godfried 1995]:

$$g_t z \approx 4\sqrt{g_s z\, \gamma \tau_L} \qquad [7]$$

Ori, *et al.* solve Eqns. [6] numerically. We have adopted their solutions, and modified them for integration through the real atmosphere rather than the exponential density profile they assume to give the SRS limit curves in the "Maneuvering Room" plots which were attached to section 5.

In particular, we utilized the most realistic of two threshold definitions they introduce: namely that SRS pulse energy has become as large as 1% of the laser pulse energy. Since threshold intensity is proportional to nepers of small signal gain normally beginning around exp(–30) for I_{so}, a choice of 10% for the limiting value would make a relatively small difference in the outccome of our calculations.

We allowed for real atmospheric profiles by separately integrating the steady state SRS gain following a prescription of Kurnit, *et al* based on the variation of T_2 with altitude (see Figures 1 and 2 of 4 attached), in order to normalize the steady state SRS gain calculated by Ori, *et al.* to these values, then letting their calculations depart into the transient regime. The attached Figure makes it clear, for example, that the first 6 km of altitude represents only a 10% effect on the overall gain integral. Steady state SRS gain actually rises with altitude at first, because temperature is going down, which results in a redistribution of the population with the various rotational states in nitrogen that favors higher gain.

They assume a source function for the first photons which are amplified at λ_s by the transient SRS gain that depends on the laser beam volume, and we have also modified their results to reflect the size of beam we intend to use in ORION.

Beam source size is a few percent effect, that can be scaled directly from beam sizes Ori, *et al.* consider without significant error. (See the Figure 3 of 4 attached to this section based on Ori, *et al.*)

The SRS threshold calculations of Ori, et al. covered numerous wavelengths from 300nm to 1μm [See Figure 4 of 4 of three attached to this section]. Therefore the only serious use of the Eqn. [4] scaling in our work was in generating the prediction for 11.1μm.

We conclude that

- SRS thresholds are very close for 530nm laser wavelength and unavoidable for shorter wavelength
- A tremendous advantage accrues from going to 11.1μm
- The 100-ps operating point we defined at the Washington kickoff meeting based on the simple "elbow" curve for SRS threshold variation that we had at that time is indeed as good a choice as the 40-ns operating point for the laser.

This laser point design will be reviewed in more detail in section 12, but its main feature was allowing us to go to about 1.5kJ pulse energy at 100ps rather than 20kJ at 40ns, which might result in a substantially cheaper laser.

Topic 5 References:

Carman, R. L., Shimizu, F., Wang, C. S. and Bloembergen, N. 1970 *Phys Rev. A* **2**, pp. 60-72

Fulghum, S. F., Trainor, D. W., Duzy, C. and Hyman, H. A. *1984 IEEE J. Quant. Electron* . **QE-20** pp. 218-22

Heeman, R. J. and Godfried, H. P. 1995 *IEEE J. Quant. Electron.* **31** pp. 358-64

Henesian, M. A., Swift, C. D. and Murray, J. R. 1985 *Opt. Lett.* **10** pp565-7

Herring, G. C., Dyer, M. J. and Bischel, W. K. 1986 *Phys. Rev. A* **34** pp. 1944-51

Pennington, D. M., Henesian, M. A., and Hellwarth, R. W., 1988 *Phys. Rev. A* **39** pp.

Kurnit, N., Ackerhalt, J. and Watkins, D. E. 1987 *Stimulated Raman Scattering in the Atmosphere*, Los Alamos white paper (unpublished)

Ori, A., Nathanson, B. and Rokni, M. 1990 *J. Phys. D.* **23** pp. 142-9

Wang, C. S. "The Stimulated Raman Process" in *Quantum Electronics: A Treatise*, H. Rabin and C. L. Tang, eds., Academic, New York pp.447-72.

$T_2 = 1/(\pi\delta\nu)$ for nitrogen, including pressure and doppler broadening effects, after Kurnit, et al. (1987)

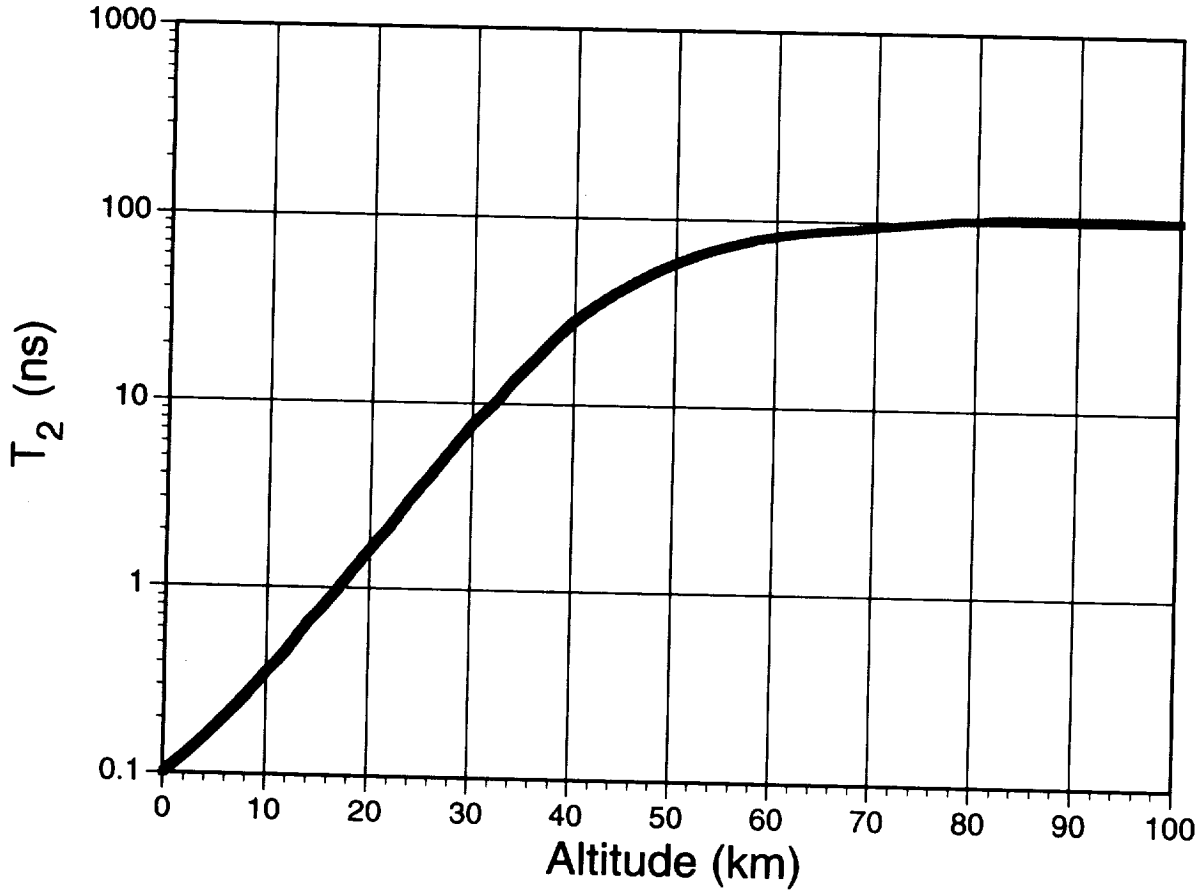

Photonic Associates
excellence in photonics

SRS Gain vs. altitude (1.06 μm)

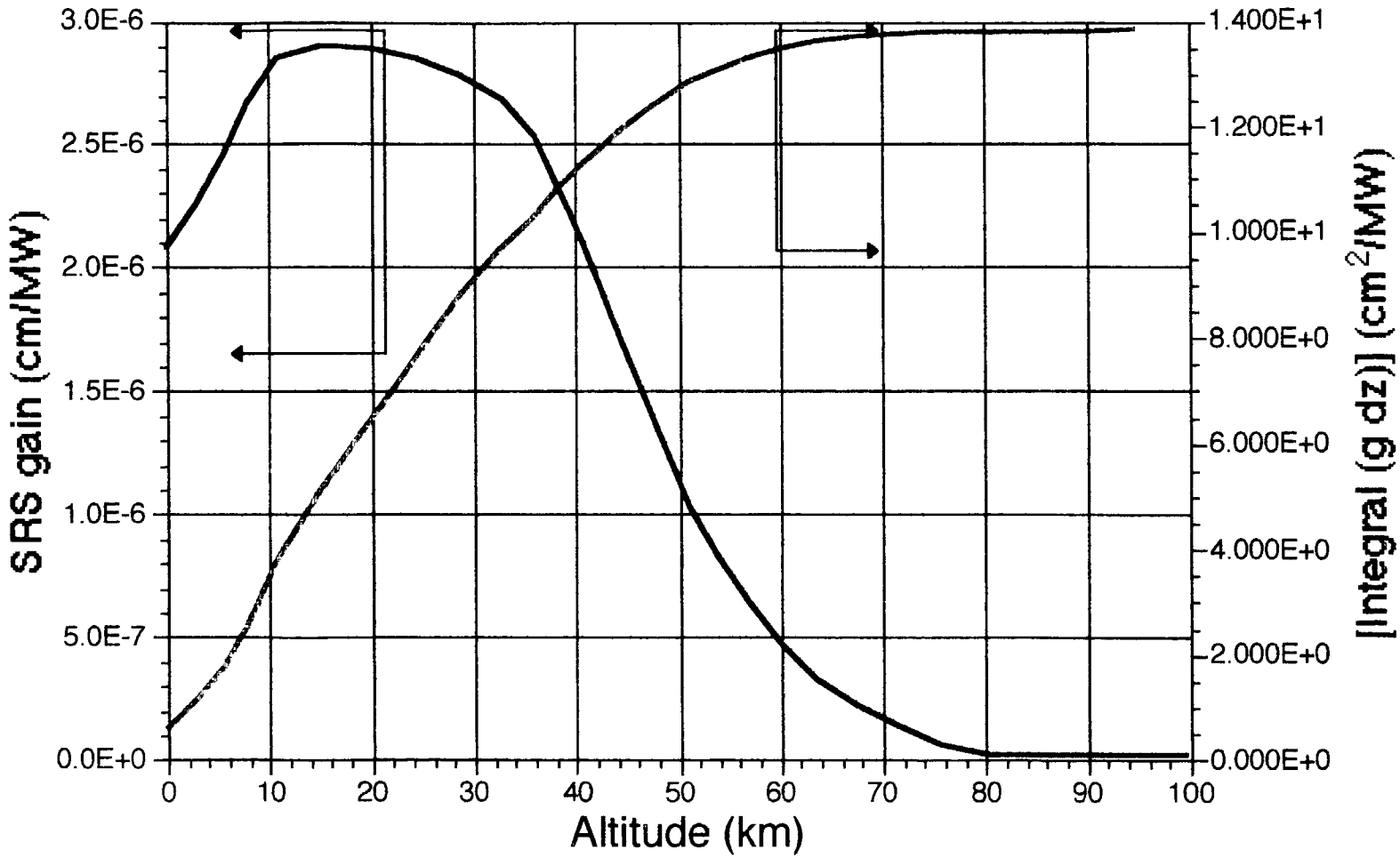

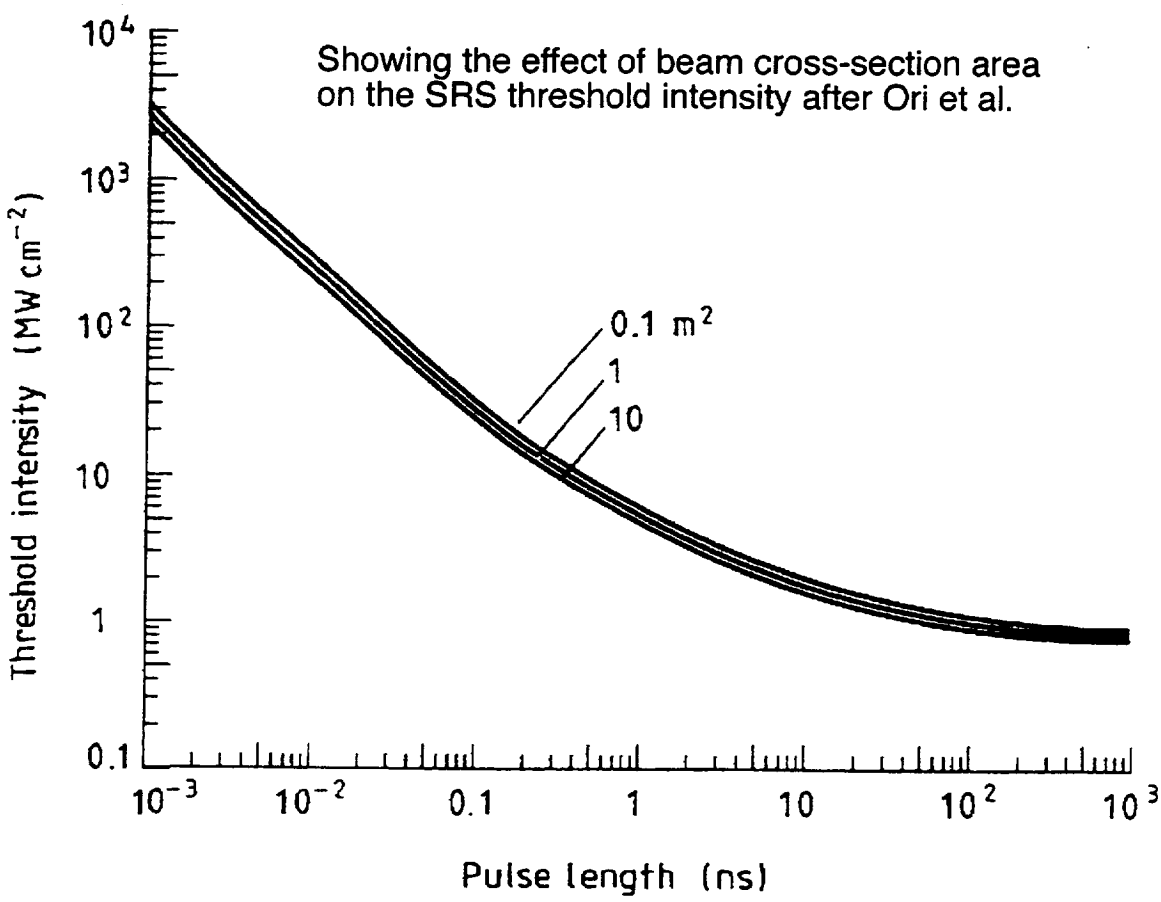
Showing the effect of beam cross-section area on the SRS threshold intensity after Ori et al.
Threshold intensity (MW cm^{-2})
10^4
10^3
10^2
10
1
0.1
0.1 m^2
1
10
10^{-3}
10^{-2}
0.1
1
10
10^2
10^3
Pulse length (ns)

SRS intensity thresholds for $1m^2$ beam area after Ori, et al.

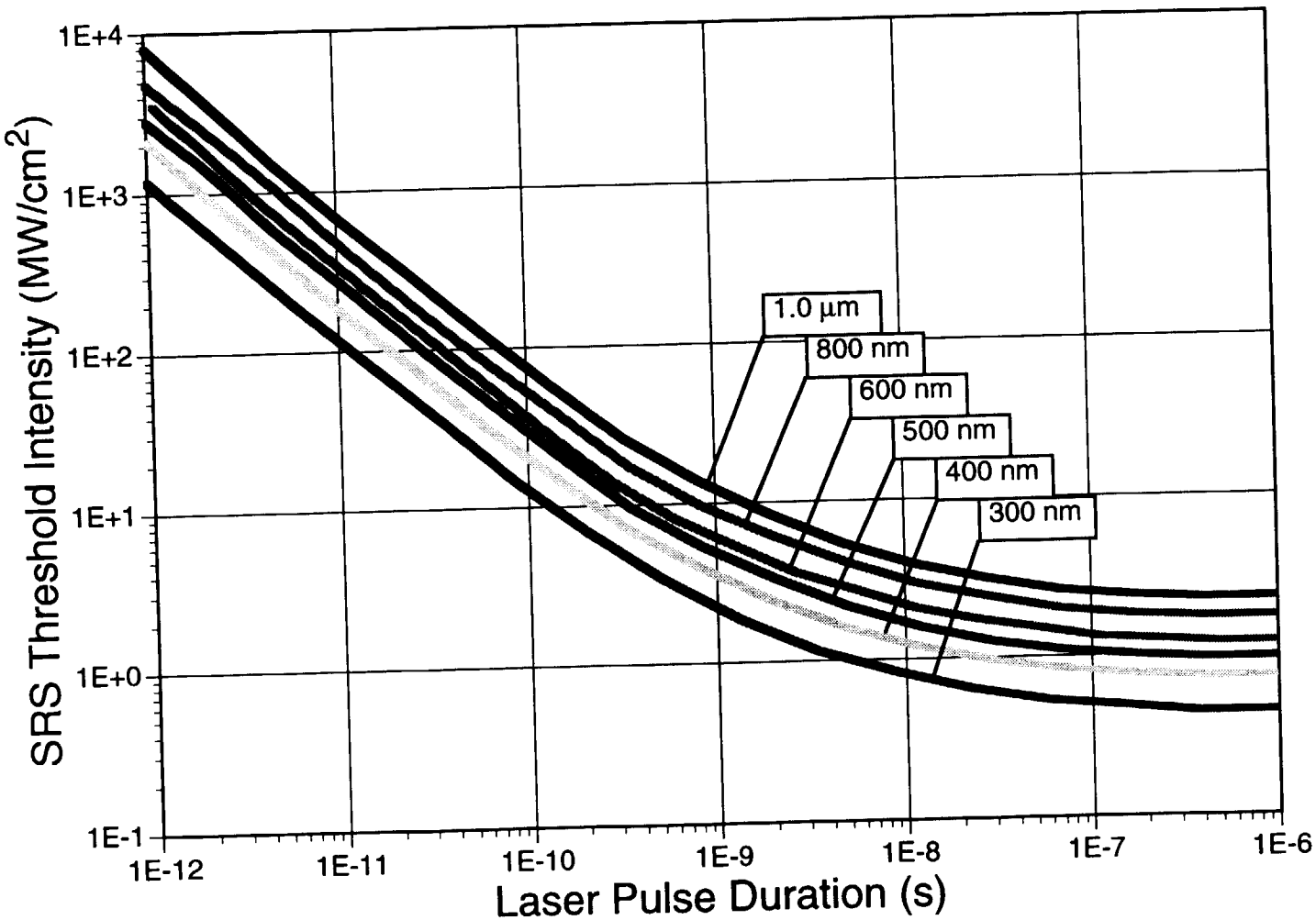

TOPIC 6: STRS LIMITS TO ORION MANEUVERING ROOM

We have now completed calculations which clearly define the limits posed by Stimulated Thermal Rayleigh Scattering (STRS) in the atmosphere to "maneuvering room" in pulsewidth and intensity for the ORION laser.

Our results show that there is more room in the direction of longer pulsewidth and lower beam intensity than we earlier believed based on simpler first-round calculations defining the STRS limits.

STRS is a fine-scale analog to whole beam thermal blooming, in which ripples in the laser beam intensity grow by producing corresponding density variations in the atmosphere which act like lenses, creating more intense ripples downstream. When gain in the direction of laser propagation is positive for these ripples, they ultimately become strong enough to form a diffraction grating which scatters the laser beam and severely degrades its intensity and optical quality.

The difference with whole beam blooming is in the scale of the effect, not in the basic physics. In a plot of intensity or refractive index across the laser beam, the spacial frequency of the STRS effect for gains of e^{30} or so will range from 30/cm to 30,000/cm [meaning ripples with wavelength from 0.2 mm to 0.2μm] depending on laser wavelength and pulse duration in the ORION application. In whole beam thermal blooming, in contrast, spacial frequency is of the order of a reciprocal beam radius, say, 0.003/cm.

The improvement in the present calculation is similar in nature to that for the improved calculations of SRS and n_2 limits which we reported earlier. In the present work, the atmosphere up to a height of 70 km was divided into 13 zones of various physical thickness ranging from 1.6 to 8.7 km, the thickness of each zone chosen to correspond to an absorption length $1/\alpha$ for the laser wavelength. Our earlier estimates of the STRS limit used just one zone with thickness equal to the atmospheric scale height. As in earlier work, the theory of J. J. Barnard [1989] was employed to analyze STRS.

This is a fairly complex problem. Barnard defines 8 distinct regions, each with completely different expressions for exponential gain G experienced by the index perturbations. These regions describe different physical effects. In each zone of the atmosphere, different regions play a dominant rôle, since so many of the physical parameters that determine the theory change by several orders of magnitude on the way to outer space, including refractive index (n-1), laser absorption coefficient α, thermal diffusivity χ, and the velocity v due to wind shear and turbulence. In our simulations, we found that the laser beam often experienced the effects of 3 of the Barnard regions on the way out of the atmosphere and, of course, which ones were engaged depended a lot on laser beam parameters. In general, the longer the wavelength, the higher the intensity which can be propagated for a given pulsewidth, just as with SRS and n_2.

Figure 1, plotted from theory for the indicated choice of parameters, and constant distortion number N_D, defined below, illustrates the complexity involved, and the specific physical effects encountered.

For clarity, we have added some nomenclature not present in Barnard's paper, plus more precise definitions of the boundaries separating the gain regions.

Notation is summarized in the inset of the Figure, but we will amplify a few definitions here at a level which will not fit the inset.

It is convenient to use dimensionless perturbation wavenumber $\kappa = k_\perp/\xi$ and laser pulsewidth $\mathcal{T} = \xi c_s \tau$, where $\xi = \sqrt{(2k/z)}$, z is the range (thickness of a particular atmospheric zone $1/\alpha$ in our case) and $k = 2\pi/\lambda$ is the laser wavenumber. These are the axes in the Figure, but corresponding "realworld" values are also shown on the opposing axes. The "distortion number" N_D is given by

$$N_D = \Gamma I_b k z \tau$$

where $$\Gamma = \frac{(\gamma-1)}{\gamma}\frac{(n-1)\alpha}{p}$$

and γ indicates the specific heat ratio. N_D is directly related to laser beam fluence $\Phi_b = I_b\tau$ and, numerically,

$$N_D = 2.826\, \Phi_b (n-1) k z (\alpha p_o/p) \qquad [1]$$

when Φ_b is expressed in J/cm^2 and α, k and z remain in cm units. Atmospheric pressure is p_o at sea level, so $\Phi_o\alpha/p$ is proportional to the heat per molecule absorbed from the laser beam.

G is the exponential gain in nepers, so that ripples at the end of a zone of thickness z have experienced a gain e^G [*not* e^{Gz}]. This is an important distinction because the dimensionless quantities κ, N_D and $\mathcal{T}$ in the following expressions implicitly contain the z-dependence in the gain expressions. For example, in Eqn. [2], $G = N_D^{1/5}\,\kappa^{4/5}\,\mathcal{T}^{2/5}$ implicitly contains $z^{2/5}$.

With this preamble, the physics regions are summarized as follows:

<u>Region 1</u>: growth due primarily to acoustics, where diffraction is unimportant

$$G_1 = 1.82 N_D^{1/5} \kappa^{4/5} \mathcal{T}^{2/5} \qquad [2]$$

Boundaries are $\mathcal{T}_1 = 0.398\left(\frac{N_D}{\kappa}\right)^{1/3}$ and $\kappa_1 = 0.678\, N_D^{1/6}\mathcal{T}^{1/3}$.

<u>Region 2</u>: growth in the acoustic regime but with sufficiently large wavenumbers κ that diffraction cannot be ignored. This is typically the regime occupied by the laser beam at sea level.

$$G_2 = 1.62 N_D^{1/4} \kappa^{1/2} \mathcal{T}^{1/2} \qquad [3]$$

Boundaries are κ_1, $\mathcal{T}_2 = 0.758 \left(\frac{N_D^{1/2}}{\kappa}\right)$ and $\mathcal{T}_3 = 0.604\, N_D^{1/6} \kappa^{1/3}$.

Region 5: longer pulse times where growth is isobaric (constant pressure) rather than acoustic, and diffraction is not important.

$$G_5 = 1.26 N_D^{1/3} \kappa^{2/3} \qquad [4]$$

Boundaries are $\mathcal{T}_1$, $\mathcal{T}_3$ and $\kappa_2 = 1.189\, N_D^{1/4}$.

Region 3: isobaric growth where diffraction is important. This is another typical region, particularly for μs- rather than ns-duration laser pulses.

Here, $$G_3 = 1.41 N_D^{1/2} \qquad [5]$$

Boundaries are $\mathcal{T}_2$, κ_2, $\mathcal{T}_{crit\,1} = \left(\frac{c_s \sqrt{N_D}}{K v}\right)$ and $\mathcal{T}_{crit\,6} = 1.41 \left(\frac{\sqrt{N_D}}{\kappa^2 x}\right)$.

Region A: sufficiently long pulse times that wind shear becomes important in helping to wash out the index perturbations. this is important at higher elevations in our problem. Where dv/dz = v/z,

$$G_A = 1.41 \left(\frac{N_D c_s \kappa}{v \mathcal{T}}\right)^{1/2} \qquad [6]$$

and the boundaries for this region are $\kappa_3 = \left(\frac{N_D\, c_s}{v\, \mathcal{T}}\right)^{1/3} \left[1+\ln\left(\frac{\mathcal{T}}{\mathcal{T}_{crit\,1}}\right)\right]^{2/3}$,

$\mathcal{T}_{crit\,2} = 1.259\, c_s \left(\frac{N_D^{1/3}}{\kappa^{1/3} v}\right)$, and $\mathcal{T}_{crit\,3} = \frac{(l\,\xi)^{2/9} N_D^{1/3} c_s}{(2\pi)^{8/9} v\, \kappa^{1/9}}$.

Region B: region A with large enough κ that diffraction is important:

$$G_B = \frac{N_D c_s}{\kappa v \mathcal{T}} \left[1+\ln\left(\frac{\mathcal{T}}{\mathcal{T}_{crit\,1}}\right)\right] \qquad [7]$$

with boundaries κ_3, $\mathcal{T}_{crit\,1}$, $\mathcal{T}_{crit\,4} = \left(\frac{(l\,\xi)^{1/6} N_D^{1/2} c_s}{(2\pi)^{2/3} v\, \kappa^{5/6}}\right) \left[1+\ln\left(\frac{\mathcal{T}}{\mathcal{T}_{crit\,1}}\right)\right]^{1/2}$ and

$\mathcal{T}_{crit\,5} = \left(\frac{N_D\, c_s}{v \times \kappa^3}\right)^{1/2} \left[1+\ln\left(\frac{\mathcal{T}}{\mathcal{T}_{crit\,1}}\right)\right]^{1/2}$.

Here, ℓ is the scale of the largest atmospheric eddies, which are taken equal to the atmospheric density scale height.

Finally, we have two regions in which negative gain is experienced because pulse times are long enough for either molecular diffusion (region 4) or turbulent diffusion (region C) to wash out the refractive index gratings faster than they are created.

$$G_4 = -x\kappa^2\mathcal{T} \qquad [8]$$

and

$$G_C = -y\kappa^{2/3}\mathcal{T} \qquad [9]$$

with boundaries given by $\mathcal{T}_{crit\ 3}$, $\mathcal{T}_{crit\ 4}$, $\mathcal{T}_{crit\ 5}$ and $\mathcal{T}_{crit\ 6}$, with a vertical boundary $\kappa_4 = \frac{2\pi}{\xi \ell^{1/4}}\left(\frac{\nu}{\chi}\right)^{3/4}$ separating the two regions from each other.

These expressions [as well as the boundary intersections] were incorporated into a computer simulation which determines, for each of the 13 atmospheric zones and a particular selection of $k_\perp$ and τ, which region of the propagation physics to apply.

Even with fixed laser parameters, N_D and ξ change with each zone so the Figure 1 plot appears to shift horizontally and vertically from zone to zone for a particular pair (κ, $\mathcal{T}$). Figure 2 shows how the same plot looks at height h = 69km, while Figure 3 shows a calculation for the same height but λ =11.1 μm.

In order to obtain a single point in the new calculations, 20 -3 0 iterations were necessary to find that combination of beam intensity I_b and ripple wavenumber $k_\perp$ which, for a chosen wavelength λ and pulse duration τ, gave $\Sigma_i G_i = 30$, as well as an absolute maximum versus variations of $k_\perp$. This was done for 5 - 6 values of τ for each of 3 wavelengths we are still considering, for each our two customary site altitudes of 0 and 6 km.

Figure 4 shows how net gain varies during a typical iteration sequence. Changes in gain are due to propagation in individual zones moving from one region to another in the propagation physics. Some of the zones encountered during the simulation are indicated.

Figures 5 and 6 show the results for vertical propagation from our customary site altitudes of 0 and 6 km, respectively. The limits posed by STRS are no longer straight lines with slope 3 on the chart, a feature of Barnard region 2, where constant gain G implies $I_b\tau^3$ = constant, as in whole-beam thermal blooming. Previously, we took the atmosphere to be one zone with laser site level pressure and absorption coefficient appropriate to the wavelength. Thickness of the single zone was one atmospheric scale height. In the present simulation, tabulations of the actual laser absorption coefficient vs. altitude [Wolf and Zissis, 1978] were used to create 13 zones between sea level and 70

km altitude, each with thickness $1/\alpha$. Due to the variation of α, physical thickness of the zones varied from 1.6 km to 8.7 km.

The main lesson to take home is that we now have more maneuvering room for the ORION laser at long pulse durations and low peak intensity.

On each plot is also drawn two "target effects" lines. These are given by Eqn. [8] from §0, and represent the constraints of achieving optimum coupling on target as laser pulsewidth varies from 100ps to 1μs for two different mirror diameters. These diameters are:

(1) The smallest feasible mirror which will avoid SRS. This mirror is 6m in diameter for 532 nm or [27 m] in diameter for 11.1μm, the two extremes of wavelength we are still considering.

(2) A mirror which is twice as large in diameter as (1).

Note that the larger mirror allows 4 times lower pulse energy W and 16 times lower peak intensity I_b in the near field of the laser beam. [see Eqn. 9, §0]

The reasons for this are straightforward: on the lower target effects line, a mirror of 4 times larger area A_b is capable of imaging the laser beam onto a target spot with 4 times smaller area A_s, giving a factor of 16 intensification in the ratio I_s/I_b. At the same time, 4 times larger A_b with 16 times smaller I_b gives just 4 times smaller pulse energy W. The slope of the line is – 0.55, as required by the analysis of §0 and §1.

Finally, Figure 7 shows in more detail the variation of laser pulse energy W along the target effects lines corresponding to the choices D_b = 6m and D_b = 12m for all 3 laser wavelengths [532 nm, 1.06 μm and 11.1 μm] we are considering. It can be seen from the Figure that, with these realistically-sized mirrors, the 11.1μm wavelength automatically requires MJ to 100's of MJ of pulse energy, for all but the very shortest pulses, and these pulses are difficult to do with CO_2 laser technology.

Summary of our findings in this section:

- We have more maneuvering room than previously thought, for long pulses and low peak intensities
- CO_2 laser technology requires huge pulse energy when coupled with mirrors of realistic size.
- A green (532 nm) laser beam at 100 ps pulse duration with a 12-m-diameter beam director can couple effectively to targets at 1500 km range with only 340 joules of pulse energy. A 60-Hz pulse repetition rate would be required to give 20kW average power, which is required to clear 1 – 10-cm debris in a reasonable time.

References:

Barnard, J. J. 1989 Appl. Opt. **28** pp. 437-445

Wolfe, W. L. and Zissis, G. J. 1978 *The Infrared Handbook* Office of Naval Research, Washington, D.C.

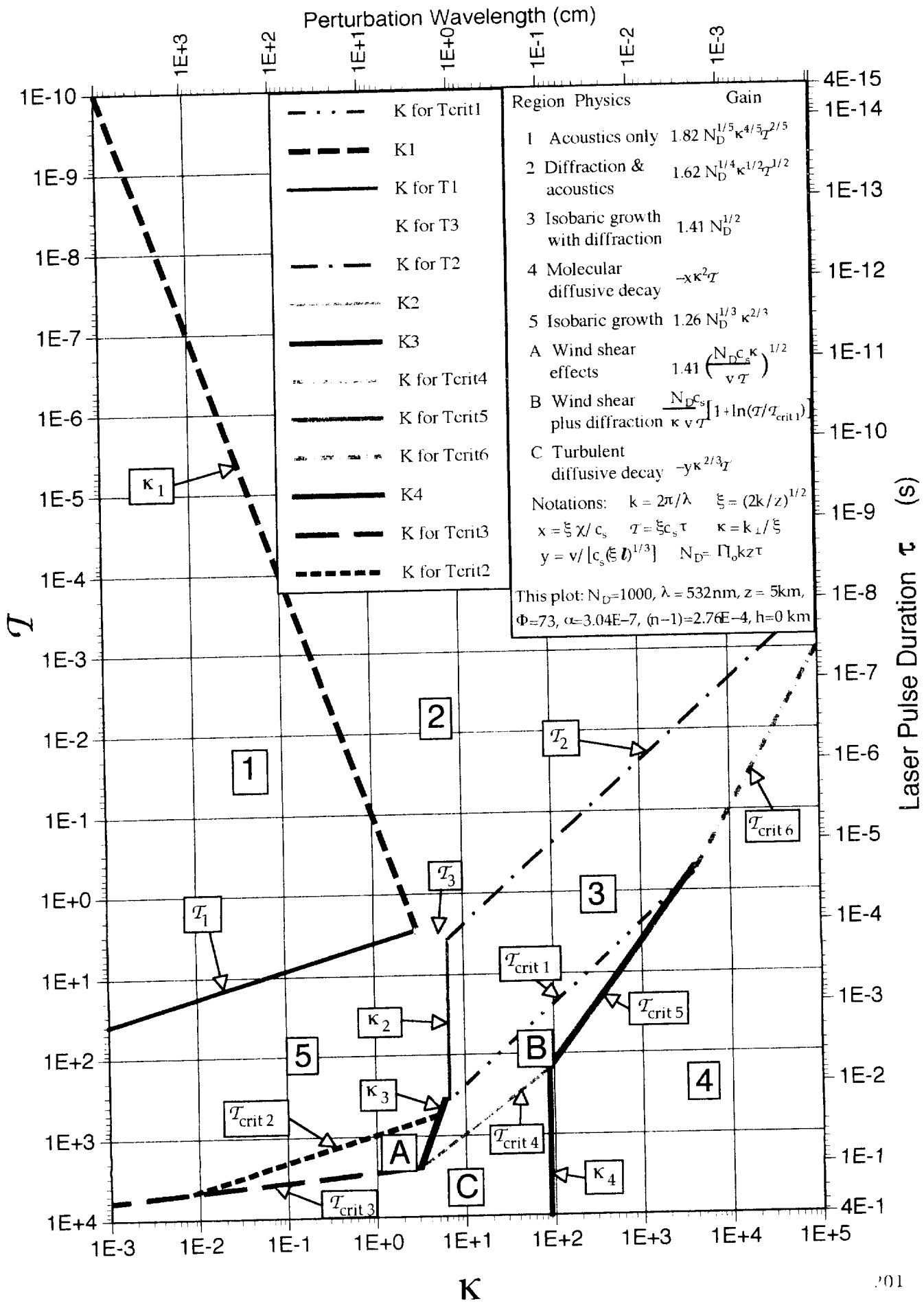
Perturbation Wavelength (cm)
1E+3
1E+2
1E+1
1E+0
1E-1
1E-2
1E-3
1E-10
1E-9
1E-8
1E-7
1E-6
1E-5
1E-4
1E-3
1E-2
1E-1
1E+0
1E+1
1E+2
1E+3
1E+4
4E-15
1E-14
1E-13
1E-12
1E-11
1E-10
1E-9
1E-8
1E-7
1E-6
1E-5
1E-4
1E-3
1E-2
4E-1
1E-3
1E-2
1E-1
1E+0
1E+1
1E+2
1E+3
1E+4
1E+5
K for Tcrit1
K1
K for T1
K for T3
K for T2
K2
K3
K for Tcrit4
K for Tcrit5
K for Tcrit6
K4
K for Tcrit3
K for Tcrit2
Region Physics Gain
1 Acoustics only 1.82 $N_D^{1/5}\kappa^{4/5}\mathcal{T}^{2/5}$
2 Diffraction & acoustics 1.62 $N_D^{1/4}\kappa^{1/2}\mathcal{T}^{1/2}$
3 Isobaric growth with diffraction 1.41 $N_D^{1/2}$
4 Molecular diffusive decay $-x\kappa^2\mathcal{T}$
5 Isobaric growth 1.26 $N_D^{1/3}\kappa^{2/3}$
A Wind shear effects 1.41 $\left(\frac{N_D c_s \kappa}{v\mathcal{T}}\right)^{1/2}$
B Wind shear plus diffraction $\frac{N_D c_s}{\kappa v \mathcal{T}}[1+\ln(\mathcal{T}/\mathcal{T}_{crit1})]$
C Turbulent diffusive decay $-y\kappa^{2/3}\mathcal{T}$
Notations: $k = 2\pi/\lambda$ $\xi = (2k/z)^{1/2}$
$x = \xi\chi/c_s$ $\mathcal{T} = \xi c_s \tau$ $\kappa = k_\perp/\xi$
$y = v/[c_s(\xi\ell)^{1/3}]$ $N_D = \Gamma_o k z \tau$
This plot: N_D=1000, λ = 532nm, z = 5km, Φ=73, α=3.04E-7, (n-1)=2.76E-4, h=0 km
$\mathcal{T}$
Laser Pulse Duration τ (s)
κ
κ_1
$\mathcal{T}_1$
$\mathcal{T}_2$
$\mathcal{T}_3$
κ_2
κ_3
κ_4
$\mathcal{T}_{crit\,1}$
$\mathcal{T}_{crit\,2}$
$\mathcal{T}_{crit\,3}$
$\mathcal{T}_{crit\,4}$
$\mathcal{T}_{crit\,5}$
$\mathcal{T}_{crit\,6}$
1
2
3
4
5
A
B
C

201

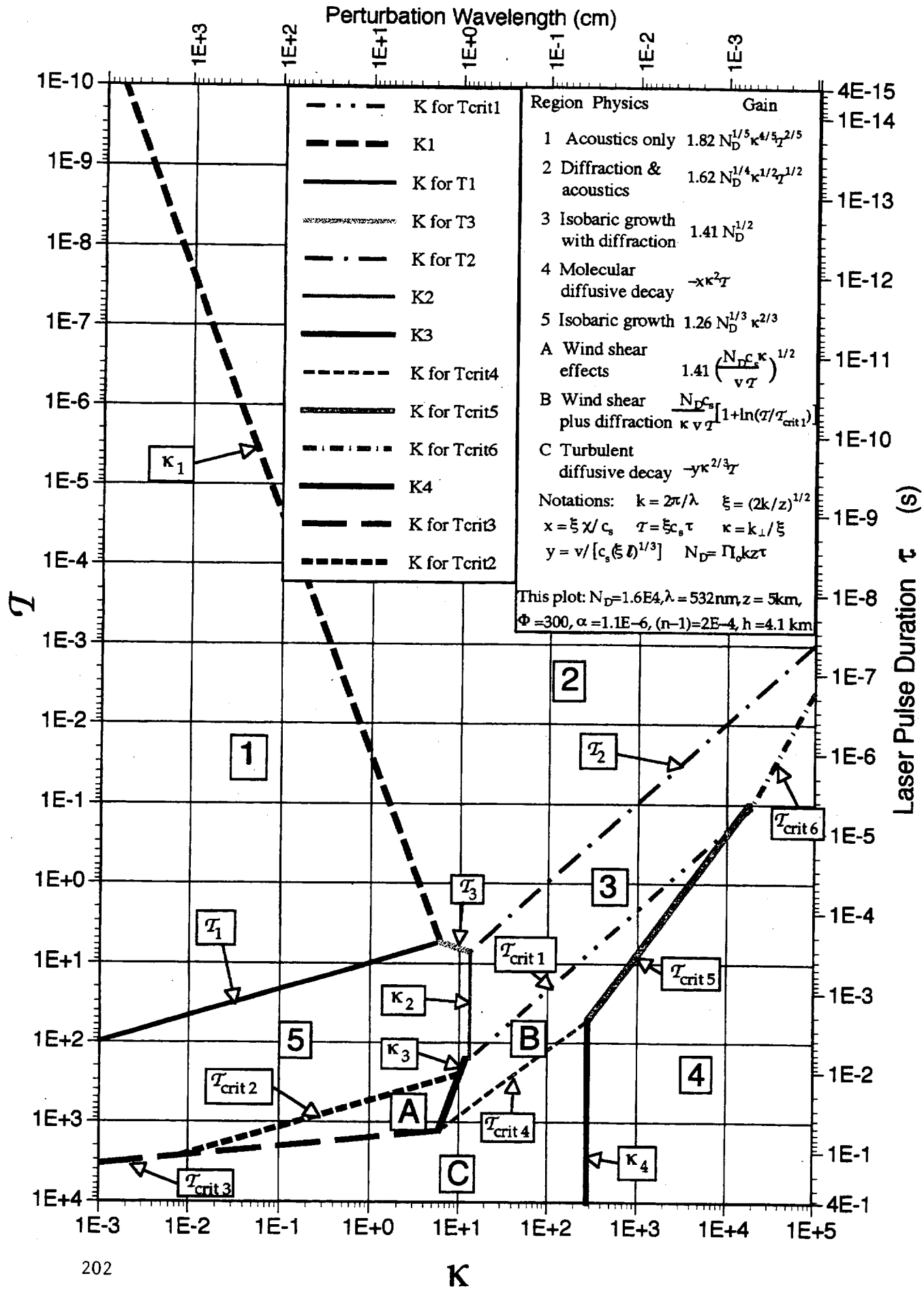
Perturbation Wavelength (cm)
1E+3
1E+2
1E+1
1E+0
1E-1
1E-2
1E-3
K for Tcrit1
K1
K for T1
K for T3
K for T2
K2
K3
K for Tcrit4
K for Tcrit5
K for Tcrit6
K4
K for Tcrit3
K for Tcrit2
Region Physics Gain
1 Acoustics only 1.82 $N_D^{1/5}\kappa^{4/5}\tau^{2/5}$
2 Diffraction & acoustics 1.62 $N_D^{1/4}\kappa^{1/2}\tau^{1/2}$
3 Isobaric growth with diffraction 1.41 $N_D^{1/2}$
4 Molecular diffusive decay $-x\kappa^2\tau$
5 Isobaric growth 1.26 $N_D^{1/3}\kappa^{2/3}$
A Wind shear effects $1.41\left(\frac{N_D c_s \kappa}{v\tau}\right)^{1/2}$
B Wind shear plus diffraction $\frac{N_D c_s}{\kappa v \tau}[1+\ln(\tau/\tau_{crit1})]$
C Turbulent diffusive decay $-y\kappa^{2/3}\tau$
Notations: $k = 2\pi/\lambda$ $\xi = (2k/z)^{1/2}$
$x = \xi\chi/c_s$ $\tau = \xi c_s \tau$ $\kappa = k_\perp/\xi$
$y = \nu/[c_s(\xi\ell)^{1/3}]$ $N_D = \Pi_o kz\tau$
This plot: N_D=1.6E4, λ = 532nm, z = 5km, Φ =300, α =1.1E-6, (n-1)=2E-4, h =4.1 km
τ
Laser Pulse Duration τ (s)
1E-10
1E-9
1E-8
1E-7
1E-6
1E-5
1E-4
1E-3
1E-2
1E-1
1E+0
1E+1
1E+2
1E+3
1E+4
4E-15
1E-14
1E-13
1E-12
1E-11
1E-10
1E-9
1E-8
1E-7
1E-6
1E-5
1E-4
1E-3
1E-2
1E-1
4E-1
1E-3
1E-2
1E-1
1E+0
1E+1
1E+2
1E+3
1E+4
1E+5
κ
κ_1
κ_2
κ_3
κ_4
τ_1
τ_2
τ_3
$\tau_{crit\,1}$
$\tau_{crit\,2}$
$\tau_{crit\,3}$
$\tau_{crit\,4}$
$\tau_{crit\,5}$
$\tau_{crit\,6}$
1
2
3
4
5
A
B
C

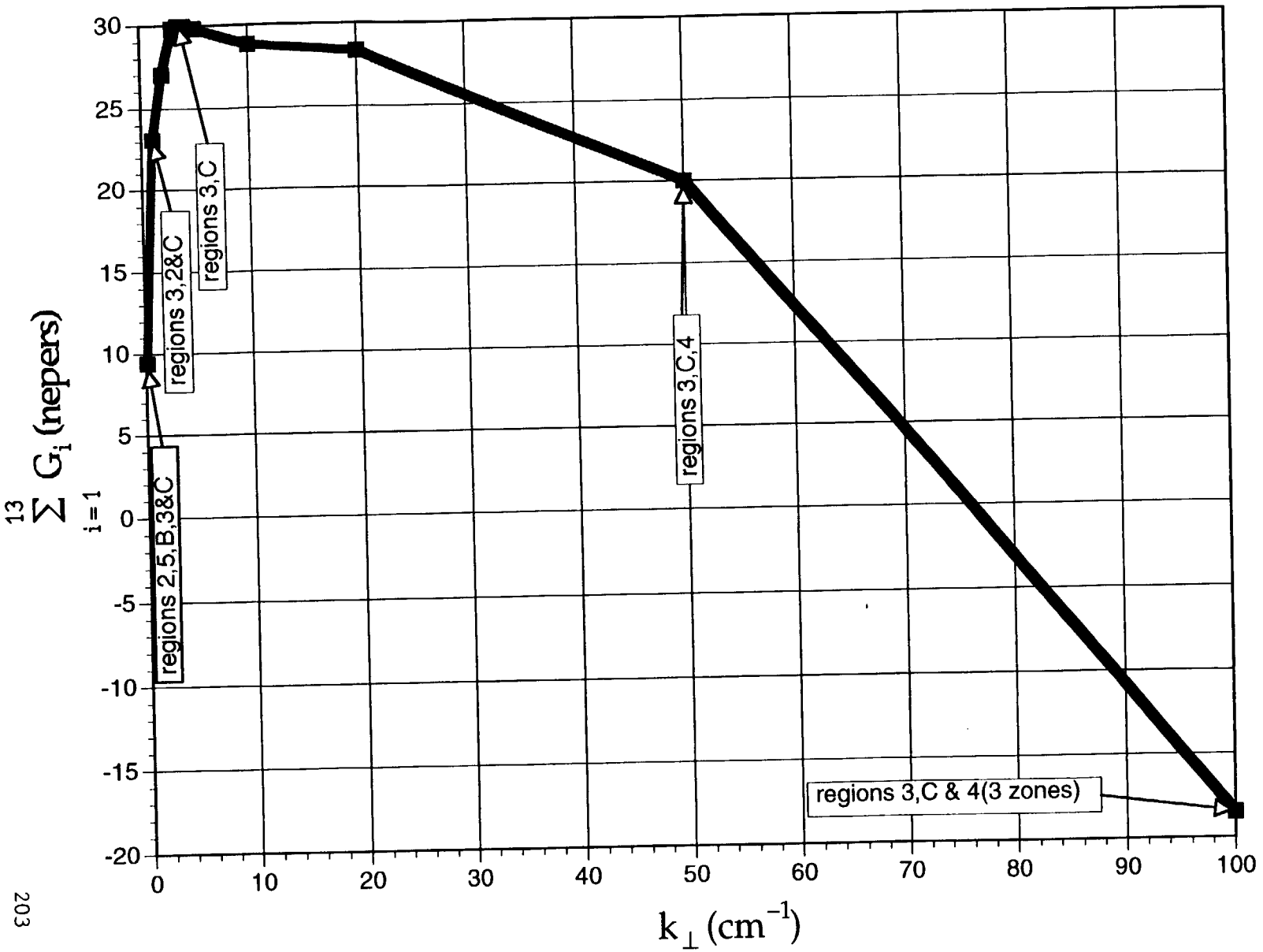
Simulation: h = 0km, I_b = 3.5E6, τ = 1E-4, λ = 11.1μm
$\sum_{i=1}^{13} G_i$ (nepers)
$k_\perp$ (cm^{-1})
regions 2,5,B,3&C
regions 3,2&C
regions 3,C
regions 3,C,4
regions 3,C & 4(3 zones)
30
25
20
15
10
5
0
-5
-10
-15
-20
0
10
20
30
40
50
60
70
80
90
100

Photonic Associates
excellence in photonics

Maneuvering Room for the ORION System limited by SRS, STRS, n_2 and other effects

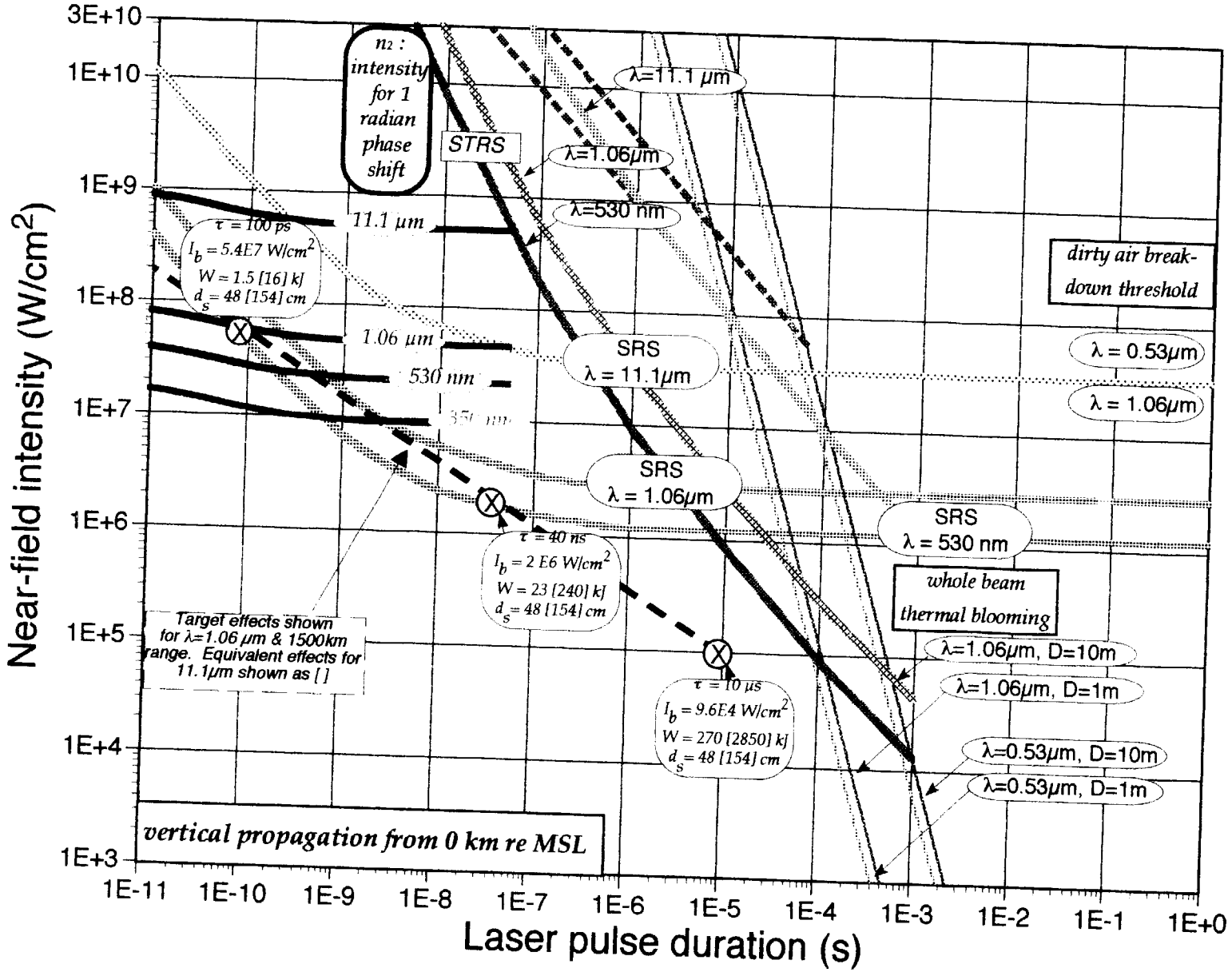

Photonic Associates
excellence in photonics

Maneuvering Room for the ORION System limited by SRS, STRS, n_2 and other effects

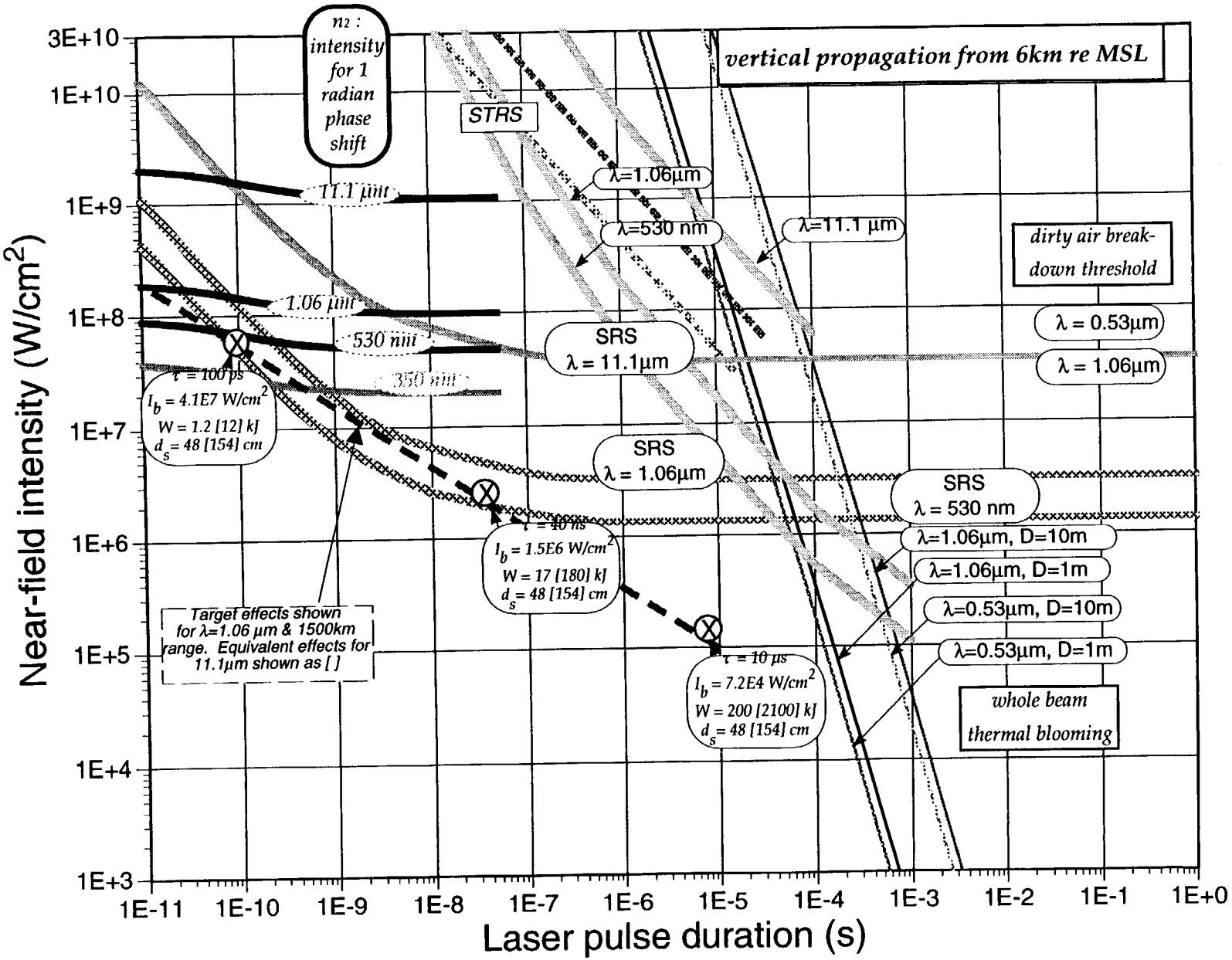

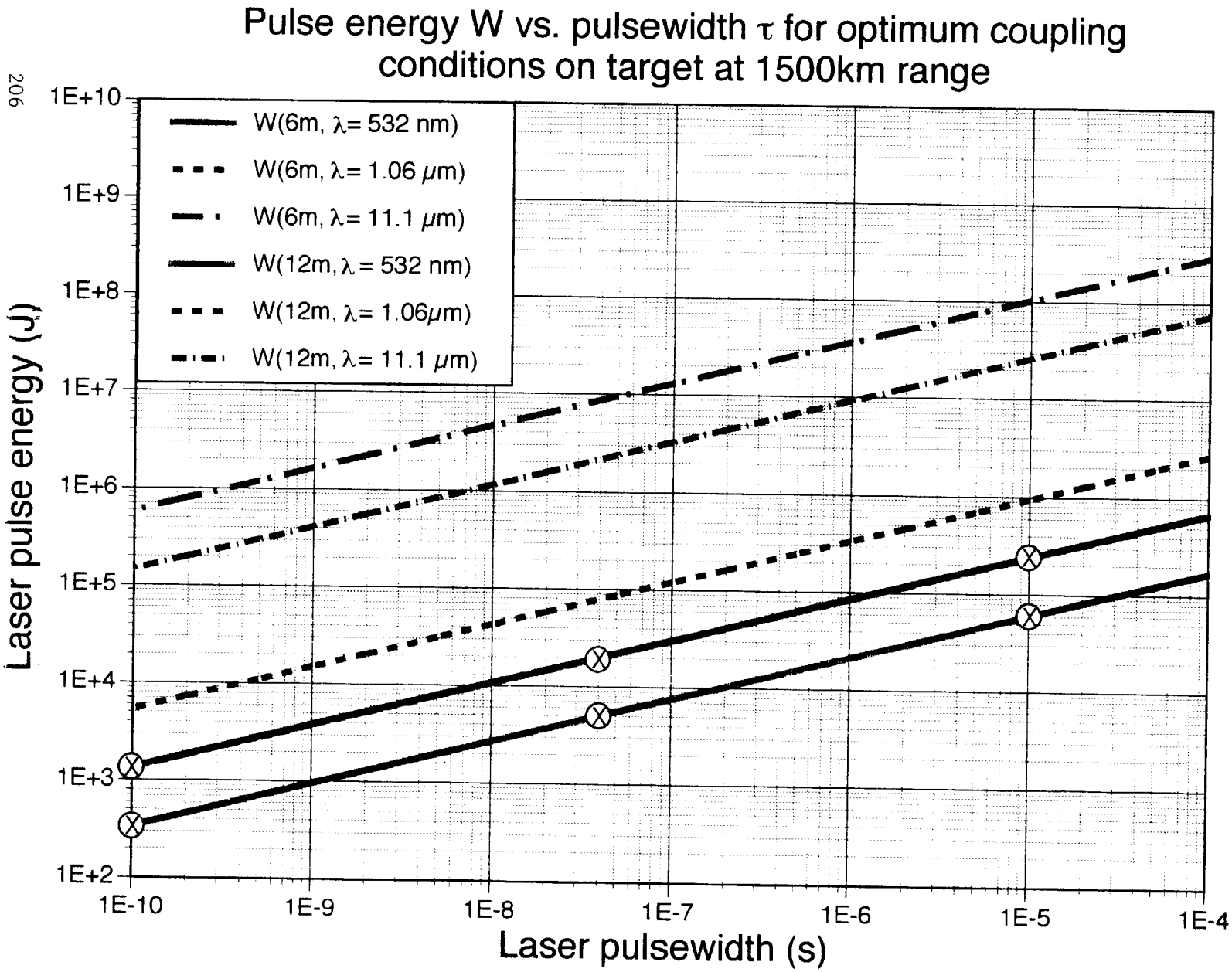
Pulse energy W vs. pulsewidth τ for optimum coupling conditions on target at 1500km range
W(6m, λ= 532 nm)
W(6m, λ= 1.06 μm)
W(6m, λ= 11.1 μm)
W(12m, λ= 532 nm)
W(12m, λ= 1.06μm)
W(12m, λ= 11.1 μm)
Laser pulse energy (J)
1E+10
1E+9
1E+8
1E+7
1E+6
1E+5
1E+4
1E+3
1E+2
1E-10
1E-9
1E-8
1E-7
1E-6
1E-5
1E-4
Laser pulsewidth (s)

TOPIC 7: GRAPHICAL METHOD FOR PICKING YOUR WAY THROUGH THE ORION PROPAGATION CHART

In previous sections (see §5 and 6), we developed the ORION "Maneuvering Room Chart", in which the limits set by such effects as Stimulated Raman Scattering (SRS), Stimulated Thermal Rayleigh Scattering (STRS), nonlinear atmospheric index (n_2), optical breakdown and whole beam thermal blooming were portrayed.

Those plots were presented as laser intensity in the atmosphere (I_b) vs. laser pulsewidth τ, following a suggestion by Reilly. This is, of course, nearfield intensity, because the farfield is typically 1 – 5,000 km distant for our problem.

On these plots, we showed a dashed line labeled "Target effects" which shows what intensity is required in the nearfield to produce optimum target coupling in the farfield (based on experimental data) for the situation we were discussing. The situation involved some combination of laser wavelength λ, range z, nearfield beam diameter D_b, etc. The connection between these parameters and the Target effects line was the relationship developed in §0:

$$I_b\tau^{1-\alpha} = \frac{C(aN)^2}{T}\left[\frac{\lambda z}{D_b^2}\right]^2 = \frac{Ca^2}{ST}\left[\frac{\lambda z}{D_b^2}\right]^2 \quad . \qquad [1]$$

where S is Strehl ratio, T is atmospheric transmission, $a = 4/\pi$, $\alpha = 0.45$ and $C = 2.3\times10^4$. It was shown elsewhere that Eqn. [1] guarantees target ignition and optimum momentum generation on the target, more or less independent of target material and wavelength in the situations we are considering. As shown in Figure 1, α is an empirical constant derived from the laser coupling literature. It makes sense physically, since α=0.5 is the value one obtains as the solution of the problem of heating the surface of a semi-infinite slab to a fixed threshold temperature. Figure 1 also reminds what we mean by "optimum coupling intensity" or fluence.

It is desirable to make a universal plot which permits the whole situation to be assessed graphically independent of special assumptions. To do this, we note that SRS and n_2, and to some extent STRS, scale inversely with wavelength, and also that fluence $\Phi_b = I_b\tau$ is probably of more direct interest than I_b, since the required laser pulse energy $W = \Phi_b*(\pi D_b^2/4)$ is directly related to hardware size and cost.

For these reasons, we plot Φ_b/λ vs. τ, modifying Eqn. [1] to read:

$$\frac{\Phi_b}{\lambda} = \frac{C\xi^2}{ST}\tau^{\alpha} \qquad [1A]$$

where

$$\xi = \frac{z\sqrt{\lambda}}{\pi D_b^2/4} \quad . \qquad [2]$$

Figure 2 is a plot of the function in Eqn. [2], and a related function ζ we will use in discussing cw laser effects later in this article.

Please refer to Figure 3 attached. Although the format may seem unfamiliar, the same data we published earlier is present, now plotted as fluence rather than intensity vs. pulsewidth.

Note the advantages: for n_2, SRS, whole beam thermal blooming and, to some extent, STRS, the boundaries set by these effects lie on top of one another for λ = 0.53, 1.06 and 11.1 μm. For the first time, we have come up with a universal plot for computing ORION propagation that is also easy to use.

Here's how to use the attached plots.

In the first place, note that wavelength is normalized to 1.0 μm, D_b to 1.0 m, and range to 1000 km (1.0 Mm) in the plots. Furthermore, we still have 3 assumptions:

- Strehl ratio S = 0.5
- Atmospheric transmission T = 0.85
- Laser repetition rate f = 100 Hz (not important until step C below)

1. Going from problem parameters to optical system parameters:

A. Determine ξ. Figure 1 allows you to do this in the normalized units, for easy transfer to the universal ORION propagation chart, Figure 3.

Please note that Eqn. [1A] works out correctly in cm and W/cm^2, but that I have done the numerical conversions involved in the normalized units for you in going between the charts (The parameter ξ in the charts is the real ξ + 100).

B. In Figure 3, interpolate between the ξ lines until you find yours. This line gives you required laser fluence vs. pulse duration.

C. In Figure 4, since you have picked a mirror (beam) diameter D_b, and you now know fluence, find pulse energy and laser cost.

2. Going from optical system parameters to problem parameters:

A. From Figure 4, pick a D_b and a laser pulse energy, defining Φ_b.

B. In Figure 3, enter your laser pulse duration and determine ξ. Figure 5 gives the same results for a high altitude site: Figure 5 shows, for 6km, a very slight improvement in the SRS limit, a slightly greater increase in the n_2 limit, and a substantial increase for STRS.

C. In Figure 2, find what range you can access with that mirror diameter and wavelength choice.

In the example shown as Illustration 2, a 1.06 μm laser with 100ps pulsewidth and 100 J pulse energy is considered. For the illustration, a 3.5-m mirror diameter is chosen, like that at the USAF Starfire Optical Range. From Figure 3, we find Φ_b = 0.001 J/cm^2, and that a 100-Hz laser with this capability should cost about $10M. From Figure 2, we find ξ=0.03. From Figure 2, this corresponds to a range of 230km, an altitude easily attained by the Shuttle, and sufficiently high that the Shuttle orbit decay time is many years. Lifetime at 230 km for 10-cm, 1-kg, spherical targets that could be deployed by the Shuttle would be about 180 days.

cw Laser Chart

In closing, it seems reasonable to see if we can develop a cw laser analog to Figure 4. The only purpose of such a plot is to facilitate range calculations. None of the effects shown in Figures 3 and 5 limit propagation except whole beam thermal blooming, and these charts are not appropriate for assessing that effect with cw lasers.

With the parameter $$\zeta = \frac{z\,\lambda}{\pi D_b^2/4} \qquad [2A]$$

the cw version of Eqn. [1] is:

$$P = \frac{\pi D_b^2}{4}\,\frac{I_s}{S\,T}\,\zeta^2 \quad . \qquad [1B]$$

In Eqn. [1B], $I_s = 1 kW/cm^2$ is the fixed intensity on target which data by O'Dean P. Judd and calculations by J. P. Reilly show is appropriate for optimum cw target coupling.

As in the pulsed case, the parameter ζ can be looked up. The only difference between ξ and ζ is an additional $\sqrt{\lambda}$ on the vertical axis of the lookup chart, Figure 2.

Figure 6 shows the resulting cw laser power and laser cost, given by J. P. Reilly's cost algorithm.

Elsewhere, we have shown that optimizing system cost gives a nearfield beam diameter D_b for the (1.3-μm) cw iodine laser case which varies from about 4.5 m at 400 km range [ζ= 0.03] to about 7.5 m at 1500 km range [ζ= 0.044]. Bear these figures in mind when reviewing Figure 6. They are totally consistent with power levels and costs given in the final Figure of §0A (rev 1) which was distributed during the Holidays.

Short pulses give optimum coupling at lowest energy

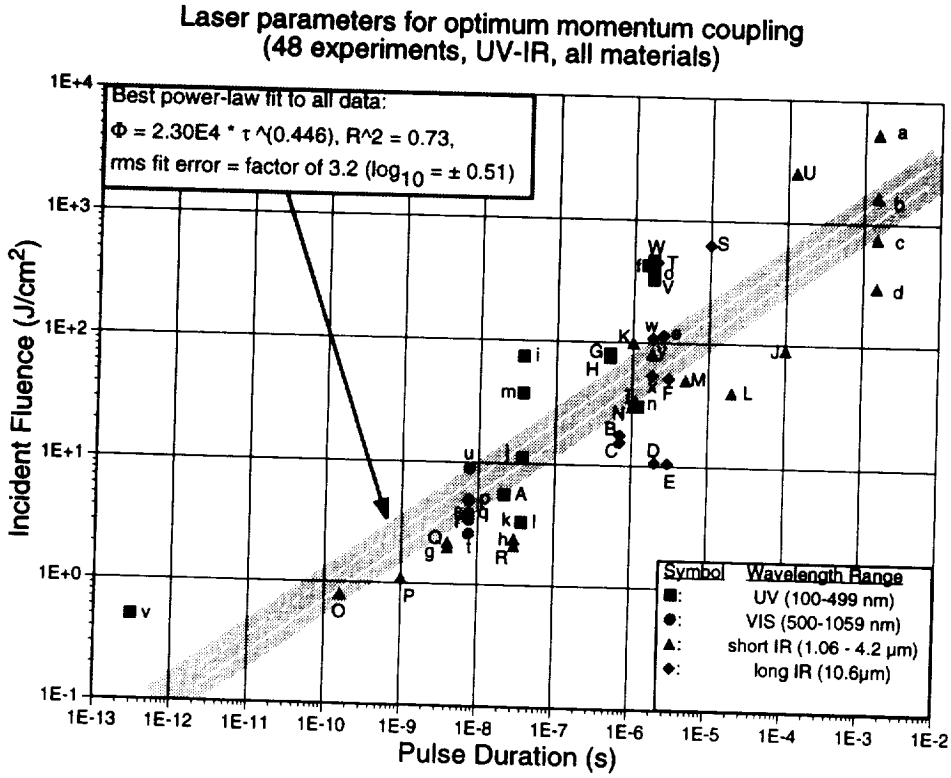

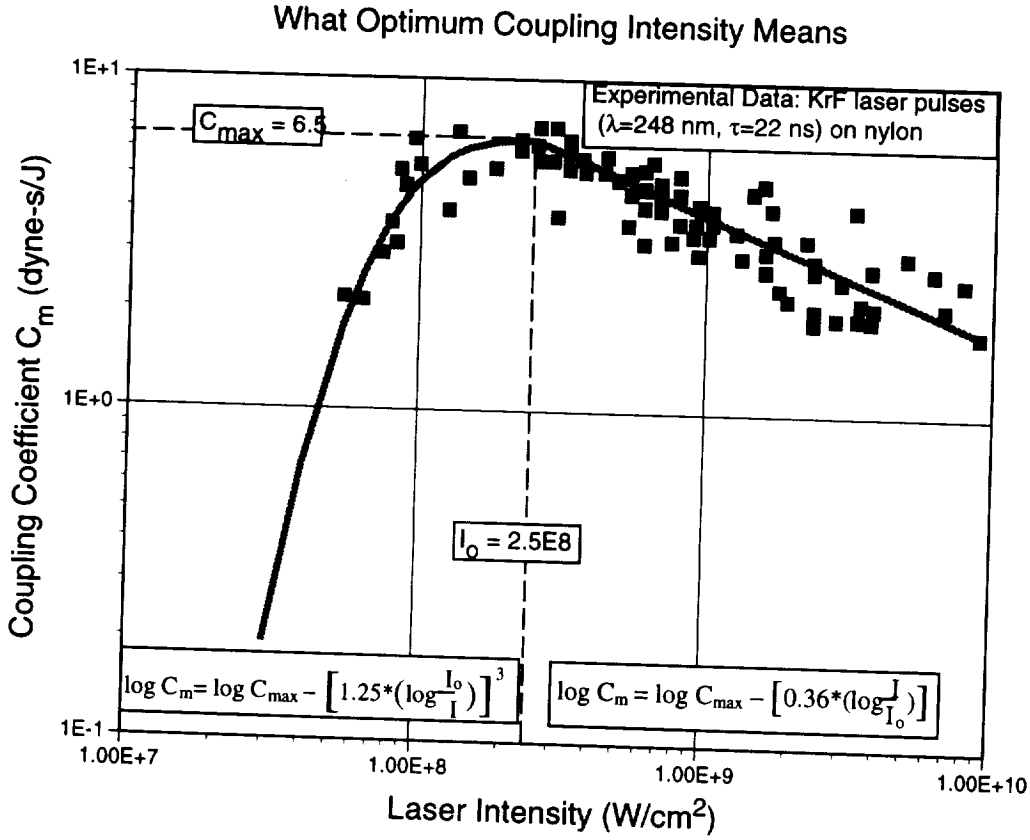

Plot of the functions ξ, ζ

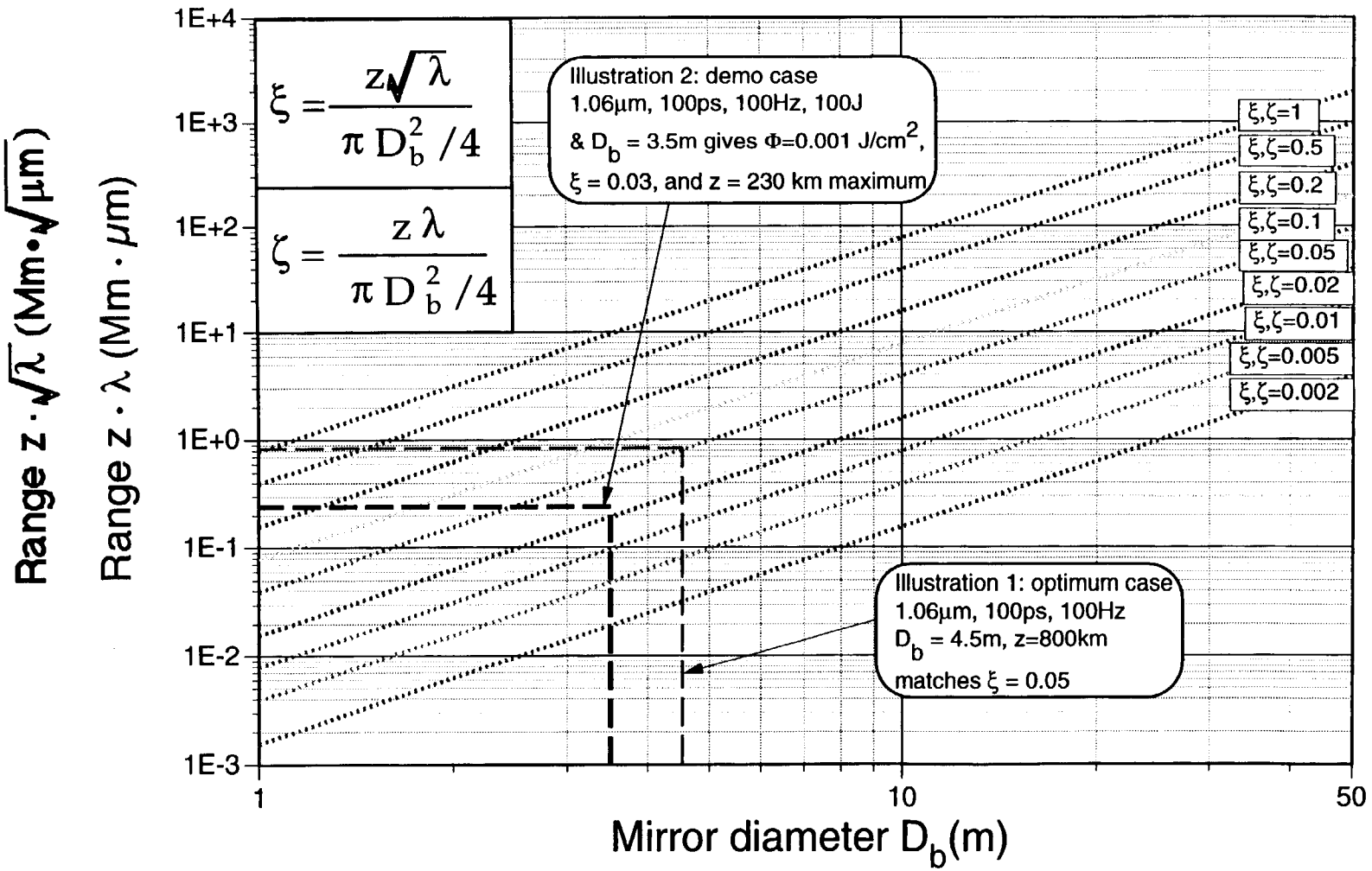

Photonic Associates
excellence in photonics

Universal ORION Propagation Chart

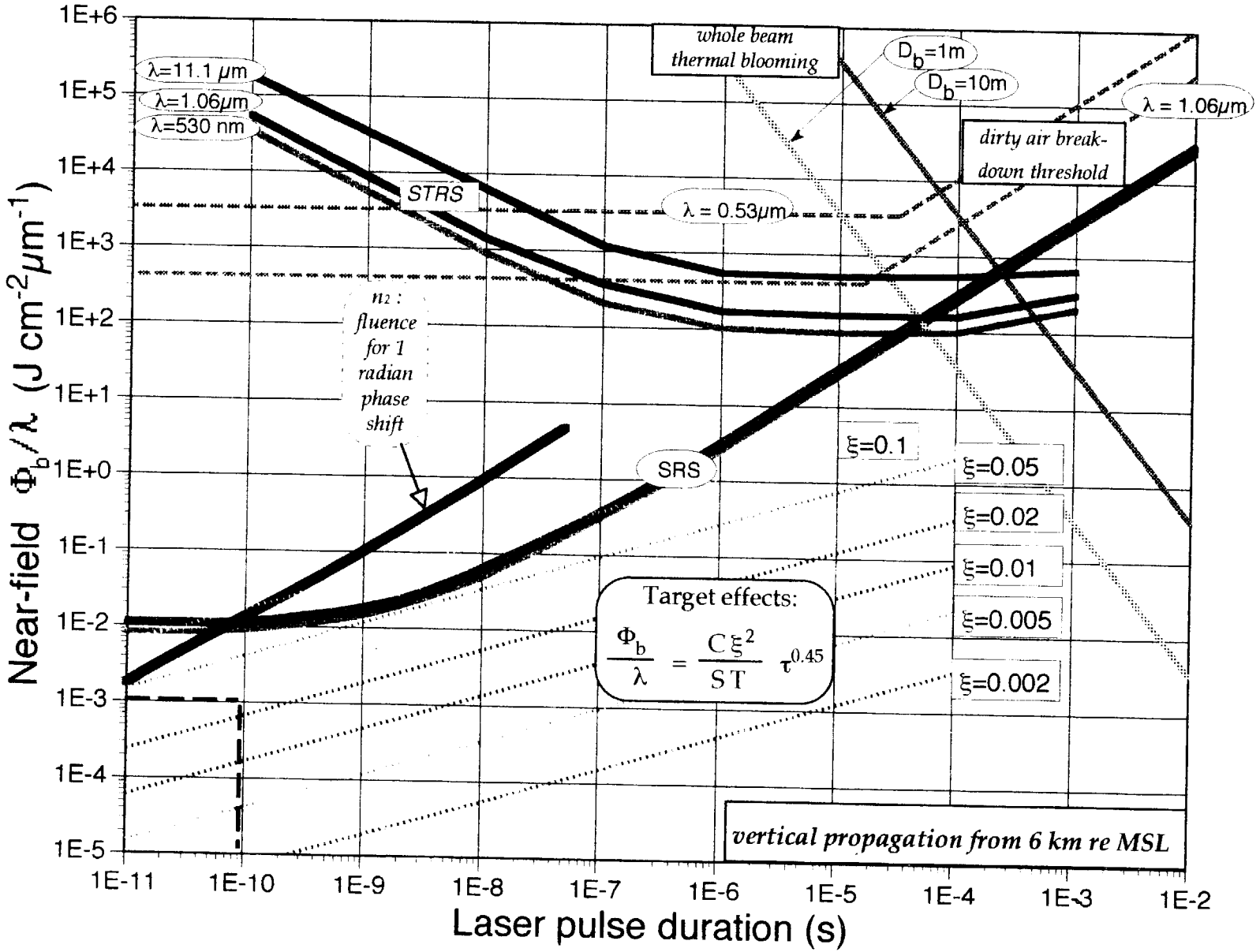

Photonic Associates
excellence in photonics

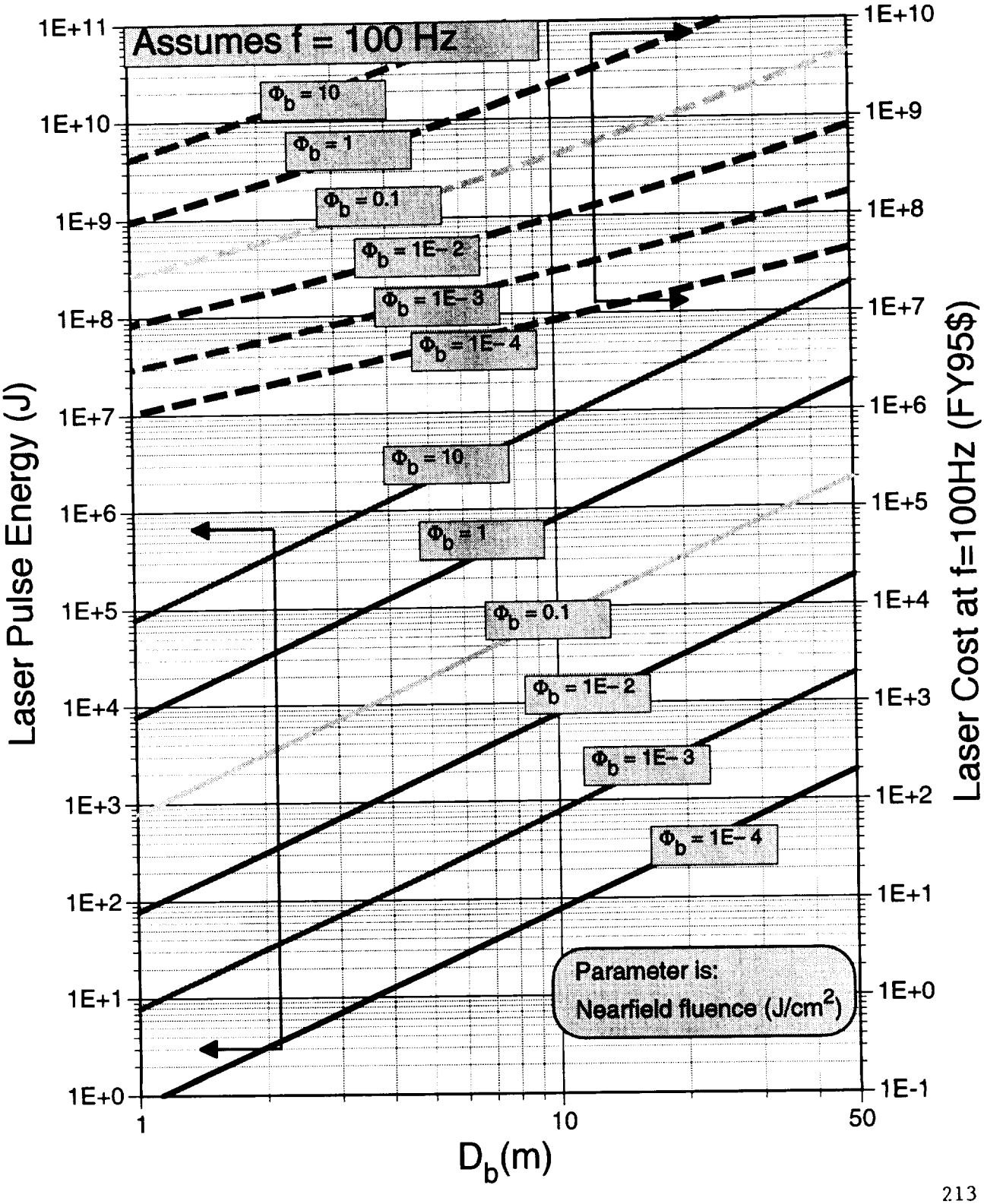

Photonic Associates
excellence in photonics

Universal ORION Propagation Chart

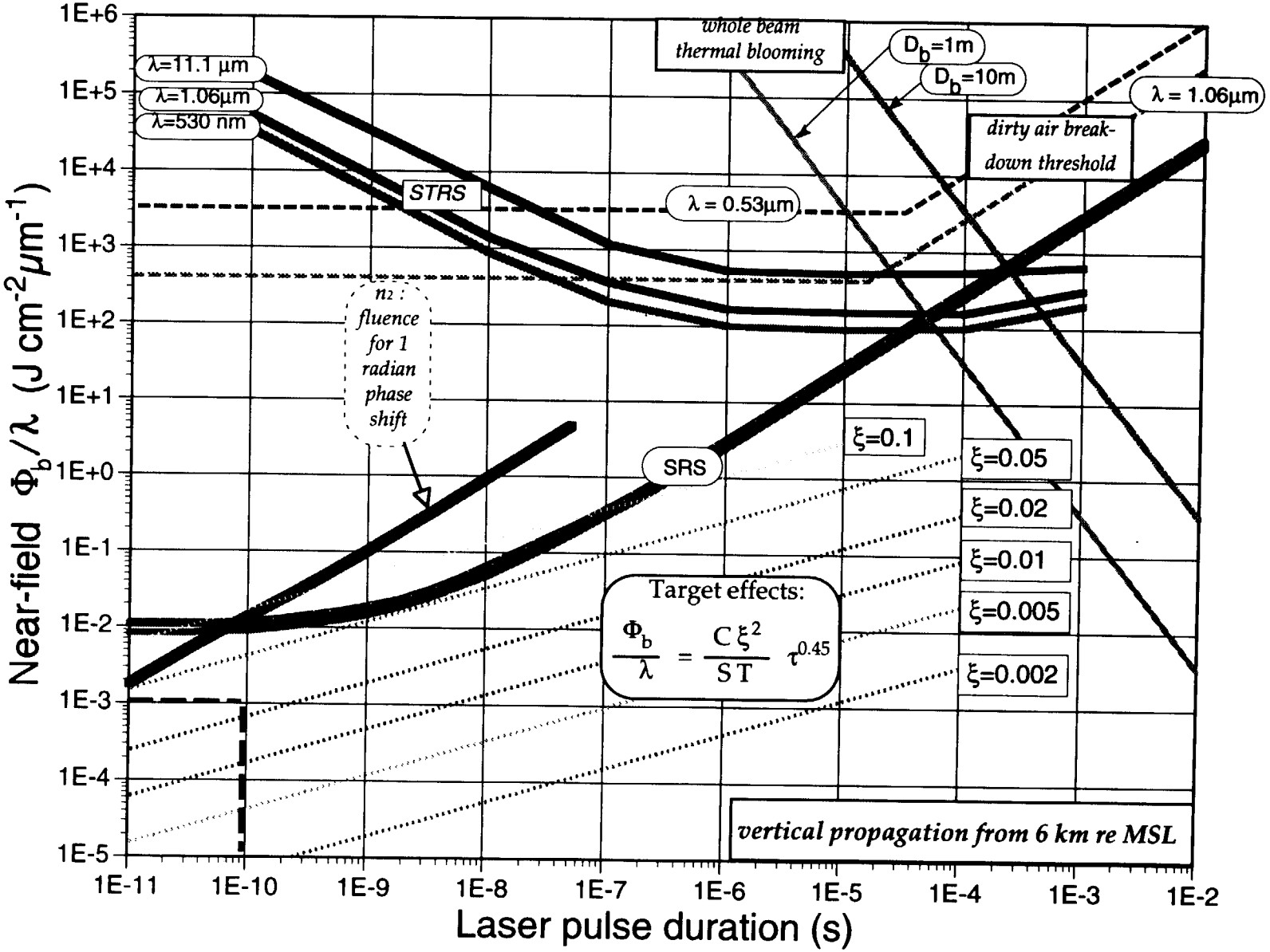

Photonic Associates
excellence in photonics

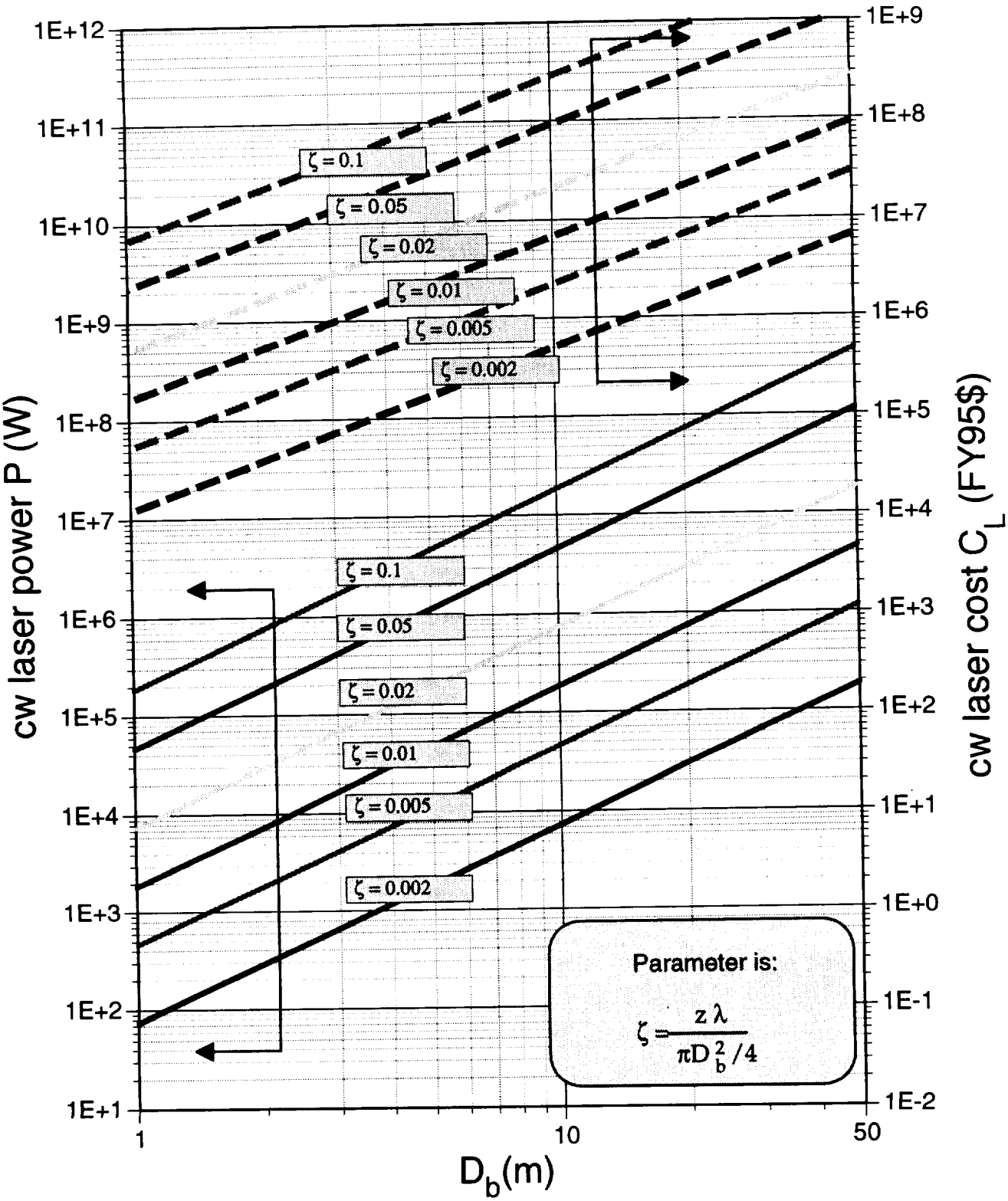

TOPIC 8: THE PRODUCT TA/M IN ORBIT, DEPENDING ON ORBITAL ELEMENTS

David Spencer provided the following table of the product T A/m of orbital lifetime and area/mass ratio as it depends on orbital elements from his "Lifetime" code.

C. Phipps also calculated the ρv^2 pressure expected on a circular orbit from the mean density represented by the CIRA 1972 Standard Atmosphere [COSPAR, 1972]. Agreement with the mean values for circular orbits provided is good. The main sources of departure from the mean lifetime are solar min/max effects on the atmospheric density. Changes in ellipticity up to 0.05 (the largest we consider) are a relatively smaller effect.

Figure 1 provides h_p vs. TA/m, which is one of the main pieces of the nomograph puzzle required for assessing laser requirements in the ORION project, others being:

- Δv_a vs h_{po} (see attached figure)
- Incident laser fluence Φ_{inc} vs $\Sigma_i v_{ai}$ ("momentum coupling coefficient" section) and
- Φ_{inc} vs on-the-ground laser parameters, from considerations being generated by other members of the ORION team, as well as limits posed by Stimulated Raman scattering and nonlinear index in the atmosphere (§4).

We have also attached a figure showing how the atmospheric scale height varies with altitude.

References:

CIRA 1972 [Committee for the COSPAR International Reference Atmosphere, Working Group 4] Akademie Verlag, Berlin

Allen, C. W. 1973, *Astrophysical Quantities, 3rd edition,* Athlone Press, London

LIFETIME TABLE BASED ON D. SPENCER 8/23 NUMERICAL INTEGRATION*

h_a(km)	h_p(km)	m (g)	T, days	T A/m (cm^2-day/g) from 1/1/99
1000	200	0.1	0.72	7.2
1000	200	1	6.83	6.8
1000	200	10	71.9	7.2
1000	200	100	492	4.9 **
1000	300	1	79.1	79.1
1000	400	1	275	275
1000	500	1	528	528
1000	600	1	875	875
1000	700	1	1550	1550
1000	800	1	5310	5310
1000	900	1	12400	12400
1000	1000	1	20570	20570
800	200	1	4.52	4.52
800	300	1	52.5	52.5
800	400	1	188	188
800	500	1	390	390
800	600	1	638	638
800	700	1	902	902
800	800	1	1280	1280
600	200	1	2.6	2.6
600	300	1	25.6	25.6
600	400	1	101	101
600	500	1	242	242
600	600	1	361	361
400	200	1	1.09	1.09
400	300	1	7.8	7.8
400	400	1	28.1	28.1
300	200	1	0.53	0.53
300	300	1	2.9	2.9
200	200	1	0.16	0.16

*: A = $1cm^2$ for all objects

**: Nonlinearity due to changing solar cycle

How much difference does it make if the impulse is applied incrementally instead of in one impulse? At perigee instead of apogee?

In §8, we computed the Δv required to lower the perigee of objects in elliptical orbits, assuming the velocity change is applied in a single impulse at apogee.

Where total energy $$H = V + E \qquad [1]$$

Potential energy $$V = -\frac{GMm}{r} \qquad [2]$$

Kinetic energy $$E = m\,v^2/2 \qquad [3]$$

and since $$e \equiv \frac{r_a - r_p}{r_a + r_p} \qquad [4]$$

Then $$H = -\frac{GMm}{2a} \qquad [5]$$

is related directly to the semimajor axis

$$a = (r_a + r_p)/2 = r_a/(1+e) \qquad [6]$$

and [1],[3] & [5],[6] give $$v_a^2 = \frac{GM(1-e)}{r_a} = \frac{2GMr_p}{r_a(r_a+r_p)} . \qquad [7]$$

Differentiating [7] gives $$\frac{d(v_a^2)}{dr_p} = \left(\frac{2GM}{r_a}\right)\left(\frac{(r_a+r_p) - r_p}{(r_a+r_p)^2}\right) = \frac{2GM}{(r_a+r_p)^2} . \qquad [8]$$

But of course $$\frac{d(v_a^2)}{dr_p} = \frac{d\left(\frac{p_a^2}{m^2}\right)}{dr_p} = \frac{2p_a\,dp_a}{m^2\,dr_p} = \frac{2v_a\,dp_a}{m\,dr_p} \qquad [9]$$

and equating [8] and [9] gives

$$\frac{dp_a}{dr_p} = \frac{m}{v_a}\frac{GM}{(r_a+r_p)^2} = \frac{m\sqrt{GMr_a}}{\sqrt{2r_p}(r_a+r_p)^{3/2}} . \qquad [10]$$

The point of this whole exercise is to integrate [10] in order to determine how much total momentum, applied in a series of increments, is required to obtain a final perigee value r_{pfinal}, starting with initial orbital parameters r_{ao} and r_{po}. This is done as follows:

$$\sum_{i=1}^{n} p_{ai} = m\sqrt{\frac{GMr_{ao}}{2}}\int_{r_{po}}^{r_{pfinal}} \frac{dr_p}{[(r_p)^{1/2}(r_a+r_p)^{3/2}]} \quad . \qquad [11]$$

The integral tables give

$$\sum_{i=1}^{n} v_{ai} = \sqrt{\frac{2GM}{r_{ao}}}\left[\frac{\sqrt{r_p}}{\sqrt{(r_{ao}+r_p)}}\right]_{r_{po}}^{r_{pfinal}} \qquad [11a]$$

as stated in the "orbital mechanics" viewgraph.

This is of course the best possible situation: that velocity increments can always be applied at apogee. Nevertheless, since we have discussed the fact that it is desirable to build a laser large enough to bring down many of the small objects in just one overhead apparition, this is a useful case to study. Note also that, to compensate for the favorable assumption, we have ignored the effects of drag during the laser application sequence.

Now, let's see how bad the worst case (Δv applied at perigee) really is.

Eqn. [11a] is symmetric with regard to exchange of subscripts. For application of Δv at perigee, the relevant expression is:

$$\sum_{i=1}^{n} v_{pi} = \sqrt{\frac{2GM}{r_{po}}}\left[\frac{\sqrt{r_a}}{\sqrt{(r_{po}+r_a)}}\right]_{r_{ao}}^{r_{afinal}} \qquad [12]$$

Figure 1 following is a plot of Δv_a required if applied as a single impulse.

Figure 2 attached is a plot of Eqns. [11a] and [12], and it is readily seen that

- There is not much difference between applying Δv incrementally and as a single impulse.
- It is <u>much</u> harder to drop the apogee by shooting the debris at perigee, than the reverse, as we claimed in §7. As an example, consider these two cases:
  1) The case h_{ao} = 1000 km, impulses applied at apogee (red solid curve). Choosing h_{po} = 500 km, we read Δv = – 82 m/s off the graph.
  2) The symmetrical case h_{po} = 500 km (green dashed line). Choosing h_{ao} = 1000 km, we read Δv = – 218 m/s off the graph, 2.65 times greater Δv this way.
- It is clear that real cases will fall somewhere between these extremes, if we have no knowledge of the particle's orbit or no convenient access to its apogee.
- Δv = –338 m/s will bring down <u>everything</u> below 1500 km, given h_p = 200 km as a definition of success.

Velocity change applied in a series of increments to reach 200 km final altitude, vs. initial altitude

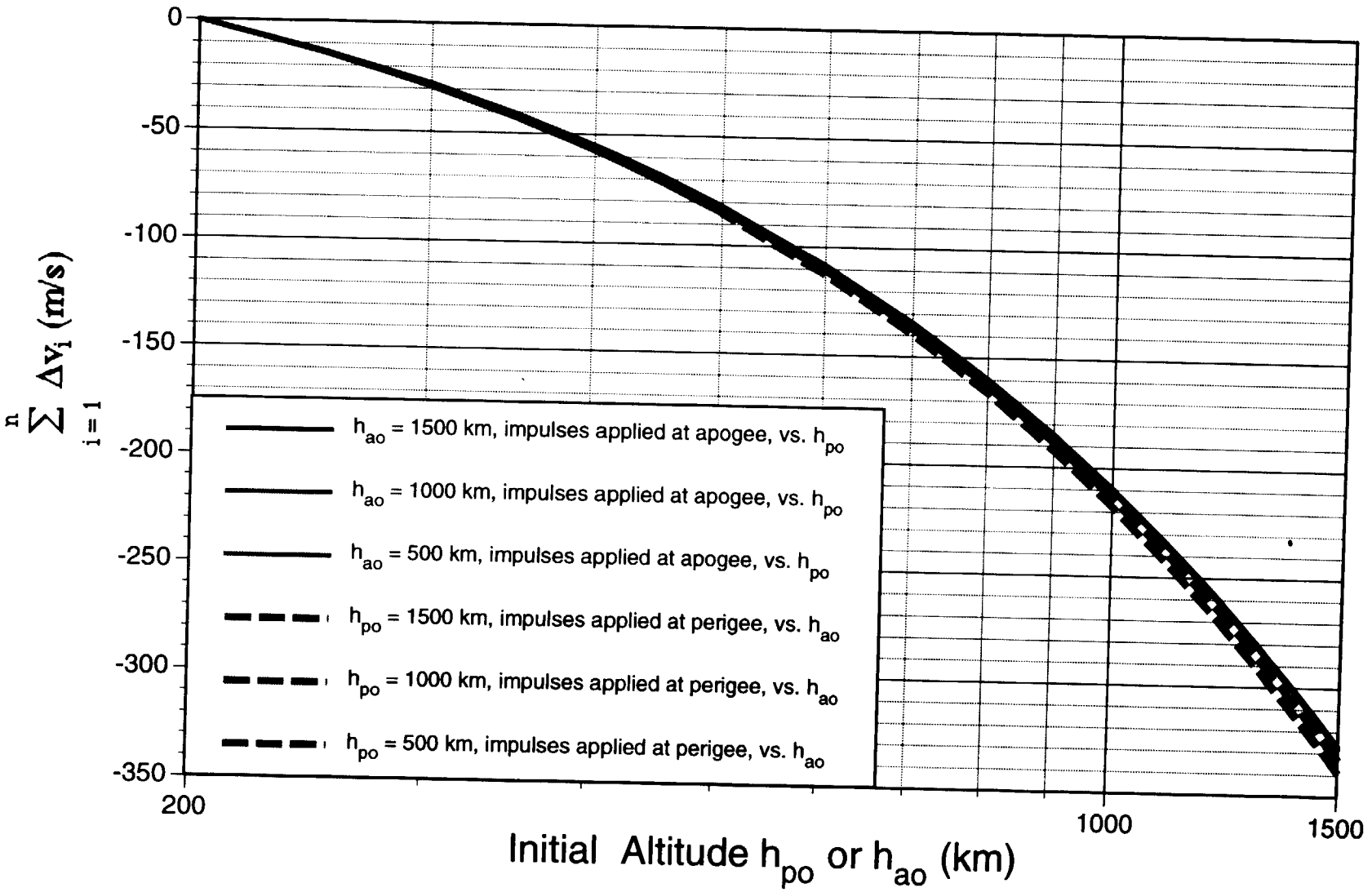

Photonic Associates
excellence in photonics

The Product TA/m in orbit, depending on orbital elements

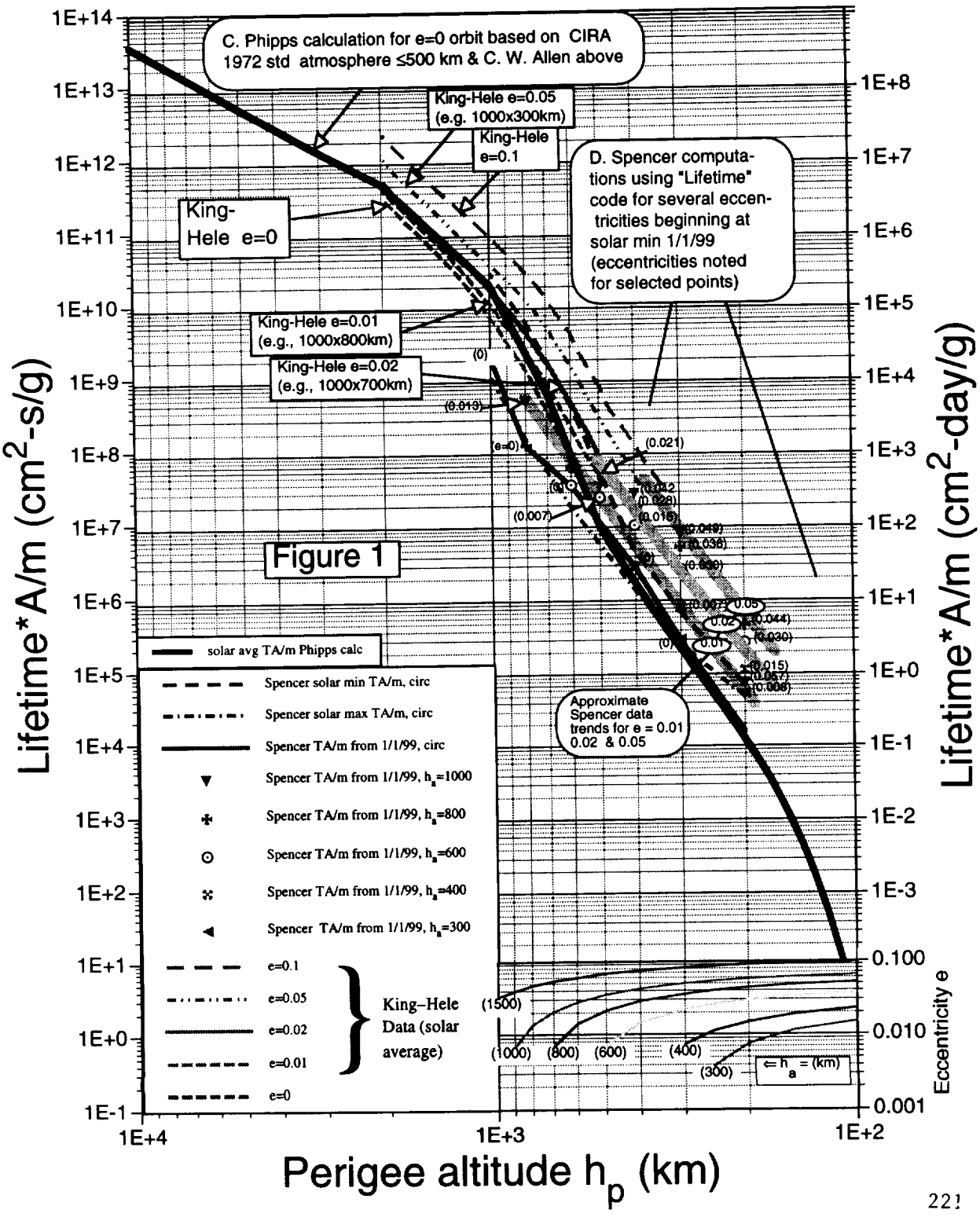

TOPIC 9: ACTIVE OPTICAL ACQUISITION AND TRACKING USING THE PUSHER LASER AS ILLUMINATOR IS A VALID OPTION

Executive Summary

We summarize the case for active optical acquisition and tracking, that is, using the pusher laser for acquiring targets instead of just identifying and ablating them after handoff from a radar. With 30kW laser average power and a 10-m diameter transmit/receive mirror, high-albedo Lambertian targets as small as 1.5cm can be acquired at 1500km range, while still searching the whole sky in 2 years.

However, it is not necessary that the receiving mirror have the same high optical quality as the transmitting mirror, which can be colocated with a much larger, low-quality receiver. In the example we will describe, a 20-m receiving mirror is able to acquire even dark (R=0.3), 1.5-cm debris particles (the smallest we need to find) at 1500 km and search the sky in 2 years. A high-quality, 6-m diameter mirror is adequate for the beam transmission task, and close to optimum size. Many targets will have narrow reflected beam profiles (such as sheet aluminum) and will be spinning, so will be easy to acquire when they point in the right direction, but very difficult otherwise, for any acquisition and tracking technique.

What are the requirements?

1. We would like to acquire and track debris targets with R >≈0.3 and d>≈1.5 cm at h ≤ 1500km.

The distinction between altitude and range is not too important since the higher, smaller targets can be pushed on radially to reduce their perigee, even though that is less efficient, because they are small.

2. We would like to scan the entire sky in 2 years or less.

3. We would like to do these things without investing in a high quality mirror larger than the ideal 6-m diameter transmitter.

4. We would like to do these things without investing in a laser with average power much larger than the ideal for pushing on the targets to clear near-Earth space – which is approximately 30kW.

Table I: Glossary

Symbol	Definition
R	Target Bond albedo: reflectivity into 2π sterrad (a hemisphere of space)
z	Target range. Always equal h in this analysis.
D_R	Receiver mirror diameter
D_T	Transmitter (beam director) mirror diameter
A	Target area (cm^2)
d	Target effective diameter (cm)
S	Strehl ratio
T	Atmospheric transmission
W	Laser pulse energy (J)
P	Laser average power (W)
τ	Laser pulse duration (s)
c	Speed of light (cm/s)
d_s	Laser spot diameter at the target
A_s	Laser footprint area at target = $\pi d_s^2/4$
Ω_s	Laser footprint solid angle = $\pi d_s^2/4z^2$
I	Peak intensity (W/cm^2) at some location
I_{opt}	Peak intensity for optimum target momentum generation per incident joule of laser light
t_m	Duration of ORION mission (s)
q	Number of targets in a specified altitude zone
$v_\perp$	Apparent target speed across the field of view
f_1	Repetition rate during 3-pulse (Hz) acquisition burst
f_2	Laser pulse repetition rate (Hz)
R_E	Radius of Earth (6378 km)
h	Target altitude
$\hbar c$	constant = 1.988E-23

How do we determine sky survey time and search spot size?

In acquisition mode, spot size at range d_s is not a free parameter, but depends on t_m, D_b, W, q, $v_\perp$, f, h and other parameters including producing the minimum necessary number of detected photons from the minimum interesting target, as well as covering the entire sky in an acceptable time, through relationships set physics and by a search **strategy**.

Strategy: with uniformly distributed targets having uniform number density per sterradian, the best strategy for detecting a fraction (1 – 1/e) of them is a random search pattern which totally covers every spot in 4π sterradians of sidereal space in time t_m, with a dwell time in each laser footprint Ω_s just long enough to detect the target (if present) and make a track. The protocol used for searching may be a picket fence or bowtie pattern as Reilly suggests in his recent memorandum, or a spiral or other pattern.

Almost all the time, a search laser of reasonable pulse energy will be looking at empty space.

Figure 1: Probability of finding any 1-20-cm Debris Particle beneath the altitude h and with d_s illustrates this fact for various debris altitudes, with basis for the calculation shown in the inset box. It is assumed that the only targets under 300km are 10 test targets deliberately placed there for the ORION demo. It will be noted that, for the existing population, a search spot as large as 100km is required to have a high probability of including any target larger than 1 cm. This is important, because it says that, most of the time we will fire the laser, not get a return, and move on. This fact makes it simple to compute ORION Sky Survey Time (Figure 3), since dwell time will be limited to the time it takes to repoint the laser beam. Plotted is the expression

$$d_s = \frac{4\,(R_E+h)}{\sqrt{q}} \qquad [1]$$

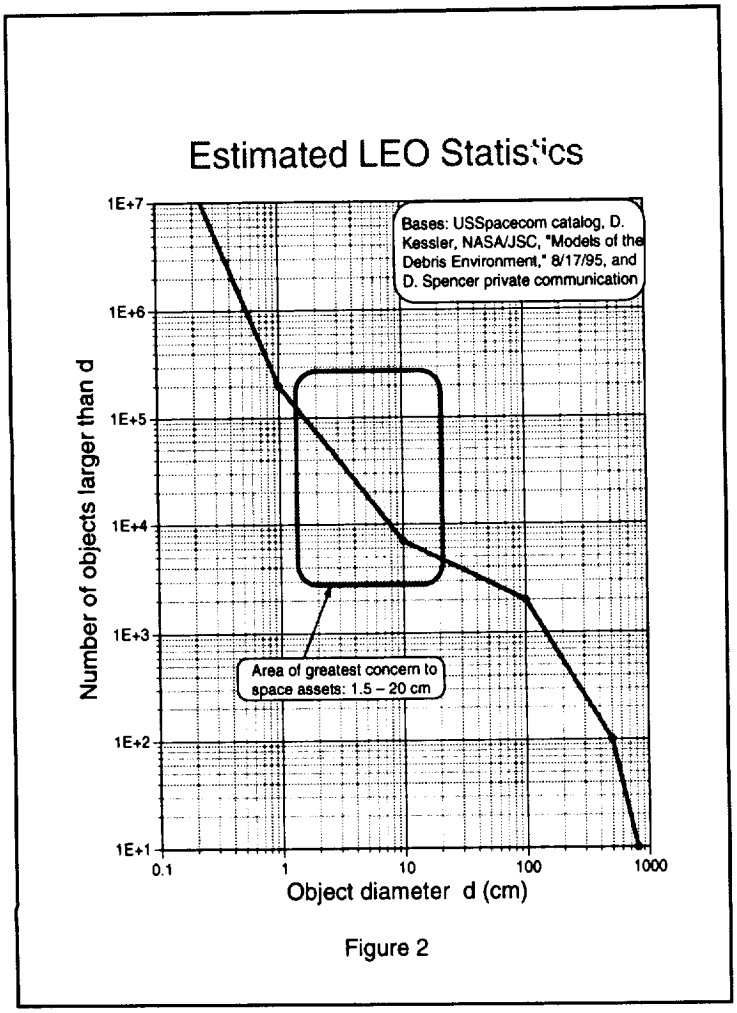

Figure 2

How do we know how many targets there are? **Figure 2: Estimated LEO Statistics** is an estimate based on information provided by Drs. Don Kessler, NASA/JSC and David Spencer, USAF/ Phillips, as well as other sources, which shows that it is reasonable to assume about 150,000 total objects in the critical 1.5 to 20-cm size range below 1500 km.

It is important to remember that, while error bars are probably a factor of two on these points, error is not accurately known because the debris number in this size range has only been sampled, in the Haystack campaign. In addition, at any time, another COSMOS event might release 70,000 more objects into LEO or a collision of large, "dead" objects might occur. The number of targets at various altitudes used in Table II and in Figure 1 is derived from this Figure by proportioning this total to the reported flux at various heights.

Table II: Assumptions for Acquisition

Pusher laser wavelength	1.06 μm
Minimum interesting target	d = 1.5 cm
T	0.85
S	0.50
R	0.30
Target number density	uniform over 4π (worst case)
Target $v_\perp$ direction	random (worst case assumption)
$v_\perp$	7.7 E5 cm/s
q(800km<h<1500km)	150k objects
q(300km<h<800km)	40k objects
q(h<300km)	10 objects (deliberately inserted for demo)
t_m	6.32E7 s (2 years)
Array quantum efficiency	20% (J. P. Reilly)
Detector quantum efficiency	65% (J. P. Reilly)

Figure 3: ORION Sky Survey Time (a correction of an earlier chart of the same name you have received) connects search spot size, target altitude (here z rather than h) and laser rep rate f to the time required to search the sky.

This Figure is used as follows: enter the Figure with an acceptable sky search time in years. Follow in the direction of the dashed line to the line for the laser rep rate, then down to the range, then back across to the required spot size. It will be seen that spot sizes of the order of 10km are necessary for reasonable search times.

Figure 4: Photons received calculator, identical to the one you received earlier (except that S = 1 for floodlight beams), shows that, if you use spots that large, you will not receive enough photons for detection except for big, bright, close targets.

This Figure is used as follows: start at the top left with spot size, turn downward at the line for target range and obtain the chart output from the bottom left axis (photons per kJ). The parameter $D_b d\sqrt{R}$ is the product of the mirror diameter D_b (here assumed the same for transmitting and receiving) in meters, target diameter in cm and the square root of its Bond albedo. For a 5-m mirror looking at an R=0.3, 1.5-cm target, $D_b d\sqrt{R} \approx 4$ is the correct line to follow. Then, a 10-km spot size for a target at 1500 km would return only 0.004 photons per kJ, that is, a 2.5-MJ pulse at the ground would be necessary to get a 10-photon return!

More realistically, if we use a 6-m mirror, W = 30kJ and 4-km spot size in the longer-term system [for 2-year sky search time], then at R = 0.3, a debris target must be 4.5 cm in size to return 10 photons.

Calculations such as this have been discouraging in the past.

Now, imagine that we have two mirrors – closely colocated – a small one with high quality to transmit and receive, and a much larger, very low quality mirror surrounding that to receive the returned photons, to take the place of the radar system.

Figure 5: Average Laser Power Required to Receive 10 photons per shot and Search Sky in 2 years shows the average power $P = f_2 * W$ required to meet thes criteria simultaneously, vs. target altitude. Two dashed horizontal lines show:

• The cutoff in detectable actively illuminated targets if we limit P to the 30kW required to bring in all the debris below 1500 km in 2 years is $D_R d\sqrt{R} = 15$ m-cm. That is, a 20-m diameter collector seeing a 1.5-cm particle with Bond albedo R = 0.25.

In other words, active laser acquisition will work with a 20-m, low quality collecting optic.

• The $D_R d\sqrt{R}$ cutoff if we were to use 3MW average power [a power level dictated by generation of useful thrust at range with a CW laser] – and dwell long enough on each spot to generate the 10 photons – is 10 times smaller. However, for CW acquisition, we can see that more received photons are required compared to the pulsed illumination case, since the target is moving and it is a streak that we must create rather than just a dot on the focal plane array.

The spot size d_s can be read off Figure 4, where it is seen that a search spot of order 4km is correct to get back 10 photons from a 30-kJ pulse. For the CW case, the target moves 77m per 10ms interval, during which the 3MW laser will also deposit 30kJ. If a 1000x1000-pixel matrix is imaging a 4-km spot at range, the target streak will be 20 pixels long, and 20 times as much illumination is required to provide detection as in the pulsed laser case. The CW laser certainly meets this requirement with 100 times more photons. However, there are concerns with thermal blooming, beam quality and target interaction. We will not analyze this case further in this memo.

Average power P is independent of search spot size d_s. Figure 5 results from combining the two equations

$$f_2 = \frac{1}{t_m}\left[\frac{4\,(R_E+h)}{d_s}\right]^2 \qquad [2]$$

and

$$W = n_{det}\frac{8\hbar c}{T^2\lambda}\left[\frac{d_s h}{D_R d\sqrt{R}}\right]^2 \qquad [3]$$

to give

$$P = \left(\frac{n_{det}}{t_m}\right)\left(\frac{8\hbar c}{T^2\lambda}\right)\left[\frac{[4(R_E+h)\,h}{D_R d\sqrt{R}}\right]^2 \qquad [4]$$

The parameter d_s contains the information about D_T, and affects the repetition frequency f_2 which is necessary through Figure 3.

In Table III, we outline the parameters for three standard active laser acquisition and tracking cases which will be discussed in the following sections.

Figure 6: Composite transmit/receive mirror site shows how this concept would work.

The only purpose of the 20-m receiving mirror is to provide enough photons to register that a debris particle is within the field of view, and tell the steerable high quality transmit/receive mirror in the center how to point *its* field of view, which might be 30 times more narrow. Again [Figure 1], most of the time, nothing will be seen. At 1 Hz, with d_s = 4km, the target detection rate at 1500 km vertical range will be 8 per hour.

It would be advisable to bury such a big mirror permanently in the earth, like the Hobby-Eberly Telescope (9 meter effective aperture, f/1.45) in Texas. Like the Arecibo radio antenna, that telescope is pointed, not by moving the mirror, but by moving the feed in 1 degree increments and then letting the Earth's rotation do the rest of the steering. Composed of 91 hexagonal segments, this is physically the world's largest primary. Yet, the total construction cost for this device is just $13.5M. A Gregorian secondary corrects spherical aberration.

Table III: Satisfying Constraints for Pusher Laser Target Acquisition

ORION System:	Demo		Near-term		Longer-term**	
Altitude h (km):	300	300	500	800	800	1500
Target diameter d (cm):	1.5	3	2	1.5	1.5	1.5
Receive mirror diameter D_R (m):	3.5	3.5	4.4	4.4	20	20
Bond albedo R:	0.3	1E4*	0.8	0.8	0.28	0.28
$D_R d\sqrt{R}$:	2.9	1.1E3	8	6	16	16
Laser pulse energy W(kJ):	1.4	1.4	9.8	9.8	30	30
d_s to return 10-photons from target (km):	0.8	330	3.6	1.6	30	4
Actual spot size d_s used (km):	0.8	30	3.6	1.6	3.3	4
Rep rate f_2 to search sky in 2 yrs (Hz):	15	0.01	1	5	1	1
Laser average power (kW):	21	0.014	9.8	50	30	30
Number of targets q (≤ h):	----	10 (TEST)	----	40E3	40E3	150E3
Detection rate for these targets (per hr.):	----	N/A: LOC. KNOWN	----	2	2	8
Actual photons received:	10	670	10	10	50	10

Table III notes:

* Target is covered with corner cube arrays (fused silica bicycle reflectors) with 1° beamwidth
** Parameters in these columns differ from those for the ORION final report Longer-term Option

Table III shows that a 30kJ pulse at 1.06μm incident on even a very dark, 1.5-cm target can return the minimum required signal from 1500 km, and a quite adequate signal from 800 km. A 100-photon signal would be obtained if the 1.5-cm target at 800 km altitude were bright rather than dark. There is not room in the Table to show all cases, but repeating the last column on the right with a 20-cm target gives 8,900 photons.

Figure 7: Photons received for several cases vs $D_R d\sqrt{R}$ treats cases given in Table III.

Our 20-m receiver would have very low optical quality compared to the Hobby telescope, and should be cheaper to make. A surface figure of order 10 waves per 10 cm (100 μrad) would be sufficient, with a 30x30 array of 2-cm image spots covering the 3-mrad field of view at the mirror's 100-m focus. A suitably small image of this array to match an array of single photon detectors can be created by a high power optic without violating the etendue theorem. Segments of such a low quality mirror could be replicated cheaply by machining, single-point-diamond-turning and mechanically polishing. The reflective coating could be applied chemically – like your bedroom mirror – or by vapor depositing aluminum on the vacuum furnace conveyor belt at PPG Industries.

The point is: it could very well be cheaper to create this mirror site than to use radar for acquisition. It is difficult to see how the total cost of the site could exceed $15M, based on the cost of the Hobby-Eberly telescope. This compares well to the $80M estimated cost of reproducing Haystack.

Now, we review detection of a moving target against a fixed background of stars (Figure 8).

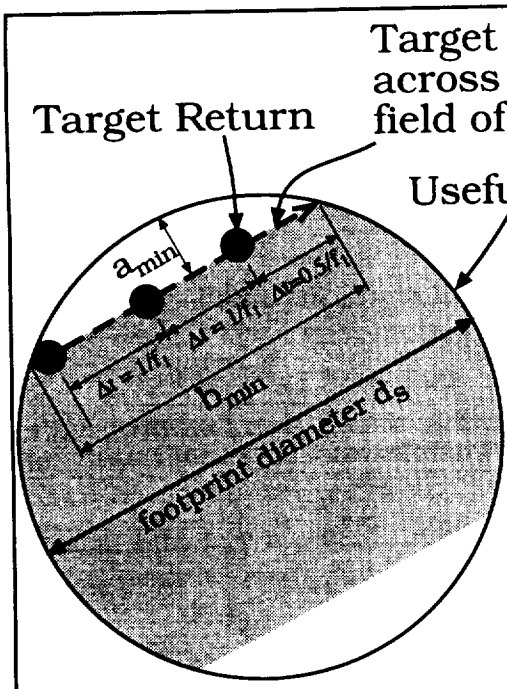

Figure 8

If a target is found in the field of view, making a reliable track requires getting 3 returns within the footprint (Figure 1), in order to establish present location and vector velocity well enough to provide the instructions needed to center the footprint on the target when the transition is made from acquisition to tracking mode.

Only rarely will this be necessary –on the rare occasions when a target is present and then only during the first few shots necessary to establish a track. So, triple pulsing will not affect average laser power.

The two corresponding pulse formats are illustrated in Figure 9. This concept first appeared as Fig. 1 of §10A in October '95.

From the formula for the fractional area of a circle enclosed by two parallel chords [Eqn. 5], we can determine that 99.3% of the detection footprint is "useful area" for track assembly purposes using our strategy, when $b_{min}/d_s = 25\%$.

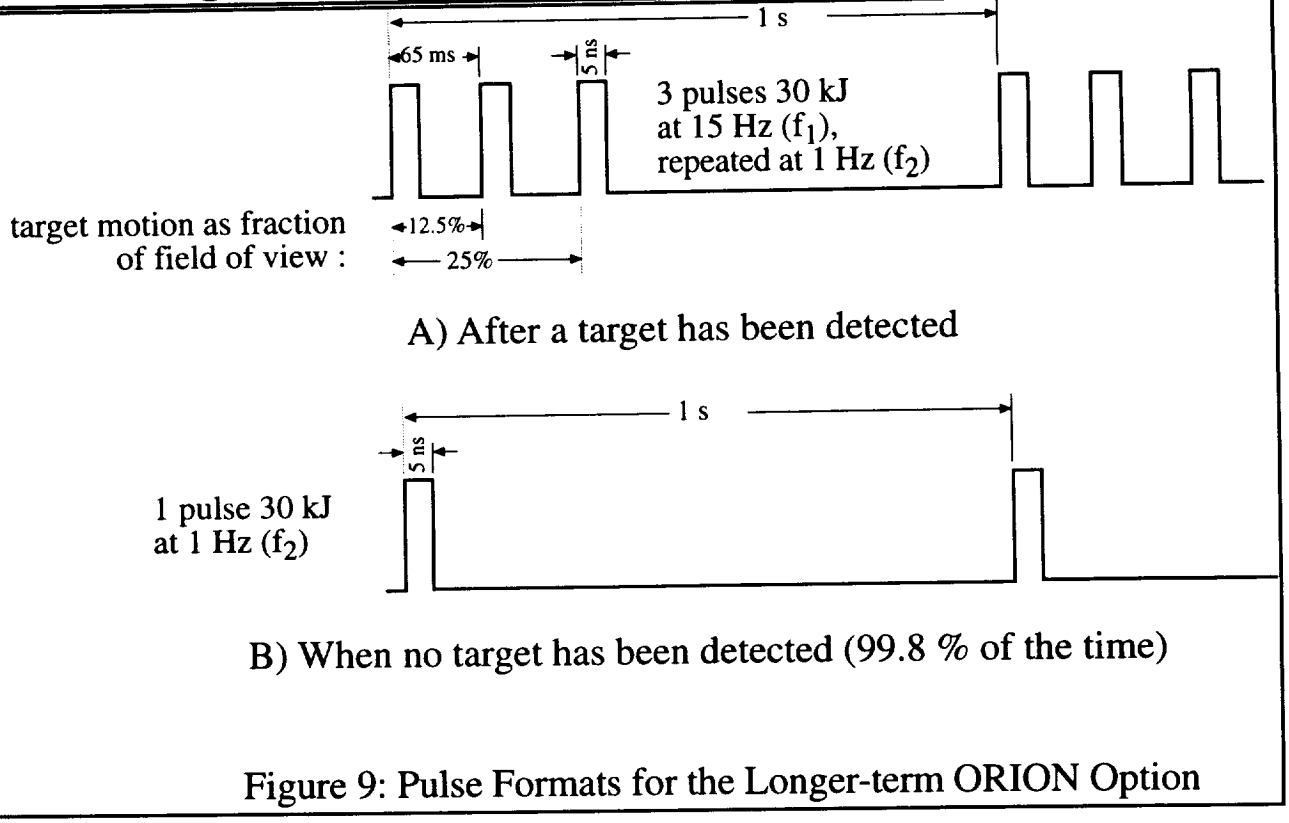

Figure 9: Pulse Formats for the Longer-term ORION Option

$$\beta = 1 - \frac{2}{\pi}\left[\sin^{-1}\left(\frac{b_{min}}{d_s}\right) - \frac{b_{min}}{d_s}\sqrt{1-\left(\frac{b_{min}}{d_s}\right)^2}\right] \qquad [5]$$

Combining this prescription with a strategy requiring that we always have 3 returns within the window, constrains the burst pulse rate to the value given by:

$$f_1 \geq \frac{10\, v_\perp}{d_s} \qquad [6]$$

for at least as long as one burst of 3 pulses. In the example shown in the Figure, this is 15Hz.

Signal to Noise ratio in the Daytime

Reilly did an excellent analysis of signal to noise ratio in his recent report, and there is no point in repeating his results here.

The only important differences in our analyses are these:

1. The specific cases he considered were limited to 3kJ pulse energy and a 3.75 m diameter collecting mirror, whereas we have considered 30kJ and 20m. These two differences have large impacts on how the rest of the problem turns out.
2. The notch filter he uses has 0.05μm bandwidth. I had assumed a bandwidth given by the time bandwidth product of the laser pulse itself: for 5ns pulses, $\Delta\lambda$= 7E-7 μm, about 5 orders of magnitude smaller than 0.05μm.
3. By limiting consideration to considerably smaller spot size at range, Reilly necessarily comes up with much higher repetition frequencies, like 1kHz, in order to cover space in a year or two. This choice leads to MW average power levels, very difficult beam director accelerations and transmit/receive interference. Our repetition rate is typically 1Hz, except when a target is detected. Then, one or two triple-pulse bursts of 15Hz are needed. Our selection of laser and beam director parameters makes it OK to have just 30kW average laser power, the same level required to remove the debris [recall Figure 5].

How would one create such a narrow pass filter? By combining commercially available interference filters such as those by Barr Associates, which have $\Delta\lambda$ as small as 7E-5 μm, with a single Fabry-Perot having a finesse of 100.

What does this affect? Nothing significant, except that one still does not have to worry about signal to background ratio (SBR) even during the day in the case we discuss herein, as one also does not in Reilly's case studies.

Why is this important? Because we consdier ($D_R d_s$) products which are as much as 180 times larger than Reilly's, giving up to 4 orders of magnitude more background signal, which depends on the square of that quantity, so it is good that we have more background rejection.

The bottom line is this: in both cases, SBR can be ignored even in the daytime, and SNR is dominated by readout, or electrical, noise. Since our signals are about the same, our SNR's will be, too.

We conclude this memorandum with a matrix summarizing the case for active laser acquisition and tracking, Table IV.

Photonic Associates
excellence in photonics

Probability of finding <u>any</u> 1–20-cm Debris Particle beneath the altitude h, and within the circle d_S

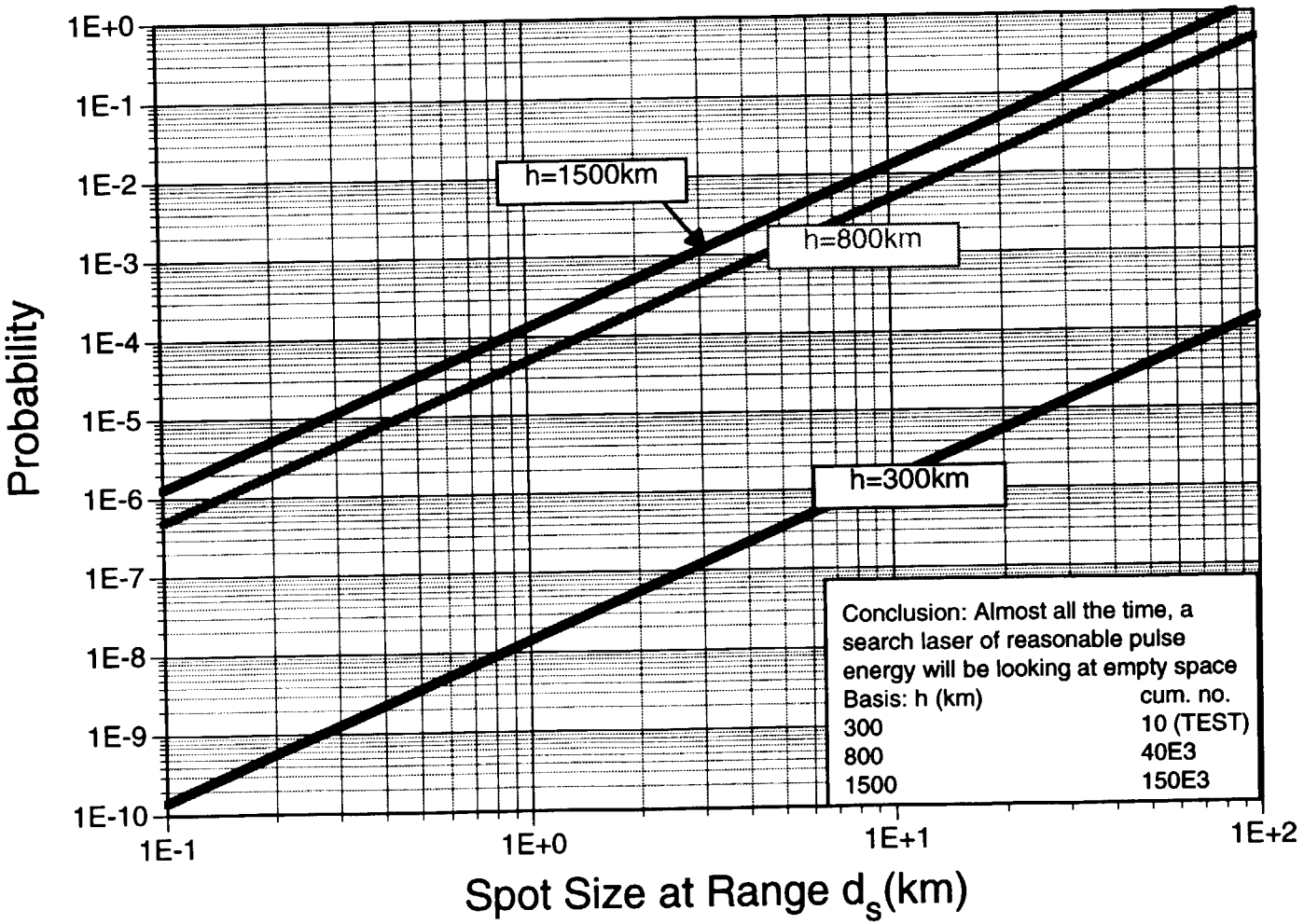

Average Laser Power Required to Receive 10 photons per shot and Search Sky in 2 years

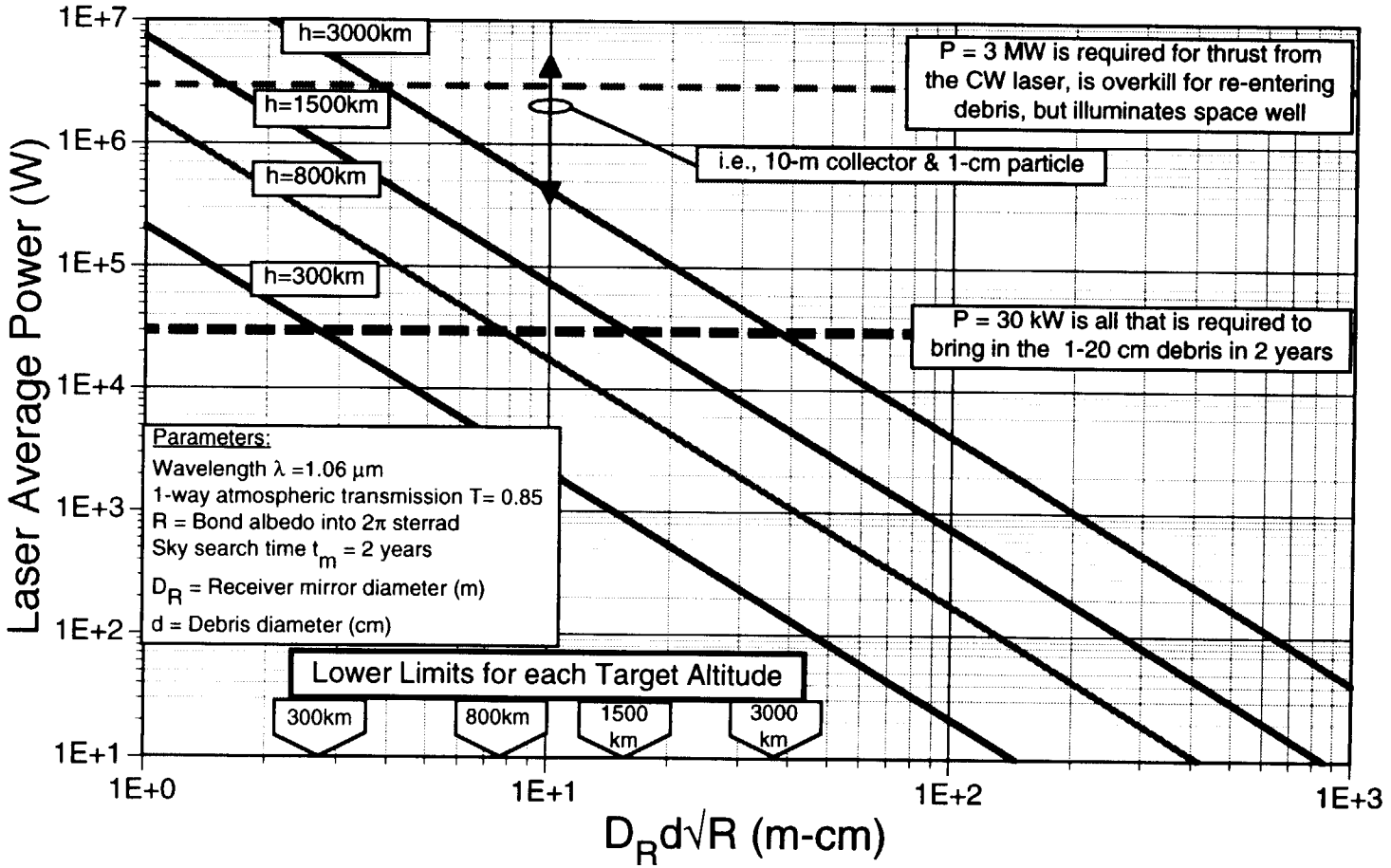

Photonic Associates
excellence in photonics

ORION Sky Survey Time

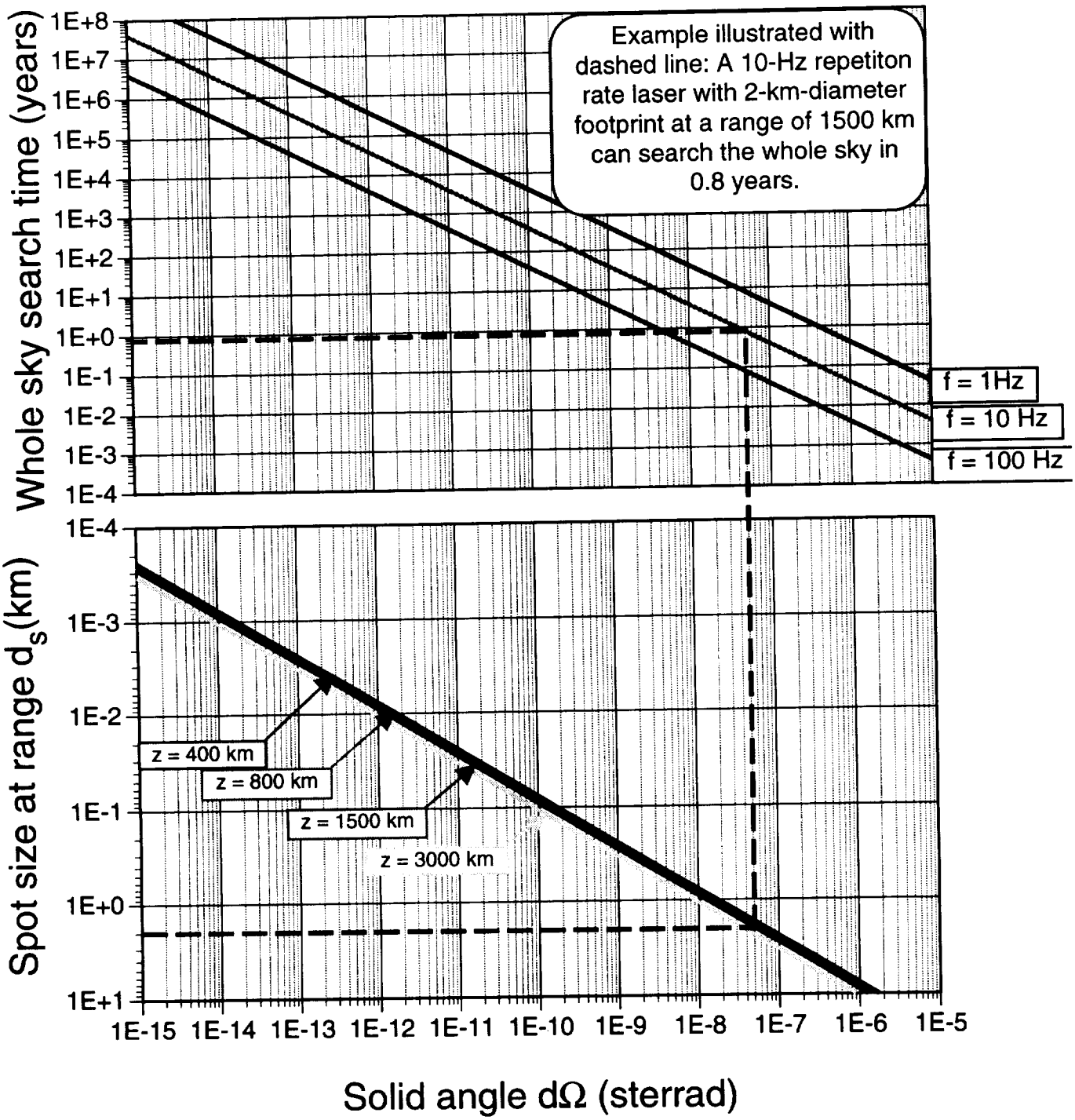

Photonic Associates
excellence in photonics

Photons received calculator

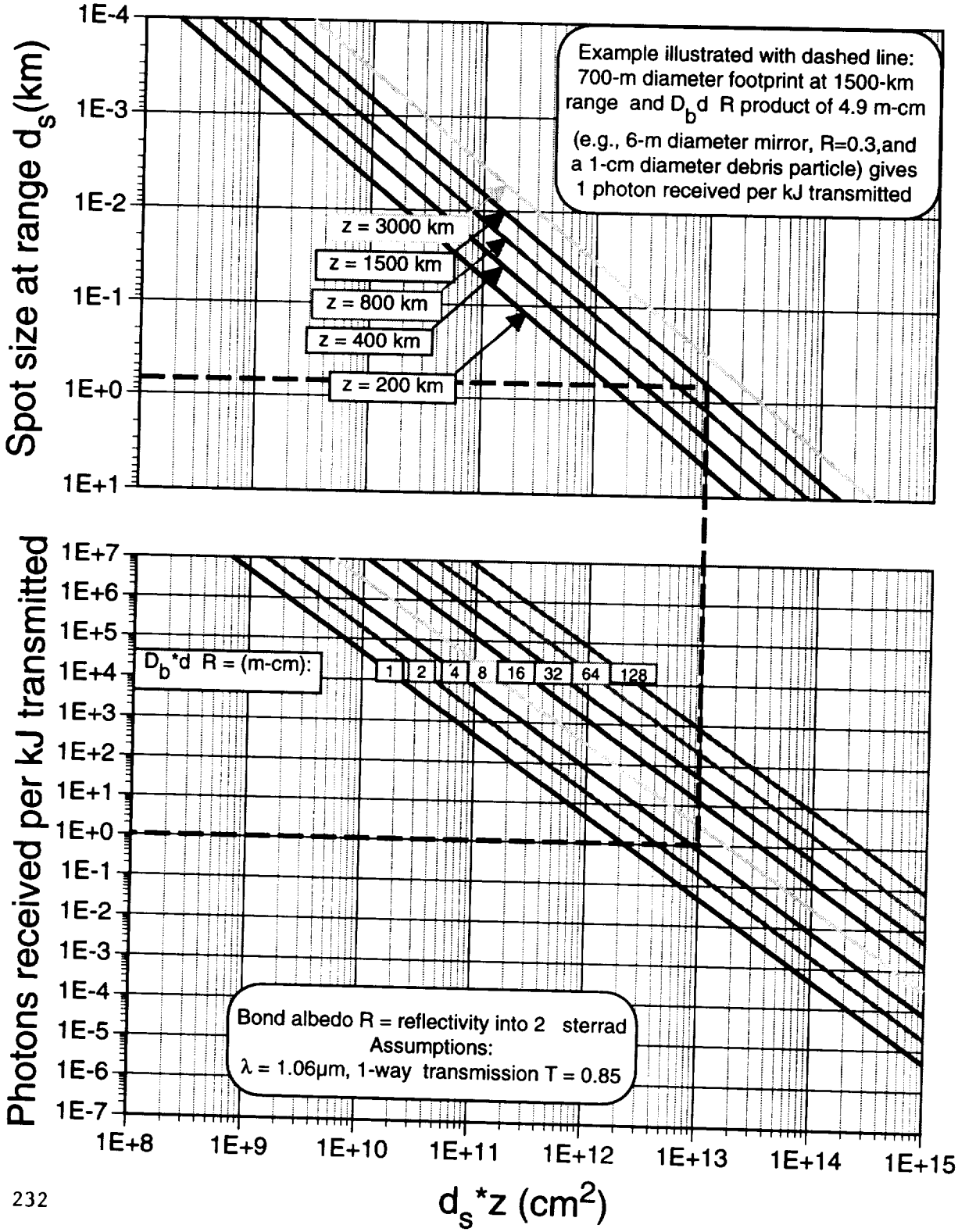

Photonic Associates
excellence in photonics

Active Laser Acquisition and Tracking Option

Laser Sensor	Search Wide Field of View	Sensitivity	Discrimination	Assessment	Operability	Adequate Signal-to-Noise Ratio	Handover
⇒	**≥0.5°**	**d=1cm h=1500km R ≥ 0.3**	**X-section Size Orbit**	**Immediate Spin Orbit**	**24 hours**	**Limited by Photon Count**	**d_s=200m**

Parameters of Active Laser A/T System which Exactly Meets all Requirements

Parameter	Value
Day/Night Operation	Yes
Transmit/Receive Mirror Diameter D_T(m)	6
Acquisition Mirror Diameter D_R(m)	20
Acquisition Detector Quantum Efficiency η_{QE}	65%
Laser Wavelength (μm)	1.06
Laser Pulse Duration (ns)	5
Laser Pulse Energy (kJ)	30
Laser Repetition Rate [search mode] (Hz)	1
Laser Repetition Rate [tracking burst] (Hz)	15
Acquisition Mirror Spot Size at Max Range (km)	4
Transmit/Receive Spot Size at Max Range (m)	Variable 150 – 0.5
Laser Average Power (kW)	30
Acquisition Mirror Type	Earth supported, segmented, non-steering with moving feed
Acquisition Mirror Surface Figure	10 waves /10 cm
Detector Notch Filter Bandwidth (nm)	7E-4

Photonic Associates
excellence in photonics

Photons received for several cases vs. $D_R d\sqrt{R}$

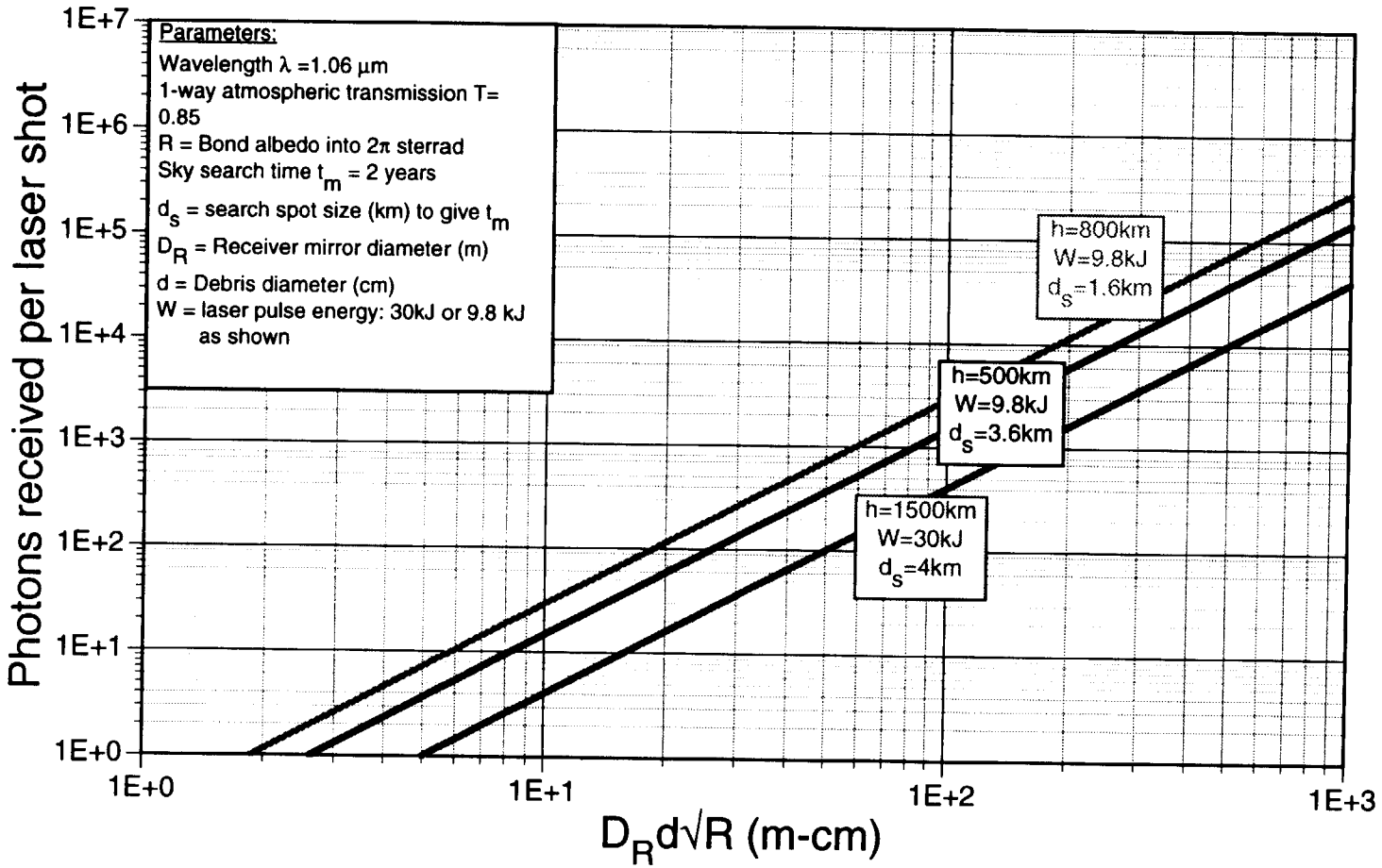

Daylight Detection

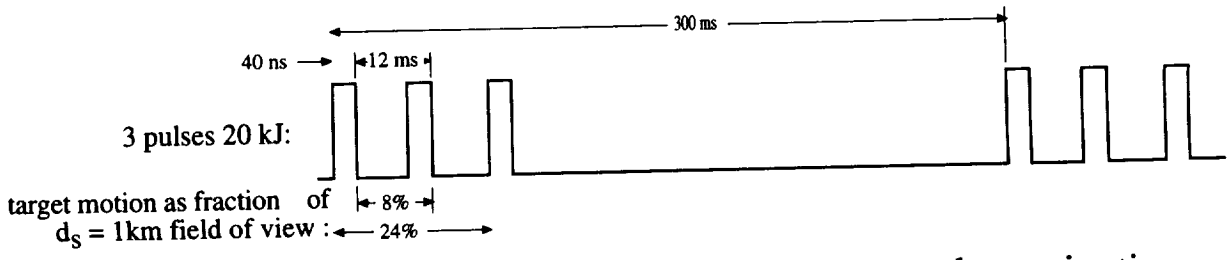

Figure 1: a pulse format to enable velocity vector determination

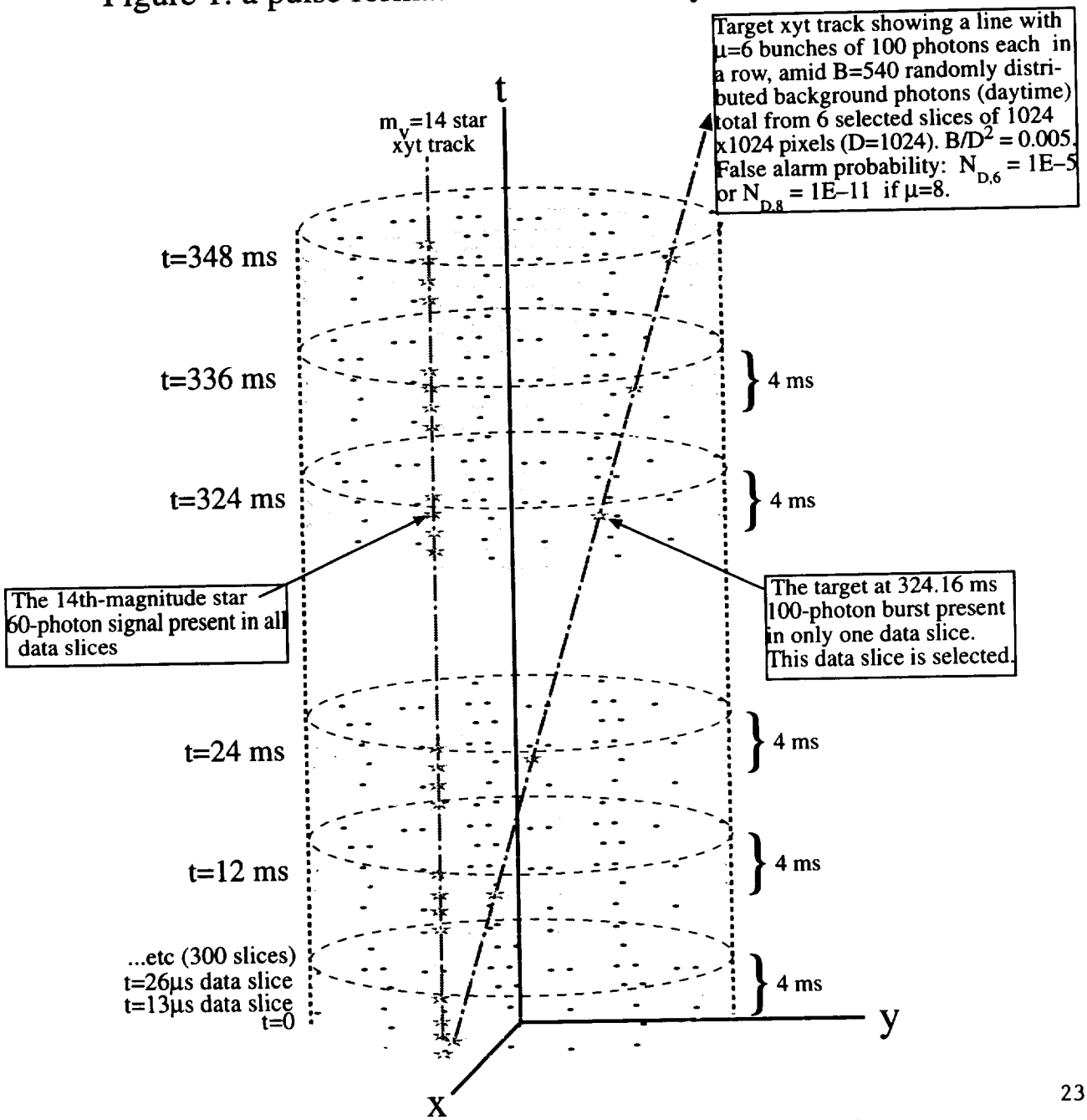

Figure 2: illustrating 3-D correlation scheme (adapted from Ho & Priedhorsky)

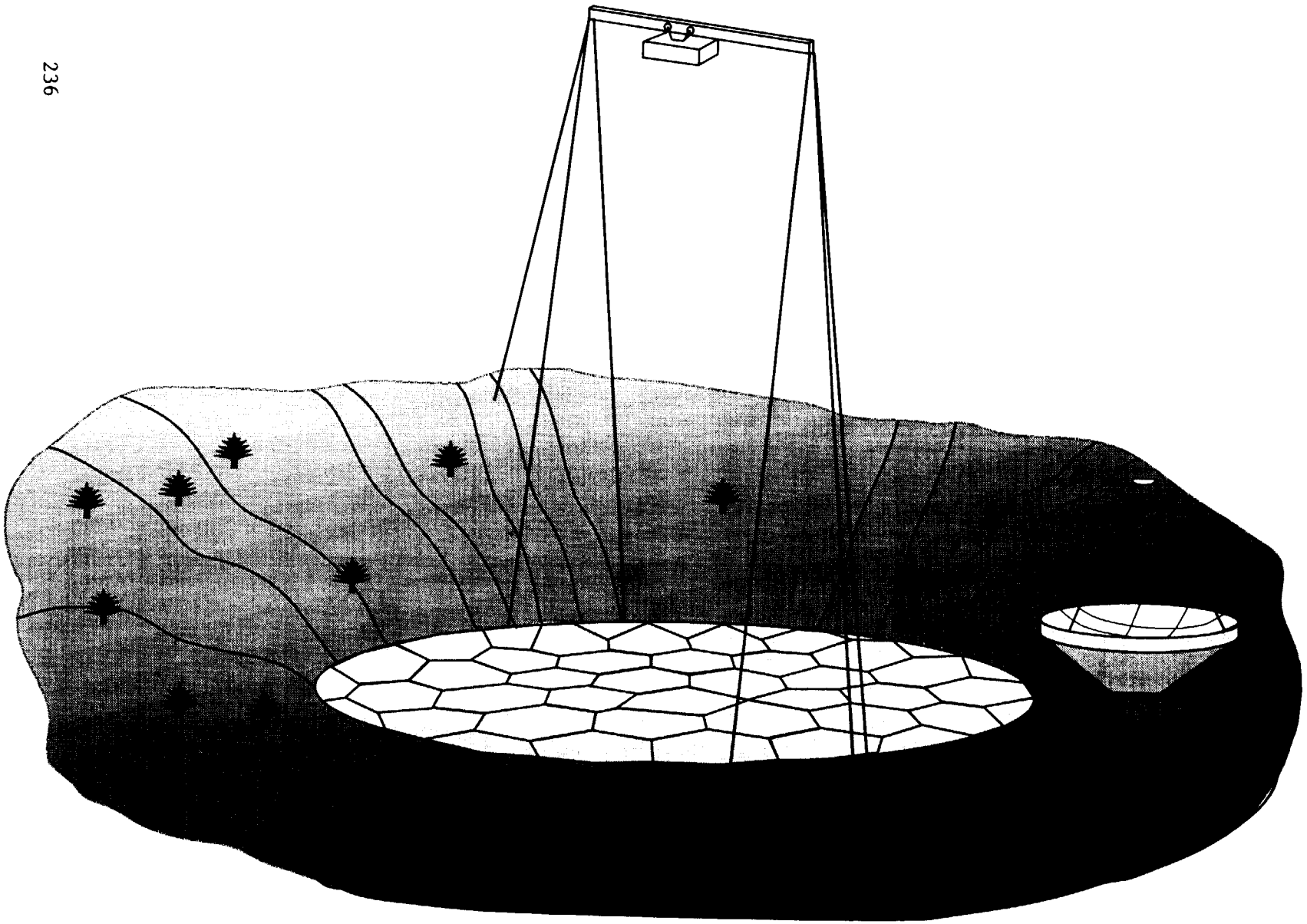

Composite Transmit/Receive Mirror Site

TOPIC 10: SUMMARIZING THE ADVANTAGES OF A SHORT-PULSE ORION SYSTEM

1. Recommendation

Based on §1, we see that a low-cost system could be built with limited range [say 600 km, just enough to protect ISSA] to begin the ORION program. It is important to start with an affordable demonstration system.

What is the short-pulse system which we propose?

Wavelength λ	1.06μm
Beam diameter in atmosphere D_b	4.2 m
Pulse length τ_p	100 ps
Nominal range z	600 km
Pulse energy W	500 J
Pulse repetition rate f	50 Hz
Laser average power P	25 kW
Spot size on target d_s	27 cm
Strehl ratio	50%
Atmosphere transmission T	85%
Product $I_b\tau_p^{0.55}$ in atmosphere	114
Beam intensity in atmosphere I_b	36 MW/cm^2
Beam intensity on target I_s	7.3 GW/cm^2
Target effects product $I_s\tau_p^{0.55}$	2.3 E4
Time to clear LEO targets ≤450km	2 -3 years
Cost	$30M

We believe the cost for such a system, if it employs the short-pulse option, could be built for $30M total, including beam director, computers and adaptive optics.

As is seen from the "100ps" point in the attached Figure, the laser and transmitting optic combination just avoids SRS conversion and serious n_2 effects in the atmosphere, even at sea level, without being overdesigned. It is well away from STRS effects. Furthermore, at 6km laser station altitude, there is a substantial safety factor with regard to these effects.

2. What are its advantages?

- Since the pulse energy is only 500 joules, it is a small laser. It is 30 times smaller than the LLNL "Beamlet". It does require special hardware, probably employing STRS/SBS cascade techniques, following the work of Pasmanik and others, to compress a nominal 20-ns laser pulse down to the required short pulse efficiently.

Photonic Associates has references, including those of the Vavilov Institute and the U.S. work, showing how this is done.

- Based on our experience, it will cost a lot less to achieve 25kW average power (which is required for debris clearing in a reasonable time) with 50-Hz, 0.5-kJ pulses than with, say, 1-Hz, 25-kJ pulses. The latter is a laser in the class of the LLNL "Beamlet". In particular, our costing algorithm says that the 450-J laser ought to cost about 5 times less than the 15-kJ Beamlet laser.

3. Scenario

A 500-J, 100-ps laser coupled with this 4.2-m mirror could create substantial effects on a debris object. Taking target "B" of our debris matrix, for example: a 5-cm-diameter object with A/m = 20 at 600 km range, B would intercept 12.9J per laser pulse. Let's assume the laser is operating in the "hot-rod" mode, and can deliver 400 pulses at 50 Hz in 8 seconds before it shuts down. With a C_m of 7.6 dyne-s/J [best guess for this carbon phenolic material], 400 laser pulses give $\Delta v = -16$ m/s, which should be easily detected by radar or other means. Note that this is about 10% of the input required to re-enter the target, depending on its orbit eccentricity.

How effective is it on typical debris target "B"?

Target material	Carbon Phenolic
Target diameter d	5 cm
Target A/m	0.7
Target mass m	28 g
Absorbed energy per shot W_{abs}	14.4 J
Coupling coefficient C_m	7.6 dyne-s/J
Velocity change per shot Δv	- 3.9 cm/s
Δv in 8 sec burst @ 50 Hz	- 15.6 m/s

4. Recommendation

It is recommended we give serious thought to this laser option, in order to obtain the lowest possible projected system cost which is consistent with an effective system.

TOPIC 11: ORION DEMO

Introduction

In recent weeks, the outline of a possible near-term ORION demonstration experiment has emerged. It is the purpose of this memo to summarize it. Participants in the dicussions have included Jim Reilly, myself, Bob Fugate at Starfire Optical Range, and Herb Friedman, John Murray, Lloyd Hackel, Brent Dane and Jerry Britten at Livermore.

Laser Equipment

Originally, Lloyd Hackel and Brent Dane were to deliver an illuminator laser and Herb Friedman a sodium guidestar to Bob Fugate. Recentlly, to support the effort in Bosnia, cuts were made in Fugate's program by which Friedman's guidestar will not be funded and Hackel's illuminator will be completed (since the money is already sunk) but not delivered.

These decisions could be reversed.

Here are summaries of the two laser systems:

Laser	Wavelength	Pulse length	Pulse energy	Rep rate	Power
Guidestar	589 nm	150 ns	6.7 mJ	30 kHz	0.2 kW

Other parameters: Smaller version installed and operating at Lick observatory.

Laser	Wavelength	Pulse length	Pulse energy	Rep rate	Power
Illuminator	530 nm	10 – 700ns	120J	10 Hz (20-s, 30 Hz burst	1.2 kW 3.6kW)

Other parameters: Output aperture 50 cm^2. Uses phase conjugation to get diffraction limited beam quality. Output (optical) frequency stable to 25kHz. Four 30-J beams, SBS wavefront beam combination in a nonlinear cell. Cost, new and installed: $4M.

This laser would be run at 1.06μm wavelength in our application.

Starfire modifications

To do the demo, Fugates's telescope would have to be modified.

There may be more, but the modifications which are easy to anticipate are in the 25-cm diameter part of the train having to do with tolerating peak laser intensity, or beam transfer.

1. Corrector plate

In its present configuration, the beam comes to a real focus in air. This can't be tolerated in the demo, because the laser would cause a spark in air. A 25-cm corrector plate (a lens) would be installed adjacent to the secondary or tertiary mirrors to solve this problem.

2. Mirror HR coatings

Parts exposed to laser flux in the 25-cm diameter part of the beam need to be recoated with a high intensity HR (high reflectance) coating. This statement includes an estimated 4 flat turning mirrors and the 1000-element rubber mirror. The latter is difficult, because it is a thin membrane which must be epoxied to the actuators before final finishing and coating. The solution is the room-temperature sol-gel coating process. This is a good and inexpensive approach even though it involves up to 23 layers. Furthermore, if damage

occurs, sol-gel coatings can be stripped and redone fairly quickly. Jerry Britten at Livermore routinely does this and already gets 1/10th wave surface figure. If the parts were dipped for each coating at slightly different azimuthal angles to the liquid surface, the 1/50th wave irregularities would add up to quite a bit less than 1/10th wave in 23 coatings.

HR coating damage threshold requirements for 25-cm diameter beam at 10ns:

Pulse energy	Surface area cm^2	Pk Intensity*	Average Power**	Avg Intensity
120	45° mirrors: 690	3.5E7 W/cm^2	3.6 kW	10 W/cm^2
120	AO mirror: 490	4.9E7 W/cm^2	3.6 kW	15 W/cm^2

* Assuming 2:1 peak to average ratio, 10 ns pulse
** During 20-second, 30 Hz burst and 2:1 peak to average ratio

Lowest damage threshold of sol-gel HR coatings under above conditions:

Pk Intensity*	Avg Intensity
1.1E9 W/cm^2	5E3 W/cm^2

In short: there is no problem with either the CW or the average power levels anticipated. The mirrors do not have to be rebuilt, just recoated.
Back when we were talking about using 100-ps pulses, there might have been a problem, but not now.

How to demonstrate acquisition and pushing

Exotic Coupling Coatings

So how is it possible that optics only twice the size of the beam at the target which we wish to damage, will not be damaged?

There are two reasons: First, damage intensities for high quality HR coatings are from 4 – 10 times higher than for common materials.

Second, we want to make the demo target "cooperative" by designing in the very best properties from our point of view. There are several specialized coatings which will generate good thrust well below the plasma formation threshold.

Reilly has recently done a number of calculations on such materials which show that, for example, arsenic should generate very good thrust at an intensity nearly 10 times below that for plasma formation, just due to intense vaporization of a low boiling material.

Furthermore, measurements I did several years ago on another low boiling material (pyroxylin) gave similar results: C_m = 33 dyne-s/J for intensities 5 times below plasma threshold.

Low orbits with Long Lifetimes

Max/Min Lifetime(days)	Orbit (km)
4/4	200 x 200
16/8	250 x 250
40/10	200 x 480
100/35	300 x 300
160/40	200 x 900

It is important to minimize target altitude, both because we want the Shuttle to be able to insert the objects, and because we want to minimize range for an easier demo using a low-energy laser. An additional reason is easy acquisition, using only active optics, that is, the same laser.

A quick glance at the lifetime graphs of § 7 shows that it is not easy to get a significant lifetime together with an orbit altitude of even as low as 300km. A value of A/m of 0.05 cm^2/g in the ram direction is about as much as we can take. Assuming this value, the Table shows what lifetimes you can get, and indicates that 300km is the minimum altitude that makes sense. Eccentric orbits would last longer, but would create a *real* debris hazard to objects already in orbit. Not to mention the added difficulty of creating such an orbit from the Shuttle.

Please see Figure 1. It is a joint Photonic Associates/New England Science & Technology invention which satisfies all the requirements. The plan would be for 10 of these targets to be dropped overboard from a getaway special package on the earliest available Shuttle flight. In a Getaway Special, a 2 cu. ft. box is permitted, and one wire to a switch which the astronaut only has to flip early in the mission. Many people have launched small satellites that way. The cost is about $75k. Target parameters are summarized in the Table at the left.

Parameter	Value
Nose mass	52 g
Tail mass	36 g
Total mass	88 g
Total cross-section facing flow	4.6 cm^2
A/m	0.05 cm^2/g
Target beam intercept area	200 - 400 cm^2
Strehl ratio	0.5
Beam footprint on target	200 cm^2
C_m	33 dyne-s/J
Atm. transmission	0.85
Fluence on target	0.6 J/cm^2
Energy on target	102 J/pulse
Δv per laser pulse	38 cm/s
Δv per 20-s 30-Hz burst of pulses	**230 m/s**

This target shoud respond magnificently!

Effects which we can demonstrate with this target

The Figure 1 target has several other useful aspects:

1. With alternating black and white fins which also alternate coupling coefficient from high to low, the laser beam will cause the target to spin at a high rate at almost any incidence angle. This solves any difficulty which might exist in measuring changes in range rate with a relatively long laser pulse.

2. The high-density ring at the front (this could also be a ball at the front, but the ring maximizes surface) moves the center of gravity well forward, so the device will have a controlled orientation parallel to the ram direction.

3. The ring at the front also provides a separate mounting surface which will not produce plasma for damage-resistant fused silica "bicycle reflectors" imitating the common ones, particularly in having 1-degree return beamwidth. Basically, this is an array of corner cubes. This device will automatically return the intercepted beam to the source independent of its orientation with a gain of 26,000 relative to an object with Bond albedo = 1.0.

Here is what we can demonstrate:

1. All-optical Acquisition and Tracking
2. Spinning the target as a minimum
3. Producing net momentum change
4. Re-entry

Concept:
Photonic Associates
Northeast Science & Technology

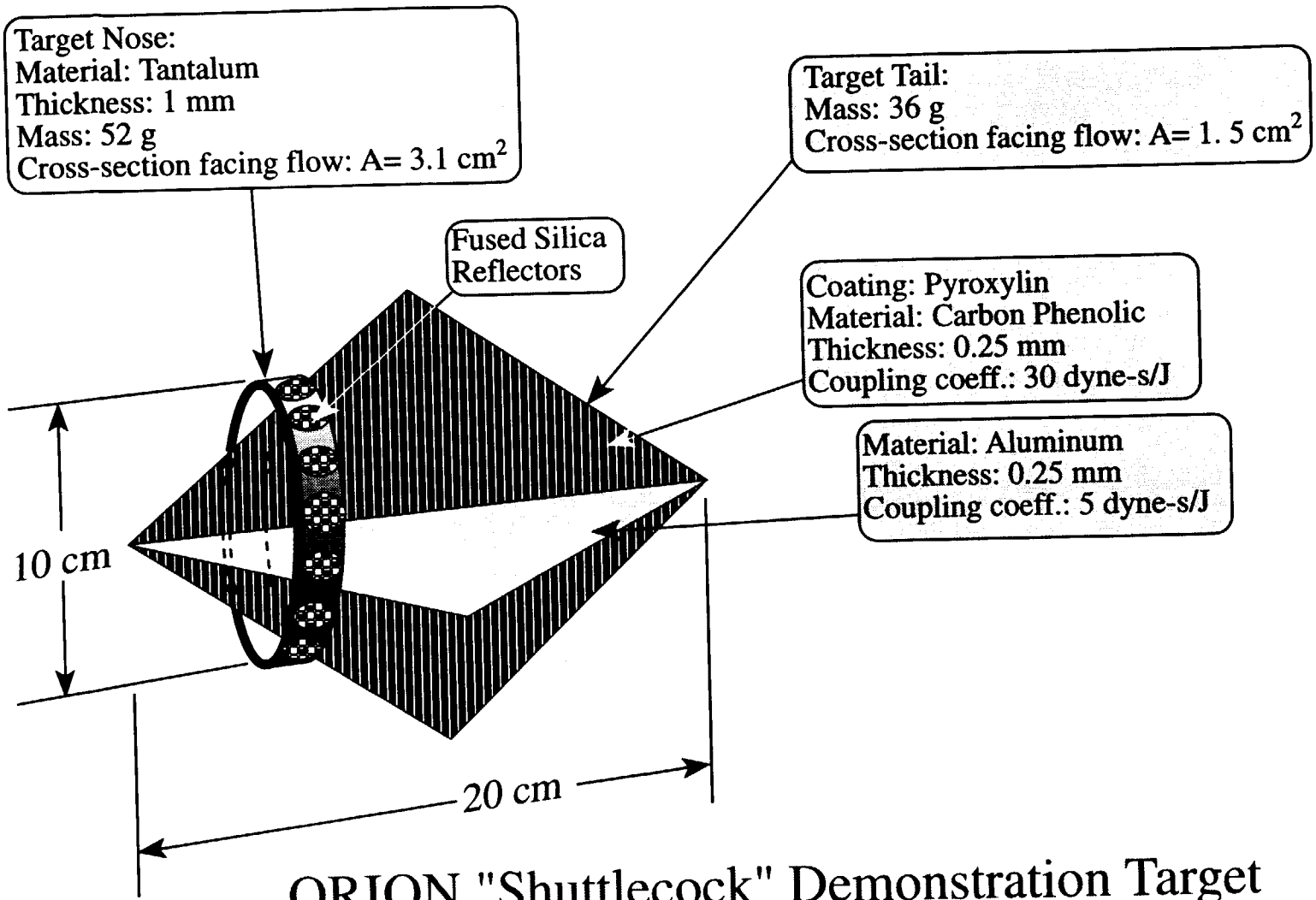

ORION "Shuttlecock" Demonstration Target

Total target mass:	88 grams
Area to mass ratio:	0.05
Lifetime on orbit:	60 days at 300km

TOPIC 12: THREE METHODS OF OBTAINING ULTRASHORT 1.06 μm LASER PULSES

In this section, we will compare the three principal methods of obtaining 100-ps pulses which have been demonstrated in the literature. Much of this work has occurred at the Lawrence Livermore Laboratory and at the Russian Vavilov Institute. Experts at either laboratory are capable of executing any of the approaches in actual hardware.

Two of these methods feature clever schemes to deliberately compress a longer pulse. Of these, one involves the use of a holographic grating pair to passively compress a so-called "chirped" large bandwidth pulse of about 10 ns duration. The second compression method uses the physics of Stimulated Brillouin Scattering (SBS), Stimulated Raman Scattering (SRS) or both in a cascade to provide passive compression.

The third method is the "brute force" approach: make a very short oscillator pulse, and amplify it in an amplifier of adequate bandwidth.

1. Holographic Gratings

The beauty of this technique is its nearly perfect energy convesion efficiency (in principle). However, the difficulty is that these gratings are limited to about 1 meter in transverse dimension by current technology. Inspection of the figure above will show that the chriped input pulse to the grating must

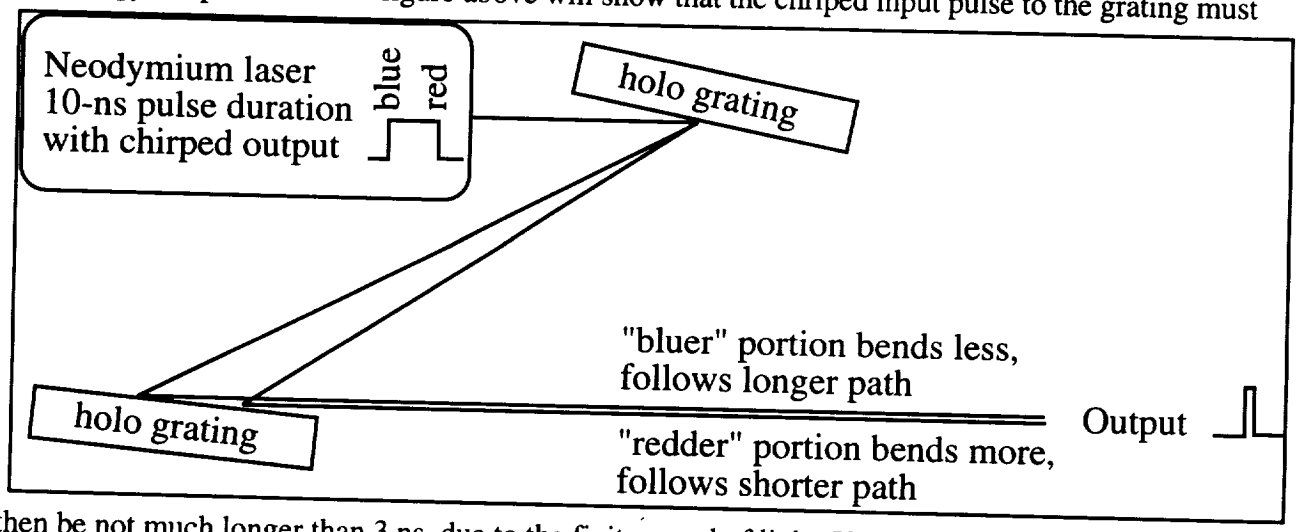

then be not much longer than 3 ns, due to the finite speed of light. Unfortunately, 3 ns is too short to get good extraction and high beam quality at the same time from a neodymium system at the present time.

2. SBS/SRS Cascade

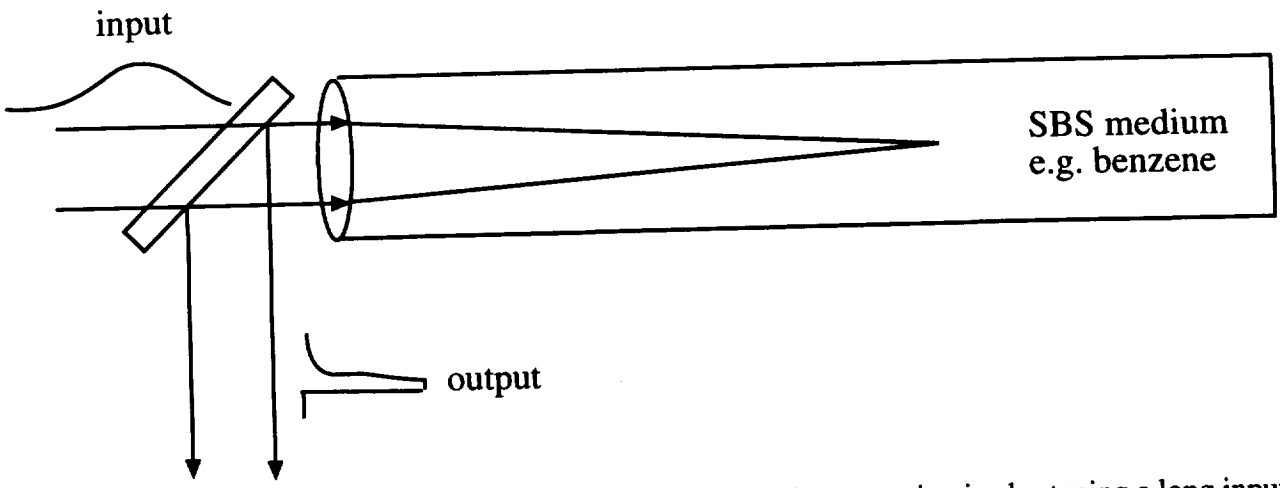

The advantage of this technique is its simplicity and totally passive operation in shortening a long input pulse, by as much as a factor of 10. The pulse reshaping that results is due to strong satruation of the input or pump wave by the leading oedge of the counterpropagating output or "Stokes" wave. A similar diagram describes the behavior of a reverse SRS pulse compressor. SBS and SRS units can be used in cascade to obtain certain desirable effects.

Total compression ratios of about 100 have been obtained, just about what we require in the ORION system (efficient conversion to 100 ps pulses which couple efficiently to the debris target, from cheap, relatively low energy 10 ns inputs).

The problem with this technique is: low efficiency. Compression ratios of 100 go along with energy efficiency which may be as low as 2%, unacceptable for ORION. Such a low efficiency would actually make it less expensive to build and use a higher energy long pulse laser.

3. Amplfiying a short oscillator pulse

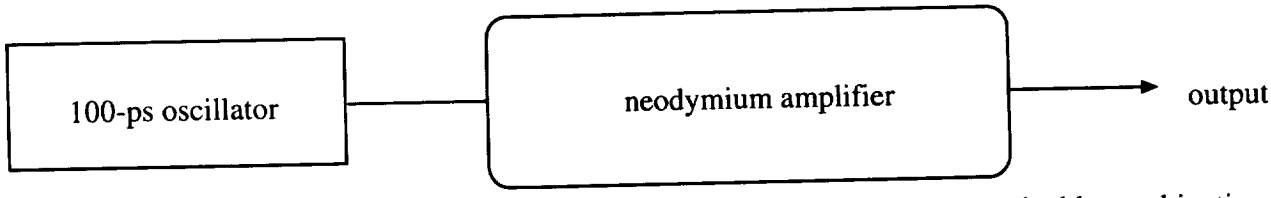

This approach is deceptively simple. It also depends, at the present time, on unattainable combinations of laser parameters. The problem is that the brightness integral or "B-integral" which determines beam breakup due to nonlinear refraction in the glass host of a solid state laser system is the same integral, apart from constants, that determines energy extraction efficiency. And, for 100-ps pulses, the result is that efficient extraction is not yet possible for 100ps pulses if high beam quality is also required.

The consequence of all this is: At this time, the best choice is a 5 or 10 ns pulse for ORION, if that pulse is generated by a solid state laser system. The situation may well improve in the next year or two as efforts at solid state laser R&D labs proceed.

TOPIC 13: FINAL ORION SYSTEM RECOMMENDATIONS

Latest info indicates 5 to 10-ns, rather than 100-ps, pulses

1. In order to address the 1 to 20-cm threat range of debris sizes in a time ≈ 2 years, the average power output of a repetitively-pulsed pusher laser must be ≈ P = fW = 30kW.

Previously, the repetition rate f and pulse energy W were free parameters in my analyses, to be driven by achieving lowest laser cost. In earlier reports, it was suggested that laser cost for a certain average power P should go down as pulse width τ decreases, and that τ=100ps looked attractive, based on encouraging statements I was getting from the Livermore laser experts.

Since December, information from Livermore has reversed that story. It now appears that $\tau \approx$5ns is the shortest-pulse laser one should use in a repetitively pulsed 20kW ORION laser. Reasons for this will be provided in detail in a subsequent report. The short version is: a lot of the requisite R&D has not yet been done. It *should* still be cheaper to use shorter pulses, but laser builders are not yet confident about doing it.

2. At the same time, it was always clear that the pusher-laser-as-illuminator idea required high energy pulses or a big receiving aperture to function effectively at significant debris range.

Final recommendation

Based on previous work plus an assessment of what can be economically built today, here is the final system we propose:

What is the system which we propose?

Wavelength λ	1.06μm
Beam diameter in atmosphere D_b	6 m
Pulse length τ_p	5 ns
Nominal pusher range z	3000 km
Pulse energy W	30 kJ
Pulse repetition rate f	1 Hz
Laser average power P	30 kW
Spot size on target d_s at max range	95 cm
Strehl ratio	50%
Atmosphere transmission T	85%
Product $I_b\tau_p^{0.55}$ in atmosphere	577
Beam intensity in atmosphere I_b	21 MW/cm^2
Beam intensity on target I_s	705 MW/cm^2
Target effects product $I_s\tau_p^{0.55}$	1.9 E4
Time to clear LEO targets ≤450km	2 -3 years
Cost	$90M

We believe such a system could be built for $90M total, including beam director, computers and adaptive optics.

Following are summary graphs for the work we have completed.

ORION Laser System Design Logic Diagram

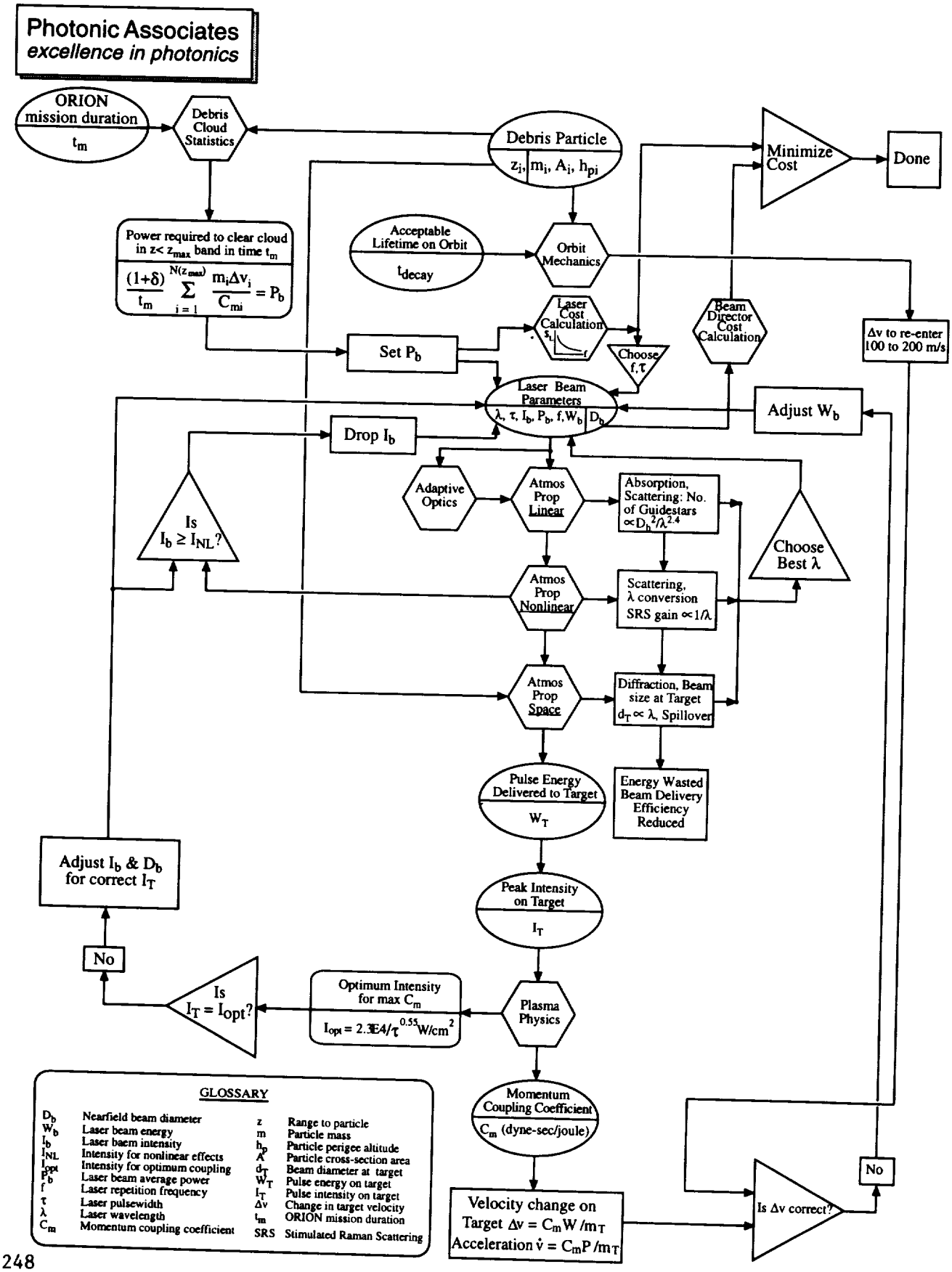

Photonic Associates
excellence in photonics

DEBRIS TARGET MATRIX

Target	A	B	C	D	E	F
Description:	Na/K sphere	Carbon phenolic fragment	MLI (plastic/Al surfaces)	Crumpled aluminum	Steel tank rib support	Steel tank
Inclination (deg)	65	87	99	30	82	60
Apogee (km) Perigee (km)	930 870	1190 610	1020 725	800 520	1500 820	1020 980
A/m (cm^2/gm) Actual size (cm)	1.75 1.0	0.7 1x5	25 0.05x30	0.37 1x5	0.15 1x10	0.13 100x100x0.2
Bond albedo	0.4	0.02	0.05/0.7	0.05/0.7	0.5	0.1
Laser spot size at range (cm)	40	40	40	40	40	40
Optimum C_m(dyne-s/J)	6±2	7.5±2	5.5±2	4±1.5	4±1.5	4±1.5
Δv required (m/s)	190	110	140	90	160	210
Est. number of targets	50k	20k	60k	10k	10k	1
Laser re-entry effort: Shine time/target [30kW](min) Retargeting time (min)	 5 0.5	 6 0.5	 0.3 0.5	 13 0.5	 9 0.5	 930 n/a
Total time all targets (yrs) Down time all targets (yrs) Cumulative time (yrs)	0.5 0.2 0.7	0.3 0.1 1.1	0.1 0.05 1.25	0.3 0.1 1.65	0.2 0.1 **1.95**	Est 1.3 (Do Not Re-enter) 3.25

Point illustrated here: 30kW of average laser power in a 40-cm spot will re-enter the 1.5 – 20-cm targets beneath 1500 km in less than 2 years

Photonic Associates
excellence in photonics

Technical Basis for Choosing ORION Laser Device (Longer-term Example)

Laser ⇒	Atmospheric Windows 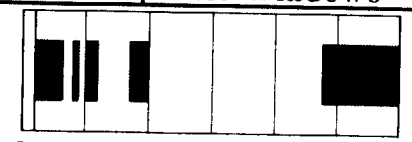	Nonlinear Effects (SRS, STRS, n_2)	Debris alt. (km)	1-20-cm clear time (yrs)	Debris Intensity (MW/cm^2)	Debris Fluence (J/cm^2)
		$\tau \geq 10ns$: $I_{atm} \leq 3 MW/cm^2$	**500-1500**	**<5**	**τ=5-10ns: 600–850**	**τ=5-10ns: 4–6**

Rep-Pulsed Laser Options	λ (μm)	Beam size at 1500 km (cm)	Laser Pulse Energy for efficient thrust (kJ)		Beam fluence in atmosphere (J/cm^2)		SRS-safe beam fluence in atmosphere (J/cm^2)		Guide-stars Needed	Cost (M$)		Laser Device Choice Basis
Pulse width: ⇒			1μs	10ns	1μs	10ns	1μs	10ns		1μs	**10ns**	
Nd solid state	0.53	24	24	3.0	0.085	0.011	2	0.04	4* (difficult)	54	**23**	* Cheaper but guidestar kluge
Nd solid state	**1.06**	**48**	**97**	**12**	**0.34**	**0.043**	**2.5**	**0.05**	**1**	**100**	**40**	**√ Best cost that works**
DF chemical	4±	180	1370	170	4.9	0.61	2.5	0.06	0	1920	290	High cost, won't work (SRS)
CO_2 gas	10.6	480	9700	1200	34	4.3	3	0.07	0	11400	1700	High cost, won't work (SRS)

CW Laser Option	Wave-length μm	1500 km beam dia (cm)	Laser Power for efficient thrust (kW)	Intensity in atmosphere (W/cm^2)	Blooming-safe intensity in atmos. (W/cm^2)	Guide-stars Needed	Cost (M$)	Basis for Laser Device Choice
Iodine gas	1.3 CW	59	3200 (power overkill necessary for thrust)	11	8?	1	68	Blooming? Beam Quality? Target interaction? Next lower cost

CHOOSE Nd:YAG FOR ORION SYSTEMS

Photonic Associates
excellence in photonics

ORION System Requirements

Laser	Atmospheric Windows	Nonlinear Effects (SRS, STRS, n_2)	Debris alt. (km)	1-20-cm clear time (yrs)	Debris Intensity (MW/cm^2)	Debris Fluence (J/cm^2)
⇒	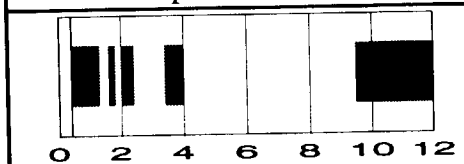	$\tau \geq 10ns$: $I_{atm} \leq 3 MW/cm^2$	500-1500	<5	τ=5-10ns: 600–850	τ=5-10ns: 4–6

Radar Sensor	Field of View	Sensitivity	Discrimination	Assessment	Operability	S/N Ratio	Handover
⇒	≥0.5°	d = 1cm h = 1500km R ≥ 0.3	X-section Orbit	Immediate Spin Orbit	24 hours	Limited by Noise	d_s = 200m

Laser Sensor	Search Wide Field of View	Sensitivity	Discrimination	Assessment	Operability	S/N Ratio	Handover
⇒	≥0.5°	d = 1cm h = 1500km R ≥ 0.3	X-section Orbit	Immediate Spin Orbit	24 hours	Limited by Photon Count	d_s = 200m

Passive Optics Sensor	Search Wide Field of View	Sensitivity	Discrimination	Assessment	Operability	Adequate Signal-to-Noise Ratio	Handover
⇒	≥0.5°	d = 1cm h = 1500km	X-section Orbit	Immediate Spin	4 hours (twilight)	Limited by Photon Count	d_s = 200m

APPENDIX E

ORION OPTICS AND TARGET ENGAGEMENT

Glenn Zeiders
The Sirius Group

ORION Optics and Target Engagement

1. Propagation and Engagement Conditions

Diffraction Requirements

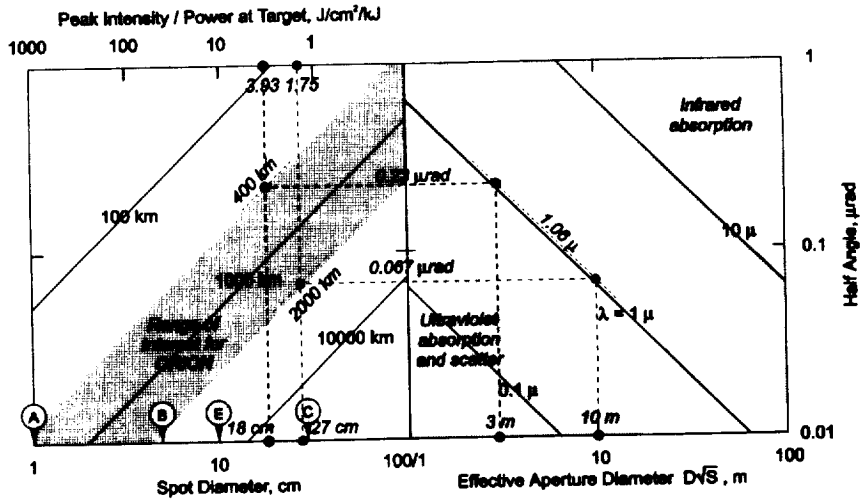

Although laser systems are normally designed to match the beam with the intended target, conditions for ORION are such that even the largest reasonable beam directors will tend to flood the sky, spreading much of the energy far beyond the relatively small debris particles. A laser beam from a finite aperture spreads by diffraction, the resulting peak intensity at range R being given by $I = P/\lambda^2R^2$ $\pi D^2/4$ $S = P/(\pi d^2/4)$ where P is the power reaching the target plane, λ is the wavelength, $\pi D^2/4$ is the transmitting area, and d is the spot size. The Strehl ratio S accounts for non-ideal propagation effects such as turbulence, and can be much less than unity in practice.

Since most of the space debris of interest for mitigation by ORION is at altitudes from 800 to 1200 km, laser spot sizes of at least 20 cm (and perhaps much larger) can be expected even with short wavelength (1.06μ for Nd:Glass lasers) and with beam directors approaching the size of today's largest astronomical telescopes. While these relatively large sizes exact a toll from the pusher lasers in view of the required output power, it will be shown that they, together with the short wavelengths and large apertures that are needed to achieve them, are nevertheless very costly in terms of both turbulence compensation and the associated sub-microradian pointing accuracy, and a more complete optimization at the system level might yet recommend operation with even larger spot sizes.

Atmospheric Turbulence and Adaptive Optics

Aside from nonlinear propagation effects that can normally be avoided by reducing peak intensity levels, the major contributor to non-ideal beam spread and loss of Strehl ratio is atmospheric turbulence (see the figure on the next page) which disrupts the beam by superimposing regions of varying refractive index (much like lenses.) Turbulence affects both telescope images and transmitted laser beams by reducing the coherence and scattering the light with short correlation scales (often reducing the effective aperture size from the full one D to a much smaller Fried scale r_0), whereas large scales tend to tilt the wavefront and steer the light. Adaptive optics attempt to counter these effects by measuring the distortion of a reference wavefront traversing the path and introducing the conjugate (opposite) distortion in the primary wavefront. The source for the reference wavefront can be, for example, a natural star, reflection from an object (like a target), or emission from a laser beacon projected from the ground. Turbulence of course varies both spatially and temporally, so correlation between the two wavefronts will be lost over increasingly large scales as any transverse displacement of their axes is increased, an effect usually referred to as anisoplanatism. The degree of correction improves as the size d of the control zones is decreased, and $d = r_0$ generally represents a useful cost-effective compromise. Such correction can be achieved with state-of-the-art segmented and/or deformable adaptive optics systems, but it should be realized that many thousands of elements will be required for the large apertures of interest for ORION – and costs for such systems

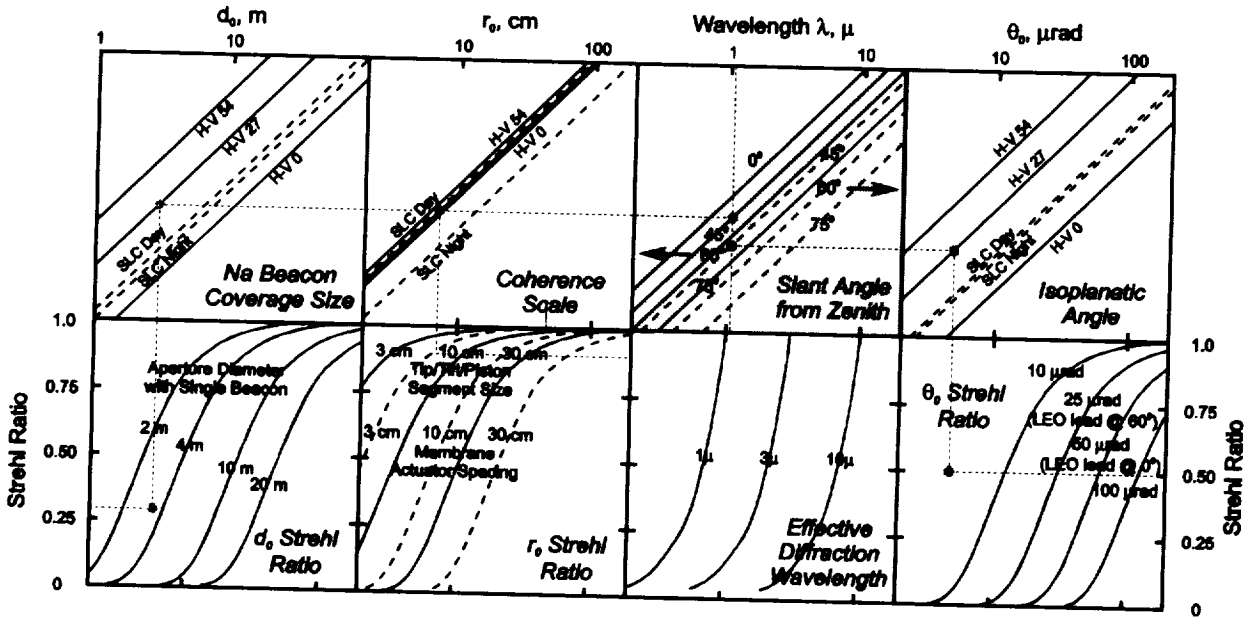

continue to be at least about $1000 per channel (although $200-$250 per channel is recommended for use as an eventual goal.)

Several typical distributions of atmospheric turbulence are shown at the right, and their effects on propagation are given in the nomogram. Turbulence always tends to be very high near the surface due to the Earth's boundary layer (dominating the contribution to r_0), but locally-severe conditions can arise at higher altitudes due to wind shear. High tropospheric winds in particular often lead to pronounced turbulence at upper altitudes, and, although the resulting strength is such that they contribute little to r_0 itself, their distance from the aperture can cause important coherence losses between paths that diverge from the aperture.

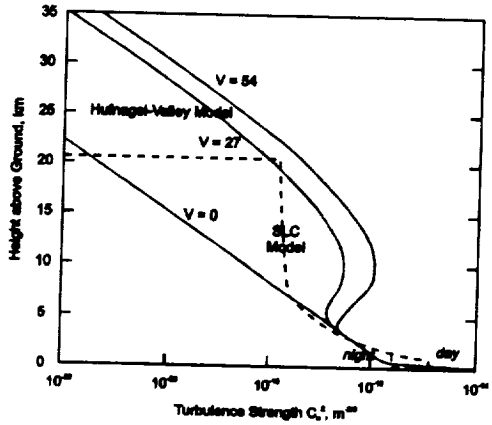

The latter effect is especially important for propagation to space because the "isoplanatic" angle over which coherence is preserved is usually much less than both the angle between the target and a sufficiently-bright natural star beacon (typically spaced several hundred microradians) and the lead-ahead angle $2v/c \cos\theta$ required to account for the distance that the target moves in the round-trip transit time for light between the ground system and the target. It is because of the lead-ahead that the "flash" from the beam impinging on a target cannot be used directly for pointing, and a properly-located artificial beacon will therefore be required to correct the outgoing laser beam.

To quantify these statements and to provide a useful example, the allowable separation between two parallel paths is related to the Fried coherence length $r_0 = 0.185(\lambda^2/\mu_0)^{3/5} = 11.2$ cm for a Kolmogorov spectral distribution, and the allowable angular separation from a point on the ground is the isoplanatic angle $\theta_0 = 0.0582\ (\lambda^2/\mu_{5/3})^{3/5} = 13.5$ μrad where $\lambda = 1.06\mu$ is the wavelength and where the turbulence moments $\mu_m = \sec^{m+1}\theta \int C_n^2\ h^m\ dh$ have been evaluated for an off-zenith angle $\theta = 30^0$ and using a "typical" HV-21 vertical profile with a pronounced high-altitude contribution. The RMS tilt produced in a path of diameter D = 3.5 m (that of the Starfire telescope) is $\theta_T = 2.47\ \sqrt{\mu_0}\ /D^{1/6} = 3.22$ μrad, while the RMS tilt difference between two paths at an angle α from the same point on the ground is given by $\Delta\theta_T\ /\alpha = 3.27\ \sqrt{\mu_2}\ /D^{7/6} = 0.00410$. Unless otherwise corrected, the value of r_0 would produce spread with a one-sigma half angle $0.45\ \lambda/r_0 = 4.27$ μrad, whereas the spread due to ideal diffraction would be only $0.45\ \lambda/D = 0.136$ μrad.

These mean from the standpoint of adaptive optics for either imaging or beaming that the reference "guidestar" must be located within the isoplanatic angle from the primary path for it to be effective, and this can generally be accomplished quite nicely for astronomical observations (at least for telescopes up to several meters in diameter) with an artificial beacon produced by laser excitation of the sodium layer at 92 km altitude. The tilt anisoplanatism is no more than (0.00410)(13.5) = 0.055 μrad in that case, so image motion will be small compared to the diffraction size. Matters, however, can become considerably more complicated when correction must be made for a laser beam targeted against a rapidly-moving distant object.

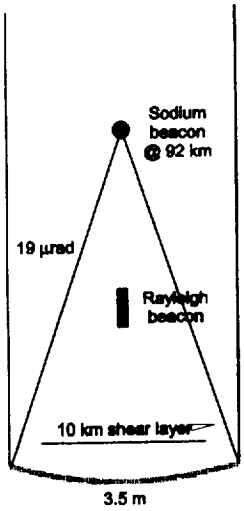

The high-altitude turbulence that most contributes to isoplanatic problems limits the effectiveness of the beacon as well because the solid angle from the beacon to the aperture does not account for all of the turbulence along the full path, even with a sodium beacon which, at 92 km altitude, is the highest artificial one that has been identified. This effect, commonly referred to as focus anisoplanatism, leads to the concept of a "beacon coverage size" d_0 that defines the largest aperture that can be covered by a single beacon (a few meters at typical conditions.) Alternatively, it also can be used to determine the number of beacons $N = (D/d_0)^2$ that would be needed for a large aperture, but each such beacon must be "tagged" to differentiate its wavefront from the others, and the multiple signals must then be "stitched" properly to produce the proper final wavefront. Unfortunately, the ability to actually use multiple beacons has lagged the theory, and there have been no truly successful demonstrations at this time. Until then, although there appear to be no fundamental reasons why multiple beacons cannot be applied, the use of an aperture larger than that which can be handled with a single beacon should be regarded for now as a very risky proposition.

The status of a number of adaptive optics systems as of 1/94 is reviewed in the table on the next page.

Engagement Profile

The engagement profile at the right shows some important characteristics of the ORION system, and serves to identify several as-yet unresolved issues. Times and angular rates are specified for a 1000 km debris altitude, but the results can easily be scaled to other altitudes.

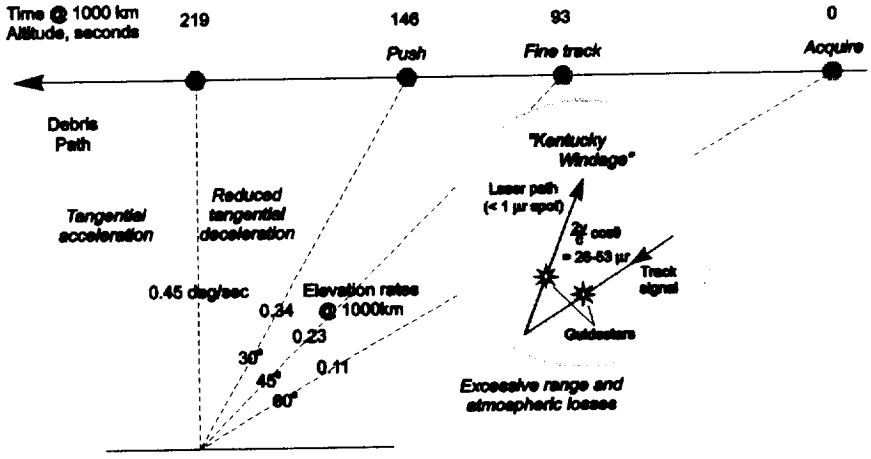

The target will typically be engaged at about 60^0 from zenith (30^0 above the horizon) because R^2 and atmospheric losses rapidly increase beyond there. Passive optical acquisition with one or more simple wide-FOV telescopes, limited by uncorrected turbulence to about 10 μrad resolution, appears to be a very viable option for ORION, and a relatively long time (93 sec @ 1000 km) is available for the acquisition system to establish track and to ensure that the target is in fact debris before possibly switching to fine track at about 45^0. The pusher laser can then commence operation, and a relatively long time will again be available before it ceases operation before zenith to avoid tangential acceleration of the target (which would increase debris lifetime.). Note that elevation rates at 1000 km are quite benign, and that rates above 1 degree/sec would only be encountered below about 450 km (azimuthal rates depend upon both the trajectory and the optical mount design, but will only be important near zenith – where operation should be avoided anyway.)

Demonstrated (D) or Functioning (F) Astronomical Adaptive Optics Systems

Operation	Telescope	Wavefront Sensor	Corrector Mirror	BW (Hz)	r □m m□	Strehl	FWHM (arcsec)	Star Mag.
ESO, COME-ON+ (F)	3.6m La Silla	7x7 subap. Shack-Hartm.	52 act DM	30	3.9 2.2 1.7 1.2	>.9 .6-.8 .26-.47 .1-.17	.22 .13-.16 .1-.16 .1-.13	<=9
U. Hawaii (F)	3.6m CFHT Mauna Kea	13 element curvature	13 seg bimorph		.85	.1	.08	.24
USAF Phillips Lab (F)	1.5m SOR	146 subap. Shack-Hartm.	241 act DM	143	.88	.25 (LE) .64 (SE) .48 (LGS)	.18 .13 .13	5.5
USAF Phillips Lab (F)	1.6m AMOS	152 subap. Shearing I/F	168 act DM					
Mt. Wilson (F)	1.52m	ACE 60 subap Shearing I/F	69 act DM	~50	.7		.125	5.9
Steward Obs. (F)	6.8m MMT Mt. Hopkins	coalign 6 images 0.7m	6 element tilt	20-100	1.2-2.2	.5	.28	14.5
Steward Obs. (F)	6.8m MMT Mt. Hopkins		6 element piston	50	2.2	.1	.08	7
Natl. Solar Obs. (D) Lockheed	0.76m Sac Pk.	6 subap. Shack-Hartm.	19 segment	300	.48			Sun
U. Durham MARTINI (D)	4.2m Herschel La Palma	19 subap. Shack-Hartm.	6 segment	20	.5	.15	.35	12.5
Inst. of Optics & Elect., China (D)	1.2m Yunnan Obs. (.37m used)	16 subap. Shearing I/F	21 act DM	65	Vis		.5-.53	3.78
ESO, COME-ON (D)	3.6m La Silla	20 subap. Shack-Hartm.	19 act DM	25	3.9 2.2 1.7	.85 .6 .3	.22 .13 .1	~7

Planned Astronomical Adaptive Optics Systems

Operation	Telescope	Wavefront Sensor	Corrector Mirror	BW (Hz)	r □m m□	Strehl	FWHM (arcsec)	Star Mag.
ESO	8m x 4 VLT	16x16 subap.	250 act DM	60	2.2	>.8		
CHFT Corp.	1.52m Meudon, France	13 element curvature	19 seg bimorph					
USAF Phillips Lab	3.5m SOR	300-1200 sub	200-1000 act	1000	1.06	.7		
USAF Phillips Lab	3.67m AMOS	300-1200 sub	~800 act	1000				
Nat. Solar Obs.	0.76m Sac Pk.		61	300-500	.5			Sun
U. Durham	4.2m Herschel La Palma	68 subap. Shack-Hartm.	76 segment	100+	.8	..2+	.05+	13+
Steward Obs.	6.8m MMT Mt. Hopkins	coalign 6 images 0.589m	6 element tilt	20	1.2-2.2			1W Na LGS
U. Chicago WCE	0.76m1.04m Yerkes Sac Pk.	60 subap. Shearing I/F	69 act DM WCE					6
U. Chicago ChAOS-97	3.5m ARC	64 subap. Shack-Hartm.	97 act DM	100	2.3	.4		13
U. Chicago ChAOS	3.5m ARC	196 subap. Shack-Hartm.	249 act DM WCE	<40	2.3	.7		12W LGS
U. Illinois	2.5m Mt. Wilson	512 subap. .351m Shearing I/F	512 seg & 30 seg	30	.5-2.5			50W LGS
NAO-SUBARU Japan	7.5m							
OAA Italy, Ohio St., Stegrd Obs.	8m x 2 Columbus/ Gemini; Mt.Graham							
Keck Obs. CARA	10m Mauna Kea							

Ref: R. Tyson, "The status of astronomical adaptive optics systems", SPIE OE Reports (Jan 1994)

The problem here is the need for "Kentucky Windage", the lead-ahead required to account for the distance traveled by the target during the elapsed time for a signal from the target to arrive at the sensor, be processed for adaptive optics correction, and then for the laser beam to return to the target. This is not a measured quantity, but, rather, must be calculated and established by dead reckoning over tens of microradians to an accuracy of the size of the laser spot (about two orders of magnitude smaller.) Unlike a duck hunter who is smart enough to use a shotgun instead of a rifle to shoot a fast-moving bird, the slowly pulsed pusher laser wants to act like a rifle, and the relative size of the lead-ahead will make it very difficult for a tracking system (active or passive) to provide the required accuracy by dead-reckoning regardless of the certainty of orbital motion – especially when the laser "rifle" is being moved about by turbulence.

Though typically only a few milliseconds, the distances are far greater than target dimensions, and the lead-ahead angle $2V/c \cos\theta$ (42.4 μrad at 30^0 and 1000 km altitude) is generally so much larger than the isoplanatic angle that the signal from the target will be useless as a beacon for the adaptive optics. A dedicated laser guidestar within the isoplanatic angle about the outgoing path (i.e., "leading" the target) will therefore be essential for reducing the beam spread, but less direct, however, is the means for handling turbulence-induced tilt because the guidestar signal is itself steered by turbulence. The debris objects of interest tend to be smaller than the beam size, and we have already shown for the case being considered that the RMS tilt angle greatly exceeds the ideal diffraction angle (by a factor of over 20), so the probability of hitting the target will be extremely low if we do not accurately measure or predict the tilt.

The most attractive option for doing so appears to be to use the target itself as a reference for tilt, accurately biasing the track and tilt data to account for the lead angle, and that should be possible because of the relatively invariant nature of orbital flight. However, it should be realized that the combination of tilt anisoplanatism and the need for highly accurate tracking data will require that the pusher beam and the optical signals from the target and the guidestar all be shared by the same aperture – a non-trivial hardware problem — because of the pronounced degradation that would otherwise result from strong low-altitude turbulence. Both the pusher beam and the target tracker must use adaptive optics to minimize spread, and their corrections will necessarily be different because their angular separation considerably exceeds the isoplanatic angle (let alone the fact that their wavelengths may be different.) All of the wavefronts will essentially tilt together at a characteristic frequency $V_T/D \approx 10$ Hz for the given conditions, so the tracking data must be rapidly processed in view of the need for accuracy to a small fraction of the large overall excursion of the tilt The small time slices required for gathering the tracking data and the need to closely synchronize it with the pusher beam strongly suggest that the target tracking illumination be provided by either a CW or very-rapidly-repped laser, probably operating at yet another wavelength to ease the difficulties of aperture-sharing. A suggested functional block diagram of the system is shown at the right to illustrate the key components and information flow. The first splitter is the only high intensity shared component beyond the basic telescope/ director. Neither the beacon nor the illuminator laser need, of course, be co-located with the pusher/sensor system.

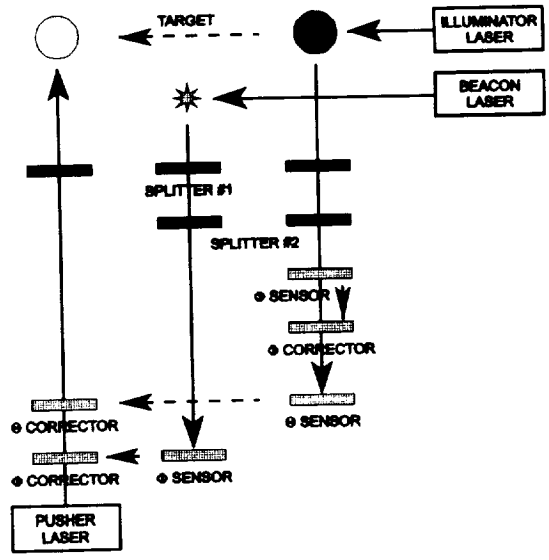

Should extrapolation of the tracking data not provide sufficiently accuracy, it may be necessary to follow the approach of the duck hunter by broadening the beam considerably (i.e., to use a "shotgun" and to accept the greatly decreased intensity) and/or to share the main aperture with a boresighted scanning laser (a CW or rapidly pulsed "machine gun") that can be continually steered to maximize return from the target. Regardless of the approach, the complications involved in boresighting with a high energy pulsed laser could prove to be so daunting that it might be worth considering the use of a far more powerful and rapidly-steered CW or highly-repped pusher laser to overcome both the lead-ahead and aperture tilt problems, probably eliminating the need for a fine tracker at the same time.

2. Large Aperture Telescopes and Beam Directors

It appears to be most likely that a large beam director will be needed for ORION to produce an acceptable spot size. Although the optical telescopes described here are not beam directors *per se*, they are large enough to be directly applicable to ORION, and each in its own right is an exceptional instrument that displays the design philosophy and cost-consciousness that will be required for orbital debris removal with ground-based lasers.

3.67M AEOS and 3.5M Starfire Telescopes

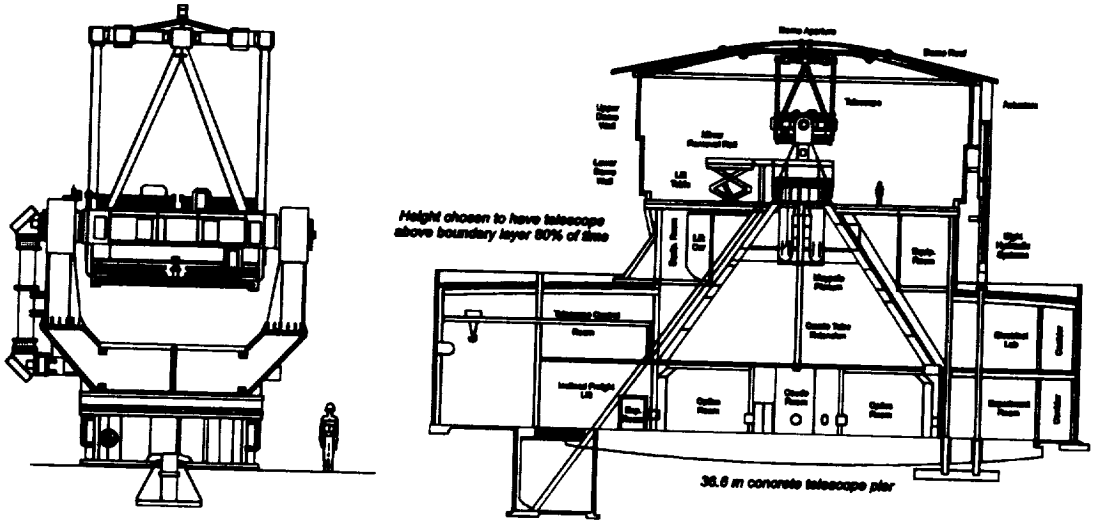

The 3.67 meter AEOS system shown above is presently under construction in Hawaii, and has extremely expensive site-related costs that do not meet our objectives, but its functionally-similar predecessor, the 3.5 meter telescope at Starfire Optical Range in Albuquerque NM, does so admirably. The 27M$ total cost of the latter included 10.5M$ for the Contraves USA optical mount and 7M$ for the primary mirror from the University of Arizona's Steward Observatory Mirror Laboratory. The very moderate telescope cost is due in large part to the use of a 4500 lb. monolithic primary mirror that broke from tradition by using a thin spun-cast borosilicate faceplate with computer-controlled actuators to compensate for deformations of the honeycomb sandwich base. Other unique features include a complete closed-cycle water heater/chiller system for precise thermal control and a protective enclosure composed of three 9 ft. high, 70 ft. diameter cylinders that collapse around the telescope to provide complete ventilation and an unobstructed view for high-speed satellite tracking. Both systems are designed to monitor a variety of space objects, and their slew rates (18.3 deg/sec in azimuth and 4.75 deg/sec in elevation) are sufficient to track even very low-altitude targets. They will eventually incorporate deformable adaptive optics at the end of the F/200 Coude paths to provide the desired resolution, but delivery of the 3.55M$ 200W sodium guide star from LLNL for SOR has been delayed by AF budget reallocation. The systems are specifically designed for imaging, and, as a minimum, the present silver-coated optics throughout the Coude path would probably have to be replaced for high-power operation. A 12 in. 5 mrad full FOV scope with an intensified camera is available for acquisition. The SOR site is located near the end of the runway of the Albuquerque International Airport, and FAA approval is required for individual shots.

10M Keck Telescopes

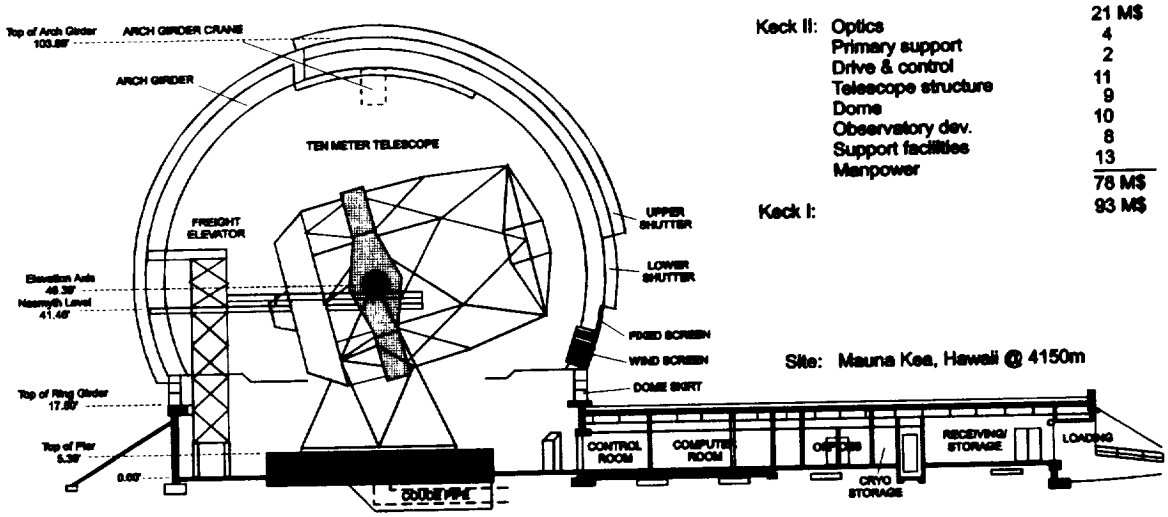

Keck II:	Optics	21 M$
	Primary support	4
	Drive & control	2
	Telescope structure	11
	Dome	9
	Observatory dev.	10
	Support facilities	8
	Manpower	13
		78 M$
Keck I:		93 M$

Site: Mauna Kea, Hawaii @ 4150m

Eventually expected to operate as an interferometer, the two 10 meter Keck astronomical telescopes on Mauna Kea in Hawaii are the largest in the world, and they again broke with conventional design tradition by each employing an array of 36 hexagonal mirror segments, each in turn actively supported on three whiffletrees with computer-controlled actuators to control distortion. The required overall parabolic figure was obtained by precisely pre-stressing each of the mirror blanks, polishing them to a spherical curvature, and then allowing them to relax to the final shape. The overall weight of the Keck telescope is 596,000 lbs, about half that of the 5 meter Hale telescope, and about three times that of the Starfire telescope (186,000 lbs.) Subsystem costs are shown in the figure, and it is quite significant that they are only about three times those of the Starfire telescope. A 349-element deformable mirror from Xinetics will be available soon to provide infrared turbulence correction (note that $d = D/\sqrt{N} = 54$ cm is much larger than typical values of r_0 in the visible.) Although designed exclusively for astronomical observations, it is interesting to note that their maximum design slew rate of 3 deg/sec ("anywhere to anywhere in under 2 minutes") would be sufficient for the needs of ORION.

High-Power Beam Director

No high-power beam directors of ORION size exist in the Western world. The telescopes described above are designed for imaging, not for beam directing, and their optical designs attest to that fact. The large primary mirrors themselves do not pose a serious problem because the flux levels on them tend to be quite low (e.g., 10 MW on a 10 meter mirror corresponds to only 0.13 W/cm^2 – one solar flux – at 1% absorption), but the smaller mirrors in the Coude path are typically subjected to 100 times or more intensity, and that will generally require more damage-resistant coatings and actively-cooled substrates. The most vulnerable elements generally tend to be those associated with the adaptive optics system, e.g. the high-power beam splitter for the wavefront sensor, and the active mirror itself (if it is in fact situated in the Coude path.) Nonlinear beam propagation becomes a major issue as well within a telescope primarily because of the high intensities in the Coude path, and a high power beam director will usually employ beam conditioning using a sealed optical system with a low absorbing flowing gas, and that in turn will require transmitting windows to isolate the gas from the surroundings.

These would represent rather extensive changes of the existing systems (which, of course, are dedicated to applications that don't need those mods), and a concept that might be suitable for a large beam director to meet the requirements of the ORION mission is the coelostat shown on the next page. This design was specifically configured to use the PAMELA segmented primary mirror concept which permits r_0-sized adaptive optic elements instead of ones reduced by the telescope magnification ratio to a few millimeters, and places them on a rigid base to minimize control-structure interactions and to allow active cooling if

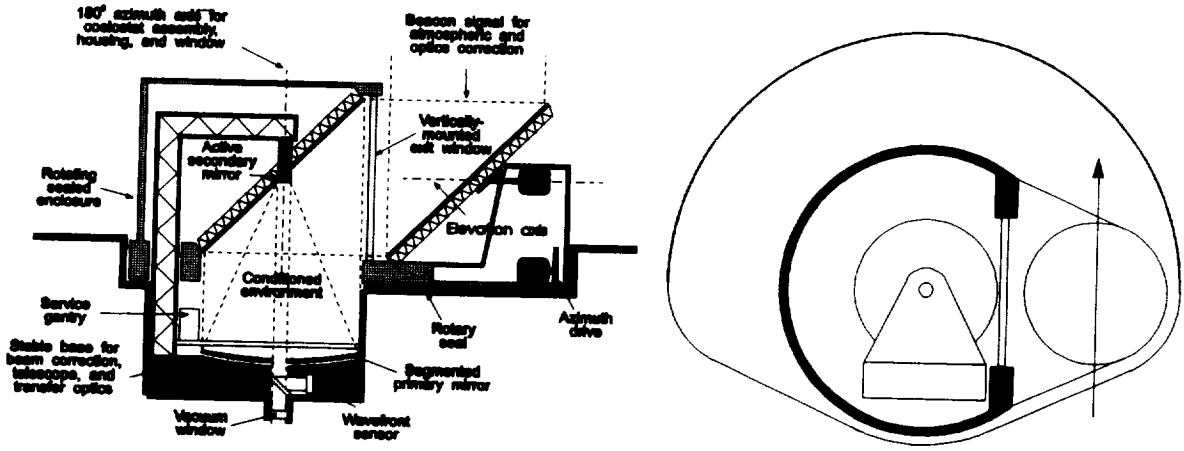

necessary. The rigid telescope structure provides stability, allows ready access throughout for thermal and electro-mechanical control, and enables the use of an active secondary for additional correction. The sealed rotating housing with a vertically-mounted window protects all of the high-value components and provides a controlled environment for the high intensity laser path. The most argumentative elements of the design are the two massive 45^0 mirrors, but they execute rather simple motion, and can be of very lightweight design with active figure correction via the adaptive optics.

Cost

The optics represent the most fundamental unit of any telescope or beam director, and scaling philosophy in the business places a premium on their total mass by assuming that other system and subsystem weights and costs are all linearly proportional to it *for similar systems*. Such scaling has little firm basis in engineering or science, but, rather, it is based on good design practice wherein improvements in one component tend to be mirrored in others because of both competition and cost-effectiveness (because relative improvements in a minor component would better be made in a major one.). An accepted rule with astronomical telescopes is, in fact, that the cost of the total telescope and mount is about twice that of the optics, and the total facility is about twice the telescope. Both the Keck and the Starfire systems fit this guideline quite well with regard to cost, but the agreement may be somewhat fortuitous in view of the disparities in telescope mass and mirror cost. The high slew rates of the Starfire telescope resulted in a much heavier telescope relative to the primary mirror, but its lightweight mirror was relatively expensive, it is thought, due to recovery of costs for spin casting development. Not to be discounted, too, is the fact that another major factor in any such system is the cost of high-tech support, and Starfire's dedicated Air Force personnel and Keck's university support probably had major impact on the very moderate overall costs.

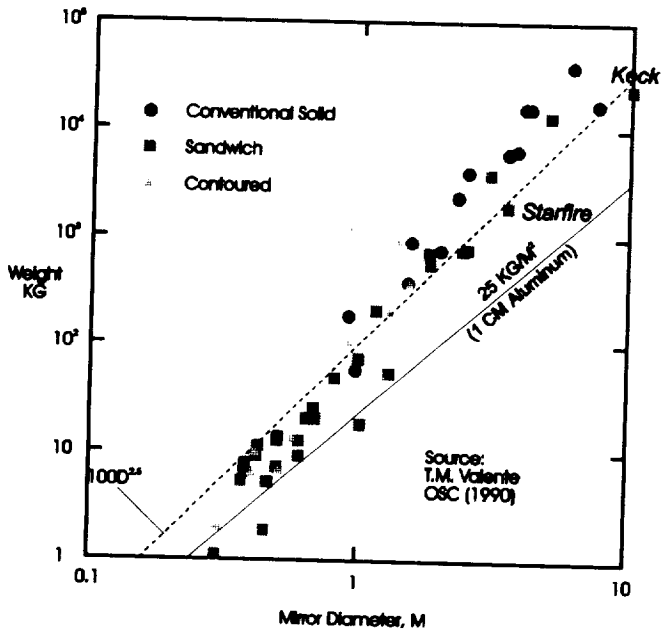

The problems associated with simple power-law scaling are shown at the right where mass is plotted for a large number of mirrors of various types of design. The Keck and Starfire mirrors themselves actually follow conventional $D^{2.6}$ scaling, but they represent lower extremes of widely scattered data, the dispersion of which can produce huge numerical differences at such large sizes. Those differences represent a major

system technology and design driver because high values can simply not be afforded, and paradigm shifts have to be made. In the interest of cost realism. As a result, the overall cost of the Keck scales almost *linearly* with D from Starfire, and a major change like the coelostat concept might perhaps be the next step that would have to be taken with radical redesign for a much larger telescope.

Economic realism dictates that means be found to continue such a scaling trend.

3. High-Energy Lasers

The choice of available lasers for the ORION mission is really quite limited because of the need to produce a beam of high energy pulses at a high duty cycle on a regular basis for long periods of time and to propagate that energy through the atmosphere to a very small spot at long ranges in space.

The CO_2 laser was the first to operate in a very high power mode, and its lower power versions today set the standard for high reliability in the industrial world, but the 10 - 11μ wavelength is prevented by diffraction from producing the target energy density needed for ORION. Another system that has attracted considerable commercial interest, partly because of its ability to actually break the chemical bonds of the material that it interacts with, is the excimer laser which operates at the other end of the wavelength spectrum in the ultraviolet and short UV; the potentially high single-pulse energy and small spot size has also caused considerable interest for use as a space-based laser weapon, but the available parameter range of pulse energy, pulse length, and rep rate don't mate well with the ORION requirements, and the short wavelengths greatly complicate the use of adaptive optics for turbulence correction. Similar arguments pertain to most of the other high energy laser systems that have been developed for military and/or industrial use (e.g., iodine @ 1.3μ, HF/DF @ 2.7 - 3.8μ, and CO @ 4.8 - 6μ), the result being that the only remaining viable candidates appear to be the neodymium glass and free electron lasers.

Solid state neodymium glass lasers are widely used for inertial confinement fusion programs because of their ability to produce high energy in relatively short pulses at short wavelength -- 1.06μ, but readily doubled and tripled for operation in the visible. Lawrence Livermore National Laboratory has led this country in the development of such lasers through the massive Shiva, Nova, and soon-to-be NIF (National Ignition Facility) systems, and their currently-operating Beamlet laser with its 20 kJ, tens of nanosecond pulses may be uniquely suited to the ORION mission if the system can be cooled for operation in a repetitively pulsed mode. A major benefit of the concentrated R&D that has gone into those systems is the availability of specialized hardware for such functions as frequency doubling, beam isolation, and cleanup, a notable example of the latter being the SBS (stimulated Brillouin scattering) mirror that has been used at LLNL to generate a phase conjugated beam for real-time cancellation of thermal distortions. Caution is simply advised that these lasers are very expensive, and their present location in the heart of California's heavily-populated Livermore Valley is less than ideal from every viewpoint for ORION. Nevertheless, LLNL has performed ground-to-space propagation from there, and they have -- or could soon have -- the capabilities on site to vividly demonstrate the debris clearing concept.

The free electron laser remains a candidate for ORION because of the advantages offered by its wide operational parameter space (including wavelength), potentially high efficiency with electron beam recovery, and excellent beam quality, but it also represents one of the most dramatic failures of the DoD high energy laser program in terms of dollars spent per kilowatt output. It has, however, been pursued far more successfully in the former Soviet Union, and it and other systems developed there might prove more suitable for orbital debris removal than would their US counterparts if certain biases by our government and its industrial partners can be overcome. The most serious technical question involving the use of an FEL for debris clearing is its ability to actually produce the desired target interaction: for example, a 200 kW FEL (e.g., the Microtron RF system proposed for near-term delivery to the U.S. by the Budker Institute in Novosibirsk) operates at about 20 MHz with about 20 psec pulses, and, regardless of the details of the macropulse format, this corresponds to no more than tens of millijoules of energy per pulse whereas target coupling requires at least tens of joules at that pulse duration.

The benefits of a well-corrected large aperture beam director for ORION cannot be understated because of the profound effect of the resulting small spot size on the laser system itself. A 10 cm spot on a target at a range of 2500 km, about the most that would be necessary to deorbit the largest concentration of orbital debris, would require an effective aperture size D√S of 32 meters at 1μ wavelength. This is clearly far beyond even the largest optical astronomical telescopes being considered today and it would require a pointing accuracy of at least 30 nanoradians, but such sizes are relatively routine with radio telescopes, the segmented optics technology exists today to populate such structures for operation at optical frequencies, and the pointing accuracies are similar to those pursued for the Strategic Defense Initiative. Instead of the tens of kilojoules/pulse that might be required with a more conventional telescope, the desired effect could be obtained with less than 1 kJ pulses from a 50 nsec laser, and this corresponds to the pulse parameters of the 20 MW induction FEL (1 kJ pulses @ 20 kHz) that was the early baseline for the SELENE system and for which the solid-state accelerator modules are already in operation at Science Research Laboratory in Somerville MA. Note that the 20 MW figure is for comparison only, and an operational ORION system using either an FEL or a glass laser could operate at far smaller PRF and power level with those kJ pulses. For near-term use, that same beam director operating against a target at 500 km would produce only a 2.5 cm spot, but the same impulse could be obtained with only a few tens of joules per pulse.

4. Space Debris Removal -- Orbital Considerations

Space debris can be deorbited by using a ground-based laser to selectively apply a velocity increment to increase ellipticity and/or to decrease energy. The reduced perigee altitude in either case will then result in increased drag and more rapid destructive re-entry. The orbital/reentry aspects of the problem are fully treated here, emphasizing physical understanding of the behavior rather than actual numerics. A simple expression for the time required by atmospheric drag to cause reentry from an arbitrary orbit is first developed, and the impulsive Δv requirements are then defined for most effectively producing reentry.

Orbital Mechanics

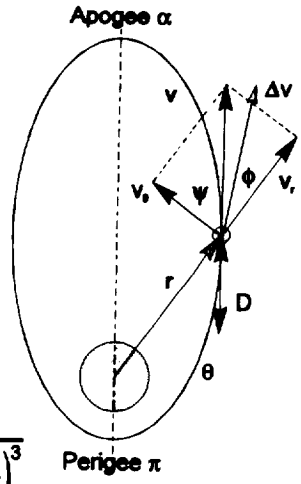

The two-body orbit problem, including drag D, is described by the equations

Radial force: $d^2r/dt^2 = dv_r/dt = v_\theta^2/r - \mu/r^2 - D/m \cos\psi$

and *Angular momentum H*: $d(rv_\theta)/dt = - Dr/m \sin\psi$,

which may be combined to give

Energy E: $d[(v_r^2 + v_\theta^2)/2 - \mu/r]/dt = - Dvr/m$ and $d^2(1/r)/d\theta^2 = \mu/H^2 - 1/r$.

It follows that the orbital parameters in vacuum (i.e., with D = 0) are given by

$$E = -\frac{\mu}{r_\alpha + r_\pi} = -\left(\frac{\mu}{H}\right)^2 \frac{1-\varepsilon^2}{2}, \quad \frac{r}{r_\pi} = \frac{1+\varepsilon}{1+\varepsilon\cos\theta}, \quad v_\pi = \sqrt{\frac{\mu}{r_\pi}(1+\varepsilon)}, \quad T = 2\pi\sqrt{\frac{1}{\mu}\left(\frac{r_\pi}{1-\varepsilon}\right)^3}$$

where $\varepsilon = (r_\alpha - r_\pi)/(r_\alpha + r_\pi)$ is the eccentricity of the orbit.

Lifetime

Atmospheric drag produces azimuthal deceleration that first reduces orbital ellipticity, and then causes the debris particle to slowly spiral inwards towards the earth until the rapidly rising density (shown on the next page) causes it to precipitously lose altitude and self-destruct. Transforming to θ as the independent variable for convenience, the reentry trajectory is described by the coupled differential equations

$$d^2(1/r)/d\theta^2 = \mu/H^2 - 1/r \quad \text{and} \quad dH/d\theta = -\rho C_D A/2m\, r^2 v.$$

The first equation remains unchanged from the vacuum case, and the second describes the rate of change of angular momentum H where the drag coefficient $C_D = 2D/\rho v^2$ for hypersonic flight is nearly a constant with the Newtonian value 2.

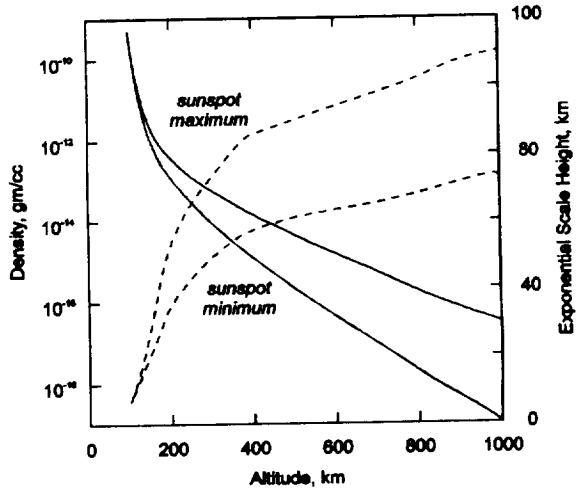

The drag is localized near perigee for an initial highly-elliptical orbit, and this essentially produces a negative tangential Δv with no change of perigee, each ensuing orbit having decreased ellipticity until a circular condition is reached with nearly the original perigee altitude. Assuming an exponential density variation which the data shows is appropriate at high altitudes, the change in angular momentum per orbit during the early stages where integrated drag is the least and most of the time is spent is given approximately by

$$-\Delta H = \int_{-\pi}^{\pi} \frac{\rho C_D A}{2m} r^2 v\, d\theta \cong \frac{\rho_* C_D A}{2m} r_* H \int_{-\pi}^{\pi} e^{-\frac{r - r_*}{L}} d\theta = \frac{r_* C_D A}{2m} r_* H \int_{-\pi}^{\pi} e^{-\frac{H^2}{\mu L} \frac{2\varepsilon \sin^2\theta/2}{(1+\varepsilon)(1+\varepsilon\cos\theta)}} d\theta$$

$$\rightarrow \frac{\rho_* C_D A}{m} r_* H \int_0^{\infty} e^{-\frac{H^2}{\mu L} \frac{\varepsilon\theta^2/2}{(1+\varepsilon)^2}} d\theta = \frac{\rho_* C_D A r_*}{m} (1+\varepsilon)\sqrt{\frac{\pi\mu L}{2\varepsilon}}\ .$$

Thus,
$$\frac{\Delta H}{T} = -\frac{\rho_* C_D A}{m}\sqrt{\frac{\pi\mu L}{2\varepsilon}} \frac{\mu}{2\pi H}(1-\varepsilon^2)^{3/2} \cong \frac{dH}{dt} = \frac{\mu r_*}{2H}\frac{d\varepsilon}{dt}$$

using the orbital period T, so, if the time spent near final circularization is small, we find the time τ to reach that condition to be given by

$$\frac{\rho_* C_D A}{m r_*}\sqrt{\frac{\mu L}{2\pi}}\,\tau = \int_0^{\varepsilon} \frac{\sqrt{\varepsilon}\, d\varepsilon}{(1-\varepsilon^2)^{3/2}} = \frac{2}{3}\varepsilon^{3/2} + \cdots .$$

In the other limit of nearly circular orbits, the equations reduce to

$$r = \frac{H^2}{\mu} \quad \text{and} \quad \frac{\rho C_D A}{m} = -\frac{2}{r^2 v}\frac{dH}{d\theta} = -\frac{1}{r^2}\frac{dr}{d\theta} = -\frac{1}{\sqrt{\mu r}}\frac{dr}{dt}$$

so that the reentry time t is given by

$$\frac{C_D A}{m}\tau = \int_{r_\infty}^{r} \frac{dr}{\rho\sqrt{\mu r}} = \frac{1}{\rho\sqrt{\mu}} \int_{r_\infty}^{r} e^{\frac{r'-r}{L}} \frac{dr'}{\sqrt{r'}} \rightarrow \frac{L}{\rho\sqrt{\mu r}}$$

and is again inversely proportional to the density in the initial circular orbit and to the ballistic coefficient $C_D A/m$.

NASA has calculated the lifetime for reentry for a variety of debris objects beginning in circular orbit, and the results are shown on the next page at the upper left (Ref: "Orbital Debris, A Technical Assessment", National Research Council, National Academy Press, 1995.) The data for all of the curves has been *replotted* beside it in terms of the parameter $A\tau/m$, and it is clear that the form accurately represents the results over the entire range, and that the results closely track the density data as predicted by the simplified model.

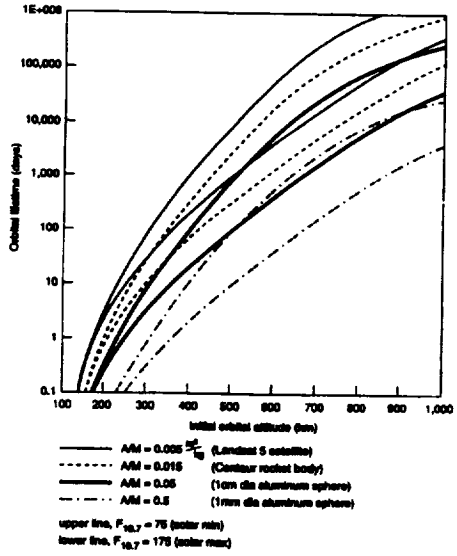

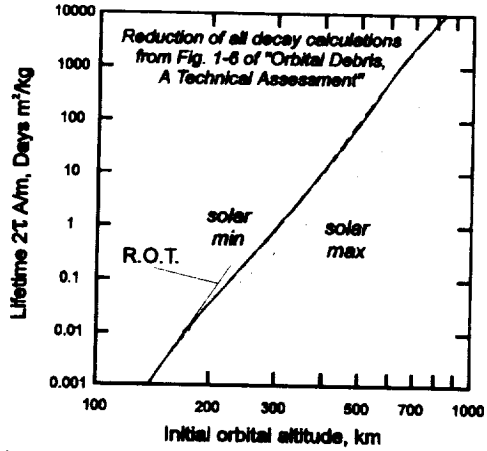

A unified picture of the reentry behavior for arbitrary initial conditions has been obtained by numerical integrating the differential equations using Mathematica and an exponential atmosphere with a constant scale height L, and representative results are shown at the right. As should be expected, highly elliptical orbits first show a decay of apogee altitude with fixed perigee, followed by an increasingly rapid decrease of perigee to an abrupt reentry. It was found that both the computational time and the memory requirements increased dramatically for "small" values of the drag parameter $\rho C_D AL/m$ and that the author's 100 MHZ Pentium slowed to a halt for values of $t\sqrt{(\mu r_\pi/L^4)}$ larger than about 10^7; those limiting drag values tended to be considerably higher than those of practical interest, but it was also found that the "final" conditions corresponded to many hundreds of orbits and that the results essentially reached asymptotic values of interest. The integration routine uses a variable step size to optimize accuracy and speed, and the quoted termination conditions reported by Mathematica when the step size essentially vanishes are therefore useful measures of the lifetimes with low drag. Those are shown below for the lowest calculated drag conditions, and it is clear that the results are quite well correlated by

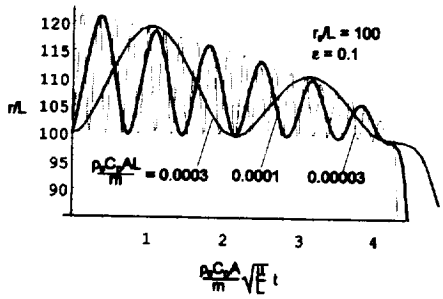

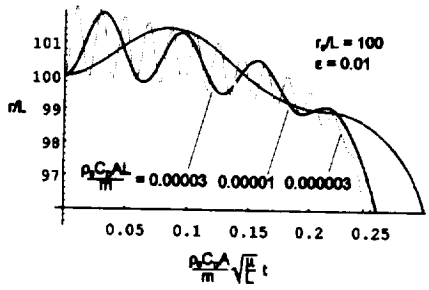

$$\frac{\rho_\pi C_D A}{mL}\sqrt{\mu r_\pi}\,t = 1 + \sqrt{2}\left(\varepsilon\frac{r_\pi}{L}\right)^{3/2}.$$

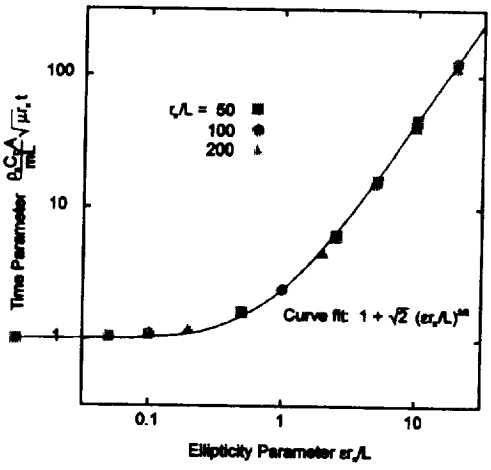

This simple summation of the circular and elliptical limits exactly matches the result given previously for circular orbits, but the elliptical term, though matching the slope, is 18% less than that calculated before (due probably to the rather liberal mathematical approximations that were made there.) The full effect of ellipticity is just to multiply the lifetime by the factor $1+\sqrt{2}(\varepsilon r_0/L)^{3/2}$, and the consequence of doing so is shown on the next page. The results appear to agree well with those of King-Hele.

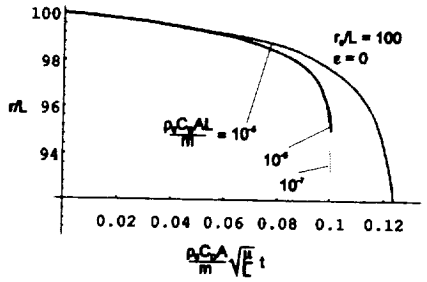

It is interesting to note from an operational viewpoint that, while the greatest concentration of debris is known to be located 800 - 1200 km above the Earth's surface, the lifetime of that material – which is relatively difficult to reach with a ground-based laser – is 10^2 - 10^4 longer than that of debris in the region near the 400+ km altitude of the high-value International Space Station Alpha.

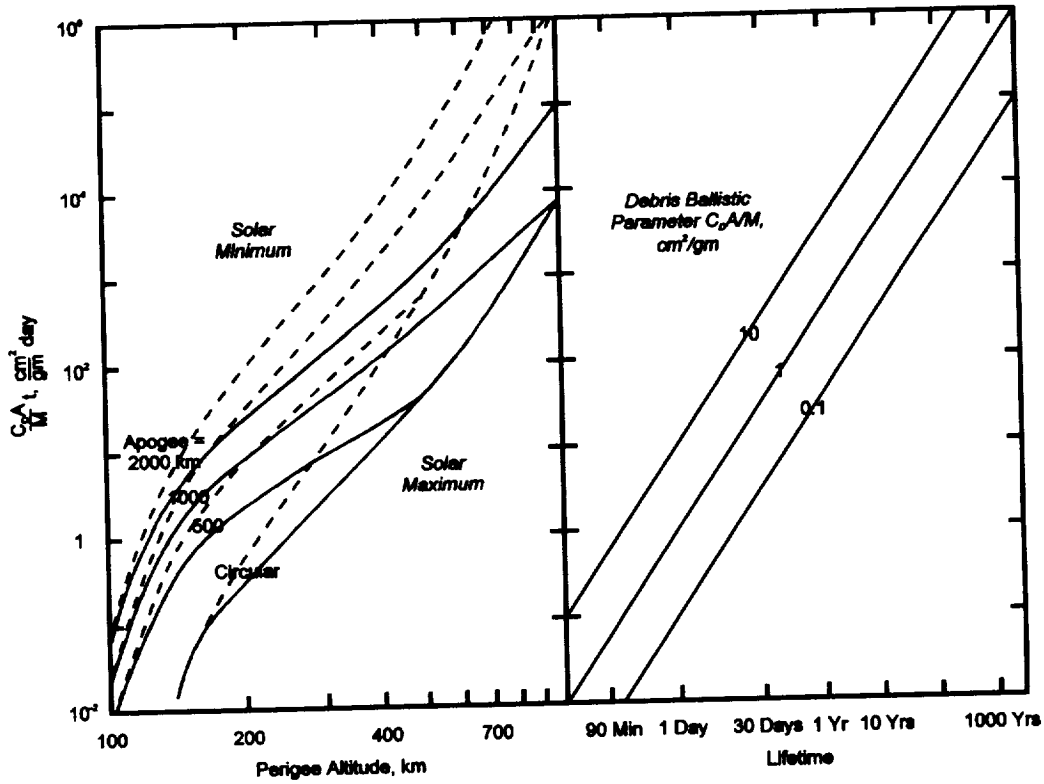

Lifetime Reduction

Pulses from a ground-based laser can effectively reduce the lifetime of a debris particle in space by ejecting a small amount of mass, partially ionizing it to create a plasma, and then by producing a pressure wave through absorption in the plasma. The wave forms across the exposed surface of the material, so the resulting force is normal to that surface. The time-integrated force from a single pulse is an impulse that in turn translates into a velocity increment, and the gross result for a train of pulses is a series of such Δv's that modify the orbit such that the integrated drag is increased and the particle more quickly reenters. To put this in perspective, Δv scales as C_mE/M, so a particle with mass M of 1 gram receives a Δv of only 0.1 mps from 1 joule of incident energy E at a coupling coefficient C_m of 10 dynes/watt; since typical orbital velocity in LEO is about 7900 mps, many such pulses will therefore be required to cause a significant change in the orbit. Although eccentricity and perigee altitude (the two orbital parameters most affecting lifetime) may be significantly affected during the exposure time, the local velocity and radial distance will change little during that period, so it is within the spirit of this analysis to treat the total impulse as purely incremental and to leave higher order effects to computer analysts.

Since each laser pulse effectively produces an incremental velocity which does not affect the local radial coordinate r but does change the other properties of the appropriate ellipse through that point, it is useful to describe the orbit in terms of its local velocity components v_r and v_θ, i.e.

$$v_r = \mu/H\ \varepsilon \sin\theta,\ \ rv_\theta = H,\ \ H^2/\mu r = 1 + \varepsilon\cos\theta.$$

Then,

$$\tan\theta = \frac{xy}{x^2 - 1}\ ,\quad \varepsilon = \sqrt{(x^2 - 1)^2 + x^2y^2}\ ,\quad \frac{r_\pi}{r} = \frac{x^2}{1 + \varepsilon}\ ,\quad x = v_\theta\sqrt{\frac{r}{\mu}}\ ,\quad y = v_r\sqrt{\frac{r}{\mu}}\ .$$

where $\sqrt{\mu/r}$, the local circular velocity, is about 7900 mps in low Earth orbit as noted above. The orbital parameters ε, θ, and r_π/r are plotted below on a "hodograph" plane using normalized velocity components x and y as coordinates, and an expanded view of that plot about (0, 1), more appropriate for nearly circular orbits, is shown on the next page. Note that the θ and ε asymmetries that are evident in the first plot for large eccentricities essentially vanish in the expanded one where conditions for small ε are described well by

$$x \cong 1 + \varepsilon/2\cos\theta\ ,\quad y \cong \varepsilon\sin\theta\ ,\quad \varepsilon^2 \cong 4(x - 1)^2 + y^2\ ,\quad \text{and}\quad \tan\theta \cong y/2(x - 1).$$

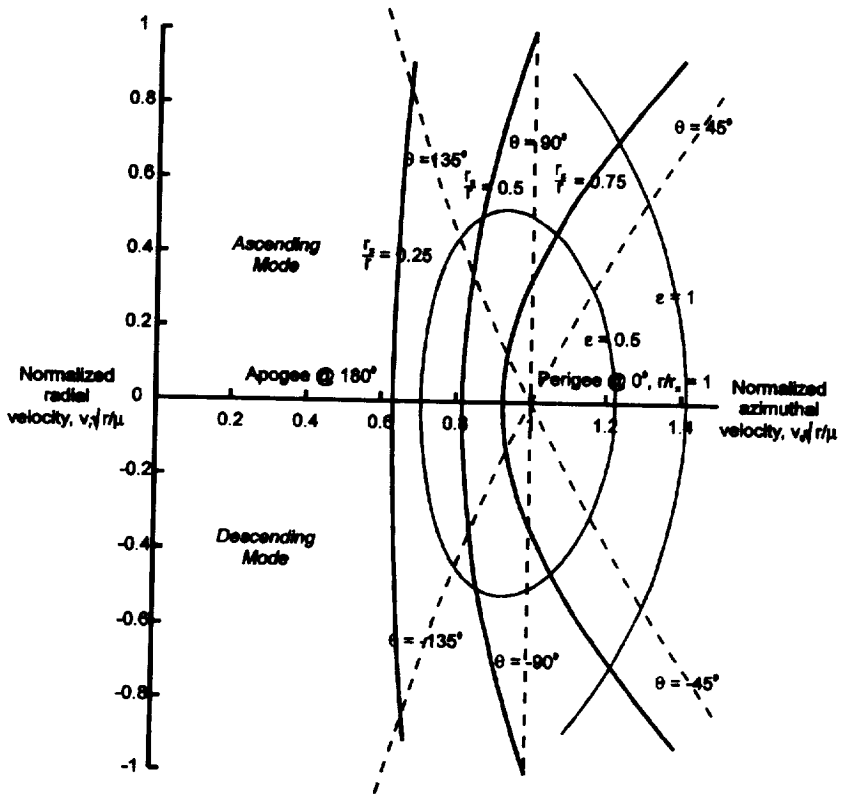

Aside from inclination angle, which is neither specified nor required in this two-dimensional analysis, a point on the hodograph plane is uniquely specified by the radial and azimuthal velocity components and the range, all of which can be measured or derived with a high-quality radar system, and those in turn (together with the inclination – that can also be measured) uniquely determine the orbit of the target. The effect of a velocity increment Δv can be graphically represented by drawing its vector with appropriate magnitude and direction from its point of origin in velocity space, and the head of the vector then defines ε, θ, and r_π/r for the new orbit. If the perturbation is truly impulsive, the radius r is unchanged and the new perigee altitude is given directly.

Curves of constant $r_\square/r$ in the first hodograph plot have been replaced in the expanded version on the next page with lifetime profiles based upon the previously derived model and given by

$$\tau = \frac{\rho C_D A}{mL}\sqrt{\mu r}\,t = [1 + (\frac{r}{L}\frac{r_\pi}{r}\varepsilon)^{3/2}]\sqrt{\frac{r}{r_\pi}}\,e^{-\frac{r}{L}(1 - \frac{r_\pi}{r})}$$

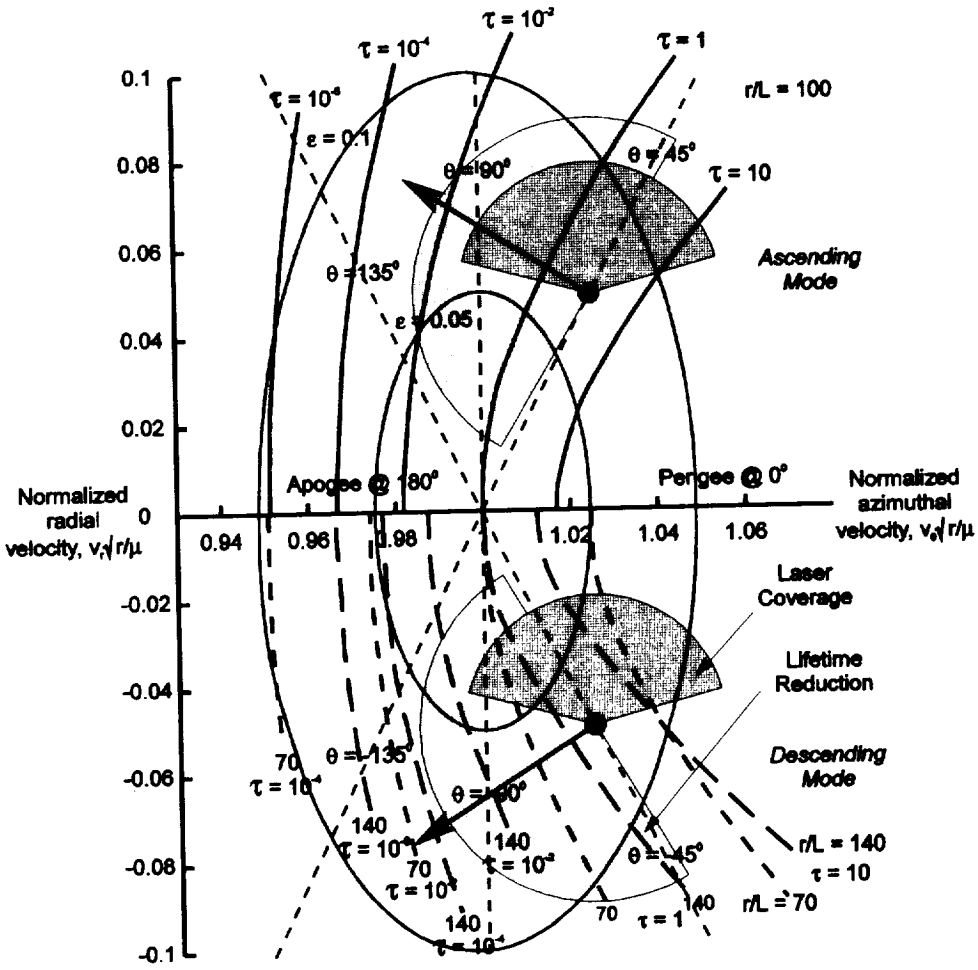

where τ is a dimensionless lifetime with its parameters evaluated at the intercept condition, and for which it is important to understand that it is ratios that are important, not the individual τ values themselves. Lifetime curves in the upper half of the figure correspond to r/L = 100, while those in the lower half are for r/L = 70 and 140; they should be understood to be symmetric about the horizontal axis, and are shown as they are simply for clarity. There is relatively little effect of changes of r/L at the right where $\theta < 90^0$ because the altitude there is very nearly that at perigee, but, otherwise, the curves are dramatically compressed as r/L decreases (meaning that lifetime is far more easily reduced.) The much closer spacing of all sets of lifetime curves for $\theta > 90^0$ in fact means that a properly directed Δv will be much more effective there than it will be near perigee, but it should be noted that the anti-azimuthal impulses of greatest benefit there will be more difficult to produce with a ground-based laser, and the propagation distances will be larger as well. Aside from laser propagation effects, the most effective application of velocity changes for lifetime reduction will be outwardly normal to the curves of constant τ in the hodograph plane. This corresponds in the physical plane to nearly radially-outward near perigee in the ascending mode to anti-azimuthal near apogee and then to nearly-radially *inward* near perigee in the descending mode. The examples shown in the expanded figure were arbitrarily selected and correspond to equivalent positions in the ascending and descending modes; the vectors point in the direction of greatest lifetime change, and the light-colored sectors depict the allowable range of impulse angles for lifetime reduction. The mean impulse for most debris objects will generally be close to the direction of the laser beam, so the angle ϕ between the impulse vector and the local radial will be limited as shown by the dark-colored sectors to about $\pm 75^0$ by atmospheric effects [as a matter of convenience for use of the graph, the vector lengths and the radii of the light and dark sectors are respectively 0.05, 0.04, and 0.03 in terms of normalized velocity.]

It should be clear from the figure that the allowable operating space (the region of overlap of the laser and lifetime sectors) for small Δv vanishes as perigee is approached in the descending mode, that it is appreciable near perigee in the ascending mode, and that it only moderately favors the ascending mode for $270^0 > \theta > 90^0$; reasonably efficient operation can be achieved anywhere in the orbit with a sufficiently high Δv. The curves must be interpreted carefully, though, because they can be misleading. In particular, while the close spacing (rapid changes) near apogee might suggest that operation would be favored there, propagation distances tend to be the longest because of both the increased altitude at apogee and the fact that larger standoff distances are required because of the reduced effectiveness of a radial Δv component. The effect of distance of closest approach on propagation range -- and therefore on target intensity and Δv -- may, in fact, be the strongest driver on the choice of engagement, and cross-range distances, in the likely event that the laser lies outside the orbital plane, may prove more demanding than will radial/axial Δv considerations (note that a LEO footprint crosses the equator every 1.5/24 = 1/16 rotation -> 2500 kms, and this can lead to a substantial cross-range distance at interesting latitudes with a highly inclined orbit.)

In view of the need imposed by the search function, atmospheric conditions, etc., to seek "targets of opportunity" with the ORION mission, it is indeed fortunate that these rules are rather loose -- but there is one that is not, and which should be strictly obeyed:

Avoid any engagement that produces a positive axial Δv component,
i.e one that acts to accelerate the debris along its path.

APPENDIX F

SELECTION OF LASER DEVICES AND NEODYMIUM GLASS LASER SYSTEM ANALYSIS

William Dent
Dent International Research, Inc.

Section 1

1.0 Selection of Laser Devices

The primary objective of this task is to survey laser devices and their associated technologies to determine what lasers might be suitable for use in clearing orbiting debris from low to medium earth orbit. The U.S. Space Station is scheduled to be launched into orbit beginning in the next two to three years. Thousands of pieces of debris from booster upper stages and defunct satellites pose a potentially serious collision threat to the Space Station and other operational satellites. A large ground-based high-energy laser is potentially capable of irradiating these pieces of debris with sufficient fluence to create enough blow-off impulse to cause the debris to de-orbit.

A high-energy laser must meet many requirements to perform this mission. Among the most important considered for this task are:

- Beam Propagation - The laser wavelength must have good atmospheric transmission characteristics, i.e., low absorption. Also, the power density in the beam for the required overall laser system parameters must be below the Stimulated Raman Scattering (SRS) and non-linear index of refraction thresholds. These parameters are determined by the laser wavelength, pulse energy, pulse length, and beam diameter.
- Average Power - The laser must be capable of producing sufficient average power to de-orbit a piece of debris in a reasonable time period.
- Single Pulse Energy - Each individual laser pulse must contain sufficient energy, when coupled with the other system parameters, to ignite a plasma on the surface of the debris creating thrust from the blow-off. Preliminary analysis indicates the required single pulse energy will be in the range of tens of kilojoules.

- Pulse Length - Target coupling and atmospheric propagation are highly dependent on the laser pulse length. Preliminary analysis indicates the pulse length should be between 100 ps and 100 ns.
- Beam Quality - Focusing on a target up to 2000 km in range with a high beam intensity requires a near-diffraction limited beam. Of particular importance is maintaining beam quality in the repetitively pulsed mode.
- Reliability - This laser will be required to operate with a large duty cycle every day for several years.
- Existing Technology - By management decree, NASA is not in the business of developing high energy laser technology. Whatever laser is chosen to perform this mission, the development and prototyping of the laser hardware will have to have been accomplished by some organization other than NASA.
- Available Technology - The laser technology NASA chooses to perform this mission must be readily available for deployment by NASA. Laser technology developed in foreign countries will only be considered if the proper business climate exists to allow NASA the opportunity to readily and reasonably acquire the hardware.
- Adaptive Optics - The compatibility of the laser system with the adaptive optics is a serious issue. Beam brightness drives the system to shorter wavelengths while the technical difficulty of constructing a large adaptive mirror pushes toward longer wavelengths.

1.1 Excimer Lasers

The near-ultraviolet wavelengths produced by excimer lasers offer the possibility of very high brightness laser systems for orbital debris removal. These lasers have been heavily researched and developed in the U.S. and other countries. In the U.S., excimer lasers have achieved average powers of several kilowatts with good beam quality. From the physics learned in these experiments, there appear to be no issues preventing the scaling of these average powers to at least the several hundred kilowatt level. Some of the issues for these lasers are:

- Low Efficiency - Typical efficiencies of excimer lasers falls in the range of two to four percent.
- Pulse Length - The natural pulse length produced by high energy excimer lasers is typically in the 500 to 1000 nanosecond region for efficient operation. Efficiently shortening the pulse length is not practical.
- Electron-Beam Pumping - Only e-beam pumping has been shown to be scaleable to high energy. E-beam sustained discharge has not been efficiently scaled to high energy. With e-beam pumping, a serious issue remains for the lifetime of the foil separating the laser cavity from the electron gun.
- Window and Coating Damage Thresholds - For near ultraviolet wavelengths and nanosecond pulses, the damage thresholds for excimer laser windows and coatings is generally 0.5 to 2.0 J/cm^2. This makes long term operation at high power difficult.
- Raman Shifting - Significant atmospheric scattering at the near ultraviolet excimer wavelengths necessitate down shifting slightly into visible wavelengths for reasonable atmospheric propagation. This is

accomplished in a high pressure hydrogen cell. The xenon fluoride wavelength of 351 nm is normally down shifted to 411 nm. This process also enhances beam clean-up.

- Adaptive Optics - The short wavelengths of excimer lasers makes correcting for atmospheric turbulence with adaptive optics extremely difficult. Also, the problems of lead angle and isoplanatic angle are severe.

Large, scaleable high average power excimer lasers have been constructed in the U.S. The EMRLD oscillator successfully produced 40 to 50 joules per pulse at 100 Hz at 353 nm with a pulse length of 600 to 700 ns and a beam quality of 1.3 times diffraction limited. Large single pulse energies of greater than ten kilojoules have been achieved by lasers such as the Aurora krypton fluoride laser at Los Alamos National Laboratory. (Reference 1)

1.2 Neodymium Glass Lasers

These solid state lasers currently produce the highest single pulse energy with short (nanosecond) pulse length of any laser. Because of this ability and their relatively short wavelength (1 micron), these lasers have been chosen by several countries around the world for inertial confinement fusion programs. Consequently, this particular laser technology has been advanced to one of the highest levels of state-of-the-art of any laser. The physics of neodymium glass is extremely well known and understood.

The largest single pulse neodymium glass laser in the world, Nova, is at Lawrence Livermore National Laboratory. This currently operating laser produces more than 100 kilojoules in one nanosecond at one micron from ten separate beam lines.

Also currently operating at Livermore is the Beamlet laser. This laser is a single beam line prototype of the neodymium glass lasers for the National Ignition Facility (NIF), scheduled to begin construction at Livermore in 1997. This system will consist of 192 separate beam lines based on the Beamlet prototype.

The Beamlet laser is potentially capable of producing a single laser pulse with sufficient energy (20 kilojoules) and short pulse length (10 to 40 nanoseconds) to ignite a plasma on a piece of orbiting debris. However, the Beamlet laser is only currently configured to be operated at the rate of one pulse per minute or less. To be of value in removing orbital debris, the Beamlet laser would need to be pulsed at the rate of approximately one pulse per second, which is far in excess of its current capability. The primary factor limiting Beamlet's repetition rate is removing heat from the laser glass slabs.

Another laser currently operating at Livermore (Reference 2) has achieved significant pulse energies (100 joules) at high repetition rates (6 pulses per second) and is being scaled up (12 pulses per second). The main feature of applicability to Beamlet from this high repetition rate laser is a Stimulated Brillouin Scattering (SBS) mirror used in this laser configuration to generate a phase conjugated beam which cancels out thermal distortions and allows the system to produce a nearly diffraction limited (1.1-1.15 times diffraction limited) beam at the high repetition rates.

If this mirror configuration could be adapted to Beamlet (Reference 3), and if the neodymium glass slabs could be adequately cooled, it is quite possible Beamlet could be modified to perform the mission of orbital debris removal.

1.3 Iodine Lasers

Single short (nanosecond) pulse high energy iodine lasers have been developed in Russia and Germany. Development in the U.S. has been limited to longer pulses (10 microseconds) at high energy (1 kilojoule). Currently in the U.S., the largest repetitively pulsed iodine laser has an output of 50 joules per pulse at a rate of one Hertz (Reference 4). This laser is currently being upgraded to 10 Hertz.

The ISKRA-V laser located at Arzamas-16 in Russia was built for inertial confinement fusion and has 12 amplifier chains. The total energy output of the system at a wavelength of 1.3 microns is 30 to 40 kilojoules in 0.4 to 2.0 nanoseconds. It was built for single pulse operation and is typically fired only once per day.

The ASTERIX IV laser located in Garching, Germany has six amplifier chains with an output of 1 to 2 kilojoules per chain with a pulse length of 0.1 to 4.0 nanoseconds. It also was constructed for single pulse operation.

1.4 Free Electron Lasers

Free Electron Lasers were first invented in the U.S. approximately 20 years ago. Since then, over two billion dollars has been spent developing these lasers at a large number of institutions. Yet the highest recorded output of any of these lasers in the U.S. has been only ten watts. However, the physics learned during these investigations and experiments indicates that these lasers have the potential for very high average power, high peak power in the micropulses of induction linear accelerator amplifiers, excellent beam quality, infinite wavelength tunability, and good efficiency.

At the Budker Institute of Nuclear Physics in Novosibirsk, Russia, a large free electron laser using a radio frequency linear accelerator has been built. This laser is reported to be capable of producing 10 to 100 kilowatts of average power in the wavelength region of 6.5 to 13 microns (Reference 5) in the near future. This laser use a race-track microtron for energy recovery, giving it a potential efficiency greater than 30 percent. It is designed to produce 10 to 30 picosecond pulses at a 2 to 45 Megahertz repetition frequency. This laser offers a high average power with good wavelength selection. However, a serious question exists concerning the ability of the micropulses to cumulatively ignite a plasma on a piece of orbiting debris due to the low energy in the individual micropulses.

1.5 Carbon Monoxide Lasers

Most of the current work in carbon monoxide lasers is taking place in Japan for industrial applications and in Russia for airborne missions. These lasers were researched in the U.S. in the '70s but were not pursued because of strong water vapor absorption of most of the laser lines. The carbon monoxide laser is the most efficient high energy laser in existence. However, for efficient operation, it must operate in the cascade mode and lase on most of its laser lines. This laser produces wavelengths from about 4.8 to 6.0 microns. When line selected to operate only on the lines that transmit well through the atmosphere at around 4.8 microns, the efficiency drops to a point that make the laser unattractive for use in the orbital debris removal mission.

1.6 Carbon Dioxide Lasers

Although there are no longer any operational pulsed high energy carbon dioxide lasers in the U.S., this laser technology is a very well developed and mature technology. This laser has high efficiency, relatively easy to build and operate, and good atmospheric transmission. However, for the mission of orbital debris removal, which requires the focusing of laser energy at a distance of over 1000 kilometers, the far infrared wavelengths of 10.6 and 11.2 microns give the carbon dioxide laser a disadvantage of a factor of more than 100 when compared to neodymium glass with a wavelength of 1.06 microns. All other factors being equal, a carbon dioxide laser would require more than 100 times the energy per pulse to create the equivalent power density on target as a neodymium glass laser.

Section 2

2.0 Neodymium Glass Laser System Analysis

After reviewing the aforementioned types of lasers and considering all of the important issues and requirements, the neodymium glass laser appears to be the most promising candidate for the orbital debris removal mission. This section will address some of the issues pertaining to this laser.

2.1 Repetitively Pulsed With SBS Mirror

The major issue for adapting neodymium glass lasers to the orbital debris removal mission is configuring them for long-term repetitively pulsed operation while maintaining good beam quality and cooling the laser glass slabs. These issues are addressed in Reference 2. Figure 1 shows a diagram of a laser amplifier using an SBS mirror for wavefront control. As long as the laser glass slab is kept reasonably cool, the SBS mirror will produce a phase conjugated reflection that will effectively cancel out thermal distortions in the glass and produce a near diffraction limited laser beam.

Figure 2 indicates the dimensions and layout of the rectangular glass slab. Figure 3 shows how the glass slab is mounted with the flashlamps and how the flashlamps and the slab are cooled with water. In this configuration, the light from the flashlamps must pass through the cooling water before entering the laser glass slab.

The output wavelength of neodymium glass can be frequency doubled with high efficiency using KD*P crystals. When implemented at high average power, the crystals must be cooled as shown in Figure 4.

Source: Reference 2

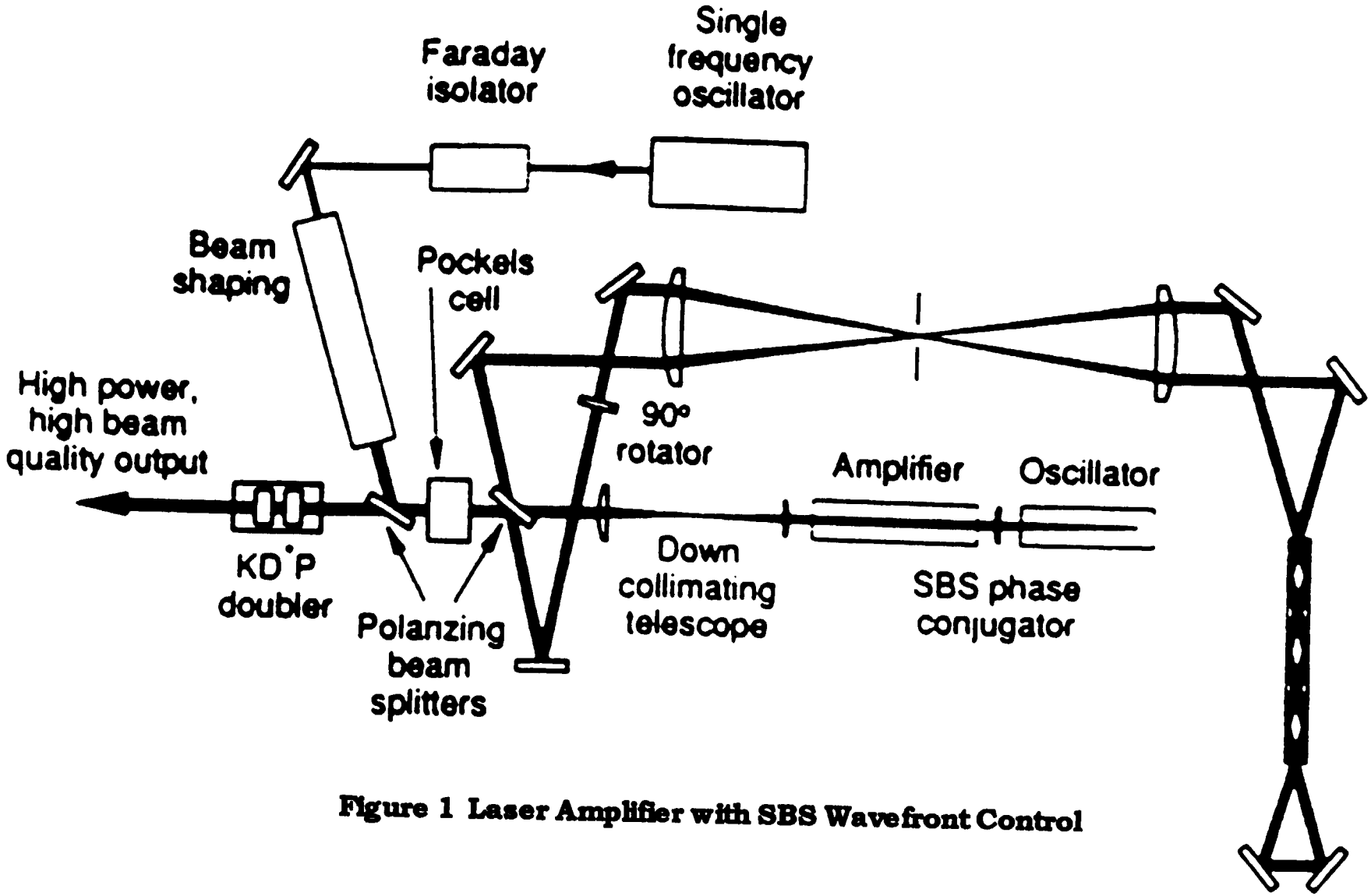

Figure 1 Laser Amplifier with SBS Wavefront Control

Figure 2 intentionally left blank

Source: Reference 2

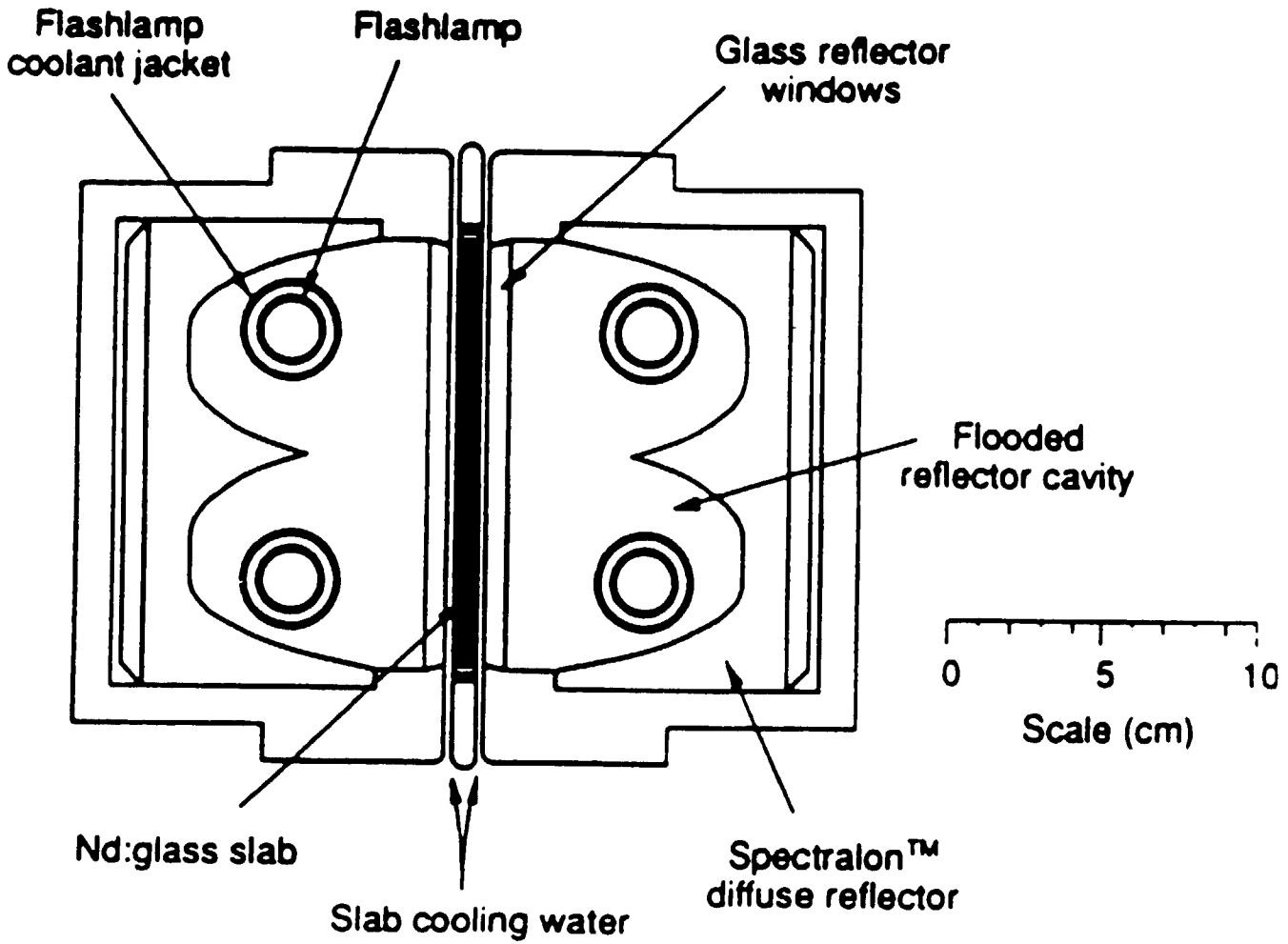

Figure 3 Flashlamps with Cooling Water

Figure 4 KD*P Doubling Crystals

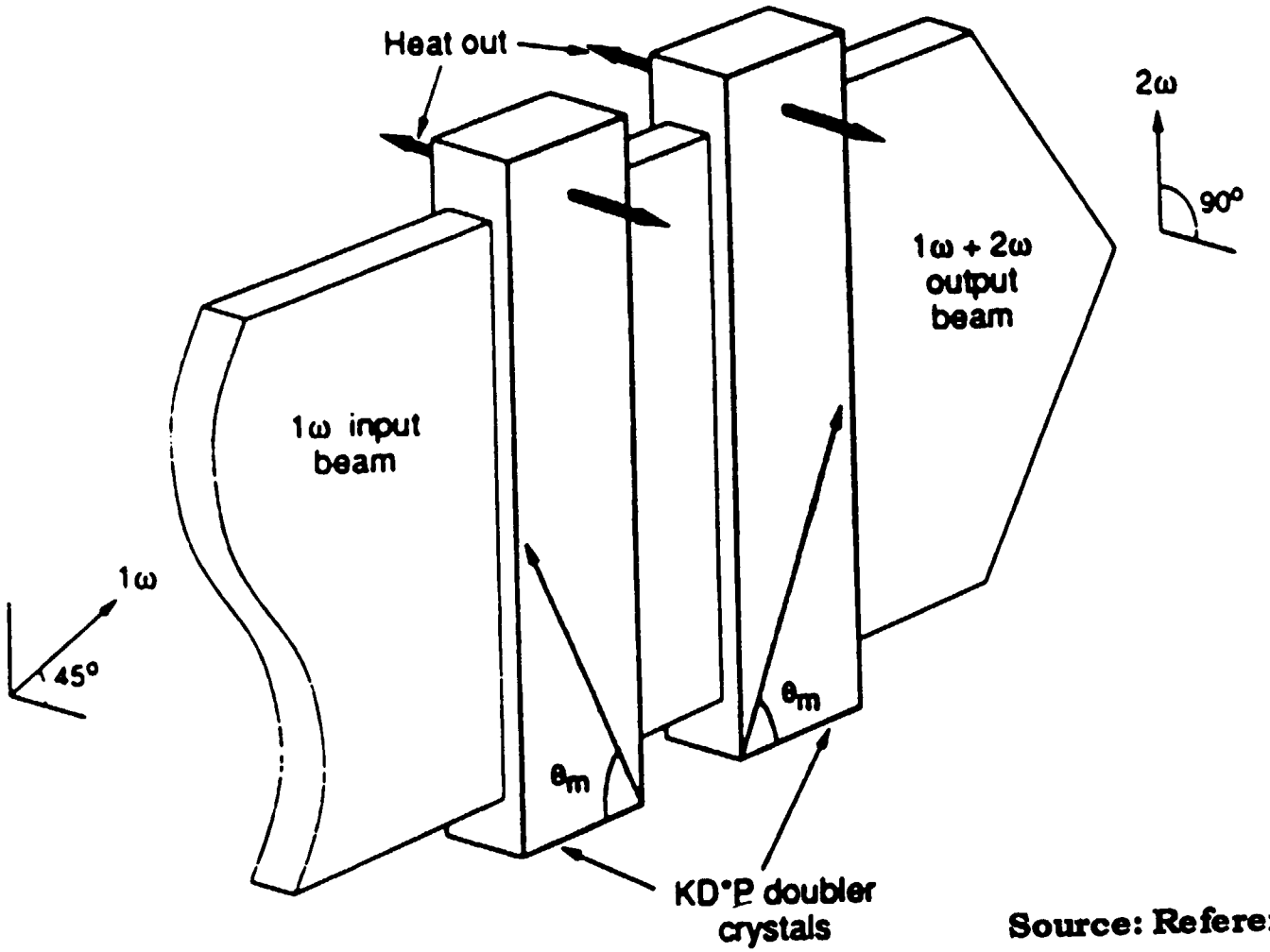

Source: Reference 2

2.2 Beamlet Prototype System Design

The most applicable laser for the orbital debris removal mission currently in existence and in operation today is probably the Beamlet laser at Lawrence Livermore National Laboratory. A schematic diagram of this laser is shown in Figure 5 (Reference 6). This laser is a single beam prototype of the laser chain designed for the NIF. A pulse is injected from a low power oscillator and a segmented back mirror adaptively adjusts to provide wavefront control to improve the beam quality.

This laser currently produces 17.3 kilojoules in 10 nanoseconds. This pulse energy may be increased by adding additional glass slabs and increasing the pulse length to maintain the peak power at a constant level well below the damage threshold of the glass surfaces.

Figure 5 Beamlet Laser System Configuration

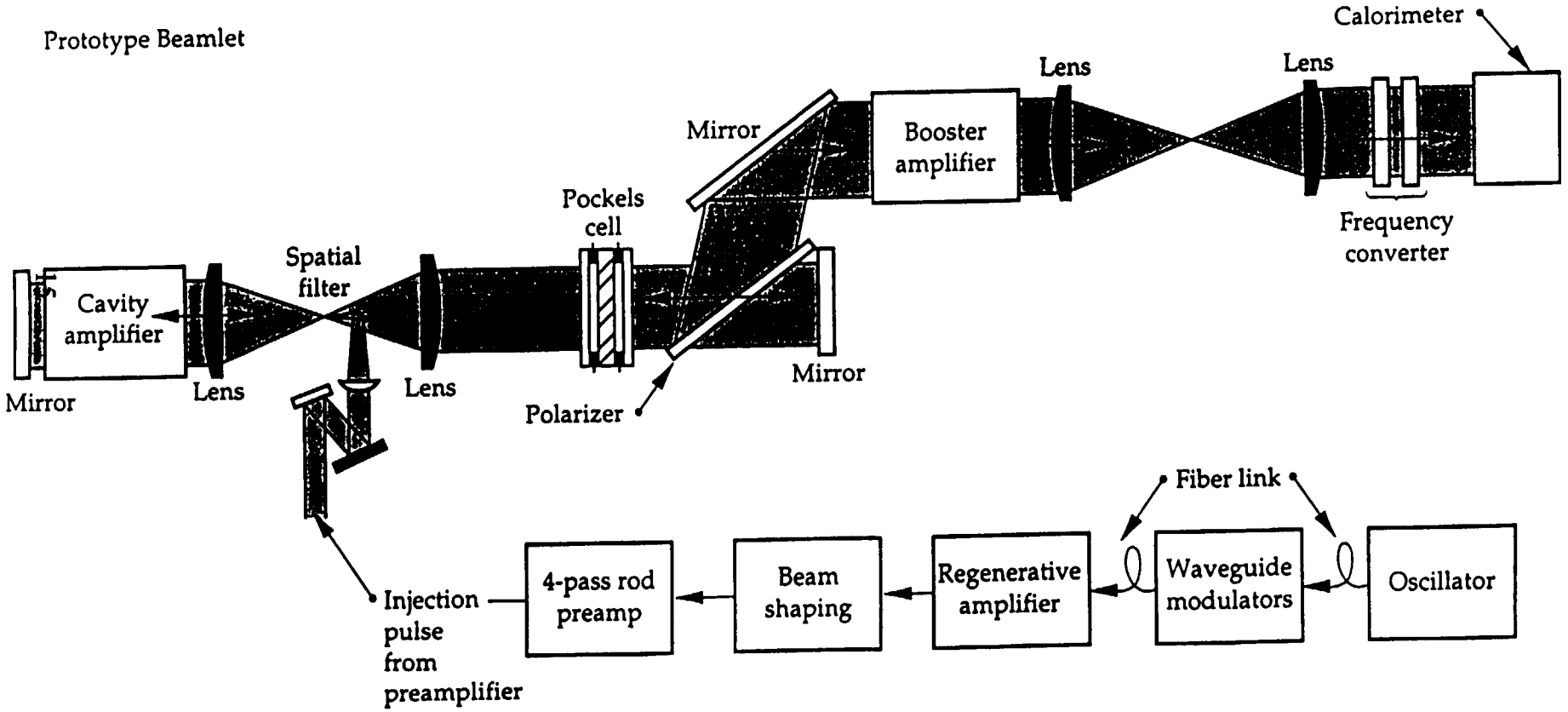

Source: Reference 6

2.3 NIF Laser System Design

The final configuration for a laser beam line of the National Ignition Facility is shown in Figure 6 (Reference 6). This configuration differs from Beamlet in that the pulse from the preamplifier is injected at the very beginning of the booster amplifiers. This allows the back cavity mirror to adaptively compensate for all the wavefront distortions though the entire system.

The current NIF design uses a segmented mirror to perform this task due to the very low planned repetition frequency. For the orbital debris removal mission, however, with its approximately one hertz repetition rate, the SBS mirror used in Reference 2 may be able to perform this function better and produce a higher beam quality.

Figure 6 NIF Laser System Configuration

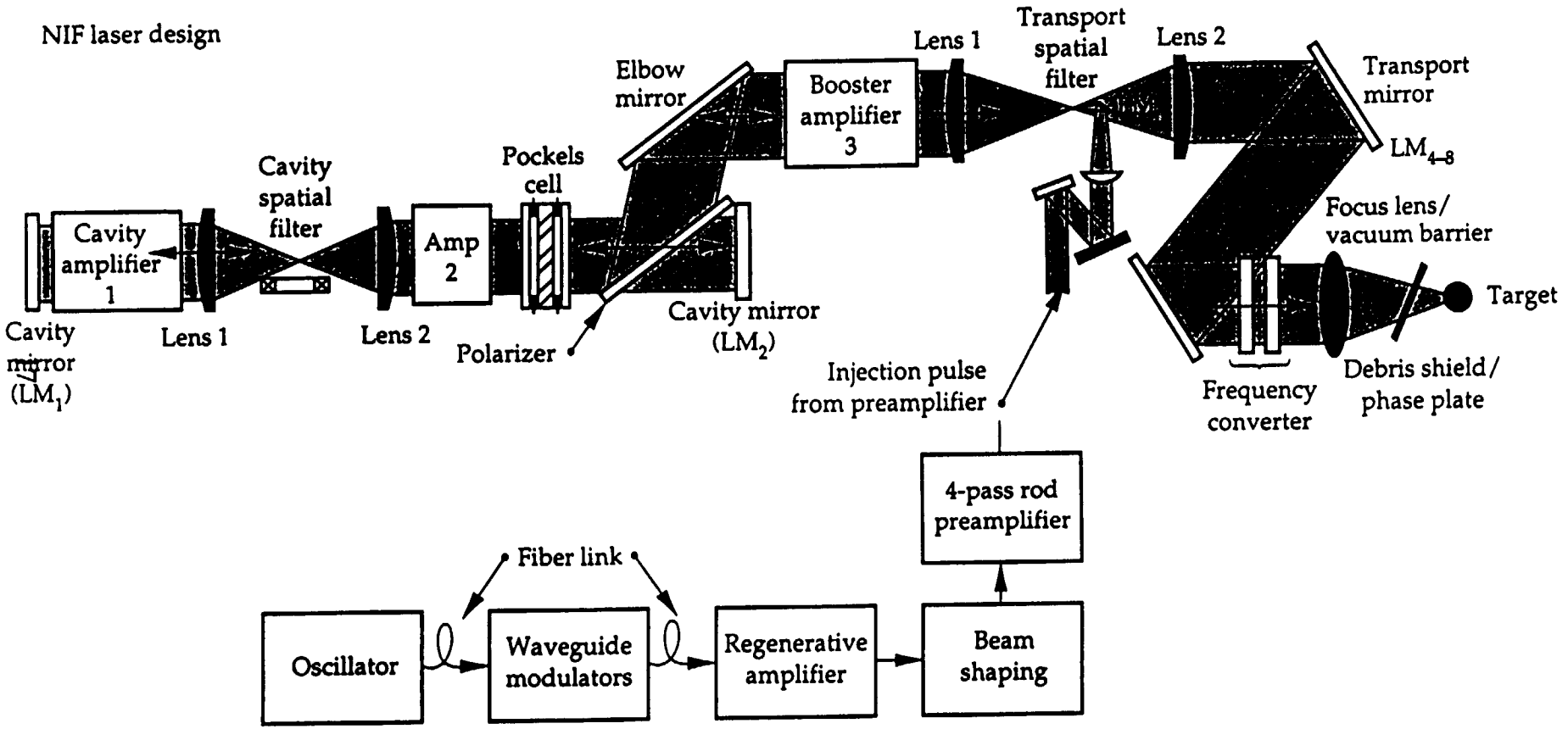

Source: Reference 6

2.4 Laser Slab Cooling Designs

A cross section of a disk amplifier in the Nova laser is shown in Figure 7(Reference 7). This diagram shows the location of the flashlamps surrounding the laser disks. This configuration is conducive to cooling the flashlamps with water, but not the laser disks. At best, the disks can be cooled by a slow flow of air through the main housing.

Figure 8 shows a configuration where the disks are cooled by gas flowing through channels on either side of the disks (Reference 8). A close-up view of these cooling channels is shown in Figure 9. These channels direct helium gas over the laser glass slab at a velocity of nearly 100 meters per second, removing heat and allowing the glass to be rapidly pulsed.

Figure 7 Disk Amplifier Cross Section

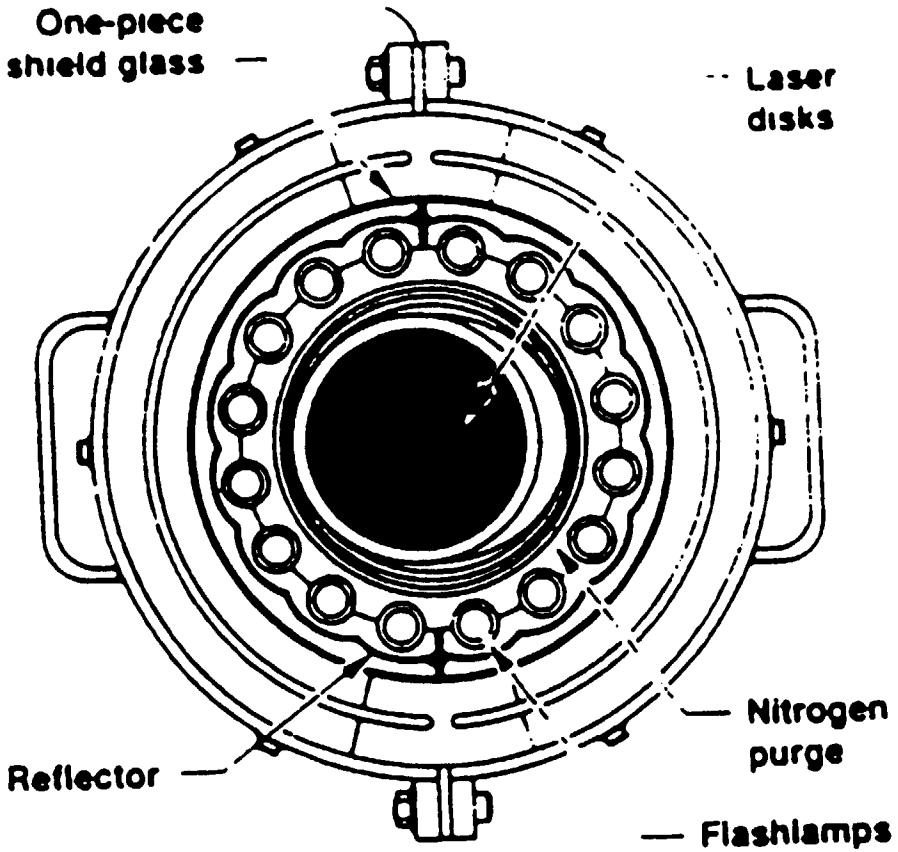

Source: Reference 7

Figure 8 Gas Cooling Flow Channels

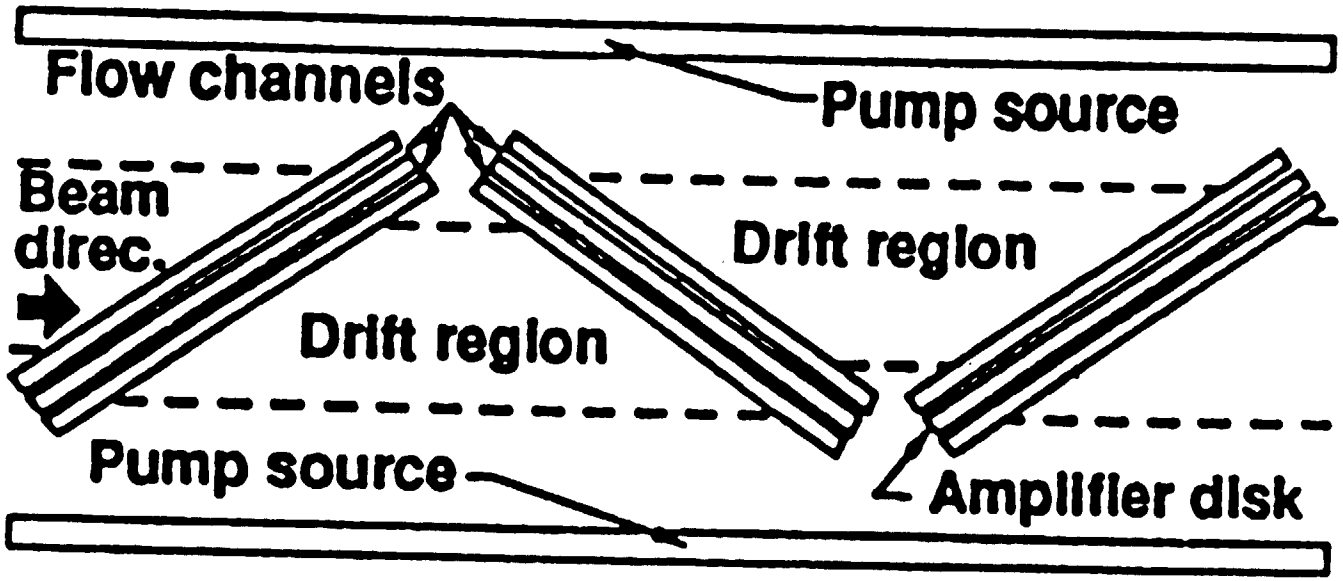

Source: Reference 8

Figure 9 Cooling Flow Geometry

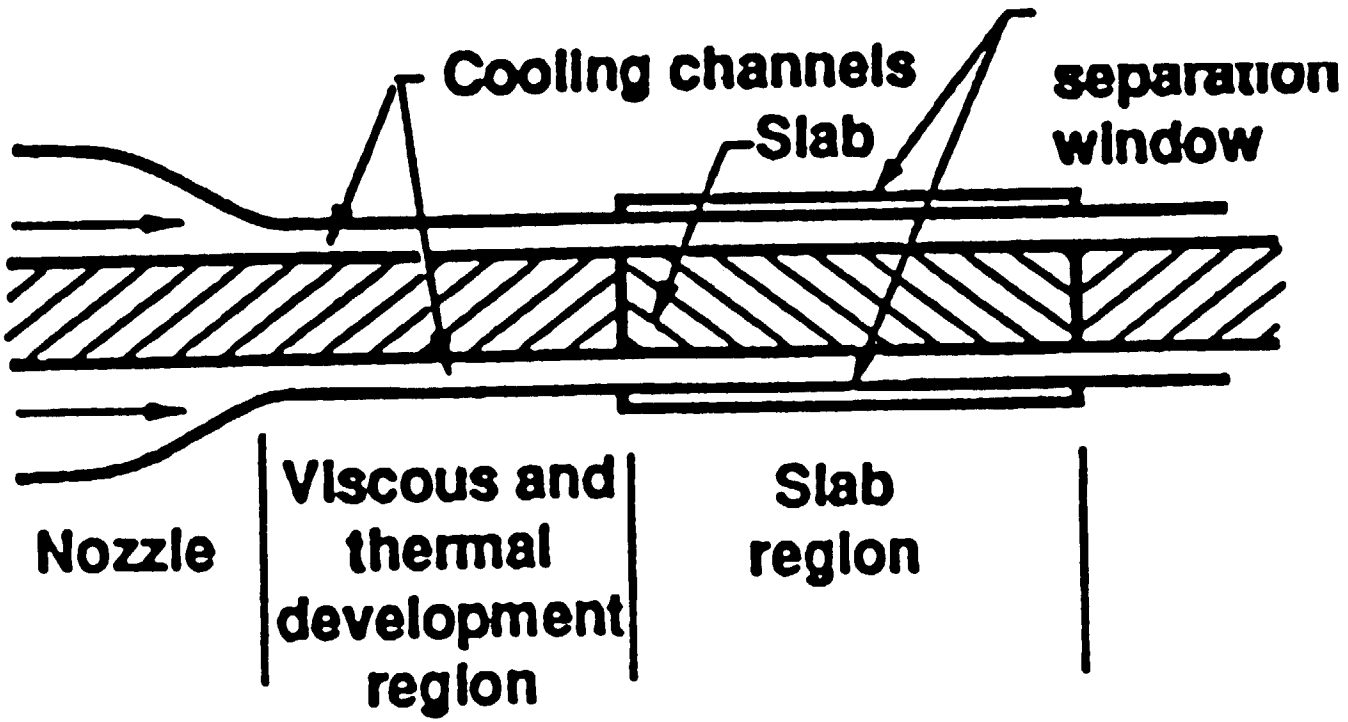

Source: Reference 8

REFERENCES

1. J.P. Reilly, Northeast Science & Technology, Private Communications, 1995.

2. C.B.Dane, L.E. Zapata, W.A.Neuman, M.A. Norton, and L.A. Hackel, "Design and Operation of a 150 W Near Diffraction-Limited Laser Amplifier with SBS Wavefront Correction", IEEE J. Quantum Electron., vol. 31, no. 1, pp. 148-163, 1995.

3. J.R. Murray, Lawrence Livermore National Laboratory, Private Communications, 1995.

4. R.A. Jones, Science Applications International Corporation, Private Communications, 1995.

5. G.I Erg et al., "Status of Novosibirsk High Power CW FEL", SPIE Vol. 2376, pp. 84-92, 1995.

6. B.M. Van Wonterghem et al., "System Description and Initial Performance Results for Beamlet", Inertial Confinement Fusion, Lawrence Livermore National Laboratory, vol. 5, no. 1, pp. 1-85, Oct.-Dec. 1994.

7. G.F. Albrecht, B. Comaskey, and L. Furu, "A 1.4-kJ Solid-State Power Oscillator with Good Beam Quality", IEEE J. Quantum Electron., vol 31, no. 1, pp. 164-168, 1995.

8. S.B. Sutton, G.F. Albrecht, and H.F. Robey, "Heat Removal in a Gas Cooled Solid-State Laser Disk Amplifier", AIAA Journal, Vol. 30, pp. 431-435, 1992.

APPENDIX G

BISTATIC DETECTION OF SPACE OBJECTS USING A COMMUNICATIONS SATELLITE SYSTEM

R.C. Raup
MIT, Lincoln Laboratories

ABSTRACT

This report considers bistatic surveillance systems that utilize an existing component of a communications satellite system. The communications satellite systems that are considered consist of a ground-based transmitter (the uplink) and one or more satellites (each with transponders). The surveillance system would detect and track other space objects. Possible surveillance system architectures include a space-to-ground system that utilizes the communications satellite as an incidental target illuminator and a ground-to-ground system that detects targets accidentally illuminated by the uplink. By reciprocity many principles of the space-to-ground system apply to a ground-to-space surveillance system that utilizes a special ground-based transmitter and the communications satellite transponder as a relay. This report emphasizes a space-to-ground surveillance system employed to detect low-earth-orbit targets.

Communications satellite transmitters operate at about 70 dB less (equivalent isotropically radiated) average power than the transmitters in most operational space-surveillance radars, so optimization of the space-to-ground surveillance system design is important. Various bistatic sensor principles, including forward-scattering enhancement of target cross section, are discussed in order to develop the intuitively best bistatic configurations. The detection performance of a bistatic sensor that relies on forward-scattering enhancement of the target cross section exhibits a weak dependence on parameters such as transmitter power and receiver aperture. The minimum detectable projected target areas are calculated for a number of hypothetical surveillance systems to illustrate the concepts.

In the near term, surveillance systems capable of detecting and tracking targets with projected areas of .1 m^2 or more in both low-earth orbit and high-earth orbit might be an appropriate technical goal. For low-earth-orbit targets the best performance might be obtained with a ground-to-ground system that utilizes the satellite uplink as a target illuminator. For high-earth-orbit targets a space-to-ground system operated at large bistatic angles might provide the best performance.

This work was sponsored by the National Aeronautics and Space Administration under Air Force Contract F19628-95-C-0002.

TABLE OF CONTENTS

LIST OF ILLUSTRATIONS

1. INTRODUCTION

A communications satellite both receives and transmits microwave radiation. These functions are accomplished by a transponder. The transponder receives the unlinked transmission from the ground, shifts it to another center frequency and downlinks it back to earth. This report concerns the question of how we could utilize an existing communications satellite system along with a specially constructed ground-based component to implement a sensor for the purpose of detecting and tracking other space objects. The hope is that some economy will be achieved by the dual usage of parts of the existing communications satellite system. Surveillance radars that make opportunistic use of existing radiation sources have been considered before. Sometimes they are called *parasitic* radars ([1], chapter 5).

If a new surveillance system needs to be built and a parasitic radar will do the job, then it might be cheaper because the transmitter already exists. For many years it has also been pointed out that because a new transmitter is not built, the operation of the parasitic radar cannot be detected. A new relevant factor follows from the modern need to conserve the radio spectrum. Independent sensor and communications systems require more bandwidth than a combined system that can share the spectral allocation. The reasons for revisiting this topic now include the promise of many new communications satellite systems operating with increased power levels.

Several architectures come to mind. The communications satellite transmission could illuminate a target and be scattered to an observer on the ground. The transmission of a special ground-based transmitter could illuminate a target and be scattered through the communications satellite transponder back to an observer on the ground. The uplink station transmission from the ground to the communications satellite could illuminate a target and be scattered back to an observer on the ground. In the last case the communications satellite is not directly involved. All of these candidate surveillance systems are worth discussing.

The candidates are all types of bistatic sensor systems. The transmitter and the receiver are not co-located.

- **space to ground** The communications satellite transmission scatters from the target. A special ground-based receiver is built to detect and track the target. The transmitter is free and an unusual bistatic geometry is realized. but we are stuck with whatever signal the communications satellite is transmitting.
- **ground to space** A special ground-based transmitter illuminates the target. Scattered radiation is boosted and relayed back to earth through the communications satellite's transponder. The communications satellite provides gain and an unusual bistatic geometry is realized, but the communications satellite's transponder must be reserved for surveillance use.

- **ground to ground** The ground-based transmitter that is providing the uplink to the communications satellite also illuminates a target. The radiation scatters to a special ground-based receiver. The transmitter is free.

This report concentrates on the space-to-ground surveillance system, but by a reciprocity principle most of the results also apply to a ground-to-space surveillance system.

Typical communications satellite transponders have bandwidths of 27 or 36 MHz and achieve a downlinked power flux of from 10^{-16} to 10^{-12} W/m^2 on the ground. These transmitters do not have the characteristics that a designer would choose for a space-based bistatic illuminator [2]. It is easy to argue that a surveillance system using a communications satellite transponder as the transmitter of a bistatic sensor to detect and track space objects would have to be carefully designed. If we were to place a modern space-surveillance radar transmitter from a ground system into geosynchronous orbit and operate it, it might place a power flux of 10^{-5} W/m^2 on the ground. Inevitably orbiting transmitters are radiating less power than an operational radar space-surveillance system typically utilizes. In fact, partly because space-based transmitters are more expensive than equivalent ground-based transmitters, the uplink transmitter in a typical communications satellite system is the most powerful transmitter in the system. Thus as the surveillance sensor model is developed in this report, various principles to optimize detection performance are uncovered and exploited. Some of these principles cannot be utilized by space surveillance systems without a space-based component. To our advantage, the power fluxes from communications satellite transmitters are larger than those produced by radio stars and the sun, two other microwave sources that have been studied as illuminators [3].

The main part of the report is found in the next section, where various tradeoffs in the surveillance system design are discussed. To validate some of the tradeoff principles an additional section is provided that includes performance curves. The report ends with a section of results and conclusions. Many relevant principles are collected together, and the detection performance of candidate surveillance systems are briefly evaluated so that this document will provide a useful reference.

2. SURVEILLANCE SYSTEM MODELING AND OPTIMIZATION

The first two sections of this part of the report involve manipulating the surveillance geometry in order to maximize the power flux at the observer. The assumption is that a larger power flux is better. More complex optimization principles require a detection model which is introduced in section 2.3. The detection model suggests that the time-bandwidth product of the surveillance system should be minimized which leads to the correlation receiver proposed in section 2.4. To implement a correlation receiver it is necessary to separate the receiver signal component due to the transmitter from the signal component due to target scatter. This separation is accomplished with the angular resolution of an antenna array described in section 2.5. Another result from the detection model justifies a particular configuration of the array which is discussed in section 2.6. The final section of this part of the report takes advantage of the fact that the target may be illuminated over several receiver antenna beamwidths to suggest methods of improving the detection performance.

2.1 The Forward-Scattering Effect

One interesting principle behind bistatic sensors is the angle diversity that can be exploited by arranging different angles between the transmitter, the target and the observer. This angle is called the *bistatic angle*. It has been known for some time that under suitable conditions a target's cross section at a bistatic angle of 180 degrees can be much larger than its cross section at a bistatic angle of zero degrees. When the bistatic angle is 180 degrees, the target's cross section is called its *forward-scattered cross section* and the phenomenon is called *forward scattering*. The case of a bistatic angle of zero is the usual *back-scattering* phenomenon, also called the *monostatic* case. Siegel [4] is often credited with showing that the forward-scattered cross section can be much larger than the monostatic cross section in the high frequency limit although the phenomenon was apparently described as early as 1908 by Mie [5].

The far forward-scattered field can be thought of as a diffraction phenomenon. It is pointed out in ([6], page 25.18) that by application of a diffraction principle (Babinet's principle) the target may be absorbing or conducting and in either case will produce a forward-scattered diffraction pattern. In [7] Glaser further argues that the behavior of the cross section near a bistatic angle of 180 degrees can be approximated by treating the projected area of the target as a uniformly illuminated aperture in an infinite plane. We can expect good agreement with these predictions when the size of the target is many times the wavelength of the radiation and the bistatic angle is very near 180 degrees. In this case, the forward-scattered cross section σ_f is given by

$$\sigma_f = \frac{4\pi A^2}{\lambda^2} \tag{1}$$

where A is the projected area of the target onto the plane normal to the line-of-sight, and λ is the wavelength of the radiation. The forward-scattered cross section falls from its peak value of σ_f as the bistatic angle becomes less than 180 degrees. The angular distance to the first null is approximately λ/d where d is the apparent extent of the target silhouette as measured in the plane of the angle.

The geometry is illustrated in figure 1. For concreteness, the values for a 20 cm diameter sphere illuminated by 20 GHz radiation are included as an example. If we specify that the target is a sphere then we also know its monostatic cross section. The ratio

$$\frac{\sigma_f}{\sigma_m} = \left(\frac{\pi d}{\lambda}\right)^2 \tag{2}$$

is the ratio of the forward-scattered cross section to the monostatic cross section for a sphere of diameter d illuminated by radiation of wavelength λ. This ratio quantifies the forward-scattering enhancement. For the 20 cm sphere and 20 GHz illumination the ratio is over 1000.

In figure 2, the value of $10\log(\sigma_f/\sigma_m)$ is plotted versus d/λ. The amount of forward-scattering enhancement increases with increasing d/λ. There are two ways to increase the ratio d/λ. We may fix λ and increase d. This says that larger targets benefit from more enhancement than small targets, a fact that is not particularly useful from a surveillance system design point of view. We would prefer that small targets with a small monostatic cross section receive most of the enhancement so that they are easier to detect. We can fix d and decrease λ, or increase the frequency of illumination, to increase the forward scattering enhancement. We have stumbled on the first useful tradeoff in a surveillance system that uses forward scattered radiation to detect a target. We will expect the surveillance system performance to increase as the frequency of illumination is increased. This will be verified through the system model later.

Even though equation 2 is specifically for a sphere and utilizes an expression that is only valid when $d \gg \lambda$, it correctly describes the qualitative effects of the phenomenon for other target shapes and smaller targets. Generally as a target's size decreases relative to the wavelength of the illuminating radiation, the forward-scattering enhancement becomes less pronounced. We need to keep the frequency of the illuminating radiation as large as we can to get an effective surveillance system.

The large forward-scattered cross sections exhibited by targets is a phenomenon that is too useful to ignore. We will explore geometries where the bistatic angle is nearly 180 degrees, expecting that this will result in a surveillance system with better detection performance against the target.

2.2 Power Flow and Geometry

We first compare the power flux that is available as bistatic scattering from a target with the power flux available through a clear reference path to the transmitter. In figure 3 the two paths are illustrated.

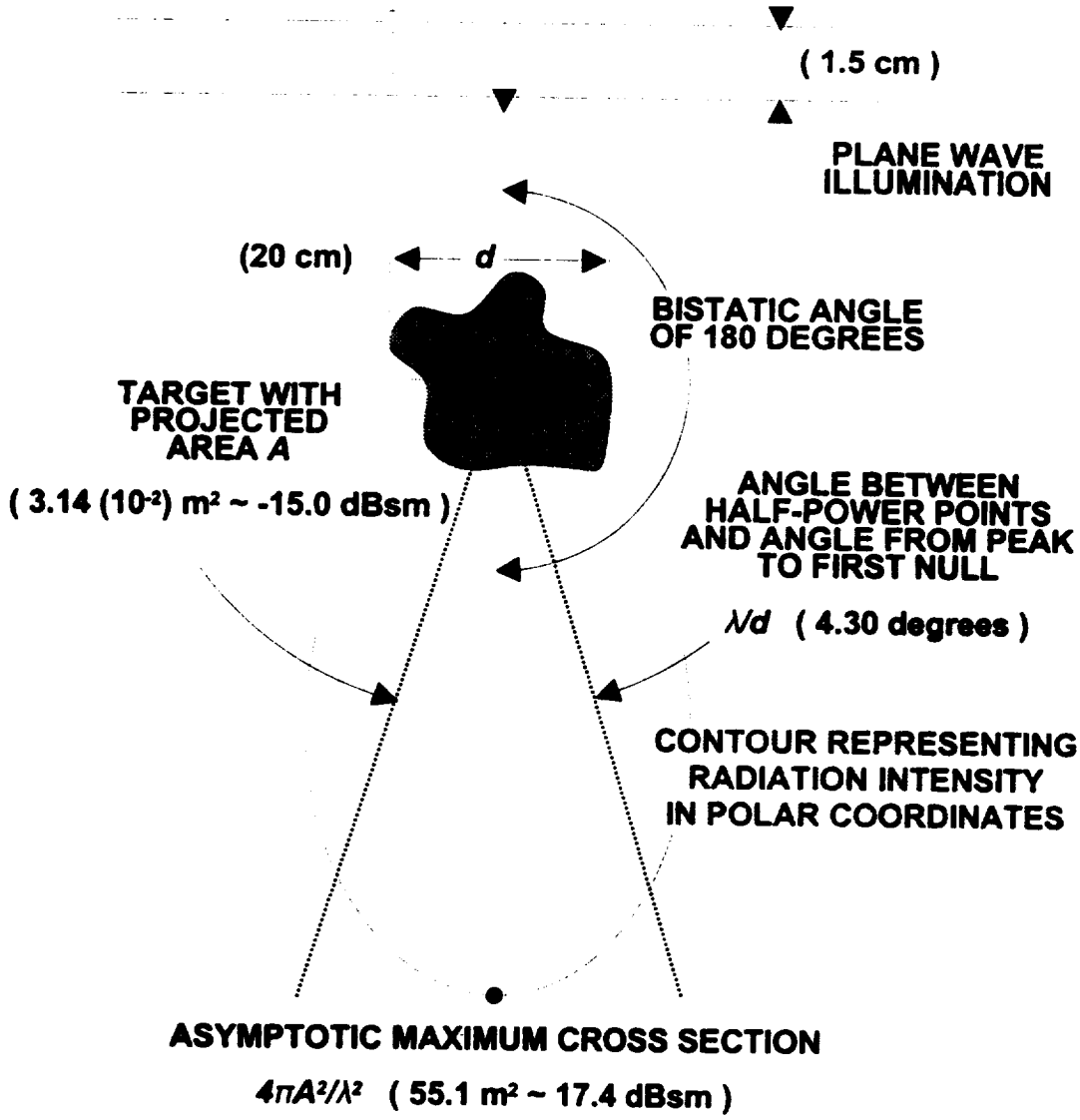

Figure 1. The cross section of a target that is large compared to the wavelength of the illuminating radiation has a much larger cross section at a bistatic angle of 180 degrees than it does at a bistatic angle of zero. The specific numerical values are for a 20 cm diameter sphere illuminated by 20 GHz radiation.

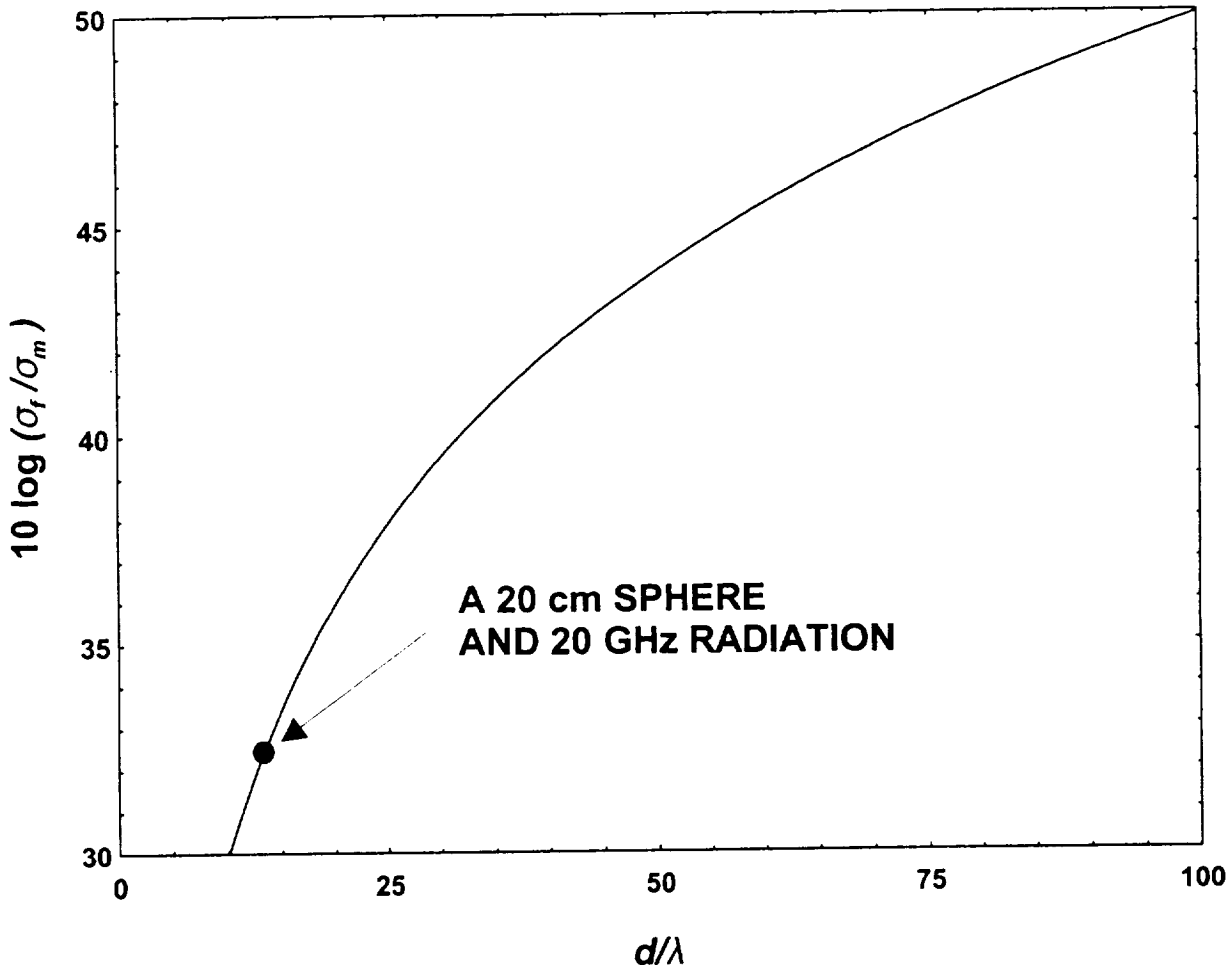

Figure 2. The forward-scattering enhancement depends on the diameter d of the sphere and the wavelength λ of the illuminating radiation. Larger targets undergo greater cross section enhancement through the forward-scattering effect than small targets. The enhancement also increases as the frequency of illumination increases.

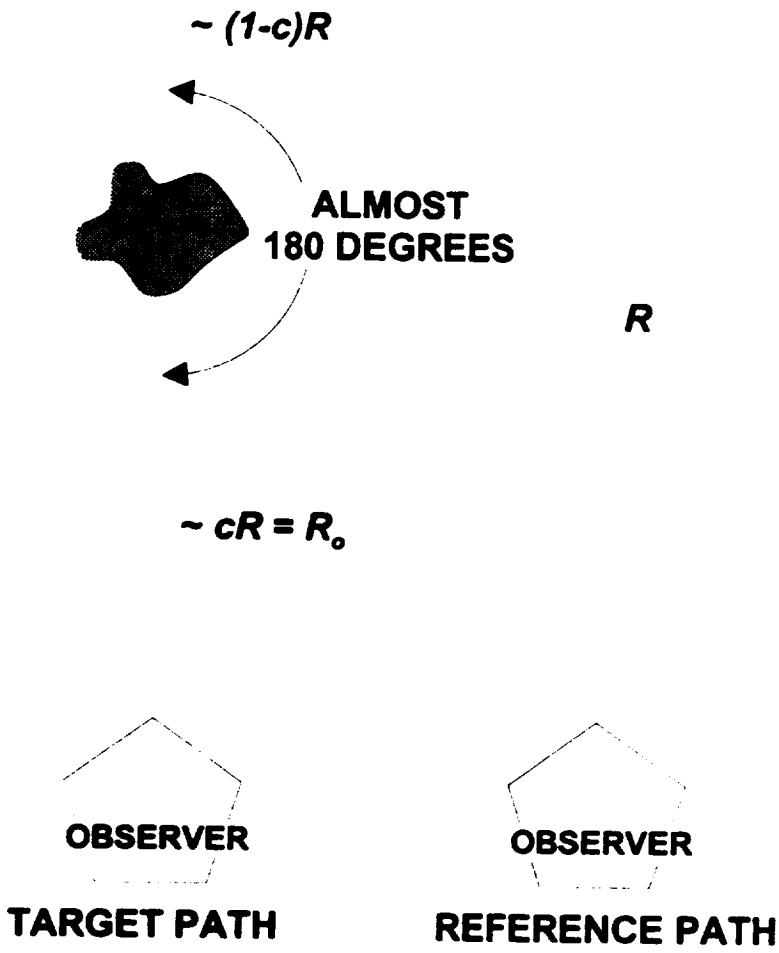

Figure 9. Power flow through a reference path and a target path are shown. The losses through the target path relative to the reference path change as the target is moved along the path or the length of the path is changed.

A reference power flux p_r seen by an observer at a distance R from a source with an equivalent isotropic radiation power (EIRP) W is

$$p_r = \frac{W}{4\pi R^2}. \tag{3}$$

The length of the reference path has been set equal to the total path length from the transmitter through the target to the observer. Thus the only difference between the two paths is due to the insertion of the target. The distance of the target from the observer is $R_o = cR$ where c takes a value between 0 and 1. The target has a cross section of σ_f. Then the power flux p_t seen by the observer *due only to the scattering effect of the target* is

$$p_t = \frac{\frac{W}{4\pi(1-c)^2R^2}\sigma_f}{4\pi c^2R^2} = \frac{W\sigma_f}{(4\pi)^2(1-c)^2c^2R^4} \tag{4}$$

The reader might wish to imagine that the target has been slightly displaced from the line-of-sight between the transmitter and the observer, and that the observer has enough angular resolution to observe the power scattered from the target independently of the power received directly from the transmitter. In this case the total path length through the target is longer than the reference path length and equation 4 becomes a lower bound on the true value.

The ratio

$$\frac{p_t}{p_r} = \frac{\sigma_f}{4\pi(1-c)^2c^2R^2} \tag{5}$$

is an indication of the power flux through the target path relative to a clear reference path in terms of the fractional height c of the target. We can think of this ratio as the penalty (or advantage) of attempting to receive the radiation through a target path instead of the clear reference path. In terms of the absolute target height R_o equation 5 becomes

$$\frac{p_t}{p_r} = \frac{\sigma_f}{4\pi(1-\frac{R_o}{R})^2R_o^2}. \tag{6}$$

Figure 4 shows graphs of $10\log(p_t/p_r)$ for $\sigma_f = 1$ as a function of c for LEO and GEO transmitters, and as a function of the transmitter height for a LEO target. The observer is on the ground. Note that the power flux scattered by the target is more than 100 dB below that which is received directly from the transmitter source. If targets with cross sections less than one square meter are considered then an additional attenuation occurs. For targets with one square centimeter of cross section the curves are 40 dB lower. Only values of c such that $.1 \leq c \leq .9$ are considered,

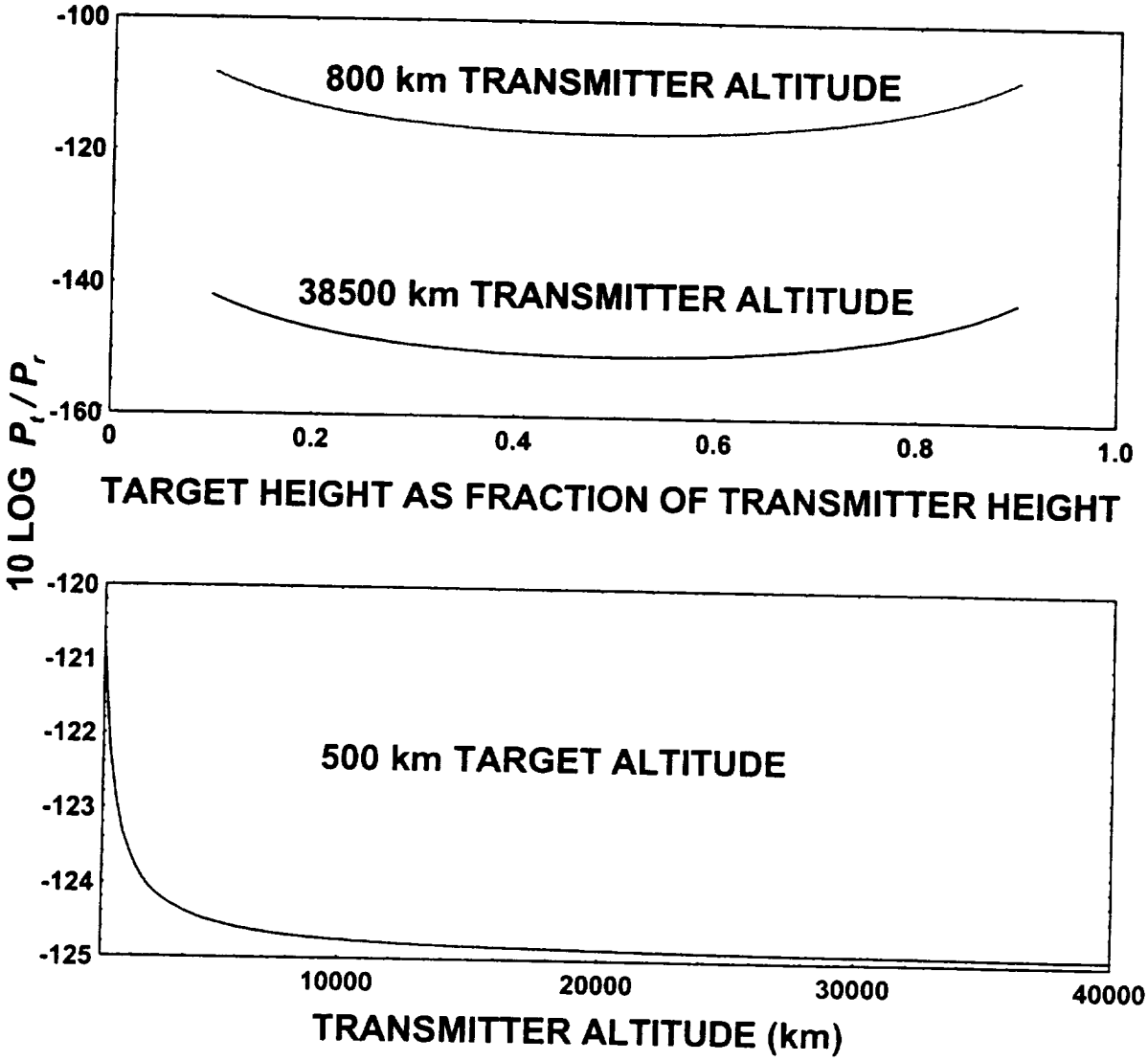

Figure 4. The power flux delivered through the target path relative to a reference path is shown as the target height and the transmitter height varies. Relative losses are smaller when the target is near the transmitter or the observer, or when the path length is shorter. The cases shown are for $\sigma_f = 1$.

because the isotropic radiation model used to obtain equations 3, 4, 5 and 6 is not valid very close to the antennas.

We have discovered a second important set of surveillance system performance factors. These factors are due to path length geometry. First, the relative losses through the target path can be reduced by observing a target near the transmitter or near the observer. The greatest relative loss occurs when the target is midway between the transmitter and the observer. The second consequence is even more interesting. Suppose that a geosynchronous transmitter and a near-earth transmitter were designed to place the same power flux at the ground level. This is reasonable if the transmissions are to be received by ground stations of similar size and cost. Let the target height be fixed. Figure 4 illustrates that the signal through the target path originating from the near-earth transmitter will be stronger even though the signals received directly from the two transmitters are of the same strength! The relative loss is a monotonic function of the transmitter altitude even though transmission power is varied to keep the direct power flux on the ground constant.

Can we design a receiver to detect the power scattered from the target? We might imagine that a receiver designed to receive the original direct communications satellite transmission would not be able to perform its communication function using a signal source that is 100 dB below the design point. The original communications satellite receiver was designed not only to detect the signal, but to demodulate the encoded data component which might represent a symbol rate of from several thousand to many million symbols per second. We only wish to detect the presence of the scatter from the target and, theoretically at least, we have all of the time that the target is visible to do it! In that sense our job is easier, but 100 dB is a large amount of loss to recover. We will need a detection model to see what really happens.

In addition, equations 5 and 6 reminds us that a large dynamic range is involved in any surveillance system that we build. When a microwave or laser radar is designed, the transmitter is almost inevitably constrained to release its energy in timed pulses. When the relatively powerful transmitter is not radiating, the receiver listens for the weak scattered return from the target. The communications satellite transmitter is a continuous-time radiator. If the communications satellite is used as a transmitter, then the radiation scattered from the target and the direct transmitter radiation fall on the observer simultaneously. The original transmission jams reception of the target scatter!

In this section we have discovered some geometric principles that can be used to increase the power flux on the ground due to the target scatter. Intuitively this could improve performance, but there are other issues to consider. Certainly the length of time that the target is illuminated by the transmitter may affect performance also. To be precise about the surveillance system's detection performance we will need a detection model. We must also remember that the assumptions of lossless processing used in the remainder of the report may not account for the difficulties that a practical design will face in the presence of the large dynamic signal range that we have documented in this section.

2.3 The Detection Model

In this section we discuss the detector. Because we would like to expose the tradeoffs among the receiver processing options that affect the time-bandwidth product characterization of the surveillance system, a simple energy detection, or radiometric, model is used. The principal parameterizations of this model are the signal energy, the noise power spectral density, the bandwidth and the observation time. It is true that additional assumptions regarding the characterization of the signal component can be used to predict better performance. For example, specific stochastic fluctuation models for target modulation could replace our bandwidth characterization. But the additional assumptions would have to be justified, and the resulting performance improvement would not change our conclusions about the suitability of the surveillance system for any purpose ([8], pages 101–106). The loss of generality that results from using specialized and incomparable detection models would also make it difficult to develop an intuitive understanding of the surveillance system tradeoffs that point us toward the best possible architecture for a particular application.

The detection problem consists of deciding between the following two hypotheses.

- **Hypothesis H_0:** Only noise is present at the detector input.
- **Hypothesis H_1:** Both signal and noise are present at the detector input.

The detector model is shown in figure 5. We make the usual assumption that the noise appears to come from an additive zero-mean Gaussian source. An early reference for the application of the model to the detection of deterministic signals is found in [9], while a more recent treatment can be found in [10], section 4.3. The following facts about the detector are taken from those references.

Suppose the input value is zero before time $t = 0$ and the detector bandwidth is B. When the detector is appropriately implemented, its output at some time $t = T$ is a chi-squared random variable whose degree of freedom is equal to twice the time-bandwidth product, or $2TB$. Under hypothesis H_0 the distribution is central, and under hypothesis H_1 the distribution has a non-centrality parameter value equal to the in-band signal energy E divided by the noise power spectral density n_0. Specifically,

$$H_0 : y(t) \sim \chi^2(0, 2TB) \qquad \text{and} \qquad H_1 : y(t) \sim \chi^2(\frac{E}{n_0}, 2TB). \tag{7}$$

In order to apply the output of the detector to the problem of deciding between H_0 and H_1 at time T, we compare the value $y(T)$ to a threshold. If $y(T)$ exceeds the threshold, then we declare H_1 to be true. Otherwise H_0 is assumed to be correct. This method is a standard one-sided binary hypothesis test. The threshold is chosen so that the probability of false alarm p_f (the probability of incorrectly choosing H_1 as true) is a small value. Then the probability of detection p_d (the probability of correctly choosing H_1 as true) is determined by the value of the non-centrality parameter E/n_0. All of these probabilities can be obtained from the distributions 7.

It will be convenient to write E/n_0 as

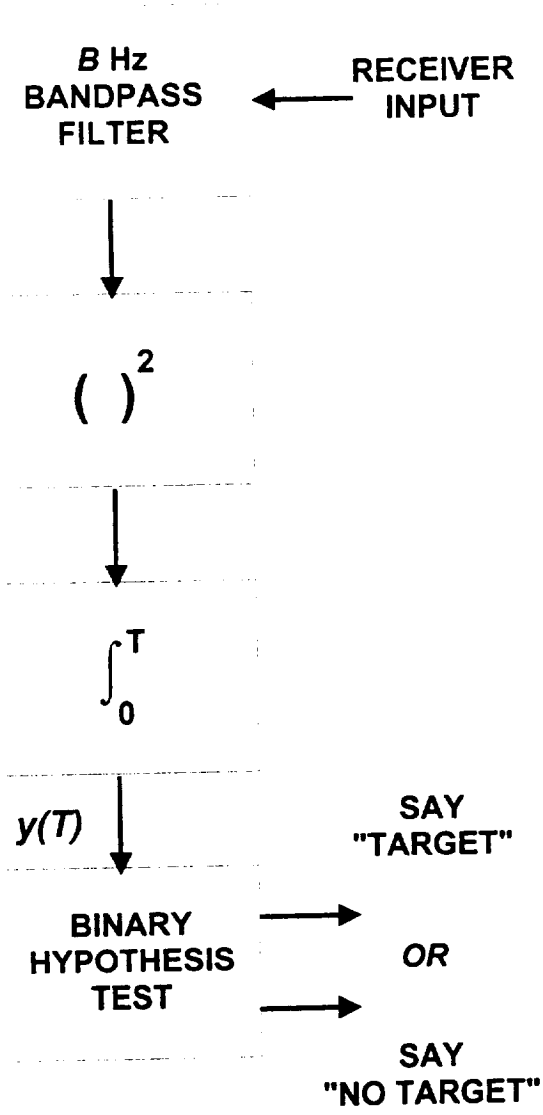

Figure 5. The detection model allows analysis of the surveillance system detection performance as a function of signal energy, noise spectral density, the bandwidth and the observation time.

$$\frac{E}{n_0} = \frac{p_t A_e T_d}{n_0} \tag{8}$$

where p_t is the power flux given by equation 4 due to target scattering that is seen by the observer, A_e is the observer's effective (antenna) aperture, and the signal energy is collected over a time duration T_d. Note that the time-bandwidth product TB that determines the distribution of $y(T)$ is characterized by a time T which represents the detector's time interval of operation. The value T_d may be less than or equal to T.

Changes in various scenario parameters will be studied in the remainder of the report. The effects on detection performance can be interpreted by understanding a few basic performance tradeoffs that are determined by the properties of the distributions 7 through manipulation of their parameters, the signal-to-noise ratio E/n_0 and the time-bandwidth product TB. For the best detection performance we want the probability of detection p_d to be as large as possible for a small given probability of false alarm p_f.

Performance improves when the signal-to-noise ratio is increased. In terms of our model, the signal-to-noise ratio can be increased by increasing the amount of signal energy collected (increasing the numerator of the right-hand side of equation 8), or by decreasing the value of the noise power spectral density n_0 (decreasing the denominator of the right-hand side of equation 8). Few readers would find this counter-intuitive. Less often considered is the fact that the detection performance can be improved by decreasing the time-bandwidth product. This feature of the problem is numerically illustrated in figure 6.

Figure 6 shows the probability of detection as a function of the time-bandwidth product for fixed values of the signal-to-noise ratio and the probability of false alarm. An increase in the time-bandwidth product increases the total noise energy, given by the product TBn_0. If not offset by an increase in signal-to-noise ratio, detection performance suffers.

On the other hand, if $T = T_d$ and the time-bandwidth product is increased by increasing the value of T, then the signal-to-noise ratio is also increased through equation 8. In this case some improvement in detection performance is observed. The greatest performance increase is obtained when the signal-to-noise ratio is increased by increasing $T_d = T$while keeping the time-bandwidth product fixed. This can be done provided that the bandwidth B is reduced accordingly. When the signal is a constant of duration T_d, its bandwidth is approximately $B = 1/T_d$, so that the time-bandwidth product TB remains unity as T_d increases with $T = T_d$.

A typical communications satellite transponder has a significant bandwidth, and although it is possible theoretically to directly apply the detection model to such signals, the large detection bandwidths would provide the worst performance of all reasonable surveillance systems. The communications satellite transponder signal has a constant amplitude, or envelope, by design so that it is possible to implement a correlation type of receiver designed to recover the constant envelope of the signal. This constant envelope can be applied to a detector with an ideal time-bandwidth value of unity. In reality the envelope will be modulated by target cross-section fluctuations due

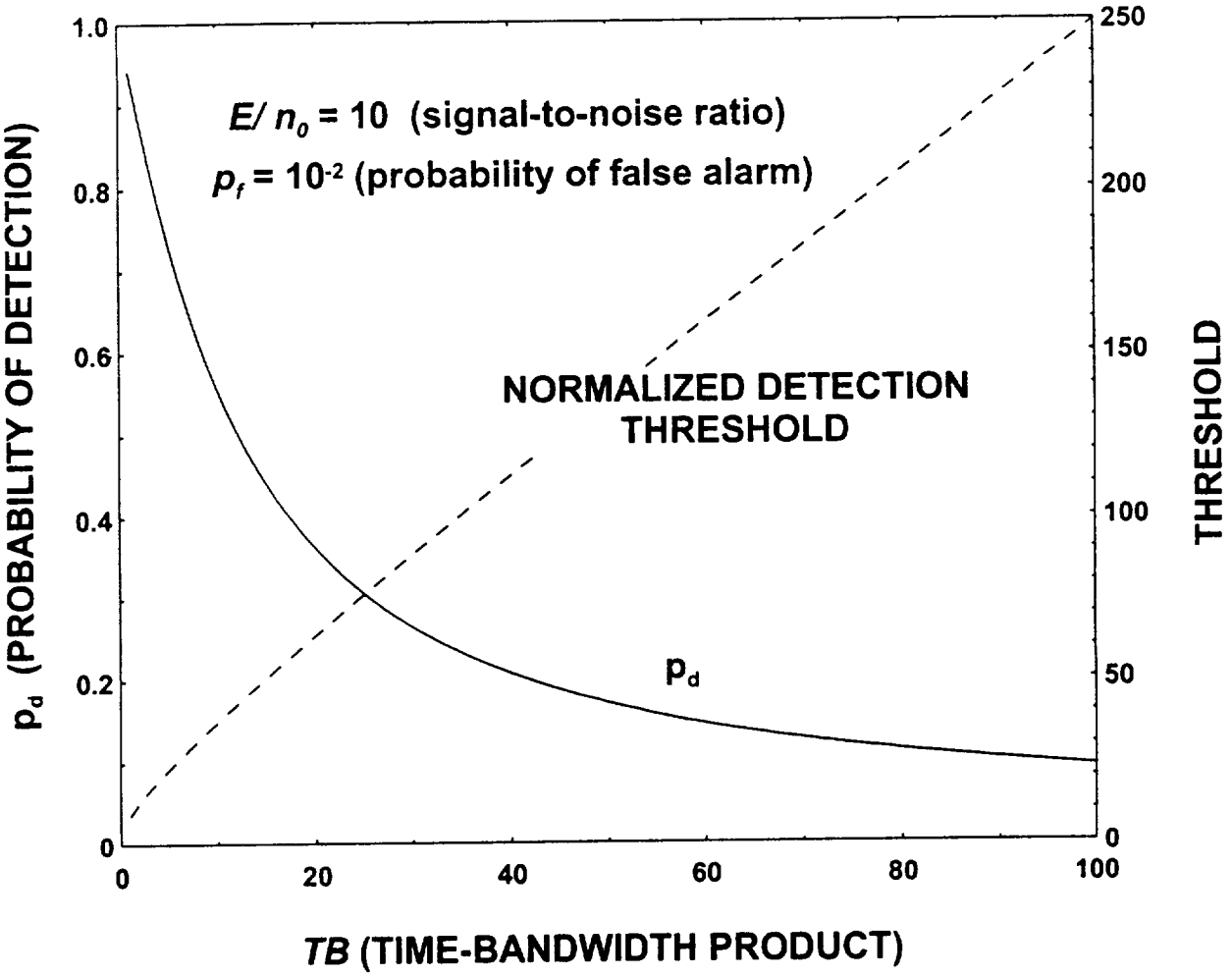

Figure 6. Changes in the time-bandwidth product causes detection performance to change. A signal-to-noise ratio of 10 provides useful detection performance only if the time-bandwidth is nearly minimum.

to the changing aspect of a rotating target and the slowly changing observation geometry, but this should be limited to a few hundred Hertz at worst.

For these reasons, only correlation receivers are considered in the remainder of the report. Other minimal time-bandwidth receiver implementations may be possible, but their detection performance cannot be significantly better. The scenario parameterization changes are limited to those that affect the signal-to-noise ratio.

2.4 The Correlation Receiver

Figure 6 shows us the folly of contemplating any large-bandwidth sensor system. Generally we must tolerate any envelope bandwidth that is due to the target cross-section fluctuation. Depending on the scattering properties of the target and changes in geometry the bandwidth could be 100 Hz or so, and quickly dominate the bandwidth due to the signal duration. The bandwidth due to the signal duration is roughly the reciprocal of the time that the target spends in the detection cell, so the smallest time-bandwidth product is unity. At all costs we must avoid the communications satellite system's modulation bandwidth which is typically 27 or 36 MHz. The time-bandwidth product can only approach unity if there is no target cross-section fluctuation because, in this case, the signal bandwidth is approximately the reciprocal of the signal duration. Thus the next principle that we employ to improve the surveillance system detection performance is to compress the available signal energy into the smallest possible bandwidth.

The principles of the correlation receiver are illustrated in figure 7. Assume that the signal due to direct transmission from the satellite transmitter and the signal due to target scatter can be separated in the receiver. A principle of separation will be discussed in section 2.5. The direct transmission from the communications satellite is received with a large signal-to-noise ratio and can presumably be recovered almost exactly. If it is appropriately delayed to account for path length difference and *mixed* with the signal component due to the target scatter, the envelope modulation of the resulting signal will be due to the target cross-section fluctuation. The resulting low-bandwidth signal can be applied to the radiation detection model.

The relative delay between the signal components due to target scatter and the direct transmission is due to the path length difference. Presumably we know where the transmitter is, so the path length through the target can be estimated, placing the target somewhere on an ellipsoid. With an estimate of the direction to the target intersecting the ellipsoid the target's position in three-dimensional space has actually been estimated.

2.5 The Antenna Array

In order to implement the correlation receiver we need to isolate the signal due to the transmitter from the signal due to target scatter. It has already been pointed out that when the communications satellite is used as the surveillance system transmitter, the radiation from the transmitter and the scattered radiation from the target will fall on the observer simultaneously. They do not result in identical signal components, but the radiation from both sources are continuous. Thus we

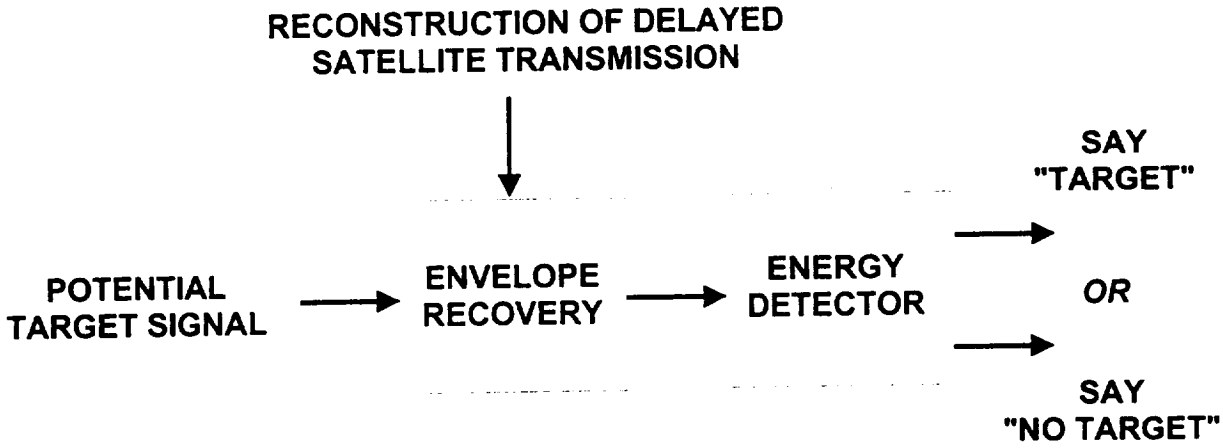

Figure 7. The signal received directly from the transmission source, which is resolved from the target in angle, is reconstructed, delayed and used to recover the envelope of the signal due to target scatter. The resulting relatively low-bandwidth signal is applied to the energy detector.

cannot trivially separate the signal due to target scattering from the signal due to the transmitter by time demultiplexing, as we would do in an active sensor with a transmitter that releases its energy in discrete pulses.

Can the two signals be separated in frequency by a simple bandpass filter? The signal due to target scattering will be Doppler shifted relative to the signal associated with the transmitting source. It is difficult to imagine cases where the Doppler shift will exceed .01% of the center radiation frequency and typically it will be much less. Because the transmission sources are communications devices carrying information, their radiation bandwidths exceed the expected Doppler shifts by a fair margin. The spectra of the transmission source radiation and the target scatter will be overlapped so we cannot separate the signal due to target scattering from the signal due to the transmitter by simple frequency demultiplexing with bandpass filters.

Angle demultiplexing remains a possibility. We have already established that the target and the transmitter as seen by the observer can be separated as much as a few degrees without seriously reducing the forward-scattering enhancement. Therefore we assume that the surveillance system employs a principle that allows the various radiation sources to be separated in angle. An antenna, or an array of antennas, with sufficient physical extent to provide the required angle resolution would suffice. We will assume a multiple element array, because it includes a single element antenna as a special case.

By reciprocity the array might be part of the transmitter or the receiver. The advantage of a ground-based transmitter and array clearly resides in the fact that the transmission waveform can be designed. In this case, the ground-based transmission scatters from the target to the communications satellite and is relayed back to earth through the satellite's transponder. Ground-based transmitters somewhat more powerful than the communications satellite transmitter can be easily built at low cost. The ground-based bistatic transmitter can still be less powerful than a conventional monostatic transmitter because of the forward-scattering enhancement. The disadvantage of the ground-based transmitter lies in the fact that a transponder would need to be reserved for the exclusive use of the space surveillance system. In the remainder of this section the space-to-ground option is assumed. The emphasis is also on the detection of LEO targets.

A conceptualized antenna array is shown in figure 8. There are N^2 parabolic elements in the

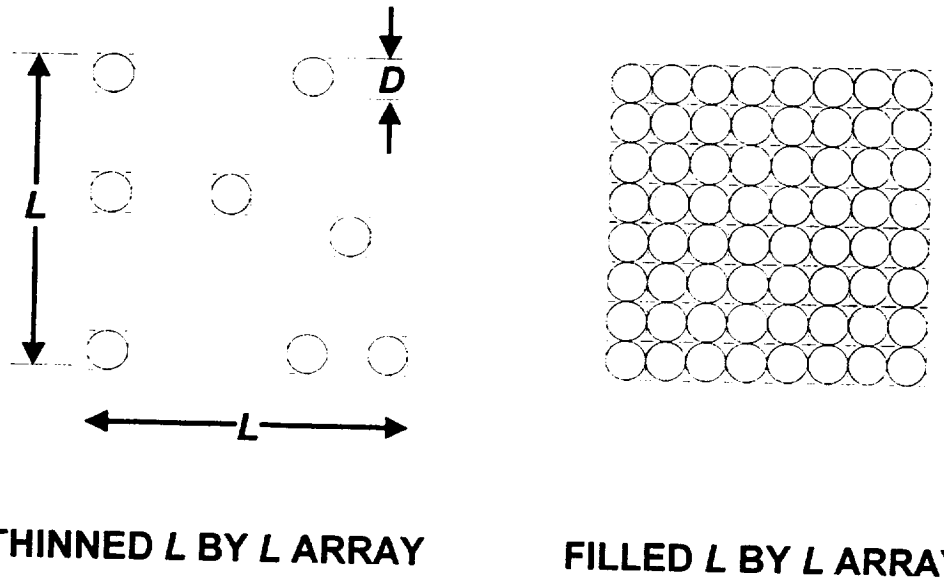

Figure 8. The conceptualized antenna array consists of a square array of parabolic elements. The best detection performance is obtained when the array is filled.

filled array, each with a physical aperture of $\pi D^2/4$. Thus the total physical aperture of the filled array is

$$A_p = \frac{N^2 \pi D^2}{4} = \frac{\pi L^2}{4} \tag{9}$$

where $L = ND$ is the size of the array. Because each side of the array is L units long, the angular resolution Δ of the array is

$$\Delta = 2\sin^{-1}\frac{\lambda}{2L} \simeq \frac{\lambda}{L} \tag{10}$$

where λ is the radiation wavelength. The approximation in equation 10 is valid for small values of angle. From aperture sampling theory the unambiguous field-of-view of the array is $N\Delta$ by $N\Delta$, and within this field-of-view N^2 distinct *beams* can be formed in parallel fairly efficiently with, say, multidimensional fast Fourier processing. When we say that two objects can be resolved in angle we mean that they are separated in angle enough to be observed in the main lobe of distinct beams, a value of approximately at least Δ.

Notice that the number of antenna elements N and their diameter D have dropped out of equations 9 and 10. Once we have decided on the type of array that we want to use, then the physical aperture and the angular resolution depend primarily on the size, or real estate, associated with the array. In the remainder of the report we will generally tradeoff aperture and angular resolution in order to investigate the detection performance of a lossless surveillance system. The tracking performance, the effect of processing losses and the cost of the surveillance system are not analyzed. These issues would be more directly affected by the tradeoffs between element size and the number of elements.

If the power flux at the antenna is specified, say in units of W/m^2, then it is tempting to multiply the power flux times the physical aperture of the antenna to determine the collected power. Because of losses this is not a good approximation of the collected power. Instead an effective aperture A_e is used to scale the power flux to obtain collected power. We write

$$A_e = \eta A_p. \tag{11}$$

For a parabolic antenna an efficiency η of .5 or greater is not uncommon.

Without justification we have completely filled the array with antenna elements that were placed closely together. We could imagine thinning the array by deleting elements in the interior of the array, or increasing the separation between antenna elements. In section 2.6 it is shown that the filled array provides better detection performance.

2.6 Aperture and Detection Time

The product of the effective aperture A_e and the target detection time T_d, the aperture-time product, can be altered by the configuration of the antenna array. We know from section 2.3 and equation 8 that if we can maximize this product without adversely affecting the values of other variables that determine the signal-to-noise ratio and the time-bandwidth product, then we can improve performance. What array characteristics maximize the aperture-time product, and hence

improve target detectability? In this section we show that a filled array is associated with the largest aperture-time product.

First we consider how to manipulate the array characteristics to increase T_d. If we continue to restrict ourselves to detection of the target within a single beam, then the detection time is limited to the time that the target is in the beam. The spot diameter of the beam s at a range R_o from the observing array of diameter L is

$$s = 2R_o \tan \frac{\Delta}{2} \simeq R_o \Delta \tag{12}$$

where the resolution Δ is given by equation 10.

If we assume that a target flies through the center of the spot at velocity v normal to the line-of-sight from the observer, then the detection time T_d is given by

$$T_d = \frac{s}{v} = \frac{2R_o}{v} \tan \frac{\Delta}{2} \simeq \frac{R_o \lambda}{vL} \tag{13}$$

Hence the target detection time depends on the size of the array, and the smaller the array the longer the detection time.

Then how can we maximize the effective aperture A_e for an array of a given size? Within the context of our simple array of parabolic elements, we obtain the maximum effective aperture by completely filling the array, placing the elements as closely as possible. We would not want to thin the array, because any such configuration leads to an array with a smaller aperture-time product. The analogy holds with other array element types.

Thus it seems clear that if we wish to increase the size of the array, then in order to maintain the largest possible aperture-time product we must add elements to the array as it grows, keeping it filled. If we want to reduce the number of elements in the array, then in order to maintain the largest possible aperture-time product we must decrease the size of the array, keeping it filled.

We can now consider how the aperture-time product changes as the filled array grows. Closer examination of equations 9, 11, and 13 reveals that

$$A_e T_d \simeq \frac{\eta \pi L R_o \lambda}{4v} \tag{14}$$

so that the aperture-time product grows about linearly with the array size L. This is less than the quadratic growth of the aperture alone because target detection time is decreasing. The consequence is that the detection performance does not grow as fast with increasing array size as in the monostatic surveillance case.

We have used the detection model to justify the previous decision in section 2.5 to fill the antenna array. In general we will want an array with the largest possible effective aperture for its physical size. Thus another principle that we will apply to the surveillance system in order to improve its detection performance will be to use antenna arrays associated with large aperture-time products.

2.7 Trajectory-Based Predetection Processing

Once we have maximized the detection performance for a target passing through a single array beam, we wish to consider how the results are extended to multiple array beams — a super-beam. Suppose that the surveillance system, when attempting to detect a target passing through a single beam, processes k independent detection tests per unit time. With a probability p_f of a false alarm from each test, the expected number of false alarms F_1 for the single beam detection system in T time units is

$$F_1 = p_f k T. \tag{15}$$

Now suppose that j possible target trajectories, each traversing exactly m array beams are postulated. For the trajectory that actually corresponds to the target motion, the duration of the signal becomes approximately mT_d, ignoring the fact that the target actually dwells a different time in each beam. The time T_d is the target dwell time in a single beam. Then the signal-to-noise ratio E/n_0 becomes

$$\frac{E}{n_0} = \frac{p_t A_e m T_d}{n_0}, \tag{16}$$

an improvement in the signal-to-noise ratio by a factor of m over the single-beam case. If we continue to assume that $T = T_d$ and that $B = 1/T$ then the time-bandwidth product remains at unity and the improvement in signal-to-noise ratio will directly improve the surveillance system detection performance.

Note however that the surveillance system is presumably now performing jk detection tests per unit time, so that the expected number of false alarms F_m for the m beam trajectory case becomes more like

$$F_m = p_f j k T, \tag{17}$$

ignoring the fact that the trajectories may not be completely independent. To keep the expected number of false alarms per unit time constant, the detection threshold could be adjusted so that the probability of false alarm is reduced to p_f/j and part of the benefit of the increased signal-to-noise ratio would be lost. Overall detection performance will still improve as the number of

beams processed before detection is increased, provided j is not too large. Another approach is to allow the false alarm rate to rise, at least a bit, and employ postdetection data processing to eliminate most of the false alarms. Our final principle for improving the detection performance of the surveillance system is therefore the application of trajectory-based predetection processing.

3. SURVEILLANCE SYSTEM PERFORMANCE

The modelling elements of the previous section may be combined to solve for the minimum detectable projected target area. Assume that

p_t is the power flux that the target scatters onto the observer.

p_r is the power flux that the illuminator could place directly on the observer,

R_i is the distance from the illuminator to the target,

R_o is the distance from the observer to the target,

R_r is the distance from the observer to the illuminator,

σ is the cross section of the target,

z is the signal-to-noise ratio E/n_0,

K is the Boltzmann constant, and

T_s is the characteristic temperature of the receiver.

Now using an isotropic scattering model as in equations 3 and 4 it is possible to write

$$p_t = \frac{p_r R_r^2 \sigma}{4\pi R_i^2 R_o^2} \tag{18}$$

so that

$$\sigma = 4\pi \left(\frac{R_i R_o}{R_r}\right)^2 \frac{p_t}{p_r}. \tag{19}$$

Equation 19 is valid for any bistatic angle. In most cases we are interested in the minimum detectable projected target area for bistatic angles near 180 degrees. This value is obtained by setting σ_f equal to the value of σ obtained from equation 19 and solving equation 1 for A. In this case we also set $R_r = R_i + R_o$ and obtain

$$A = \frac{R_i R_o \lambda}{R_i + R_o} \sqrt{\frac{p_t}{p_r}} \tag{20}$$

By definition of the receiver system temperature

$$n_0 = K T_s, \tag{21}$$

and from equation 16

$$p_t = \frac{zn_0}{A_e m T_d}. \tag{22}$$

With substitutions from equations 9, 11, 13, 22 and 21 it is possible to obtain the minimum detectable target cross section from equation 19 or the minimum detectable projected target area from equation 20. The value of z used should be the one that provides the smallest acceptable probability of detection for a given rate of false alarm.

The graphs in this section are obtained with the exact forms of equations 10, 12 and 13, but the small angle approximations available for those equations yield a simple approximation for equations 19 and 20. We obtain

$$\sigma \simeq 16 \left(\frac{R_i}{R_r}\right)^2 \frac{R_o K T_s z v}{\eta L p_r m \lambda} \tag{23}$$

and

$$A \simeq 2 \frac{R_i}{R_i + R_o} \sqrt{\frac{R_o K T_s z v \lambda}{\pi \eta L p_r m}}. \tag{24}$$

We recall that

λ is the radiation wavelength,

η is the antenna efficiency,

L is the size of the L by L antenna array,

m is the number of array beams processed for detection, and

v is the velocity of the target through the beam center and normal to the observation bore-sight.

From equation 24 it is easy to see the approximate dependency of the minimum detectable projected target area on most of the variables. In most cases there is an inverse square-root dependence. Only the dependence on distances remains a bit obscure.

3.1 The Baseline System

We will vary the parameters that characterize the surveillance system, but we wish to specify a baseline system that will be used as a design reference point. The approach throughout has been to use simple enough assumptions that the basic principles that determine the surveillance system performance can be studied, and the tradeoffs understood. The numerical predictions of

performance will inevitably appear to be a lower bound, but our goal is to be correct within a factor of two or three in calculating a minimum detectable projected target area under various conditions.

RECEIVER

- lossless single-beam processing
- from 1 by 1 meter to 100 by 100 meter antenna array
- signal-to-noise ratio z of 10
- time-bandwidth product of unity
- antenna efficiency η of .5
- system temperature T_s of 100 degrees Kelvin
- boresight elevation of about 90 degrees

TARGET

- 500 km height
- 7 km/s velocity normal to boresight
- bistatic angle nearly 180 degrees

TRANSMITTER

- 800 km height
- 20 GHz carrier frequency
- 10^{-12} W/m^2 on the ground
- illuminates target as necessary

The baseline surveillance system is a LEO system, looking at LEO targets between the transmitter and the receiver at bistatic angles of about 180 degrees. The bistatic angle is assumed to be so large that the maximum forward-scattered cross-section enhancement is obtained.

The transmitter is at 800 km altitude and places 10^{-12} W/m^2 on the ground. Although many existing communications satellite systems produce lower flux levels, some produce more. We assume that whenever the target is within the beam of the receiving antenna, the target is being illuminated by the transmitter. This requires at least some good operational procedures, and in some cases the antenna pattern of the transmitter may not be adequate. However, communications satellites usually have the smallest antennas, and hence the widest beams, making it easier to satisfy this assumption than if orbiting antennas were as large as communications engineers would like.

The baseline target is at 500 km altitude. Its projected area is unspecified. We will calculate the minimum value of the projected area in order to achieve at least 10 dB signal-to-noise ratio as various parameters are varied. It is unlikely that a target will be traveling exactly 7 km/s through the center of the receiver's antenna beam, yet this is what we assume. Some targets will be moving

faster, some slower, because the receiver is presumably tracking the transmitter. It could be easier to detect targets moving almost parallel to the transmitter because their relative velocity through the moving beam will be slower than $\bar{7}$ km/s.

Processing in the receiver is assumed to be lossless, and so the minimum detectable projected target area that we calculate will be a goal, rather than a guarantee. The antenna array size is varied in each performance graph from 1 to 100 meters, the latter size being exceptionally large. At the projected target areas that we calculate, barely 10 dB signal-to-noise ratio is achieved. In reality most operational surveillance systems operate at larger values. Referring to figure 6 we see that for the probabilities of false alarm and target detection to be at all reasonable at this signal-to-noise ratio, we must assume a time-bandwidth product of unity. Commonly the target would be said to be *coherent*. Antenna efficiency and system noise temperature at the surveillance system frequency of 20 GHz are slightly optimistic also, at .5 and 100 degrees Kelvin respectively.

3.2 Parametric System Performance

Here we consider, numerically, tradeoffs in simple surveillance system parameters. The parameters varied are of physical interest at the system level. Their variation affects the detection performance through the signal-to-noise ratio and the time-bandwidth product as detailed in section 2. Although in most cases we have already argued what the effect of each variation will be, it is important to test those arguments with the numerical model. For example, we know from figure 4 that moving the transmitter of a surveillance system with a fixed power flux at the ground level from LEO to GEO will increase the losses through the target path relative to a clear reference path. But the receiver antenna beam is wider at high altitude and the HEO target will move through the beam more slowly than a LEO target, increasing the signal duration available for detection processing. These are conflicting effects and we will have to apply the full detection model to see what happens.

In figure 9 the lossless detection performance of the LEO baseline surveillance system is shown. Our assumptions allow the computation of both a minimum detectable target cross section and a minimum detectable target projected area. The two quantities are related through the forward scattering equation 1. The effect of forward scattering is significant unless the projected target areas are so small that d/λ approaches unity. In the later graphs, when the baseline surveillance system is compared to other systems, only the minimum detectable target projected areas are graphed as one baseline variable is changed.

One of the simplest effects to anticipate is that communications satellite systems that place a larger power flux on the ground will be more effective illuminators for the surveillance system. The detection performance is shown in figure 10 for three different flux levels. Most of the existing communications satellite systems place 10^{-12} W/m^2 or less on the ground. This is the baseline value. However some existing systems produce larger flux values. Communications satellite systems that produce larger flux values can provide a more reliable service. The economics of commercial

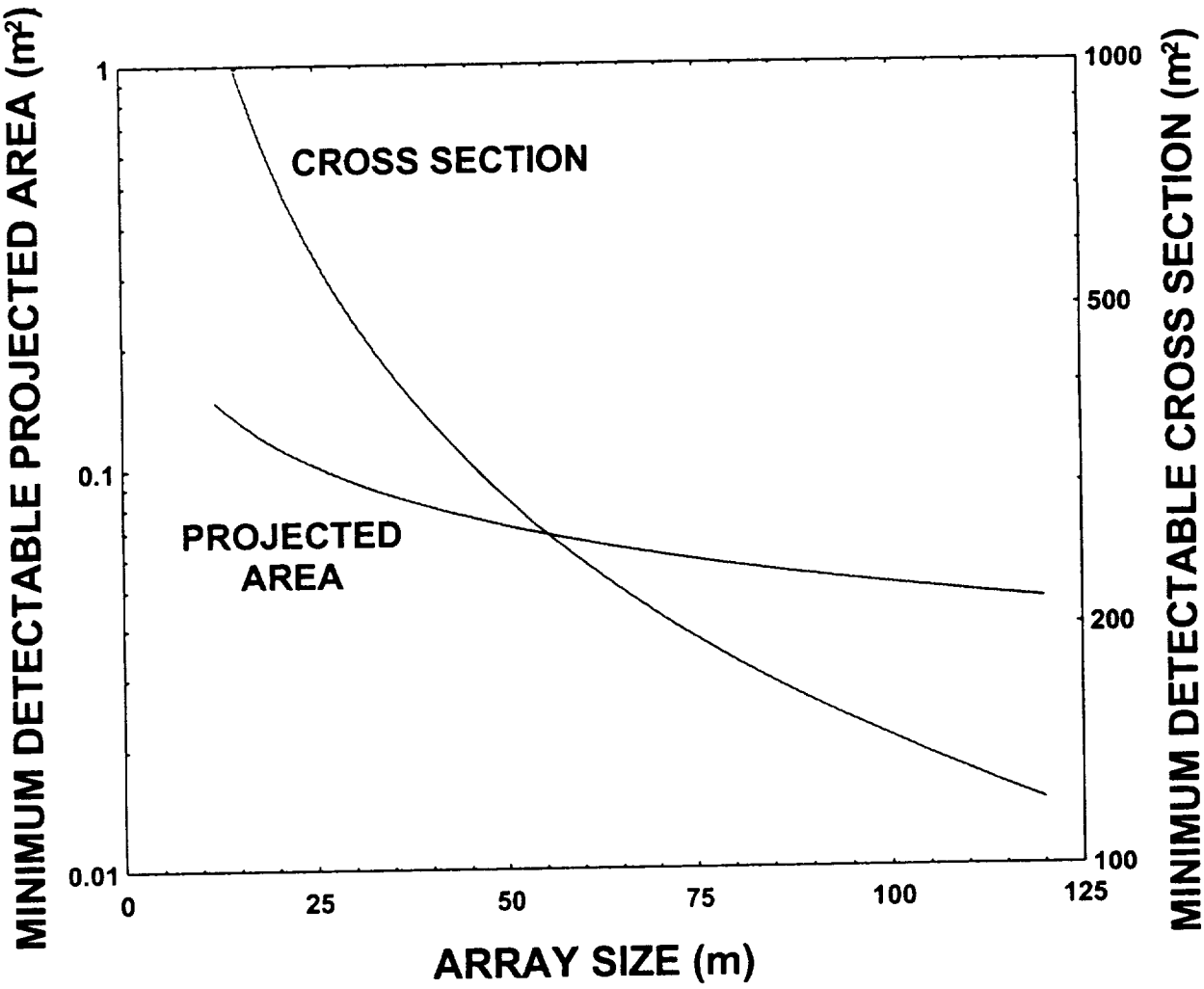

Figure 9. The forward-scattering effect significantly improves the surveillance system's detection performance. The observed cross section is much greater than the target's projected area.

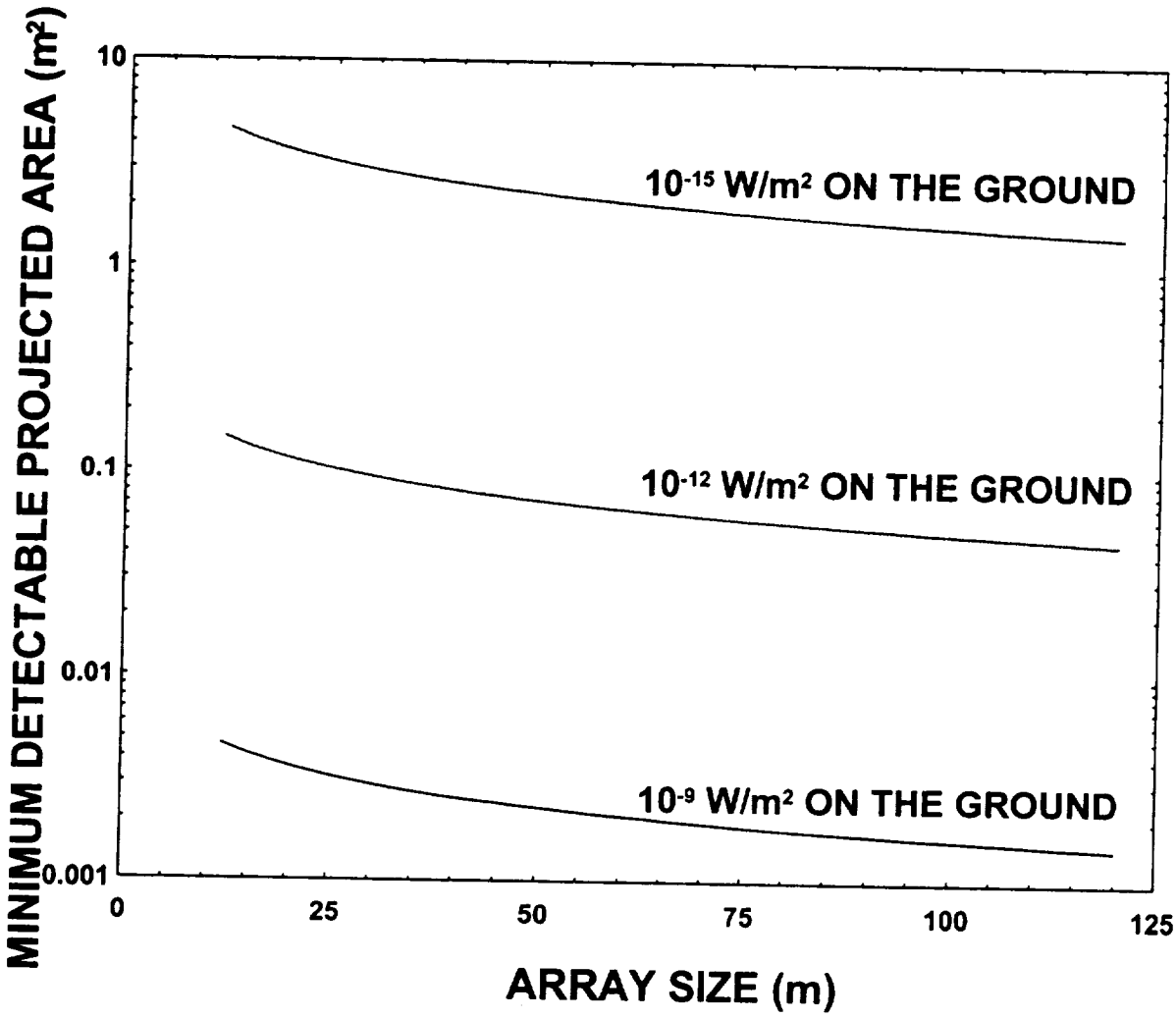

Figure 10. There do not appear to be any current communications satellite systems that place as much as 10^{-9} W/m^2 on the ground.

mobile communications demand that the number of accidentally terminated services be reduced, so power fluxes will probably increase in the future.

Equation 2 predicts that increasing the radiation frequency will improve performance. The effect is shown numerically in figure 11. Communications satellite systems will probably not operate

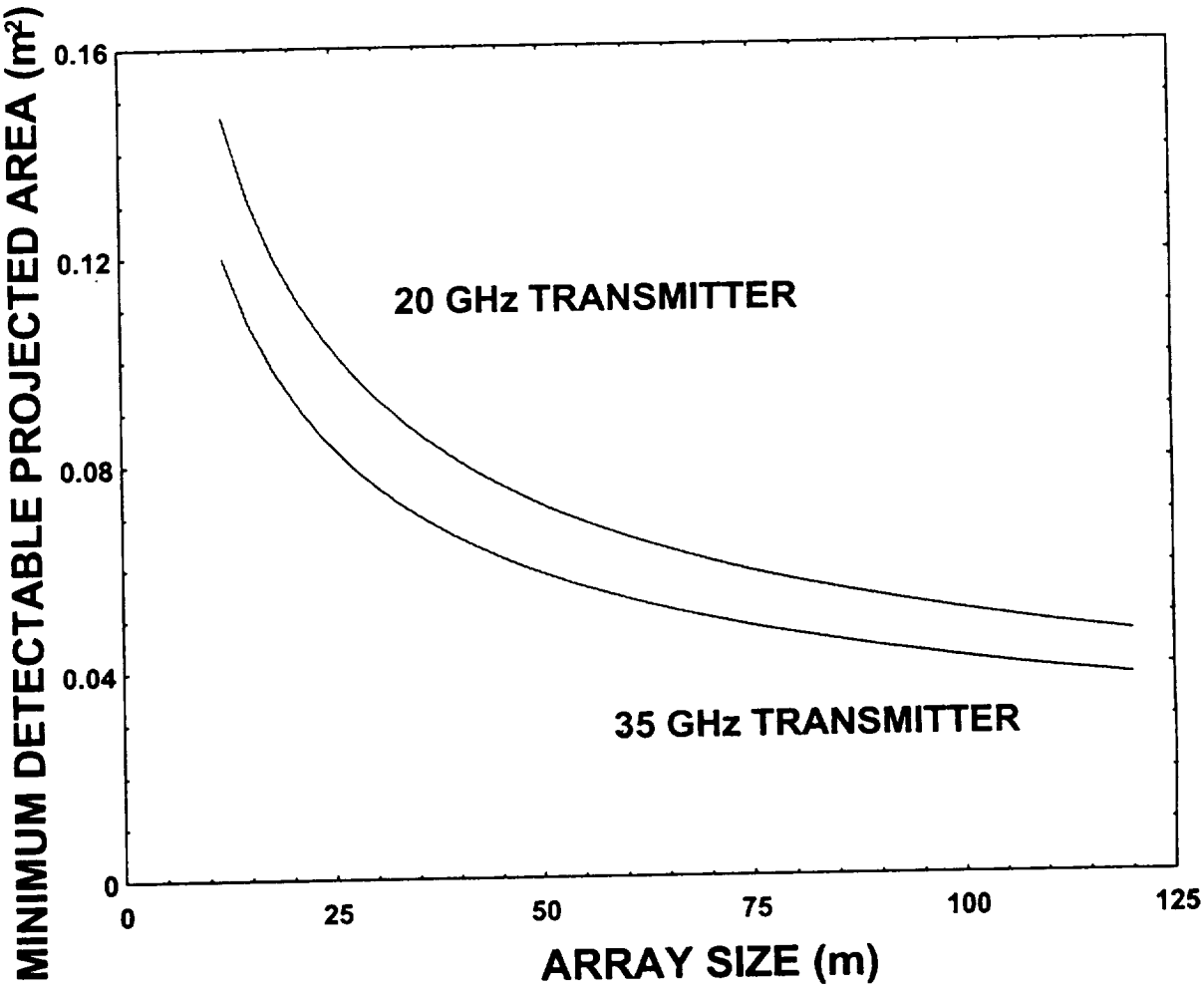

Figure 11. In the near term, communications satellite systems with frequencies as high as 30 GHz may be routinely built.

much over 30 GHz for the foreseeable future. This frequency does not provide a large advantage over the baseline assumption of 20 GHz. The advantage of searching for targets near the transmitter can be seen in figure 12. This effect is predicted by equation 5 which shows that path losses will

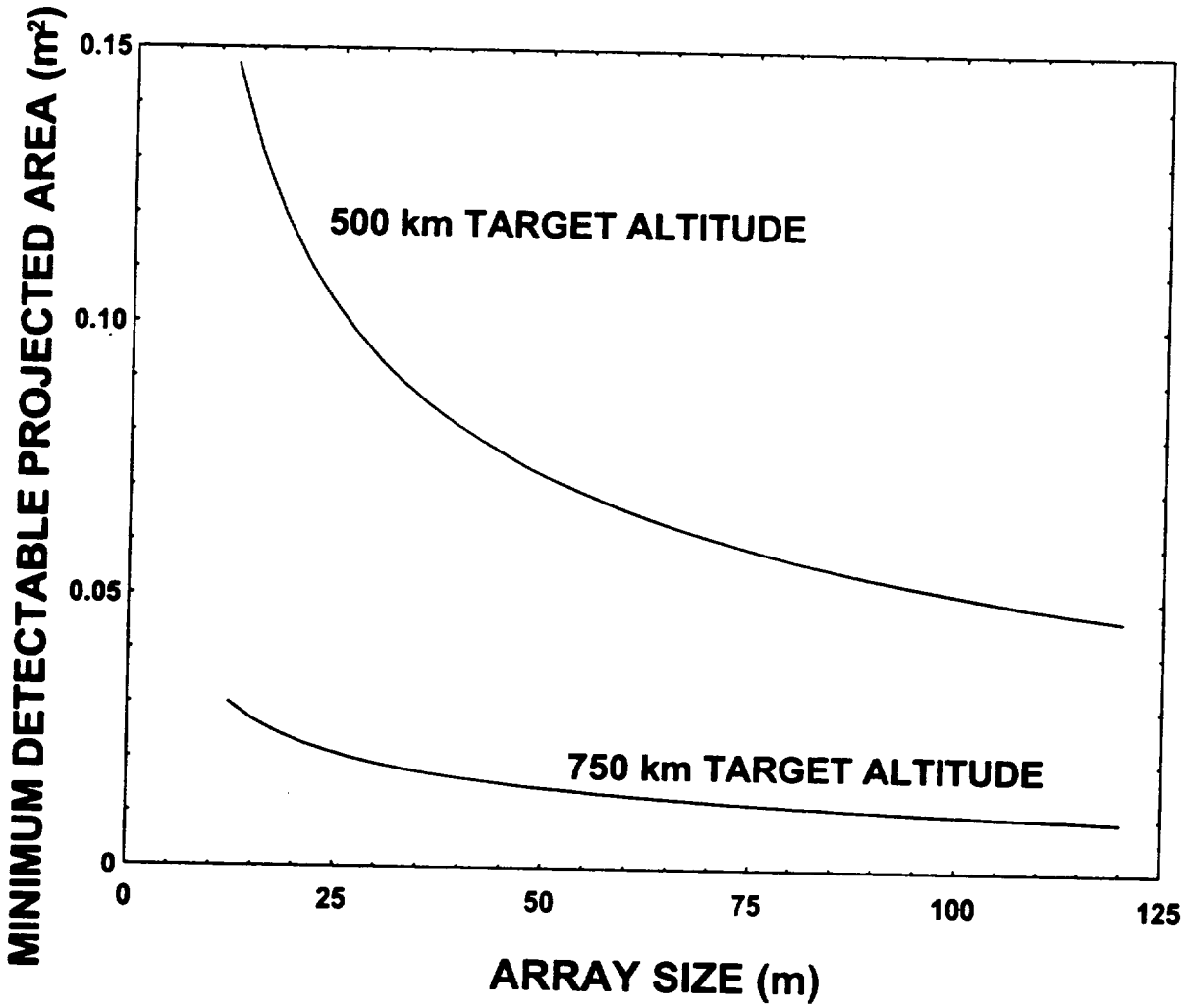

Figure 12. Improved performance is obtained when the target is 50 km from the transmitter instead of 300 km. Since the bistatic angle is nearly 180 degrees, there is no significant change in the total propagation path length in the two cases. The transmitter altitude is 800 km.

be less when the target is near either the transmitter or the observer. Remember that we have assumed that the target is illuminated as long as necessary for it to pass through the receiver antenna beam. This assumption may be challenged as the target nears the transmitter. Also if

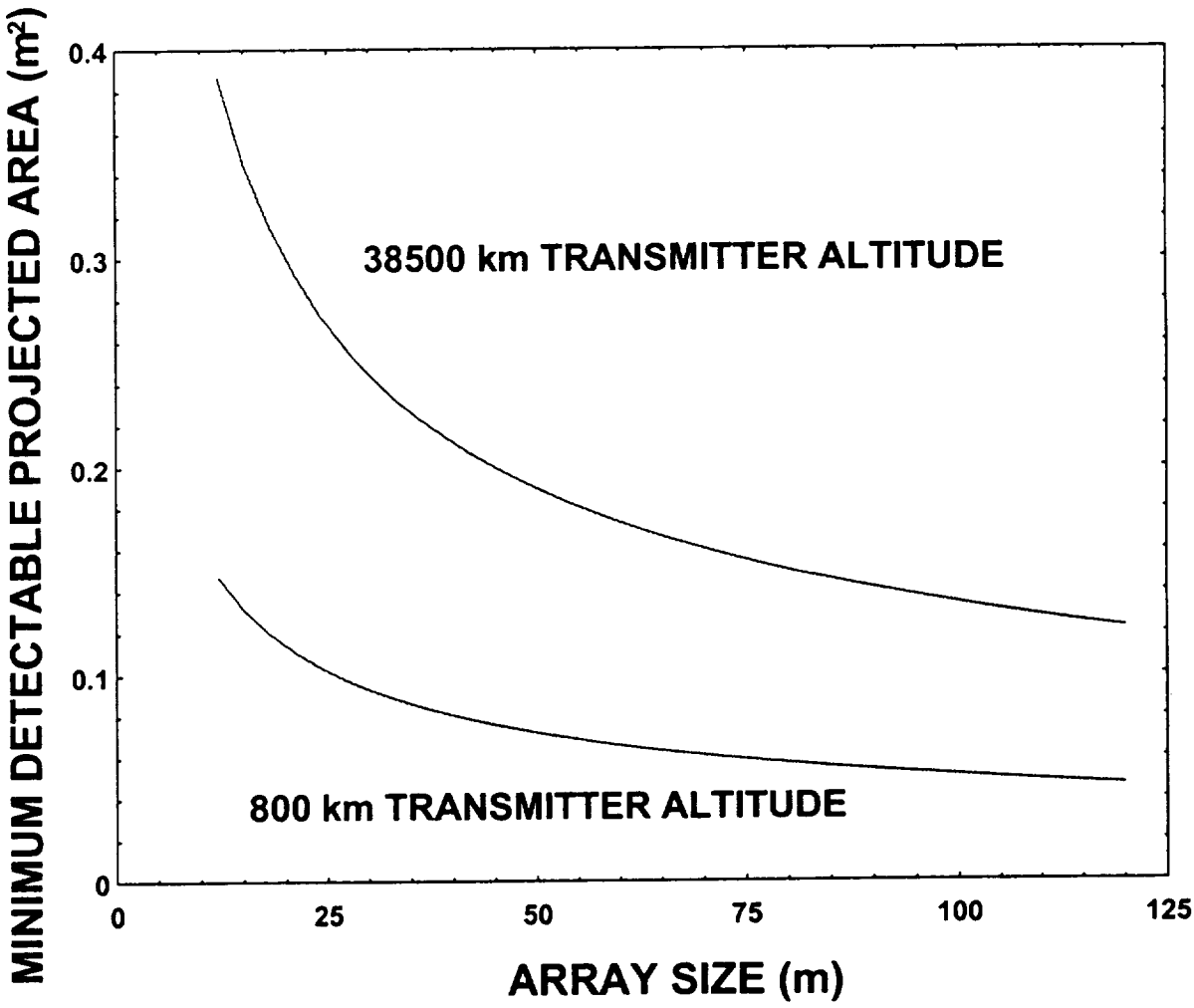

Figure 13. Moving the transmitter from LEO to GEO will decrease the LEO target detection performance, even though the GEO transmitter is assumed to be more powerful so that it places the same power flux on the ground as the LEO transmitter. The target altitude is 500 km.

we restrict ourselves to targets near the transmitter we will encounter larger processing losses (the target and the transmitter will be separated less in angle from the observer's viewpoint) and we will see fewer targets due to the smaller volume of space that is searched. Equation 6 also predicts that a LEO transmitter might be more effective than a GEO transmitter even though both transmitters put the same power flux on the ground. The effect can be seen in figure 13.

In section 2.7 it was argued that the time for detection could be extended by trajectory-based processing assumptions. The resulting performance improvement is optimistic because it does not take into account the false alarm rate which will increase to a new value depending on how the trajectory assumptions are incorporated into the detection scheme. The scheme is only possible because, in some cases, the target will be illuminated by the transmitter for a period of time longer than the time that the target stays in one beamwidth of the receiver antenna. This is not generally the case for a monostatic sensor with the transmission and reception antenna patterns nearly identical. The effect is shown in figure 14. Its application might be ultimately limited by the illumination geometry, or by computational restrictions.

Figure 15 compares several hypothetical surveillance systems. We have discussed a number of bistatic sensor optimization principles. It is interesting to see what happens in the following surveillance systems as many of the variables are changed together from one system to the next. We have already discussed the baseline surveillance system, which uses a LEO transmitter radiating 10^{-12} W/m^2 onto the ground from 800 km altitude. The target passes through a single beamwidth of the receiver antenna at 500 km altitude and at 7 km/s.

The Advanced Communications Technology Satellite (ACTS) is an unusually powerful communications satellite (60 dBW EIRP) in GEO. The ACTS satellite can put more than 10^{-11} W/m^2 on the ground. Because of its greater power and the fact that HEO targets can be expected to spend a longer time in the receiver antenna beamwidth than a LEO target, the ACTS might be used to detect HEO targets smaller than the LEO targets detectable by the baseline surveillance system. These additional factors governing the ACTS scenario overcome the tendency of a LEO surveillance system to perform more poorly as the transmitter altitude is raised. The target is 5000 km from the communications satellite transmitter that is at 38500 km altitude and the target is assumed to be traveling at 3 km/s through the receiver antenna beam. The frequency of operation is the same as the baseline 20 GHz.

The U.S. NAVSTAR GPS and the Russian GLONASS satellites have been considered as illuminators for an air-defense system, for example in [11]. These satellites have similar attributes as illuminators. They orbit at about 20,000 km altitude, radiate from about 1200 MHz to 1600 MHz, and place about 10^{-16} W/m^2 at ground level. The increased altitude, lower frequencies, lower flux levels and change in the fractional height of the LEO target are all disadvantages compared to the baseline system. The GPS and GLONASS satellites could not be used to detect LEO targets smaller than about 10 m^2. Used as illuminators for air-defense the fractional height disadvantage is somewhat mitigated and detection performance improves.

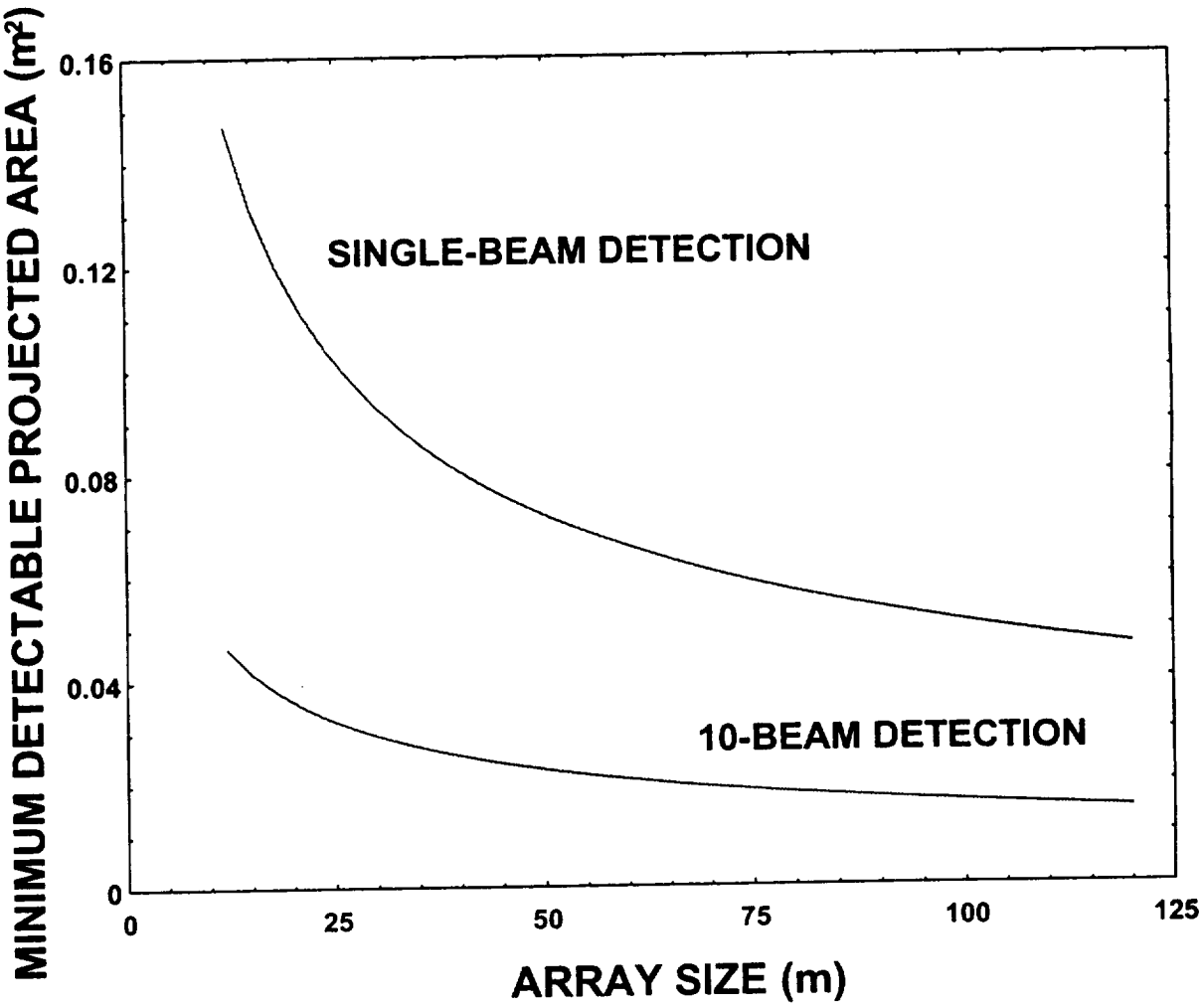

Figure 14. If the target is illuminated over several receiver beamwidths, then an improvement in detection performance can be gained by attempting detection over several beamwidths. The false alarm rate will also increase to a new value that depends on details of the implementation unless a smaller probability of target detection is tolerated, so the improvement shown is optimistic.

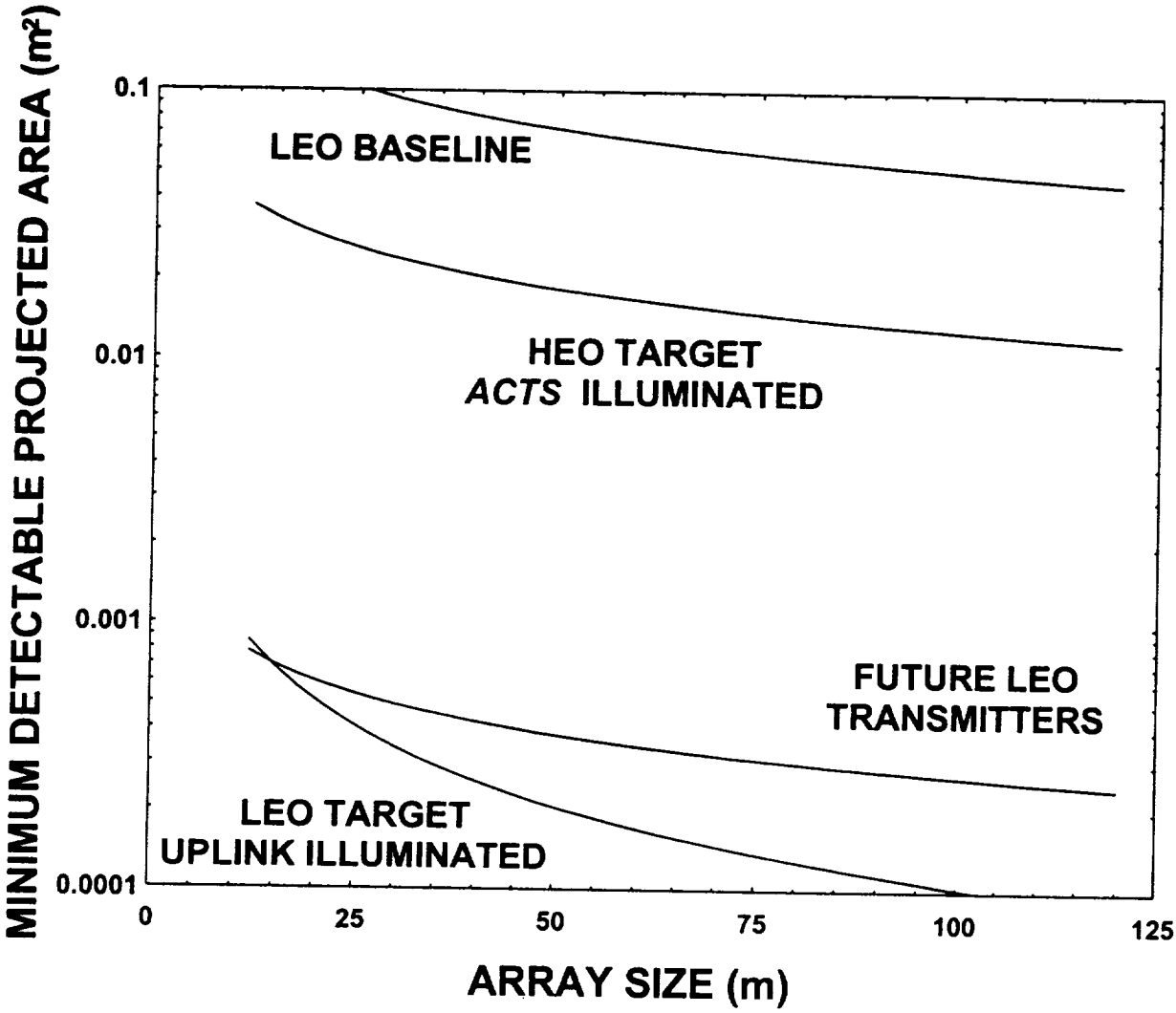

Figure 15. By postulating a number of surveillance systems that each utilize some of the principles outlined in section 2 several possibilities for detecting targets of .1 m^2 projected area or smaller are possible.

If future LEO communications satellite place larger power fluxes on the ground at 30 GHz, they will be more useful for the detection of LEO targets than the baseline surveillance system. The future LEO surveillance system is illuminating a target 50 km away, a relatively small distance, from an altitude of 800 km. The proposed communications satellite transmitter can put 10^{-10} W/m^2 on the ground. The example further supposes that a target trajectory passing through 10 receiver beamwidths at 7 km/s was observed and, as usual, processing was lossless.

The biggest surprise concerns how well the ground-to-ground surveillance system will work with very low-altitude targets. The uplink transmitter parameters are similar to those found in [12], section 9.2. The relatively good performance is due to the fact that uplink transmitters for GEO communications satellites are fairly powerful (75 dBW EIRP) compared to communications satellite transmitters, and the target is only at a 500 km altitude traveling at 7 km/s. This uplink transmitter is assumed to radiate at the baseline frequency value of 20 GHz. Because large bistatic angles cannot be realized for the ground-to-ground surveillance system, it was assumed that the target cross section and the projected area of the target are the same in this case. The hypothetical system does not perform as well as an operational space surveillance radar because the uplink transmitter is 30 dB or more less powerful.

Calculations for the latter two surveillance systems yield minimum detectable projected target areas below .001 m^2. This implies that the characteristic dimension of the smallest detectable targets for these surveillance systems are on the order of the radiation wavelength. This represents a fundamental limit of the modeling ideas employed. We might be suspicious of calculations for postulated surveillance systems that yield smaller minimum detectable area values unless higher frequencies were employed.

To obtain sharper results it is necessary to include processing losses for particular implementations and to include more subtle effects of geometry. We have assumed that the target is illuminated for as long as it stays in the receiver's antenna beam and that forward-scattering enhancement is always available. We have assumed that the target travels through the center of the beam at 3 km/s in HEO and at 7 km/s in LEO in order to determine the time available for target detection. Miller [13] has correctly pointed out that the requirement for a large bistatic angle might determine a different value for the detection time and significantly effect the surveillance coverage in general.

4. DISCUSSION

4.1 Summary

We have considered the detection performance of a number of bistatic sensor systems that make opportunistic use of existing communications satellites. This report has emphasized a space-to-ground surveillance system that uses an existing communications satellite transmitter to incidentally illuminate a target while the satellite is performing its normal (probably commercial) communications function. A special receiver would be needed on the ground to complete the surveillance system. State-of-the-art communications satellites put between 10^{-16} and 10^{-12} W/m^2 on the ground. A space-surveillance radar transmitter, if it could be operated in orbit, could place a flux of 10^{-5} W/m^2 on the ground from GEO. Thus the bistatic surveillance systems under consideration are underpowered by operational radar space-surveillance standards and their design must be optimized.

Besides utilizing an existing piece of communications equipment, the surveillance concept also allows for a variety of interesting bistatic geometries. As discussed in section 2.1 the largest target cross section is typically seen at a bistatic angle of 180 degrees. At a bistatic angle of 180 degrees, a 20 cm diameter sphere illuminated at 20 GHz exhibits a cross section that is 32 dB greater than its monostatic cross section. Similar enhancements are expected for complex targets of similar size. The enhancement effect is not significant (and the model is not necessarily valid) unless the ratio d/λ is much greater than one, where d is the characteristic dimension of the target and λ is the wavelength of the radiation.[1] The enhancement effect decreases as the size of the object decreases for a fixed illumination wavelength. Nevertheless, bistatic geometries where the transmitter, target and observer are nearly colinear can provide a useful cross section advantage. The enhancement increases with increasing frequency. The enhancement also remains significant within a few degrees of its maximum for typical targets and illuminating frequencies. The forward-scattering enhancement effect lead us to consider observation geometries with large bistatic angles.

The power received directly from the transmitter will be more than 100 dB greater than the scattered power received from the target in all cases of interest. This large dynamic range places a burden on any processing system that must handle the combined responses from the transmitter and the target. By analyzing a simple power flow model that assumes only the forward scattering geometry in section 2.2 we found that the power flux at the observer due to the target scattering is increased by searching for targets of a given size near the transmission source or near the observer. Power flux due to target scattering is at a minimum when the target is equidistant from the transmitter and the observer. Communications satellite systems at various altitudes tend to put the same power on the ground to provide a constant quality of service for ground stations of fixed

[1]This restriction actually affects the performance of all microwave sensing systems somehow, and is not particularly a weakness of the bistatic sensors examined in this report.

design and size. We found that the ratio of the power received via scattering from the target to the power received through a clear reference path from the transmitter to the observer increases as the distance between the observer and the transmitter decreases. Thus, for example, if two communications satellite systems are designed to put 10^{-12} W/m^2 on the ground, one operating from LEO and one from GEO, the bistatic surveillance system using the LEO transmitter will have better detection performance. These are peculiarities of purely geometric properties.

We discovered the preceding tradeoffs without discussing the detection model. We assumed that if a tradeoff increased the target-scattered power flux at the observer, detection performance would improve. In order to investigate more complex phenomenon including the effect of the duration of the target illumination, we chose a basic energy detection model in section 2.3 with a performance determined by the signal-to-noise ratio and the time-bandwidth product. Generally detection performance improves if either the signal-to-noise ratio is increased or the time-bandwidth product is decreased while the other quantity is held constant.

Transponder bandwidths dominate the bandwidth of the scattered radiation, having 27 and 36 MHz bandwidths typically. Using the detection model we observed that the bandwidth of the surveillance system should be reduced to as small a value as possible. This leads to the postulation of a correlation receiver in section 2.4 that could recover the signal envelope and reduce the required bandwidth to at least the reciprocal of the signal duration but no more than the 100 Hz or so bandwidth due to target cross-section fluctuation. Other minimum time-bandwidth receiver implementations would exhibit similar detection performance.

The signal component associated with the transmitter illumination and the potential signal due to target scattering must be separately available in order to implement the correlation receiver, which is based on a signal mixing principle. This signal separation can be accomplished by resolving the potential target and the communications satellite transmission in angle. Angle resolution can be accomplished by a beam-forming antenna array as proposed in section 2.5, possibly with sidelobe cancellation techniques. Using the detection model we discussed maximization of the aperture-time product in section 2.6, as determined by the array configuration, to improve surveillance system detection performance. The antenna array model that we proposed was general enough to show that no matter how many antenna array elements are used, the array should not be thinned (the array elements should not be moved further away from each other than necessary). Removing elements from the array, or separating the elements would cause the aperture-time product to be reduced.

The minimum detectable projected target area was calculated in section 3.2 to demonstrate the preceding tradeoff analyses. Most of these calculations were based on an assumption that the detection time was limited by the time that the target takes to fly through a single fixed antenna beam. By assuming possible trajectories for the target, signal energy can be collected over multiple array antenna beams before detection, improving the detection performance. This is a useful concept, discussed in section 2.7, when the target is illuminated longer than it requires to pass through a single receiver antenna beam. This approach does not make sense in an active

staring monostatic sensor that has an illumination antenna pattern that is nearly the same as its receiver antenna pattern.

Ignoring processing losses, in the near term it appears that a reasonable technical goal for a surveillance system based on these principles might be the detection and tracking of .1 m^2 area targets. This is about 3 orders of magnitude larger than the projected areas of the 1 cm LEO targets that generally elude the current space-surveillance system. A GEO communications satellite such as the ACTS can provide a capability for GEO targets also. Perhaps surprising, the performance of a ground-to-ground surveillance system that accidentally illuminates LEO targets with the communications satellite system uplink transmitter might provide the best near-term LEO performance.

In the future communications satellite systems may be placing 10^{-10} W/m^2 or more on the ground in urban areas in order to reduce the number of blocked and accidentally terminated transmissions to hand-held terminals with omnidirectional antennas. Their frequencies of operation may rise to 30 GHz to utilize new portions of the spectrum and also to reduce the antenna size requirements. Both of these future developments would improve the performance of the space-to-ground surveillance system.

The minimum detectable projected target areas under some assumptions were small enough that the characteristic sizes of the smallest targets were on the order of a radiation wavelength. This condition can be regarded as a practical limit of conventional microwave surveillance sensors. Under such conditions the cross section of the target is not guaranteed to be simply related to its projected area.

4.2 Potential Applications

As evidenced by figure 15, there are a number of possible parasitic systems that could detect and track *payload* and *rocket-body* class targets in LEO or HEO, in fact anywhere that there is a suitable transmitter nearby. We assume that all viable architectures use an existing transmitter because of its cost to build and maintain, in space or on the ground. It might come as a surprise that these flea-powered systems could be used at all, considering the expensive and powerful transmission hardware that is used in the current space-surveillance system. These parasitic systems utilize transmitters with peak power equal to their average power, generally the simplest and most inexpensive way to deliver power to a load. A transmitter in a monostatic radar operating at 10% duty cycle must be designed to deliver peak powers 10 times greater than the system's average illumination power, increasing its cost and complexity. Also, as evidenced by equation 1 and figure 9, forward-scattering enhancement provides a significant cross-section advantage. Thus if nothing else, thinking about the technologies needed to implement these parasitic systems might lead to more efficient and less expensive surveillance radars.

4.2.1 Ground-to-Ground Systems

The smallest technical risk is associated with a ground-to-ground surveillance system using the communications satellite uplink as a LEO target illuminator. Except for the wideband continuous-time illumination, the system need not be very different from existing multistatic and monostatic systems. The system is operated at small bistatic angles. Forward scattering enhancement is not involved. Therefore placing the receiver over the horizon from the transmitter, or anywhere that it is sufficiently shielded, should make it possible to recover the weak scatter from the target without being jammed by the uplink. In order to implement an envelope detection type of receiver as discussed in section 2.4, some arrangement might be made to obtain a reference signal from a cooperative uplink. Another possibility is to receive the downlinked signal from the illuminated communications satellite transponder which is at a different (typically lower) frequency and translate it to obtain the local receiver reference signal.

The ground-to-ground system is limited to the detection of LEO targets and its coverage of the LEO environment is limited. A more interesting system might combine a ground-to-ground system with a space-to-ground system for illumination of HEO targets and a larger number of LEO targets than those illuminated by the uplink alone. The space-to-ground system, which utilizes forward scattering enhancement, faces additional technical challenges. This scheme could utilize all of the transmitters in a given communications satellite system.

4.2.2 Space-to-Ground Systems

In section 2.2 it was shown that the sensitivity of a bistatic radar can be expected to improve as the target nears the transmitter or receiver. Therefore space-to-ground systems that utilize a GEO communications satellite transmitter are best used to detect and track targets in HEO or LEO, while LEO communications satellites are best used to illuminate LEO targets. Here by *best* is meant the situation that allows the detection and tracking of the smallest targets. Such parasitic bistatic radars will not be as sensitive as existing monostatic surveillance radars because the transmitters have much less average power. Improving the performance of these space-to-ground systems involves a technical risk that follows from the need to take advantage of forward scattering enhancement.

It is well known that the target has the greatest cross section, and hence the smallest targets are detectable, at a bistatic angle near 180 degrees, as discussed in section 2.1. The effect persists within a few degrees of the optimum geometry. This advantage is very pronounced when the target dimension is many wavelengths, but goes away as the target size decreases to a wavelength. Thus the forward scattering geometry is only advantageous when the system sensitivity is not great enough to detect targets on the order of a wavelength at small bistatic angles anyway. We found from figure 9 that typical space-to-ground system sensitivities are such that forward scattering does provide an advantage, without it the smallest targets that can be detected are many wavelengths in size. Therefore we consider the forward scattering case and its technical risk further.

When the receiver, target and transmitter are nearly colinear in order to utilize the forward scattering enhancement, recovering the weak target scatter in the presence of the strong direct illuminator radiation must be considered. The scatter from the target is much weaker than the direct illumination on the receiver as evidenced by figure 4. Typical schemes for recovering the weak target scatter rely on the fact that the forward scattering enhancement persists at bistatic angles slightly less than 180 degrees, when the transmitter, target and receiver are not quite positioned along the same line.

There are several ways to exploit the slight non-colinearity. In a one scheme, the transmitter transmits a sinusoid, so that the Doppler shift in the scattered return from a target allows it to be separated from the direct transmission with a bandpass filter. The relative Doppler shift in the target scatter vanishes of course as the target crosses the line between the transmitter and receiver, hence the non-colinearity is required. Another common scheme pulses the transmitter so that the scatter from a target arrives at the receiver while the transmitter is turned off. Of course there is no relative time delay between the target scatter and the direct transmission when the target lies directly on the line between the transmitter and receiver. Again the non-colinearity is required. These are examples of schemes that allow the target scatter, at more than 100 dB below the power received directly from the transmitter, to be recovered without being jammed in the receiver by the direct illuminator transmission. An excellent overview with references is found in [14], particularly section 1.4.

If an existing communications satellite is utilized, its transmissions will be neither pulsed nor sinusoidal. It radiates a wideband waveform continuously. The missing technology is a demonstration of the ability to operate parasitic radars at very large bistatic angles with a wideband continuously radiating illuminator. No reference providing evidence that this technology has been demonstrated was found by the author. In a very recent article, Koch and Westphal [11] have only succeeded in recording the power fluctuations that occur in a Global Positioning System satellite receiver as large aircraft and spacecraft pass between the transmitter and the receiver. Furthermore their accomplishment is not unique.

In this report one possible solution employing angle diversity was suggested in sections 2.4 and 2.5. Angle diversity is a way of taking advantage of the slightly non-colinear relationship among the positions of the transmitter, target and receiver. Other solutions may be possible. In any case it is very important to remember that any solution must embody a minimal time-bandwidth receiving system. As illustrated in figure 6, a system with larger time-bandwidth product is likely to perform so poorly that the forward-scattering advantage will be lost anyway and the designer might as well fall back to the case of small bistatic angles.

4.3 Small Aperture Space-to-Ground Systems

In section 2.5 where the antenna array model is described, it is stated that only the size of the array directly affects the target detection capability. The minimum detectable projected target areas can be achieved with a single element antenna as well as an array of the same size with many

elements, provided that the in both cases the receiver is equally implementable. A single element antenna is simpler than an array.

Also note from the approximate expression 24 and, say, figure 15 that the minimum detectable projected target areas do not depend strongly on the antenna size so that a system with one square meter of aperture will be able to see objects with an area only ten times greater than an object detectable with a 100 meter by 100 meter array! Such objects might have characteristic dimensions only slightly more than 3 times the dimensions of the smallest object detectable by the system with the 100 by 100 meter array! When put his way, it becomes interesting to think about a parasitic space-to-ground surveillance system with a small dish antenna that would fit in a truck, for example.[2]

How could we implement the system without a large number of elements? The answer will not be determined in this report. However, because of the large intensity difference at the receiver between the target scatter and the direct transmitter illumination, nulling may play a role. Suppose, only for example, that a single antenna is aligned to receive the direct transmission from the illuminating satellite with maximum gain. A second identical antenna might be aligned so that its maximum gain is achieved at an angle corresponding to an angle of minimum gain for the first antenna. The second antenna achieves some rejection of the signal contribution due to direct illumination by the communications satellite. Furthermore, the signals from the two antennas can be combined to adaptively null this contribution from the second antenna beyond the amount of rejection due only to the antenna patterns. Further signal-to-clutter improvement might be achieved by processing that takes advantage of the structure of the signal associated with the illuminator, typically frequency modulation. The final signal-to-clutter ratio that could be achieved would limit the performance of the small aperture system. Only two small antenna elements have been used, hence the complexity of the antenna array is minimal.

4.4 Conclusions

Several architectures for a parasitic radar that utilizes an existing component of a satellite communications system seem possible for the detection and tracking of payload and rocket-body size targets. For LEO targets the best detection performance will probably be obtained with a ground-to-ground system that uses a satellite uplink as a target illuminator. For greater surveillance coverage, including HEO, a space-to-ground system utilizing a communications satellite transmitter

[2]From equation 24 it is clear that the minimum detectable projected target area depends weakly on many variables. Improvements in system temperature, transmitter power, antenna array size and so forth are rewarded by only a square-root improvement in the detectable area. For this reason the use of multiple illuminating sources and wide-band receivers is also an expensive way to improve the detection performance, although technically not difficult to imagine.

and forward scattering enhancement might be postulated, but the illuminator tends to jam detection of the weak target scatter in the receiver at large bistatic angles.

A demonstration of a receiving system that operates at large bistatic angles with wide-band continuous-time illumination of the target appears to be the new technology that is required for a space-to-ground system. There is only a weak dependence of the detection performance of this system on antenna array size, so smaller and relatively inexpensive systems become interesting. The required technology can be demonstrated by achieving reasonable signal-to-clutter ratios in a small aperture space-to-ground system.

REFERENCES

1. L. J. Cantafio. *Space-Based Radar Handbook.* Norwood, Massachusetts: Artech House, 1989.
2. Y. Hsu and D. Lorti, "Spaceborne bistatic radar—an overview," *IEEE Proceedings*, vol. 133, pp. 642–648, December 1986.
3. G. W. Preston, "The theory of stellar radar," Memorandum RM-3167-PR, Rand Corporation, May 1962.
4. K. Siegel, "Bistatic radars and forward scattering," in *Proc. Nat. Conf. Aeronaut. Electron.*, pp. 286–290, May 1958.
5. G. Mie, "Beitrage zur optik truber medien speziell kolloidaler metalosungen," *Annalen der Physik*, no. 25, pp. 377–445, 1908.
6. M. I. Skolnik, *Radar Handbook.* New York: McGraw-Hill Book Company, 1990.
7. J. I. Glaser, "Bistatic rcs of complex objects near forward scatter," *IEEE Trans.*, vol. AES-21, pp. 70–78, 1985.
8. N. Levanon, *Radar Principles.* New York: John Wiley and Sons, 1988.
9. H. Urkowitz, "Energy detection of unknown deterministic signals," *Proc. IEEE*, vol. 55, pp. 523–531, April 1967.
10. D. J. Torrieri, *Principles of Secure Communications Systems.* Boston: Artech House, 1992.
11. V. Koch and R. Westphal, "New approach to a multistatic passive radar sensor for air/space defense," *IEEE AES Magazine*, vol. 10, pp. 24–32, November 1995.
12. R. L. Douglas, *Satellite Communications Technology.* Englewood Cliffs, New Jersey: Prentice Hall, 1988.
13. R. W. Miller private communication.
14. N. J. Willis, *Bistatic Radar.* Boston: Artech House, 1991.

APPROVAL

PROJECT ORION: ORBITAL DEBRIS REMOVAL USING GROUND-BASED SENSORS AND LASERS

By J.W. Campbell

The information in this report has been reviewed for technical content. Review of any information concerning Department of Defense or nuclear energy activities or programs has been made by the MSFC Security Classification Officer. This report, in its entirety, has been determined to be unclassified.

A. ROTH
Director, Program Development Office

☆U.S. GOVERNMENT PRINTING OFFICE—1996—532-128/40059

REPORT DOCUMENTATION PAGE

Form Approved
OMB No. 0704-0188

1. AGENCY USE ONLY (Leave Blank)	2. REPORT DATE	3. REPORT TYPE AND DATES COVERED
	October 1996	Technical Memorandum

4. TITLE AND SUBTITLE

Project ORION: Orbital Debris Removal Using Ground-Based Sensors and Lasers

5. FUNDING NUMBERS

6. AUTHOR(S)

J.W. Campbell, Project Manager

7. PERFORMING ORGANIZATION NAME(S) AND ADDRESS(ES)

George C. Marshall Space Flight Center
Marshall Space Flight Center, Alabama 35812

8. PERFORMING ORGANIZATON REPORT NUMBERS

9. SPONSORING/MONITORING AGENCY NAME(S) AND ADDRESS(ES)

National Aeronautics and Space Administration
Washington, DC 20546-0001

10. SPONSORING/MONITORING AGENCY REPORT NUMBER

NASA TM-108522

11. SUPPLEMENTARY NOTES

Prepared by Program Development Office.

12a. DISTRIBUTION/AVAILABILITY STATEMENT

Unclassified-Unlimited

12b. DISTRIBUTION CODE

13. ABSTRACT *(Maximum 200 words)*

About 100,000 pieces of 1- to 10-cm debris in low-Earth orbit are too small to track reliably but large enough to cripple or destroy spacecraft. The ORION team studied the feasibility of removing the debris with ground-based laser impulses. Photoablation experiments were surveyed and applied to likely debris materials. Laser intensities needed for debris orbit modification call for pulses on the order of 10kJ or continuous wave lasers on the order of 1 MW. Adaptive optics are necessary to correct for atmospheric turbulence. Wavelength and pulse duration windows were found that limit beam degradation due to nonlinear atmospheric processes. Debris can be detected and located to within about 10 microrads with existing radar and passive optical technology. Fine targeting would be accomplished with laser illumination, which might also be used for detection. Bistatic detection with communications satellites may also be possible. We recommend that existing technology be used to demonstrate the concept at a loss of about $20 million. We calculate that an installation to clear altitudes up to 800 km of 1- to 10-cm debris over 2 years of operation would cost about $80 million. Clearing altitudes up to 1,500 km would take about 3 years and cost about $160 million.

14. SUBJECT TERMS

orbital debris removal, orbital debris detection, laser atmospheric propagation, laser impulse

15. NUMBER OF PAGES

348

16. PRICE CODE

NTIS

17. SECURITY CLASSIFICATION	18. SECURITY CLASSIFICATION OF THIS PAGE	19. SECURITY CLASSIFICATION OF ABSTRACT	20. LIMITATION OF ABSTRACT
Unclassified	Unclassified	Unclassified	Unlimited